

# Talanta

The International Journal of Pure and Applied Analytical Chemistry

---

## Editors-in-Chief

**Professor G.D. Christian**, University of Washington, Department of Chemistry, 36 Bagely Hall, P.O. Box 351700, Seattle, WA 98195-1700, U.S.A.

**Professor J.-M. Kauffmann**, Université Libre de Bruxelles, Institut de Pharmacie, Campus de la Plaine, C.P. 205/6, Boulevard du Triomphe, B-1050 Bruxelles, Belgium

## Associate Editors

**Professor J.-H. Wang**, Research Center for Analytical Sciences, Northeastern University, Box 332, Shenyang 110004, China

**Professor J.L. Burguera**, Los Andes University, IVAIQUIM, Faculty of Sciences, P.O. Box 542, 5101-A Mérida, Venezuela.

## Assistant Editors

**Dr R.E. Synovec**, Department of Chemistry, University of Washington, Box 351700, Seattle, WA 98195-1700, U.S.A.

**Professor J.-C. Vire**, Université Libre de Bruxelles, Institut de Pharmacie, Campus de la Plaine, C.P. 205/6, Boulevard du Triomphe, B-1050 Bruxelles, Belgium

## Talanta

R. Apak (Istanbul, Turkey)  
E. Bakker (Auburn, AL, U.S.A.)  
D. Barceló (Barcelona, Spain)  
B. Birch (Luton, UK)  
K. S. Booksh (Tempe, AZ, U.S.A.)  
J.-L. Capelo-Martinez (Caparica, Portugal)  
Z. Cai (Kowloon, Hong Kong)  
S. Cosnier (Grenoble, France)  
D. Diamond (Dublin, Ireland)  
W. Frenzel (Berlin, Germany)  
A.G. Gonzales (Seville, Spain)  
E.H. Hansen (Lyngby, Denmark)  
P. de B. Harrington (OH, U.S.A.)

A. Ho (Hsin-chu, Taiwan)  
J. Kalivas (Pocatella, ID, U.S.A.)  
B. Karlberg (Stockholm, Sweden)  
J.-M. Lin (Beijing, China)  
Y. Lin (Richland, WA, U.S.A.)  
M.D. Luque de Caastro (Cordoba, Spain)  
I.D. McKelvie (Victoria, Australia)  
S. Motomizu (Okayama, Japan)  
D. Nacapricha (Bangkok, Thailand)  
J.-M. Pingarron (Madrid, Spain)  
E. Pretsch (Zürich, Switzerland)  
W. Schuhmann (Bochum, Germany)  
M. Shamsipur (Kermanshah, Iran)

M. Silva (Porto Alegre, Brazil)  
P. Solich (Hradec Králové, Czech Republic)  
K. Suzuki (Yokohama, Japan)  
D.G. Themelis (Thessaloniki, Greece)  
D.L. Tsalev (Sofia, Bulgaria)  
Y. van der Heyden (Belgium)  
B. Walczak (Katowice, Poland)  
J. Wang (Tempe, AZ, U.S.A.)  
J.D. Winefordner (Gainesville, U.S.A.)  
Xiu-Ping Yan (Tianjin, China)  
E.A.G. Zagatto (Piracicaba, SP, Brazil)

---

Copyright © 2007 Elsevier B.V. All rights reserved

**Publication information:** *Talanta* (ISSN 0039-9140). For 2007, volumes 71–73 are scheduled for publication. Subscription prices are available upon request from the Publisher or from the Regional Sales Office nearest you or from this journal's website (<http://www.elsevier.com/locate/talanta>). Further information is available on this journal and other Elsevier products through Elsevier's website: (<http://www.elsevier.com>). Subscriptions are accepted on a prepaid basis only and are entered on a calendar year basis. Issues are sent by standard mail (surface within Europe, air delivery outside Europe). Priority rates are available upon request. Claims for missing issues should be made within six months of the date of dispatch.

**Orders, claims, and journal enquiries:** please contact the Customer Service Department at the Regional Sales Office nearest you:

**Orlando:** Elsevier, Customer Service Department, 6277 Sea Harbor Drive, Orlando, FL 32887-480 USA; phone: (+1) (877) 8397126 [toll free number for US customers], or (+1) (407) 3454020 [customers outside US]; fax: (+1) (407) 3631354; e-mail: [usjcs@elsevier.com](mailto:usjcs@elsevier.com)

**Amsterdam:** Elsevier, Customer Service Department, PO Box 211, 1000 AE Amsterdam, The Netherlands; phone: (+31) (20) 4853757; fax: (+31) (20) 4853432; e-mail: [nlinfo-f@elsevier.com](mailto:nlinfo-f@elsevier.com)

**Tokyo:** Elsevier, Customer Service Department, 4F Higashi-Azabu, 1-Chome Bldg, 1-9-15 Higashi-Azabu, Minato-ku, Tokyo 106-0044, Japan; phone: (+81) (3) 5561 5037; fax: (+81) (3) 5561 5047; e-mail: [jp.info@elsevier.com](mailto:jp.info@elsevier.com)

**Singapore:** Elsevier, Customer Service Department, 3 Killiney Road, #08-01 Winsland House I, Singapore 239519; phone: (+65) 63490222; fax: (+65) 67331510; e-mail: [asiainfo@elsevier.com](mailto:asiainfo@elsevier.com)

**USA mailing notice:** *Talanta* (ISSN 0039-9140) is published monthly by Elsevier B.V. (P.O. Box 211, 1000 AE Amsterdam, The Netherlands). Annual subscription price in the USA US\$ 3,818 (valid in North, Central and South America), including air speed delivery. Application to mail at periodical postage rate is paid at Rathway, NJ and additional mailing offices.

**USA POSTMASTER:** Send address changes to *Talanta*, Publications Expediting Inc., 200 Meacham Avenue, Elmont, NY 11003.

**AIRFREIGHT AND MAILING** in the USA by Publications Expediting Inc., 200 Meacham Avenue, Elmont, NY 11003.

## FTIR analysis and monitoring of synthetic aviation engine oils

Mike J. Adams<sup>a,\*</sup>, Melissa J. Romeo<sup>a</sup>, Paul Rawson<sup>b</sup>

<sup>a</sup> School of Applied Sciences (Applied Chemistry), RMIT University,  
Melbourne, Victoria 3001, Australia

<sup>b</sup> Defence Science and Technology Organisation, Platform Sciences Laboratory,  
Fishermans Bend, Melbourne, Victoria 3207, Australia

Received 1 February 2007; received in revised form 18 April 2007; accepted 18 April 2007

Available online 27 April 2007

### Abstract

Synthetic turbine oils from military aircraft engines were analysed for antioxidant content and total acid number using infrared (IR) spectroscopy. Two-dimensional IR correlation analysis was employed to investigate and interpret observed trends in the spectra, as acid was formed and antioxidant species were depleted in the oils, as a function of aging and engine wear. Principal components and partial least squares algorithms were used and compared for the development of calibration and prediction models. Transmission IR spectrometry is demonstrated to be effective for the analysis and monitoring of synthetic aviation turbine engine oils and shown to provide rapid and accurate information as compared with traditional analytical techniques and methods.

© 2007 Elsevier B.V. All rights reserved.

**Keywords:** Synthetic turbine engine oil; Infrared spectroscopy; Principal components regression; Partial least squares; Total acid number; Antioxidants; 2D IR correlation spectroscopy

### 1. Introduction

Oil is vital for maintaining optimum engine performance [1]. It protects the engine from the effects of heat, pressure, corrosion, oxidation and contamination, it acts as a lubricant by providing a fluid barrier between moving parts, reducing friction and wear, and oil serves to clean the interior of the engine by removing dirt, wear and combustion contaminants. Oil also serves to cool an engine by increasing heat dissipation, further reducing wear and preventing the entry of contaminants. Because of the different operating conditions and loads to which the engines are subjected, there are many differences between the oils used in the automotive and aviation industry and a complex approval process exists for ensuring that materials used in aviation applications are manufactured to relevant standards. Aviation engines are made of lightweight alloys, and operate over a wider temperature range than normal automotive engines. As a consequence of this, oils used in aviation engines are generally complex synthetic mixtures. Compared with automotive

oils they operate at a different viscosity and contain additives developed to cope with the specific high performance needs of aviation engines [2].

It is imperative that aviation engine oil is monitored on a regular basis, to identify impurities arising from the engine and to determine the concentration of specific additives that may become depleted through general use. For example, oils highly depleted in added antioxidant have the potential to damage aircraft lubrication systems and shorten the life expectancy of the engine or transmission system [2]. Typical antioxidants added to oils are phenylamines such as PAN (phenyl- $\alpha$ -naphthylamine, C<sub>16</sub>H<sub>13</sub>N) [3]. These materials are generally lipophilic solids that serve as radical scavengers in the auto-oxidation of lubricants, and such additives are usually present in fresh oils at a concentration of about 1–2% [3].

Two important oil parameters that require regular monitoring are the concentration of antioxidant present in the oil and the so-called total acid number (TAN) of the oil. The latter indicates the degree to which oil has broken down and is a measure of the useful life remaining for the oil. When oil degrades, chiefly by oxidation, the oxidation by-products are acidic, and so measuring the acidity of oil (and comparing it to an initial value) is a good indicator of the suitability of the oil for further service [4].

\* Corresponding author. Tel.: +61 3 9925 3358; fax: +61 3 9925 3747.  
E-mail address: [mike.adams@rmit.edu.au](mailto:mike.adams@rmit.edu.au) (M.J. Adams).

TAN is the measure of the weak organic and strong inorganic acids formed in oil. The magnitude of the TAN value is proportional to the amount of acidic constituents in the oil and is defined as the specific quantity, in mg, of base (potassium hydroxide) required to neutralize the acid in 1 g of oil [5]. Common acids formed in aviation turbine oils are carboxylic acids, predominantly C7 and C9, but also butyric (butanoic) acid and valeric acid, which arise from the hydrolysis of esters, and phosphoric acid which originates from the hydrolysis of organic phosphates. If acids are allowed to accumulate in the oil there is a danger that they will corrode the metallic engine components. Magnesium, commonly used in engine and transmission components to reduce system weight, is particularly susceptible to this form of corrosion [2].

Traditionally oil condition monitoring is performed using a range of chemical and physical tests; TAN by titration with potassium hydroxide, and antioxidant concentrations by liquid chromatography [5]. Such methods are time consuming and, in the case of TAN determinations, require relatively large volumes of sample. As an alternative, the use of FTIR spectrometry to monitor fuel and engine oil condition has received considerable attention in the literature [2,4,6–10]. Thus, Pavoni et al. have reported the use of fixed-path length transmission studies, with principal components analysis and partial least squares regression analysis, to determine physico-chemical properties of gasoline (including density, Research Octane Number, aromatic content, etc.) [7]. Navotny-Farkas and Bohme have similarly employed FTIR as a replacement technique for the traditional methods of chemical analysis of industrial lubricants [9], and Wooton has reviewed the application of spectroscopic methods in the fuels and lubrication industry [10]. The determination of Acid Number and Base Number in lubricants by FTIR has been reported by van de Voort et al. [4,6]. These authors overcame the matrix effects commonly encountered with IR spectrometry of unknown, complex mixtures by using signal transduction and differential spectroscopy. By this method trifluoroacetic acid and potassium phthalimide were used as stoichiometric reagents to provide IR absorption signals proportional to the basic and acidic constituents present in oils. Samples were diluted with 1-propanol then split in half with one sub-sample treated with reagent and the other treated with a blank reagent. The spectrum of each sub-sample was recorded and the differential spectrum obtained to ratio out the invariant spectral contributions from the sample. The authors reported excellent correlation between the IR results (using peak height measurements of the C=O and COO<sup>-</sup> vibration absorptions) and those from standard, titrimetric methods, with the spectrometric technique providing advantages of requiring smaller size, greater speed of analysis, and lower environmental impact by the reagents used. These authors have described a similar method for the quantitative determination of moisture in lubricants [8].

The apparent complexity of these previous studies employing IR techniques, involving the use of added reagents to provide an indirect determination of analytes, arises because of the complex and varying types and structure of oils used in different engines. The variability in oil matrix composition associated with different engine types, and different lubricant manufacturers, makes a

single, direct IR technique suitable for all types of oil difficult to achieve. However, if only a single type of oil is studied (as here, and as is the case if a single engine oil system is monitored during performance) then the variability in matrix composition is reduced and subsequent spectral interference effects minimized.

Non-spectrometric methods have also received attention and conductivity measurements for monitoring engine oil condition have been reported by Wang [11].

In the study described here two properties, TAN (total acid number) and antioxidant concentration, of a turbine engine oil from a military aircraft were determined using FTIR spectroscopy with multiple regression, principal components (PC) and partial least squares (PLS), algorithms employed for the development of calibration, prediction, and validation models. In addition to these quantitative analyses, results are presented of the application of two-dimensional IR correlation spectroscopy [12] as a technique for studying the dynamic processes and interpreting the spectral data obtained during oil degradation.

## 2. Experimental

### 2.1. Samples

The oil samples examined were taken from a military aircraft (type F111 TF30 engine oil system). The oil is a synthetic product containing synthetic polyol esters based on a mixture of 95% C<sub>5</sub>–C<sub>10</sub> fatty acid esters of pentaerythritol and dipentaerythritol and containing, when fresh, approximately 2% added antioxidant [2]. A total of 176 oil samples were examined, representing a wide range of TAN and antioxidant concentration values as might typically be encountered in monitoring military aircraft engine oil condition over a prolonged period of use.

### 2.2. Data collection

Infrared spectra of the engine oil samples were collected in fixed-path length potassium bromide cells, mounted in a FTIR spectrometer (Model Spectrum 2000, Perkin-Elmer, UK). The spectra were recorded in transmission mode using one of several cells of path lengths ranging from 0.1126 mm to 0.1173 mm, and to correct for this all spectra were converted to absorbance spectra and normalized to a constant path-length prior to data analysis. Spectra were acquired over the spectral range 4000–500 cm<sup>-1</sup> at 2 cm<sup>-1</sup> spectral resolution, 16 scans per sample were co-added. Spectra were signal averaged to 5 cm<sup>-1</sup> resolution, converted to JCAMP format and imported into Matlab 7.1 (CEANET Pty., Ltd., Sydney, Australia) for preprocessing, multivariate statistical analysis, and two-dimensional correlation analysis. Calibration model development was conducted using the PLS toolbox (Version 3.5, Eigenvector Research Inc., WA, USA) in Matlab, and both principal components (PC) and partial least squares (PLS) regression techniques were evaluated. Model validation was undertaken using the leave-one-out method in which each sample in turn is removed from the set used to build the model and subsequently used to derive a predicted value, the total of the errors for all samples treated this way provides the validation error. The pre-

dictive performance of models was assessed using samples not employed in model development.

### 2.3. Reference methods

Each oil sample was analysed by conventional, reference methods to provide TAN values and antioxidant concentration values. TAN reference values were determined by titration of the oil with potassium hydroxide as per ASTM D664 [13]. The antioxidant content of each sample was determined by HPLC [14]. Briefly, a 20  $\mu\text{L}$  sample was injected on to a 250 mm silica packed column and eluted using a 96% isooctane and 4% ethyl acetate solvent mix. A UV detector, at 265 nm, was employed to detect and determine total antioxidant concentration.

### 2.4. Data preprocessing

Following normalization to constant path-length, the spectral data were mean-centred prior to model development and no other pre-processing of the data was undertaken for quantitative analysis. It should be noted that although baseline correction using, for example, second derivative transformation of spectral data or multiplicative scatter correction [15], is often employed in quantitative IR analysis, no observable advantages were gained by using the technique here. By retaining spectral data in a non-transformed mode spectral bands are more easily recognized, and interpretation of latent variables can be much clearer.

## 3. Results and discussion

An initial study included an examination of how the recorded IR spectra reflected the changes in oil composition as a function of its aging and use. Fig. 1 illustrates typical infrared spectra obtained from samples of engine oil at different stages of use.

When fresh, the oil has a relatively high antioxidant concentration and a low free-acid (TAN) value. During use as the oil wears, the concentration of antioxidant decreases and the TAN value rises. However, at all stages the concentrations of the antioxidant and acids are relatively low compared with the bulk oil components and the spectra are dominated by the features associated with the matrix. Qualitative and quantitative data analysis was subsequently undertaken on infrared

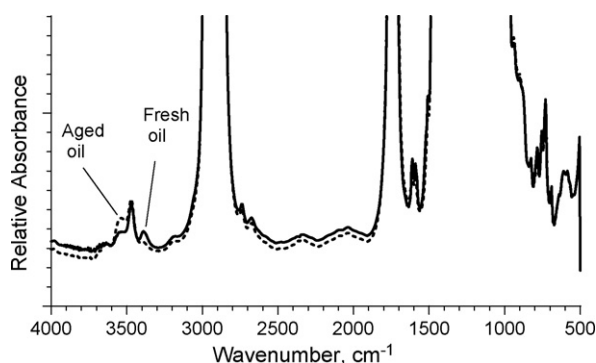


Fig. 1. Typical infrared spectra from samples of aviation engine oil, fresh (-) and aged (- - -).

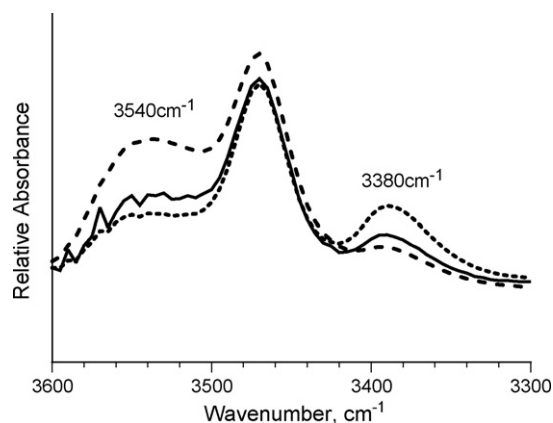


Fig. 2. Oil samples having a high TAN value (- - -) and a high antioxidant value (· · ·), compared with the average spectrum (—) for the samples examined.

data from a non-saturated region of the spectrum, away from steep absorption shoulders. One region often quoted in the literature as suitable for quantitative analysis is the region 1750–1550  $\text{cm}^{-1}$  [4,8]. Under the experimental conditions described here the spectral window found to provide best results was the region 3600–3200  $\text{cm}^{-1}$ . Regions 1630–1540  $\text{cm}^{-1}$ , and 800–650  $\text{cm}^{-1}$  also exhibited visible changes in spectral profile with aging of the samples but including data from these regions was found not to improve quantitative analysis.

In general, antioxidant concentration and measured TAN value follow inverse trends with oil age and for the 176 samples examined here the correlation coefficient between the two sets of reference values is  $-0.74$ . In Fig. 2 selected spectra are illustrated of samples having significant differences in TAN values and samples with different antioxidant concentrations, along with the mean spectrum from all samples examined. The visible differences in these spectra confirm that IR spectrometry is sufficiently sensitive for monitoring the changing composition of the oil as it performs in an engine. The nature of this relationship between these sample characteristics as provided from the IR spectra can be illustrated by calculation and examination of the so-called two-dimensional (2D) spectral correlation matrices.

Noda and co-workers pioneered the application and interpretation of two-dimensional correlation spectroscopy [12,16]. The full theory associated with the method has been presented in these and other publications and the technique has been applied to a diverse range of problems. Its application alongside more conventional chemometric methods (such as calibration modeling) has received less attention although Yung et al. have discussed its use with factor analysis [17] and Segtnan et al. have employed principal components analysis and 2D near-infrared correlation spectroscopy for studying water structure [18].

For a series of spectra recorded as a function of time or changing composition, then the generalized 2D correlation spectroscopy concept allows the data to be described by synchronous and asynchronous spectral features [12,19], as given by the central formula,

$$\mathbf{X}(v_1, v_2) = \Phi(v_1, v_2) + i\Psi(v_1, v_2) \quad (1)$$

$\mathbf{X}(v_1, v_2)$  describes the variation of spectral intensity as a function of time or compositional change at two different spectral variables  $v_1$  and  $v_2$ , and  $\Phi$  and  $\Psi$  are, respectively the orthogonal real (synchronous) and imaginary (asynchronous) components.

Noda and Ozaki [12] have demonstrated that the synchronous 2D correlation spectrum is concisely represented by the product of the mean-centred spectra matrix and its transpose.

$$\Phi(v_1, v_2) = \frac{1}{m-1} \mathbf{X}^T \mathbf{X} \quad (2)$$

The asynchronous correlation spectrum can be derived from,

$$\Psi(v_1, v_2) = \frac{1}{m-1} \mathbf{X}^T \mathbf{N} \mathbf{X} \quad (3)$$

where  $m$  is the number of spectra in the series examined, and  $\mathbf{N}$  is referred to as the Hilbert–Noda transformation matrix, given by

$$N_{j,k} = \begin{cases} 0 & \text{if } j = k \\ 1/\pi(k-j) & \text{otherwise} \end{cases} \quad (4)$$

It is apparent from Eq. (2) that for mean-centred data the synchronous correlation matrix describes the covariance matrix between the spectral variables of spectra recorded as a sequential series. By orthogonalising the mean-centred spectra with the Hilbert–Noda transform matrix (Eq. (3)) all linear relationships in the data are zeroed and only non-linear effects are displayed in the asynchronous matrix [12]. Asynchronicity is observed only when two signals are not totally proportional to each other and a non-linear relationship exists. Originally, the methodology underlying 2D correlation spectroscopy was developed to describe the changes observed in dynamic spectral data, i.e., when the data matrix,  $\mathbf{X}$ , represents a series of spectra changing with time and arranged in chronological order. However, the dynamic variable need not be time but can be, for example, concentration of a spectrally active species. Thus, Wang et al.

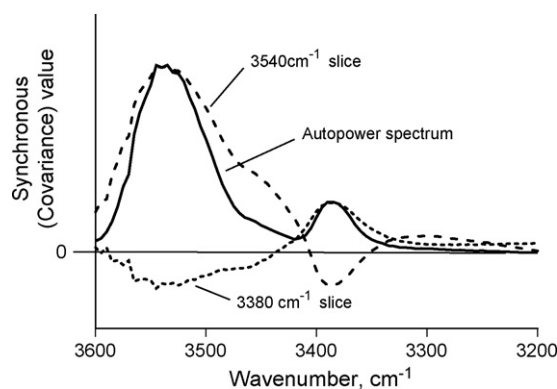


Fig. 4. The autopower spectrum (—) from the synchronous 2D correlation matrix, and slices taken through this matrix at 3380  $\text{cm}^{-1}$  (...) and 3540  $\text{cm}^{-1}$  (---).

have examined near-infrared 2D spectral correlation analysis of changing protein and fat concentrations in milk [20].

The mean-centred infrared spectral data were ranked according to known antioxidant concentration and the results of applying Eqs. (2) and (3) are illustrated in Fig. 3a and b as contour plots along with the average oil spectrum to aid identification of the features displayed in the 2D matrix.

In Fig. 3a the synchronous (covariance) spectral matrix is displayed. The symmetric nature of the synchronous matrix about its leading diagonal is evident.

The values occupying this diagonal provide the so-called autopower spectrum [12]. The autopower spectrum has been observed to be similar to the first principal component [21], which is not surprising since both extract and highlight regions of maximum change in the data relative to the mean spectrum. The autopower spectrum from this spectral data is shown in Fig. 4, and autopeaks, which are always positive, occur at 3540  $\text{cm}^{-1}$  and 3380  $\text{cm}^{-1}$ . These peaks correspond to the regions of major change in spectral intensity observed during the observation interval, in

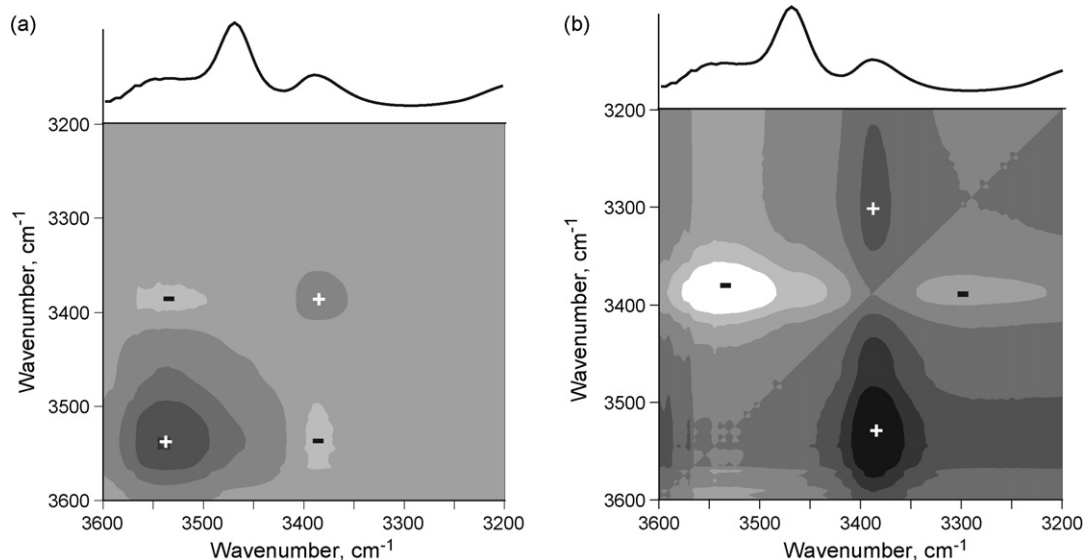


Fig. 3. (a) Synchronous correlation matrix, from spectra ranked according to antioxidant concentration and (b) the asynchronous correlation matrix.

this case as the oil ages and the antioxidant concentration decreases.

The relationship between these spectral features is highlighted in the observed off diagonal negative peaks present in Fig. 3a, at  $3540\text{ cm}^{-1}/3380\text{ cm}^{-1}$ , and correspondingly at  $3380\text{ cm}^{-1}/3540\text{ cm}^{-1}$ , indicating a negative covariance (correlation) between the intensities of the IR peaks at these positions. This inverse relationship is evident in the ‘slice’ spectra of Fig. 4, where vertical slices from the synchronous matrix at  $3380\text{ cm}^{-1}$  and  $3540\text{ cm}^{-1}$  are displayed.

Further information concerning the changes in the recorded spectra is obtained from examination of the asynchronous matrix, displayed in Fig. 3b. This matrix is antisymmetric about the leading diagonal, and has no autopeaks. Fig. 3b shows peaks at off-diagonal positions, at  $3380\text{ cm}^{-1}/3540\text{ cm}^{-1}$  (and  $3540\text{ cm}^{-1}/3380\text{ cm}^{-1}$ ). The presence of these features indicates that the species responsible for these bands are out of phase (non-linear) with respect to each other’s rate of change. Thus, these absorption bands are negatively correlated (that at  $3540\text{ cm}^{-1}$  increasing whilst the peak at  $3380\text{ cm}^{-1}$  is decreasing) but the changes are not occurring at the same rate. The relative signs of these peaks would also serve to suggest that the peak at  $3380\text{ cm}^{-1}$  was changing (decreasing) at a faster rate than that at  $3540\text{ cm}^{-1}$  was increasing [12].

These qualitative results and observations can be interpreted in terms of the species present in the samples. Phenylamines, such as PAN, are substituted aromatic hydrocarbons and are typical antioxidant additives in lubricants. The observed absorption band at  $3380\text{ cm}^{-1}$  that decreases with increasing age and degradation of the oil is consistent with the medium intensity N–H stretch band associated with aromatic secondary amines in a non-polar environment [2,22]. The other significant feature in the series of recorded IR spectra is the band at  $3580\text{ cm}^{-1}$  that increases in intensity with age of the oil. This band is likely due to O–H stretch from carboxylic acid monomers [22] that are common products formed as the oil undergoes oxidation. The lack of significant spectral features around  $2600\text{ cm}^{-1}$  [22] and the fact that including other spectral regions did not improve TAN value prediction accuracy implies that there is little free phosphoric acid in these samples.

### 3.1. Calibration models

Of the 176 samples, 120 were used to develop calibration models with the calculated calibration error (RMSEC) used to indicate the goodness of fit between the predicted and known analyte values, and the validation error (RMSEV) value used to indicate how the model behaves with samples not included in calibration development. Although useful in model development RMSEV provides a biased estimate of future behavior of the calibration model [15], and the remaining 56 samples not used in model development were used for determining prediction errors (RMSEP). These statistics are defined by,

$$\text{error} = \sqrt{\frac{\sum_{i=1}^M (\tilde{y}_i - \hat{y}_i)^2}{M}} \quad (5)$$

Table 1

Performance of calibration models for the determination of antioxidant concentration in aviation oil

Wavenumber range	Model	No. of factors	RMSEC	RMSEV	RMSEP
3200–3600 $\text{cm}^{-1}$	PC	8	0.037	0.040	0.040
	PLS	8	0.029	0.030	0.035

where  $\tilde{y}_i$  and  $\hat{y}_i$  represent the measured and reference values for the  $i$ th sample, respectively. For RMSEC,  $M$  is the number of samples used in developing the calibration model ( $M = 119$ ), for RMSEV it is the number of samples used in validation ( $M = 120$ ) using the leave-one-out procedure, and for RMSEP  $M$  is the number of samples kept aside for examining the predictive ability of the model ( $M = 56$ ).

The distribution of analyte concentration values in the samples examined was quite evenly spread across the range and the 56 prediction samples were selected randomly and uniformly from the 176 samples available.

The major changes in the spectra were observed in the region  $3600\text{--}3200\text{ cm}^{-1}$  as discussed above, and for the calibration models developed and examined here data from other regions was not found to improve the performance of the models and these data were not included. Using the selected spectral range and  $5\text{ cm}^{-1}$  resolution allowed each sample to be represented by 81 absorbance data points.

### 3.2. Antioxidant analysis

The results using principal components and partial least squares models for estimation of antioxidant concentration are summarized in Table 1.

For both schemes the minimum RMSEV value was attained with eight factors (latent variables) included in the models. The relative performance of the different models, PC versus PLS regression, can be accounted for by the PLS algorithm including the dependent variable (analyte concentration) in the matrix decomposition and factor extraction stages of the numerical analysis. This is not the case with PC regression, which relies on the magnitude of the variance of independent variables alone in determining which factor to add to the model. The predictive performance of the PLS model, using the 56 samples with eight latent variables, is illustrated in Fig. 5(a); the correlation coefficient between measured and predicted antioxidant concentration values is 0.993.

### 3.3. Total acid number

The total acid number of an oil represents an oil property rather than a specific component such as, for example, an antioxidant concentration. As with the determination of antioxidant content, the determination of TAN value was conducted by examining the region  $3600\text{--}3200\text{ cm}^{-1}$  using both PC and PLS regression techniques. A summary of results using these models is provided in Table 2, and again 8-factor models were determined to provide the most parsimonious results. The per-

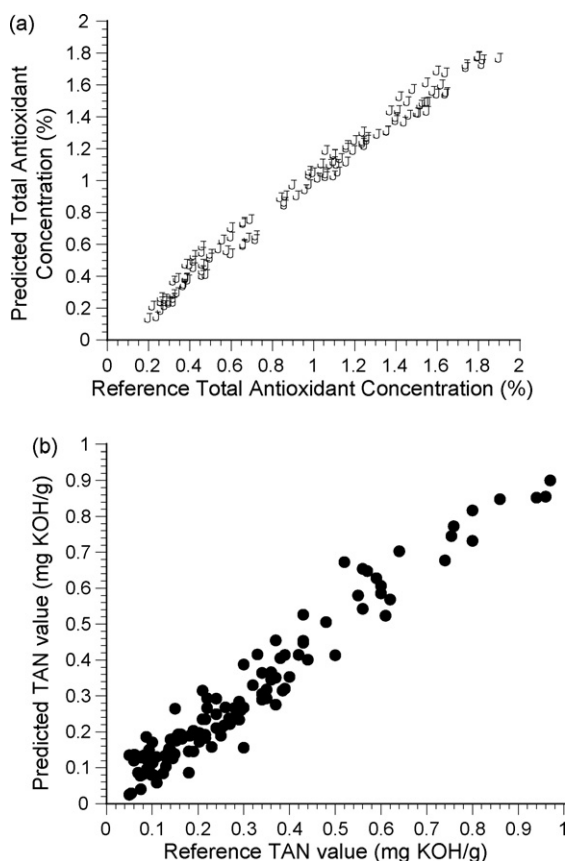


Fig. 5. Predicted, using PLS models, vs. reference values for (a) concentration of antioxidant and (b) TAN values, for aviation oils.

Table 2  
Performance of PLSR models for the determination of TAN of aviation oils

Wavenumber range	Model	No. of factors	RMSEC	RMSEV	RMSEP
3200–3600 $\text{cm}^{-1}$	PC	8	0.062	0.068	0.060
	PLS	8	0.050	0.057	0.048

formance of the 8-factor PLS model illustrated in Fig. 5(b); the correlation coefficient between measured and predicted TAN values is 0.972.

The residuals in the calibration data, for both the antioxidant and TAN analyses, were visually examined and for both analytes the residuals exhibited no discernable pattern as a function of analyte concentration. Similarly, there was no significant difference between the range of residuals for the calibration and validation samples for these analytes.

#### 4. Conclusion

Infrared spectrometry can provide a useful alternative to conventional analytical methods for monitoring aging of oil samples from aviation engines. By restricting the application to the role of monitoring a specific oil type in a specific engine, as here, rather than analysis of the many oil types on the market, then the problems associated with variable interfering components is largely overcome and the

technique provides a rapid and versatile means of process control. Both antioxidant concentration and total acid number of aviation oils are amenable to assessment by FTIR with relative error of determination of less than 10% across a wide range of values typically encountered in such samples.

The calibration models examined to predict TAN value and antioxidant concentration produce prediction errors comparable to the more traditional methods. In all cases reported here the error is small compared to the observed change in these analytes during use of the oil [2].

By treating component concentration as a dynamic variable the technique of two-dimensional correlation spectroscopy has been applied to the FTIR data and the results obtained provide insight into the variables used in the construction and use of multivariate calibration models.

#### Acknowledgments

The authors would like to thank the Defence Science & Technology Organisation (DSTO) Melbourne, Australia for access to samples and providing reference analytical values.

#### References

- [1] J.G. Speight, Handbook of Petroleum Product Analysis, Wiley Interscience, New Jersey, 2002, p. 214.
- [2] P. Rawson, G. Morris, FTIR Based Oil condition Monitoring for Synthetic Turbine Oils, DSTO-TR-1467, Melbourne, Australia, 2003.
- [3] C. Winder, J.-C. Balouet, Environ. Res. Sec. A 89 (2002) 146–164.
- [4] F.R. van de Voort, J. Sedman, V. Yaylayan, C. Saint Laurent, Appl. Spec. 57 (2003) 1425–1431.
- [5] Lubrication and Oil Analysis Dictionary, <http://www.oilanalysis.com/dictionary/>, 2003.
- [6] J. Dong, F.R. van der Voort, A.A. Ismail, E. Akochi-Koble, D. Pinchuk, Lubr. Eng. 56 (2000) 12–20.
- [7] B. Pavoni, N. Rado, R. Piazza, S. Frignani, Ann. Di Chim. 94 (2004) 521–532.
- [8] F.R. van de Voort, J. Sedman, V. Yaylayan, C. Saint Laurent, C. Mucciardi, Appl. Spec. 58 (2004) 193–198.
- [9] F. Navotny-Farkus, W. Bohme, Petrol. Coal 44 (2001) 84–86.
- [10] D.L. Wooton, Appl. Spec. Rev. 36 (2001) 315–332.
- [11] S.S. Wang, Sens. Actuator B 86 (2002) 122–126.
- [12] I. Noda, Y. Ozaki, Two Dimensional Correlation Spectroscopy—Applications in Vibrational and Optical Spectroscopy, John Wiley and Sons, Chichester, UK, 2004.
- [13] ASTM International, <http://www.astm.org/>, 2003.
- [14] P. Rawson, Personal Communication DSTO, Fishermans Bend, Victoria, Australia, 2006.
- [15] T. Naes, T. Isaksson, T. Fearn, T. Davies, Multivariate Calibration and Classification, NIR Publications, Chichester, UK, 2002.
- [16] I. Noda, Vibrat. Spectrosc. 36 (2004) 143–165.
- [17] Y.M. Yung, S.B. Kim, I. Noda, Appl. Spectrosc. 57 (2003) 850–857.
- [18] V.H. Segtnan, S. Sasic, T. Isaksson, Y. Ozaki, Anal. Chem. 73 (2001) 3153–3161.
- [19] I. Noda, A.E. Dowrey, C. Marcott, G.M. Story, Y. Ozaki, Appl. Spectrosc. 54 (2000) 236A.
- [20] Y. Wang, R. Tsenkova, M. Amari, F. Terada, T. Hayashi, A. Abe, Y. Ozaki, Anal. Mag. 26 (1998) M64–M69.
- [21] K. Murayama, B. Czarnik-Matusewicz, Y. Wu, R. Tsenkova, Y. Ozaki, Appl. Spectrosc. 54 (2000) 978.
- [22] G. Socrates, Infrared Characteristic Group Frequencies, John Wiley and Sons, Chichester, UK, 1994.

Review

# Hyphenation of flow injection/sequential injection with chemical hydride/vapor generation atomic fluorescence spectrometry

Ming-Li Chen<sup>a</sup>, Ai-Mei Zou<sup>a</sup>, Yong-Liang Yu<sup>a</sup>, Rong-Huan He<sup>b,\*</sup>

<sup>a</sup> Research Center for Analytical Sciences, Northeastern University, Box 332, Shenyang 110004, China

<sup>b</sup> Department of Chemistry, Northeastern University, Box 332, Shenyang 110004, China

Received 20 March 2007; received in revised form 17 April 2007; accepted 18 April 2007

Available online 27 April 2007

## Abstract

The dominant role played by flow injection/sequential injection (FI/SI, including lab-on-valve, LOV) in automatic on-line sample pretreatments coupling to various detection techniques is amply demonstrated by the large number of publications it has given rise to. Among these, its hyphenation with hydride/vapor generation atomic fluorescence spectrometry (HG/VG-AFS) has become one of the most attractive sub-branches during the last years, attributed not only to the high sensitivity of this technique, but also to the superb separation capability of hydride/vapor forming elements from complex sample matrices. In addition, it also provides potentials for the speciation of the elements of interest.

It is worth mentioning that quite a few novel developments of sample pretreatment have emerged recently, which attracted extensive attentions from the related fields of research. The aim of this mini-review is thus to illustrate the state-of-the-art progress of implementing flow injection/sequential injection and miniaturized lab-on-valve systems for on-line hydride/vapor generation separation and preconcentration of vapor forming elements followed with detection by atomic fluorescence spectrometry, within the period from 2004 up to now. Future perspectives in this field are also discussed. © 2007 Elsevier B.V. All rights reserved.

**Keywords:** Flow injection; Sequential injection; Lab-on-valve; Hydride/vapor generation atomic fluorescence spectrometry

## Contents

1. Introduction .....	599
2. On-line hydride/vapor generation atomic fluorescence spectrometric determination of metal species from complex matrices .....	600
2.1. The recent development of flow injection/sequential injection hydride/vapor generation with detection by atomic fluorescence spectrometry .....	600
2.2. Simultaneous determination of multi-elements with flow injection hydride/vapor generation atomic fluorescence spectrometry .....	602
2.3. Miscellaneous flow injection/sequential injection hydride/vapor generation approaches employed for special sample matrices .....	603
3. Conclusions and perspectives .....	604
References .....	605

## 1. Introduction

In modern analytical methodologies, sample pretreatment has been recognized as a bottle-neck of the success to the entire analytical procedure [1]. Therefore, efficient separation/preconcentration protocols are highly appreci-

ated especially for complex sample matrices. Chemical hydride/vapor generation (HG/VG) is an elegant approach which can readily separate the species of interest from the undesirable matrix components. Moreover the introduction of the hydride/vapor into the atomization cell eliminates the need of a nebulizer, and therefore improves the atomization efficiency of the analytes [2]. Atomic fluorescence spectrometry (AFS), as a flow through detector, is well compatible with on-line hydride/vapor generation systems, therefore is most suitable for measuring hydride/vapor forming species. Obviously, AFS

\* Corresponding author. Tel.: +86 24 83683429; fax: +86 24 83676698.  
E-mail address: [herh@mail.neu.edu.cn](mailto:herh@mail.neu.edu.cn) (R.-H. He).



possesses the figures of merit of high sensitivity for most of the vapor forming elements, ease of operation and low cost, and minimized interfering effects comparing to ICPMS and some other instruments. The capability of simultaneous multi-element quantification well facilitated the determination of a series of hydride/vapor forming elements by employing HG/VG-AFS [3].

The detection capability of hydride/vapor generation atomic fluorescence spectrometry is, however, still frequently restricted by the coexisting matrix components especially the transition metal species when analysing real-world samples. Thus an appropriate sample pretreatment step is needed in order to isolate the interfering species before hydride/vapor generation process and the ensuing AFS detection. It is obvious that the most effective approach for completely eliminating the matrix effects should encompass the separation of the analytes from the sample matrix components. At this point, flow injection/sequential injection is undoubtedly a prominent choice, which not only facilitates automatic on-line operation, but also minimizes potential sample contamination [4].

This review presents an up-to-date progress of the implementation of flow injection/sequential injection in facilitating on-line hydride/vapor generation with detection by AFS since 2004. In this context, the frequently employed on-line hydride/vapor generation schemes are discussed, including FI/SI on-line HG/VG separation/preconcentration coupled with AFS (where LOV-bead injection schemes incorporating a renewable micro-column for on-line hydride/vapor generation interfaced to AFS detection is addressed as a useful supplement), simultaneous determination of multi-elements of vapor forming nature with FI/SI-HG/VG-AFS, as well as the determination of vapor forming species in special sample matrices by adopting FI-HG/VG-AFS. It is worthwhile mentioning that atomic fluorescence spectrometry has been a well developed and widely used technique in China. Therefore, a large part of the contributions involved in this mini-review is attributed to Chinese researchers.

## 2. On-line hydride/vapor generation atomic fluorescence spectrometric determination of metal species from complex matrices

During the last few years a large amount of investigations were focused on the hyphenation of flow injection/sequential injection hydride/vapor generation sample clean-up to atomic fluorescence spectrometry. In Sections 2.1–2.3, pertinent details about on-line hydride/vapor generation for the determination of vapor forming metal species are presented. Special emphasis is on some of the novel separation/preconcentration systems along with the development of innovative AFS detection protocols.

### 2.1. The recent development of flow injection/sequential injection hydride/vapor generation with detection by atomic fluorescence spectrometry

It is well documented that the combination of flow injection/sequential injection and hydride/vapor generation is among

the most efficient sample clean-up approaches, which in addition to the high sensitivity of atomic fluorescence spectrometric determination offers excellent detection capability for the hydride/vapor forming elements with satisfactory selectivity. Within the time span of the present review, some exciting achievements in the development of novel sample pretreatment methodologies were reported, as illustrated in Table 1. Some of the prominent characteristics of these procedures are given.

A method for analysing different species of selenium was proposed by performing the speciation of inorganic selenium with an on-line system [5], where Se(IV) was co-precipitated with lanthanum hydroxide and was collected by using a PTFE beads packed micro-column. The collected co-precipitate was dissolved with a certain amount of hydrochloric acid which was afterwards employed for hydride generation and AFS detection. Se(VI) was reduced to Se(IV) with hydrochloric acid and a similar co-precipitating procedure was followed in order to obtain the total amount of selenium, and the amount of Se(VI) was finally achieved by subtraction.

The existence of dimethylselenium (DMSe) and dimethyldiselenium (DMDS) tend to cause serious interference on the determination of Se(IV) by hydride generation atomic fluorescence spectrometry. A flow injection separation and preconcentration system coupled to HG-AFS was therefore developed by on-line co-precipitation in a PTFE knotted reactor to eliminate the interference suffered from organoselenium [6]. Hydrochloric acid was used to dissolve the precipitate and merge with  $\text{KBH}_4$  solution for HG-AFS detection. The interference of DMSe and DMDS on the Se(IV) determination by conventional HG-AFS and its elimination by the developed separation and preconcentration system were evaluated. Another on-line preconcentration coupled with hydride generation atomic fluorescence spectrometric system demonstrated that Se(IV) could be selectively determined in aqueous solution by on-line formation of Se(IV)–pyrrolidinedithiocarbamate (PDC) complex in HCl medium [7]. The neutral charged complex was adsorbed onto the surface of PTFE fiber in a micro-column, which was afterwards eluted with  $\text{KBH}_4$  in KOH solution and used for hydride generation by merging with an acid stream.

Lead in environmental and biological sample matrices was determined with a procedure of on-line solid phase extraction separation and preconcentration [8]. A micro-column packed with iminodiacetate chelating resin was employed for retaining trace level of lead, which was afterwards eluted with a small volume of hydrochloric acid followed by hydride generation with reduction by tetrahydroborate in the presence of ferricyanide as an oxidizing/sensitizing reagent.

A gas–liquid generator was specially designed for mercury non-aqueous hydride generation. The mercury reacted with  $\text{KI-HNO}_3 + \text{CS}(\text{NH}_2)_2$  was on-line extracted into tri-butylphosphate and thereafter the hydride was generated with sodium tetrahydroborate in *N,N*-dimethylformamide and anhydrous acetic acid followed by AFS quantification [9]. An interesting procedure for the separation and non-chromatographic speciation of mercury was described [10], where ammonium diethyl dithiophosphate (for  $\text{Hg}^{2+}$ ) and dithizone (for  $\text{CH}_3\text{Hg}^+$ ) were used as dual selective complexing agents to develop a novel

Table 1

Various flow injection/sequential injection separation and preconcentration schemes for hydride/vapor generation elements as interfaced to AFS

On-line pretreatment protocols	Means for collection of analytes	Elements and samples	References
Precipitation/coprecipitation	On a PTFE beads packed micro-column	Se in reference human hair materials and environmental water samples	[5]
	On the inner wall of PTFE knotted reactor	CH <sub>3</sub> Hg <sup>+</sup> or Hg <sup>2+</sup> in biological and water samples	[10]
	On the inner wall of PTFE knotted reactor	Se in reference tea materials	[6]
	Sequential/bead injection lab-on-valve incorporating a renewable C18 micro-column	Cd in biological and water samples	[18]
Solid phase extraction	Micro-column packed with PTFE fiber	Se in certified reference water samples	[7]
	Micro-column packed with iminodiacetate chelating resin	Pb in frozen cattle blood, human hair water samples	[8]
	Column packed with an anion-exchange resin (Amberlite IRA-410)	As in reference solid and water materials	[11]
	Anion-exchange resin (D201) packed column	Cd in certified soil reference materials	[16]
	Column packed with Cyanex 923 immobilized PTFE powder	Tea standard reference materials	[15]
	Bead injection-LOV with anion-exchanger as sorbent	As in environmental waters	[19]
Solvent extraction	Sequential extraction procedure (from solid to aqueous)	As in certified soil reference materials	[12]
	Extraction (from aqueous to organic phase and vapor generation in organic phase)	Hg in soil and geological samples	[9]

flow injection on-line sorption separation and preconcentration system by adsorbing both complexes onto the inner wall of a PTFE knotted reactor. The retained complexes were then eluted by using 15% (v/v) hydrochloric acid. The speciation of Hg<sup>2+</sup> and CH<sub>3</sub>Hg<sup>+</sup> was thereafter carried out by hydride generation followed by AFS determination. The flow manifold is illustrated in Fig. 1.

Hydride generation technique has found wide applications in the determination of trace levels of arsenic in various sample matrices. Inorganic arsenic was on-line preconcentrated on a column packed with Amberlite IRA-410 using a multi-syringe flow injection system and determined by HG-AFS [11], and a five-fold improvement of detection sensitivity was achieved by using this approach over a similar technique developed previously by the same group of authors. By employing K<sub>2</sub>S<sub>2</sub>O<sub>8</sub> solution as the oxidizing reagent for the oxidation of As(III) and organic arsenic species into As(V) at room temperature, a new flow injection on-line sequential extraction procedure coupled with HG-AFS was developed for rapid and automatic fractionation of arsenic in soil samples [12]. The methodology involved a three-step sequential extraction procedure with deionized water, KOH solution, and HCl solution. The technique offers several advantages, which include high speed, decreased sample/reagent consumption, minimized risk of sample contamination as well as analyte loss.

The hydride/vapor generation of cadmium tends to suffer from severe interferences arising from the coexisting species, thus the experimental conditions are generally much more critical as compared to other vapor forming elements, e.g., mercury, arsenic and selenium [13,14]. Therefore, on-line removal/separation of the interfering components is undoubtedly an ideal choice. Recently, an on-line solid phase extraction procedure was developed for the preconcentration of cadmium from tea samples [15]. Cadmium was retained on a micro-

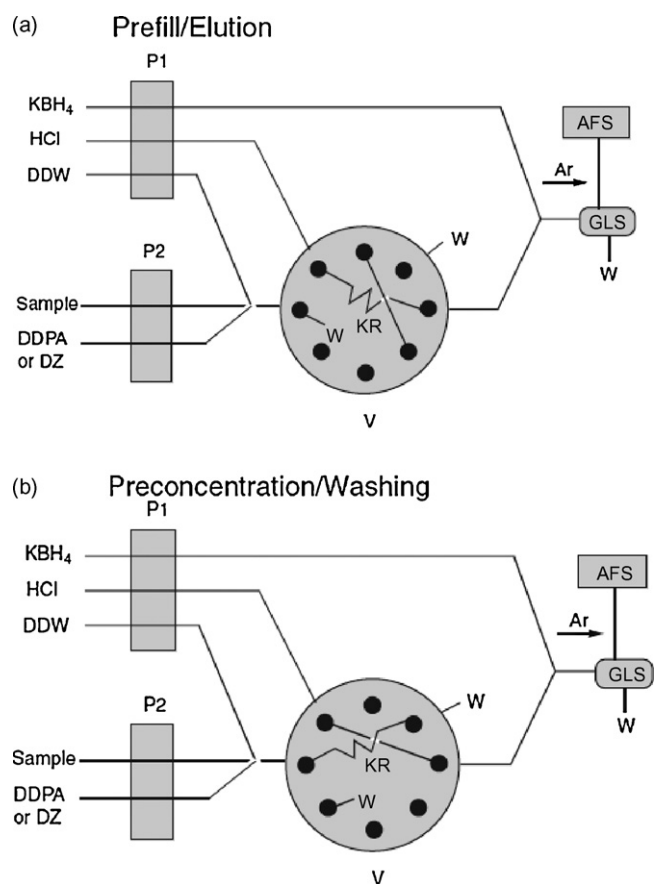


Fig. 1. The FI flow manifold for on-line sorption preconcentration of mercury coupled with CVG-AFS (from Ref. [10], with permission by Elsevier B.V.).

column packed with Cyanex 923 attached PTFE powders, while other matrix ions or interfering ions were removed. The retained cadmium was afterward eluted from the column by using an eluent containing  $\text{Co}^{2+}$  and sulphuric acid, and the eluate was employed for the ensuing AFS detection. Another procedure was reported to effectively separate ultra-trace amount of cadmium in the presence of more than  $10^4$  fold of coexisting metal species [16], where cadmium was retained by using an anion exchange resin packed micro-column, while the majority of the interfering metal species remained in the original solution and were therefore eliminated. The cadmium was eluted from the column with ammonia, and the ensuing hydride generation process was facilitated by merging with a hydrochloric acid stream followed by AFS detection. The system was applied for the analyses of a series of geological standard reference materials.

The third generation of flow injection, i.e., the so-called micro-sequential injection lab-on-valve ( $\mu\text{SI-LOV}$ ) system, has opened up new avenues in chemical analysis regarding sample processing [17]. An on-line co-precipitation separation/preconcentration approach was developed for the determination of ultra-trace cadmium, by using a sequential/bead injection lab-on-valve system incorporating a renewable micro-column packed with C18 immobilized copolymeric micro-beads [18]. The flow manifold was illustrated in Fig. 2. The proposed operating procedure includes separation/preconcentration by adsorbing the co-precipitate onto the C18 surface, co-precipitate dissolution and hydride generation. The on-line renewal of the packed micro-column in the lab-on-valve system well avoided the malfunctions of the column, arising from the build up of flow impedance and consequently the deterioration of collection efficiency. With a sampling volume of 500  $\mu\text{l}$ , quantitative retention of cadmium was achieved, along with an enrichment factor of 9.8 and a detection limit of  $3.5 \text{ ng l}^{-1}$ , as the authors claimed. The procedure was validated analyzing cadmium in a few certified reference materials.

Very recently, another interesting marriage between lab-on-valve/bead-injection and HG-AFS for the assay of trace-level metalloids was reported [19]. Employing quantitative pre-oxidation of As(III) to As(V) by means of permanganate, the method involves preconcentration of arsenate at pH 10 on a renewable anion exchanger packed micro-column. The analyte species was afterward stripped out and concurrently pre-reduced

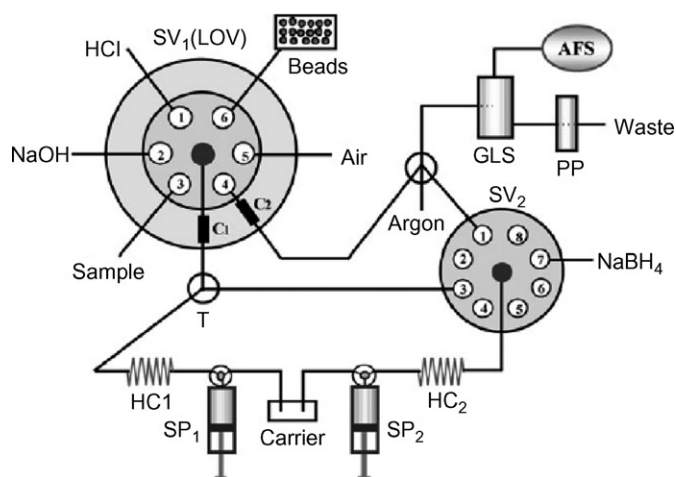


Fig. 2. Flow manifold of the sequential/bead injection LOV system coupled to HG-AFS. SP1, SP2: syringe pumps; SV1: LOV; SV2: 8-port selection valve; PP: peristaltic pump; GLS: phase separator; HC1, HC2: holding coils; C1, C2: renewable column positions; T: connector (from Ref. [18], by permission of The Royal Society of Chemistry).

by KI in a HCl medium. The eluate was downstream merged with sodium tetrahydroborate for generation of arsine, which was subsequently quantified by AFS. The proposed procedure is characterized by a high tolerance to metal species and interfering hydride-forming elements.

## 2.2. Simultaneous determination of multi-elements with flow injection hydride/vapor generation atomic fluorescence spectrometry

Atomic fluorescence spectrometry has been extensively used for the determination of hydride-forming elements, by taking advantages of high sensitivity, wide linear dynamic range, high sampling frequency as well as ease of operation and low cost. But when comparing to hydride generation atomic absorption spectrometry, the main advantage of HG-AFS is the potentials for simultaneous determination of multi-elements.

When conducting literature survey, it could be readily recognized that only very few publications were located concerning simultaneous determination of multi-elements, as compared to those handling the quantification of individual species. Table 2 illustrated some of the approaches for multi-element analysis,

Table 2  
Various flow injection schemes for simultaneous determination of hydride/vapor forming elements as interfaced to AFS

Species determined	Procedures for sample clean-up	Samples	References
As and Se	Acid digestion of the samples in a microwave digestion system, using hydrochloric hydroxylamine as pre-reducer	Chinese medicinal herbs	[21]
As and Sb	Soxhlet extraction method with a methanol–water system	Chinese herbal medicines	[20]
Cd and Zn	Microwave digestion with $\text{Co}^{2+}$ and 8-hydroxyquinoline as enhancement reagents	Certified reference materials of soil, cabbage, peach leaf, rice flour and tea	[2]
As, Sb, Se and Bi	HCl for the reduction of Se(VI), while As(V) and Sb(V) was reduced by thiourea	Certified biological reference materials	[22]

while pertinent details and discussions related to these procedures are presented in the following.

A recent study reported a new method for simultaneous determination of trace arsenic and antimony in Chinese herbal medicines by hydride generation-double channel atomic fluorescence spectrometry with a Soxhlet extraction system and an *n*-octanol-water extraction system [20]. The authors claimed that the concentration ratios of *n*-octanol-soluble As or Sb to water-soluble As or Sb were related to the kinds of medicine and the acidity of the decoction. Soxhlet extraction was found to be an effective method for plants pretreatment for determination of arsenic and antimony species in Chinese herbs.

Another procedure indicated that the presence of both tartaric acid and hydrochloric acid can facilitate the simultaneous generation of hydrides of selenium and arsenic, and the hydrochloric hydroxylamine had a favorable effect on the efficiency of hydride generation of total arsenic, but similar phenomenon was not observed for the hydride generation of selenium, to the authors' experience [21].

Four hydride-forming elements, i.e., arsenic, antimony, bismuth and selenium, were simultaneously determined by hydride generation-four-channel non-dispersive atomic fluorescence spectrometry, and the proposed method was applied to the determination of these elements in a series of Chinese certified biological reference materials [22]. Fig. 3 shows the schematic diagram of the four-channel non-dispersive AFS employed in this study. The high-powered hollow cathode lamps were operated in high lamp current, providing high intensity of radiation, which improved the stability and offered a longer lifetime. A solar blind photomultiplier was used as the detector in the non-dispersive detection system. Thiourea was used as a pre-reduction agent for pentavalent arsenic and antimony, and at the same time, acted as a masking agent for the elimination or

minimization the interferences on the determination of hydride-forming elements from the coexisting metal species, e.g., Fe, Cu and Ni. Even Zn and Cd were simultaneously evaluated by AFS coupled with an intermittent flow vapor generation system. The enhancement reagents were crucial to the chemical vapor generation of these two elements, where complexing reagents such as phenanthroline and 8-hydroxyquinoline played important roles [2].

### 2.3. Miscellaneous flow injection/sequential injection hydride/vapor generation approaches employed for special sample matrices

Most of the commercially available AFS instrument are equipped with one or two peristaltic and/or syringe pumps as intermittent or continuous flow-reactor for hydride/vapor generation. The pumps well facilitated automatic operation of the entire system. Practically, one could perform on-line sample pretreatment by using a peripheral flow injection or sequential injection system, followed by hydride/vapor generation and AFS determination. It is also quite common to carry out off-line sample clean-up served as a front-end of the ensuing HG-AFS operation. A recent study reported the determination of five hydride-forming elements in milk samples, e.g., arsenic, antimony, selenium, tellurium and bismuth, by employing slurry sampling [23].

Recently, an electromagnetic induction-assisted heating on-line oxidation system coupled to atomic fluorescence spectrometry was developed for the determination of total and inorganic mercury in fish samples [24]. Inorganic or total mercury could be determined with a same flow manifold by employing potassium peroxodisulphate as the oxidizing agent to decompose organo-mercury compounds. The experimental parameters governing on-line digestion efficiency were investigated. Previously, the same group developed an electromagnetic induction oven as the heating source for on-line sample digestion [25]. The proposed method was successfully applied to the determination of total mercury in cigarette by atomic fluorescence spectrometry equipped with an intermittent flow reactor. Another interesting work reported for the first time was the determination of trace arsenic in the skeleton fossils by utilizing hydride generation atomic fluorescence spectrometry [26]. The samples were digested with aqua regia in a boiling water bath. The analytical results indicated that the arsenic concentrations were exceptionally high in all of the skeleton fossil samples investigated. The obtained results might provide useful information for revealing the mystery of the mass extinction of the dinosaur fauna.

Tetrahydroborate has been widely employed for hydride and vapor generation in a hydrochloric acid medium. It is, however, not feasible for some of the species of higher oxidation states, e.g., Se(VI), As(V), and thus appropriate reduction process is a pre-requisite for the analysis of such species. Thiourea was employed as a reduction reagent for on-line pre-reduction of selenium (VI) followed by hydride generation in the  $\text{KBH}_4/\text{NaOH-HCl}$  system. The authors reported that the HG efficiency of Se(VI) was significantly improved, which was even

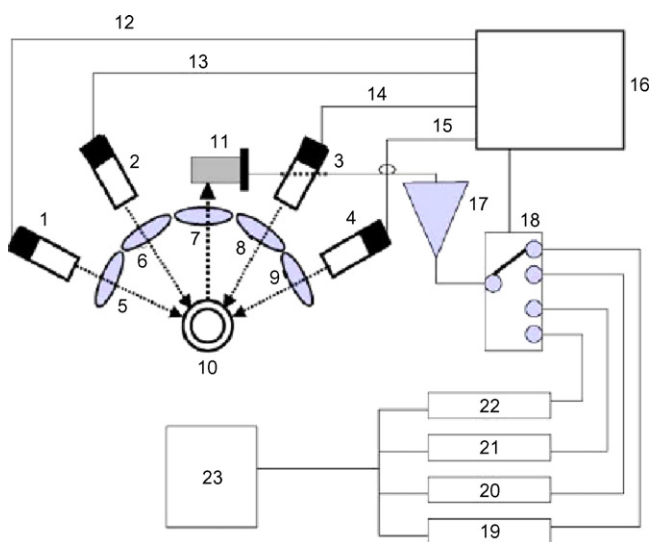


Fig. 3. The schematic diagram of the four-channel non-dispersive atomic fluorescence spectrometer used. (1–4) High-power hollow cathode lamp; (5–9) lens; (10) atomizer; (11) solar blind photo-multiplier; (12–15) lamp source controlling; (16) modulated pulsed generator and controller; (17) multiplier; (18) electro-switch; (19–22) channel signal processor; (23) computer (from Ref. [22], courtesy Elsevier B.V.).

higher than that obtained by using a same amount of Se(IV) in the conventional HG system [27]. This procedure was validated by analyzing total selenium and selenium species in certified reference material NIST 1946. It was further applied to selenium speciation in cultured garlic samples. The same group of authors also reported the pre-reduction of As(V) to As(III) by using thiourea and ascorbic acid as the reducing reagents, and the pre-oxidation of Pb(II) to Pb(IV) with  $K_3Fe(CN)_6$  and tartaric acid as the oxidizing reagents [28]. In the mean time, the reducing and oxidizing reagents served as masking reagents for alleviating the potential interferences arising from the coexisting transition metal species during the vapor generation process.

Selenium content in vegetables was determined by hydride generation atomic fluorescence spectrometry [29] after the samples were digested by enclosing  $H_2SO_4$ ,  $HNO_3$ ,  $H_2O_2$ ,  $V_2O_5$  and HF inside a piece of PTFE tube. Another procedure for the determination of selenium in plant and peat samples by hydride generation-atomic fluorescence spectrometry was developed [30]. Dried samples were digested with nitric acid and hydrogen peroxide in closed, pressurized PTFE vessels in a microwave oven. Se(VI) was directly reduced to Se(IV) in the undiluted digestion solutions after addition of hydrochloric acid in a microwave oven. The analytical procedure was critically evaluated by analyzing two certified plant reference materials as well as three peat reference materials.

An automated sequential injection hydride generation atomic fluorescence spectrometric method was developed, with the aim of screening blood lead levels for Chinese citizens, especially for children [31]. Lead hydride was generated from acid solution, with potassium ferricyanide as an oxidizing agent, by reacting with alkaline tetrahydroborate solution. The hydride was separated from the reaction medium in a gas–liquid separator and swept directly into the atomizer. A thorough scrutiny was made of the various factors, including the modification of the AFS instrument and related parameters, the various wet digestion protocols, the variables of the flow system and the reaction conditions. The accuracy and practical applicability of the procedure were validated by analyzing certified reference materials of frozen cattle blood GBW 09139 and GBW 09140, and further demonstrated by spiking recoveries of lead in human whole blood samples.

When real-world sample matrices were pretreated, it is always necessary to convert the species of interest to a chemical form suitable for hydride/vapor generation. In this respect, ultraviolet irradiation has been proved to be a useful approach. In an alkaline medium, the pretreatment of seawater by continuous-flow hydride generation-atomic fluorescence spectrometry was employed for the determination of total arsenic [32]. This sample pretreatment is meant to convert non-reducible arsenic into inorganic forms to facilitate hydride generation. The behaviors of four hydride-reactive arsenic species, i.e., As(III), As(V), monoethylarsonic acid (MMA), dimethylarsinic acid (DMA), and arsenobetaine (AsB) were studied. The authors claimed that UV irradiation at pH 1 resulted in the conversion of all species into As(V) with the exception of AsB and DMA. While conversions of DMA and AsB into As(V) were observed at pH 11 in less than 30 min under UV irradiation.

An online UV/TiO<sub>2</sub> photocatalysis reduction device was developed for online reduction of Se(VI) [33]. Nano-TiO<sub>2</sub> was prepared by sol–gel process, which was coated onto the surface of a glass fiber fixed in the central part of a quartz capillary to achieve the on-line reduction of Se(VI) under UV-irradiation in a flow system. The vapor generation efficiency of Se(VI) was improved up to 53.3% compared with that in a  $KBH_4/HCl$  VG-AFS system, and was about two orders of magnitude higher than that obtained by using a same UV-irradiation system in the absence of nano-TiO<sub>2</sub>.

A new photochemical reaction for mercury vapor generation coupled to atomic fluorescence spectrometry was described for the speciation analysis of inorganic mercury and organic methylmercury in aqueous solution [34]. The system simply used a single reagent, i.e., formic acid, to react with  $Hg^{2+}$  or MeHg in aqueous solution under natural light or ultraviolet irradiation for the generation of cold mercury vapor, which was subsequently detected by AFS. This method was validated by determination of mercury in a certified reference material of water sample. Another technique was reported for direct vapor generation of mercury species on nano TiO<sub>2</sub> under UV irradiation in the presence of a mixture of formic acid and sodium formate as a hole scavenger [35]. The procedure was applied for the determination of mercury species by atomic fluorescence spectrometry with a newly designed UV/TiO<sub>2</sub> photocatalysis reaction device (UV/TiO<sub>2</sub> PCRDR) as an effective sample introduction unit.

### 3. Conclusions and perspectives

It is obvious from the above discussions that the determination of hydride/vapor forming elements can be well facilitated by FI/SI hydride generation atomic fluorescence spectrometry. On-line separation and preconcentration procedures can effectively eliminate the interfering effects from matrix components, and offer pertinent improvements of sensitivity. So far the coupling of on-line sample pretreatment protocols with HG-AFS has not yet been investigated thoroughly. There are therefore still some vacant areas need to be further exploited. For instance, more selective and more effective preconcentration procedures are highly expected, which deserve pertinent attentions to be focused on.

Micro sequential injection lab-on-valve system has proven to be an excellent front-end for downscaling the level of fluidic manipulation and sample pretreatment, thus the integration of hydride/vapor generation and fluorescence detection onto a lab-on-valve will definitely open up avenues for novel applications of atomic fluorescence spectrometry [36].

It is well known that so far some 20 vapor forming elements could be determined by using atomic fluorescence spectrometry, future investigations should be directed to exploit vapor generation approaches for metal species out of this scope. Although very few literatures demonstrated that on-line vapor generation AFS is equally effective for the determination of some metals that cannot form hydride [37], more efforts are obviously required in this field in order to extend the list of vapor forming elements.

## References

- [1] J.-H. Wang, E.H. Hansen, Trends Anal. Chem. 22 (2003) 836.
- [2] H.-W. Sun, R. Suo, Anal. Chim. Acta 509 (2004) 71.
- [3] Y.-K. Lu, H.-W. Sun, C.-G. Yuan, X.-P. Yan, Anal. Chem. 74 (2002) 1525.
- [4] Z.-L. Fang, Flow Injection Separation and Preconcentration, VCH, Weinheim, 1993.
- [5] X.-D. Tang, Z.-R. Xu, J.-H. Wang, Spectrochim. Acta Part B 60 (2005) 1580.
- [6] H. Wu, Y. Jin, Y.-Q. Shi, S.-P. Bi, Talanta 71 (2007) 1762.
- [7] C.-Y. Lu, X.-P. Yan, Z.-P. Zhang, Z.-P. Wang, L.-W. Liu, J. Anal. Atom. Spectrom. 19 (2004) 277.
- [8] Z. Wan, Z.-R. Xu, J.-H. Wang, Analyst 131 (2006) 141.
- [9] X. Guo, C.-G. Zheng, Z.-X. Jin, Z.-Y. Tang, Microchim. Acta 148 (2004) 221.
- [10] H. Wu, Y. Jin, W.-Y. Han, Q. Miao, S.-P. Bi, Spectrochim. Acta Part B 61 (2006) 831.
- [11] L.O. Leal, N.V. Semenova, R. Forteza, V. Cerda, Talanta 64 (2004) 1335.
- [12] L.-M. Dong, X.-P. Yan, Talanta 65 (2005) 627.
- [13] X.-W. Guo, X.-M. Guo, J. Anal. Atom. Spectrom. 10 (1995) 987.
- [14] T.-J. Hwang, S.-J. Jiang, J. Anal. Atom. Spectrom. 12 (1997) 579.
- [15] T.-C. Duan, X.-J. Song, D. Jin, H.-F. Li, J.-W. Xu, H.-T. Chen, Talanta 67 (2005) 968.
- [16] Z.-X. Li, L.-P. Zhou, Anal. Sci. 22 (2006) 123.
- [17] J.-H. Wang, E.-H. Hansen, Trends Anal. Chem. 22 (2003) 225.
- [18] Y. Wang, M.-L. Chen, J.-H. Wang, J. Anal. Atom. Spectrom. 21 (2006) 535.
- [19] X.-B. Long, M. Miro, E.H. Hansen, J.M. Estela, V. Cerda, Anal. Chem. 78 (2006) 8290.
- [20] H.-W. Sun, F.-X. Qiao, R. Suo, L.-X. Li, S.-X. Liang, Anal. Chim. Acta 505 (2004) 255.
- [21] Z.-F. Liu, H.-W. Sun, S.-G. Shen, L.-Q. Li, H.-M. Shi, Anal. Chim. Acta 550 (2005) 151.
- [22] Z.-X. Li, Y.-A. Guo, Talanta 65 (2005) 1318.
- [23] P. Cava-Montesinos, M.L. Cervera, A. Pastor, M. de la Guardia, Talanta 62 (2004) 175.
- [24] L.-J. Shao, W.-E. Gan, Q.-D. Su, Anal. Chim. Acta 562 (2006) 128.
- [25] L.-J. Shao, W.-E. Gan, W.-B. Zhang, Q.-D. Su, J. Anal. Atom. Spectrom. 20 (2005) 1296.
- [26] Z.-D. Zhou, H. Luo, X.-D. Hou, G. Li, K. Li, Microchem. J. 77 (2004) 29.
- [27] J.-H. Qiu, Q.-Q. Wang, Y.-N. Ma, L.-M. Yang, B.-L. Huang, Spectrochim. Acta Part B 61 (2006) 803.
- [28] J. Liang, Q.-Q. Wang, B.-L. Huang, Anal. Sci. 20 (2004) 85.
- [29] P. Smrkolj, V. Stibilj, Anal. Chim. Acta 512 (2004) 11.
- [30] J.B. Garcia, M. Krachler, B. Chen, W. Shoty, Anal. Chim. Acta 534 (2005) 255.
- [31] J.-H. Wang, Y.-L. Yu, Z. Du, Z.-L. Fang, J. Anal. Atom. Spectrom. 19 (2004) 1559.
- [32] E. Castro, I. Lavilla, C. Bendicho, Talanta 71 (2007) 51.
- [33] Q.-Q. Wang, J. Liang, J.-H. Qiu, B.-L. Huang, J. Anal. Atom. Spectrom. 19 (2004) 715.
- [34] C.-B. Zheng, Y. Li, Y.-H. He, Q. Ma, X.-D. Hou, J. Anal. Atom. Spectrom. 20 (2005) 746.
- [35] Y.-M. Yin, J. Liang, L.-M. Yang, Q.-Q. Wang, J. Anal. Atom. Spectrom. 22 (2007) 330.
- [36] Y.-L. Yu, Z. Du, J.-H. Wang, J. Anal. Atom. Spectrom. 22 (2007) 650.
- [37] Z.-X. Li, J. Anal. Atom. Spectrom. 21 (2006) 435.

## Photo-induced chemiluminescence-based determination of diphenamid by using a multicommutated flow system

A. Czescik<sup>a</sup>, D. López Malo<sup>a</sup>, M.J. Duart<sup>b</sup>, L. Lahuerta Zamora<sup>c</sup>,  
G.M. Antón Fos<sup>c</sup>, J. Martínez Calatayud<sup>a,\*</sup>

<sup>a</sup> Department of Analytical Chemistry, University of Valencia, Valencia, Spain

<sup>b</sup> Departamento de Ingeniería, División de Farmacia y Tecnología Farmacéutica, Facultad de Farmacia, Universidad Miguel Hernández, Alicante, Spain

<sup>c</sup> Department of Chemistry, Biochemistry and Molecular Biology, University Cardenal Herrera-CEU, Moncada (Valencia), Spain

Received 14 December 2006; received in revised form 18 April 2007; accepted 30 April 2007

Available online 10 May 2007

### Abstract

This manuscript deals with the application of molecular connectivity calculations to predict the photo-induced chemiluminescent behaviour of the family of herbicides grouped as amides. Several compounds of this group were theoretically studied by means of a general discriminant equation formerly obtained, being 18 of them (plus eight from the chloroacetanilide sub-group) predicted with a high probability as photo-induced chemiluminescent. Empirical confirmation of the chemiluminometric behaviour was performed with some few commercially available amide herbicides.

On the basis of these results, a new multicommutation-photo-chemiluminescent method is proposed for the determination of the diphenamid. The method is based on the photodegradation of the pesticide and then the resulting photo-fragment solutions are oxidized by  $K_3[Fe(CN)_6]$  in sodium hydroxide medium, at room temperature and 80 °C, for the photodegradation and chemiluminometric oxidation, respectively. The studied calibration up to 5.0 mg l<sup>-1</sup>, revealed a linear dynamic graph up to 20 mg l<sup>-1</sup>. The reproducibility between days resulted in a R.S.D. (in slope %) of 2.8 ( $n=5$ ) and the repeatability with a %R.S.D. ( $n=20$ ) of 4.3. LOD ( $s/n=3$ ) of 1 µg l<sup>-1</sup> and sample throughput of 20 h<sup>-1</sup>. The influence of foreign compounds is also tested and the optimized flow assembly is applied to different kind of samples.

© 2007 Elsevier B.V. All rights reserved.

**Keywords:** Chemiluminescence; Photo-induced chemiluminescence; Multicommutation; Diphenamid; Amide herbicides

### 1. Introduction

Diphenamid is the *N,N*-dimethyl- $\alpha$ -phenylbenzeneacetamide and its molecular structure is depicted in Fig. 1. This herbicide belongs to the group of the substituted amide herbicides [1], which are usually used to control seedling weeds prior to, or immediately following emergence. This group, made from aniline treated with organic acids, is formed by a certain number of components all of them used very often due to persistence, efficacy and selectivity when applied to pre-emergence field trials [2,3]. Persistence of these herbicides is generally fairly short; however, many of them are susceptible to leaching and have been found as contaminants in ground water.

A relevant member of this herbicide family is diphenamid which is used as a selective pre-emergence surface-applied herbicide for control of annual grasses and broadleaf weeds in peanuts, tobacco seedbeds, field tobacco, tomatoes and peppers, okra, irish potatoes, sweet potatoes, cotton, soybeans, strawberries, blackberry and raspberry (nonbearing), apple and peach trees, orange, lime and cherry trees (nonbearing), pine seedbeds, dichondra, iceplant, bermudagrass lawns and other ornamental plants. Light rainfall or sprinkler irrigation following diphenamid application will improve its control of weeds.

Diphenamid will be released in the environment during its use as an herbicide. If released to soil, the loss of diphenamid will occur primarily due to biodegradation, as certain species of soil fungi are capable of metabolizing diphenamid. The loss due to volatilization and photolysis should not be important; it is nonvolatile and appears to be relatively stable in sunlight. Depending on soil characteristics and rainfall, the persistence of

\* Tel.: +34 96 354 40 62; fax: +34 96 354 40 62.

E-mail address: [jose.martinez@uv.es](mailto:jose.martinez@uv.es) (J.M. Calatayud).

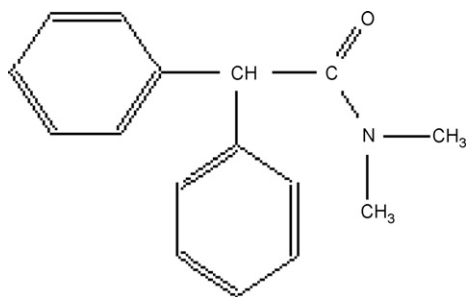


Fig. 1. Molecular structure of diphenamid.

diphenamid in soil may be 3–8 months. Microorganisms appear to play a significant role in degradation of diphenamid in soil [4].

Most reported methods for the analytical determination of diphenamid are dealing with chromatographic, liquid or gas, separation. A mixture of pesticides including diphenamid were determined by chromatography–spectrometric detection [5].

The couple gas chromatography–mass spectrometry has been applied to three kinds of Korean domestic crops, namely: *Chrysanthemum coronarium*, *Perilla japonica*, leaf, and *Lactuca scariola*, which are very popular vegetables eaten raw in Korea [6]. Gas chromatography–mass spectrometry-FTI spectrometry and high-performance liquid chromatographic have also been applied to characterization of di- and monoisomers of diphenamid [7]. Other published procedure is a Micromass Technical Note—particle beam LC/MS analysis of pesticides including determination of diphenamid in ground water [8]. The analysis of some pesticide residues in foodstuffs have been solved by applying capillary gas chromatography with mass-spectrometric detection [9]. A method for the determination of residues of pesticides in fruits and vegetables is based on two different strategies, gas chromatography–mass spectrometry and liquid chromatography with fluorescence detection, respectively. The method has been used for analysis of various fruits and vegetables, such as apple, banana, cabbage, carrot, cucumber, lettuce, orange, pear, pepper and pineapple [10].

This paper deals on an analytical strategy applied to determination of pesticides in samples of environmental interest in which is coupled a “clean chemistry” procedure as is the UV-irradiation with a high sensitivity detector, the luminometer. The automated assembly belongs to the new and emergent continuous-flow methodology known as multicommutation which manifolds can be adapted to different analytical problems. This versatility is possible as the required changes in the configuration of the flow manifold are only a logical reconfiguration via software; it even can be used to implement a separation procedure in a post-column format to increase the selectivity.

On the other hand, molecular topology, which relies on mathematical analysis, has clearly proved in recent times capable of identifying and characterizing molecular structures. Once the molecular structures with a unique profile excluding others have been established, they can be correlated with a number of physical, chemical and biological properties.

Molecular topology has recently been used to construct mathematical models capable of predicting whether a given compound will exhibit photo-induced chemiluminescence. A large body of pesticides was experimentally tested in a continuous-flow assembly furnished with a UV lamp. The results were used to calculate a discriminant function, the accuracy of which was checked on a control group consisting of pesticides not used in establishing the equation [11]. This equation has been used in the present paper to predict the photo-induced chemiluminescence of the substituted amide herbicides group. According to these predictive mathematical results, diphenamid was selected as a test-substance of the group to develop a new photo-induced determination.

To the author’s knowledge, this is the first report dealing with the chemiluminescent behaviour of diphenamid and also the first using a continuous-flow methodology for its automated determination. As far as the authors know this is the first attempt to determine diphenamid dealing on nonchromatographic procedures.

## 2. Experimental

### 2.1. Reagents and apparatus

All reagents used were analytically pure unless stated otherwise. Solutions were prepared in purified water by reverse osmosis and then deionised (18 M $\Omega$ cm) with a Sybron/Barnstead Nanopure II water purification system provided with a fibber filter of 0.2  $\mu$ m pore-size.

The diphenamid and the other assayed pesticides were from Dr. Ehrenstorfer (98.8% purity, diphenamid). Other chemicals were strong inorganic acids and alkalis, oxidants as  $\text{KMnO}_4$ ,  $\text{Ce}(\text{NH}_4)_2(\text{NO}_3)_6$ ,  $\text{H}_2\text{O}_2$ ,  $\text{K}_3\text{Fe}(\text{CN})_6$  (all of them from Panreac, Spain); tensoactives and sensitizers: Triton X-100, *N,N*-dimethylformamide and  $\text{Na}_2\text{B}_4\text{O}_7 \cdot 10\text{H}_2\text{O}$  from Panreac;  $\beta$ -cyclodextrine (Fluka, Buchs, Switzerland); sodium dodecyl sulphate and hexadecylpyridinium chloride from Fluka;  $\text{NH}_3$ ,  $\text{Na}_2\text{HPO}_4$ ,  $\text{NH}_4\text{Cl}$ ,  $\text{FeSO}_4$ ,  $\text{FeNO}_3 \cdot 9\text{H}_2\text{O}$  and sodium acetate from Probus;  $\text{H}_2\text{O}_2$ , ethanol and acetonitrile from Prolabo and Merck;  $\text{KH}_2\text{PO}_4$ ,  $\text{NaOH}$ ,  $\text{HCl}$  and acetic acid from J.T. Baker.

### 2.2. Flow assembly

The equipment was periodically tested by means of a chemiluminescent system based on the oxidation of the Aldicarb by  $7 \times 10^{-4} \text{ mol l}^{-1} \text{ MnO}_4^-$  in  $2.0 \text{ mol l}^{-1} \text{ H}_2\text{SO}_4$ . The test was performed twice every day, before and after the studies with the diphenamid and according to the procedure published elsewhere [12].

The continuous-flow manifold is depicted in Fig. 2 and it consisted of a PTFE coil of 0.8 mm internal diameter; a Gilson (Worthington, OH, USA) Minipuls 2 peristaltic pump provided with pump tubing from Elkay Elreann (Galway, CO, USA); and three Model 161T031 solenoid valves (NRResearch, Northboro, MA, USA). The photoreactor consisted of a 150 cm length and 0.8 mm internal diameter PTFE tubing (from Omnifit) helically coiled around a 15 W low-pressure mercury lamp (Sylvania)



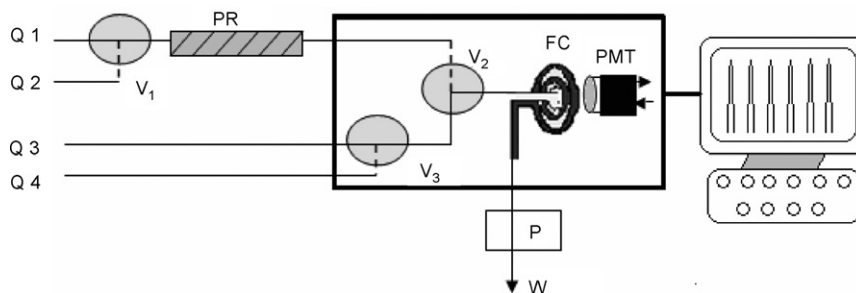


Fig. 2. Multicommutation continuous-flow assembly for the photodegradation-chemiluminescent determination of diphenamid. Q<sub>1</sub>, pesticide solution; Q<sub>2</sub>, suitable medium for the UV-irradiation; Q<sub>3</sub>, oxidant in basic medium solution; Q<sub>4</sub>, pure water; P, peristaltic pump; PMT, photomultiplier tube; V<sub>1</sub>, V<sub>2</sub> and V<sub>3</sub>, solenoid valves; FC, flow-cell; PR, photo-reactor.

for germicidal use. The flow cell was a flat-spiral quartz tube of 1 mm internal diameter and 3 cm total diameter backed by aluminium foil as a mirror for maximum light collection.

The photo-detector package was a P30CWAD5F-29 Type 9125 photomultiplier tube (PMT) supplied by Electron Tubes operating at 1280 V; it was located in a laboratory-made light-tight box. The output was fed to a computer equipped with a counter-timer, also supplied by Electron Tubes.

### 2.3. Procedures

#### 2.3.1. Preparation of the diphenamid solutions

An aqueous stock solution of 50 mg l<sup>-1</sup> of diphenamid was prepared by exactly weighing and dissolving it in purified water with a help of an ultrasonic bath. The stock solution was protected against room light and stored into the fridge. The working standard solutions were prepared daily by diluting the stock solution and protected against light.

#### 2.3.2. Preparation of samples

One human urine sample and several water samples of different type were collected from different places: namely, tap water, surface water and commercially available bottled water. Samples were collected in plastic flasks at 4 °C and analysed before 24 h. No sample pre-treatment was required. All samples were spiked with the required volume of the stock solution (10 mg l<sup>-1</sup> diphenamid).

#### 2.3.3. Optimization of experimental variables

Chemical and flow variables were optimized by using a sequentially combined methodology. First, chemical variables (*viz.* oxidant, photodegradation medium, surfactants, sensitizers, temperature and photodegradation time) were optimized by using the univariate method to provide a more systematic and comprehensive information on the chemical process; then, flow variables (*viz.* segment size and number, and flow-rate) were optimized with the modified simplex method (MSM), a multivariate approach [13–15].

Two consecutive simplex series were developed, the range of each variable used in the second being restricted to the region that gave the best results in the first. Then, three of the higher vertices were chosen for a new, extensive ( $n = 16$ ) comparative study leading to the selection of the output resulting in the best

compromise between sensitivity (peak height), throughput (peak base width) and reproducibility. Finally, the previously optimized chemical variables were refined by using the optimum values of the flow variables.

Application of the sequential methodology was completed with a study of the robustness of the proposed method.

## 3. Results and discussion

### 3.1. Preliminary studies of the light-induced chemiluminescence in amide herbicides by molecular connectivity

As formerly published [11], a set of structurally heterogeneous pesticides was studied. These comprise an inactive group, which do not present chemiluminescence with or without UV-irradiation; and an active group formed by compounds, which either increased dramatically the CL-response with irradiation, or turns into chemiluminescent ones after irradiation. From an analytical point of view the most interesting photo-induced chemiluminescent (Ph-CL) effects are included in the second group and these pesticides are suitable for developing new and sensitive chemiluminescent analytical procedures. Each group was separated in two groups, the training and the test group. Based on this, the obtained discriminant function was validated; then the discriminant ability was validated by a “cross validation” test. For details see Ref. [11].

Compounds from substituted amide herbicides were theoretically studied by means of the discriminant equation, being 17 of them predicted as Ph-CL with a high probability. See Table 1 for results. Several amide herbicides were preliminarily screened to check whether irradiation caused a substantial increase in their ability to emit luminescence upon oxidation according to the procedure and flow assembly described elsewhere [16].

The evaluation of these results lead us to select diphenamid for further work as an interesting compound and the one presenting very high chemiluminescence emission intensities.

### 3.2. Preliminary tests on the kinetic stability of aqueous diphenamid solutions

The initial tests were used to determine the kinetic stability of aqueous diphenamid. To this end, a solution containing a

Table 1  
Prediction of the photo-induced/chemiluminescent behaviour for amide herbicides

Allidochlor	–
Beflubutamid	+
Benzadox	+
Benzipram	+
Bromobutide	+
Cafenstrole	+
CDEA	–
Cyprazole	–
Dimethenamid	+
Diphenamid	+
Epronaz	–
Etnipromid	+
Fentrazamid	+
Flupoxam	+
Fomesafen	–
Halosafen	–
Isocarbamid	–
Isoxaben	+
Napropamide	+
Naptalam	+
Pethoxamid	+
Propyzamid	+
Quinonamid	+
Tebutam	+

50 mg l<sup>-1</sup> concentration of the herbicide was prepared and stored refrigerated in the dark at 4 °C prior to periodic recording of its UV–vis spectrum from 200 to 500 nm over a period of 6 consecutive days. The spectra thus obtained exhibited virtually no difference.

### 3.3. Photodegradation tests

#### 3.3.1. Influence of the medium

The previous aqueous solution of diphenamid was merged with various photodegradation media (see Fig. 3) including 1 × 10<sup>-3</sup> mol l<sup>-1</sup> NaOH, 0.05% H<sub>2</sub>O<sub>2</sub>, 6 × 10<sup>-5</sup> mol l<sup>-1</sup> Fe(III) and 6 × 10<sup>-5</sup> mol l<sup>-1</sup> Fe(II), and the oxidant (KMnO<sub>4</sub> in H<sub>2</sub>SO<sub>4</sub>). As can be seen from Fig. 3, the maximum chemiluminescence emission was obtained with Fe(II) and, especially, Fe(III)—which was thus chosen for subsequent tests.

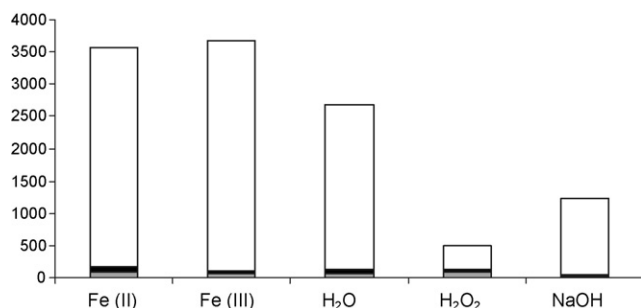


Fig. 3. Influence on the chemiluminescent outputs of the different media tested in the UV-irradiation. Black box, lamp OFF.

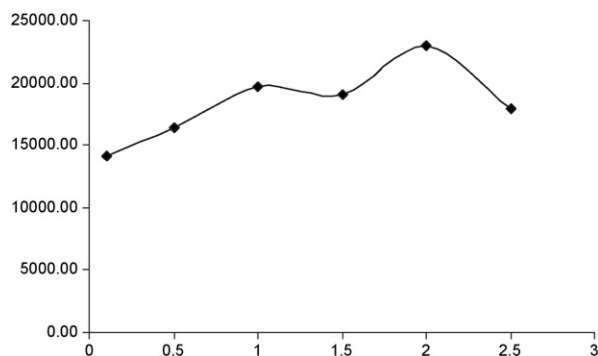


Fig. 4. Influence of different concentration of NaOH on the oxidation.

#### 3.4. Influence of the oxidant on the chemiluminescence emission

The preliminary screening was performed with a single oxidant: potassium permanganate. Subsequent tests included various strong oxidants that were used in combination with the chosen photodegradation medium and the lamp ON or OFF. The oxidants studied included 4 × 10<sup>-4</sup> mol l<sup>-1</sup> KMnO<sub>4</sub> or 6 × 10<sup>-3</sup> mol l<sup>-1</sup> Ce(IV) (both in 1.5 mol l<sup>-1</sup> H<sub>2</sub>SO<sub>4</sub>); and 6 × 10<sup>-3</sup> mol l<sup>-1</sup> Fe(CN)<sub>6</sub><sup>3-</sup> and 4 × 10<sup>-2</sup> mol l<sup>-1</sup> *N*-bromosuccinimide (both in 1.5 mol l<sup>-1</sup> NaOH). The emission intensity obtained with them was as follows (with the intensity measured with the lamp OFF): 1226 (0) with Ce(IV), 22,386 (130) with Fe(CN)<sub>6</sub><sup>3-</sup>, 8562 (92) with KMnO<sub>4</sub> and 1908 (49) with *N*-bromosuccinimide. Each result was the difference between the blank and analyte signals as obtained with the lamp OFF in both cases. As can be seen, the ratio of the signal for ferricyanide to that for permanganate were invariably 2.6.

The next test was intended to expose the influence of the oxidant concentration, which was examined over the range of 0.01–0.1 mol l<sup>-1</sup> Fe(CN)<sub>6</sub><sup>3-</sup>. The strongest signals were observed in the region 0.04–0.06 mol l<sup>-1</sup> and peaked at ca. 0.05 mol l<sup>-1</sup>, which was thus chosen for subsequent tests.

Once the most effective oxidant and concentration were selected, we examined the influence of the alkali concentration over the range of 0.1–2.5 mol l<sup>-1</sup> NaOH. The chemiluminescent signal was found to increase with increasing NaOH concentration up to 2.0 mol l<sup>-1</sup>, beyond which it started to decrease. See Fig. 4.

#### 3.5. Influence of the photodegradation medium

This test examined the influence of the concentration of Fe(III) ion as the optimum choice of photodegradation medium. To this end, an aqueous solution of the analyte was supplied with variable volumes of the Fe(III) solution in order to obtain a final analyte concentration of 10 mg l<sup>-1</sup> and one of Fe(III) over the range of 10<sup>-4</sup> to 10<sup>-2</sup> mol l<sup>-1</sup>. As can be seen from Fig. 5, this variable had a critical influence; thus, the signal rose abruptly up to an Fe(III) concentration of 5 × 10<sup>-4</sup> mol l<sup>-1</sup> and then decreased, also abruptly.

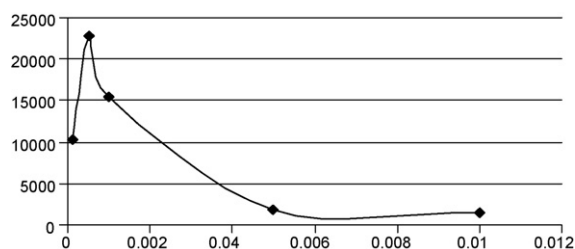


Fig. 5. Influence of different concentration of Fe(III) on the photodegradation process.

### 3.6. Influence of the presence of external chemicals: organized media and sensitizers

The presence of reagents such as surfactants and sensitizers can have a strong effect on the photodegradation and chemiluminescence processes, and alter (increase or decrease) the chemiluminescence intensity as a result. Micelle-forming agents and surfactants were used at concentrations above their critical micelle concentration (cmc). Tests were performed by merging the analyte solution with that of the agent. The substances tested and the results they provided (with the difference

from the pure analyte solution, at a  $5 \text{ mg l}^{-1}$ ) are depicted in Fig. 6a.

No signal was found to exceed the reference signal, and only that for Triton X-100 came close to it (71%). Therefore, no micellar agent or surfactant was used in subsequent tests.

We then tested various fluorophores commonly used to boost chemiluminescence. These compounds act by using the energy transferred by one or more products of the analyte upon excitation to become excited. Then, they return to their ground state by returning the energy previously received. Their usefulness lies in the high efficiency with which they can return to the ground state via radiation mechanisms. The fluorophores studied included 20% 2-propanol, 20% acetonitrile, 5% dimethylformamide, 5% ethanol, 0.5% formic acid and  $1 \times 10^{-4} \text{ mol l}^{-1}$  quinine sulphate, which were added to a  $5 \text{ mg l}^{-1}$  solution of diphenamid. Only quinine provided results close to the reference values—albeit somewhat lower (see Fig. 6b).

### 3.7. Influence of temperature

Temperature changes have complex, contradictory effects on the behaviour of chemiluminescent systems. Thus, an increased

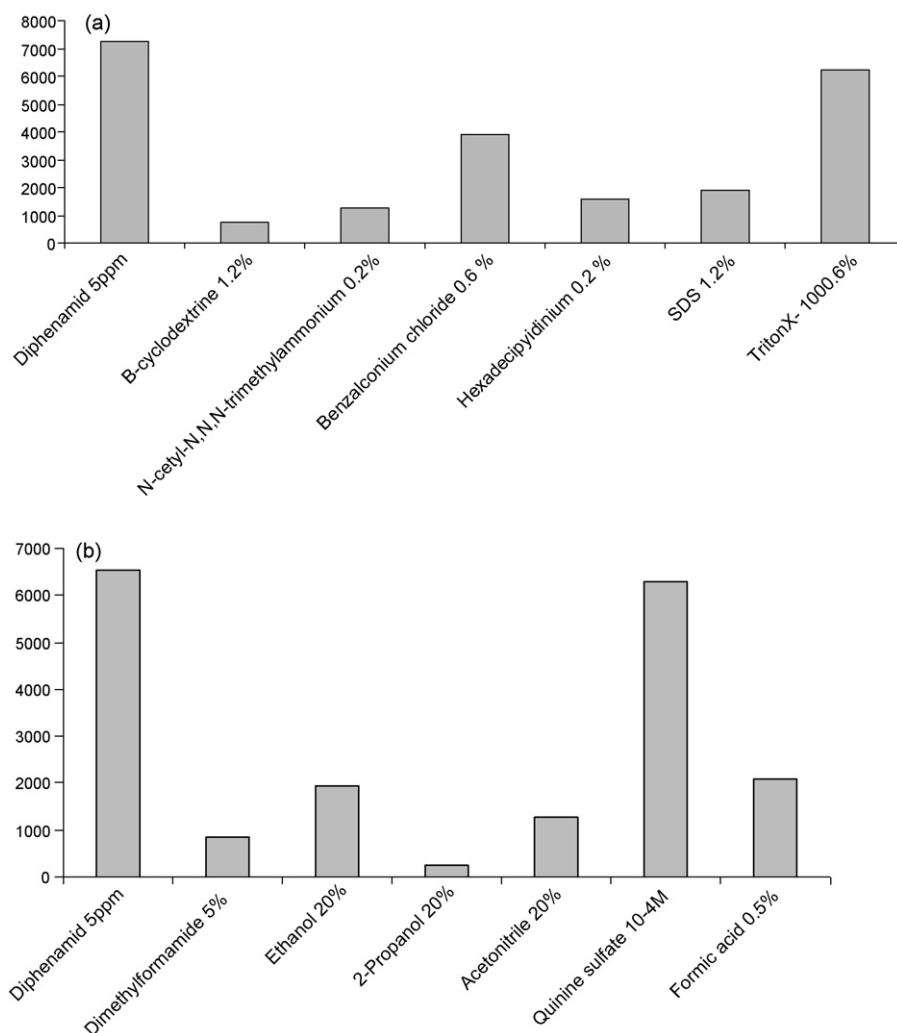


Fig. 6. Influence of different external reagents, sensitizers and organized media. (a) Influence of different organized media and (b) different sensitizers tested.

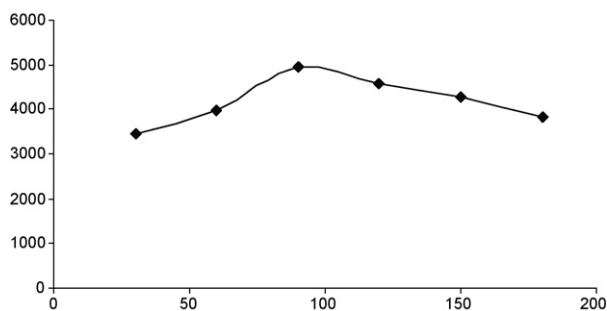


Fig. 7. Influence of different time of photodegradation.

temperature can facilitate oxidation via a favourable effect on its kinetics and equilibrium; however, it can also have an adverse effect on emission by facilitating de-excitation via nonradiative mechanisms [17]. In addition, it can have similar kinetic and equilibrium-related effects on the chemiluminescent reaction.

The influence of temperature on the photodegradation and chemiluminescence results was examined separately. In one test, the PTFE tubes carrying the sample and photodegradation medium were immersed in a Tectron 200 water bath at temperatures from room level to 80 °C. In the other, the tube immersed in the water bath was that containing the oxidant. Results seemed contradictory; as the outputs decreased when increased the irradiation process, the outputs increased with the temperature increase on the chemiluminescent oxidation. Based on them, we chose room temperature for the photodegradation medium and 80 °C for the oxidant.

### 3.8. Influence of the photodegradation time

This variable is very important, as the fragments exposed to the oxidant in order to generate the chemiluminescence are usually intermediates of the overall degradation process caused by absorption of the electromagnetic energy irradiated by the lamp. We studied the effect of times from 30 to 180 s. The chemiluminescent signal was found to increase with increasing time up to 90 s, beyond which it decreased (Fig. 7). A photodegradation time of 90 s was therefore chosen for subsequent tests.

### 3.9. Influence of hydrodynamic variables

The flow-rate and the segment length and number, were optimized by using the modified simplex method (MSM) over the following ranges: 100–999 (arbitrary units coinciding with the rotation speed of the peristaltic pump drum as shown on the display) for the flow-rate; 20–40 for the number of sample segments supplied via valve  $V_2$  and 0.1–0.5 for their size; and 0.4–0.8 for the size of the oxidant segments. Valves  $V_1$  and  $V_3$  were not studied. The pesticide concentration used was 5 mg l<sup>-1</sup>.

The experimental sequence involved two optimization series. The first was used to set the limits for each variable based on the results of the previous tests and the second to adjust the ranges of the variables in accordance with the results of the first series. The best three vertices were selected in terms of peak height and used in separate iterative series in order to identify that pro-

Table 2

Finally selected set of parameters

$V_1$	0, 50*(0.4, 0.2), 0.5
$V_2$	0, 30, 90, 36*(0.6, 0.4), 0.5
$V_3$	105, 53
$t_{\text{cycle}}$	180 s

The final total flow-rate was 10 ml min<sup>-1</sup>.

viding the best compromise between sensitivity (peak height), reproducibility (R.S.D.) and throughput (peak base height). See Table 2 for selected set of parameters.

### 3.10. Chemical robustness of the proposed method

Validating a method usually involves assessing its robustness as a means of refining the optimized results [18]. Method robustness is given little consideration by academia, but highly regarded by regulatory bodies such as ICH and FDA. A robust method is one capable of responding accurately to changes in the experimental conditions. Therefore, assessing robustness entails altering some experimental variables (particularly those set by the operator).

The robustness of our method was determined by using a univariate procedure to change each variable around the value chosen as optimal. The first variable studied was the oxidant concentration, which was examined over the range of 0.03–0.07 mol l<sup>-1</sup>. The peak height obtained at 0.04 mol l<sup>-1</sup> was slightly greater than that at 0.05 mol l<sup>-1</sup>, so the former concentration was adopted for further testing. The standard deviation relative to the peak at 0.04 mol l<sup>-1</sup> was 18%, 19% and 16% for 0.03, 0.06 and 0.07 mol l<sup>-1</sup>, respectively.

The influence of small changes ( $\pm 10\%$ ) in concentration of the oxidation medium, NaOH, was examined at three different concentrations of pesticide; the standard deviation thus obtained never exceeding 5%.

The Fe(III) concentration was found to be a critical variable. As a result, the deviation obtained with respect to the optimum value ( $5 \times 10^{-4}$  mol l<sup>-1</sup>) was 12% at  $4 \times 10^{-4}$  mol l<sup>-1</sup> and 10% at  $6 \times 10^{-4}$  mol l<sup>-1</sup>.

## 4. Analytical figures of merit

### 4.1. Calibration graphs, limit of detection, reproducibility, repeatability and throughput

The dynamic range was found to be between  $5 \times 10^{-3}$  and 20 mg l<sup>-1</sup> of diphenamid, and fitted with the equation  $I = -101.37x^2 + 4003.1x - 586.06$  with a correlation coefficient of 0.9978, where  $I$  is the chemiluminescent emission in counts and  $x$  is the pesticide concentration in mg l<sup>-1</sup>. The average equation was obtained from five independent calibration graphs, performed with freshly prepared solutions on 5 different days.

The lineal behaviour was observed over the range of  $5 \times 10^{-3}$  to 5 mg l<sup>-1</sup>, fitting with the equation  $I = 3277.6x + 81.142$  with a correlation coefficient of 0.9994.

The limit of detection was 1 µg l<sup>-1</sup> and which was defined as three-times the blank output height average and was empir-

ically established by decreasing the concentration of injected diphenamid until this relationship was reached.

The reproducibility of the slope of the calibration curve (or relative standard deviation in experiments performed in different days and freshly prepared solutions), was determined from 0.01 to 5 mg l<sup>-1</sup>. The mean slope from five independent calibrations of diphenamid was 3256.04 with a R.S.D. 2.8%.

The R.S.D. for the peaks, which is a measure of repeatability was determined by using 16 consecutive sample aliquots of 0.5 mg l<sup>-1</sup> and it was 4.3%. The maximum sample throughput was calculated from the average of base-peak wide (20 replicates) containing 0.5 mg l<sup>-1</sup> of diphenamid; obtained result was 20 h<sup>-1</sup>.

#### 4.2. Influence of interferences

The analytical features of the proposed method and its tolerance to potential interferences accompanying diphenamid in water samples and human urine were studied for different concentrations of the potential interference tested (maximum 500 mg l<sup>-1</sup>) and a concentration of pesticide of 0.5 mg l<sup>-1</sup>. Foreign compounds were not considered as interference when the calculated relative error versus the reference (solution containing only 0.5 mg l<sup>-1</sup> of pesticide) was less than ±5%. See results in Table 3.

Most critical interference was presented by Mn<sup>2+</sup>, Cr<sup>3+</sup>, NH<sub>4</sub><sup>+</sup> and Fe<sup>3+</sup>. Therefore, for application to water samples and urine, these cations and some anions like: Cl<sup>-</sup>, SO<sub>4</sub><sup>2-</sup>,

Table 3  
Study of interferences

Interferents	C (mg l <sup>-1</sup> )	Recovery (%)
(a) Influence of foreign compounds		
Inorganic cations		
Fe <sup>3+</sup>	50	-1.2
NH <sub>4</sub> <sup>+</sup>	50	-4.2
Mn <sup>2+</sup>	10	-1.1
K <sup>+</sup>	100	-4.9
Na <sup>+</sup>	200	-4.9
Zn <sup>2+</sup>	100	-3.2
Mg <sup>2+</sup>	100	-4.8
Cr <sup>3+</sup>	10	-1.3
Cu <sup>2+</sup>	100	+3.1
Ca <sup>2+</sup>	100	-2.5
Inorganic anions		
H <sub>2</sub> PO <sub>4</sub> <sup>-</sup>	100	-1.6
Cl <sup>-</sup>	100	-2.7
SO <sub>4</sub> <sup>2-</sup>	100	+3.1
NO <sub>2</sub> <sup>-</sup>	100	4.8
NO <sub>3</sub> <sup>-</sup>	200	-3.2
CO <sub>3</sub> <sup>2-</sup>	10	-1.2
(b) Influence of most critical interferents after passage through the ion exchange column		
Fe <sup>3+</sup> , Mn <sup>2+</sup> , NH <sub>4</sub> <sup>+</sup> , Cr <sup>3+</sup>	500	4.7
SO <sub>4</sub> <sup>2-</sup> , H <sub>2</sub> PO <sub>4</sub> <sup>-</sup> , Cl <sup>-</sup> , CO <sub>3</sub> <sup>2-</sup>	500	4.7
NO <sub>2</sub> <sup>-</sup> (boil)	500	2.9

The aqueous solutions were prepared from salts of sodium or chloride for anions and cations, respectively.

Table 4  
Origins and recoveries of the spiked water samples and urine

Type of sample	Origin of the samples	Recovery (%) (n = 3)
Residual water	0°26'19.057"W and 39°27'10.642"N (Xirivella, Valencia, Spain)	101 ± 5
Underground water	1°9'9.993"W and 39°31'22.096"N (San Antonio, Valencia, Spain)	98 ± 1
Mineral water	Trade mark Ague de Bejis, Castellon, Spain	100 ± 3
Tap water	University of Valencia, Valencia, Spain	103 ± 3
Human urine	-	101.9 ± 0.8

CO<sub>3</sub><sup>2-</sup> should be removed by passage through appropriate ion-exchange resins; Duolite A-102 (Fluka) (anionic) or Duolite C20 (Probus, cationic).

The exchangers were prepared by packing Omnifit 5 cm × 4 mm i.d. methacrylate chromatographic columns with the resins. Prior to use, each column was conditioned by passage of a 0.1 mol l<sup>-1</sup> NaOH or HCl solution. To remove the interferences were prepared solutions containing 0.5 mg l<sup>-1</sup> of the pesticide and 500 mg l<sup>-1</sup> of the corresponding interferent to be tested. All the results were quite favourable.

Other interferent was nitrite under 100 mg l<sup>-1</sup>; these anions can be easily removed. A solution containing 0.5 mg l<sup>-1</sup> of diphenamid and 500 mg l<sup>-1</sup> of nitrite was gently heated during 10 min; no error was observed. See the results in Table 3.

#### 4.3. Application of the method to real samples

The applicability of the proposed method, based on a photoreaction and the chemiluminescence phenomenon, was checked by analysing samples which were human urine and different types and origin of water. All samples were spiked with 1 mg l<sup>-1</sup> of diphenamid. Analysed samples were as illustrated in Table 4. Origins and recoveries of the spiked water samples and urine are also depicted in this table.

## 5. Conclusions

The molecular connectivity is an interesting tool to predict the photo-induced chemiluminescence; it has been applied to amide pesticide family and the result is a new, automated, simple, sensitive, and precise method for the determination of herbicide diphenamid. The method is performed by a continuous-flow manifold of the type of the emergent multicommutation methodology.

The method is based on the on-line UV-irradiation of diphenamid in presence of Fe(III) medium. As far as the authors know this is the first attempt to determine diphenamid out of the chromatographic procedures. Then, the photo-fragments are oxidized by hexacyanoferrate(III) in NaOH medium and the resultant chemiluminescent intensity is measured. The method allows a sample throughput 20 h<sup>-1</sup>. It is reasonably robust (chemical robustness) being the Fe(III) concentration the only

critical parameter as it is usual in this kind of photo-induced emission methods influenced by the Fe(III) presence.

### Acknowledgement

One of the authors, D. López Malo, thanks Caja de Ahorros del Mediterráneo, CAM, the pre-doctoral scholarship CAM-Investigación, Convocatoria 2005.

### References

- [1] [http://www.alanwood.net/pesticides/class\\_herbicides.html#amide\\_herbicides](http://www.alanwood.net/pesticides/class_herbicides.html#amide_herbicides).
- [2] <http://wssa.allenpress.com/wssaonline/?request=get-abstract&issn=0890-037X&volume=017&issue=02&page=0381>.
- [3] <http://www.fr.iucr.org/e/issues/2006/03/00/ww6469/ww6469.pdf#search=%22amide%20herbicides%20%22>.
- [4] Weed Science Society of America, Herbicide Handbook Committee, Herbicide Handbook of the Weed Science Society of America, 5th ed., Weed Science Society of America, Champaign, IL, 1983, 515 pp.
- [5] J. Dalluge, R.J.J. Vreuls, J. Beens, U.A.T. Brinkman, J. Separ. Sci. 25 (2002) 201.
- [6] O.K. Chun, H.G. Kang, M.H. Kim, J. AOAC Int. 86 (2003) 823.
- [7] L. Sojak, A. Perjessy, R. Kubinec, J. Cambalikova, A.G. Guimanini, G. Verardo, M.M. Magnan, J. Chromatogr. A 878 (2000) 235.
- [8] C.J. Miles, D.R. Doerge, S. Bajic, Micromass Technical Note, 202, January 2001, 4.
- [9] H.J. Stan, J. Chromatogr. A 892 (2000) 347.
- [10] J. Fillion, F. Sauve, J. Selwyn, J. AOAC Int. 83 (2000) 698.
- [11] I. Sahuquillo Ricart, M.J. Duart, G.M. Antón Fos, L. Lahuerta Zamora, J.V. García Mateo, J. Martínez Calatayud, Talanta 72 (2007) 378.
- [12] M. Palomeque, J.A. García Bautista, M. Catalá Icardo, J.V. García Mateo, J. Martínez Calatayud, Anal. Chim. Acta 512 (2004) 149.
- [13] L.A. Yabro, S.N. Derming, Anal. Chim. Acta 73 (1974) 1043.
- [14] S.L. Morgan, S.N. Derming, Anal. Chem. 46 (1974) 1170.
- [15] J.A. Nelder, R. Mead, Computer 7 (1965) 308.
- [16] Y. Fuster Mestre, L. Lahuerta Zamora, J. Martínez Calatayud, Luminescence 15 (2000) 1.
- [17] J. Martínez Calatayud, Flow Injection Analysis of Pharmaceuticals. Automation in the Laboratory, Taylor and Francis, Cambridge, 1996.
- [18] I.S. Krull, S. Swartz, Anal. Lett. 32 (1999) 1067.

# Development of a solid phase extraction procedure for HPLC–DAD determination of several angiotensin II receptor antagonists in human urine using mixture design

N. Ferreirós, G. Iriarte, R.M. Alonso\*, R.M. Jiménez

*Departamento de Química Analítica, Facultad de Ciencia y Tecnología, Universidad del País Vasco/EHU, Apdo 644, 48080 Bilbao, Spain*

Received 5 February 2007; received in revised form 20 April 2007; accepted 30 April 2007

Available online 13 May 2007

## Abstract

The optimisation of a solid phase extraction procedure involves several variables whose influence has been widely studied. However, in most cases, only process variables are taken into account. In this work, the influence of those process variables together with the fact of using mixtures of solvents during the elution step of the solid phase extraction of four angiotensin II receptor antagonist drugs has been studied. Since the influence on the extraction efficiency of several process variables were simultaneously tested, a D-optimal design was constructed. The composition of the elution solvent (a mixture of methanol, acetonitrile, ethanol and acetone at different proportions from 0 to 100% each solvent), the percentage and pH of the buffer solution added to the urine samples at the beginning of the extraction procedure; the percentage of the organic component and the volume of the washing solution, the drying time and the volume of the elution solvent were the studied variables. The chromatographic separation was carried out by gradient elution mode with 0.026% trifluoroacetic acid (TFA) in the organic phase and 0.031% TFA in the aqueous phase using an Atlantis dC18, 100 mm × 3.9 mm I.D. chromatographic column at a flow rate of 1 mL/min and a column temperature of  $35 \pm 0.2$  °C. For detection a diode array detector set at 232 nm was used. The extraction procedure for spiked human urine samples was developed using C8 cartridges, phosphate buffer pH 6.8 as conditioning agent, a drying step of 10 min, a washing step with methanol–phosphate buffer (20:80, v/v) and methanol as eluent. Recovery percentages obtained: 84% for eprosartan, 74% for telmisartan, 74% for irbesartan and 89% for valsartan allow the determination of these drugs concentration levels in urine.

© 2007 Elsevier B.V. All rights reserved.

**Keywords:** SPE; ARA-II; Mixture design; Optimisation; PLS

## 1. Introduction

Eprosartan, telmisartan, irbesartan and valsartan are highly selective, non-peptide angiotensin-II receptor antagonists (ARA-II). These compounds have been shown to inhibit angiotensin II induced vasoconstriction in preclinical species and cause reductions in systolic and diastolic blood pressure at peak effect after dosing in clinical patients [1,2]. As the rest of drugs of this family, they are safe and effective agents for the treatment of hypertension and heart failure, either alone, or together with diuretics. Because of this, they have been proposed as an alternative to the more traditional angiotensin-converting enzyme (ACE) inhibitors.

The development of analytical methods for the determination of ARA-II is crucial for the study of the antihypertensive efficacy of these single dose drugs during the inter dosage range, since they would allow the monitorization of their biologic concentration levels.

There are some works dealing with the determination of ARA-II in pharmaceuticals and biological samples. Hillaert and coworkers [3–5] have described some electrophoretic and chromatographic screening methods for several ARA-II alone or in combination with diuretics in pharmaceuticals. Other authors [6–22] have developed methods to separate ARA-II in biological fluids such as plasma and urine. But none of these include eprosartan in human urine. Since telmisartan, irbesartan and valsartan are also widely prescribed ARA-II drugs in the treatment of hypertension and their administered doses are higher than those of other ARA-II such as candesartan (16 mg/day) or losartan (50 mg/day), it is expected to determine their urine

\* Corresponding author. Tel.: +34 94 601 2686; fax: +34 94 601 3500.  
E-mail address: [rosamaria.alonso@ehu.es](mailto:rosamaria.alonso@ehu.es) (R.M. Alonso).

concentration levels. Only in the case of telmisartan, the administered dose can be lower (20, 40 or 80 mg/day) than the other studied drugs. Besides, telmisartan, irbesartan and valsartan have not been previously determined by using HPLC–DAD or together with eprosartan. Thus, the development of simultaneous extraction for eprosartan, telmisartan, irbesartan and valsartan from urine for further determination by HPLC–DAD based on a previously validated chromatographic method for eprosartan in human plasma samples, [23] has been performed. Experimental design was used to optimise the clean-up procedure of urine samples. This chemometric tool has been successfully applied to the optimisation of the parameters of interest in chromatography and related techniques (electrochromatography and electrophoresis) [24–27]. In chemometric approaches, experimental measurements are performed in such a way that all factors vary together. An objective function is utilised in which the analyst introduces the desired criteria (selectivity, resolution, time of analysis . . .).

The aim of actual optimisation strategies is to obtain the largest quality information while carrying out a limited number of experiments. The great number of chromatographic parameters and the relationship between them rule out the possibility of empirical optimisation by trial and error or intentional variation of one or two parameters. These intentional variations fail to take interactions between two or more parameters into account. But, although it suffers from severe limitations such as the success in the optimisation procedure mainly relays on the starting conditions and the researcher's experience, one variable-at-a-time optimisation method is still nowadays very popular and extremely used in analytical applications. This traditional methodology may become erratic and, which is more important, possible synergetic effects among variables are not considered at all.

Use of experimental design combined with analysis of variance, and simplex or multisimplex methods are much more reliable and avoid the limitations mentioned above.

The purpose of multivariate data analysis is to extract information from a data table. The data can be collected from various sources or designed with a specific purpose in mind. The objectives of experimental design are the following: efficiency (get more information from fewer experiments), and focusing (collect only the information you really need) [28].

Experimental design is a strategy to gather empirical knowledge based on the analysis of experimental data and not on theoretical models. To build a design, it is necessary to define an objective to the experiment. In the case that at least three design variables define a mixture, these are called mixture variables, for which the variations are controlled in an experimental or D-optimal mixture design and a constraint is applied on:

$$X_1 + X_2 + \dots + X_n = S$$

where  $X_i$  represent the ingredients of the mixture, and  $S$  is the total amount of the mixture. In most cases,  $S$  is equal to 100%.

There are three types of classical mixture designs: simplex-lattice design, simplex-centroid design and axial design.

If there are only mixture variables, and their ranges of variation define a simplex, a choice between a simplex-lattice design, a simplex-centroid design or an axial design must be done. If

the mixture region is not a simplex, or if mixture variables with process variables are combined, the design will be built according to the D-optimal principle, which consists in a sub-set of candidate points which define a maximal volume region in the multidimensional space. This principle aims at minimizing the condition number. In a D-optimal mixture design, multilinear relationships can be defined between mixture and process variables. For screening purposes, a linear model, optionally with interactions, must be chosen. When the optimisation is the study purpose, interactions and squares must be included.

Designed data can be analysed using general statistics, principal component analysis (PCA), principal component regression (PCR), partial least squares (PLS) or multiple linear regression (MLR).

PLS is a method for relating the variations in one or several response variables ( $Y$ -variables) to the variations of several predictors ( $X$ -variables), with explanatory or predictive purposes. Partial least squares regression is a bilinear modelling method where information in the original  $X$ -data is projected onto a small number of underlying ("latent") variables called PLS components. The  $Y$ -data are actively used in estimating the "latent" variables to ensure that the first components are those that are most relevant for predicting the  $Y$ -variables. Interpretation of the relationship between  $X$ -data and  $Y$ -data is then simplified as this relationship is concentrated on the smallest possible number of components [29].

In PLS two different versions can be employed: PLS1, the version with only one  $Y$ -variable, and PLS2, the one in which several  $Y$ -variables are modelled simultaneously, thus taking advantage of possible correlations or co-linearity between  $Y$ -variables.

This article accomplishes the development of a solid phase extraction procedure for eprosartan, telmisartan, irbesartan and valsartan in human urine samples. In this case, a mixture design must be used, due to the fact that a mixture of four solvents as the elution liquid was tested and some process variables were also studied. A D-optimal mixture design was constructed upon the basis of other Solid Phase Extraction (SPE) procedure designed in our laboratory for the extraction of eprosartan in human plasma samples [30].

## 2. Experimental

### 2.1. Materials and reagents

Eprosartan {(E)-3-[2-butyl-1-[(4-carboxy-phenyl)methyl]-1H-imidazol-5-yl]-2-[(2-thienyl)-methyl]propenoic acid}, provided as mesylate salt, telmisartan {4'-[[4-methyl-6-(1-methyl-2-benzimidazolyl)-2-propyl-1-benzimidazolyl]methyl]-2-biphenylcarboxylic acid}, irbesartan {2-butyl-3-[[2'-(1H-tetrazol-5-yl)(1,1'-biphenyl)-4-yl]methyl]-1,3-diazaspiro[4,4]non-1-en-4-one}, valsartan {*N*-(1-oxopentyl)-*N*-[[2'-(1H-tetrazol-5-yl)[1,1'-biphenyl]-4-yl]methyl]-valine} and the internal standard EXP3174 {2-*n*-butyl-4-chloro-1-[[2'-(1H-tetrazol-5-yl)[1,1'-biphenyl]-4-yl]methyl]-1H-imidazole-5-carboxylic acid} were kindly supplied by Solvay Pharma (Barcelona, Spain), Boehringer Ingelheim (Ingelheim, Germany), Sanofi-Synthelabo (Montpellier, France), Novartis



Table 1  
Gradient elution conditions

Time (min)	ACN 0.026% TFA	H <sub>2</sub> O 0.031% TFA
0	30	70
8	30	70
12	45	55
16	45	55
20	30	70

Pharma (Basel, Switzerland) and Merck (New Jersey, USA), respectively. Reagent grade trifluoroacetic acid (TFA), di-sodium tetraborate decahydrate, potassium hydroxide, hydrochloric acid and sodium di and monohydrogen phosphate were purchased from Merck (Darmstadt, Germany). HPLC grade acetonitrile and methanol were obtained from Scharlab (Barcelona, Spain). Reagent grade absolute ethanol and acetone were purchased from Panreac (Barcelona, Spain). Purified water from a Milli-Q Element A10 water system (Millipore, Bedford, MA, USA) was used in the preparation of buffer and reagent solutions. SPE C8 cartridges (100 mg bed packing, 1 mL volume capacity) were purchased from Varian (Harbour City, CA, USA). Drug-free control human urine was obtained from healthy volunteers.

## 2.2. Apparatus

The chromatographic system consisted of a Waters (Milford, MA, USA) Alliance Model 2695 separation module and a Waters 996 diode array detector. Chromatograms were recorded by means of a computer and were treated with the aid of the software Empower from Waters.

A Waters Atlantis dC18, 100 mm × 3.9 mm I.D., 3 μm, 100 Å column was used to perform separation. It was thermostated at 35 ± 0.2 °C. Previous to the analytical column, a Waters μBondapak C18 guard column 10 μm was placed to prevent column degradation.

The clean-up procedure consisted of solid-phase extraction and was performed using a vacuum manifold system from Supelco (Bellefonte, PA, USA) coupled to a vacuum pump from Millipore (Bedford, MA, USA).

pH of solutions was measured with a Crison GLP 22 pH-meter (Barcelona, Spain) using a Crison glass-combined electrode model 52-02 (Barcelona, Spain) with reference system Ag/AgCl and electrolyte KCl 3 M saturated in AgCl.

Urine extracted samples were evaporated to dryness under a nitrogen stream using a Zymark Turbovap evaporator LV (Barcelona, Spain).

Urine samples were centrifuged in a 5804R Eppendorf refrigerated centrifuge (Hamburg, Germany).

## 2.3. Preparation of standard solutions and spiked urine samples

All compounds were supplied as solid, white powders, which were used to prepare stock solutions of 1 mg/mL of each compound in methanol. These solutions were used to prepare the

working solutions as follows. A 70 μg/mL working solution of eprosartan, telmisartan, irbesartan and valsartan was prepared in 100% methanol (mixture solution). A 50 μg/mL working solution of a metabolite of losartan (EXP 3174), used as internal standard, was also prepared following the same procedure. These solutions were used to spike the blank urine samples. All solutions were stored at refrigerator temperature and protected from light.

For the SPE optimisation, blank urine samples were daily spiked to achieve drug concentrations of 2.1 μg/mL of each drug and 1.5 μg/mL of the internal standard.

## 2.4. Extraction procedure of urine samples

0.5 mL aliquots of blank urine samples were spiked with the working solutions of the studied ARA-II compounds (eprosartan, telmisartan, irbesartan and valsartan) to achieve a concentration of 2.1 μg/mL. An aliquot (0.2 mL) of phosphate buffer pH 6.8, 50 mM was added to all samples, which was followed by brief vortex mixing and centrifugation for 5 min in a high speed centrifuge (10,000 r.p.m.) refrigerated at 4 °C.

The SPE cartridges were conditioned with 2 mL of methanol, followed by 2 mL of phosphate buffer (50 mM, pH 6.8). The urine samples were applied to the cartridges manually and washed with 1 mL methanol–phosphate buffer solution (20:80, v/v), followed by a 10 min drying period at high vacuum. The cartridges were then eluted with 2 mL of methanol. After the elution step, the appropriate volume of the internal standard working solution to achieve a concentration of 1.5 μg/mL was added. The eluent was evaporated to dryness under nitrogen at 60 °C. The residue was reconstituted with 100 μL of mobile phase (acetonitrile 0.026% TFA:water 0.031% TFA, 30:70, v/v), vortex mixed, filtered with a 0.45 μm syringe filter and transferred to auto sampler vials. Twenty microliter aliquots were injected into the HPLC system for analysis.

Table 2  
Variables and levels considered for the optimisation of the SPE procedure for eprosartan, telmisartan, irbesartan and valsartan in human urine

	Studied ranges	
	Low value	High value
	<i>Mixture variables</i>	
Methanol (%)	0	100
Acetonitrile (%)	0	100
Acetone (%)	0	100
Ethanol (%)	0	100
	<i>Process variables</i>	
Initial buffer (%)	20	50
pH conditioning buffer	6	10
Composition washing sol. (% organic solvent)	0	30
Washing sol. volume (mL)	0.5	2
Drying time (min)	5	15
Elution sol. volume (mL)	0.5	2

Table 3  
The 32-run, four-factor, two level D-optimal design proposed by The Unscrambler software and the obtained recovery percentages

Exp.	Methanol (%)	ACN (%)	Acetone (%)	Ethanol (%)	pH conditioning	Initial buffer (%)	Washing sol. Volume (mL)	Organic sol. (%)	Drying time (min)	Elution sol. Volume (mL)	Eprosartan	Telmisartan	Irbesartan	Valsartan
1	0	1	0	0	10	20	0.5	0	5	0.5	0.00	3.05	55.71	13.23
2	0	0	1	0	6	50	0.5	0	5	0.5	0.00	67.44	74.86	81.71
3	1	0	0	0	6	20	2	0	5	0.5	82.46	73.18	74.37	83.72
4	0	0	0	1	10	50	2	0	5	0.5	73.73	69.71	57.19	78.57
5	0	0	0	1	6	20	0.5	30	5	0.5	19.28	77.37	76.65	75.51
6	0	1	0	0	6	50	0.5	30	5	0.5	0.00	70.89	19.54	2.61
7	0	1	0	0	10	20	2	30	5	0.5	0.00	0.00	0.00	0.00
8	0	0	1	0	10	50	2	30	5	0.5	0.00	0.00	0.00	0.00
9	0	1	0	0	6	20	0.5	0	15	0.5	0.00	61.53	66.21	48.44
10	1	0	0	0	10	50	0.5	0	15	0.5	97.22	84.07	77.29	93.01
11	0	0	1	0	10	20	2	0	15	0.5	0.00	0.00	26.75	0.00
12	0	0	0	1	6	50	2	0	15	0.5	69.84	74.74	71.84	71.28
13	0	0	0	1	10	20	0.5	30	15	0.5	0.00	67.34	69.31	1.99
14	0	0	1	0	6	50	0.5	30	15	0.5	5.92	85.72	85.43	2.77
15	1	0	0	0	6	20	2	30	15	0.5	36.64	79.82	80.59	80.64
16	0	0	0	1	6	20	0.5	0	5	2	0.00	64.35	64.12	69.28
17	0	0	0	1	10	20	2	0	5	2	97.05	89.16	82.28	138.83
18	0	1	0	0	6	50	2	0	5	2	79.81	72.30	73.86	88.88
19	0	0	1	0	10	20	0.5	30	5	2	0.00	30.34	18.86	0.00
20	1	0	0	0	10	50	0.5	30	5	2	29.88	89.09	89.40	100.33
21	0	0	0	1	6	50	2	30	5	2	0.00	83.06	82.20	0.00
22	1	0	0	0	10	20	0.5	0	15	2	38.16	91.39	72.77	95.81
23	1	0	0	0	6	50	0.5	0	15	2	0.00	81.40	79.83	86.13
24	0	0	1	0	10	50	0.5	0	15	2	0.00	0.00	62.85	0.00
25	0	0	1	0	6	20	2	0	15	2	79.63	71.81	71.80	79.93
26	0	1	0	0	6	20	0.5	30	15	2	0.00	79.12	18.03	0.00
27	0	0	0	1	10	50	0.5	30	15	2	0.00	69.86	64.04	0.00
28	0	0	0	1	10	20	2	30	15	2	0.00	72.22	11.74	0.00
29	1	0	0	0	10	50	2	30	15	2	7.48	89.38	71.05	95.36
30	0.25	0.25	0.25	0.25	8	35	1.25	15	10	1.25	64.38	72.22	66.79	81.46
31	0.25	0.25	0.25	0.25	8	35	1.25	15	10	1.25	62.90	68.30	64.75	80.50
32	0.25	0.25	0.25	0.25	8	35	1.25	15	10	1.25	63.41	64.79	60.00	81.40

## 2.5. Chromatographic conditions

The mobile phase consisted of a mixture of acetonitrile 0.026% TFA and water 0.031% TFA and was delivered in gra-

dient mode at a flow rate of 1 mL/min. The gradient is shown in Table 1. Before using, the mobile phase was passed through a 0.45  $\mu\text{m}$  membrane filter from Millipore (Bedford, MA, USA) and degassed in an ultrasonic bath. The chromatographic separa-

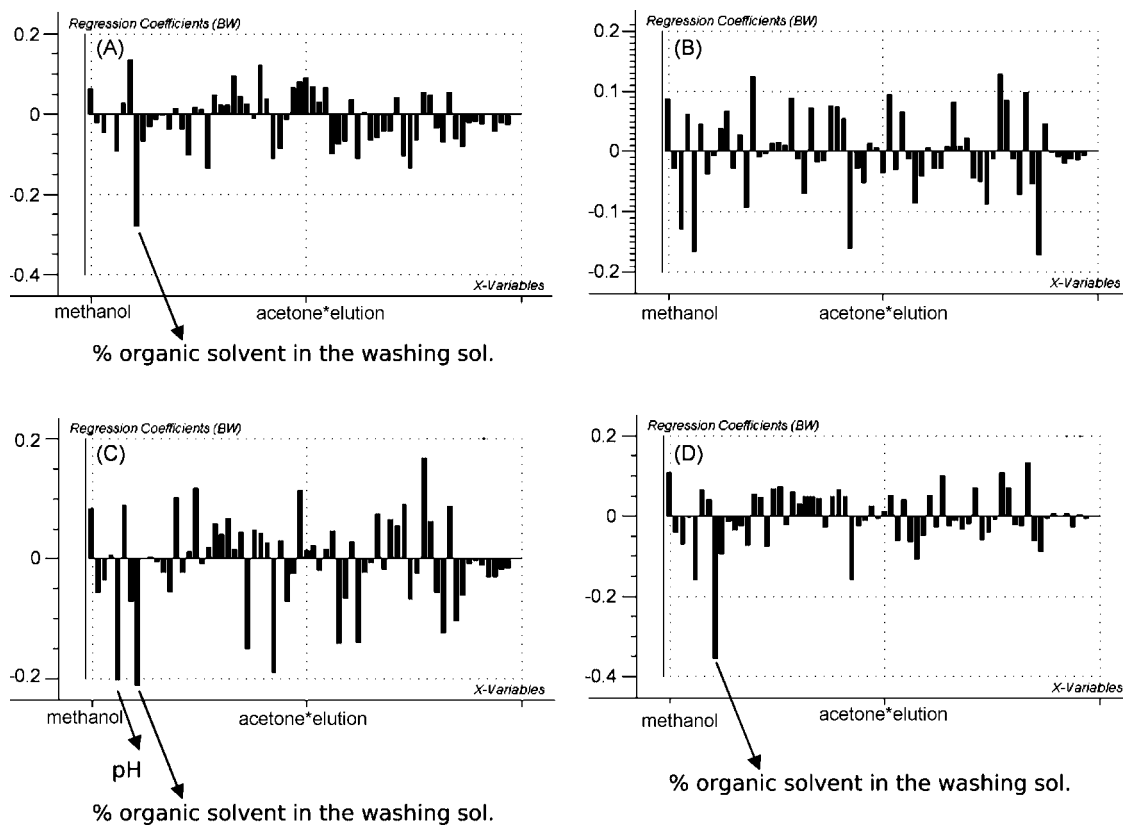


Fig. 1. Regression coefficients for the studied factors and their interactions obtained by treating the D-optimal design data with PLS-2. The significant variables for eprosartan (A), telmisartan (B), irbesartan (C) and valsartan (D) were those whose regression coefficient was larger than 0.2 in absolute value.

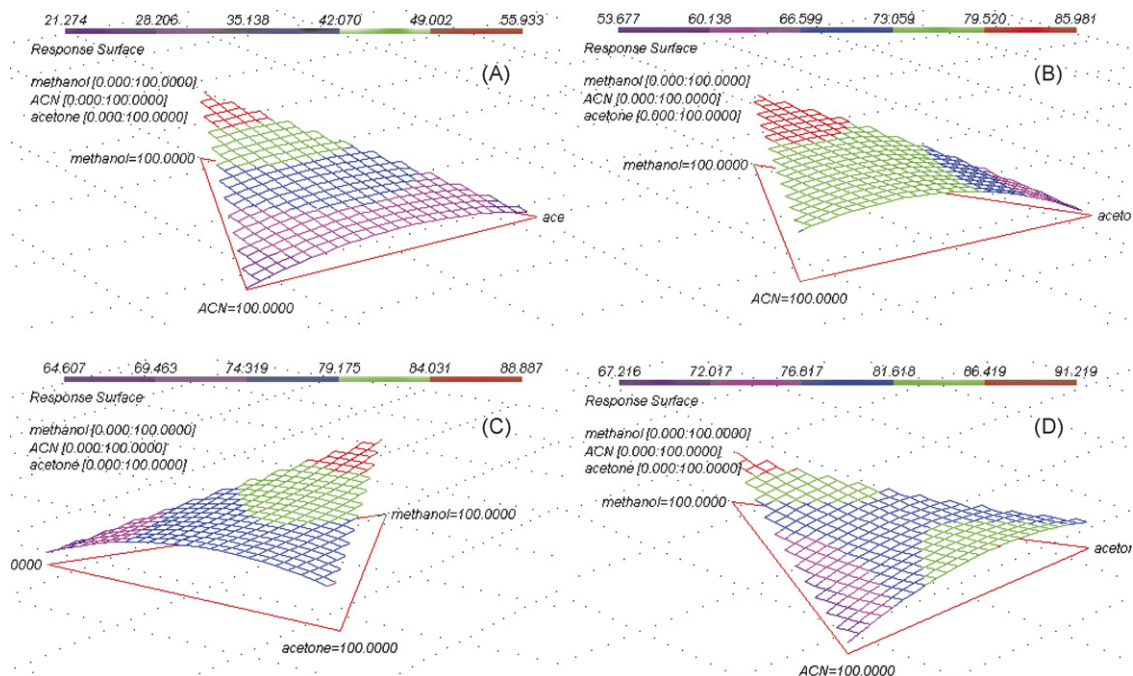


Fig. 2. Response surfaces for the mixture variables for eprosartan (A), telmisartan (B), irbesartan (C) and valsartan (V).

tion was performed at  $35 \pm 0.2^\circ\text{C}$  and the analytes and internal standard were monitored photometrically at 232 nm.

2.6. Recovery and repeatability of the extraction procedure

The repeatability and efficiency of the extraction procedure were determined by extracting replicate spiked urine samples ( $n = 6$ ).

The extraction efficiency, expressed in terms of percentage of recovery, was estimated by comparing the peak area of each compound in spiked urine samples with that from the blank urine samples to which the compounds were added before the evaporation step. Data were collected as peak areas and peak

areas ratio of eprosartan, telmisartan, irbesartan and valsartan against IS was considered for all the calculations.

The repeatability of the extraction was expressed as percentage of relative standard deviation (%R.S.D.):

$$\left[ \%R.S.D. = \left( \frac{\text{standard deviation}}{\text{mean of the recoveries}} \right) \times 100 \right].$$

2.7. Selectivity of the extraction procedure

Selectivity of the assay was established with six independent sources of blank urine samples, and comparing these with control urine spiked with the studied compounds. The

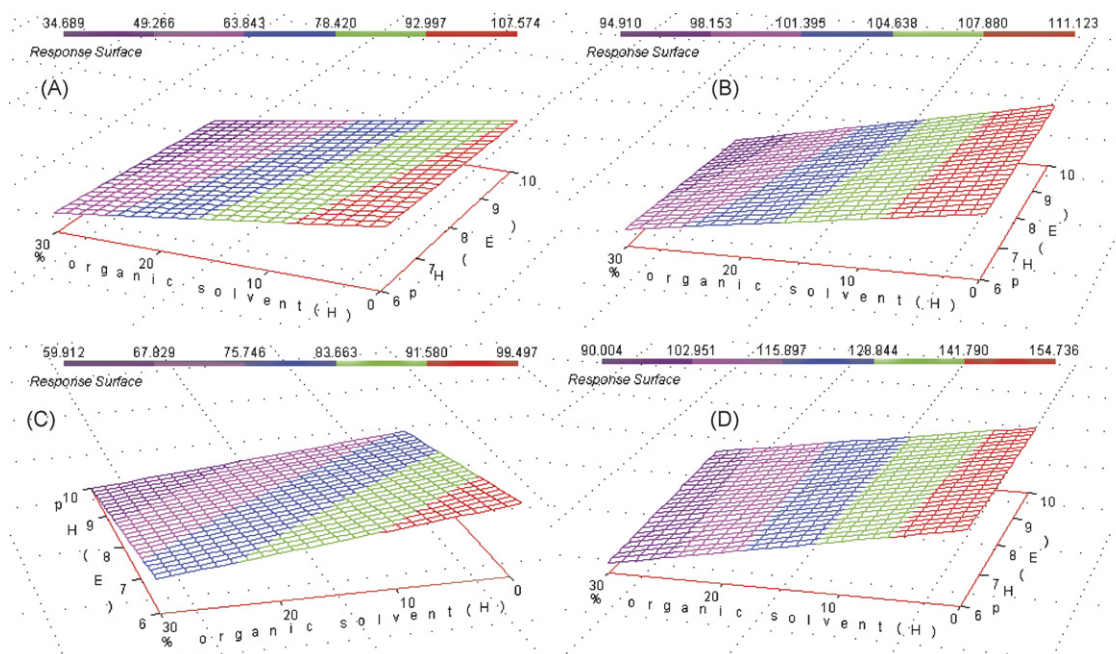


Fig. 3. Response surfaces for the process variables: pH and organic solvent percentage of the washing solution for eprosartan (A), telmisartan (B), irbesartan (C) and valsartan (V).

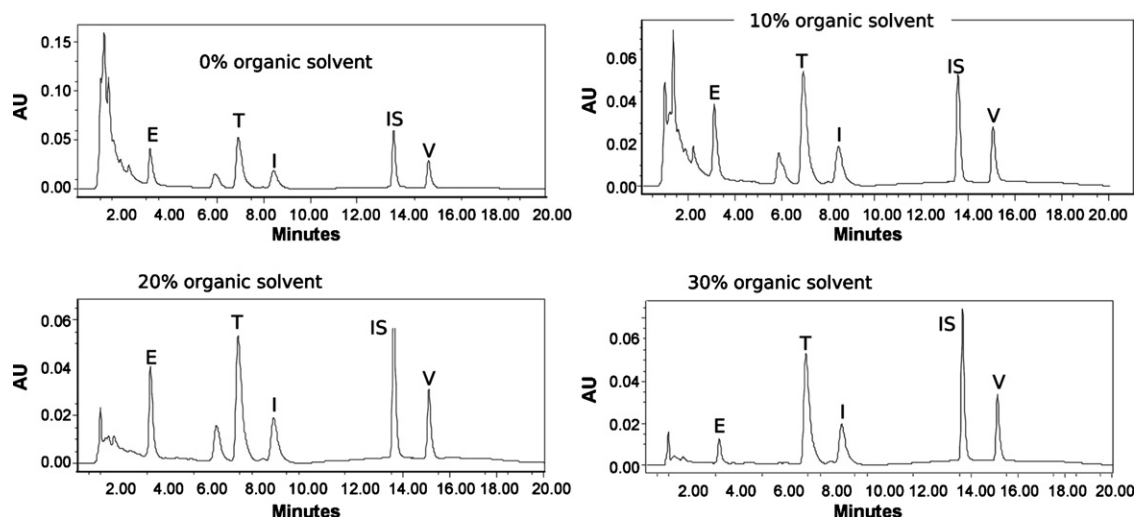


Fig. 4. Chromatograms of extracted urine samples spiked with eprosartan (E), telmisartan (T), irbesartan (I) and valsartan (V) (2.1  $\mu\text{g/mL}$ ) and the IS (1.5  $\mu\text{g/mL}$ ) obtained during the SPE procedure for different percentages of methanol in the washing solution.

chromatograms were visually inspected for interfering chromatographic peaks from urine endogenous substances.

### 3. Results and discussion

Mixture design is a useful chemometric tool which decreases the number of experiments when procedures involving mixture of components are studied [31,32].

There are several factors which affect the extraction procedure. As a mixture of four solvents was studied as elution solvent, the studied variables were classified in two different groups: mixture variables and process variables. Both of them were chosen upon the basis of a previous SPE procedure developed for eprosartan in human plasma [23].

The possible combinations of methanol, acetonitrile, ethanol and acetone were studied from 0 to 100% each solvent in the mixture composition. These four organic solvents constituted the mixture variables. Among the process variables these were included: percentage and pH of the buffer solution which must be added to the urine samples at the beginning of the extraction procedure to get the same pH value in all the processed samples; the percentage of the organic component in the washing solution and the volume of this solution which must be employed in the washing step; the drying time and the volume of the elution solvent. All the variables are shown in Table 2.

The experimental domain, in which the D-optimal design was constructed, was chosen on the basis on the previously mentioned work dealing with the determination of eprosartan in human plasma and the experience of our research laboratory.

Although the plasma samples were conditioned with a buffer solution with a pH value of 2, for the extraction of urine samples, the use of basic conditioning buffers get cleaner extracts than acidic buffers. Therefore, the pH values range was set between 6 and 10.

The used organic solvents were selected upon the basis on their polarity, from the most polar methanol to acetonitrile, ethanol and acetone.

A 32-run, four-factor, two level D-optimal design was proposed by The Unscrambler software (Camo, Norway) in order to study the influence of the variables described in Table 2 on the solid phase extraction of eprosartan, telmisartan, irbesartan and valsartan from human urine samples. The carried out experiments and the measured responses (in terms of recovery percentage) are shown in Table 3. To calculate the responses, the same SPE conditions were applied to blank urine samples spiked with the analytes at the beginning of the extraction procedure and to blank urine samples spiked with the analytes just before evaporation step. In all cases, the IS was added just before evaporation.

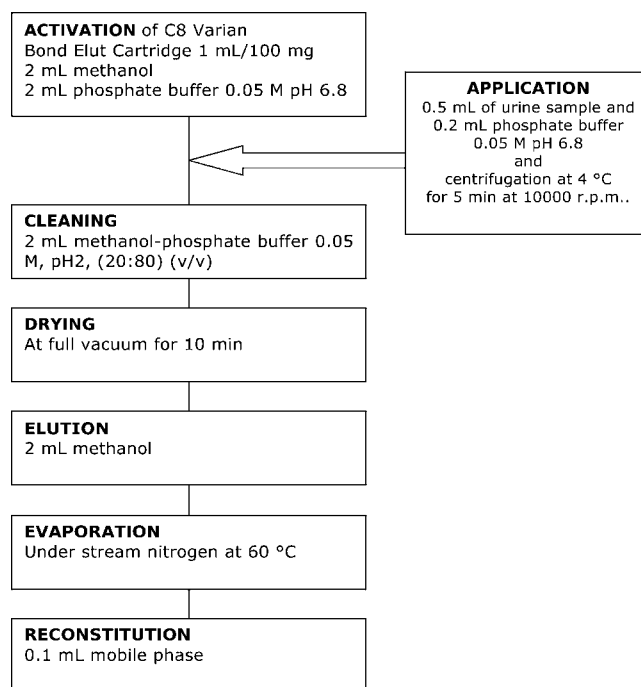
In all the proposed experiments, the elution solvent (or mixture of solvents) was also used as the organic solvent mixed with the buffer solution to compose the washing solution.

The obtained results were treated using The Unscrambler software and PLS-2 regression, leverage correction; and interactions and squares were taken into account to predict the model on the basis of the studied responses.

The data treatment by PLS-2 allows plotting all the studied factors, their interactions and their squares to test if those have any kind of influence on the studied response and if this influence is positive or negative. A regression coefficient is calculated for each variable or interaction and in the case of the calculated value for each coefficient is larger the 0.2 in absolute value, if the studied variables have been normalised; then, the effect of that variable is most probably significant. If the regression coefficient is smaller than 0.1 in absolute value, then the effect is negligible. Between 0.1 and 0.2, no certain conclusions can be drawn. The regression coefficients for each analyte and each studied factor are plotted in Fig. 1. As it could be predicted, the most important variable is the percentage of organic solvent in the washing step and it has a negative influence because when the proportion of the organic solvent in the washing solution increases, the analytes are eluted from the column during the washing step.

To study the influence of the solvent mixtures and the other process variables and in order to choose the most adequate values for obtaining the greater extraction efficiency, the response surfaces shown in Fig. 2 were constructed. As it can be seen in the plot, the highest extraction efficiency for all the drugs was achieved when methanol was used as elution solvent and mixtures of solvents did not show better results.

In the case of process variables, several interactions can be observed. As an example, in Fig. 3 the response surfaces corresponding to the influence on the studied response of the pH value of the conditioning buffer and the composition of organic solvent in the washing solution are shown. As it can be seen, the lowest percentage of the organic solvent in the washing step achieves the best extraction efficiency but it must be consid-



Scheme 1. Optimised SPE procedure for urine samples containing eprosartan, telmisartan, irbesartan and valsartan.

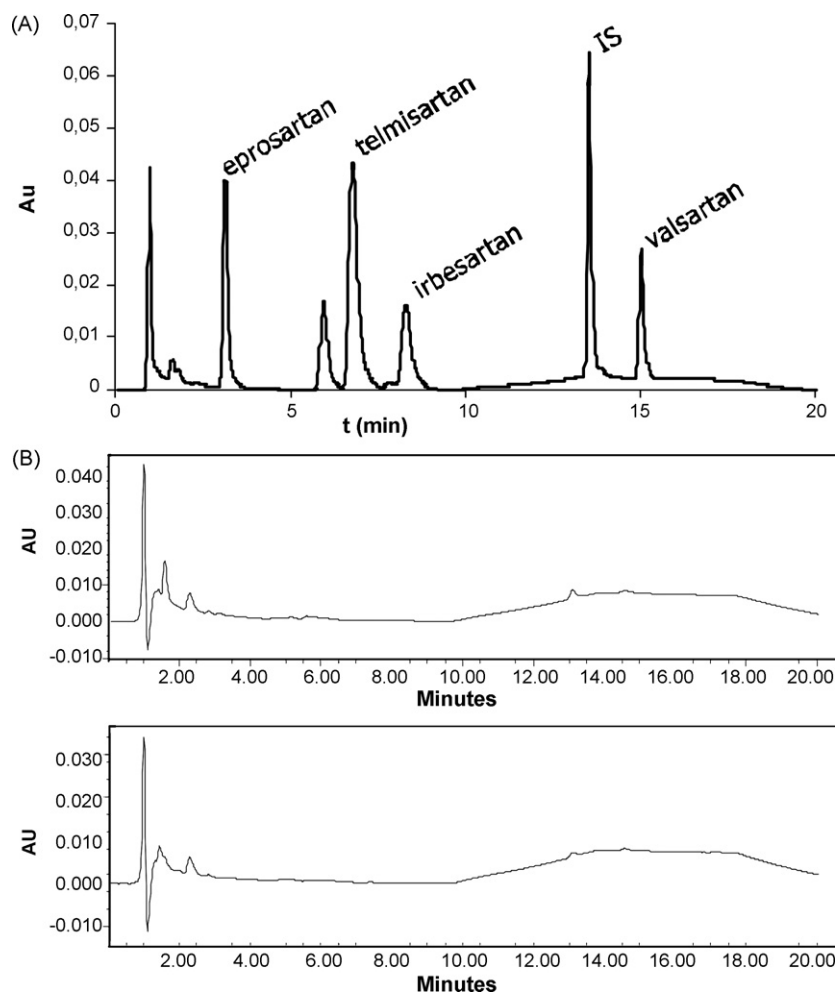


Fig. 5. Chromatograms corresponding to: (A) an extracted urine sample in the optimised conditions (the sample was spiked with eprosartan, telmisartan, irbesartan and valsartan in concentration  $2.1 \mu\text{g/mL}$  and the IS  $1.5 \mu\text{g/mL}$ ) and (B) two blank urine samples extracted following the same procedure.

ered that in urine samples, there are a lot of polar endogenous compounds which interfere in the chromatographic separation of the studied compounds. To choose the best percentage of organic solvent in the composition of the washing solution, several washing solutions were tested which contained from 0 to 30% of the organic component. The chromatograms corresponding to these extracted urine samples are shown in Fig. 4. From these results, a washing solution containing a 20% of organic solvent was used.

The optimised conditions were fixed in the following values: pH of the conditioning buffer 6.8, because the use of low values in the studied pH range gave rise to better recovery percentages. The washing and elution volumes were fixed in 2 mL and the drying time, in 10 min. 0.2 mL (40% of sample volume) as conditioning buffer solution was added to the sample, to assure the same pH values in all the extracted samples.

All the extraction conditions are summarised in Scheme 1.

The calculated extraction efficiency (in terms of recovery percentage) was  $84 \pm 2$  for eprosartan,  $74 \pm 2$  for telmisartan,  $74 \pm 1$  for irbesartan and  $89 \pm 1$  for valsartan, for spiked urine samples ( $2.1 \mu\text{g/mL}$  each analyte) extracted in the optimised conditions. In all cases, the R.S.D. was less than 5%.

The repeatability of the extraction, in terms of R.S.D., did not exceed the 10% in any case.

In Fig. 5, the chromatograms corresponding to an extracted urine sample spiked with the studied analytes and several blank urine samples extracted under the optimised conditions are shown. The proposed procedure has been successfully applied to urine samples obtained from hypertensive patients in treatment with eprosartan and valsartan (600 and 160 mg/day). A percentage between 0.04 and 1.85%, and 4 and 7% of the ingested drug was, respectively, recovered.

#### 4. Conclusions

Chemometric approach allows reducing the number of experiments needed for optimisation of extraction procedure and chromatographic separation, as well as the attainment of a true optimum set of conditions.

The HPLC–DAD developed method by using gradient elution mode, achieved the separation of eprosartan, telmisartan, irbesartan and valsartan and the internal standard EXP 3174 in human urine samples in 16 min, by using an Atlantis dC18 column  $100 \text{ mm} \times 3.9 \text{ mm I.D.}$ ,  $100 \text{ \AA}$ ,  $3 \mu\text{m}$ , and a mobile phase

of water 0.031% TFA and ACN 0.026% TFA. The whole analytical procedure (extraction and separation for six samples by duplicate) can be carried out in 1 h. This fact makes the method suitable for applying it to routine analysis.

The extraction recoveries obtained are lower than those obtained with other methods described in bibliography. Values of recoveries by using SPE of 78% for telmisartan [9], 89.3 and 97.9% for irbesartan and valsartan, respectively, [6] or by solid phase microextraction: 96.4, 94.7 and 89.4% for telmisartan, irbesartan and valsartan, respectively, [21] were obtained. But it has been taken into account that there is no a SPE procedure for urine samples including the four studied analytes. The different properties of the studied substances led us to adopt some agreements, usual practice in the development of screening methods.

The application of the developed SPE procedure allows the determination of the expected ARA-II drugs concentration levels in urine.

The developed SPE procedure together with the chromatographic separation can be applied to the quantitation of eprosartan, telmisartan, irbesartan and valsartan by HPLC–DAD in human urine. Therefore, the urine excreted percentage of the administered dose for each compound can be calculated and used for renal excretion studies.

## Acknowledgements

Authors thank the Ministry of Education and University of Basque Country for financial support (CTQ 2006-11285; UPV 00171.310-15359/2003) and Dr. N. Etxebarria for his help with experimental design. N. Ferreirós thanks the Ministry of Education for a FPU grant and G. Iriarte the UPV/EHU for his predoctoral grant.

## References

- [1] J.H. Bauer, G.P. Reams, *Arch. Intern. Med.* 155 (1995) 1361.
- [2] G.L. Plosker, R.H. Foster, *Drugs* 60 (2000) 177.
- [3] S. Hillaert, W. Van den Bossche, *J. Chromatogr. A* 979 (2002) 323.
- [4] S. Hillaert, W. Van den Bossche, *J. Pharm. Biomed. Anal.* 31 (2003) 329.
- [5] S. Hillaert, T.R.M. De Beer, J.O. De Beer, W. Van den Bossche, *J. Chromatogr. A* 984 (2003) 135.
- [6] L. Gonzalez, R.M. Alonso, R.M. Jimenez, *Chromatographia* 52 (2000) 735.
- [7] E. Cagigal, L. Gonzalez, R.M. Alonso, R.M. Jimenez, *Talanta* 54 (2001) 1121.
- [8] L. Gonzalez, J.A. Lopez, R.M. Alonso, R.M. Jimenez, *J. Chromatogr. A* 949 (2002) 49.
- [9] N. Torrealday, L. Gonzalez, R.M. Alonso, R.M. Jimenez, E. Ortiz Lastra, *J. Pharm. Biomed. Anal.* 32 (2003) 847.
- [10] D.E. Lundberg, R.C. Person, S. Knox, M.J. Cyronak, *J. Chromatogr. B* 707 (1998) 328.
- [11] C.I. Furtek, M.W. Lo, *J. Chromatogr. B: Biomed. Sci. Appl.* 573 (1992) 295.
- [12] J.W. Lee, W. Naidong, T. Johnson, A. Dzerk, T. Miyabayashi, M. Motohashi, *J. Chromatogr. B: Biomed. Sci. Appl.* 670 (1995) 287.
- [13] T. Miyabayashi, T. Okuda, M. Motohashi, K. Izawa, T. Yashiki, *J. Chromatogr. B: Biomed. Sci. Appl.* 677 (1996) 123.
- [14] D. Farthing, D. Sica, I. Fakhry, A. Pedro, T.W.B. Gehr, *J. Chromatogr. B: Biomed. Sci. Appl.* 704 (1997) 374.
- [15] M.A. Ritter, C.I. Furtek, M.W. Lo, WaiF M., *J. Pharm. Biomed. Anal.* 15 (1997) 1021.
- [16] S.Y. Chang, D.B. Whigan, N.N. Vachharajani, R. Patel, *J. Chromatogr. B* 702 (1997) 149.
- [17] H.H. Maurer, T. Kraemer, J.W. Arlt, *Therap. Drug Monitor.* 20 (1998) 706.
- [18] A. Soldner, H. Spahn-Langguth, E. Mutschler, *J. Pharm. Biomed. Anal.* 16 (1998) 863.
- [19] H. Stenhoff, P.O. Lagerstrom, C. Andersen, *J. Chromatogr. B: Biomed. Sci. Appl.* 731 (1999) 411.
- [20] M. Polinko, K. Riffel, H. Song, M.W. Lo, *J. Pharm. Biomed. Anal.* 33 (2003) 73.
- [21] J. Nie, M. Zhang, Y. Fan, Y. Wen, B. Xiang, Y.O. Feng, *J. Chromatogr. B* 828 (2005) 62.
- [22] M. Zhang, F. Wei, Y.F. Zhang, J. Nie, Y.O. Feng, *J. Chromatogr. A* 1102 (2006) 294.
- [23] N. Ferreirós, G. Iriarte, R.M. Alonso, R.M. Jiménez, E. Ortiz, *J. Chromatogr. A* 1119 (2006) 309.
- [24] A.M. Siouffi, R. Phan-Tan-Luu, *J. Chromatogr. A* 892 (2000) 75.
- [25] E. Marengo, V. Gianotti, S. Angioi, M.C. Gennaro, *J. Chromatogr. A* 1029 (2004) 57.
- [26] Y.P. Zhang, X.J. Li, Z.B. Yuan, *Microchem. J.* 73 (2002) 307.
- [27] L. González, U. Akesolo, R.M. Jiménez, R.M. Alonso, *Electrophoresis* 23 (2002) 223–229.
- [28] <http://www.camo.no>.
- [29] K.H. Esbensen, *Multivariate Data Analysis – In Practice*. (fifth ed.) CAMO 2001.
- [30] N. Ferreirós, G. Iriarte, R.M. Alonso, R.M. Jiménez, *Talanta* 69 (2006) 747.
- [31] Y. El-Malah, S. Nazzal, N.M. Khanfar, *Drug Dev. Ind. Pharm.* 32 (2006) 1207.
- [32] S. Furlanetto, S. Orlandini, A.M. Marras, P. Mura, S. Pinzauti, *Electrophoresis* 27 (2006) 805.

# Metal furnace heated by flame as a hydride atomizer for atomic absorption spectrometry: Sb determination in environmental and pharmaceutical samples

Eduardo Costa Figueiredo<sup>a</sup>, Jiří Dědina<sup>b</sup>, Marco Aurélio Zezzi Arruda<sup>a,\*</sup>

<sup>a</sup> *Universidade Estadual de Campinas, Institute of Chemistry, Department of Analytical Chemistry, P.O. Box 6154, 13084-862 Campinas, SP, Brazil*

<sup>b</sup> *Academy of Sciences of the Czech Republic, Institute of Analytical Chemistry, v.v.i. Vídeňská 1083, CZ-142 20 Prague, Czech Republic*

Received 1 February 2007; received in revised form 3 April 2007; accepted 8 April 2007

Available online 24 April 2007

## Abstract

The present work describes a metallic hydride atomizer for atomic absorption spectrometry, by evaluating the performance of the Inconel 600<sup>®</sup> tube. For this purpose, stibine was used as the model volatile compound and antimony determination in river and lake sediments and in pharmaceutical samples was carried out to assess the metal furnace performance. Some parameters are evaluated such as those referring to the generation and transport of the hydride (such as  $\text{KBH}_4$  and acid concentrations, carrier gas flow rate, injected volume, etc.), as well as those referring to the metal furnace (such as tube hole area, flame composition, long-term stability, etc.). The method presents linear Sb concentration from 2 to 80  $\mu\text{g L}^{-1}$  range ( $r > 0.998$ ;  $n = 3$ ) and the analytical frequency of *ca.* 140  $\text{h}^{-1}$ . The limit of detection (LOD) is 0.23  $\mu\text{g L}^{-1}$  and the precision, expressed as R.S.D., is less than 5% (40  $\mu\text{g L}^{-1}$ ;  $n = 10$ ). The accuracy is evaluated through the reference materials, and the results are similar at 95% confidence level according to the *t*-test.

© 2007 Elsevier B.V. All rights reserved.

**Keywords:** Hydride generation; Atomic absorption spectrometry; Metal furnace; Meglumine antimoniate; River sediment; Lake sediment

## 1. Introduction

Following the first report on the hydride generation atomic absorption spectrometry (HG-AAS) by Holak [1], the unquestionable advantages of the technique led to its application to virtually all elements forming volatile hydrides [2].

For on-line hydride atomization conventional externally heated quartz tube atomizers (QTA) [3–6] are currently almost exclusively employed devices. An exception is the application of the W-coil atomizer [7,8], which was adapted from the initial idea of Berndt and Schaldach [9]. The usual design of the conventional externally heated QTA is a T-tube with the horizontal arm (optical tube) of the T aligned in the optical path of the spectrometer. The central arm of the T-tube serves for delivery of hydrides carried by a gas flow from a generator [2]. The optical tube is heated either using an electrical resistance device or the acetylene–air flame (700–1100 °C).

Grinberg et al. [10] suggested a modified “holed” externally heated QTA (HQTA) differing from the usual design only in having five holes (o.d. 2 mm) drilled along the length of the optical tube which was heated by the acetylene–air flame, which improved the selectivity and sensitivity, except for As, where a fivefold reduction on sensitivity was observed. The authors explained the good performance of HQTA in terms of resistance to concomitants by a hydrogen radical rich environment.

In general, conventional externally heated QTA presents high sensitivity as well as a lower background noise is attained, improving the limit of detection (LOD). However, there are also fundamental limitations inherent to QTA: poor linearity (or even a rollover) of the calibration curves and low resistance towards atomization interferences. To overcome these drawbacks, Dědina and Matousek [11] proposed a multiple microflame QTA (MMQTA), based on a recurrent atomization of analyte in multiple clouds of hydrogen radicals in the optical tube. Even though the multiatomizer eliminated calibration curvature and yielded one to two orders of magnitude better related to concomitant effects than the conventional externally heated QTA [11,12], its performance was not still ideal [12]. Addition-

\* Corresponding author. Tel.: +55 19 3521 3089; fax: +55 19 3521 3023.  
E-mail address: [zezzi@iqm.unicamp.br](mailto:zezzi@iqm.unicamp.br) (M.A.Z. Arruda).



ally, the temperature of QTA is limited by the thermal durability of quartz up to around 1100 °C [2].

In the same year of the multiple microflame QTA preposition, Gáspár and Berndt [13], proposed the thermospray flame furnace atomic absorption spectrometry (TS-FF-AAS), and as well commented by the authors “Up to now, only gaseous compounds could be introduced completely into flame-heated cell. The classic examples for this are the determination of the hydride-forming elements . . .”. In such technique, a Ni tube is coupled on the burner head of a FAAS spectrometer and the sample is introduced into the tube by ceramic capillary heated by the flame. Its main advantage is the complete introduction of the sample in the Ni tube, reaching sensitivity compatible with electrothermal atomic absorption spectrometry (ETAAS).

Due to those drawbacks already commented when QTA is used, the advantages for working with microflames (as MMQTA or TS-FF-AAS) [11,14–18] as well as the different reaction environment when compared metallic tube and quartz tubes, the aim of the present work was to test the feasibility of the metal furnace for hydride generation atomic absorption spectrometry. Stibine was chosen as the model of volatile compound and antimony determination in river and lake sediments and in pharmaceutical samples was employed to assess the metal furnace performance.

## 2. Experimental

### 2.1. Instrumentation

The proposed system was built-up by an Ismatec peristaltic pump (IPC-12, Glattzbrugg, Switzerland) and a homemade three-piece injector-commutator device of the polymethacrylate [19]. Polyethylene tubes (0.8 mm i.d.) were used as transmission lines and Tygon® tubes for propelling the solutions.

A Perkin-Elmer model AAnalyst 300 flame atomic absorption spectrometry (Norwalk, USA) equipped with deuterium lamp background correction was used for Sb determinations. Electrodeless discharge lamp was used as a primary source and the operating conditions were those recommended by manufacturer.

High purity deionized water was obtained from a Millipore model Milli-Q Plus water purification unit and a Provecto Analítica microwave oven, model DGT Plus (Jundiaí, Brazil), was used for sample decomposition.

### 2.2. Reagents and solutions

All solutions were prepared with deionized water (18.2 MΩ cm) and with analytical reagent grade. The glassware was kept in a 10% (v/v) HCl for 24 h with posterior cleaning with ultra-pure water.

A 100 mg L<sup>-1</sup> Sb stock solutions was prepared dissolving appropriate mass of the C<sub>4</sub>H<sub>4</sub>KO<sub>7</sub>Sb·1/2H<sub>2</sub>O in 1 mol L<sup>-1</sup> HCl. Reference Sb solutions (5–80 µg L<sup>-1</sup>) were daily prepared by serial dilution of the stock solution also in 1 mol L<sup>-1</sup> HCl.

Table 1  
Heating program for sediments samples decomposition using microwave oven

Stage	Time (min)	Power (W)
1	3	200
2	5	400
3	5	600
4	20	700
5	2	80

A 1.0% (m/v) KBH<sub>4</sub> (Vetec, Brazil) solution was prepared in 0.8% (m/v) NaOH (Merck, Darmstadt, Germany), and kept under refrigeration up to two weeks after its preparation.

### 2.3. Samples

Meglumine antimoniate samples were obtained from the Regional Health Bureau Alfenas – Minas Gerais State. This samples were diluted (1:2,500,000) with 1 mol L<sup>-1</sup> HCl, and treated with 5% (m/v) KI for Sb(V) reduction.

Masses of 150 and 250 mg for river (BCR-320) and lake (IAEA-SL-1) sediment samples, respectively, were mineralized using microwave oven (MW). For both samples, 10 mL *aqua regia* and 5 mL HF were used. Pre-digestion period of 30 min was carried out, followed by the heating program as in Table 1. After the mineralization, the samples were heated almost to dryness and the volumes completed to 10 mL with 1 mol L<sup>-1</sup> HCl. To promote the reduction of Sb(V) to Sb(III), a treatment with 5% (m/v) KI was made.

### 2.4. Hydride generator and metal furnace atomizer

The proposed system is based on the reaction between BH<sub>4</sub><sup>-</sup> and Sb(III) in a 1 mol L<sup>-1</sup> HCl. Stibine its then generated and inserted into a gas liquid separator [7,8], where it is carried by an argon constant flow. Then it is atomized in an Inconel 600® tube atomizer fixed above the burner of the spectrometer (Fig. 1). The approximately Inconel 600® tube composition is >72% (m/m) Ni, 14–17% (m/m) Cr and 6–10% (m/m) Fe, and its dimension is similar to that of Ni tube commonly used in the TS-FF-AAS [13–18].

Fig. 1A shows the system in the sampling position, where the L<sub>1</sub> (samples) and L<sub>2</sub> (KBH<sub>4</sub>) loops are filled. Volumes of both loops, L<sub>1</sub> and L<sub>2</sub> were always kept the same. When the central part of the injector is switched to the alternative position (Fig. 1B), the volumes contained in both L<sub>1</sub> and L<sub>2</sub> loops are transported by C<sub>1</sub> and C<sub>2</sub> carrier (deionized water) through the analytical pathway.

The sample (in acidic medium) receives the KBH<sub>4</sub> solution in the x confluence point and proceeds for the reactor (R), where the hydride is formed by the reaction among BH<sub>4</sub><sup>-</sup> in acidic medium and Sb(III) present in the standard/sample. Then, the antimony hydride is transported to the gas–liquid separator (GLS) and carried by an argon constant flow rate (1 L min<sup>-1</sup>) to its upper part. The remained sample is aspirated through a lateral hole in the GLS, being then discarded. Finally, the antimony hydride reaches the ceramic capillary, and it is directly introduced into

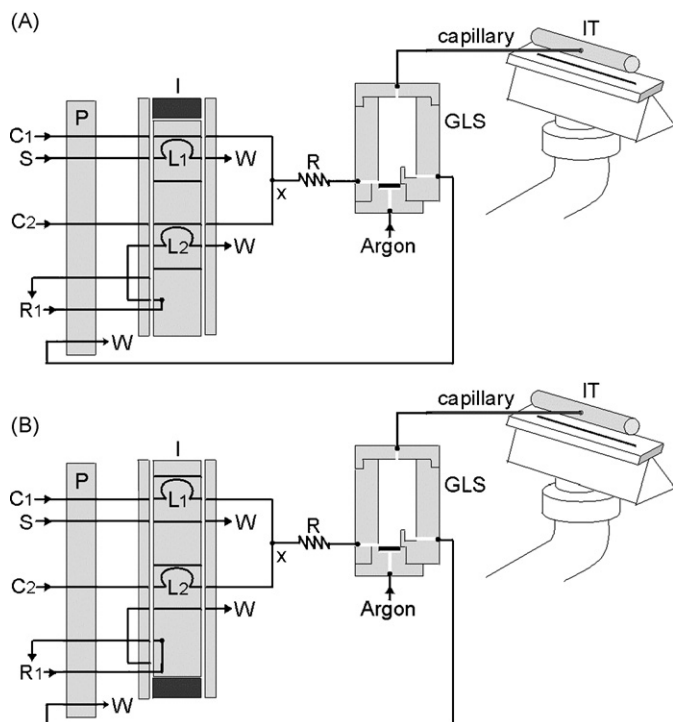


Fig. 1. Hydride generation system comprises a peristaltic pump (P), an injector commutator (I), a gas liquid separator (GLS), ceramic capillary and Inconel<sup>®</sup> tube (IT). (A) System in the sampling position, filling the loops (L1 and L2). R1 = 1.0% (m/v)  $\text{KBH}_4$  in 0.8% (m/v) NaOH, C1 and C2 = deionized water (carrier solution) at  $13 \text{ mL min}^{-1}$ , S = standards/samples, R = reactor, x = confluence point, argon at  $1 \text{ L min}^{-1}$ , W = waste. (B) System in the injection position.

the hot Inconel 600<sup>®</sup> tube through a lateral hole [13]. The tube coupled on the flame has six holes in the face addressed to the burner, allowing the partial flame penetration inside of the tube, and promoting the Sb atomization.

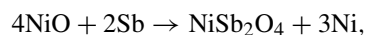
### 3. Results and discussion

#### 3.1. Optimization of the variables

The optimizations of the chemical and physical variables were performed in a univariate way, by maximizing the integrated absorbance of a  $40 \mu\text{g L}^{-1}$  standard solution.

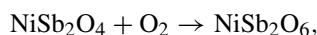
##### 3.1.1. The nature of the tube

As the nickel tube is commonly used in the TS-FF-AAS technique [13–18], it was also applied as atomizer in such purpose, but it yielded a poor sensitivity (*ca.* 40% when compared with the Inconel 600<sup>®</sup> tube) and precision (*ca.* 20% R.S.D.). Such fact can be attributed to the  $\text{NiSb}_2\text{O}_4$  and/or  $\text{NiSb}_2\text{O}_6$  formation [20], according to Eqs. (1) and (2), as follow



$$\Delta G^\circ_f = -988.3 + 0.3472T (\text{K}) \pm 4.2 \text{ kJ mol}^{-1} (769 - 931 \text{ K})$$

(1)



$$\Delta G^\circ_f = -406.6 + 0.2010T (\text{K}) \pm 0.2 \text{ kJ mol}^{-1} (894 - 1138 \text{ K})$$

(2)

Subsequently, the performance of the tube furnace built-in by Inconel 600<sup>®</sup> was investigated with the same dimensions to those used when worked with the nickel tube [13–18]. The results achieved were encouraging. However, increase in the results (in terms of integrated absorbance) was observed after each injection of the  $40 \mu\text{g L}^{-1}$  Sb standard. At least 30 injections were necessary for signal stabilization, suggesting a gradual change in the tube surface. Such behavior can be explained due to the gradual formation of both ternary oxides as exemplified in the Eqs. (1) and (2). Apparently, a decrease in the nickel concentration on the tube surface for signal stabilization was necessary, being the intensity of the signal maintained during the sequence of the experiments.

From this fact, an experiment was performed to investigate the modification of the Inconel 600<sup>®</sup> tube and its durability. In this way, the tube surface was now treated by injecting a  $40 \text{ mg L}^{-1}$  Sb standard, followed by a blank solution (four sequential injections). Excellent signal stability was obtained with such procedure: 200 injections of the  $40 \mu\text{g L}^{-1}$  Sb standard yielded R.S.D. of only 1.3%.

Scanning electron microscopy and X-ray fluorescence were employed to characterize changes of the inner surface of the Inconel 600<sup>®</sup> tube due to its treatment with  $40 \text{ mg L}^{-1}$  Sb standard. Fig. 2 illustrates the change in the morphology of the material. Additionally, we can point out changes in the quantities of nickel, chromium and iron, before and just after tube treatment using  $40 \text{ mg L}^{-1}$  Sb standard. While in the new Inconel 600<sup>®</sup> tube, the nickel quantity was about 75% (m/m), it decreases to 71 and 62% (m/m), respectively, for both lateral and upper regions of the tube evaluated, probably due to ternary oxides formed as exemplified in the Eqs. (1) and (2) and commented above. The upper region is that with a higher flame incidence. On the other hand, chromium was increase (15% (m/m) – new tube) to 19 and 25% (m/m), for both lateral and upper regions of the tube, respectively. Finally, iron contents also increase (8% (m/m) – new tube) to 11% (m/m) – upper region of the tube. It should be highlighted that the tube became greenish during the experiment, indicating the presence of  $\text{Cr}_2\text{O}_3$ , which has a higher melting point ( $2435^\circ\text{C}$ ) than  $\text{Ni}_2\text{O}_3$  ( $1984^\circ\text{C}$ ) or  $\text{NiO}$  ( $1955^\circ\text{C}$ ) [21]. This behavior indicates that a new environment formed inside the tube plays an important role in the antimony atomization, once that the sensitivity was 10-fold increased at this new condition.

##### 3.1.2. Nature and concentration of the mineral acid

Some mineral acids such as HCl,  $\text{H}_2\text{SO}_4$  and  $\text{HNO}_3$  were tested due to the possibility of their use for sample mineralization. The acid concentrations were evaluated from 0.1 to

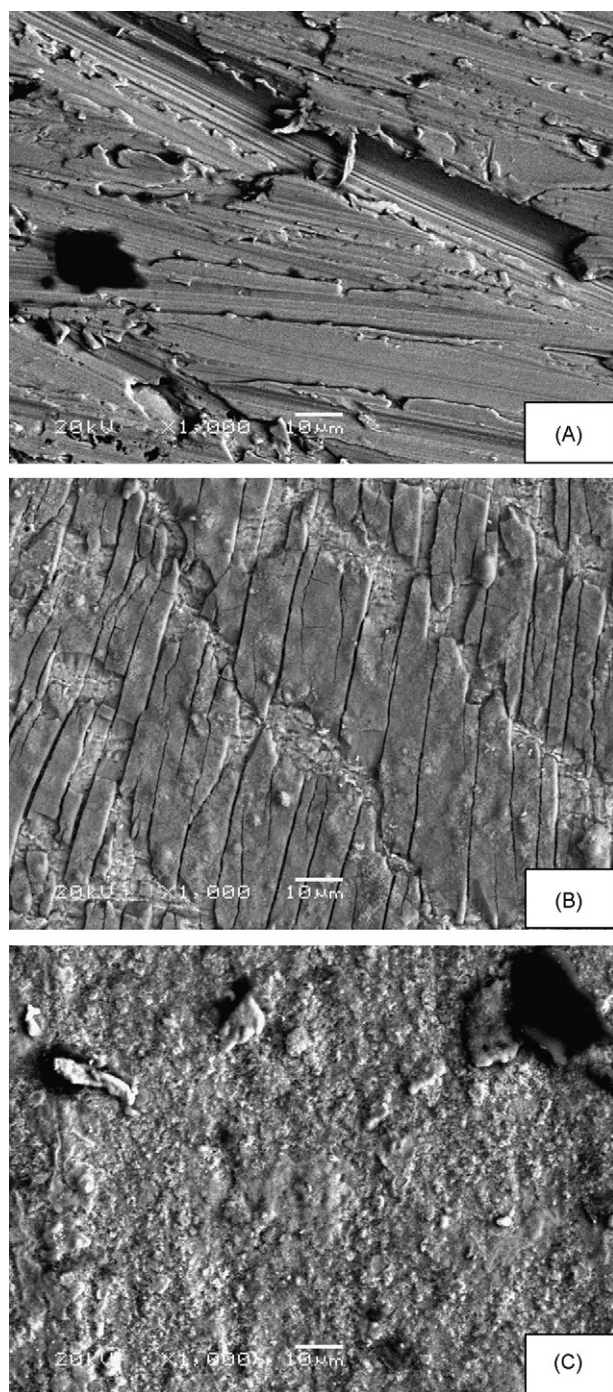


Fig. 2. Scanning electron micrography (SEM) of the Inconel<sup>®</sup> tube ( $\times 1000$ ). (A) New Inconel<sup>®</sup> tube, (B) lateral, and (C) upper region of the tube. The (B) and (C) micrographies were obtained from the same tube and just after the tube treatment.

$4.0 \text{ mol L}^{-1}$  range and the results are presented in the Fig. 3. As one can see, the behavior of  $\text{H}_2\text{SO}_4$  and  $\text{HCl}$  was similar from  $1.0$  to  $4.0 \text{ mol L}^{-1}$  concentrations. However, due to the good precision (R.S.D. as  $2.6\%$ ) obtained when  $\text{HCl}$  was employed, the  $1.0 \text{ mol L}^{-1}$   $\text{HCl}$  concentration was selected. Lower results for  $\text{HNO}_3$  are compatible with often reported interferences of nitrogen oxides with  $\text{HG-AAS}$  determinations of antimony [2]. Nitrogen oxide interferences are observed also in determina-

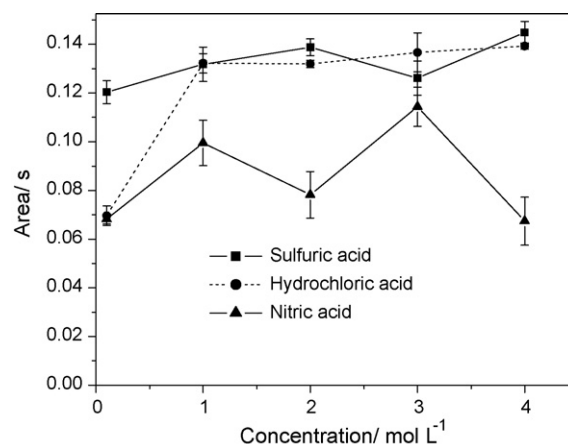


Fig. 3. Influence of nature and concentration of the acid on the analytical response.

tions of other hydride forming elements [2,22], however, their mechanisms are not known.

### 3.1.3. $\text{KBH}_4$ concentration

The  $\text{KBH}_4$  concentration was tested in the range from  $0.1$  to  $2.0\%$  (m/v) in the solution stabilized with  $0.8\%$  (m/v)  $\text{NaOH}$ . The optimum concentration, selected for further measurements, was  $1.0\%$  yielding integrated absorbance of *ca.*  $0.30 \text{ s}$ . There was a decrease in the analytical signal ( $0.14 \text{ s}$ ) at lower concentrations compatible to lower efficiency of hydride generation. Concentrations above  $1.0\%$  caused impaired signal repeatability as well as slight signal decrease (*ca.*  $0.27 \text{ s}$ ), obviously due to enhanced production of hydrogen.

### 3.1.4. Reactor length

Too short reactor might cause incomplete hydride release [2] but too long reactor increases risk of analyte losses. A study to evaluate the reactor length influence in the analytical response was therefore made. The reactor length was varied from  $10$  to  $90 \text{ cm}$ , and the best analytical signal was obtained with  $50 \text{ cm}$  length (*ca.*  $0.36 \text{ s}$ ). Reactor lengths of  $70$  and  $90 \text{ cm}$  also produced similar signals than those with  $50 \text{ cm}$  reactor. In this way,  $50 \text{ cm}$  reactor length was selected for future tests.

### 3.1.5. Injected volume

The  $L_1$  and  $L_2$  loop volumes ( $300$ ,  $600$ ,  $900$ ,  $1200$ ,  $1500$  and  $2000 \mu\text{L}$ ) were simultaneously studied. The integrated absorbance signal was directly proportional to the sample volume, which can be varied depending on the necessary sensitivity for each determination. The volume of  $2000 \mu\text{L}$  (*ca.*  $0.73 \text{ s}$ ) was then selected for further measurements.

### 3.1.6. Carrier solution flow rate

The influence of the carrier flow solutions was checked from  $10$  to  $14.5 \text{ mL min}^{-1}$ . The obtained results did not present differences larger than  $10\%$ . Thus, the peak profile was used as a choice criterion, being the selection made as a function of the peak symmetry, as well as the shortest time of the signal to return to the baseline, which directly contributes for improv-

ing the analytical frequency of the method. The flow rate of  $13 \text{ mL min}^{-1}$  was selected for further measurements as the compromise between sample throughput (lower flow rates resulted in broader peaks decreasing the throughput) and signal repeatability (higher flow rates resulted in higher internal pressure impairing the precision – R.S.D. > 15% for the flow rate of  $14.5 \text{ mL min}^{-1}$ ).

### 3.1.7. Argon flow rate

The carrier flow gas was also studied from  $0.1$  to  $4.0 \text{ L min}^{-1}$ , presenting significant influence in the analytical signal. The flow rate presented an inversely proportional tendency with integrated absorbance. However, at very low flow rate, there was an enlargement of the peaks (with an excessive tail). Thus,  $1.0 \text{ L min}^{-1}$  carrier flow was selected as working condition (*ca.*  $1.57 \text{ s}$ ). On the other hand, the possible explanation to lower analytical signals at higher carrier gas flow rate is the dilution of the hydride inside the tube and/or its quick expulsion from the metal tube.

### 3.1.8. The Inconel 600<sup>®</sup> tube area

The tube coupled on the flame has six holes in the face addressed to the burner. A study to verify the influence of the hole area in the analytical response was made, because it can strongly influence the atomization. For this study, five tubes were used, presenting six similar holes, each one with  $3.3$ ,  $6.6$ ,  $10$ ,  $13.3$  and  $20 \text{ mm}^2$  of area, with  $20$ ,  $40$ ,  $60$ ,  $80$  and  $120 \text{ mm}^2$  of total drilled area, respectively. Another tube without holes was also tested.

A difference of *ca.* 22% can be observed from Fig. 4, when compared the tubes with  $40$  and  $80 \text{ mm}^2$  of total drilled area. However, when compared those tubes with  $20$ ,  $40$  and  $60 \text{ mm}^2$  (best results), only slight differences were found (*ca.* 1.7%). As there were no statistical differences between  $40$  and  $60 \text{ mm}^2$ , the last area was chosen for further experiments.

A tube without hole was also tested, however the results obtained were not promising, once that the R.S.D. of the measurements was as high as 30%. It can be attributed due to the lack of the carrier gas inside the tube, being the analyte randomly atomized and transported to outside of the tube.

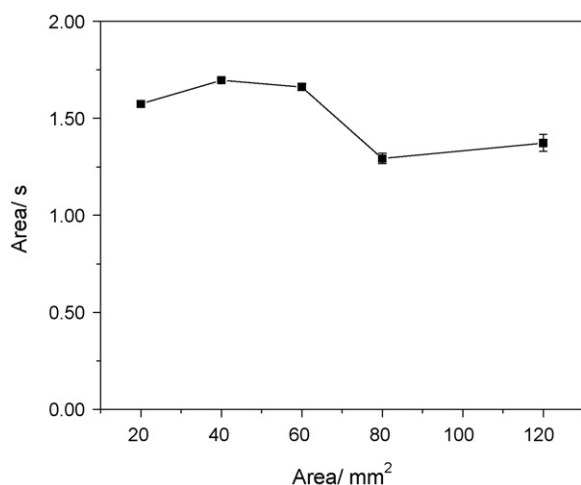


Fig. 4. Influence of the drilled hole area on the analytical response using tubes with  $20$ ,  $40$ ,  $60$ ,  $80$  and  $120 \text{ mm}^2$  of total hole.

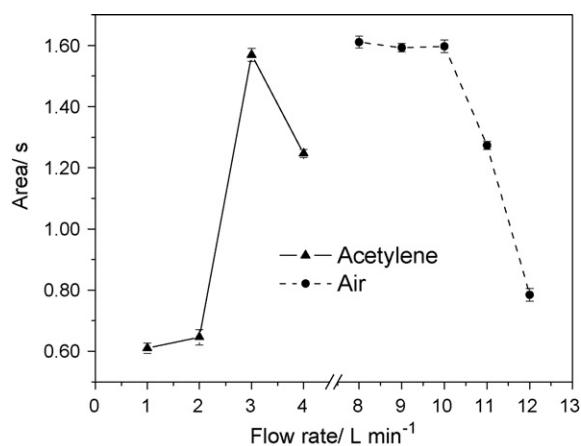


Fig. 5. Influence of the flame composition on the analytical response.

### 3.1.9. Capillary

Two ceramic capillaries with different internal diameters ( $0.5$  and  $1.0 \text{ mm}$ ) were tested. Only slight differences in the analytical signal (R.S.D. < 4%) were observed, and the selection criterion was then attributed to the best signal profile in terms of symmetry as well as the highest analytical frequency ( $127$  and  $140$  signals per hour using  $0.5$  and  $1.0 \text{ mm}$  capillary, respectively). In this way, the broader capillary – with  $1.0 \text{ mm}$  i.d. was then therefore selected for further experiments.

### 3.1.10. Flame composition

The Fig. 5 shows the influence of acetylene flow rate at air flow rate of  $10 \text{ L min}^{-1}$  and the influence of air flow rate at acetylene flow rate of  $3 \text{ L min}^{-1}$ . The optimum flame composition, selected for further measurements, was therefore  $3 \text{ L min}^{-1}$  of acetylene and  $10 \text{ L min}^{-1}$  of air. It should be highlighted that this is a strongly reducing flame. As illustrated in Fig. 5, changing the flame composition towards more oxidizing conditions resulted in a pronounced sensitivity loss in spite of higher tube temperature. This behavior indicates strong evidence that the atomization mechanism is analogous to that in QTA due to the interaction of hydride molecules with highly energetic hydrogen radicals (H radicals), as treated in detail by Dědina and Tsalev [2]. The fact that the holes drilled to the bottom of the tube have the beneficial effect on the signal suggest that H-radicals, formed preferentially in the reducing flame, penetrating through holes to the analytical volume facilitate analyte atomization. The metal tube atomizers obviously require higher H-radical supply than QTA for complete analyte atomization. The reason is probably the higher H-radical recombination rate on the metal surface compared to the quartz surface. The marked sensitivity drop under more oxidizing flame compositions can be attributed to the lower production of H-radicals and/or to the enhanced free analyte atom reaction with oxygen.

### 3.2. Temperature of the Inconel 600<sup>®</sup> tube

The temperature on the tube surface was obtained using an optical pyrometer. It was checked in five points as presented in the Fig. 6. A slightly lower temperature, by around  $15 \text{ }^\circ\text{C}$ , in

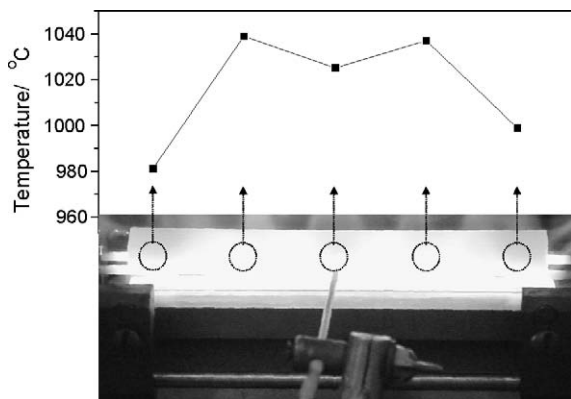


Fig. 6. Distribution of the temperature along the Inconel<sup>®</sup> tube.

the central point should be attributed to the cooling effect of the carrier gas introduced to the tube just in such position. The more pronounced temperature drop (60 °C) close to tube ends suggests a lower efficient heating.

### 3.3. Concomitants

Concomitant effects of selected species were studied by comparing signals of 20  $\mu\text{g L}^{-1}$  Sb standard solution with that of the same analyte concentration in the presence of concomitants. No masking agent was used in this test, and the concomitant effect was only considered when the recoveries were  $> \pm 10\%$ . As one can see in the selectivity chart (Table 2), Fe, Se, Ni and Bi caused the main interferences due to the low recoveries in the 1:100, 1:100, 1:100 and 1:1 proportions, respectively. Such interferences can be attributed either in the liquid [2,23] or in the gaseous phases [2]. Specifically related to Bi (the most problematic concomitant), it presents the capacity of decomposing stibine in the gaseous phase by forming bi- or polymolecular species with antimony at high flame temperatures [24]. So, in order to improve selectivity, a masking agent is commonly used (e.g. KI, thiourea), mainly if such concomitants effects are present in the hydride generation step [25].

### 3.4. Figures of merit

The proposed method presents linear Sb concentration from 2 to 80  $\mu\text{g L}^{-1}$  range ( $r > 0.998$ ;  $n = 3$ ) and the analytical frequency of  $ca. 140 \text{ h}^{-1}$ . The limit of quantification (LOQ) was of 0.75  $\mu\text{g L}^{-1}$  (according to the IUPAC recommendations) [26] and the precision, expressed as R.S.D., was less than 5% (40  $\mu\text{g L}^{-1}$ ;  $n = 10$ ). The accuracy was evaluated through the reference materials.

### 3.5. Analytical applications

Fig. 7 shows the analytical signals for blank solution ( $n = 10$ ), 2, 5, 20, 40, 60 and 80  $\mu\text{g L}^{-1}$  Sb standard solution ( $n = 3$ ), three meglumine antimoniate ( $n = 3$ ), one river sediment ( $n = 3$ ) and one lake sediment samples ( $n = 3$ ), respectively. The meglumine antimoniate samples were also analyzed by FAAS, and no signif-

Table 2  
Selectivity chart for determination of 20  $\mu\text{g L}^{-1}$  Sb ( $n = 3$ )

Element	Interferent/Sb ratio	Recovery (%)
Fe	1	96
	100	55
Mg	200	93
	1000	58
Ca	200	97
	1000	110
Mn	200	109
	1000	105
Zn	200	97
	1000	54
K	200	104
	1000	61
Cu	200	110
	1000	41
Pb	200	91
	1000	61
Co	100	97
	200	77
Cr	200	98
	1000	95
Al	200	106
	1000	58
As	200	92
	1000	70
Se	1	103
	100	79
Cd	100	108
	200	76
Ni	1	110
	100	84
Ba	200	104
	1000	54
Sn	200	108
	1000	66
Bi	1	46
	200	31

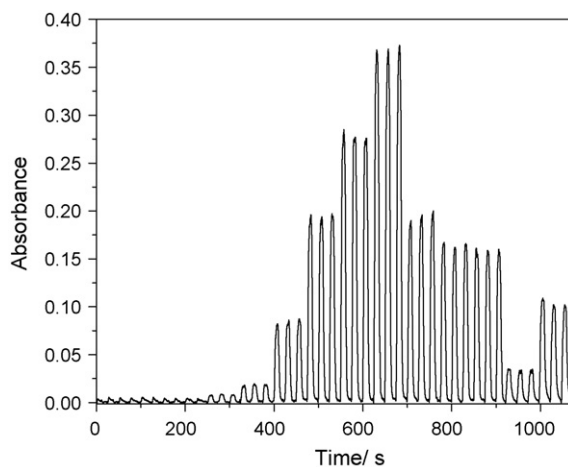


Fig. 7. Analytical signals from blank ( $n = 10$ ), 2, 5, 20, 40, 60 and 80  $\mu\text{g L}^{-1}$  Sb standard solution ( $n = 3$ ), three meglumine antimoniate ( $n = 3$ ), one river sediment ( $n = 3$ ) and one lake sediment sample ( $n = 3$ ).

Table 3

Sb concentration ( $\bar{x} \pm \text{S.D.}$ ) in meglumine antimoniate samples (MA) and reference materials, determined by proposed method (PM) and by FAAS

Samples	PM	FAAS	Reference value
MA 1 <sup>a</sup>	108 ± 4	98 ± 1	–
MA 2 <sup>a</sup>	92 ± 3	96 ± 2	–
MA 3 <sup>a</sup>	92 ± 6	95 ± 1	–
MA 4 <sup>a</sup>	95 ± 5	96 ± 2	–
BCR-320 <sup>b</sup>	0.54 ± 0.02	–	0.6 <sup>c</sup>
IAEA-SL-1 <sup>b</sup>	1.33 ± 0.05	–	1.31 ± 0.12

<sup>a</sup> Values expressed as mg mL<sup>-1</sup>.

<sup>b</sup> Values expressed as mg kg<sup>-1</sup>.

<sup>c</sup> Uncertainty not expressed.

icant differences on the results were achieved at 95% confidence levels, according to the *t*-test, when compared both sets of the results (Table 3).

#### 4. Conclusions

The initial purpose, that was to test the feasibility of the metal furnace for hydride generation atomic absorption spectrometry was greatly attained, once that the performance of the metal furnace as well as the proposed method for antimony determination can be compared, or even better, to others methods proposed in the literature (see Table 4). Related to the figures of merit of the proposed method using the metal furnace Inconel 600<sup>®</sup>, good LOD, sensitivity, selectivity, analytical frequency, linear range, precision and accuracy were attained. This last one was checked by using reference materials for river and lake sediments, as well as alternative technique for pharmaceutical samples.

As a 10-fold increase on sensitivity was achieved by treating the metallic tube with antimony, such new environment formed inside the tube plays an important role in the antimony atomization. After the treatment, changes in the concentrations, mainly for nickel and chromium were detected, and due to the results obtained antimony was better atomized in such environment, which presents higher chromium contents (probably as Cr<sub>2</sub>O<sub>3</sub>,

the most stable chromium oxide form), such species however, does not participate, apparently, in the antimony atomization at the temperature employed in this work.

In this way, metallic atomizers can be considered an elegant and complementary alternative related to hydrides techniques because new environments can be used in the hydride decomposition, once that each one is defined according to the constituents of the alloy used. In view of such fact, a vast field of investigations according to new reactions involved in each environment could be opened, enlarging the studies and the potentialities on hydride generation. Additionally, due to its physical constitution, metallic tubes are much more resistant to shocks than others atomizers already proposed for hydride atomization, which can be a welcome characteristic, mainly for routine laboratories due to the dynamic of the work as well as its lifetime is limited only due to material fatigue. Specifically to this application, its lifetime was higher than 2000 h. If necessary, the facility of the tube pretreatment is another interesting point, as presented in this work, as well as its long-term stability. Finally, due to such characteristics of the metal furnace in addition its low cost (*ca.* US\$ 7 each tube), possible tendencies of using metals as atomizers, besides those common hydride forms, could also be the atomization of those volatile forms of transition and noble metals, due to some difficulty achieved for this task [27].

#### Acknowledgements

The authors thank to the Fundação de Amparo à Pesquisa do Estado de São Paulo (FAPESP, São Paulo, Brazil), the Conselho Nacional de Desenvolvimento Científico e Tecnológico (CNPq, Brasília, Brazil), the Coordenação de Aperfeiçoamento de Pessoal de Nível Superior (CAPES, Brasília, Brazil) and the Grant Agency of the AS CR (Project No. A400310507) for financial support and fellowships.

#### References

- [1] W. Holak, *Anal. Chem.* 41 (1969) 1712.
- [2] J. Dědina, D.L. Tsalev, *Hydride Generation Atomic Absorption Spectrometry*, Wiley & Sons, Inc., Chichester, 1995.
- [3] D.K. Korkmaz, N. Ertas, O.Y. Ataman, *Spectrochim. Acta, Part B* 57 (2002) 571.
- [4] D.K. Korkmaz, J. Dědina, O.Y. Ataman, *J. Anal. At. Spectrom.* 19 (2004) 255.
- [5] D.K. Korkmaz, C. Demir, F. Aydin, O.Y. Ataman, *J. Anal. At. Spectrom.* 20 (2005) 46.
- [6] J. Kratzer, J. Dědina, *Spectrochim. Acta, Part B* 60 (2005) 859.
- [7] A.S. Ribeiro, M.A.Z. Arruda, S. Cadore, *Spectrochim. Acta, Part B* 57 (2002) 2113.
- [8] A.S. Ribeiro, M.A.Z. Arruda, S. Cadore, *J. Anal. At. Spectrom.* 17 (2002) 1516.
- [9] H. Berndt, G. Schaldach, *J. Anal. At. Spectrom.* 3 (1988) 709.
- [10] P. Grinberg, I. Takase, R.C. de Campos, *J. Anal. At. Spectrom.* 14 (1999) 827.
- [11] J. Dědina, T. Matousek, *J. Anal. At. Spectrom.* 15 (2000) 301.
- [12] T. Matousek, J. Dědina, A. Selecka, *Spectrochim. Acta, Part B* 57 (2002) 451.
- [13] A. Gáspár, H. Berndt, *Spectrochim. Acta, Part B* 55 (2000) 587.
- [14] E.R. Pereira-Filho, H. Berndt, M.A.Z. Arruda, *J. Anal. At. Spectrom.* 17 (2002) 1308.

Table 4

Comparison of the limit of detection (LOD) among different methods used in the Sb determination and the proposed method

Technique	LOD ( $\mu\text{g L}^{-1}$ )	References
FAAS	1600	[28]
Spectrophotometry	200	[29]
TS-FF-AAS	40	[28]
ETAAS	2.5	[30]
ICP OES	0.7	[31]
HG-AAS	1.0 and 0.5 <sup>a</sup>	[32]
ASP <sup>b</sup>	0.3	[33]
HG-AAS	0.23	This work
HQTA-HG-AAS	0.18	[10]
HG-AAS	0.13	[4]
ICP-MS	0.01	[34]
Pre-concentration HG-AAS	0.004	[4]
HG-AFS	0.008	[35]

<sup>a</sup> For Sb(III) and Sb(V), respectively.

<sup>b</sup> Anodic stripping potentiometry.

- [15] M.G. Pereira, E.R. Pereira-Filho, H. Berndt, M.A.Z. Arruda, *Spectrochim. Acta, Part B* 59 (2004) 515.
- [16] C.R.T. Tarley, E.C. Figueiredo, G.D. Matos, *Anal. Sci.* 21 (2005) 1337.
- [17] C.C. Nascentes, M.Y. Kamogawa, K.G. Fernandes, M.A.Z. Arruda, A.R.A. Nogueira, J.A. Nóbrega, *Spectrochim. Acta, Part B* 60 (2005) 749.
- [18] C.R.T. Tarley, M.A.Z. Arruda, *Anal. Lett.* 38 (2005) 1427.
- [19] H. Bergamin, E.A.G. Zagatto, F.J. Krug, B.F. Reis, *Anal. Chim. Acta* 101 (1978) 17.
- [20] K. Swaminathan, O.M. Sreedharan, *J. Alloys Compd.* 292 (1999) 100.
- [21] N.N. Greenwood, A. Earnshaw, *Chemistry of the Elements*, 2nd ed., Butterworth Heinemann, London, 1997.
- [22] D.L. Nunes, E.P. dos Santos, J.S. Barin, S.R. Mortari, V.L. Dressler, E.M.M. Flores, *Spectrochim. Acta, Part B* 60 (2001) 731.
- [23] A. D'Ulivo, V. Loreti, M. Onor, E. Pitzalis, R. Zamboni, *Anal. Chem.* 75 (2003) 2591.
- [24] M.T. Martínez-Soria, J.S. Asensio, *J. Anal. At. Spectrom.* 10 (1995) 975.
- [25] P. Pohl, W. Zyrnicki, *Anal. Chim. Acta* 468 (2002) 71.
- [26] Analytical Methods Committee, *Analyst* 112 (1987) 199.
- [27] A.S. Luna, R.E. Sturgeon, R.C. de Campos, *Anal. Chem.* 72 (2000) 3523.
- [28] J. Davies, H. Berndt, *Anal. Chim. Acta* 479 (2003) 215.
- [29] S. Rath, W.F. Jardim, J.G. Dórea, *Fresenius J. Anal. Chem.* 358 (1997) 548.
- [30] R.J. Cassella, B.A.R.S. Barbosa, R.E. Santelli, A.T. Rangel, *Anal. Bioanal. Chem.* 379 (2004) 66.
- [31] M.J. Harmse, R.I. McCrindle, *J. Anal. At. Spectrom.* 17 (2002) 1411.
- [32] Y.P. Peña, O. Vielma, J.L. Burguera, M. Burguera, C. Rondón, P. Carrero, *Talanta* 55 (2001) 743.
- [33] S.B. Adeloju, T.M. Young, D. Jagner, G.E. Batley, *Analyst* 123 (1998) 1871.
- [34] A. Asfaw, G. Wibetoe, *J. Anal. At. Spectrom.* 21 (2006) 1027.
- [35] B. Chen, M. Krachler, W. Shotyk, *J. Anal. At. Spectrom.* 18 (2003) 1256.

## Colorimetric detection of fluoride in an aqueous solution using Zr(IV)–EDTA complex and a novel hemicyanine dye

Xia Gao, Hong Zheng\*, Gui-qin Shang, Jin-Gou Xu\*

*Key Laboratory of Analytical Sciences, Ministry of Education, Department of Chemistry, College of Chemistry and Chemical Engineering, Xiamen University, Xiamen 361005, China*

Received 15 February 2007; received in revised form 29 April 2007; accepted 30 April 2007

Available online 16 May 2007

### Abstract

A new highly sensitive and selective colorimetric method for fluoride determination in water is described. The novel reagent used is a hemicyanine dye (**HC**), which forms a stable complex with Zr–EDTA, the fluoride-binding site, through the hydroxyl groups. The hemicyanine-chelating Zr–EDTA complex (**HC–Zr–EDTA**) is ready to react with fluoride ion to release **HC**. This result in remarkable color change of the sensing solutions from red ( $\lambda_{\max} = 513 \text{ nm}$ ) to yellow ( $\lambda_{\max} = 427 \text{ nm}$ ) at pH 4.40. When applied to the colorimetric determination of fluoride ions, a linear range from  $3.0 \times 10^{-6}$  to  $5.0 \times 10^{-5} \text{ mol/L}$  and a detection limit of  $2.8 \times 10^{-6} \text{ mol/L}$  with a correlation coefficient of 0.9993 can be achieved under the optimized conditions. Because of the specific affinity of fluorides for the [Zr–EDTA], there is little interference by other ions. This method has been successfully applied to the determination of fluorides in toothpaste samples.

© 2007 Elsevier B.V. All rights reserved.

*Keywords:* Fluoride; Hemicyanine; Spectrophotometric

### 1. Introduction

Anions play an important role in a wide range of chemical and biological processes, and considerable attention has been focused on the design of host molecules that can recognize and sense anion species selectively through electrochemical or optical responses [1,2]. Among these anions, fluoride, which is often involved in biological, environmental, supramolecular sciences and lots of industrial processes, is of great interest in designing artificial anion receptors due to its unique properties of relatively small size and stronger electronegativity compared to other halogens. Many molecular chemosensors have been developed for fluoride with the use of a variety of signaling mechanisms such as competitive binding [3], photo-induced electron transfer (PET) [4], excited state proton transfer (ESPT) [5], excimer/exciple formation [6], and intramolecular charge transfer [7]. Spectrophotometric method is widely accepted due to its simplicity, low cost and reliability, and important efforts have been focused

on synthesizing and investigating new reagents for the colorimetric determination of fluoride ions [8]. However, some of these systems use organic solvents as the detection medium because these sensors generally rely on hydrogen bonding or electrostatic interactions for the recognition of the target [8c,8d], therefore, the application of these systems to practical water samples requires tedious solvent extraction procedures and the phase transfer catalysts. Hence, a practical fluoridesensing system is desirable to overcome the above shortcomings and apply to the direct detection of fluoride ion in aqueous media.

Many metal-dye complexes of La(III), Ce(III) and Zr(IV) have been applied to the colorimetric determination of fluoride ion [9]; however, most of these systems lack chemical stability or cost much time in color development. Zr–EDTA has been reported to strongly bind fluoride by ligand-exchanging with coordinated water molecules [10]. Based on this knowledge, Matsunaga and co-workers have reported a new colorimetric method for the detection of fluorides [11a], in which fluoride ion replaces Pyrocatechol Violet (PV) molecules in ternary complex of PV–Zr–EDTA by ligand-exchanging with high specificity. During the study of water-soluble cyanine in our laboratory, we discovered a novel hemicyanine (**HC**) that showed an obvi-

\* Corresponding authors.  
*E-mail addresses:* [hzheng@xmu.edu.cn](mailto:hzheng@xmu.edu.cn) (H. Zheng),  
[jgxu@xmu.edu.cn](mailto:jgxu@xmu.edu.cn) (J.-G. Xu).



ous complexation with Zr–EDTA. Moreover, the relatively large molar absorptivity of **HC** makes it an excellent chromogenic indicator. Based on the fact above-mentioned, a more sensitive system for the colorimetric determination of fluoride was developed. The principle of this method is that **HC** shows a new absorption peak at 513 nm upon binding to Zr–EDTA and the **HC**–Zr–EDTA complex exhibits a large absorbance changes leading to great sensitivity in the presence of fluoride ions by the ligand-exchanging reactions between fluoride ions and **HC**. Interference of foreign anions is negligible and higher sensitivity is resulted by the proposed method.

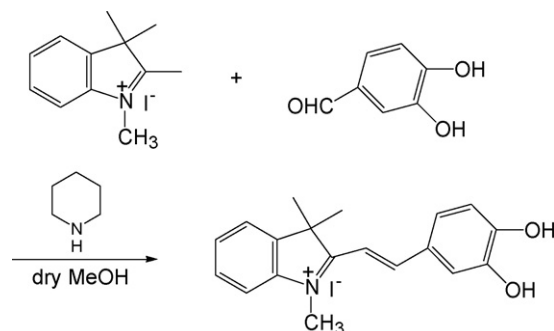
## 2. Experimental

A Beckman DU 7400 absorption spectrophotometer and a 1.0 cm quartz cell were used for absorption study; corrected fluorescence spectra were measured on a Hitachi F-4500 fluorescence spectrophotometer with a 1.0 cm quartz cell; pH was measured with a Model pHs-301 meter (Xiamen, China). All experiments were conducted in DMSO/water (3/7, v/v) solutions at pH 4.40 at room temperature of ca. 25 °C.

1, 2, 3, 3,-Tetramethyl-3H-indolium iodide and 3, 4-dihydroxybenzaldehyde were obtained from Aldrich, other reagents were received from Shanghai Chemicals Group Company as analytical grade or better and used without further purification. Twice-deionized water was further distilled in the presence of  $\text{KMnO}_4$ . Standard solution containing  $1.0 \times 10^{-2}$  mol/L fluoride was prepared by dissolving 42.0 mg NaF in 100 mL distilled water. The  $[\text{Zr}(\text{H}_2\text{O})_2\text{EDTA}]$  white crystal was prepared from  $\text{Zr}(\text{NO}_3)_4$  according to the reported procedure [12] and a  $1.0 \times 10^{-2}$  mol/L stock solution of the complex was prepared in distilled water and stored at 4 °C for the future use.

The hemicyanine dye (**HC**) was synthesized and purified as Scheme 1 [13]:

0.50 g (1.7 mmol) 1, 2, 3, 3,-tetramethyl-3H-indolium iodide and 0.23 g (1.7 mmol) 3, 4-dihydroxybenzaldehyde were dissolved in dry methanol, the reaction mixture was refluxed for 4 h under  $\text{N}_2$  atmosphere after adding 82.0  $\mu\text{L}$  dry piperidine. The solvent was removed first and the residue was purified by recrystallization with methanol to afford **HC** (0.125 g, yield: 25%). The purity of **HC** was confirmed by MS,  $^1\text{H}$  NMR and  $^{13}\text{C}$  NMR spectra as follows:



Scheme 1. Synthesis of the hemicyanine dye.

$^1\text{H}$  NMR ( $d_6$ -DMSO, 400 MHz)  $\delta$  1.763 (s, 6H), 4.070 (s, 3H), 6.934 (d,  $J=8$  Hz, 1H), 7.362 (d,  $J=16$  Hz, 1H), 7.551–7.588 (m, 2H), 7.606–7.626 (m, 2H), 7.835 (d,  $J=6.8$  Hz, 2H), 8.289 (d,  $J=16$  Hz, 1H), 9.384 (s, 1H), 10.612 (s, 1H).

$^{13}\text{C}$  NMR ( $d_6$ -DMSO, 100 MHz)  $\delta$  26.224, 34.280, 52.010, 109.314, 114.901, 116.586, 117.115, 123.229, 126.658, 126.981, 128.969, 129.290, 142.389, 143.526, 146.669, 153.526, 154.441, 181.338.

ESI mass spectrometry,  $m/z$ : 295.4 ( $\text{M}-\text{I}^- + 1$ ).

**HC** was then dissolved in methanol to make a  $1.0 \times 10^{-3}$  mol/L stock solution and stored at 4 °C for the future use.

### 2.1. General procedure

Into a 10.0 mL volumetric flask, transfer 1.0 mL of NaAc–HAc buffer solution (pH 4.40, 0.20 mol/L), an appropriate volume of fluoride solution, 3.0 mL of DMSO and 0.10 mL  $1.0 \times 10^{-3}$  mol/L  $[\text{Zr}(\text{H}_2\text{O})_2\text{EDTA}]$  standard solution in turn. The mixture was diluted to 10.0 mL with distilled water and mixed thoroughly. Then 0.10 mL  $1.0 \times 10^{-3}$  mol/L **HC** standard solution was added and mixed thoroughly once again. After incubation for 15 min, the absorbance of the sample (A) and the blank ( $A_0$ ) (prepared in a similar manner without fluoride ions) were measured at 513 nm.

## 3. Results and discussion

### 3.1. The spectral characteristics of **HC**–Zr–EDTA

It was reported that ethylenediamine- $N,N,N',N'$ -tetraacetic acid (EDTA) formed a remarkably stable 1:1 complex with Zr(IV) with a stability constant  $\log K = 29$  [14]. This high stability constant suggested that the complex could be present in aqueous solution over a wide pH range without any hydrolysis. Even though the  $[\text{Zr}(\text{H}_2\text{O})_2\text{EDTA}]$  complex was fairly stable, some new ternary complex still could be formed by easy replacement of the water molecules bound to Zr(IV) with various bidentate ligands [15–17]. Since hemicyanine dye (**HC**) has a catechol-type chelating group, a good bidentate ligand for Zr(IV) [11], hence we attempt to use **HC** as the indicator to assemble a new fluoride-sensing probe, **HC**–Zr–EDTA.

The  $\text{pK}_{a1}$  value of **HC** was determined to be 7.34 by photometric titration in aqueous solution. The changes of the absorption spectra of **HC** solutions with increasing concentration of Zr–EDTA at pH 4.40 are shown in Fig. 1a. The Job's plot (Fig. 1b) suggested that a 1:1 complex form between **HC** and Zr–EDTA. Therefore, we selected 1:1 as the ratio of Zr–EDTA to **HC** to fabricate the probe for further studies.

As shown in Fig. 1a, free **HC** in DMSO/water (3/7, v/v) solution exhibited a light yellow color with the maximum absorption wavelength at 427 nm ( $\epsilon = 38,000$  L/(mol cm)). However, the color changed to red gradually after addition of  $[\text{Zr}(\text{H}_2\text{O})_2\text{EDTA}]$  stock solution and the maximum absorption wavelength shifted to 513 nm ( $\epsilon = 69,000$  L/(mol cm)) with the decline of the absorption peak at 427 nm. The color reaction is

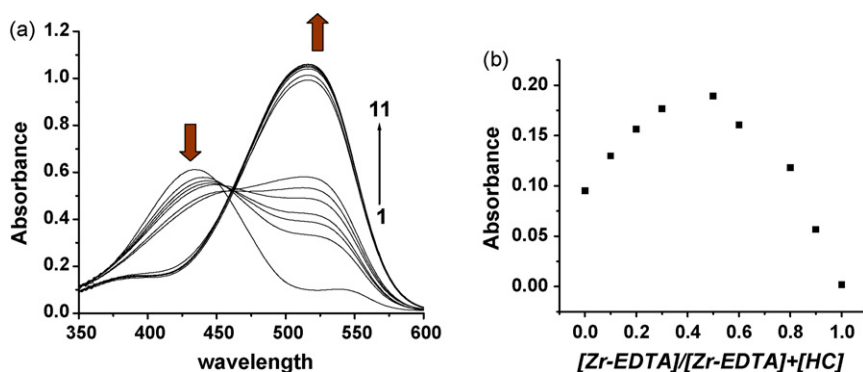
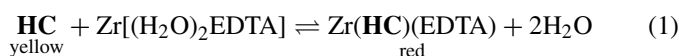


Fig. 1. (a) Absorption spectra of **HC** in the absence (curve 1) and presence of Zr-EDTA (curves 2–11). Concentration of Zr-EDTA (from curves 2 to 11,  $\times 10^{-5}$  mol/L): 0.1; 0.3; 0.5; 0.7; 0.9; 1.0; 2.0; 3.0; 4.0; 5.0.  $[\text{HC}] = 1.0 \times 10^{-5}$  mol/L. (b) Job's plot for **HC**-Zr-EDTA system at 513 nm. Total concentration of **HC** and Zr-EDTA was kept constant at  $1.0 \times 10^{-5}$  mol/L.

expressed as follows:



The conditional formation constant of Eq. (1) was determined to be  $2.0 \times 10^5$  L/mol (pH=4.40) at 298 K by analysis of the molar ratio plots. Along with the changes of absorption spectra, the fluorescence intensity of **HC** at 540 nm also decreased upon excitation at 440 nm (the figure was not given). This phenomenon was ascribed to the formation of **HC**-Zr-EDTA complex since the fluorescence intensity of free **HC** at 540 nm was significantly high under the same conditions.

### 3.2. The spectral evolutions with fluoride titration

The spectral evolution of the **HC**-Zr-EDTA sensing solutions titrated with fluorides is shown in Fig. 2a. It can be seen that the absorbance at 513 nm gradually decreased while the absorbance at 427 nm restored with the increase of the fluorides added, accompanying a spectral shift of the system from the absorption spectrum of **HC**-Zr-EDTA to that of free **HC**. This absorption response induced by the addition of fluorides was attributed to the replacement of **HC** by fluoride ions as

expressed in Scheme 2. This could also be proved by the restored fluorescence at 540 nm (Fig. 2b), the characteristic fluorescence of free **HC**.

### 3.3. Optimization of the experimental conditions

#### 3.3.1. Effect of pH

The effect of pH on the detection of fluoride ion is shown in Fig. 3. It can be seen from Fig. 3 that an optimal value of  $\Delta A$  ( $\Delta A = A_0 - A$ ) can be obtained over the pH range from 4.20 to 4.60, where  $A_0$  and  $A$  are the absorbance of **HC**-Zr-EDTA solution at 513 nm in the absence and presence of fluoride ions, respectively. As a result, the HAC-NaAc buffer (pH 4.40) was selected for further study.

#### 3.3.2. Effects of **HC** concentration and incubation time

The effect of **HC** concentration on the determination of fluorides was investigated. When concentrations of all the other reagents were kept constant at  $1.0 \times 10^{-5}$  mol/L, the  $\Delta A$  increased with the increasing amount of **HC**. However, when the concentration of **HC** exceeded  $1.0 \times 10^{-5}$  mol/L, the  $A_0$  increased remarkably. Thus, a concentration of  $1.0 \times 10^{-5}$  mol/L for **HC** was recommended. Under these optimized conditions,

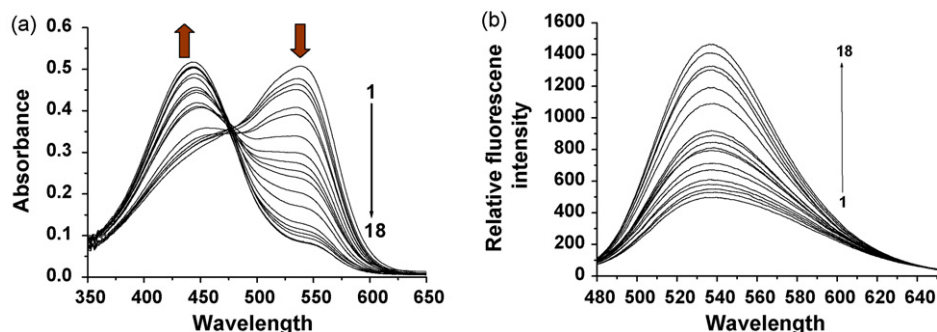
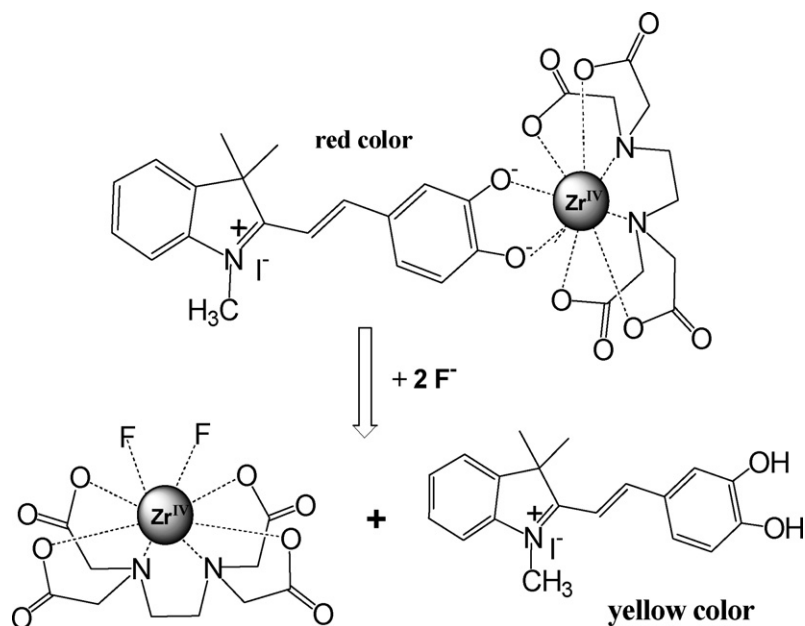


Fig. 2. (a) Absorption spectra of **HC**-Zr-EDTA in the absence (curve 1) and presence (curve 2–18) of  $\text{F}^-$  in DMSO/water solution (3/7, v/v) at pH 4.40 (acetate buffer).  $[\text{HC}] = 1.0 \times 10^{-5}$  mol/L;  $[\text{Zr-EDTA}] = 1.0 \times 10^{-5}$  mol/L. Concentration of  $\text{F}^-$  (from curves 2 to 18,  $\times 10^{-4}$  mol/L): 0.03; 0.05; 0.07; 0.09; 0.2; 0.4; 0.6; 0.8; 1.0; 2.0; 3.0; 4.0; 5.0; 6.0; 7.0; 8.0; 9.0. (b) Fluorescence spectra of **HC**-Zr-EDTA in the absence (curve 1) and presence (curve 2–18) of  $\text{F}^-$  in DMSO/water solution (3/7, v/v) at pH 4.40 (acetate buffer).  $[\text{HC}] = 1.0 \times 10^{-5}$  mol/L;  $[\text{Zr-EDTA}] = 1.0 \times 10^{-5}$  mol/L, concentration of  $\text{F}^-$  (from curves 2 to 18,  $\times 10^{-4}$  mol/L): 0.03; 0.05; 0.07; 0.09; 0.2; 0.4; 0.6; 0.8; 1.0; 2.0; 3.0; 4.0; 5.0; 6.0; 7.0; 8.0; 9.0.



Scheme 2. Ligand-exchange reaction between HC–Zr–EDTA and fluoride ion.

the effect of incubation time on the  $\Delta A$  was also tested (Fig. 4), and the results showed that the system reached equilibrium in 15 min and remained constant for at least 60 min. So incubation for 15 min was chosen for this study.

### 3.3.3. Effects of organic solvents

Effects of some water-soluble organic solvents on the determination of fluoride ion were checked. Results showed that higher sensitivity could be obtained in H<sub>2</sub>O/DMSO (70/30, v/v) solution. Therefore, an aqueous solution containing 30% DMSO was selected for further research.

### 3.3.4. Effect of ionic strength

The effect of ionic strength on the assay was investigated by adding the strong electrolyte such as sodium chloride (Table 1). Results indicated that NaCl had rather low effect on the determination of  $1.0 \times 10^{-5}$  mol/L F<sup>-</sup> even the final concentration

of the salt up to 0.10 mol/L and 1.0 mol/L of sodium chloride only caused ca. –12.7% relative error.

### 3.4. Selectivity and interference of foreign ions

The selective spectroscopic behavior of the sensing system towards background anions was investigated by UV-vis measurements. Fig. 5a shows the representative chromogenic behavior of the sensing system towards the tested anions in aqueous solutions. One can see that HC–Zr–EDTA exhibits rather strong absorption at 513 nm (designated as the blank) and the absorption behavior of the sensing system is almost unaffected upon addition of 10.0 equiv of the tested background anions. However, only the addition of fluoride ion resulted in a rapid decrease of the absorption of HC–Zr–EDTA at 513 nm, which

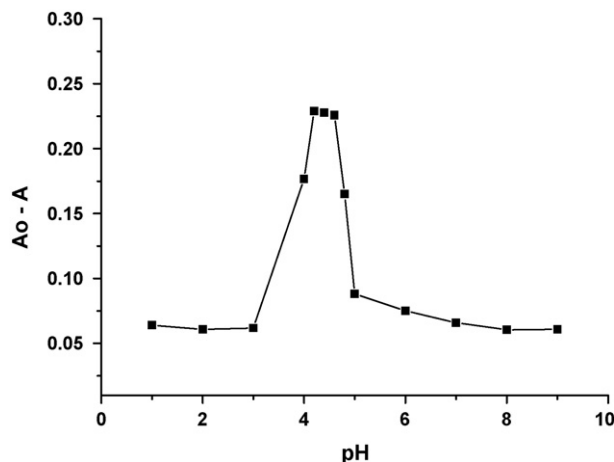


Fig. 3. Effect of pH on  $\Delta A$  at 513 nm. [F<sup>-</sup>] =  $1.0 \times 10^{-4}$  mol/L; [HC] =  $1.0 \times 10^{-5}$  mol/L; [Zr–EDTA] =  $1.0 \times 10^{-5}$  mol/L.

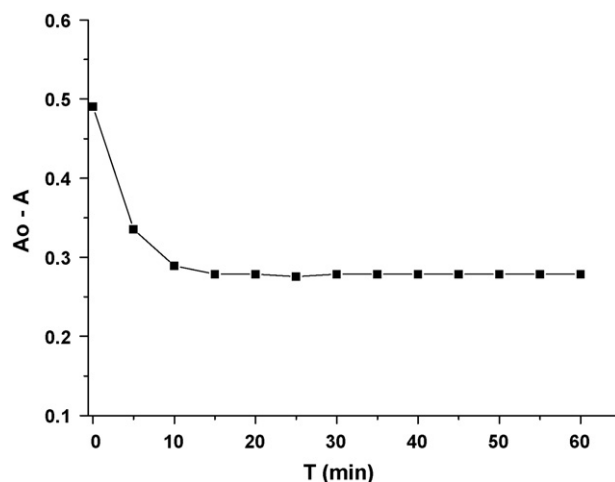


Fig. 4. Effect of reaction time on the absorption response of HC–Zr–EDTA system to fluoride. [HC] =  $1.0 \times 10^{-5}$  mol/L; [Zr–EDTA] =  $1.0 \times 10^{-5}$  mol/L; [F<sup>-</sup>] =  $5.0 \times 10^{-5}$  mol/L.

Table 1  
Tolerance of foreign substances for the determination of  $1.0 \times 10^{-5}$  mol/L fluoride

Foreign ions	Coexisting concentration (mol/L)	Relative error caused (%)
None		0
NaCl	1.0	-12.7
NaCl	0.1	-3.08
NaCl	0.05	-2.12
NaCl	0.02	-0.8
Cl <sup>-</sup>	$1.0 \times 10^{-3}$	-0.12
Br <sup>-</sup>	$1.0 \times 10^{-3}$	-0.75
I <sup>-</sup>	$1.0 \times 10^{-3}$	2.60
HS <sup>-</sup>	$1.0 \times 10^{-3}$	6.20
SCN <sup>-</sup>	$1.0 \times 10^{-3}$	5.60
NO <sub>3</sub> <sup>-</sup>	$1.0 \times 10^{-3}$	3.70
HCO <sub>3</sub> <sup>-</sup>	$1.0 \times 10^{-3}$	2.60
SO <sub>4</sub> <sup>2-</sup>	$1.0 \times 10^{-3}$	-1.87
HSO <sub>3</sub> <sup>-</sup>	$1.0 \times 10^{-3}$	0.50
H <sub>2</sub> PO <sub>4</sub> <sup>-</sup>	$1.0 \times 10^{-3}$	-0.94
P <sub>2</sub> O <sub>7</sub> <sup>4-</sup>	$1.0 \times 10^{-3}$	-1.62
SDS	$4.0 \times 10^{-3}$	-7.03
CTAB	$1.0 \times 10^{-3}$	2.11
TX-100	$3.0 \times 10^{-4}$	0.62
Propionic	$1.0 \times 10^{-4}$	-1.72
Tartaric	$1.0 \times 10^{-4}$	-1.75
Citric	$3.0 \times 10^{-4}$	-1.79
H <sub>2</sub> O <sub>2</sub>	$1.0 \times 10^{-4}$	2.27
Al <sup>3+</sup> (+EDTA)	$1.0 \times 10^{-5}$ ( $1.0 \times 10^{-4}$ )	-20.80(4.20)
Fe <sup>3+</sup> (+EDTA)	$1.0 \times 10^{-5}$ ( $1.0 \times 10^{-4}$ )	-15.4(0.20)
Cu <sup>2+</sup> (+EDTA)	$1.0 \times 10^{-5}$ ( $1.0 \times 10^{-4}$ )	10.36(4.58)

indicated the high selectivity for the spectrophotometric determination of F<sup>-</sup>. Meanwhile, the color changes of the sensing system towards these anions are shown in Fig. 5b. It can be seen that only F<sup>-</sup> induces the color change from red to yellow which indicates that the method can indeed serve as a selective and sensitive semi-quantitative indicator for F<sup>-</sup> by “naked-eye detection”.

The effects of coexisting foreign ions including some anions and related metal ions on the determination of fluoride ion were

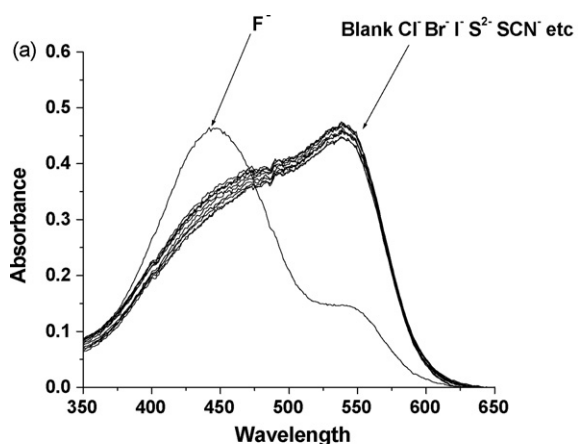


Fig. 5. (a) Absorbance response of HC-Zr-EDTA system to various anions (Cl<sup>-</sup>, Br<sup>-</sup>, I<sup>-</sup>, HS<sup>-</sup>, F<sup>-</sup>, NO<sub>3</sub><sup>-</sup>, HCO<sub>3</sub><sup>-</sup>, HSO<sub>3</sub><sup>-</sup>, H<sub>2</sub>PO<sub>4</sub><sup>-</sup> and SCN<sup>-</sup>;  $1.0 \times 10^{-4}$  mol/L) in DMSO/water solution (3/7, v/v) at pH 4.40 (acetate buffer). [HC] =  $1.0 \times 10^{-5}$  mol/L, [Zr-EDTA] =  $1.0 \times 10^{-5}$  mol/L. (b) Chromogenic response of HC-Zr-EDTA to various anions ( $1.0 \times 10^{-4}$  mol/L) in DMSO/water solution (3/7, v/v) at pH 4.40 (acetate buffer). [HC] =  $1.0 \times 10^{-5}$  mol/L, [Zr-EDTA] =  $1.0 \times 10^{-5}$  mol/L. From left to right (A to K): no anion (blank), Cl<sup>-</sup>, Br<sup>-</sup>, I<sup>-</sup>, F<sup>-</sup>, HS<sup>-</sup>, NO<sub>3</sub><sup>-</sup>, HCO<sub>3</sub><sup>-</sup>, HSO<sub>3</sub><sup>-</sup>, H<sub>2</sub>PO<sub>4</sub><sup>-</sup> and SCN<sup>-</sup>.

also studied. The tolerated concentrations of these foreign ions causing a relative error less than  $\pm 10\%$  are listed in Table 1.

From Table 1, we can see that the tested ions have little interference with the determination. The relatively high concentrations of tested anions that can be tolerated are explained by the high affinity and reacting specificity of fluoride with Zr-EDTA. Among the tested metal cations including Li<sup>+</sup>, Na<sup>+</sup>, K<sup>+</sup>, Ca<sup>2+</sup>, Al<sup>3+</sup>, Mg<sup>2+</sup>, Ba<sup>2+</sup>, Cu<sup>2+</sup>, Pb<sup>2+</sup>, Cd<sup>2+</sup>, Hg<sup>2+</sup>, Fe<sup>3+</sup>, Zn<sup>2+</sup>, Mn<sup>2+</sup>, Al<sup>3+</sup>, Cu<sup>2+</sup> and Fe<sup>3+</sup>, only Al<sup>3+</sup>, Cu<sup>2+</sup> and Fe<sup>3+</sup> appreciably interfered with the determination due to their competing complexation for HC with Zr(IV) ion (data are not shown except for Al<sup>3+</sup>, Cu<sup>2+</sup> and Fe<sup>3+</sup>). However, it was found that further addition of EDTA masked these cations to some extent.

### 3.5. Calibration graphs and analysis of samples

The titration curves of the sensing system with the standard solution of fluoride were constructed under the optimal condi-

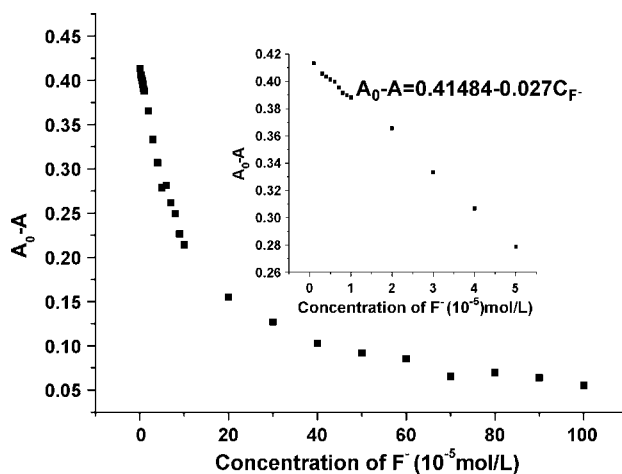


Fig. 6. Calibration graphs for the determination of F<sup>-</sup> ion in DMSO/water solution (3/7, v/v) at pH 4.40 (acetate buffer). [HC] =  $1.0 \times 10^{-5}$  mol/L; [Zr-EDTA] =  $1.0 \times 10^{-5}$  mol/L.

Table 2  
Analytical results of toothpaste samples

Samples	Proposed method found <sup>a</sup> (10 <sup>-5</sup> mol/L)	F <sup>-</sup> , added (10 <sup>-5</sup> mol/L)	F <sup>-</sup> , found (10 <sup>-5</sup> mol/L)	Average recovery (%)	F <sup>-</sup> ISE method; found <sup>a</sup> (10 <sup>-5</sup> mol/L)
1	1.05 ± 0.1	1.00	2.07	102.0	1.08 ± 0.1
2	1.16 ± 0.1	1.00	2.15	98.5	1.21 ± 0.1

<sup>a</sup> The analytical samples of toothpaste were prepared by resolving 1.0 g toothpaste into 50 mL distilled water and stirring for 2 h at 60 °C in a polypropylene breaker, filtering the solution to eliminate the solid residue, then further washing the solid residue with some distilled water, finally incorporating the filtrates and making the volume with distilled water to 100 mL. The above solution was further diluted by 50-fold to provide the analytical sample solution.

tions. The results showed that the absorbance of **HC**–Zr–EDTA at 513 nm decreased with the increment of F<sup>-</sup> concentration, changing from 0.43 in the absence of F<sup>-</sup> to 0.08 after 1.0 × 10<sup>-3</sup> mol/L F<sup>-</sup> treatment. That means the decrease of the absorbance is over 4/5. The linear equation of calibration curve (Fig. 6) was  $\Delta A = 0.41484 - 0.027 C_{F^-}$ , with a correlation coefficient of 0.9993 ( $N = 12$ , S.D. = 0.0017) when a **HC** concentration of 1.0 × 10<sup>-5</sup> mol/L used. The linear range of quantitative determination for F<sup>-</sup> was determined to be 3.0 × 10<sup>-6</sup> to 5.0 × 10<sup>-5</sup> mol/L with a detection limit of 2.8 × 10<sup>-6</sup> mol/L.

In order to check the potential applicability, this method was applied to the quantitative determination of fluoride in commercial toothpaste (*Crest*<sup>®</sup>, **P&G**, in Guangzhou, China). In our experiment, two commercial toothpaste samples were collected and treated to get the sample solutions according to the literature [18] (see footnote in Table 2), and then the sample solutions were diluted 50-fold for experimental uses. The determination results by this method and by the F<sup>-</sup> ion-selective electrode (ISE) method [19] are shown in Table 2. It is noticeable that the determination results by the proposed method are very close to those obtained by ISE method. All the results indicate that the proposed method is sensitive and reliable.

#### 4. Conclusions

In summary, a novel colorimetric method for the determination of fluoride was developed based on the selective ligand-exchange between fluoride and a catechol-type hemicyanine dye. Besides its high sensitivity and specificity, the semi-quantitative determination by “naked-eye detection” is possible. The selectivity, sensitivity, rapidity and simplicity of the present method make it possible to use the probe as a novel sensor material for the detection of F<sup>-</sup> ion by absorption spectrometry in aqueous solution.

#### Acknowledgments

This work was supported by the Science Research Foundation of Xiamen University (No.E43011) and the National Natural Science Foundation of China (No.20275033).

#### References

- [1] E. Bianchi, K. Bowman-James, E. Garcia-Espana (Eds.), *Supramolecular Chemistry of Anions*, Wiley–VCH, New York, 1997.
- [2] R. Martinez-Manez, F. Sancenon, *Chem. Rev.* 103 (2003) 4419.
- [3] C. Minero, G. Mariella, U. Maurino, E. Pelizzetti, *Langmuir* 16 (2000) 2632.
- [4] (a) T. Gunnlaugsson, P.E. Kruger, T.C. Lee, R. Parkesh, F.M. Pfeffer, G. Hussey, *Tetrahedron Lett.* 44 (2003) 6575;  
(b) V. Thiagarajan, P. Ramamurthy, D. Thirumalai, V.T. Ramakrishnan, *Org. Lett.* 7 (2005) 657.
- [5] Y.G. Zhao, B.G. Zhang, C.Y. Duan, Z.H. Lin, Q.J. Meng, *New J. Chem.* 30 (2006) 1207.
- [6] (a) J.S. Wu, J.H. Zhou, P.F. Wang, X.H. Zhang, S.K. Wu, *Org. Lett.* 7 (2005) 2133;  
(b) S.K. Kim, J.H. Bok, R.A. Bartsch, J.Y. Lee, J.S. Kim, *Org. Lett.* 7 (2005) 4839.
- [7] (a) F.Y. Wu, Z. Li, Z.C. Wen, N. Zhou, Y.F. Zhao, Y.B. Jiang, *Org. Lett.* 4 (2002) 3203;  
(b) F.Y. Wu, Y.B. Jiang, *Chem. Phys. Lett.* 355 (2002) 438;  
(c) B. Liu, H. Tian, *Chem. Lett.* 34 (2005) 686.
- [8] (a) C.Q. Zhu, J.L. Chen, H. Zheng, Y.Q. Wu, J.G. Xu, *Anal. Chim. Acta.*, 539 (2005) 311;  
(b) S. Watanabe, H. Seguchi, K. Yoshida, K. Kifune, T. Tadakib, H. Shiozaki, *Tetrahedron Lett.* 46 (2005) 8827;  
(c) Z.H. Lin, S.J. Qu, C.Y. Duan, B.G. Zhang, Z.P. Bai, *Chem. Commun.* (2006) 624;  
(d) E.j. Cho, B.j. Ryu, Y.J. Lee, K.C. Nam, *Org. Lett.* 7 (2005) 2607.
- [9] (a) R. Belcher, M.A. Leonard, T.S. West, *J. Chem. Soc.* (1959) 3577;  
(b) S.S. Yamamura, M.A. Wade, J.H. Sikes, *Anal. Chem.* 34 (1962) 1308;  
(c) T. Lay, T.S. West, *Anal. Chem.* 43 (1971) 136.
- [10] (a) A. Yuchi, N. Hokari, H. Kerao, G. Nakagawa, *Inorg. Chem.* 29 (1990) 136;  
(b) P.D. Beer, P.A. Gale, *Angew. Chem. Int. Ed.* 4 (2001) 486.
- [11] (a) T. Balaji, H. Matsunaga, *Anal. Sci.* 21 (2005) 973;  
(b) Y. Takahashi, D.A.P. Tanaka, H. Matsunaga, T.M. Suzuki, *J. Chem. Soc., Perkin Trans. 2* (2002) 759;  
(c) H. Matsunaga, C. Kanno, H. Yamada, Y. Takahashi, T.M. Suzuki, *Talanta* 68 (2006) 1000.
- [12] H.G. Langer, *J. Inorg. Nucl. Chem.* 36 (1964) 59.
- [13] A.P. Phillips, *J. Org. Chem.* 12 (1947) 333.
- [14] A.E. Martell, R.M. Smith, *Critical Stability Constants*, 1, Plenum Press, New York and London, 1974, p. 207.
- [15] B.J. Intorre, A.E. Martell, *J. Am. Chem. Soc.* 83 (1964) 3618.
- [16] A. Yuchi, T. Ban, H. Wada, G. Nakagawa, *Inorg. Chem.* 29 (1990) 136.
- [17] T.M. Suzuki, D.A.P. Tanaka, M.L. Tanco, M. Kanesato, T. Yokoyama, *J. Environ. Monit.* 2 (2000) 550.
- [18] T.L. Daines, K.W. Morse, *J. Chem. Educ.* 51 (1974) 680.
- [19] J.H. Xu, J.H. Zhao, H.W. Wang, *Chinese J. Health Technol.* 11 (2001) 165.

# Determination of complex formation constants by phase sensitive alternating current polarography: Cadmium–polymethacrylic acid and cadmium–polygalacturonic acid

Anna Maria Garrigosa, Rui Gusmão, Cristina Ariño\*,  
José Manuel Díaz-Cruz, Miquel Esteban

*Departament de Química Analítica, Universitat de Barcelona, Martí i Franquès 1-11, E-08028 Barcelona, Spain*

Received 21 February 2007; received in revised form 12 April 2007; accepted 30 April 2007

Available online 10 May 2007

## Abstract

The use of phase sensitive alternating current polarography (ACP) for the evaluation of complex formation constants of systems where electrodic adsorption is present has been proposed. The applicability of the technique implies the previous selection of the phase angle where contribution of capacitive current is minimized. This is made using Multivariate Curve Resolution by Alternating Least Squares (MCR-ALS) in the analysis of ACP measurements at different phase angles. The method is checked by the study of the complexation of Cd by polymethacrylic (PMA) and polygalacturonic (PGA) acids, and the optimal phase angles have been *ca.*  $-10^\circ$  for Cd–PMA and *ca.*  $-15^\circ$  for Cd–PGA systems. The goodness of phase sensitive ACP has been demonstrated comparing the determined complex formation constants with those obtained by reverse pulse polarography, a technique that minimizes the electrode adsorption effects on the measured currents.

© 2007 Elsevier B.V. All rights reserved.

**Keywords:** Phase sensitive alternating current polarography; Complex formation constants; Cadmium; Electrodic adsorption; Polymethacrylic acid; Polygalacturonic acid

## 1. Introduction

Voltammetric techniques have been widely used on the study of the distribution of metal compounds in natural waters due to their high sensitivity and to the dependence of the voltammetric signal on the nature of the different species involved. In these media, metal ions are found associated to different ligands (simple monomeric ones, macromolecules, colloids, etc.) forming complexes. Voltammetric techniques have been applied successfully in the evaluation of complexation parameters using methodologies based on the postulation of a theoretical physicochemical model for both the electrodic reaction and the complexation process and its further analytical or numerical resolution. The fitting of the parameters of that model to experimental data provides information about metal complexation in different kind of systems [1,2]. The applicability of mod-

els requires the fulfilment of the hypothesis assumed in their formulation. Among them, absence of adsorption phenomena is a typical assumption and it is of great relevance.

When adsorption of the ligand on the electrode (and sometimes, induced adsorption of the metal ion) is not negligible, the majority of the models described in the literature are not suitable. Their direct application to data obtained in the presence of adsorption yield anomalous complexation constant values [3,4], and the larger it is the more erroneous the results. This is because adsorption affects the electrode-solution interphase and, consequently, the total currents and the potential shifts measured. To avoid this problem, the use of reverse pulse polarography (RPP) is recommended, since previous investigations have shown that, although the potential values are affected by adsorption phenomena, the limiting current values are not influenced [5]. However, this technique is not enough sensitive to be applied on the study of metal complexation at concentration levels close to those in natural media. By this reason, phase sensitive alternating current polarography (ACP) appears as a reliable alternative to RPP for solving the problem of lack of sensitivity but addressing properly

\* Corresponding author. Tel.: +34 93 402 15 45; fax: +34 93 402 12 33.  
E-mail address: [cristina.arino@ub.edu](mailto:cristina.arino@ub.edu) (C. Ariño).

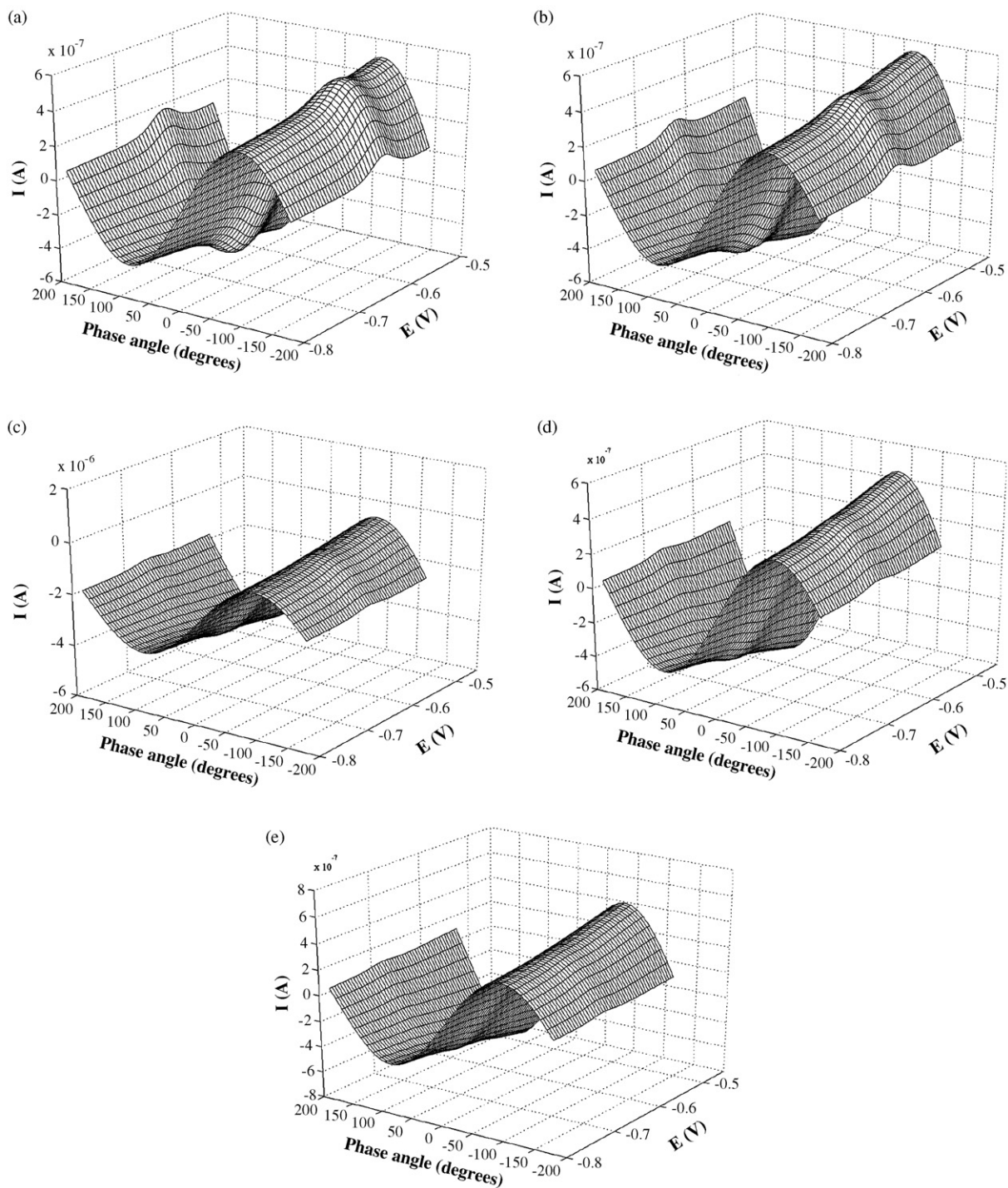


Fig. 1. AC polarograms measured at different phase angles of solutions containing  $10^{-5} \text{ mol L}^{-1}$  Cd(II) in  $0.1 \text{ mol L}^{-1}$   $\text{KNO}_3$  at different PMA concentrations: (a) 0, (b)  $1.5 \times 10^{-4}$ , (c)  $3 \times 10^{-4}$ , (d)  $7 \times 10^{-4}$  and (e)  $3 \times 10^{-3} \text{ mol L}^{-1}$ .

adsorption effect. This is because ACP can discriminate between the capacitive (or charging) ( $I_c$ ) and the faradaic ( $I_f$ ) currents if measurements are made at the convenient phase angle relative to the applied AC potential function [6–9]. However, the selection of the proper phase angle to yield complete discrimination is not a trivial task [9].

In a previous work, an accurate method, based on the application of Multivariate Curve Resolution with Alternating Least

Squares (MCR-ALS) to series of AC polarograms measured at different phase angles, has been proposed to establish the phase angle where  $I_c$  is minimized [10]. With the aim to check the applicability of the method for complexation studies of systems where adsorption on the electrode is present, a comparative study by RPP and ACP at different phase angles is reported. In this study, Cd(II) has been chosen as metal ion, and polymethacrylic (PMA) and polygalacturonic (PGA) acids

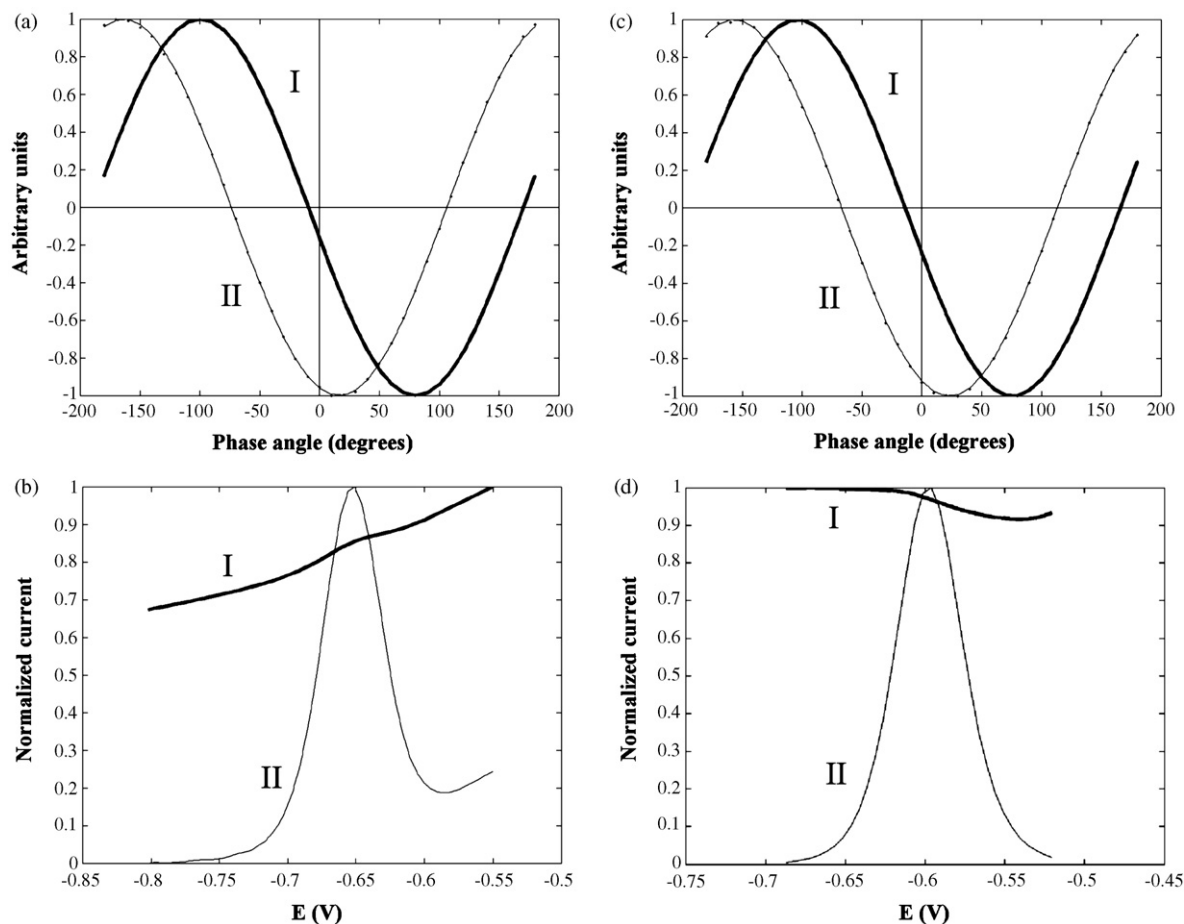


Fig. 2. Pure voltammograms (second row) and evolution of capacitive and faradaic currents with phase angle (first row) obtained in the MCR-ALS decomposition of data matrices from  $10^{-5} \text{ mol L}^{-1} \text{ Cd(II)}-3.0 \times 10^{-4} \text{ mol L}^{-1} \text{ PMA}$  (a and b) and  $10^{-5} \text{ mol L}^{-1} \text{ Cd(II)}-2.0 \times 10^{-3} \text{ mol L}^{-1} \text{ PGA}$  (c and d), using the constrains of non-negativity for voltammograms and peak shape for the faradaic component of the current. I represents capacitive component and II faradaic component.

as ligands, which have been considered because of their homogeneity and macromolecular characteristics. In addition, both systems have shown evidences to be adsorbed on a mercury electrode [11,12]. Complexation constants have been determined by application of the voltammetric model developed by de Jong et al. for metal–macromolecular systems [13–15]. The goodness of the phase sensitive ACP based method is checked by comparing the results obtained with those by RPP that is a technique with adsorption-independent currents, and by DPP, a technique greatly affected by adsorption processes on the electrode, or

by ACP at a phase angle of  $45^\circ$  where capacitive current is present.

It must be pointed out that direct application of this approach is only valid for moderate adsorption, that is, when adsorption only affects capacitive currents and the non-faradaic contribution of the adsorbed species predominates. In those cases an approximation described previously must be applied [16]. Then, the current measured at the selected phase angle must be corrected by a contribution due to the reduction of the metal contained on the adsorption layer.

Table 1  
Phase angle values where capacitive and faradaic currents are minimized for Cd–PMA and Cd–PGA systems at:  $10^{-5} \text{ mol L}^{-1}$  of Cd(II) and  $0.1 \text{ mol L}^{-1}$  of  $\text{KNO}_3$  and pH 6.5 (Cd–PMA) and  $0.01 \text{ mol L}^{-1}$  of  $\text{KNO}_3$  and pH 6.0 (Cd–PGA)

[PMA] ( $\text{mol L}^{-1}$ )	[PGA] ( $\text{mol L}^{-1}$ )	$\varphi$ ( $I_c$ minimum)	$\varphi$ ( $I_f$ minimum)	Lack of fit (%)
0	–	$-9.6^\circ$	$-58.8^\circ$	0.1
$1.4 \times 10^{-4}$	–	$-9.9^\circ$	$-69.6^\circ$	0.5
$3.0 \times 10^{-4}$	–	$-9.7^\circ$	$-72.9^\circ$	0.1
$7.2 \times 10^{-4}$	–	$-9.6^\circ$	$-76.8^\circ$	0.1
$3.0 \times 10^{-3}$	–	$-11.2^\circ$	$-81.3^\circ$	0.7
–	0	$-13.9^\circ$	$-64.9^\circ$	0.3
–	$2.0 \times 10^{-3}$	$-14.1^\circ$	$-66.8^\circ$	0.7
–	$4.0 \times 10^{-3}$	$-15.2^\circ$	$-60.9^\circ$	1.1
–	$6.0 \times 10^{-3}$	$-15.1^\circ$	$-66.0^\circ$	0.8



## 2. Selection of the optimal phase angle by MCR-ALS

Theoretically, in ACP the capacitive current ( $I_c$ ) is  $90^\circ$  out of phase respect to the applied AC potential, whereas the faradaic current ( $I_f$ ) is usually  $45^\circ$  (or less) out of phase [6–9]. Then, in principle complete discrimination of  $I_f$  against  $I_c$  should be possible measuring currents either in phase with the applied AC potential or at  $180^\circ$  out of phase. However, the selection of this angle is not so clear, as Smith discussed in detail [9], because the capacitive current is not the same in the presence that in the absence of faradaic processes. This is the reason why a method based on MCR-ALS analysis was recently proposed [10]. MCR-ALS can discriminate between different contributions that independently affect to the signals, in this case,  $I_f$  and  $I_c$ . This method implies the construction of a data matrix ( $\mathbf{I}$ ) from AC polarograms measured at different angles, and its mathematical decomposition in a product of two abstract matrices,  $\vartheta$  and  $\mathbf{V}$ , that explain the variation of the two current components ( $I_f$  and  $I_c$ ) with phase angle and potential, respectively. The analysis of  $\vartheta$  allows to deduce the angle at which charging current is minimized; so, in principle, it is possible to obtain signals without the  $I_c$  contribution, thus minimizing the influence of electrodic adsorption, useful for the evaluation of complexation parameters. A more detailed description of the procedure can be found in [10].

## 3. Experimental

### 3.1. Chemicals and instrumentation

Polymethacrylic acid was provided by BDH, with an average molecular mass of  $26,000 \text{ g mol}^{-1}$ . Polygalacturonic acid from orange was provided by Sigma with an average molecular mass of  $21,000 \text{ g mol}^{-1}$ . PMA and PGA stock solutions of *ca.*  $0.1$  and  $0.01 \text{ mol L}^{-1}$ , respectively (in monomeric units) were prepared by dilution, and the total number of carboxylic groups was determined by conductometric acid–base titration. Both solutions were stored in the dark at  $4^\circ\text{C}$  to prevent decomposition.

All other reagents were analytical-reagent grade from Merck. Cd(II) stock solution was prepared from  $\text{Cd}(\text{NO}_3)_2 \cdot 4\text{H}_2\text{O}$  and standardised complexometrically.  $\text{KNO}_3$  was used as supporting electrolyte, and  $\text{HNO}_3$  and  $\text{KOH}$  were used for partial neutralization or in conductometric titrations.

Polarographic measurements were performed in a Metrohm-757 VA Computrace attached to a personal computer with data acquisition software also from Metrohm. The working, reference and auxiliary electrodes were a static mercury drop electrode (SMDE) with a drop area of  $0.6 \text{ mm}^2$ , an  $\text{Ag}/\text{AgCl}$ ,  $\text{KCl}$  ( $3 \text{ mol L}^{-1}$ ) and a glassy carbon, respectively, all of them from Metrohm. Double distilled Hg is used. The quality of Hg is of great importance in ACP measurements, because small amounts of impurities greatly affect the double layer capacity.

Unless otherwise indicated, instrumental parameters were drop time of 1 s and scan rate of  $0.005 \text{ V s}^{-1}$  for both ACP and RPP; pulse amplitude of 4 or 10 mV, modulation time of 0.1 s and frequency of the sinusoidal applied potential of 50 Hz in ACP; and pulse time of 0.04 s in RPP.

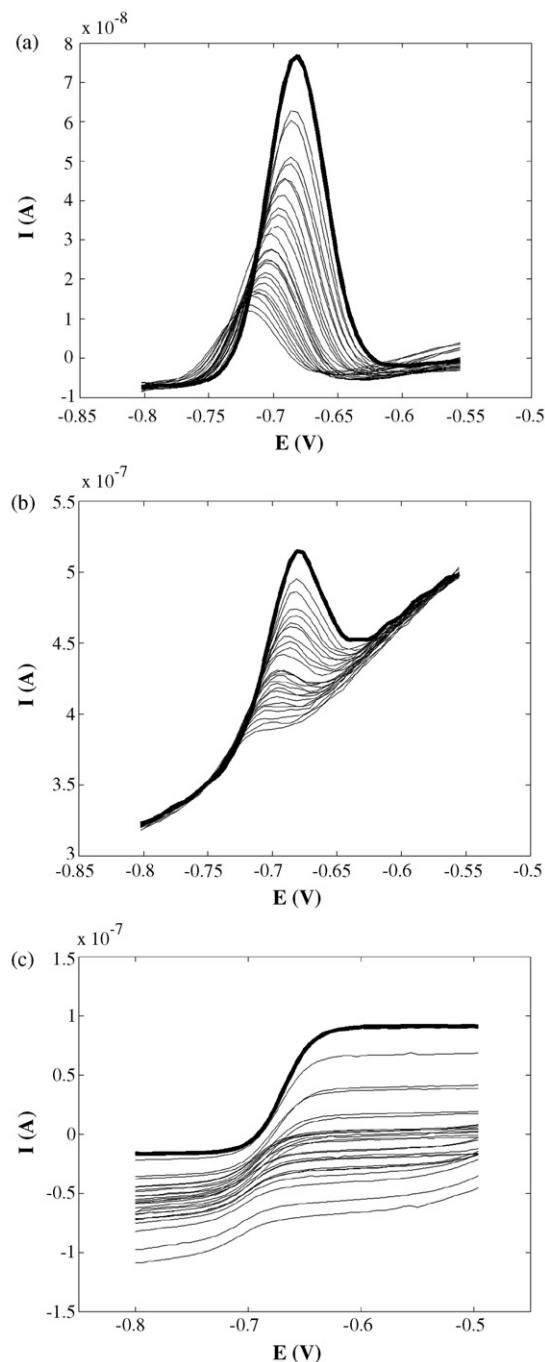


Fig. 3. AC polarograms at  $-10^\circ$  (a) and at  $45^\circ$  (b) and RP polarograms (c) measured during the titration of  $10^{-5} \text{ mol L}^{-1}$  Cd(II) solution with  $5 \times 10^{-2} \text{ mol L}^{-1}$  PMA at pH 6.5 in  $0.1 \text{ mol L}^{-1}$   $\text{KNO}_3$ .

pH measurements were made with an Orion SA 720 pH-meter, and conductometric titrations of PMA and PGA solutions were carried out with an Orion 120 Conductometer coupled to a Metrohm 665 Dosimat.

### 3.2. Phase angle selection

Measurements were carefully planned to have a detailed picture of the behaviour at different phase angles and at different extensions of the cadmium complexation pro-

cess. Aliquots containing  $10^{-5} \text{ mol L}^{-1}$  Cd(II), 0.1 or  $0.01 \text{ mol L}^{-1}$   $\text{KNO}_3$ , and different concentrations of deprotonated groups of PMA or PGA were placed in the voltammetric cell, and deaerated with  $\text{N}_2$  for 20 min. Then, successive phase sensitive AC polarograms were measured at different phase angle from  $-180^\circ$  to  $180^\circ$  (36 angles in steps of  $10^\circ$ ).

### 3.3. Voltammetric titrations

Twenty five milliliters of a  $10^{-5} \text{ mol L}^{-1}$  Cd(II) solution were placed in the voltammetric cell at fix ionic strength ( $\text{KNO}_3$ ) and pH (6.5 for PMA and 6 for PGA), and deaerated with pure  $\text{N}_2$  for 20 min. Then, RP and AC polarograms were recorded to obtain both the limiting ( $I_{\text{lim}}$ ) and peak ( $I_p$ ) current values in the absence of ligand. Further, successive additions of a  $5 \times 10^{-2} \text{ mol L}^{-1}$  PMA or  $5 \times 10^{-3} \text{ mol L}^{-1}$  PGA solution were made, making sure that an excess of ligand was present, as compared to the metal concentration. This is a condition for the proper application of the voltammetric model by de Jong et al. [13–15]. After each addition, RP and AC polarograms were recorded to obtain  $I_{\text{lim}}$  and  $I_p$  values in the presence of ligand. For the Cd–PGA system, DP polarograms have been also carried out in each addition, and the peak current values also acquired.

Since the complexation constants of PMA and PGA are especially sensitive to the counterion concentration [17] and the pH value [18], all the experiments have been performed at constant  $\text{K}^+$  concentration and controlled pH.

### 3.4. Data treatment

AC polarograms were smoothed and converted into data matrices using home-made programs implemented in MATLAB [19]. MCR-ALS analysis of data was carried out and optimal phase angle was evaluated through several home-made programs also implemented in MATLAB.

In the case of the Cd–PMA and Cd–PGA voltammetric titrations by RPP, ACP, and/or DPP, polarograms were also smoothed and current values measured by means of home-made programs implemented in MATLAB. The non-linear regression data analysis program Tablecurve 2D [20] was used to fit the experimental results to the equations of the model [13–15], which allows the evaluation of the complexation parameters.

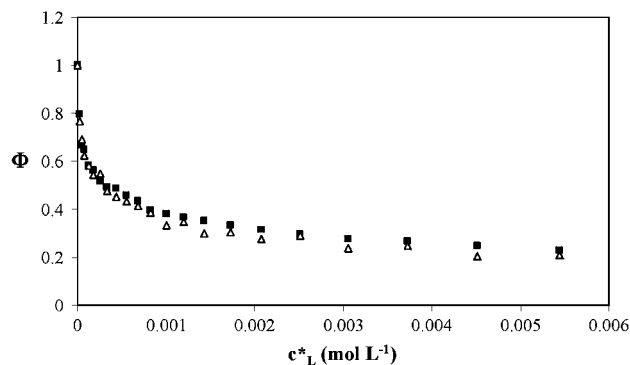


Fig. 4.  $\Phi$  vs.  $c_L^*$  plots for RPP (■) and AC (△) titrations of  $10^{-5} \text{ mol L}^{-1}$  Cd(II) with  $5 \times 10^{-2} \text{ mol L}^{-1}$  PMA at pH 6.5 in  $0.1 \text{ mol L}^{-1}$   $\text{KNO}_3$ .

## 4. Results and discussion

### 4.1. Phase angle selection

Fig. 1 shows, as an example, the experimental polarograms obtained at different phase angles of solutions with different Cd:PMA ratios. These experimental polarograms are comparable to those obtained for the Cd–PGA system. Data matrices clearly illustrate that, independently of the ligand concentration, the total current has a sinusoidal variation with the phase angle. These figures show that Cd(II) reduction peaks appear superimposed to the baseline and, as expected for a labile and macromolecular complex, when ligand concentration increases, peak current decreases while peak potential moves to more negative values.

Previous to the application of MCR-ALS to experimental data in Fig. 1, Singular Value Decomposition (SVD) [10] of those matrices shows that two components are responsible of the current variations with phase angle, independently from the studied system; these components are  $I_f$  and  $I_c$ . MCR-ALS yields the pure polarograms (matrix  $\mathbf{V}$ ), corresponding to faradaic and capacitive currents, and also the dependence of these currents with phase angle (matrix  $\vartheta$ ). Fig. 2 shows, as an example, the results obtained in the MCR-ALS treatment of data matrices corresponding to two cases of Cd(II)–PMA and Cd(II)–PGA solutions. Unitary voltammograms (second row in Fig. 2 also show the characteristic shape for the faradaic Cd(II) reduction peak (signal II) and for the capacitive baseline current (signal I). From  $\vartheta$  matrices, the phase angle values where  $I_c$  are minimized are evaluated, and the values obtained are shown in Table 1.

Table 2  
Complexation parameters of Cd–PMA and Cd–PGA systems determined by RPP, ACP and DPP

System	Technique	$\log K$	$\varepsilon$	$\log K$ at a fixed $\varepsilon$ value
Cd–PMA ( $\mu = 0.1 \text{ mol L}^{-1}$ , pH 6.5)	RPP	$4.23 \pm 0.03$	$0.069 \pm 0.006$	$4.22 \pm 0.03^a$
	ACP- $10^\circ$	$4.19 \pm 0.04$	$0.069 \pm 0.007$	$4.22 \pm 0.04^a$
	ACP $45^\circ$	$4.48 \pm 0.03$	$0.054 \pm 0.006$	$4.59 \pm 0.07^a$
Cd–PGA ( $\mu = 0.01 \text{ mol L}^{-1}$ , pH 6.0)	RPP	$4.38 \pm 0.02$	$0.079 \pm 0.009$	$4.38 \pm 0.02^b$
	ACP- $15^\circ$	$4.35 \pm 0.03$	$0.10 \pm 0.01$	$4.31 \pm 0.02^b$
	DPP	$4.18 \pm 0.02$	$0.066 \pm 0.008$	$4.21 \pm 0.01^b$

<sup>a</sup> For Cd–PMA system, fixed  $\varepsilon$  value of 0.069.

<sup>b</sup> For Cd–PGA system, fixed  $\varepsilon$  value of 0.081.

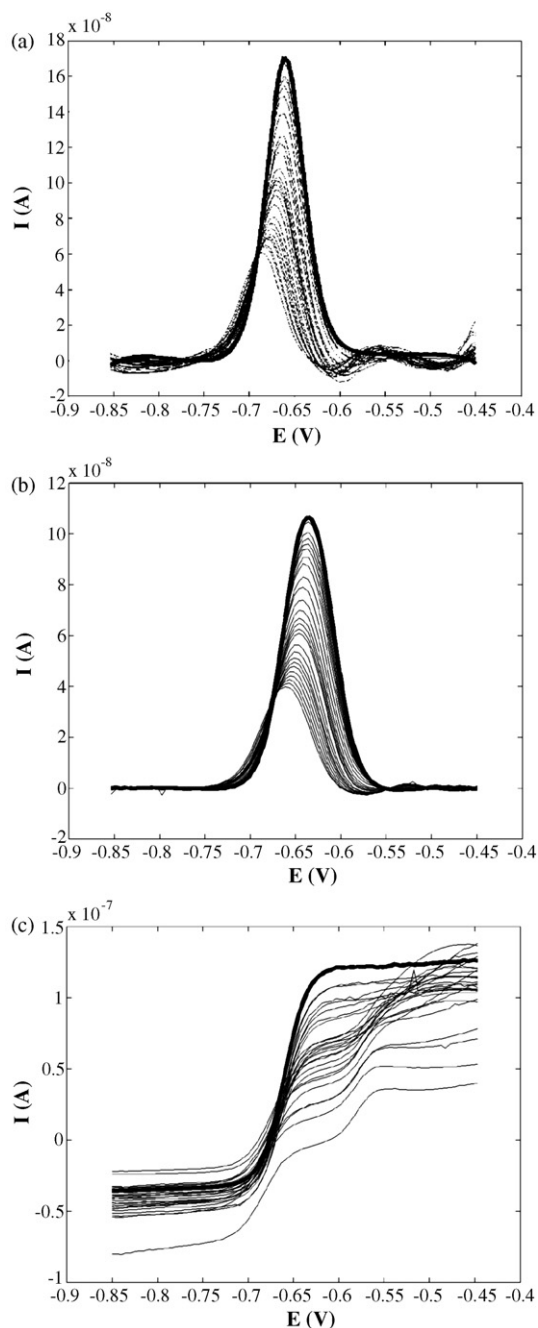


Fig. 5. AC polarograms at  $-15^\circ$  (a), DP (b) and RP polarograms (c) measured during the titration of  $10^{-5} \text{ mol L}^{-1}$  Cd(II) solution with  $5 \times 10^{-3} \text{ mol L}^{-1}$  PGA at pH 6 in  $0.01 \text{ mol L}^{-1}$   $\text{KNO}_3$ .

Phase angles of  $-10^\circ$  for the Cd–PMA system and of  $-15^\circ$  for the Cd–PGA system seem to be the most convenient to measure currents free of capacitive contribution and consequently the more convenient to evaluate complexation constants through this technique. The lack of fit (LOF) of this treatment is between 0.2 and 1% in all the cases, showing the goodness of the fitting. The difference with the theoretically expected value of  $0^\circ$  is due to the influence that faradaic processes and instrumentation have on the double layer capacity, as it has been already explained in previous works [9,10].

## 4.2. Evaluation of stability constants

### 4.2.1. The Cd–PMA system

To validate the goodness of measurements by ACP at the phase angle of  $-10^\circ$  for the determination of complexation parameters, voltammetric titrations by this technique (ACP at  $-10^\circ$ ) have been made. These results have been compared with those obtained by RPP (a technique where currents are not affected by adsorption, as mentioned above) and with those obtained by ACP at  $45^\circ$ , an angle where the total current has both faradaic and capacitive contributions (Fig. 3). If AC( $-10^\circ$ ) and AC( $45^\circ$ ) polarograms are compared (Fig. 3a and b), an important contribution of residual current is observed on polarograms measured at  $45^\circ$ , that is basically capacitive. In all cases, the labile and macromolecular character of the formed complexes produces limiting or peak current decreases and peak or half-wave potential shifts to more negative potentials (respect to the reduction of metal ion alone) when PMA concentration increases [2,13–15].

As it has been mentioned above, the model of de Jong et al. [13–15] is the most convenient for the study of these complex systems. According to this model, the normalized current  $\Phi$ , defined as  $\Phi = I/I_0$ , where  $I$  and  $I_0$  are the limiting or peak currents measured in the presence and in the absence of ligand, respectively, and related to the formation constant of the complex,  $K$ , through [13–15]:

$$\Phi = \frac{(1 + \varepsilon K c_L^*)^{1/2}}{(1 + K c_L^*)^{1/2}} \quad (1)$$

where  $\varepsilon$  is the ratio between  $D_{ML}$  and  $D_M$  (diffusion coefficients of the complex and the metal ion, respectively) and  $c_L^*$  is the bulk ligand concentration of the binding groups (carboxylate). Fig. 4 shows the  $\Phi$  versus  $c_L^*$  plots obtained by RPP and ACP at  $-10^\circ$ . The complexation parameters obtained from the fitting of the parameters of Eq. (1) to the experimental data are shown in Table 2, showing a good agreement between  $\log K$  values obtained from RPP and ACP at  $-10^\circ$ . As expected, the  $\log K$  value obtained from AC at  $45^\circ$  is different of those obtained by ACP( $-10^\circ$ ) and RPP, because of the influence of adsorption on current values [3,4]. This fact corroborates that, in systems with moderate adsorption processes on the electrode surface, measurements by ACP at an angle where current is free from the influence of capacitive current are a good alternative to RPP.

### 4.2.2. The Cd–PGA system

A similar study has been made with the Cd–PGA system, but including DPP measurements. Fig. 5 shows polarograms obtained in ACP( $-15^\circ$ ), RPP and DPP titrations. Again, all the polarograms present the expected behaviour for labile and macromolecular complexation. The application of the de Jong et al. [13–15] model to the experimental data yields the complexation constants shown in Table 2, where a good agreement between values obtained by RPP and ACP( $-15^\circ$ ) is observed. As expected, the complexation constant value obtained by DPP suffers of some deviation because DPP is affected by adsorp-

tion, thus corroborating the goodness of AC, at the angle where capacitive current is minimized, in this kind of studies.

Concerning to  $\varepsilon$  values, they are similar with each other and quite reasonable taking into account the molecular weight of the ligands. Anyway, if an  $\varepsilon$  value is fixed during the fitting of Eq. (1), the resulting log  $K$  values are still closer to each other, except for measurements by ACP(45°) and DPP, which maintain their differences as a consequence of adsorption (Table 2).

## 5. Conclusions

The use of the chemometric method MCR-ALS allows us to discriminate between the capacitive ( $I_c$ ) and the faradaic contribution ( $I_f$ ) of the ACP current through the accurate selection of the phase angle where  $I_c$  is minimized. For Cd–PMA and Cd–PGA systems, the optimal phase angle is between  $-10^\circ$  and  $-15^\circ$ , and the goodness of the method has been demonstrated through the comparative study of both systems by RPP and ACP at  $-10^\circ$ – $-15^\circ$ . The formation constant ( $K$ ) determined by ACP at  $-10^\circ$  in the presence of moderate adsorption is comparable to the one obtained by RPP (reference technique) in both systems. In addition, the log  $K$  values measured in conditions with adsorption influence are significantly different, and therefore confirming phase sensitive ACP as a convenient technique in the determination of complexation constants if measurements are made at the phase angle where capacitive contribution is minimized.

## Acknowledgements

The authors gratefully acknowledge financial support from the Spanish Ministerio de Educación y Ciencia (project BQU2006-14385-CO2-01). This research is a part of the activities of SIBA-TEQ group (2005SGR00186 and 2001SGR-

00056) from the Generalitat of Catalonia. Anna M. Garrigosa thanks the Spanish Ministerio de Educación y Ciencia for her Ph.D. grant.

## References

- [1] D.R. Crow, *Polarography of Metal Complexes*, Academic Press, London, 1969.
- [2] M. Esteban, C. Ariño, J.M. Díaz-Cruz, E. Casassas, *Trends Anal. Chem.* 12 (1993) 276.
- [3] E. Casassas, C. Ariño, *J. Electroanal. Chem.* 213 (1986) 235.
- [4] J. Puy, F. Mas, J.M. Díaz-Cruz, M. Esteban, E. Casassas, *Anal. Chim. Acta* 268 (1992) 261.
- [5] J. Galceran, D. Reñé, J. Salvador, J. Puy, M. Esteban, F. Mas, *J. Electroanal. Chem.* 375 (1994) 307.
- [6] A.M. Bond, *Anal. Chem.* 45 (1973) 2026.
- [7] A.M. Bond, *Modern Polarographic Methods in Analytical Chemistry*, Marcel Dekker, New York, 1980.
- [8] A.M. Bond, I.D. Heritage, *J. Electroanal. Chem.* 222 (1987) 35.
- [9] D.E. Smith, *Crit. Rev. Anal. Chem.* 2 (1971) 247.
- [10] A.M. Garrigosa, A. Alberich, C. Ariño, J.M. Díaz-Cruz, M. Esteban, *Electroanalysis* 18 (2006) 2405.
- [11] J.M. Díaz-Cruz, C. Ariño, M. Esteban, E. Casassas, *Electroanalysis* 3 (1991) 299.
- [12] A.M. Nadal, C. Ariño, M. Esteban, E. Casassas, *Electroanalysis* 3 (1991) 309.
- [13] H.G. de Jong, H.P. van Leeuwen, K. Holub, *J. Electroanal. Chem.* 234 (1987) 1.
- [14] H.G. de Jong, H.P. van Leeuwen, *J. Electroanal. Chem.* 234 (1987) 17.
- [15] H.G. de Jong, H.P. van Leeuwen, *J. Electroanal. Chem.* 235 (1987) 1.
- [16] A.M. Garrigosa, C. Ariño, J.M. Díaz-Cruz, M. Esteban, *Electroanalysis* 18 (2006) 1215.
- [17] M.A.G.T. van den Hoop, H.P. van Leeuwen, *Anal. Chim. Acta* 273 (1993) 275.
- [18] J.M. Díaz-Cruz, M. Esteban, M.A.G.T. van den Hoop, H.P. van Leeuwen, *Anal. Chim. Acta* 264 (1992) 163.
- [19] MATLAB Version 7.3, Maths Works Inc., Natick, MA, 2006.
- [20] Table Curve 2D, Jandel Scientific, 1994.

# Content uniformity of pharmaceutical solid dosage forms by near infrared hyperspectral imaging: A feasibility study

Christelle Gendrin<sup>a,b,\*</sup>, Yves Roggo<sup>a</sup>, Christophe Collet<sup>b</sup>

<sup>a</sup> *F. Hoffmann-La Roche A.G., Basel, Switzerland*

<sup>b</sup> *LSIIT – UMR CNRS 7005, Strasbourg University, 67000 Strasbourg, France*

Received 16 January 2007; received in revised form 12 April 2007; accepted 30 April 2007

Available online 10 May 2007

## Abstract

Near-infrared imaging systems simultaneously record spectral and spatial information. Each measurement generates a data cube containing several thousand spectra. Chemometric methods are therefore required to extract qualitative and quantitative information. The aim of this study was to determine the feasibility of quantifying active pharmaceutical ingredient (API) and excipient content in pharmaceutical formulations using hyperspectral imaging.

Two kinds of tablets with a range of API content were analysed: a binary mixture of API and cellulose, and a pharmaceutical formulation with seven different compounds. Two pixel sizes, 10  $\mu\text{m}/\text{pixel}$  and 40  $\mu\text{m}/\text{pixel}$ , were compared, together with two types of spectral pretreatment: standard normal variate (SNV) normalization and Savitzky–Golay smoothing. Two methods of extracting concentrations were compared: the partial least squares 2 (PLS2) algorithm, which predicts the content of several compounds simultaneously, and the multivariate classical least squares (CLS) algorithm based on pure compound reference spectra without calibration.

Best content predictions were achieved using 40  $\mu\text{m}/\text{pixel}$  resolution and the PLS2 method with SNV normalized spectra. However, the CLS method extracted distribution maps with higher contrast and was less sensitive to noisy spectra and outliers; its API predictions were also highly correlated to real content, indicating the feasibility of predicting API content using hyperspectral imaging without calibration.

© 2007 Elsevier B.V. All rights reserved.

**Keywords:** Active pharmaceutical ingredient; Content uniformity; Chemical imaging; Excipient; Near infrared spectroscopy; Quantification; Classical/Partial least squares; Process analytical technology

## 1. Introduction

Since 2002, the Food and Drug Administration's process analytical technology initiative has promoted the integration throughout the manufacturing process of tools and techniques that ensure final product quality [1]. Near-infrared (NIR) spectroscopy is a prime example [2,3]. Focal plane array (FPA) detectors that can acquire multiple spatially located NIR spectra simultaneously have recently been developed to visualize compound distribution. They are combined with tunable filters [4] for wavelength selection and microscopes with different objectives for varying spatial resolution and scanning area. The combination of spectroscopy for compound characterization and imaging for spatial localization in NIR-chemical imaging (NIR-

CI) [5] has had pharmaceutical applications such as mapping compound distribution [6–9] to test for homogeneity or to detect counterfeits.

NIR-CI generates data cubes that require chemometric to extract the relevant qualitative and quantitative information. Qualitative analyses of NIR hyperspectral images in pharmaceutical applications [10,11] have mainly addressed compound distribution and sample homogeneity. This information could not be extracted by classical NIR spectroscopy because the quantification is performed on the integration of a signal over the sample surface and the spatial information is lost. Nevertheless, quantification is also of interest. The main advantage of NIR imaging is that the analysis of a large area of the sample is possible. The aim is to obtain statistical and quantitative parameters describing the hypercube for further comparisons. For quantification classical partial least squares (PLS) regression has been used to predict the concentration [12,13] of several compounds simultaneously in binary and ternary mixtures with

\* Corresponding author.

E-mail address: [christelle.gendrin@roche.com](mailto:christelle.gendrin@roche.com) (C. Gendrin).



factors and the pharmaceutical tablet model with three factors. API and excipient concentrations were predicted using the PLS2 model in each pixel, i.e. in each spectra, of the data cubes. The content of the entire tablet was calculated by averaging those pixel predictions.

## 2.6. CLS

Multivariate analysis was chosen for its ability to extract chemical distribution maps from whole wavelengths. After the data cube ( $x^* y^* \lambda^*$ ) was unfolded into a two-dimensional matrix  $\mathbf{X} = ((x^* y^*)^* \lambda^*)$ , matrix  $\mathbf{X}$  was decomposed into the product of two matrices,  $\mathbf{C}$  and  $\mathbf{S}^T$ :  $\mathbf{X} = \mathbf{C}\mathbf{S}^T + \mathbf{E}$ , where  $\mathbf{E}$  is the error matrix. The rows in  $\mathbf{S}^T$  contained the pure compound signals, and the columns in  $\mathbf{C}$  their related concentration profiles or unfolded distribution map. The relative concentration matrix  $\mathbf{C}$  was extracted using CLS. This method consists in minimizing the error sum of squares  $\|\mathbf{X} - \mathbf{C}\mathbf{S}^T\|$ .  $\mathbf{C}$  was estimated by the pseudo-inverse  $\mathbf{C} = \mathbf{X}\mathbf{S}(\mathbf{S}^T\mathbf{S})^{-1}$ .

The concentration of compound  $j$  was calculated as follows:

$$C_j = 100 \times \frac{\sum_i C_{i,j}}{\sum_{i,j} C_{i,j}}$$

## 2.7. Statistical indicators

Four predicted concentrations were collected with both algorithms at each actual concentration. Methods were compared using linear regression. Accuracy of prediction was evaluated by slope, intercept, correlation coefficient of the linear regression and an additional measure of model error: the root mean square error of prediction (RMSEP), calculated as follows:

$$\text{RMSEP} = \sqrt{\frac{\sum_{i=1}^n (\hat{C}_i - C_i)^2}{n - 1}}$$

where  $\hat{C}$  is the estimated concentration,  $C$  the real concentration, and  $n$  the total sample number ( $n = 44$ ).

## 3. Results and discussion

### 3.1. Reference spectra

#### 3.1.1. Binary mixtures

The NIR normalized (SNV) reference spectra (Fig. 1) showed two main peaks for API<sub>1</sub> at 1670 nm and 1720 nm due to C–H first overtone. Both were sharper than the three broad cellulose peaks at [1400–1600 nm] due to O–H first overtone, and at [1870–1990] nm and [1990–2210] nm due to O–H combinations. Spectral features appeared to differ sufficiently between the two compounds to permit accurate prediction.

#### 3.1.2. Pharmaceutical tablets

Normalized (SNV) reference spectra for the three main compounds (Fig. 2) showed sharp but more numerous API<sub>2</sub>

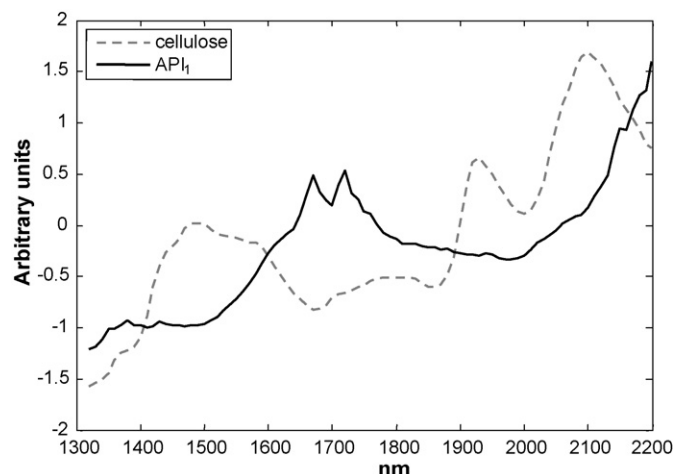


Fig. 1. Binary mixtures: markedly distinct normalized reference spectra for cellulose and API<sub>1</sub> after standard normal variate pretreatment.

peaks between 1600 and 1780 nm due to C–H first overtone, with an additional peak at 2140 nm (N–H combinations). Lactose peaks were located at nearly the same wavelengths as those of cellulose. Since API<sub>2</sub> peaks did not overlap with excipient peaks, separation appeared feasible. However, discrimination between lactose and cellulose appeared more difficult.

### 3.2. Mean spectra

Data cube mean spectra of the eleven different concentrations showed clear spectral variation with API<sub>1</sub> concentration in the binary mixtures (Fig. 3, arrowed), with finer variation around 1650 and 2140 nm (the location of the API<sub>2</sub> peaks) in the pharmaceutical tablets (Fig. 4). The differences in spectral variation clearly reflected the different concentration ranges used (increments of 10 and 1%, respectively) and the number of compounds in the formulation. Concentration estimates were therefore judged to be more accurate in binary mixtures.

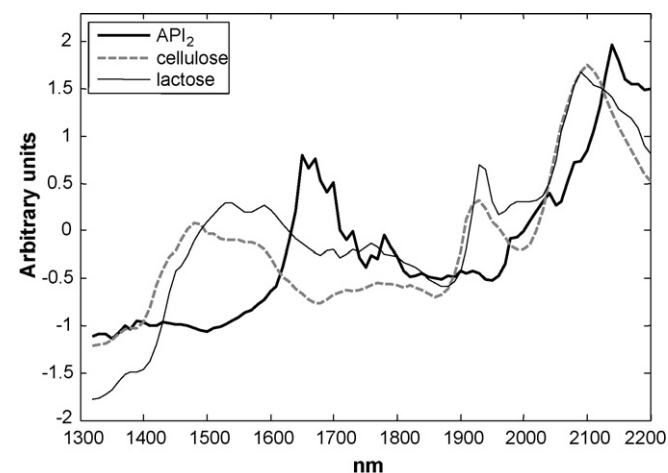


Fig. 2. Pharmaceutical tablets: normalized reference spectra (after standard normal variate pretreatment) of API<sub>2</sub>, cellulose and lactose.

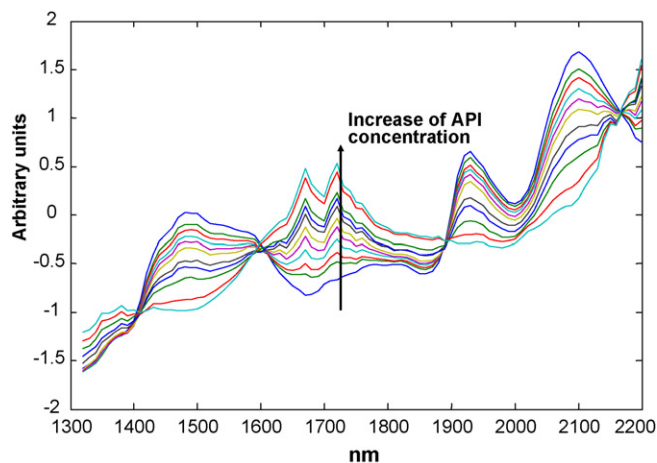


Fig. 3. Binary mixtures: normalized mean data cube spectra across the API<sub>1</sub> concentration range demonstrate marked concentration-dependent variation (arrow).

### 3.3. Concentration predictions

#### 3.3.1. Results

**3.3.1.1. Binary mixtures.** Both pretreatments and both algorithms proved highly accurate (Table 2), with correlations >0.99 and slopes >0.93. However, accuracy was greater with PLS2. Use of the 40 μm/pixel objective improved the statistical indicators whereas derivative pretreatment slightly decreased them: with both methods linearity was poorer with normalized spectra followed by derivative pretreatment than with normalized spectra only. Linear regression of API<sub>1</sub> content with PLS2 and CLS using both objectives and SNV pretreatment only is shown in Fig. 5.

**3.3.1.2. Pharmaceutical tablets.** With the PLS2 algorithm, normalized-only absorbance spectra gave more accurate results than derivative spectra as shown by slope, correlation coefficient and RMSEP. Predictions were reliable for both API<sub>2</sub> and excipients (Table 3).

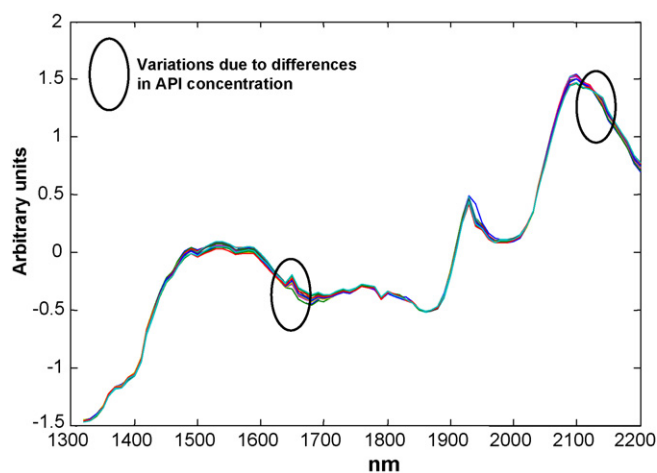


Fig. 4. Pharmaceutical tablets: normalized mean data cube spectra across the API<sub>2</sub> concentration range demonstrate minor concentration-dependent variation (circles).

With the CLS algorithm, the derivative clearly enhanced the accuracy of API<sub>2</sub> prediction. With the normalized absorbance spectra, slopes were only 0.618 with the 10 μm/pixel objective and 0.439 with the 40 μm/pixel objective, while RMSEP values exceeded 2%. With the second derivative, API<sub>2</sub> predictions were as accurate as with PLS2 (correlations >0.995 and RMSEP ≈ 0.4%). Excipient predictions were poorer, with low correlations (<0.6), adverse linear statistical indicators (slopes and intercepts far from 0 and 1, respectively), and high RMSEP values (some exceeding 10%), indicating that predictions of lactose and cellulose content using CLS are unreliable. As with the binary mixtures, use of the 40 μm/pixel objective enhanced the accuracy of both methods (Fig. 6).

#### 3.3.2. Discussion

**3.3.2.1. Pretreatments.** When PLS2 was used, statistical results were slightly poorer with the derivative, possibly due to spectral noise.

Use of the derivative with CLS gave slightly poorer results with binary mixtures and significantly improved those with pharmaceutical tablets versus normalized-only spectra. Because spectral features differed so strikingly in binary mixtures, content could be extracted simply from the absorbance spectra, and the algorithm achieved greater accuracy. Pharmaceutical tablets, on the other hand, contained more compounds, resulting in spectral overlap, especially between cellulose and lactose (Fig. 2), with the result that the derivative enhanced spectral variation and concentrations were more readily extracted using the CLS algorithm.

**3.3.2.2. Objectives.** Imaging experiments involve a choice between small pixel size for detecting finer particles and large pixel size for scanning a larger and more representative sample area. Having both high spatial resolution and reliable quantification would be of interest in case of micronized powders.

For binary mixtures, the content predictions were of the same accuracy with both objectives. For the 7 compounds pharmaceutical tablets, the results showed that content predictions were more accurate with the 40 μm/pixel objective. Noticeably, the distribution of API<sub>2</sub> predictions in pharmaceutical tablets using CLS or PLS2, the second derivative and the 10 μm/pixel objective showed larger error bars with the 5 and 8% tablets than at other contents (Fig. 6a and b) compared to similar error bars at all contents with the 40 μm/pixel objective (Fig. 6c and d). This is an indication of inhomogeneity. Effectively, if agglomerates are present on the sample surface and are scanned under the 10 μm/pixel objective this could produce overestimated or underestimated concentrations, hence a larger min–max range. Indeed, when considering API<sub>2</sub> distributions maps with 5% API (Fig. 7), agglomerates are revealed, which support the hypothesis of inhomogeneity.

Those results with binary mixtures and 7 compounds pharmaceutical tablets lead to the conclusion that the 40 μm/pixel objective which scans a larger surface is more accurate for content uniformity. Nevertheless, when the sample is homogeneous the 10 μm/pixel objective can give also reliable concentration.



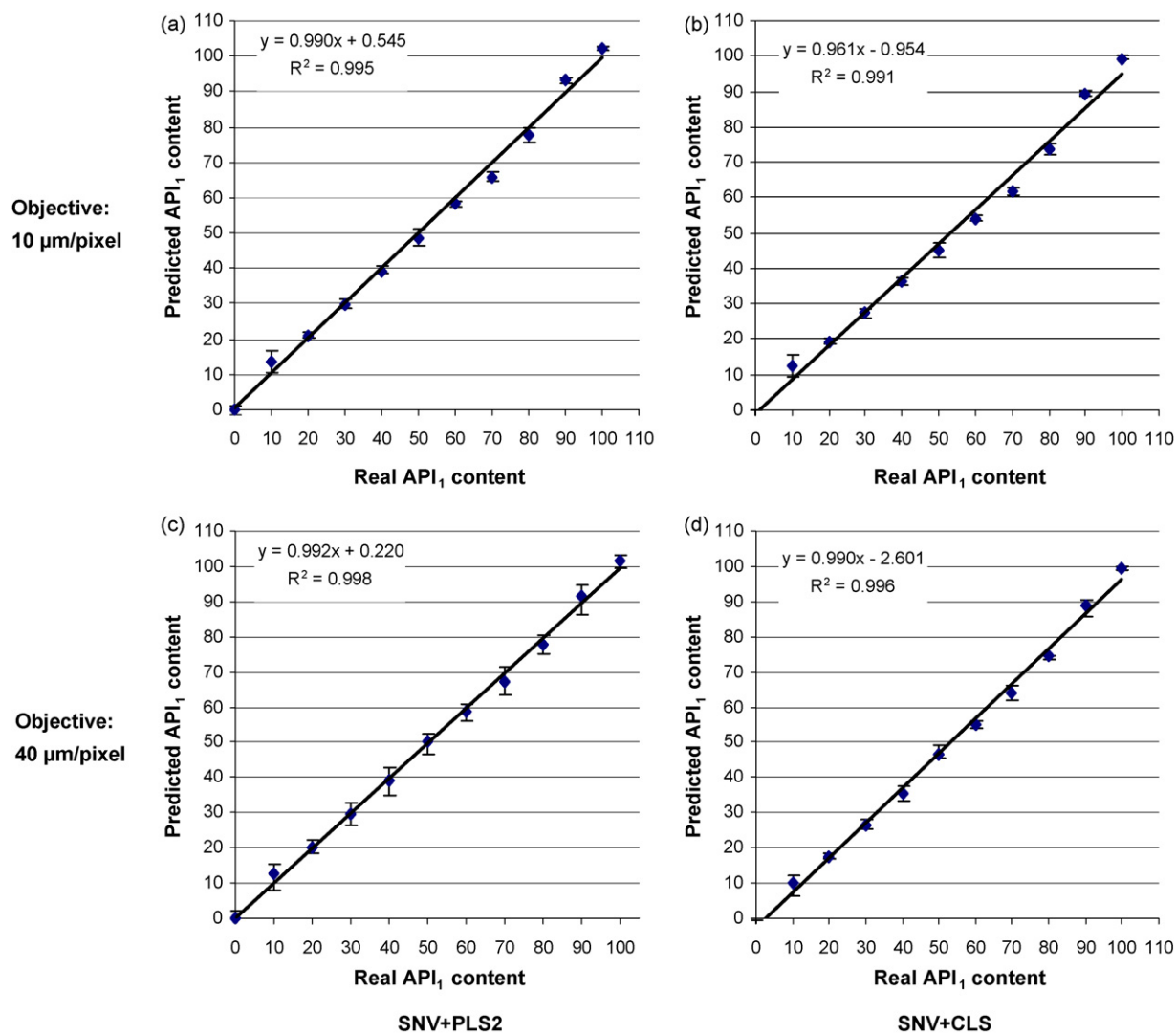


Fig. 5. Binary mixtures: prediction using PLS2 (a and c) and CLS (b and d) on normalized spectra, showing satisfactory results with both algorithms and objectives, although regression linearity is slightly better with the 40  $\mu\text{m}/\text{pixel}$  objective. Points: mean predicted value; error bars: min–max concentration range.

Table 2  
Prediction of API<sub>1</sub> and cellulose content in binary mixtures (units: %)

Objective ( $\mu\text{m}/\text{pixel}$ )	Prediction parameter	PLS2				CLS			
		SNV		SNV + SG (9/3) 1 <sup>st</sup> derivative		SNV		SNV + SG (9/3) 1 <sup>st</sup> derivative	
		API	Cellulose	API	Cellulose	API	Cellulose	API	Cellulose
10	Slope	0.990	0.988	0.991	0.987	0.961	–	0.936	–
	Intercept	0.545	0.395	-0.029	0.073	-0.954	4.828	1.665	4.768
	Correlation	0.995	0.989	0.993	0.979	0.991	–	0.990	–
	RMSEP	2.766	3.776	3.024	5.238	4.644	–	4.294	–
40	Slope	0.992	0.988	0.996	0.987	0.990	–	0.971	–
	Intercept	0.220	0.650	0.080	0.497	-2.601	3.632	-0.237	3.134
	Correlation	0.998	0.994	0.993	0.987	0.996	–	0.994	–
	RMSEP	3.219	3.678	3.184	4.868	4.234	–	3.438	–

Best predictions (shaded) were achieved with the 40  $\mu\text{m}/\text{pixel}$  objective and SNV pretreatment only. CLS and PLS2 predictions were similar. With the CLS algorithm, cellulose parameters (except intercept) were identical to those of the API due to complementarity of the calculated concentrations.

Table 3  
Prediction of API<sub>2</sub>, cellulose and lactose content in pharmaceutical tablets (units: %)

Objective ( $\mu\text{m}/\text{pixel}$ )	Prediction parameter	PLS 2						CLS					
		SNV			SNV + SG (9/3) 2 <sup>nd</sup> derivative			SNV			SNV + SG (9/3) 2 <sup>nd</sup> derivative		
		API	Cellulose	Lactose	API	Cellulose	Lactose	API	Cellulose	Lactose	API	Cellulose	Lactose
10	Slope	0.988	0.987	0.986	0.996	0.972	0.967	0.689	1327	0.029	1.037	1.531	0.543
	Intercept	-0.17	0.544	0.531	-0.019	1.512	1.579	-0.279	-22.652	53.278	0.279	-16.935	12.429
	Correlation	0.992	0.994	0.994	0.997	0.994	0.993	0.998	0.626	0.001	0.997	0.552	0.116
	RMSEP	0.704	0.325	0.3	0.554	0.421	0.398	2.272	7.799	11.387	0.898	10.373	9.332
40	Slope	0.989	0.933	0.935	1.069	0.954	0.955	0.644	0.766	0.533	0.978	0.964	1.022
	Intercept	-0.032	3.284	2.889	-0.401	2.028	1.827	-2.861	9.421	29.032	-0.065	9.622	-7.061
	Correlation	0.996	0.991	0.993	0.994	0.975	0.974	0.988	0.567	0.375	0.998	0.595	0.599
	RMSEP	0.439	0.302	0.268	0.583	0.546	0.501	5.119	2.934	9.095	0.429	8.720	6.911

Best predictions (shaded) were achieved using the 40  $\mu\text{m}/\text{pixel}$  objective and SNV pretreatment only with PLS2, followed by derivatized spectra with CLS. API predictions with CLS approximated to those with PLS2 but cellulose and lactose contents were unreliable.

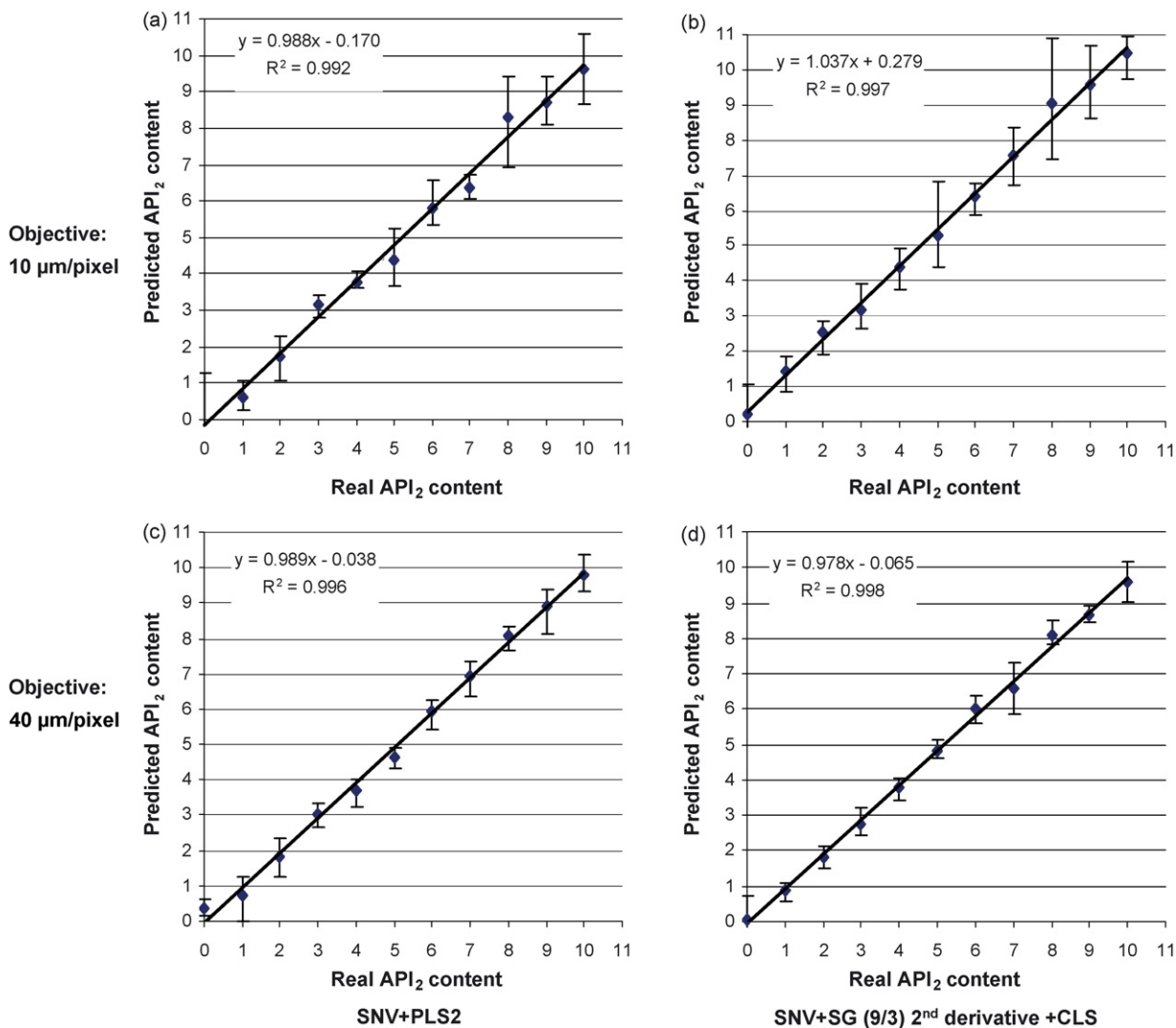


Fig. 6. Pharmaceutical tablets: prediction using PLS2 on normalized spectra (a and c) and CLS on normalized and second derivative (SG 9/3) spectra (b and d), showing better results and regression linearity with the 40  $\mu\text{m}/\text{pixel}$  objective. Points: mean predicted value; error bars: min–max concentration range.

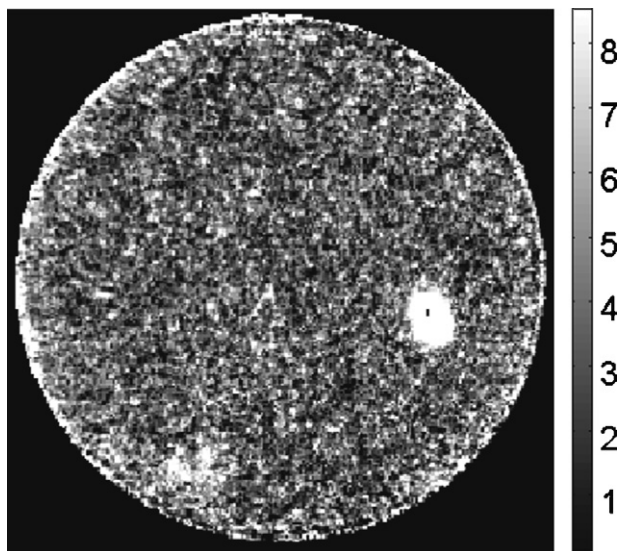


Fig. 7. Pharmaceutical tablet, 5% active pharmaceutical ingredient (API<sub>2</sub>), 40  $\mu\text{m}$ /pixel objective: API<sub>2</sub> distribution map extracted using classical least squares from second derivative spectra. The API<sub>2</sub> spot on the tablet surface indicates a homogeneity problem. White/black pixels: high/low API<sub>2</sub> concentration.

The choice of the field of view depends both of the sample size but also of its particle sizes.

**3.3.2.3. PLS2 versus CLS.** PLS2 has proven a reliable quantification method with NIR spectroscopy. In this study, it was both faster and more accurate. However a disadvantage is that a whole concentration range must first be run to calibrate the PLS2 model for future predictions.

Fig. 8 shows the distributions of the predicted concentrations for PLS2 (top) and CLS (bottom) algorithms for the main compounds (left: API, middle: cellulose, right: lactose). The color scale links a gray level in the image to a predicted concentration, linearly from black which corresponds to a low concentration to white which corresponds to a high concentration. The maps extracted with PLS2 did not feature cellulose or lactose, and contrast was low (Fig. 8a, middle and right). Higher values were located at the tablet edge, where spectra are noisier because of physical distortions and can be considered as outliers, leading to inaccurate concentration calculations. Moreover, negative API concentrations were predicted (cf. color scheme of Fig. 8a, left). Other PLS2 predictions were tried by selecting a  $140 \times 140$  pixel square in mid-tablet, thus avoiding the incorporation of outlier spectra in the model and predictions, but the predictions were not significantly more accurate and distribution maps remained the same (i.e. no distribution of particles could have been drawn).

CLS, on the other hand, accurately predicted API in both types of sample. Its advantage is that it requires only the reference spectra of the pure compounds, as is often the case with pharmaceutical samples. This results in accurate API content prediction without the need for calibration. Excipient prediction was less accurate than with PLS2 but tended to increase with derivative spectra, giving an approximation of relative content. Poor prediction of cellulose and lactose was caused by the narrow real content range (cellulose: 52–46%; lactose: 47–42%) and the similarities in spectral features [14]. Another explanation for the difference between real and predicted concentrations was the presence of minor compounds not taken into account in content computation because of their low levels. Maps of excipient (and API<sub>2</sub>) distribution extracted by CLS showed apparent

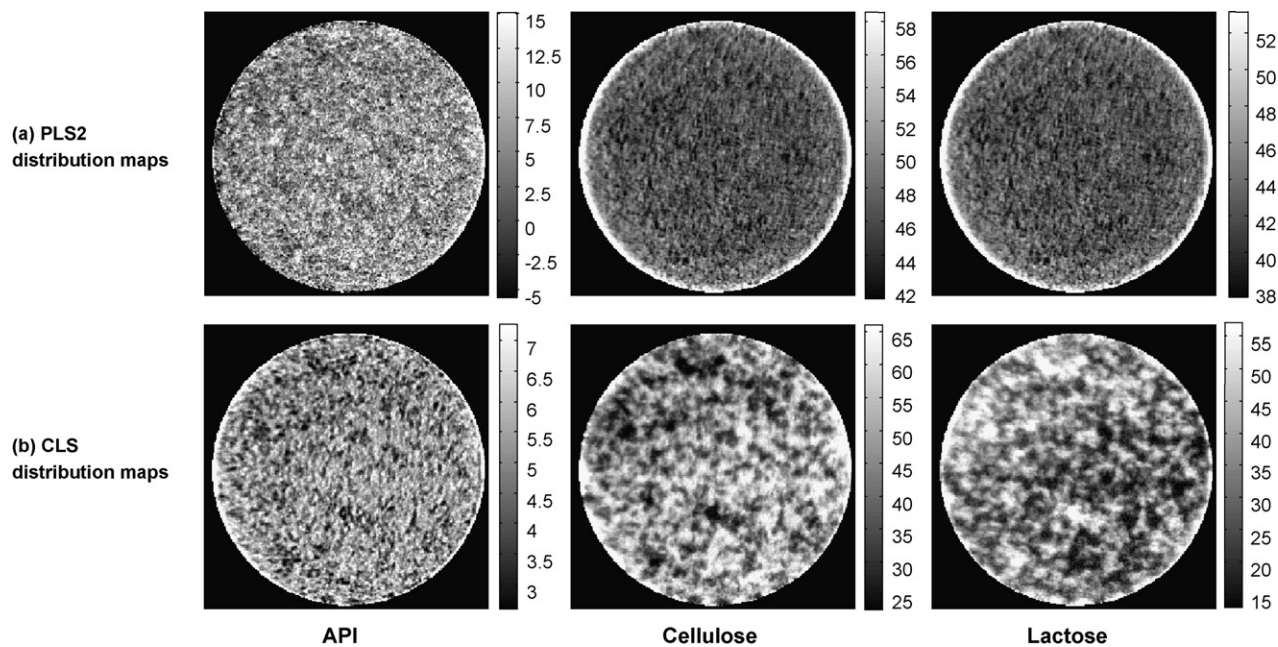


Fig. 8. Pharmaceutical tablet, 7% API<sub>2</sub>, 40  $\mu\text{m}$ /pixel objective: distribution maps of API<sub>2</sub> (left), cellulose (middle), lactose (right) using PLS2 (a) and CLS (b). API<sub>2</sub> is present over all the tablet surface. In the PLS2 regression outlier spectra are present on the tablet border in the cellulose and lactose maps, which are better extracted using CLS. PLS2 also gives some negative API<sub>2</sub> prediction values. White/black pixels: high/low API<sub>2</sub> concentration.

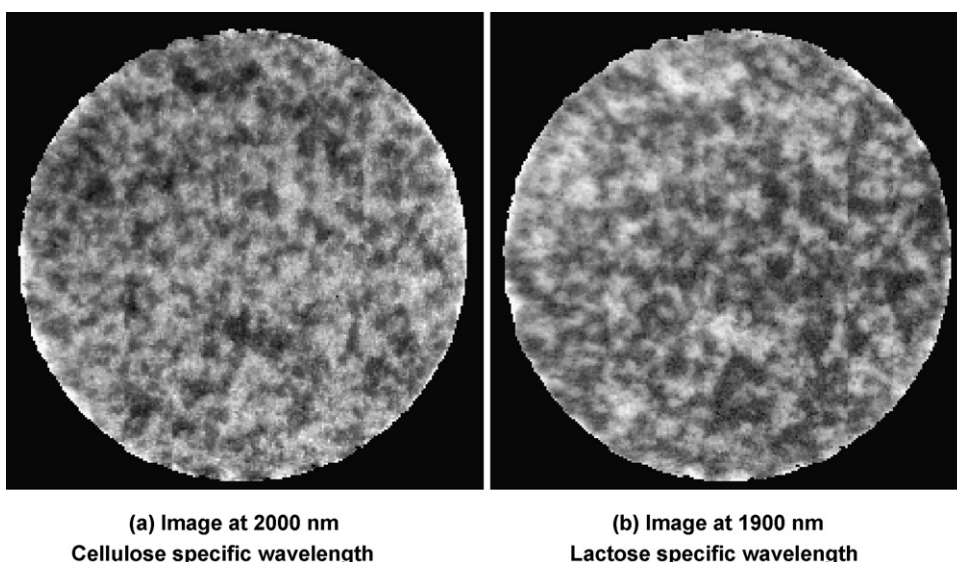


Fig. 9. Images at specific wavelengths showing the same distributions of cellulose and lactose as in Fig. 8b, proving that classical least squares can extract correct distribution maps. White/black pixels: high/low signal intensity.

homogeneity in the pharmaceutical tablet containing 7% API (Fig. 8b). Cellulose and lactose particles agglomerated but API particles were present all over the sample surface.

The distribution maps extracted by CLS were validated against images at specific wavelengths: 2000 nm, specific for cellulose (Fig. 9a), and 1900 nm, specific for lactose (Fig. 9b). Similarity between CLS and specific wavelength distribution maps indicates reliable extraction by CLS. Where the three distribution maps were available, surface distributions could be shown in a single image (Fig. 10).

PLS and CLS provide accurate predictions of API content. However, distribution maps provided by CLS are more interpretable for the analyst.

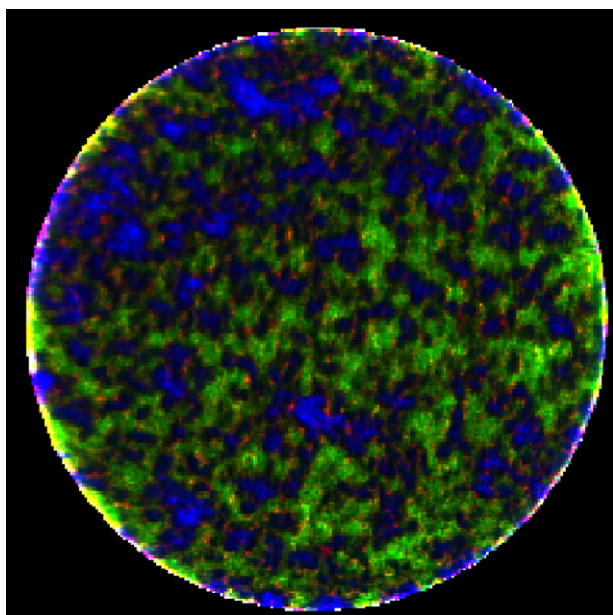


Fig. 10. Tablet reconstruction. White (green in color image): cellulose; black (blue in color image): lactose; grey (red in color image): active pharmaceutical ingredient.

#### 4. Conclusions

In this study comparing PLS2 and CLS for predicting API and excipient content in binary mixtures and pharmaceutical tablets, PLS2 proved more accurate, but CLS also provided reliable predictions of API. Noise worsened prediction with PLS2 when using derivative spectra with both types of sample. However, the derivative procedure increased the accuracy of CLS predictions in samples comprising more than two compounds with overlapping spectral features. The 40  $\mu\text{m}/\text{pixel}$  objective scanned the whole sample area, i.e. a more representative surface, giving better prediction results. However, the 10  $\mu\text{m}/\text{pixel}$  objective can also give good predictions for homogeneous batches and thus provide both high spatial resolution and reliable API concentration.

The study message is that testing API for content uniformity in pharmaceutical samples using NIR imaging based simply on knowledge of the reference spectra is feasible. One outlook of this work would be to test algorithms which use both reference spectra and positivity constraints in order to avoid predictions of negative concentrations and therefore improving the accuracy of the results.

#### Acknowledgments

The authors would like to thank Jérôme Hirtzlin (F. Hoffmann-La Roche) for his help in tablet production.

#### References

- [1] <http://www.fda.gov/cder/OPS/PAT.htm>.
- [2] M. Blanco, R. Gozalez Bano, E. Bertran, Talanta 56 (2002) 203–212.
- [3] Y. Roggo, C. Roeseler, M. Ulmschneider, J. Pharm. Biomed. Anal. 36 (2004) 777–786.
- [4] N. Gat, H.S. Szu, M. Vetterli, W.J. Campbell, J.R. Buss, Proc. SPIE 4056 (2000) 50–64.
- [5] E.N. Lewis, J.E. Carroll, F. Clarke, NIR News 12 (2001) 16–18.

- [6] K.A. Bakeev, *Process Analytical Technology*, Blackwell Publishing, Oxford, 2005.
- [7] F. Clarke, *Vib. Spectrosc.* 34 (2004) 25–35.
- [8] Y. Roggo, A. Edmond, P. Chalus, M. Ulmschneider, *Anal. Chim. Acta* 535 (2005) 79–87.
- [9] Y. Roggo, N. Jent, A. Edmond, P. Chalus, M. Ulmschneider, *Eur. J. Pharm. Biopharm.* 61 (2005) 100–110.
- [10] B.J. Westenberg, C.D. Ellison, A.S. Fussner, S. Jenney, R.E. Kolinski, T.G. Lipe, R.C. Lyon, T.W. Moore, L.K. Reville, A.P. Smith, *Int. J. Pharm.* 306 (2005) 56–70.
- [11] R.C. Lyon, D.S. Lester, E.N. Lewis, E. Lee, L.X. Yu, E.H. Jefferson, A.S. Hussain, *AAPS PharmSciTech* 3 (2002) E17.
- [12] J. Burger, P. Geladi, *Analyst* 131 (2006) 1152–1160.
- [13] N. Jovanovic, A. Gerich, A. Bouchard, W. Jiskoot, *Pharm. Res.* 23 (2006) 2002–2013.
- [14] T.N. Harald Martens, *Multivariate Calibration*, John Wiley & Sons, Chichester, 1991.
- [15] M.K. Antoon, J.H. Koenig, J.L. Koenig, *Appl. Spectrosc.* 31 (1977) 518–524.
- [16] M. Salmain, A. Varenne, A. Vessières, G. Jaouen, *Appl. Spectrosc.* 52 (1998) 1383–1390.
- [17] D.M. Haaland, W.B. Chambers, M.R. Keenan, D.K. Melgaard, *Appl. Spectrosc.* 54 (2000) 1291–1302.

# A fluorescence spectroscopic study of the interaction between epristeride and bovin serum albumine and its analytical application

Aiqin Gong, Xiashi Zhu\*, Yanyan Hu, Suhai Yu

*College of Chemistry & Chemical Engineering, Yangzhou University, Yangzhou 225002, China*

Received 9 January 2007; received in revised form 5 April 2007; accepted 19 April 2007

Available online 5 May 2007

## Abstract

A new spectrofluorimetric method to determine epristeride (EP) has been developed, which based on the EP has a strong ability to quench the intrinsic fluorescence of bovine serum albumin (BSA). There was the relationship between the fluorescence quenching intensity of BSA ( $\Delta F = F_{\text{BSA}} - F_{\text{BSA-EP}}$ ) and the concentration EP. The quenching mechanism was investigated with the quenching type, the association constants, the number of binding sites and basic thermodynamic parameters. The method had been successfully applied to the analysis of EP in real samples and the obtained results were in good agreement with the results of official method-HPLC.

© 2007 Elsevier B.V. All rights reserved.

**Keywords:** Epristeride; Bovine serum albumin; Fluorescence quenching; Spectroscopy

## 1. Introduction

The transport of drugs in vertebrates is usually shouldered by serum albumins. Drugs interactions at protein binding level would significantly affect the apparent distribution volume of the drugs and also affect the elimination rate of drugs. Therefore, investigating the interaction of drugs and serum albumins was significant for knowing the transport and distribution of drugs in body, and for clarifying the action mechanism and pharmaceutical dynamics. For example, Huang et al. studied the interaction of streptomycin sulfate and BSA using flow-injection analysis [1]. Kamat examined the interaction between fluoroquinolones and bovine serum album [2]. Kandagal et al. had investigated the binding mechanism of an anticancer drug with human serum albumin [3]. Wei et al. studied the association behaviors between biliverdin and bovine serum albumin by fluorescence spectroscopy [4]. The transport of drugs in vertebrates was usually shouldered by serum albumins. Drugs interactions at protein binding level would significantly affect the apparent distribution volume of

the drugs and also affect the elimination rate of drugs. Therefore, the interaction of drugs and serum albumins was significant for knowing the transport and distribution of drugs in body, and for clarifying the action mechanism and pharmaceutical dynamics [1–4]. Epristeride [17  $\beta$ -(*N*-*tert*-butyl carboxamido)-androst-3,5-diene-3-carboxylic acid], a 5 $\alpha$ -reductase inhibitor, can decrease prostate size and improve symptoms in men with benign prostatic hyperplasia (Fig. 1) [5–7]. Many researches indicated that the mechanism of action of EP was to inhibit the conversion of testosterone to dihydrotestosterone in the prostate by forming a three-component complex with 5 $\alpha$ -reductase and NADP<sup>+</sup>, so plasma dihydrotestosterone level is decreased and prostatic hyperplasia is inhibited [5,7,8,6,9,10]. Paper [11] determined EP in serum with high performance liquid chromatography. But until now there were seemingly no papers reported to research the interaction of EP with serum albumins. In this paper, the interaction of EP with bovine serum albumin was investigated with spectrum analysis. The mechanism of EP–BSA was discussed from (1) the quenching type; (2) the association constants and the number of binding sites and (3) the basic thermodynamic parameters were obtained. It was synchronously found that the fluorescence quenching degree of BSA ( $\Delta F$ ) had a good relationship with the concentration of EP within the range of 2.0–40.0  $\mu\text{g/mL}$ , so a new spectrofluor-

\* Corresponding author. Tel.: +86 514 7975244; fax: +86 514 7975244.  
E-mail addresses: [xszhu@yzu.edu.cn](mailto:xszhu@yzu.edu.cn), [zhuxiashi@sina.com](mailto:zhuxiashi@sina.com) (X. Zhu).

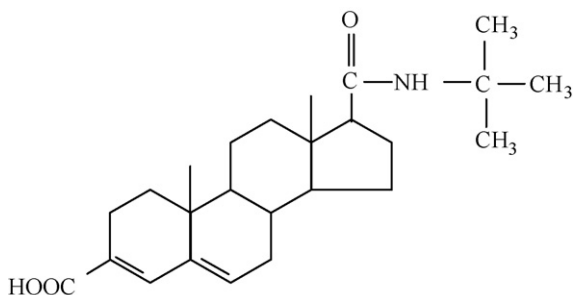


Fig. 1. The structure of epristeride.

rimetric method to determine EP was developed. The proposed method had been successfully applied to analyze EP in real samples and the obtained results were in good agreement with the results of official method, HPLC [12].

## 2. Experimental

### 2.1. Apparatus

A Hitachi F-4500 spectrofluorimeter (Japan) was used for all the fluorescence measurement, with excitation and emission slits at 2.5 nm,  $\lambda_{\text{ex}} = 280$  nm and 1-cm quartz cell. The pH was measured on a pH S-25 pH-meter (Shanghai, China). All absorption spectral recordings and absorbance measurements were performed on a UV 2501 spectrophotometer (Shimadzu, Japan).

### 2.2. Chemicals

Epristeride standard and epristeride tablets (Batch number: 20060401, labeled value: 5 mg/tablet, which excipients included lactose, starch, avicel, methylcellulose and magnesium stearate, were kindly provided by Jiangsu Lianhuan pharmaceutical corporation limited. Bovine serum albumin was purchased from the company of Guoyao (Shanghai, China). All other materials were of analytical reagent grade. Water was distilled, deionised.

A standard bovine serum albumin (BSA) (molecular weight of 65,000) solution of 2.00 mg/mL was prepared by dissolving 0.2 g pure samples in water and making up the volume to 100 mL in a calibration flask and kept in the cool, dark. Lower concentration solutions were prepared by serial dilution.

Epristeride standard solution of 1.00 mg/mL was prepared by dissolving 0.0500 g of epristeride in 50 mL of anhydrous ethanol and kept in the cool, dark.

0.1 mol/L phosphate buffer solution of pH = 7.4 was prepared by dissolving appropriate amounts of  $\text{NaH}_2\text{PO}_4\text{-NaOH}$ .

### 2.3. Procedures

#### 2.3.1. Sample preparation

Ten tablets of epristeride was weighed and crushed, and then sample powder of about one tablet was accurately weighed and placed in a 50 mL of beaker and dissolved with anhydrous ethanol. Insoluble excipient was removed by filtration through

a 0.45  $\mu\text{m}$  membrane filter. The filtered solution was diluted to 50 mL with anhydrous ethanol.

For serum samples, venous blood samples from mice at different time points were collected into heparinized plastic tubes, upon oral administration of 30 mg EP of 1 kg healthy mice. After immediate chilling, the serum was separated by centrifugation at 4 °C within 15 min. The samples were stored at -20 °C until the assay.

#### 2.3.2. Fluorescence and UV spectrum

In a 25 mL volumetric flask, 1.0 mL 2.00 mg/mL of BSA solution, 10.0 mL of phosphate buffer solution (pH = 7.4) and adequate EP standard or sample solution were added, and the solution was diluted to the mark with distilled water. The fluorescence spectra of BSA in the presence or absence of EP were recorded in the range of 250–550 nm with  $\lambda_{\text{ex}} = 280$  nm. The UV spectrum of BSA in the presence or absence of EP was made in the range of 200–320 nm.

Standard addition method was applied to analyze EP in serum samples.

## 3. Results and discussion

### 3.1. Fluorescence quenching of BSA induced by EP in physiological condition

The fluorescence spectra of BSA were recorded before and after incubation with a series concentration of EP in physiological condition (pH = 7.4) at  $\lambda_{\text{ex}} = 280$  nm (Fig. 2). It could be seen from Fig. 2 that there was no fluorescence emission for EP at the range measured and the fluorescence intensity of BSA decreased gradually with the increase of EP concentration without changing the emission maximum and shape of the peaks. These results indicated that there were interactions between EP and BSA. The fluorescence quenching effect was due to the formation of non-fluorescent complexes [13].

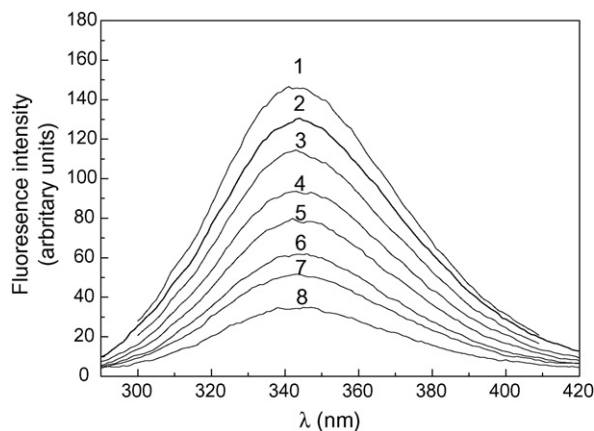


Fig. 2. Fluorescence spectra of BSA  $c_{\text{BSA}} = 80.0 \mu\text{g/mL}$ .  $c_{\text{EP}}$  was at 0.0  $\mu\text{g/mL}$  (1), 2.0  $\mu\text{g/mL}$  (2), 4.0  $\mu\text{g/mL}$  (3), 8.0  $\mu\text{g/mL}$  (4), 12.0  $\mu\text{g/mL}$  (5), 16.0  $\mu\text{g/mL}$  (6), 20.0  $\mu\text{g/mL}$  (7), 28.0  $\mu\text{g/mL}$  (8).

### 3.2. The interaction of drug and protein

The fluorescence intensity of fluorescence substance could be decreased by quenchers such as many drugs or small molecule organic compounds. The intrinsic fluorescence of BSA comes from tryptophan and tyrosyl amino acid residues of its structure. The changes of fluorescence or absorption spectra of BSA reflect the interaction of drugs and macromolecule protein. In this paper the interaction of BSA and EP was discussed from following aspects.

#### 3.2.1. Influence of pH on the drug–protein interaction

The influence of the buffer systems (HAc–NH<sub>4</sub>Ac, NH<sub>3</sub>–NH<sub>4</sub>Cl, citric acid–sodium hydrogen phosphate, NaH<sub>2</sub>PO<sub>4</sub>–NaOH and Tris–hydrochloric acid) and the pH value on the drug–protein interaction was examined from pH = 3.0 to 8.5. The results showed that the fluorescence quenching degree almost had no change in different buffer system and pH region. The buffer of NaH<sub>2</sub>PO<sub>4</sub>–NaOH and the physiological pH 7.4 were chosen for following investigation. The results showed that  $\Delta F$  reached a maximum value when the buffer solution was 10.0 mL. Therefore, a 10.0 mL buffer solution was selected as suitable for the optimized method.

The variation of the EP form in different pH could be reflected by its spectra (Fig. 3). It could be seen from Fig. 3 the absorption spectra of EP shifted with pH. It was known there was carboxyl in EP molecule structure (Fig. 1). The group would ionize when increasing pH. The maximum absorption of EP was 276 nm at pH 3.0. The carboxyl in EP was ionized gradually with the increased and the  $\lambda_{\max}$  shifted blue, and the curves of 1, 2 and 3 (pH = 3.0, 4.0, 5.0, respectively) came possible mainly from its molecule form. When pH > 6.0, the carboxyl was almost ionized so the  $\lambda_{\max}$  was almost no variation ( $\lambda_{\max} = 266$  nm), the curves of 4, 5 and 6 (pH = 6.0, 7.4, 9.0, respectively) were mainly its absorption spectra of ion forms. According front research, it was also known the pH value was almost no influence on the interaction of EP with BSA. So it may be concluded that EP molecule and its ion could react with BSA. But under physio-

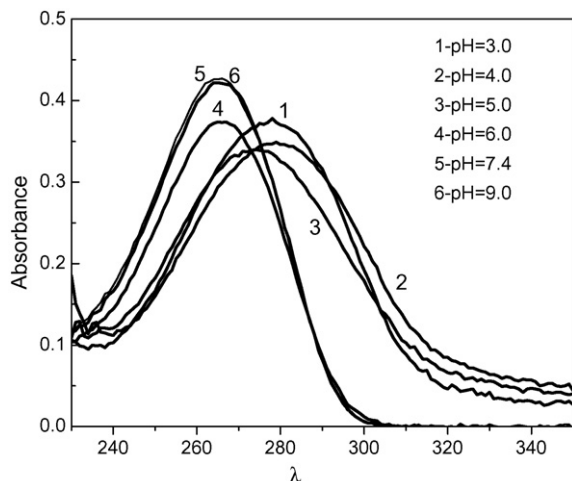


Fig. 3. The absorption spectra of EP under different pH ( $c_{EP} = 8.0 \mu\text{g/mL}$ ).

logical condition the main form of EP reacting with BSA was its ion form.

#### 3.2.2. Quenching type

Generally speaking, the fluorescence quenching is the procedure that could weaken the fluorescence intensity of fluorescence substance, such as excited-state reaction, molecule rearrange, energy transfer, ground state complex formation and collision quenching. It is necessary to know quenching procedure and type for researching the mechanism of quenching. Quenching types often include static and dynamic quenching. The dynamic quenching is that the fluorescence substance collides with quencher, which brings out the decrease of quantum yield and the weak of fluorescence strength. The static quenching is initiated from the formation of non-fluorescent compound. The quenching type was differentiated as follows:

1. The UV absorption spectra of fluorescence substance in the presence of quencher. For dynamic quenching, the absorption spectra of fluorescence substance was not changed only excite-state fluorescence molecule was influenced by quenchers; but for static quenching, a compound is formed between ground state of fluorescence substance and quencher, therefore the absorption spectra of fluorescence substance would be influenced [14].

In this paper, The UV absorption spectra of BSA with or without EP was recorded under pH = 7.4 (Fig. 5). It could be seen from Fig. 4 that the absorption intensity of BSA was enhanced with EP increased. The UV absorption spectrum of BSA was changed due to form a ground state complex (EP–BSA). From this it could be deduced that the fluorescence quenching type of BSA initiated by EP was static quenching.

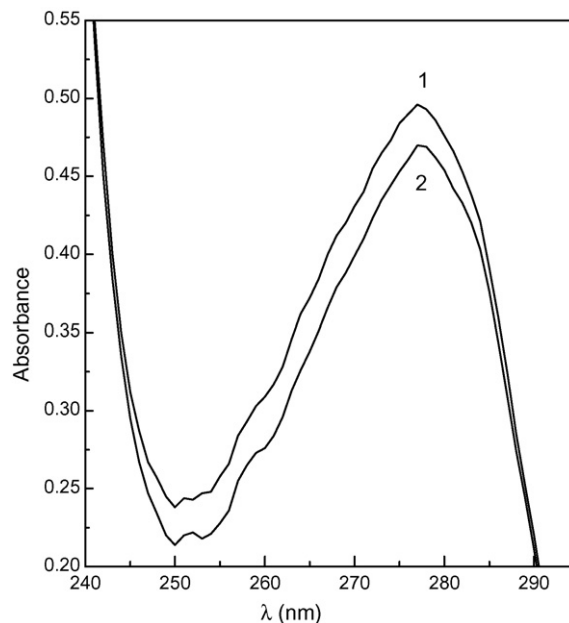


Fig. 4. Effect of EP on UV absorption spectrum of BSA.  $c_{BSA} = 0.8 \text{ mg/mL}$ ;  $c_{EP} = 6.2 \mu\text{g/mL}$ ; (1) absorption spectrum of BSA in the presence of EP; (2) absorption spectrum of BSA.



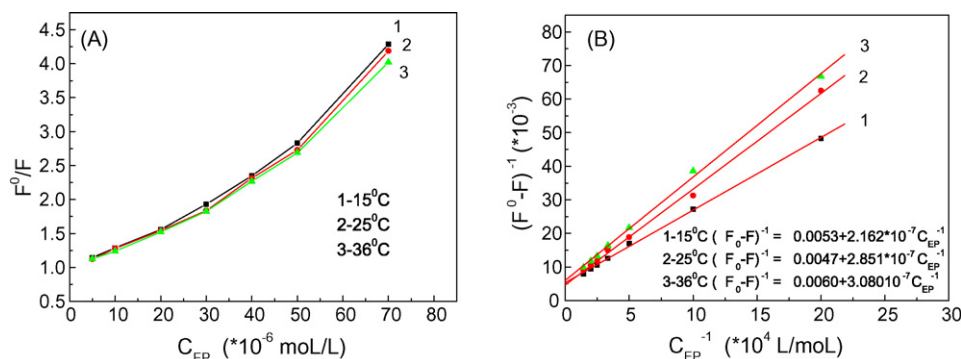


Fig. 5. The Stern–Volmer (A) and Lineweaver–Burk (B) curves at different temperatures ( $c_{\text{BSA}}$ : 80.0  $\mu\text{g/mL}$ ).

2. The fluorescence quenching spectra of fluorescence substance. The fluorescence quenching spectra and quenching type could be analyzed by Stern–Volmer Eq. (1) and Lineweaver–Burk Eq. (2) [15]:

$$\frac{F_0}{F} = 1 + K_{\text{sv}}C_{\text{Q}} = 1 + K_{\text{q}}\tau_0C_{\text{Q}} \quad (1)$$

$$\frac{1}{F_0 - F} = \frac{1}{F_0 + 1/(K_{\text{LB}}F_0C_{\text{Q}})} \quad (2)$$

Among them,  $F_0$  and  $F$  were the fluorescence intensities of BSA in the absence and presence of EP respectively,  $K_{\text{sv}}$  was the Stern–Volmer quenching constant,  $C_{\text{Q}}$  was the concentration of quencher,  $K_{\text{q}}$  is the quenching rate constant,  $\tau_0$  is the average lifetime of the protein without the quencher and  $K_{\text{LB}}$  is static quenching constant.

Within certain concentration, the curve of  $F_0/F$  versus  $C_{\text{Q}}$  (Stern–Volmer curve) would be linear if the quenching type is single static or dynamic quenching [8]; similarly, the curve of  $(F_0 - F)^{-1}$  versus  $C_{\text{Q}}^{-1}$  (Lineweaver–Burk curve) would be linear [16] for static quenching. If the quenching type is combined quenching (both static and dynamic), the Stern–Volmer plot is an upward curvature [1].

The Stern–Volmer curves of EP–BSA in different temperatures were shown in Fig. 5A. It could be seen that when the concentration of EP was lower, the Stern–Volmer curves was linear, while the concentration of EP was higher, the Stern–Volmer curves was upward bent. It illustrated that the quenching type was probable single quenching (static or dynamic quenching) at lower EP concentration. But at higher EP concentration a combined quenching (both static and dynamic) would be obtained.

The Fig. 5B listed the Lineweaver–Burk curves. From Fig. 5B it was known that under certain EP concentration, the curve of  $(F_0 - F)^{-1}$  versus  $C_{\text{Q}}^{-1}$  was linear. All these represented there were obviously characters of static quenching.

3. The effect of temperature on  $K_{\text{sv}}$ . The  $K_{\text{sv}}$  values decrease with an increase in temperature for static quenching, but the reverse effect would be observed for dynamic quenching [1,10].

In this study the values of  $K_{\text{sv}}$  were found to be  $(4.66 \pm 0.033) \times 10^4$  (15 °C),  $(4.57 \pm 0.041) \times 10^4$  (25 °C),

$(4.31 \pm 0.028) \times 10^4$  (36 °C)L/mol. It indicated that the possible fluorescence quenching mechanism of BSA by EP was a static quenching procedure and revealed the formation of a complex between EP and BSA.

4. The quenching rate constants,  $K_{\text{q}}$  ( $K_{\text{q}} = K_{\text{sv}}/\tau_0$ ). As a rule, the maximum scatter collision quenching constant,  $K_{\text{q,r}}$  of various quenchers with the biopolymer was  $2 \times 10^{10}$  L/mol s [1,16], and the value of  $\tau_0$  of the biopolymer was  $10^{-8}$  s [17]. If the  $K_{\text{q}} > K_{\text{q,r}}$ , the fluorescence quenching of biopolymer surely not come from dynamic quenching. In this paper, the  $K_{\text{sv}}$  was  $10^4$  L/mol and the  $K_{\text{q}}$  was the order of  $10^{12}$  L/mol s. Obviously, the  $K_{\text{q}}$  value of protein quenching procedure initiated by EP was greater than the  $K_{\text{q,r}}$  of the scattered procedure. This indicated that the quenching was not initiated from dynamic collision but from the formation of a compound.

### 3.2.3. Binding constants and the number of binding sites

On the assumption that the fluorescence quenching of protein was a static quenching process, i.e. the fluorescence quenching came from a complex formation between protein and quencher, then the equilibrium between free and bound molecule could be given by the following equation [1,18]:

$$\frac{\text{Log}(F_0 - F)}{F} = \text{log } K + n \text{ log } C_{\text{Q}} \quad (3)$$

where  $K$  was the binding constant, reflecting the reaction degree of BSA and EP;  $n$  was the number of binding sites, specifying the number of EP bound to a BSA macromolecule. Thus, a plot of  $\text{Log}(F_0 - F)/F$  versus  $\text{log } c_{\text{EP}}$  could be used to determine  $K$  and  $n$ .

The  $K$  and  $n$  at different temperature were listed in Table 1. It was found that the binding constant decreased with an increase in temperature, resulting in a reduction of the stability of the

Table 1  
Binding constant  $K$  and the number of binding sites  $n$

Temperature (°C)	$K^a$ ( $\times 10^5$ L/mol)	$n^a$
25	$2.589 \pm 0.038$	$1.198 \pm 0.051$
36	$2.293 \pm 0.046$	$1.192 \pm 0.036$

<sup>a</sup> Average value of three determinations.

Table 2  
Thermodynamic parameters

Temperature (°C)	$\Delta H^\circ$ (kJ/mol)	$\Delta S^\circ$ (J/mol K)	$\Delta G^\circ$ (kJ/mol)
15		70.94 ± 0.045	-28.88 ± 0.002
25	-8.45 ± 0.067	75.27 ± 0.058	-30.88 ± 0.005
36		75.24 ± 0.033	-31.70 ± 0.003

EP–BSA complex. Meanwhile, from the data  $n$  ( $n \approx 1$ ) it may be inferred that there was one independent class of binding sites on BSA for EP.

Besides, the number of binding sites  $n$  was also examined by molar ration method. The conclusion was in agreement with the result of fluorescence method.

### 3.2.4. Types of interaction force between EP and BSA

Considering the dependence of binding constant  $K$  (EP–BSA) on temperature, a thermodynamic process was considered to be responsible for the formation of a complex. Therefore, some thermodynamic parameters dependent on temperature such as enthalpy change  $\Delta H^\circ$ , entropy change  $\Delta S^\circ$  and free energy change  $\Delta G^\circ$  were used in order to further characterize the interaction between EP and BSA. Among these parameters,  $\Delta G^\circ$  reflects the possibility of reaction, and  $\Delta H^\circ$  and  $\Delta S^\circ$  are the main evidences to determine acting forces. Usually the acting forces between a small molecule and macromolecule include hydrogen bonds, van der Waals forces, electrostatic forces and hydrophobic interaction forces. When temperature varies in a small range, the  $\Delta H^\circ$  could be considered as a constant, then through binding constant  $K$ , the thermodynamic parameters are evaluated using the following equations:

$$\Delta G^\circ = \Delta H^\circ - T \Delta S^\circ \quad (4)$$

$$\Delta G^\circ = -RT \ln K^\circ \quad (5)$$

$$\ln \left( \frac{K_2}{K_1} \right) = \left( \frac{\Delta H^\circ}{R} \right) \left( \frac{1}{T_1} - \frac{1}{T_2} \right) \quad (6)$$

The  $\Delta H^\circ$ ,  $\Delta G^\circ$  and  $\Delta S^\circ$  at different temperature were shown in Table 2.  $\Delta G^\circ < 0$  clarified there was an automatic reaction happened between EP and BSA.  $\Delta S^\circ > 0$  and  $\Delta H^\circ < 0$  showed that both hydrogen bonds and hydrophobic interaction forces played a role in the binding of EP to BSA [1,18,19].

## 4. Analytical applications

In this work, it was found the fluorescence quenching degree of BSA had a good relationship with the concentration of EP in the range of 2.0–40.0  $\mu\text{g/mL}$ . Hence, a new fluorescence method to determine EP was introduced.

### 4.1. Analytical performance

From Fig. 5, it was known the linearity of Lineweaver–Burk double-reciprocal curve was better than Stern–Volmer curve. Therefore, Lineweaver–Burk double-reciprocal curve was used as working curve for the analysis of EP. Under the experimental

Table 3  
Recoveries of EP from real samples ( $n = 3$ )

Sample	Added ( $\mu\text{g mL}^{-1}$ )	Found ( $\mu\text{g mL}^{-1}$ )	Recovery (%)	R.S.D. (%)
EP tablet	0.0	4.0	–	0.6
	4.0	8.1	102.5	1.8
	6.0	9.8	96.7	1.1
	8.0	11.6	95.0	1.2
Human serum <sup>a</sup>	0.0	–	–	–
	4.0	3.9	97.5	2.3
	6.0	5.7	95.0	1.2
	8.0	7.8	97.5	1.5
Mice serum-1 <sup>b</sup>	0.0	14.3	–	0.9
	4.0	18.5	101.0	1.2
	6.0	20.4	100.5	2.1
	8.0	21.5	96.4	1.1
Mice serum-2	0.0	3.4	–	1.3
	4.0	6.9	93.2	0.8
	6.0	9.2	97.9	1.2
	8.0	10.7	93.9	1.3
Mice serum-2	0.0	3.3	–	1.6
	4.0	7.1	97.3	1.6
	6.0	8.9	95.7	1.1
	8.0	10.9	96.5	1.6

<sup>a</sup> Human serum was kindly provided by healthy volunteers, in which there was no EP.

<sup>b</sup> Mice serum was collected at different time points (3, 4, and 5 h) after oral administration.

conditions, the calibration curve equation was  $(F_0 - F)^{-1} = 4.69 \times 10^{-3} + 1.14 \times 10^{-4} c_{\text{EP}}^{-1}$  ( $c_{\text{EP}}$ , mg/mL),  $r = 0.9989$ . The detection limit estimated ( $S/N = 3$ ) was 0.28  $\mu\text{g/mL}$  and the limit of quantification was 2.0  $\mu\text{g/mL}$ .

The recoveries were obtained based on spiking different levels of concentration of EP into EP tablet and serum sample. The average recoveries of the proposed method were 93.2–102.5% (Table 3).

### 4.2. Effect of potential interferences

A study was carried out on the effects of foreign interferences on the determination of EP (8.0  $\mu\text{g/mL}$ ). With a relative error of less than  $\pm 5\%$ , the tolerance limits for the foreign substance were shown in Table 4.

Table 4  
Tolerance limits of interfering ions ( $\mu\text{g/mL}$ )

Tested ions	Tolerance limit	Tested ions	Tolerance limit
$\text{Ca}^{2+}$	20	$\text{Cr}^{3+}$	8
$\text{Mg}^{2+}$	120	$\text{Mn}^{2+}$	20
$\text{Pb}^{2+}$	6	$\text{CH}_3\text{COO}^-$	600
$\text{Zn}^{2+}$	16	$\text{NH}_4^+$	>2000
$\text{Cd}^{2+}$	20	Citric acid	>2000
$\text{Fe}^{3+}$	0.8	Glucose	>2000
$\text{Al}^{3+}$	8	Lactose	>2000
$\text{SO}_4^{2-}$	400	Sucrose	>2000
$\text{Cu}^{2+}$	1.2 <sup>a</sup>		

<sup>a</sup> In the presence of 8.0 mg/mL trisodium citrate.

Table 5  
Determination of EP in pharmaceutical products and serum ( $n=3$ )

Sample	EP found	R.S.D. (%)
EP tablet <sup>a</sup> -1	5.06 ± 0.04 (mg/tablet)	0.6
EP tablet <sup>a</sup> -2	5.09 ± 0.04 (mg/tablet)	0.5
EP tablet <sup>a</sup> -3	4.99 ± 0.03 (mg/tablet)	0.4
Mice serum <sup>b</sup> -1	0.36 ± 0.003 (mg/mL)	0.9
Mice serum <sup>b</sup> -2	0.084 ± 0.001 (mg/mL)	1.3
Mice serum <sup>b</sup> -3	0.083 ± 0.001 (mg/mL)	1.6

<sup>a</sup> The production date was different.

<sup>b</sup> The collected time of samples was different.

#### 4.3. Analysis of EP in pharmaceutical formulations and serum

The proposed method was applied for the determination of EP in pharmaceutical formulation and mice serum (Table 5). For EP tablet the results obtained by the proposed method were in good agreement with the target value (5 mg/tablet) and the official method (HPLC), which found EP tablet concentration was  $4.98 \pm 0.01$  mg/tablet. The *t*-test method was used to do a significant difference test for these data, and it was found that the data of both methods did not have significant difference.

#### 5. Conclusions

In this paper, the reaction of BSA and EP was first investigated by spectroscopic method. The fluorescence of BSA was quenched by EP with static quenching mechanism. The association constants, the number of binding sites and basic thermodynamic parameters were determined. A new fluorescence analysis of EP was established based on the fluorescence quenching degree of BSA had a good relationship with the con-

centration of EP. The biological significance of this work was evident since albumin serves as a carrier molecule for multiple drugs and the interaction of EP and albumin was not characterized so far. Hence, the report had a great significance in pharmacology and clinical medicine as well as methodology.

#### References

- [1] Y.-M. Huang, Z.-J. Zhang, D.-J. Zhang, J.G. Lv, *Talanta* 53 (2001) 835–841.
- [2] B.P. Kamat, *J. Pharm. Biomed. Anal.* 39 (2005) 1046–1050.
- [3] P.B. Kandagal, S. Ashoka, J. Seetharamappa, S.M.T. Shaikh, Y. Jadegoud, O.B. Ijare, *J. Pharm. Biomed. Anal.* 41 (2006) 393–399.
- [4] Y.-L. Wei, J.-Q. Li, C. Dong, S.-M. Shuang, D.-S. Liu, C.W. Huie, *Talanta* 70 (2006) 377–382.
- [5] Z.-Y. Sun, H.-Y. Wu, M.-Y. Wang, Z.-H. Tu, *Eur. J. Pharmacol.* 371 (1999) 227–233.
- [6] P.R. Audet, N.H. Baine, L.J. Benincosa, *Drugs Fut.* 19 (1994) 646–650.
- [7] M.A. Levy, M. Brandt, K.M. Sheedy, J.T. Dinh, D.A. Holt, L.M. Garrison, D.J. Bergsma, B.W. Metcalf, *J. Steroid Biochem. Mol. Biol.* 48 (1994) 197–206.
- [8] M. Ranjan, P. Diffley, G. Stephen, D. Price, T.J. Walton, R.P. Newton, *Life Sci.* 71 (2002) 115–126.
- [9] J.-H. Wu, Y. Zhu, Z.-Y. Sun, *Yaoxue Jinzhan (Chinese)* 26 (2002) 55–57.
- [10] L.-H. Qian, X.-L. Wang, Z.-H. Tu, *Acta Pharmacol. Sinica* 22 (2001) 847–850.
- [11] V.K. Boppana, C. Miller-Stein, G.R. Rhodes, *J. Chromatogr. A* 631 (1993).
- [12] Chinese Pharmaceutical Standard WS1-(X-075)-20032.
- [13] G.-Z. Chen, X.-Z. Huang, J.-G. Xu, *Spectrofluorimetric Analytical Method [M]*, second ed., Science Press, Beijing, 1990, p. 122.
- [14] X.-W. Zhang, F.-L. Zhao, K.-A. Li, *Chem. J. Chin. Univ.* 20 (1999) 1063–1067.
- [15] H.-L. Guan, H.-P. Yuan, Z.-T. Pan, *J. Instrum. Anal. (Chin.)* 25 (2006) 25–28.
- [16] W.R. Ware, *J. Phys. Chem.* 66 (1962) 445–448.
- [17] J.R. Lakowicz, G. Weber, *Biochemistry* 12 (1973) 4161–4170.
- [18] C.-N. Yan, Y.-F. Shanguan, Z.-T. Pan, Y. Liu, S.-S. Qu, *Chin. J. Anal. Chem.* 32 (2004) 317–319.
- [19] D.P. Ross, S. Subramanian, *Biochemistry* 20 (1981) 3096–3102.

# Rapid analysis of pseudolaric acids in Cortex Pseudolaricis and related medicinal products by high performance liquid chromatography

Quan-Bin Han, Yue-Keung Yip, Nian-Yun Yang, Lina Wong, Chun-Feng Qiao, Jing-Zheng Song, Hillary Yiu, Hong-Xi Xu\*

Chinese Medicine Laboratory, Hong Kong Jockey Club Institute of Chinese Medicine, Hong Kong, China

Received 8 February 2007; received in revised form 27 April 2007; accepted 30 April 2007

Available online 10 May 2007

## Abstract

A simple, rapid, reverse-phase high performance liquid chromatographic method was developed for the quantitative analysis of pseudolaric acids in Cortex Pseudolaricis and its related medicinal products. With a C<sub>18</sub> analytical column (4.6 mm × 150 mm i.d.), five pseudolaric acids, namely pseudolaric acids A–C, pseudolaric acid A-*O*-β-D-glucopyranoside and pseudolaric acid B-*O*-β-D-glucopyranoside, were well separated within 7 min. Acetonitrile and 0.10% acetic acid were used as the mobile phase in a gradient program. The UV detection wavelength was set at 260 nm. The detection limits and quantification limits ranged in 8.26–16.66 ng/ml and 27.54–55.53 ng/ml, respectively. The intra- and inter-day variations were less than 1% for all five compounds. The recovery of all spiked pseudolaric acids ranged from 99.1% to 101.9%. Compared to existing analytical methods, this new method not only used two more important chemical markers but also provided a fivefold reduction in analysis time. In addition, the extraction method of herb sample was also modified by an orthogonal array experiment on three variable parameters: extraction time, solvent volume, and extraction cycles. The optimized extraction method was much simpler and could be efficiently used to analyse large set of herbal materials and related medicinal products. Nineteen herb samples collected from different regions of China and five related products were examined with this new analytical method. The results showed that this method is effective in distinguishing adulterants and unqualified products. © 2007 Elsevier B.V. All rights reserved.

**Keywords:** *Pseudolarix kaempferi* Gord.; Cortex Pseudolaricis; Pseudolaric acids; Quality control; HPLC

## 1. Introduction

Recently, the problems concerning the quality control of herbal products have gained public attention. Due to the complex chemistry and great variation of the medicinal herbs, it is a big challenge to control the quality of each herbal material on the market with the current analytical technologies. To achieve this goal, quick and efficient assessments of large sets of raw herbs and products are much desired. Great efforts have been made to improve analytical methods for quality control on herbal materials [1–5]. In our current study, we have developed a high-throughput analytical method to quality control the herbal material and products of Cortex Pseudolaricis.

Cortex Pseudolaricis, known as “Tujinpi” in Chinese medicine, is the root bark of *Pseudolarix kaempferi* Gord. (Pinaceae). It is native to China and has long been used as a remedy for fungi infection of skin [6,7]. The ethanol extract of Cortex kaempferi was reported to be active against dermatomycoses [6]. A number of diterpenoids have been isolated from Cortex Pseudolaricis including pseudolaric acids A–C (PAA, PAB, and PAC) and two glucosides, pseudolaric acid A-*O*-β-D-glucopyranoside (PAAG) and pseudolaric acid B-*O*-β-D-glucopyranoside (PABG) (Fig. 1) [8–10]. Some of these compounds, such as pseudolaric acids A and B, demonstrated antifungal [6,11], antifertility [12] and cytotoxic activities [13–15]. Many studies have found that pseudolaric acid B, one of the major components in the herb, has antifungal activity against the *Candida* and *Torulopsis* species, which are common pathogens in immunocompromised patients [15]. It has also been reported that pseudolaric acids B had significant cytotoxicity against different tumor cell lines such as CNS cancer TE671, melanoma SK-MEL-5, ovarian cancer A2780, gastric

\* Corresponding author. Tel.: +852 3406 2873; fax: +852 3551 7333.  
E-mail address: [xuhongxi@hkjicm.org](mailto:xuhongxi@hkjicm.org) (H.-X. Xu).

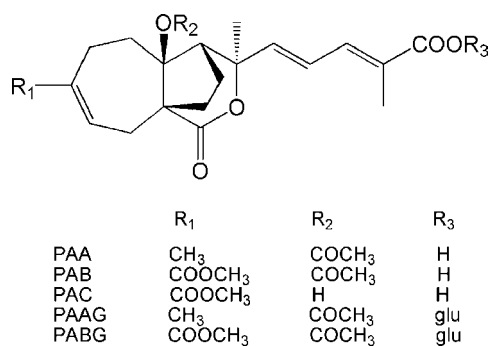


Fig. 1. Structure of the five standard compounds in the study.

cancer AGS and leukemia HL-60 [13,16,17] and pseudolaric acids A and B caused the death of rat embryos by decreasing blood flow in both endo- and myo-metrium [18]. Recently, it was reported that the cytotoxicity of pseudolaric acid B was related to inducing apoptosis [16,19,20] and inhibiting angiogenesis [21–23]. The anti-angiogenesis cytotoxic drug has been used as the target in chemotherapy, which highly increased survival rates. These diterpenoids were therefore targeted as potential antitumor drugs. In addition, Cortex Pseudolaricis has been widely used by Chinese medicine practitioners for the cure of different skin infections. Some related Chinese medicine preparation, for example, ‘ONCE OK Spray’, claimed to be effective in the treatment of different kinds of tinea, such as athlete’s foot, and were popularly used. Chinese Pharmacopoeia 2005 classified it as a toxic herb and does not recommend oral administration.

Since the genus *Pseudolarix* has only this species, the plant resource is not very rich. Its adulterants are often found in the market; they look morphologically similar to the authentic herbs and are difficult to distinguish [24]. The chromatographic analytical method is often used as a chemical authentication tool. In literatures [24–26], the TLC scanning and HPLC method were most widely used for analysis of these bioactive pseudolaric acids. While providing excellent resolution, these existing methods had several shortcomings. First, they used only pseudolaric acids A–C as the chemical markers, without including two important major glycosides, PAAG and PABG. These compounds can easily be converted to PAA and PAB by hydrolysis and therefore should be examined together. Second, the 1-h reflux extraction was required for their sample preparation and thus not practicable for high-throughput analysis in the quality control of herbal material and products. Third, long analysis times resulted in inefficiency, as they required the use of large volumes of solvents and instrument time that could have otherwise been used for other analysis. A quick, easy, high-throughput, and more comprehensive method with significantly shorter HPLC analysis time is required to facilitate more extensive studies with large sample sets. The specific objective of this study was to develop an improved method for the analysis of pseudolaric acids using commonly available HPLC equipment in order to reduce total analysis time, thereby improving efficiency, reducing analytical costs, and increasing sample throughput.

## 2. Experimental

### 2.1. Chemical and reagents

PAA and PABG were isolated from the root bark of *Pseudolarix kaempferi* Gord. by our laboratory. Three reference standards, PAA, PAB and PAC, were purchased from the National Institute for the Control of Pharmaceutical and Biological Products of China (NICPBP, China). Their structures were established based on spectroscopic data including NMR analysis. Their purities were all determined to be over 95% by HPLC-DAD analysis. These five pseudolaric acids were very stable in methanol. Methanol (MeOH) (HPLC grade) was purchased from Duksan chemical Co., Ltd. Acetonitrile (ACN) (HPLC grade), acetic acid (HAc) (HPLC grade) and silica gel H (200–300 mesh) were purchased from International Laboratory Ltd. (USA), respectively. HPLC-grade water was obtained from a Millipore Milli-Q Reagent Water System. An Elma Transsonic 700/H ultra-sonicator was used for extraction.

Nineteen samples of Cortex Pseudolaricis were collected from different provinces in the People’s Republic of China. Their microscopic identification was performed by Dr. Chun-Feng Qiao, Chinese Medicine Laboratory, Hong Kong Jockey Club Institute of Chinese Medicine (HKJCICM), Shatin, Hong Kong. Eight herb samples were identified as adulterants. The voucher species were deposited at HKJCICM. The five products of Cortex Pseudolaricis were bought in Hong Kong.

### 2.2. Instrumentation

HPLC analysis was carried out by a Waters 2695 Separations Module HPLC system and a Waters 2996 Photodiode Array Detector. Acquisitions were made using Empower Pro software version 5.00.00.00. LC separation was performed on a Waters SunFire™ C18 separation column (5 μm, 4.6 mm × 150 mm) at 25 °C under UV detection at 260 nm, using acetonitrile and 0.10% acetic acid in water as mobile phase under gradient program with a flow of 1 ml/min—0–3 min: 40% ACN → 60% ACN; 3–4 min: 60% ACN → 85% ACN; 4–7 min: 100% ACN → 100% ACN.

### 2.3. Sample preparation

The standard stock solutions containing all five pseudolaric acids at a concentration of 2.00 mg/ml each were prepared in methanol. They were diluted with methanol to obtain working standard solutions at a concentration of 1.00 mg/ml and 0.50 mg/ml. All standard solutions were stored at 4 °C in the dark.

The herbal samples of Cortex Pseudolaricis collected from different regions of China were pulverized. 0.50 g of powder was accurately weighed and placed into a 20 ml volumetric flask. Then, 10 ml methanol was added. Thereafter, the flask was ultra-sonicated for 30 min and the supernatant was transferred to a 10 ml flask. The extraction was repeated and all the supernatants were combined into the 20 ml volumetric flask. About 1 ml methanol was used to rinse the 10 ml flask and to makeup

the final volume. Three aliquots of the solution (20  $\mu$ l each) were analyzed by HPLC-DAD system after being filtered through a 0.2  $\mu$ m syringe membrane filter. Five products of Cortex Pseudolaricis in three different dosage forms were tested in this study. The spray and liquid proprietary samples were directly analyzed after filtration. The powder-form preparations were extracted and checked using the same method as the herbal samples.

#### 2.4. Method validation

The linearity validation was performed on the mixture of the five known concentration standard solutions with reference to the content ratios among different standards in herbal samples. The standard mixture then went through a twofold serial dilution to obtain seven standard mixtures with different concentrations. The standard mixtures were injected into HPLC system in triplicates. A calibration curve was constructed by linear regression of the detector response of each analyte (peak area) versus the analyte concentration.

The precision was evaluated by calculating the intra- and inter-day relative standard deviation (R.S.D.) in triplicate. The intra-day precision was referred as the repeatability of the assay and examined within 1 day ( $n = 3$ ), while the inter-day precision was determined on 5-day intervals ( $n = 5$ ).

The recovery for the five pseudolaric acids of this method was examined on fortified samples at different concentrations. The contents of the five pseudolaric acids in sample were estimated according to their respective calibration curve. A different amount of the five standard compounds was spiked into the sample at 0.7-, 1.0-, and 1.3-fold of the estimated mass of each analyte, respectively. Six parallel samples were prepared for each spike operation. Then, the spiked samples were extracted and analyzed as described above in triplicate. The recovery for each analyte was evaluated by comparing the mass difference of the analyte between the spiked samples and the original sample with the nominal mass of the analyte spiked in the fortified samples.

The limit of detection (LOD) and limit of quantitation (LOQ) for each analyte were calculated with the standard on the basis of a signal-to-noise ratio (S/N) of 3 and 10, respectively.

### 3. Result and discussion

#### 3.1. Optimization of the extraction method

The extraction method recorded in Chinese Pharmacopoeia 2005 included a time-consuming operation of reflux (1 h) [24], and therefore was not practicable to test large sample sets. A simpler and quicker extraction method was necessary for high-throughput analysis of herb samples. We compared the operations of reflux and ultra-sonication by HPLC analysis. Both methods showed similar extraction capability in terms of the contents of five pseudolaric acids when the extraction time and solvent volume were set at 1 h and 50 ml methanol. It was suggested that the ultra-sonication could be a simple alternative to reflux. Then, we optimized the ultra-sonication operation. Three different parameters (three variables each) of extraction were

Table 1  
Orthogonal array design to optimize the ultra-sonic extraction of herb sample

Group <sup>a</sup>	Extraction parameters		
	Extract cycles <sup>b</sup> , A	Time, B (min)	Methanol, C (ml)
1	1	10	10
2	1	20	25
3	1	30	50
4	2	10	25
5	2	20	50
6	2	30	10
7	3	10	50
8	3	20	10
9	3	30	25

<sup>a</sup> Nine groups having different combinations of parameters during the sample extraction. Each group contained 0.5 g of Cortex Pseudolaricis powder as the starting material, three batches were done ( $n = 3$ ).

<sup>b</sup> The residue after the first extraction was reextracted by the same volume of methanol for the same time as listed in the individual group.

studied by an orthogonal array design of  $L_9$  ( $3^4$ ). Extracts from nine groups having variations in three parameters of extractions including extraction time, solvent volume, and extraction cycles, were established in triplicate as displayed in Table 1.

Five chemical markers were determined in these extracts and showed similar variation under nine different extractions. These different parameters were analyzed statistically and the results were summarized in Table 2. The duration of extraction and the number of repeated extractions were two crucial parameters for the higher yield of all five markers ( $P < 0.01$ ), while extraction volume was a subordinate factor ( $P > 0.05$ ). Furthermore, two extraction cycles and three extraction cycles showed similar effects on the yield, and their differences were not statis-

Table 2  
Analyses of variances in the extraction

Index	Source of variation <sup>a</sup>	$F^b$	$P^c$	Optimized parameters
PABG	A	94.33	<0.01 <sup>d</sup>	2 cycles
	B	50.23	<0.01	30 min
	C	0.71	>0.05	10 ml
PAC	A	36.73	<0.01 <sup>d</sup>	2 cycles
	B	15.64	<0.01	30 min
	C	1.22	>0.05	10 ml
PAAG	A	49.36	<0.01 <sup>d</sup>	2 cycles
	B	26.17	<0.01	30 min
	C	2.43	>0.05	10 ml
PAB	A	186.53	<0.01 <sup>d</sup>	2 cycles
	B	164.09	<0.01	30 min
	C	0.42	>0.05	10 ml
PAA	A	88.55	<0.01 <sup>d</sup>	2 cycles
	B	46.58	<0.01	30 min
	C	1.21	>0.05	10 ml

<sup>a</sup> The calibration was repeated in triplicate ( $n = 3$ ).

<sup>b</sup> Calibrated by using SPSS statistical software, where  $F_{0.01}(2,18) = 7.2148$ ;  $F_{0.05}(2,18) = 4.5597$ .

<sup>c</sup> Level of significance.

<sup>d</sup> The differences between two cycles and three cycles are not statistically significant,  $P < 0.02$ .

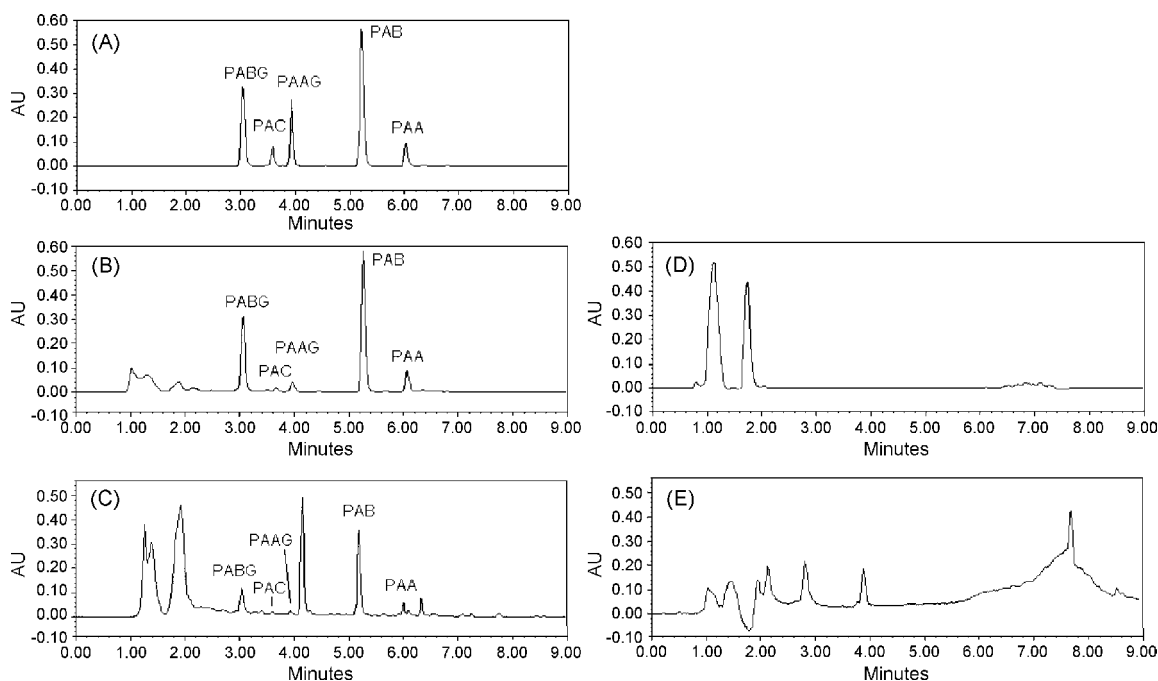


Fig. 2. Representative chromatograms for reference standards mixture (A), reference herb sample No. 19 (B), drug sample no. 1 (drug-1) (C), adulterant herbal sample (D), and unqualified drug sample (E). HPLC conditions: column, Waters SunFire™ C18 separation column (5  $\mu$ m, 4.6 mm  $\times$  150 mm); column temperature, 25 °C; mobile phase, ACN–0.1% HAc; gradient program: 0–3 min: 40% ACN  $\rightarrow$  60% ACN; 3–4 min: 60% ACN  $\rightarrow$  85% ACN; 4–7 min: 100% ACN  $\rightarrow$  100% ACN; flow rate, 1 ml/min.

tically significant ( $P < 0.02$ ). Therefore, the optimized extraction parameters should be two cycles, 30 min extraction, and 10 ml. In contrast with the previously reported methods [24], this new ultra-sonication extraction can quickly and simultaneously prepare the extraction and is therefore more practicable for large herb sample sets.

### 3.2. Chromatograms

Representative chromatograms for five standard pseudolaric acids and herb samples were shown in Fig. 2. As shown in Fig. 2A, all five standard pseudolaric acids were successfully eluted in 7 min with baseline separation. Fig. 2B exhibits that other constituents of the herb sample did not interfere with the analysis of these five target pseudolaric acids. The retention times were  $3.08 \pm 0.05$  min for PABG,  $3.63 \pm 0.05$  min for PAC,  $3.99 \pm 0.05$  min for PAAG,  $5.21 \pm 0.05$  min for PAB, and  $6.01 \pm 0.05$  min for PAA, respectively. Component peaks in samples were identified based on the retention times and UV spectrums of reference standards. The analysis time for all five chemical markers was significantly shortened, due to the appli-

cation of a shorter analytical column and a modified elution gradient.

### 3.3. Validation

The experimental results showed that the peak area of each standard was linearly correlated to the concentration within a certain range. The equations and the linear ranges were listed in Table 3. The LOD and LOQ for each standard compound were also summarized in Table 3. The LOD ranged from 8.26 ng/ml for PAB to 16.66 ng/ml for PAAG and the LOQ from 27.54 ng/ml for PAB to 55.53 ng/ml for PAAG.

The precision was estimated on the standard compounds of a set of triplicate samples with the same concentration. Table 4 summarizes the relative standard deviation for pseudolaric acids A, B, C and PAAG and PABG at different concentrations. The R.S.D. of intra-day and inter-day precisions were less than 1%. The precisions of the newly developed analytical method were excellent.

Appropriate amount of each standard was spiked into samples with known concentrations of five analytes to give fortified

Table 3  
Linear equations, limits of detection (LOD), and limit of quantitation (LOQ) for five pseudolaric acids ( $y$  = peak area;  $x$  = concentration of pseudolaric acids)

Pseudolaric acids	Linear equation	$r^2$	Linearity range ( $\mu$ g/ml)	LOD (ng/ml, S/N = 3)	LOQ (ng/ml, S/N = 10)
PABG	$y = 13853x + 3762.8$	0.9999	3.60–230.66	11.61	38.69
PAC	$y = 17564x + 601.17$	0.9997	0.15–9.76	9.07	30.24
PAAG	$y = 9597.9x + 331.36$	0.9998	0.61–38.98	16.66	55.53
PAB	$y = 19546x + 8429.1$	0.9999	4.29–274.50	8.26	27.54
PAA	$y = 20685x - 1431.6$	0.9997	0.64–40.77	8.27	27.56

Table 4  
Summary of assay precisions for pseudolaric acids in three triplicate samples for each of concentrations (6.25 mg/ml, 12.5 mg/ml, and 25 mg/ml)

Pseudolaric acids	Sample concentration (mg/ml)	Intra-day precision (n = 3)		Inter-day precision (n = 5)	
		Mean amount of analyte (μg/g)	R.S.D. (%)	Mean amount of analyte (μg/g)	R.S.D. (%)
PABG	6.25	1126.25	0.02	1126.44	0.02
	12.5	2270.68	0.18	2272.40	0.07
	25	4535.39	0.18	4539.66	0.10
PAC	6.25	40.61	0.01	40.65	0.13
	12.5	82.70	0.03	82.64	0.06
	25	166.61	0.16	166.61	0.01
PAAG	6.25	192.66	0.03	192.69	0.04
	12.5	386.84	0.03	386.89	0.01
	25	771.30	0.82	775.06	0.65
PAB	6.25	1327.00	0.04	1327.28	0.02
	12.5	2679.97	0.17	2675.93	0.02
	25	5348.39	0.60	5358.87	0.21
PAA	6.25	187.46	0.06	187.48	0.01
	12.5	371.93	0.06	372.30	0.20
	25	739.45	0.46	740.80	0.24

samples. These fortified samples were processed and measured as described in Section 2.3 and the recovery for the five pseudolaric acids was calculated. As shown in Table 5, the recovery of these spiked standards ranged from 98.2% to 103.4% and was satisfactory.

### 3.4. Method performance in assay of samples

Nineteen samples of the root bark of *Pseudolarix kaempferi* were assayed in triplicate using the analytical procedure described above. They were mainly collected from two provinces in China: Henan and Jiangsu. The sample from Hong Kong and the reference herb from NICBPB were also included. As shown in Table 6, all 5 targeted compounds can only be

found in 11 samples (Fig. 2B). All samples were similar in physical appearance and therefore difficult to authenticate. After microscopic identification, eight of the samples were identified not to be Cortex Pseudolaricis. One of them was Cortex Kadsura Radicis (Root bark of Kadsura Radicis, Magnoliaceae family) and the others were definitely adulterants but needed further identification. The herbs used in a certain region might be different from that in another, even though they have the same name. This 'same name different herb' situation is fairly common and can sometimes cause serious adulteration of medicinal herbs. In this study, all the five tested proprietary products were labeled as Cortex Pseudolaricis remedy, but only one was found to contain the herb (Fig. 2C and E). It was also proved that this new analytical method was efficient for the

Table 5  
Recovery of spiked pseudolaric acids in herbal material

Pseudolaric acids	Original (mg/ml)	Spiked (mg/ml)	Found (mg/ml)	Recovery (%)	Mean (%)	R.S.D. (%)
PABG	56.47	23.69	80.43 ± 0.05	101.1	100.7	0.44
		57.66	114.52 ± 0.11	100.7		
		97.79	154.49 ± 0.12	100.2		
PAC	2.07	0.98	3.09 ± 0.03	103.4	101.9	1.32
		2.43	4.53 ± 0.06	101.4		
		4.20	6.30 ± 0.08	100.8		
PAAG	9.62	4.01	13.67 ± 0.04	100.8	100.5	0.29
		9.76	19.42 ± 0.05	100.3		
		16.57	26.24 ± 0.10	100.3		
PAB	66.53	28.30	95.29 ± 0.12	101.6	101.0	0.59
		68.49	135.58 ± 0.13	100.8		
		116.53	183.61 ± 0.18	100.5		
PAA	9.28	4.25	13.45 ± 0.03	98.2	99.1	0.72
		10.31	19.52 ± 0.06	99.4		
		17.40	26.60 ± 0.07	99.6		



Table 6

The contents of the five pseudolaric acids in samples of Cortex Pseudolaricis (mean  $\pm$  R.S.D.,  $\mu\text{g/g}$ ,  $n = 3$ )

Sample no.	Collected from	PABG ( $\mu\text{g/g}$ )	PAC ( $\mu\text{g/g}$ )	PAAG ( $\mu\text{g/g}$ )	PAB ( $\mu\text{g/g}$ )	PAA ( $\mu\text{g/g}$ )
1	Henan	757.69 $\pm$ 29.66	331.54 $\pm$ 13.0	33.18 $\pm$ 0.44	7313.10 $\pm$ 150.01	886.58 $\pm$ 30.14
2	Jiangsu	3988.50 $\pm$ 101.37	203.37 $\pm$ 11.42	551.22 $\pm$ 22.01	4828.92 $\pm$ 132.38	584.65 $\pm$ 25.21
3	Jiangsu	4212.47 $\pm$ 112.07	248.27 $\pm$ 12.02	756.70 $\pm$ 45.28	4956.10 $\pm$ 128.00	642.93 $\pm$ 21.15
4	Jiangsu	6362.91 $\pm$ 201.21	1044.34 $\pm$ 34.15	714.12 $\pm$ 19.48	5566.86 $\pm$ 157.24	588.29 $\pm$ 20.38
5	Jiangsu	672.83 $\pm$ 18.29	985.26 $\pm$ 40.45	43.36 $\pm$ 1.56	5255.20 $\pm$ 135.21	571.13 $\pm$ 17.61
6	Jiangsu	3729.21 $\pm$ 88.05	186.88 $\pm$ 5.58	562.61 $\pm$ 25.06	6567.14 $\pm$ 155.04	854.18 $\pm$ 26.05
7	Jiangsu	2003.19 $\pm$ 62.10	421.02 $\pm$ 15.19	290.51 $\pm$ 11.01	4057.27 $\pm$ 111.02	568.81 $\pm$ 16.60
8	Jiangsu	4350.81 $\pm$ 103.18	413.48 $\pm$ 14.25	914.59 $\pm$ 32.34	4260.23 $\pm$ 114.17	554.03 $\pm$ 14.04
9	Jiangsu	2179.02 $\pm$ 45.04	390.47 $\pm$ 13.09	539.00 $\pm$ 21.42	5882.06 $\pm$ 137.13	779.62 $\pm$ 16.05
10	Shanxi	6839.92 $\pm$ 156.22	116.42 $\pm$ 1.54	918.40 $\pm$ 30.29	4722.03 $\pm$ 133.16	532.09 $\pm$ 12.38
11	NICPBP	4218.49 $\pm$ 123.22	404.79 $\pm$ 3.17	648.21 $\pm$ 17.06	5742.08 $\pm$ 135.23	657.29 $\pm$ 18.04
12	Drug-1	183.27 $\pm$ 4.37	12.01 $\pm$ 0.27	35.77 $\pm$ 0.61	383.38 $\pm$ 2.05	35.34 $\pm$ 0.84

quality control of Cortex Pseudolaricis and its related products.

Furthermore, according to Table 6, the contents of the five standard compounds ranged from 672.83  $\mu\text{g/g}$  to 6839.92  $\mu\text{g/g}$  for PABG, 116.42  $\mu\text{g/g}$  to 1044.34  $\mu\text{g/g}$  for PAC, 33.18  $\mu\text{g/g}$  to 918.40  $\mu\text{g/g}$  for PAAG, 4057.27  $\mu\text{g/g}$  to 7313.10  $\mu\text{g/g}$  for PAB and 532.09  $\mu\text{g/g}$  to 886.58  $\mu\text{g/g}$  for PAA. The total content of the five compounds ranged from 7340.81  $\mu\text{g/g}$  to 14276.51  $\mu\text{g/g}$ . Besides the known major bioactive ingredient PAB, its glycoside PABG was shown to be a major constituent since its content was even higher than PAB in the sample from Shanxi. Among the five compounds, two glucosides had the widest content variation range. This may be due to the fact that some herbs might have been washed with water or treated with different processes after harvesting. Since these two glycosides were water-soluble, they could easily be washed away, thereby reducing the amount. On the other hand, the varied glycoside contents might have affected the contents of their aglycones because of a possible transformation between the two. Similar transformations can also be found in other herbs. For example, the herbal material of Fructus Psoraleae always showed a significant variation of its major components, namely psoralen, isopsoralen and their related glycosides. However, after complete hydrolysis, the glycosides were converted into psoralen and isopsoralen, the contents of which increased to a much stable level [27]. Compared to the previously reported analytical methods [24], the newly established HPLC analysis was able to determine not only the well-known pseudolaric acids but also their glycosides, and therefore more capable and comprehensive.

#### 4. Conclusion

The method developed in this study provided a quick, comprehensive and accurate identification and quality control of Cortex Pseudolaricis and its related products using five bioactive markers. Calibration and reproducibility data indicate that this rapid, high-throughput HPLC method is repeatable, reproducible, and sensitive. This method not only represented a fivefold reduction in total analysis time (7 min, as opposed to 30 min, on average) but also covered two more important chem-

ical markers. Furthermore, the sample preparation was much simpler, and therefore available for high-throughput sample tests in QC of herbal material and drug production. This new method was successfully used to evaluate the quality of Cortex pseudolaricis and its related products and efficiently identify adulterants and unqualified products.

#### Acknowledgement

This research was funded by the Hong Kong Jockey Club Charities Trust.

#### References

- [1] C. Rivasseau, A.M. Boisson, G. Mongéard, G. Couram, O. Bastien, R. Bligny, J. Chromatogr. A 1129 (2006) 283.
- [2] P.Q. Tranchida, M.L. Presti, R. Costa, P. Dugo, G. Dugo, L. Mondello, J. Chromatogr. A 1103 (2006) 162.
- [3] S.P. Ip, C.T. Che, J. Chromatogr. A 1135 (2006) 241.
- [4] G.H. Lu, K. Chan, C.L. Chan, K. Leung, Z.H. Jiang, Z.Z. Zhao, J. Chromatogr. A 1046 (2004) 101.
- [5] H.B. Xiao, M. Krucker, K. Albert, X.M. Liang, J. Chromatogr. A 1032 (2004) 117.
- [6] J.X. Wu, R.S. Hu, G.L. Yang, J. Chin. Dermatol. 8 (1960) 18.
- [7] J.H. Tang, X.X. Zhang, W. Liu, G.L. Wang, J. Liaoning Norm. Univ. 28 (2005) 3.
- [8] Z.L. Li, D.J. Pan, C.Q. Hu, Q.L. Wu, S.S. Yang, G.Y. Xu, Acta Chim. Sin. 40 (1982) 447.
- [9] Z.L. Li, K. Chen, D.J. Pan, G.Y. Xu, Acta Chim. Sin. 43 (1985) 786.
- [10] Z.L. Li, D.J. Pan, Q.L. Wu, G.Y. Xu, Acta Chim. Sin. 40 (1982) 757.
- [11] B.N. Zhou, B.P. Ying, G.Q. Song, Z.X. Chen, J. Han, Y.F. Yan, Plant. Med. 47 (1983) 35.
- [12] J.Y. Ma, Acta Acad. Med. Shanghai 15 (1988) 208.
- [13] D.J. Pan, Z.L. Li, C.Q. Hu, K. Chen, J.J. Chang, K.H. Lee, Plant. Med. 56 (1990) 383.
- [14] B. Liu, H. Chen, Z.-Y. Lei, P.-F. Yu, B. Xiong, J. Asian Nat. Prod. Res. 8 (2006) 241.
- [15] E. Li, A.M. Clark, C.D. Hufford, J. Nat. Prod. 58 (1995) 57.
- [16] K.S. Li, X.F. Gu, P. Li, Y. Zhang, Y.S. Zhao, Z.J. Yao, N.Q. Qu, B.Y. Wang, World J. Gastroenterol. 11 (2005) 7555.
- [17] M. Zhang, X. Mo, X.Y. Chen, L.Z. Li, Chin. Tradit. Herb. Drugs 33 (2002) 533.
- [18] W.C. Wang, Z.P. Pu, A. Koo, W.S. Chen, Acta Pharmacol. Sin. 12 (1991) 423.
- [19] X.F. Gong, M.W. Wang, Z. Wu, S.I. Tashiro, S. Onodera, T. Ikejima, Exp. Mol. Med. 36 (2004) 551.

- [20] X. Gong, M.W. Wang, S.I. Tashiro, S. Onodera, T. Ikejima, *Arch. Pharm. Res.* 28 (2005) 68.
- [21] Y.G. Tong, X.W. Zhang, M.Y. Geng, J.M. Yue, X.L. Xin, F. Tian, X. Shen, L.J. Tong, M.H. Li, C. Zhang, W.H. Li, L.P. Lin, J. Ding, *Mol. Pharm. Fast Forw.* 10 (2006) 1124.
- [22] M.H. Li, Z.H. Miao, W.F. Tan, J.M. Yue, C. Zhang, L.P. Lin, X.W. Zhang, J. Ding, *Clin. Cancer Res.* 10 (2004) 8266.
- [23] W.F. Tan, X.W. Zhang, M.H. Li, J.M. Yue, Y. Chen, L.P. Lin, J. Ding, *Eur. J. Pharmacol.* 499 (2004) 219.
- [24] The Pharmacopoeia Committee of China, *The Chinese Pharmacopoeia*, vol. I, The Chemical Industry Publishing House, 2005, p. 14.
- [25] X.F. Zhai, Z.R. Zhang, G.H. Li, W.J. Sun, *Chin. Tradit. Herb. Drugs* 35 (2004) 93.
- [26] C.F. Qiao, Q.B. Han, J.Z. Song, S.F. Mo, C. Tai, H.X. Xu, *Food & Drug Anal.* 14 (2006) 353.
- [27] C.F. Qiao, Q.B. Han, J.Z. Song, S.F. Mo, L.D. Kong, H.F. Kung, H.X. Xu, *Chem. Pharm. Bull.* 54 (2006) 887.

## Plasmid DNA isolation using amino-silica coated magnetic nanoparticles (ASMNPs)

Xiaoxiao He, Hailing Huo, Kemin Wang\*,  
Weihong Tan, Ping Gong, Jia Ge

State Key Laboratory of Chemo/Biosensing and Chemometrics, Engineering Center for biomedicine, Institute of Life Science & Biological Technology, Key Laboratory for Bio-Nanotechnology and Molecule Engineering of Hunan Province, Changsha 410082, PR China

Received 12 February 2007; received in revised form 26 April 2007; accepted 30 April 2007

Available online 22 May 2007

### Abstract

A simple and efficient approach for the rapid isolation of plasmid DNA from crude cell lysates has been described. The approach took advantage of the amino-modified silica coated magnetic nanoparticles (ASMNPs) with positive zeta potential at neutral pH and superparamagnetism under the external magnetic fields. As a demonstration, the pEGFP-N3 plasmid has been concentrated and isolated from the *E. coli* DH5 $\alpha$  transformed with pEGFP-N3 plasmid through electrostatic binding between the positive charge of the amino group of ASMNPs and the negative charge of the phosphate groups of the plasmid DNA. Then the pEGFP-N3 plasmid has been released easily and quickly from the pEGFP-N3 plasmid–ASMNPs complexes with 3 M NaCl. The entire procedure could be carried out by the aid of external magnetic fields in 15 min and eliminate the need of phenol, cesium chloride gradients or other noxious reagents and complexes operation. Moreover, the pEGFP-N3 plasmid obtained by this approach retains biological activity that can be suitable for restriction enzyme digestion and cells transfection with expression of green fluorescence protein. © 2007 Elsevier B.V. All rights reserved.

**Keywords:** Amino-silica coated magnetic nanoparticles (ASMNPs); pEGFP-N3 plasmid–ASMNPs complexes; Isolation of plasmid DNA

### 1. Introduction

The isolation of high quality, biologically active plasmid DNA is extremely important in the field of biotechnology. And the demand for efficient production methods of plasmid DNA has increased vastly for its widely applications in gene therapy [1], gene vaccine [2,3], DNA sequence [4,5] and so on. The early developed traditional of plasmid isolation method rely on phenol/chloroform technique. The method is classical but with some disadvantages such as toxicity and complexes operation. So there were several methods have been developed gradually to improve the isolation of plasmid DNA such as agarose gel electrophoresis extraction, column chromatography,

selective adsorption using solid phase supports and so on [4]. Among these methods, solid phase supports to isolate plasmid DNA was commonly used for its simplicity and practicality. There were many works have been reported for the isolation of DNA basing on the principle of solid surface adsorption of DNA in the presence of binding agents [6–19]. And silica has been widely selected as one of effective solid phases to purify plasmid DNA for its several features of straightforward synthesis, easily modification and biocompatibility [4,10,18]. Silica matrix-based kits for rapid isolation of plasmid DNA are also commercially available (e.g., Invitrogen, Qiagen). However, the binding agents are indispensable by using of silica as solid phase for adsorption and isolation of plasmid DNA in the reported works.

Recently, novel amino-modified silica nanoparticles (ASNPs) and amino-modified silica coated magnetic nanoparticles (ASMNPs) have been developed in our research group [20–28]. The two kinds of nanoparticles displayed positive surface charge at neutral pH. Pure plasmid DNA could be bind to ASNPs easily without need of extra binding agents and could

\* Corresponding author at: State Key Laboratory of Chemo/Biosensing and Chemometrics, Engineering Center for biomedicine, Institute of Life Science & Biological Technology, Key Laboratory for Bio-Nanotechnology and Molecule Engineering of Hunan Province, Changsha 410082, PR China. Tel: +86 731 8821566; fax: +86 731 8821566.

E-mail address: [kmwang@hnu.cn](mailto:kmwang@hnu.cn) (K. Wang).

be protected from cleavage [20]. Basing on this principle, an approach for the isolation of plasmid DNA from crude bacterial lysates has been reported in this article. ASMNPs behaving positive zeta potential at neutral pH and superparamagnetism were selected as solid phase supports. pEGFP-N3 plasmid has been successfully concentrated and purified from the *E. coli* DH5 $\alpha$  transformed with pEGFP-N3 plasmid under the magnetic fields. The combination and release of pEGFP-N3 plasmid with ASMNPs from crude *E. coli* DH5 $\alpha$  lysates has been investigated. The purified pEGFP-N3 plasmid was then tested for purity and bioactivity through its use in a number of downstream applications.

## 2. Experimental

### 2.1. Reagents and materials

*N*-( $\beta$ -Aminoethyl)- $\gamma$ -aminopropyl-triethoxysilane (AEAPS) was purchased from Hubei Wuhan University Silicone New Material Co., Ltd. Biowest agarose was distributed by Shanghai Yito Enterprise Company Limited. EcoRI and HindIII were purchased from Beijing Dingguo Biotechnology Co. Ltd. Sofast<sup>TM</sup> Transfection Reagent was obtained from Xiamen Sunma Biotechnology Co. Ltd. COS-7 cell line was offered by cell culture lab of our research group. All other reagents were of analytical grade and used without further isolation. Solutions were prepared with Nanopure water (Barnstead/Thermolyne, Dubuque, IA).

### 2.2. Instruments

The ASMNPs were measured with Transmission Electron Microscope (TEM) (JEOL JEM-1230). Malvern Zetasizer 3000HS (Malvern, England) was used to measure the Zeta potential of ASMNPs. UV–vis measurements were carried out by DU-800 Spectrophotometer (Beakman, America). The fluorescence of GFP in cells was observed by fluorescence microscopy (Nikon TE300, Japan).

### 2.3. Experimental details

#### 2.3.1. Preparation and characterization of the ASMNPs

The ASMNPs were prepared by water-in-oil microemulsion technique as reported before [20,26]. Suspension of magnetic Fe<sub>3</sub>O<sub>4</sub> ferrofluid was first synthesized by precipitation from appropriate mixture solution of ferrous sulfate and ferric chloride with ammonia according to the reported method [29]. Then 150  $\mu$ l of 40 mM aqueous magnetic Fe<sub>3</sub>O<sub>4</sub> ferrofluid solution was added to the microemulsion composed of 1.8 ml of Triton X-100, 1.4 ml of *n*-hexanol, 7.5 ml of cyclohexane. In the presence of TEOS and AEAPS (3:1 volume ratio), polymerization reaction was initiated by adding 200  $\mu$ l concentrated NH<sub>4</sub>OH. The reaction was allowed to continue for 24 h to produce ASMNPs. Then, the ASMNPs were isolated by magnetic separation and washed with ethanol and water for several times to remove all remainders and surfactant molecules. At the same time, the silica coated magnetic nanoparticles (SMNPs)

were also prepared with no hydrolysis of AEAPS for control experiments. The obtained ASMNPs were suspended in water for further application. The morphology and diameter of ASMNPs was analyzed with TEM. The Zeta potential of ASMNPs and SMNPs was measured by using Malvern Zetasizer 3000HS.

#### 2.3.2. The incubation and lysis of the *E. coli* DH5 $\alpha$ transformed with pEGFP-N3 plasmid

A single colony of *E. coli* DH5 $\alpha$  transformed with pEGFP-N3 plasmid was inoculated into 2–5 ml of Luria Broth (LB). This culture was grown for 6–8 h at 37 °C with rapid agitation, and then used to inoculate 250 ml of LB containing 60  $\mu$ g/ml ampicillin. The culture was incubated at 37 °C overnight for the colony formation. Then the *E. coli* DH5 $\alpha$  culture were placed into centrifuge tube and harvested with 4000  $\times$  *g* for 15 min at 4 °C. In order to isolate pEGFP-N3 plasmid by using ASMNPs, effective lysis of harvested *E. coli* DH5 $\alpha$  must be first completed before plasmid isolation by using the alkaline lysis method that is most commonly used methods for lysing bacteria [30]. Briefly, the harvested *E. coli* DH5 $\alpha$  pellet was washed with STE (0.1 mol/l NaCl; 10 mmol/l Tris–HCl (pH 8.0); 1 mmol/l EDTA) and then centrifuged at 4000  $\times$  *g* for 15 min at 4 °C. The supernatant was removed. Then, solution I (50 mmol/l glucose; 25 mmol/l Tris–HCl (pH 8.0); 10 mmol/l EDTA), lysozyme and solution II (0.2 M NaOH; 1% SDS) were all added to the tube. Five minutes later, ice-cold solution III (5 mol/l KAc 60 ml, glacial acetic acid 11.5 ml, ultrapure water 28.5 ml) was added to the tube and then centrifuged at 13,000  $\times$  *g* for 20 min at 4 °C. RNase A was lastly added to the supernatant and was incubated at 37 °C for 30 min to get the crude *E. coli* DH5 $\alpha$  lysates for further application.

#### 2.3.3. The isolation of pEGFP-N3 plasmid from crude *E. coli* DH5 $\alpha$ lysates using ASMNPs

**2.3.3.1. Combination analysis of pEGFP-N3 plasmid with ASMNPs.** A 100  $\mu$ l crude *E. coli* DH5 $\alpha$  lysates was removed and transferred to a 1.5-ml micro-centrifuge tube, and an equal volume ASMNPs suspension with concentration of 3.6 mg/ml was added. The mixture was agitated gently at room temperature for 1, 10 and 30 min, respectively. At the same time, a control sample was prepared that 100  $\mu$ l crude *E. coli* DH5 $\alpha$  lysates was added to 100  $\mu$ l negative potential of silica coated magnetic nanoparticles at neutral pH with concentration of 3.6 mg/ml. The combination of the pEGFP-N3 plasmid with ASMNPs was analyzed with agarose gel electrophoresis.

**2.3.3.2. The release of pEGFP-N3 plasmid from the pEGFP-N3 plasmid–ASMNPs complexes.** A 100  $\mu$ l crude *E. coli* DH5 $\alpha$  lysates was removed and transferred to a 1.5-ml micro-centrifuge tube, and an equal volume ASMNPs suspension with concentration of 3.6 mg/ml was added. The complexes of pEGFP-N3 plasmid–ASMNPs were obtained as the aforementioned step and were washed with 70% ethanol and PBS, respectively. And then the complexes of pEGFP-N3 plasmid–ASMNPs were eluted with 3 M NaCl as the followed process. 100  $\mu$ l of 3 M NaCl was added to the washed pEGFP-N3

plasmid–ASMNPs complexes and incubated at room temperature for some time. Then the ASMNPs were immobilized again using magnetic rack. The eluent was removed and retained for further analysis.

Here, different incubation time of NaCl with pEGFP-N3 plasmid–ASMNPs complexes has been also investigated. Five same samples of ethanol and PBS washed pEGFP-N3 plasmid–ASMNPs complexes were prepared. Then 100  $\mu$ l 3 M NaCl was added to every sample respectively, and the incubation time of NaCl with pEGFP-N3 plasmid–ASMNPs complexes was 60, 30, 10, 5 and 1 min, respectively. Then the ASMNPs were immobilized via external magnetic field and the supernatant was removed to five tubes. The released pEGFP-N3 plasmid was analyzed using UV–vis spectrum.

**2.3.3.3. The isolation efficiency of ASMNPs for pEGFP-N3 plasmid.** The isolation efficiency of ASMNPs for pEGFP-N3 plasmid was tested by comparison with the traditional phenol/chloroform method. A 100  $\mu$ l crude *E. coli* DH5 $\alpha$  lysates was removed and transferred to a 1.5-ml micro-centrifuge tube for pEGFP-N3 plasmid isolation using ASMNPs. Another 100  $\mu$ l crude *E. coli* DH5 $\alpha$  lysates was removed and transferred to a 1.5-ml micro-centrifuge tube for pEGFP-N3 plasmid isolation using traditional phenol/chloroform method. The plasmid DNA that isolated by using the two different methods was suspended with equal volume buffer and was analyzed by UV–vis spectra analysis.

**2.3.3.4. Bioactivity of the isolated pEGFP-N3 plasmid using ASMNPs.** The bioactivity of the isolated pEGFP-N3 plasmid using ASMNPs was analyzed through its use in two downstream applications, including restriction enzyme digestion (EcoRI, HindIII) and transfection of COS-7 cells for expressing of green fluorescence protein (GFP). For restriction enzyme digestion, the pEGFP-N3 plasmid was first desalted using ethanol and was dissolved in TE, then 1.6  $\mu$ g of pEGFP-N3 plasmid was digested with appropriate amount of EcoRI and HindIII, respectively for 1 h at 37  $^{\circ}$ C. The products were analyzed using agarose gel electrophoresis.

For transfection, approximately  $1 \times 10^5$  COS-7 cells were seeded in six-well plates on the RPMI1640 (GIBCO USA) medium with 10% fetal calf serum at 37  $^{\circ}$ C with 5% CO<sub>2</sub> atmosphere until the cover rate reached 70%. Sofast<sup>TM</sup> transfection reagent transfections were performed. A suitable isolated pEGFP-N3 plasmid using ASMNPs suspended in culture medium was mixed with 5  $\mu$ l Sofast<sup>TM</sup> transfection to obtain Sofast–pEGFP-N3 plasmid complexes. Then the Sofast–pEGFP-N3 plasmid complexes were added to the culture medium containing COS-7 cells. After 24 h incubation, the transfected COS-7 cells were observed with fluorescence microscopy.

### 3. Results and discussions

#### 3.1. Characterization of ASMNPs

The ASMNPs were prepared using water-in-oil (W/O) reverse microemulsion technique that was one of the most rec-

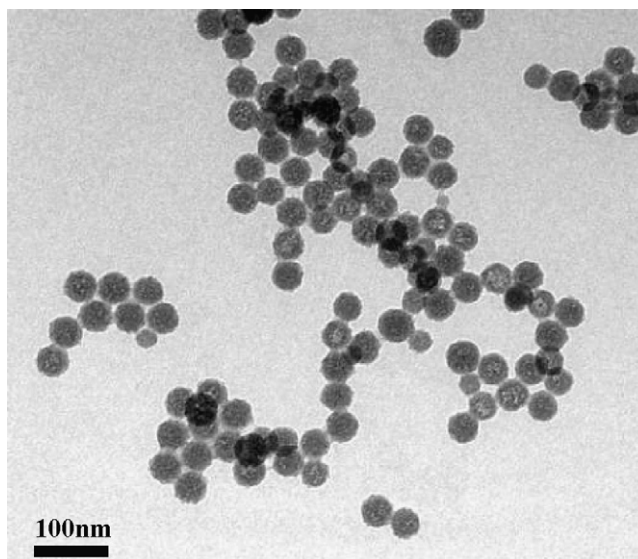


Fig. 1. TEM image of ASMNPs.

ognized methods in our group for preparation of core-shell nanoparticles. The TEM image of ASMNPs was shown in Fig. 1. From the image, we can acquire that the diameters of ASMNPs were about  $45 \pm 5$  nm and the particles were global and non-aggregative. The zeta potential of ASMNPs has also been determined by using a Malvern Zetasizer. The results showed that the zeta potential of ASMNPs at neutral pH was 33.5 mV, which indicated the ASMNPs display a positive surface charge at neutral pH due to the presence of amino groups on the surface of ASMNPs. So they could be used to isolate plasmid DNA in the form of plasmid DNA–ASMNPs complexes that was accomplished through electrostatic binding between the positive charge of the amino group and the negative charge of the phosphate groups of the plasmid DNA.

#### 3.2. The isolation of pEGFP-N3 plasmid from crude *E. coli* DH5 $\alpha$ lysates using ASMNPs

##### 3.2.1. Combination of the pEGFP-N3 plasmid with ASMNPs

A 100  $\mu$ l of ASMNPs suspension and 100  $\mu$ l crude *E. coli* DH5 $\alpha$  lysates were mixed well and reacted at room temperature for 1, 10 and 30 min, respectively. On the control experiments, a 100  $\mu$ l negative SMNPs suspension and 100  $\mu$ l crude *E. coli* DH5 $\alpha$  lysates were mixed well and reacted at room temperature for 30 min. The pure ASMNPs suspension, the pure SMNPs suspension, the mixture of ASMNPs incubated with crude *E. coli* DH5 $\alpha$  lysates for different time and the mixture of SMNPs incubated with crude *E. coli* DH5 $\alpha$  lysates were all analyzed with agarose gel electrophoresis. The results of the agarose gel electrophoresis were shown in Fig. 2. Lane 1 was pEGFP-N3 plasmid that was isolated by using traditional phenol/chloroform method. Lanes 2 and 3 were the pure ASMNPs and SMNPs suspension. Lane 4 was the *E. coli* DH5 $\alpha$  lysates that were incubated with SMNPs. Lanes 5, 6, and 7 were mixture of ASMNPs incubated with the crude *E. coli* DH5 $\alpha$  lysates for 30, 10 and 1 min,

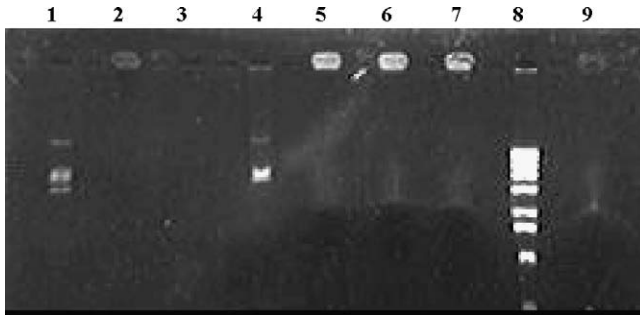


Fig. 2. Agarose gel electrophoresis of plasmid DNA and pEGFP-N3 plasmid–ASMNPs complexes. Lanes 1, 2, 3, 4, 5, 6, 7, 8 and 9 were represented pure pEGFP-N3 plasmid isolated using phenol/chloroform method, pure ASMNPs suspension, pure SMNPs suspension, *E. coli* DH5 $\alpha$  lysates that were incubated with SMNPs; mixture of ASMNPs and bacterial lysates after incubation for 30 min, mixture of ASMNPs and bacterial lysates after incubation for 10 min, mixture of ASMNPs and bacterial lysates after incubation for 1 min, 1 kb DNA marker and supernatant of the mixture of ASMNPs and bacterial lysates after the nanoparticles was immobilized.

respectively. Lane 8 was a marker DNA. Lane 9 was the supernatant of the mixture of ASMNPs and crude *E. coli* DH5 $\alpha$  after the ASMNPs was immobilized. During the electrophoresis, pure pEGFP-N3 plasmid moved in the electric field, but pEGFP-N3 plasmid–ASMNPs complexes stayed around the sample pore. With the ethidium bromide for visualization, fluorescence of plasmid DNA could be clearly observed. The results from the agarose gel electrophoresis showed the sample pore of lanes 2 and 3 were not fluorescent which demonstrated clearly those

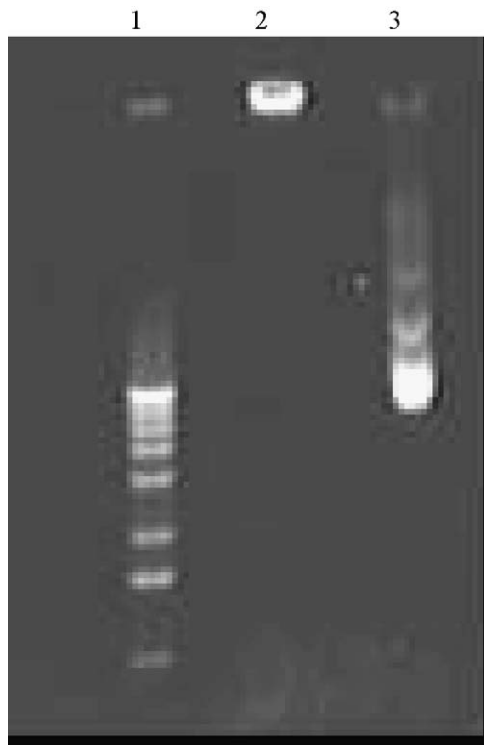


Fig. 3. Agarose gel electrophoresis of pEGFP-N3 plasmid isolated from bacterial lysates using ASMNPs. Lanes 1, 2 and 3 were represented 1 kb DNA marker; pEGFP-N3 plasmid–ASMNPs complexes, released pEGFP-N3 plasmid from pEGFP-N3 plasmid–ASMNPs complexes.

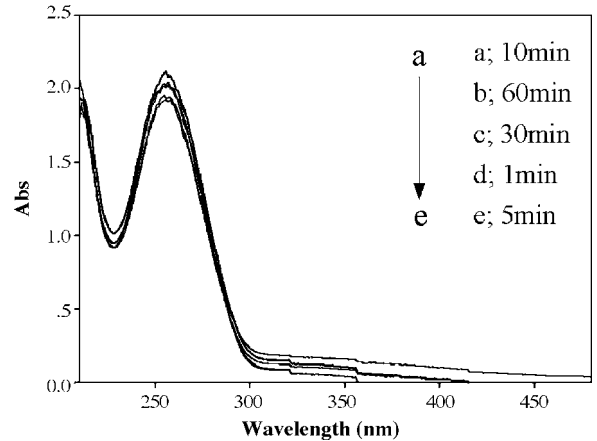


Fig. 4. The UV–vis absorption spectra of the released pEGFP-N3 plasmid those were eluted from pEGFP-N3 plasmid–ASMNPs complexes by 3 M NaCl with different incubation time.

ASMNPs and SMNPs had no obvious autofluorescence. But the fluorescence in the sample pore of lanes 5, 6, and 7 were fluorescent, which implied that the ASMNPs have bound pEGFP-N3 plasmid and formed pEGFP-N3 plasmid–ASMNPs complexes. And the incubation time of the ASMNPs with crude *E. coli* DH5 $\alpha$  lysates would not affect the binding obviously, which indicated the ASMNPs could bind the pEGFP-N3 plasmid of *E. coli* DH5 $\alpha$  lysates quickly. However, when *E. coli* DH5 $\alpha$  lysates were incubated with SMNPs, electrophoresis results showed that there was no fluorescence of pEGFP-N3 plasmid in the sample pore but in agar gel. The DNA that stained in the agar gel of lane 4 was similar with the pEGFP-N3 plasmid isolated by using traditional phenol/chloroform method as that stained in lane 1. There was no fluorescence of pEGFP-N3 plasmid in lane 9. All of the above-mentioned agarose gel electrophoresis results displayed that the positive ASMNPs could combine the pEGFP-N3 plasmid from the *E. coli* DH5 $\alpha$  lysates by ion-pairing formation between the positive charges of the ASMNPs and the negative charges of the plasmid DNA. And this combination was rapidly.

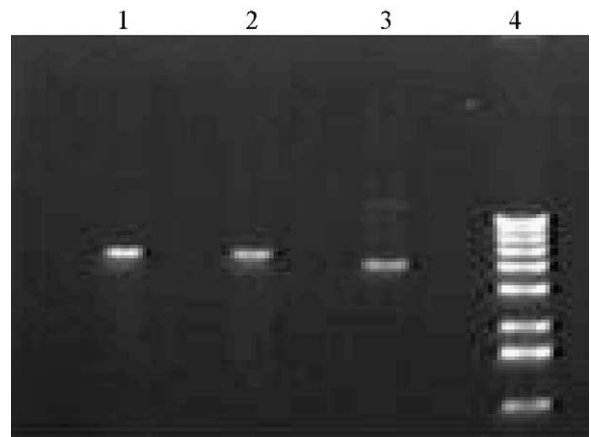


Fig. 5. Agarose gel electrophoresis of isolated pEGFP-N3 plasmid using ASMNPs digested with EcoRI and HindIII. Lanes 1, 2, 3 and 4 were represented isolated pEGFP-N3 plasmid using ASMNPs digested with EcoRI, isolated pEGFP-N3 plasmid using ASMNPs digested with HindIII, desalted ASMNPs-isolated pEGFP-N3 plasmid and 1 kb DNA Marker.

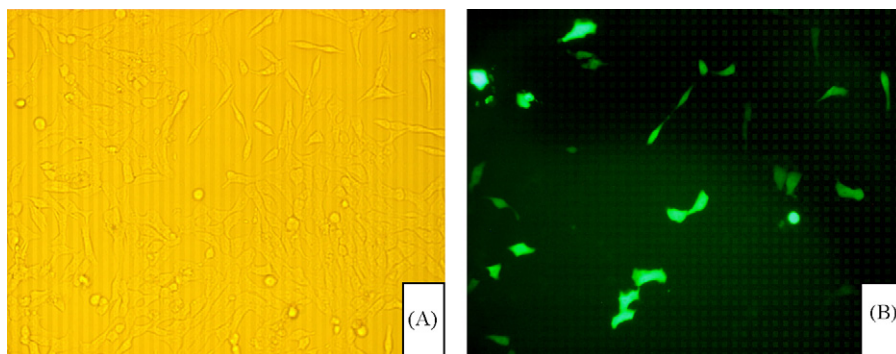


Fig. 6. Expression of isolated pEGFP-N3 plasmid using ASMNPs in COS-7 cells. (A) Optical image of the cells; (B) fluorescence image of the cells.

### 3.2.2. The release of the plasmid DNA from the pEGFP-N3 plasmid–ASMNPs complexes

The bound pEGFP-N3 plasmid was released from the pEGFP-N3 plasmid–ASMNPs complexes using 3 M NaCl. As shown in Fig. 3, lane 1 was the DNA marker. Lane 2 was the ASMNPs that incubated with *E. coli* DH5 $\alpha$  lysates for 30 min and washed with PBS buffer. And lane 3 was the eluent of pEGFP-N3 plasmid–ASMNPs complexes with 3 M NaCl. The results from agarose gel electrophoresis implied that pEGFP-N3 plasmid could be washed off from the pEGFP-N3 plasmid–ASMNPs complexes by using 3 M NaCl and still retained its normal structure.

Because the above results illustrated that the pEGFP-N3 plasmid could be released from the pEGFP-N3 plasmid–ASMNPs complexes, we proceeded to investigate the release time. The released plasmid DNA from five pEGFP-N3 plasmid–ASMNPs complexes samples that were incubated in 3 M NaCl for 60, 30, 10, 5 and 1 min, respectively was analyzed with UV–vis spectrum. As shown in Fig. 4, the results demonstrated that the absorption of the released plasmid DNA from the five pEGFP-N3 plasmid–ASMNPs complexes samples was not different obviously, which indicated the release of the plasmid DNA from the pEGFP-N3 plasmid–ASMNPs complexes was rapidly and 1 min was enough.

### 3.2.3. The isolation efficiency of the ASMNPs for pEGFP-N3 plasmid

A favorable method for the isolation of plasmid DNA must be rapid and efficient. We have noted that the approach was rapid. Here the isolation efficiency of this method was compared with the traditional phenol/chloroform method. We have calculated that about 55  $\mu$ g pEGFP-N3 plasmid could be isolated from 1 ml prepared bacterial lysates using ASMNPs (3.6 mg/ml), and the average OD<sub>260</sub>/OD<sub>280</sub> ration was 1.9, indicating that the DNA was of a high purity with negligible protein contamination. However, there was only about 35  $\mu$ g pEGFP-N3 plasmid that had been isolated from the same volume bacterial lysates by using phenol/chloroform method. Then the yield of pEGFP-N3 plasmid extracted using ASMNPs was on average 1.6-fold greater than that using the traditional phenol/chloroform method. So we can conclude that this method was not only rapid but also efficient.

### 3.2.4. The bioactivity of the isolated pEGFP-N3 plasmid using ASMNPs

Because the above studies showed that pEGFP-N3 plasmid could be isolated from bacterial cell lysates rapidly and efficiently by use of ASMNPs, we proceeded to test the bioactivity of the isolated pEGFP-N3 plasmid. In order to detect whether the isolated pEGFP-N3 plasmid was still active, here we reported two further applications of the purified pEGFP-N3 plasmid.

Firstly, the isolated pEGFP-N3 plasmid was desalted by ethanol and was dissolved in TE (0.03745  $\mu$ g/ $\mu$ l). Then EcoRI and HindIII were used respectively to digest the desalted isolated pEGFP-N3 plasmid. Fig. 5 was a gel picture of the result. Lanes 1 and 2 were the isolated pEGFP-N3 plasmid digested by the EcoRI and HindIII, respectively. Lane 3 was the desalted isolated pEGFP-N3 plasmid. It was well known that undigested plasmid DNA was superhelix DNA, and it would become linear DNA after restriction enzyme digestion. The results from the agarose gel electrophoresis showed that the move rate of the isolated pEGFP-N3 plasmid was different with the restriction enzyme digested isolated pEGFP-N3 plasmid. It can be seen clearly that the isolated pEGFP-N3 plasmid using ASMNPs could be fully digested with the enzyme. The result indicated that the pEGFP-N3 plasmid was sufficiently pure and free of crude cell lysates.

To further prove the bioactivity of the isolated pEGFP-N3 plasmid using ASMNPs, we tested the function of the plasmid DNA in a cellular environment. If pEGFP-N3 plasmid is delivered into cells and is still functional, green fluorescence protein (GFP) will be synthesized in the cells through the expression of pEGFP-N3 gene and then can be imaged in real time with fluorescence microscopy. As shown in Fig. 6, the green fluorescence was obviously seen in the cell dish. The result indicated that the isolated pEGFP-N3 plasmid using ASMNPs was able to maintain a high degree of biological activity.

## 4. Conclusions

Plasmid DNA can be isolated from the crude bacteria efficiently by use of ASMNPs through the formation of plasmid DNA–ASMNPs complexes and released easily with 3 M NaCl. From the downstream application of the isolated plasmid DNA, it can be seen that the isolated plasmid DNA retains biological activity. Furthermore, all of the operation can be finished under

the external magnetic fields. The results reported here open up new perspectives for ASMNPs and will have great potential in isolation of genome.

### Acknowledgements

This work was partially supported by the National Key Basic Research Program (2002CB513100-10), Key Project Foundation of China Education Ministry (107084), Key Project of International Technologies Collaboration Program of China (2003DF000039), Program for New Century Excellent Talents in University (NCET), National Science Foundation of PR China (90606003, 20405005) and Outstanding Youth Foundation of Hunan Province (06JJ10004).

### References

- [1] G.J. Nable, Z.Y. Yang, E.G. Nabel, K. Bishop, M. Marquet, P.L. Felgner, D. Gordon, A.E. Chang, *Ann. NY Acad. Sci.* 772 (1995) 227.
- [2] H.T. Maecker, G. Hansen, D.M. Walter, R.H. DeKruyff, S. Levy, D.T. Umetsu, *J. Immunol.* 166 (2001) 959.
- [3] T. Jiang, M. Yu, B.C. Fan, S.P. Chen, H.Y. Duan, Y.Q. Deng, W.M. Peng, Q.Y. Zhu, E.D. Qing, *Chin. J. Biochem. Mol. Biol.* 19 (2003) 278.
- [4] D.A. Dederich, G. Okwuonu, T. Garner, A. Denn, A. Sutton, M. Escotto, A. Martindale, O. Delgado, D.M. Muzny, R.A. Gibbs, M.L. Metzker, *Nucleic Acids Res.* 30 (2002) e32.
- [5] C.J. Elkin, P.M. Richardson, H.M. Fourcade, N.M. Hammon, M.J. Pollard, P.F. Predki, T. Glavina, T.L. Hawkins, *Genome Res.* 11 (2001) 1269.
- [6] B. Vogelstein, D. Gillespie, *Proc. Natl. Acad. Sci.* 76 (1979) 615.
- [7] M.A. Marko, R. Chipperfield, H.C. Birnboim, *Anal. Biochem.* 121 (1982) 382.
- [8] T.L. Hawkins, T. O'Connor-Morin, A. Roy, C. Santillan, *Nucleic Acids Res.* 22 (1994) 4543.
- [9] M.J. Davies, J.I. Taylor, N. Sachsinger, I.J. Bruce, *Anal. Biochem.* 262 (1998) 92.
- [10] M. Engelstein, T.J. Aldredge, D. Madan, J.H. Smith, J.I. Mao, D.S. Smith, P.W. Rice, *Microb. Comp. Genomics* 3 (1998) 237.
- [11] M. Itoh, T. Kitsunai, J. Akiyama, K. Shibata, M. Izawa, J. Kawai, Y. Tomaru, P. Carninci, Y. Shibata, Y. Ozawa, M. Muramatsu, Y. Okazaki, Y. Hayashizaki, *Genome Res.* 9 (1999) 463.
- [12] J.I. Taylor, C.D. Hurst, M.J. Davies, N. Sachsinger, I.J. Bruce, *J. Chromatogr. A* 890 (2000) 159.
- [13] M.C. Breadmore, K.A. Wolfe, I.G. Arcibal, W.K. Leung, D. Dickson, B.C. Giordano, M.E. Power, J.P. Ferrance, S.H. Feldman, P.M. Norris, J.P. Landers, *Anal. Chem.* 75 (2003) 1880.
- [14] Z.M. Saiyed, C. Bochiwal, H. Gorasia, S.D. Telang, C.N. Ramchand, *Anal. Biochem.* 356 (2006) 306.
- [15] C.L. Chiang, C.S. Sung, C.Y. Chen, *J. Magn. Magn. Mater.* 305 (2006) 483.
- [16] C.L. Chiang, C.S. Sung, *J. Magn. Magn. Mater.* 302 (2006) 7.
- [17] M.J. Archer, B.C. Lin, Z. Wang, D.A. Stenger, *Anal. Biochem.* 355 (2006) 285.
- [18] J. Wen, C. Guillo, J.P. Ferrance, J.P. Landers, *Anal. Chem.* 78 (2006) 1673.
- [19] Z.M. Saiyed, M. Parasramka, S.D. Telang, C.N. Ramchand, *Anal. Biochem.* 363 (2007) 288.
- [20] X.X. He, K.M. Wang, W.H. Tan, B. Liu, X. Lin, C.M. He, D. Li, S.S. Huang, J. Li, *J. Am. Chem. Soc.* 125 (2003) 7168.
- [21] X.X. He, K.M. Wang, W.H. Tan, X. Lin, L. Chen, X.H. Chen, *Rev. Mater. Sci.* 5 (2003) 375.
- [22] X.X. He, K.M. Wang, D. Li, W.H. Tan, C.M. He, S.S. Huang, B. Liu, X. Lin, X.H. Chen, *J. Disper. Sci. Technol.* 24 (2003) 633.
- [23] X.X. He, K.M. Wang, W.H. Tan, X. Lin, S.S. Huang, D. Li, C.M. He, J. Li, *Chin. Sci. Bull.* 48 (2003) 223.
- [24] X.X. He, X. Lin, K.M. Wang, W.H. Tan, L. Chen, P. Wu, Y. Yuan, *Encyclopedia Nanosci. Nanotechnol.* 1 (2004) 235.
- [25] W.H. Tan, K.M. Wang, X.X. He, X.J. Zhao, T. Drake, L. Wang, R.P. Bagwe, *Med. Res. Rev.* 24 (2004) 621.
- [26] P. Ashtari, X.X. He, K.M. Wang, P. Gong, *Talanta* 67 (2005) 548.
- [27] X.L. Xing, X.X. He, J.F. Peng, K.M. Wang, W.H. Tan, *J. Nanosci. Nanotechnol.* 5 (2005) 1688.
- [28] X.X. He, J.Y. Chen, K.M. Wang, D.L. Qin, W.H. Tan, *Talanta* 72 (2007) 1519.
- [29] R. Massart, *IEEE Trans. Magn.* 17 (1981) 1247.
- [30] J. Sambrook, D.W. Russell, *Molecular Cloning: A Laboratory Manual*, vol. 1, Cold Spring Harbor Laboratory Press, New York, 2001, p. 32.



# Identity confirmation of drugs and explosives in ion mobility spectrometry using a secondary drift gas

Abu B. Kanu, Herbert H. Hill Jr. \*

*Department of Chemistry, Washington State University, Pullman, WA 99164-4630, USA*

Received 28 June 2006; received in revised form 26 April 2007; accepted 27 April 2007

Available online 22 May 2007

## Abstract

This work demonstrated the potential of using a secondary drift gas of differing polarizability from the primary drift gas for confirmation of a positive response for drugs or explosives by ion mobility spectrometry (IMS). The gas phase mobilities of response ions for selected drugs and explosives were measured in four drift gases. The drift gases chosen for this study were air, nitrogen, carbon dioxide and nitrous oxide providing a range of polarizability and molecular weights. Four other drift gases (helium, neon, argon and sulfur hexafluoride) were also investigated but design limitations of the commercial instrument prevented their use for this application. When ion mobility was plotted against drift gas polarizability, the resulting slopes were often unique for individual ions, indicating that selectivity factors between any two analytes varied with the choice of drift gas. In some cases, drugs like THC and heroin, which are unresolved in air or nitrogen, were well resolved in carbon dioxide or nitrous oxide. © 2007 Elsevier B.V. All rights reserved.

*Keywords:* Ion mobility spectrometry; Explosives; Drugs; False positives; Confirmatory tests

## 1. Introduction

First introduced as an analytical technique in the late 1960s for the detection of trace quantities of organic vapors [1,2], ion mobility spectrometry (IMS) has developed into one of the primary analytical methods used for the detection of explosives [3–18], drugs [19–24] and chemical warfare agents [25,26]. For a more complete discussion of IMS as a detection method for explosives and drugs of abuse see reference [27].

Despite years of development, IMS instruments, when applied to real samples, still experience false positive responses [27]. A false positive response rate less than 0.05 is currently the Department of Homeland Security goal for identification of explosives ([www.dhs.gov/xres/](http://www.dhs.gov/xres/)). In general false positive responses occur when a compound or mixtures of compounds ionize and drift similar to the target compound. In these cases, the instrument indicates the presence of an explosive or drug when in fact none were present. In order to ensure the absence of the target, more sophisticated analytical tests must be performed as well as comprehensive searches of luggage or containers. Thus,

false positive responses cost both time and money. The development of simple methods that can serve as confirmatory tests for currently available commercial IMS systems would reduce the level of false positives and aid the identification of explosives, drugs and chemical warfare agents in the field. The hypothesis of this paper is that the use of an alternate drift gas, with polarizability different from that of air, may provide a simple test which can be used in the field to confirm or refute a positive response for drugs or explosives.

The use of drift gas polarizability to alter the separation of ions in an IMS was first reported in 1986 [28]. A study by Rokushika et al. using carbon dioxide and nitrogen as drift gases demonstrated that, under the normal operating conditions of an IMS, separation of reactant ion and product ion peaks were possible when carbon dioxide was used as the drift gas [28]. Prior to this investigation, the only data available in the literature for IMS studies in carbon dioxide was performed at 25 °C [29]. At this temperature all reactant ions in carbon dioxide were observed to produce essentially the same reduced mobility constant. Large clusters were formed around the core ion such that both size and shape of the ion clusters were only weakly dependent on the identity of the core ion. The conclusion from this early, low temperature, studies was that mobility of ions in carbon dioxide is largely independent of the ion species so long as the pressure

\* Corresponding author. Tel.: +1 509 335 5648; fax: +1 509 335 8867.  
E-mail address: [hhill@wsu.edu](mailto:hhill@wsu.edu) (H.H. Hill Jr.).

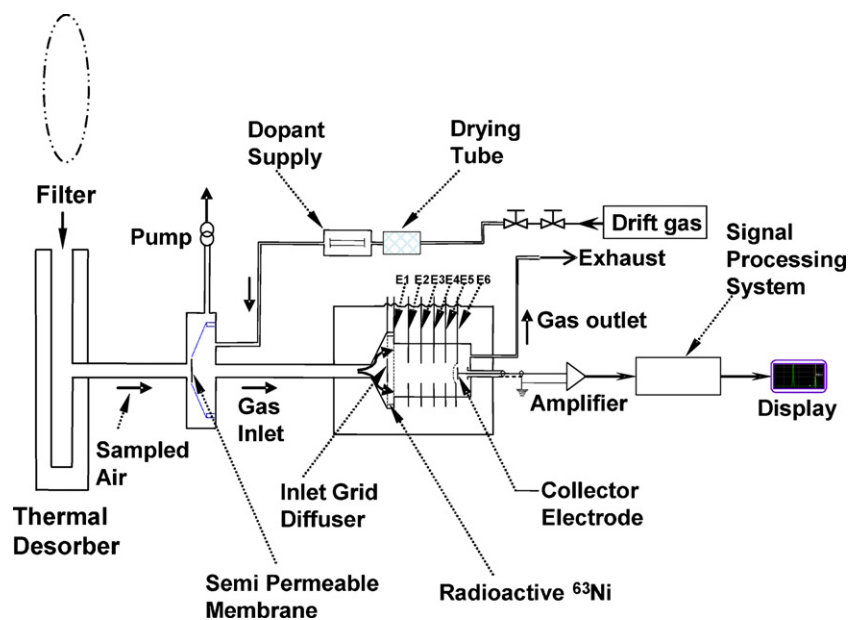


Fig. 1. Schematic cross-sectional view of the modified open loop IMS Itemiser unit fitted with a thermal desorber.

is greater than 100 Torr and therefore carbon dioxide was considered to be inadequate as a drift gas for IMS. With the 1986 investigation by Rokushika et al., it became clear that at higher temperatures carbon dioxide could be used as a drift gas for IMS.

In ion mobility spectrometry, the separation factor is defined as the ratio of the mobility ( $K_1$ ) of the faster drifting ion (low drift time,  $t_{d1}$ ) to the mobility ( $K_2$ ) of the slower drifting ion (high drift time,  $t_{d2}$ )

$$\alpha = \frac{K_1}{K_2} = \frac{t_{d2}}{t_{d1}}$$

The use of different drift gases to alter separation factors ( $\alpha$ ) in IMS was first demonstrated by Ashbury and Hill [30]. Using helium, argon, nitrogen and carbon dioxide, they demonstrated that separation factors could be altered by using drift gases of different polarizabilities. Matz et al. used helium, argon, nitrogen and carbon dioxide to investigate the ion mobility behavior for cocaine/metabolites, amphetamines, benzodiazepines and peptides [31]. They demonstrated that ion mobility separations of various drugs could be achieved in some drift gases which were not possible in others. Other studies used helium, the smallest and least polarizable drift gas, to derive a theoretical understanding of the interaction between an ion and a gas [32–34]. Karpas and Berant on the other hand, demonstrated that, for a homologous series of compounds, drift times in a highly polarizable gas can be predicted from those measured in a weakly polarizable drift gas [35]. Russell and co-workers, also demonstrated that the polarizability of gases for molecules from similar classes such as peptides had little effect on separation factors [36].

Thus, for small, dissimilar molecules such as drugs and explosives, it may be possible to use alternate drift gases as a rapid field confirmatory test with commercial IMS instruments, reducing the false positive response rate in the trace detection of drugs and explosives. To test this hypothesis, reduced mobilities of explosives and drugs were measured in different drift gases with a

commercially available IMS instrument typical of that used in the field.

## 2. Experimental

### 2.1. Instrumentation

The IMS used in this study was a commercially available ion mobility spectrometer called “The Itemiser” (GE Security, Wilmington, MA). A schematic of the IMS as it was operated in this study is shown in Fig. 1. The IMS was modified to an open loop system for operation with the different drift gases by disconnecting the pump used to recycle the drift gas flow and connecting the gas pneumatics directly to pressurized gas tanks containing the drift gas of choice.

Eight drift gases (air, nitrogen, carbon dioxide, nitrous oxide, helium, neon, argon and sulfur hexafluoride) were investigated. Table 1 lists the molecular weight and polarizability of the drift gases studied. The drift gases were doped with low concentrations of ammonia (for drug selective detection) or methylene dichloride (for explosive selective detection).

Table 1  
Molecular weight and polarizability of drift gases

Drift gas	MWt/g mol <sup>-1</sup>	Polarizability (10 <sup>-24</sup> cm <sup>3</sup> ) <sup>a</sup>
Helium	4	0.21
Neon	20	0.40
Nitrogen	28	1.74
Air	28.8	1.71
Argon	40	1.64
Carbon dioxide	44	2.91
Nitrous oxide	44	3.03
Sulfur hexafluoride	146	6.54

<sup>a</sup> As tabulated in CRC Handbook of Chemistry and Physics, 70th ed., D.R. Lide Ed., CRC Press, Boca Raton, FL, 1989.

Sample introduction into the instrument was achieved by pipetting 1  $\mu\text{L}$  sample onto sampling filters (GE Security, Wilmington, MA) made from silicone elastomeric membrane (50  $\mu\text{m}$  thick  $\times$  90 mm wide). After solvent evaporation, a filter containing the known quantity of sample was inserted into the instrument's thermal desorber. Samples were introduced into the spectrometer by volatilization in a thermal desorption chamber attached to the front end of the instrument. For these investigations the desorber was operated at 220  $^{\circ}\text{C}$ . Desorbed vapors were drawn into the IMS through a semi-permeable silicone membrane (part no. PA005007, GE Security). The membrane protected the IMS tube from contamination by excluding particulate matter from the system and minimizing the amount of moisture entering the IMS tube.

Sample molecules passing through the membrane were carried into the detector by the drift gas. Contrary to most IMS instrument, in the Itemiser design the drift gas flowed in the same direction as the ions migrated. The drift gas (and the neutral analytes) flowed through an ionization chamber, 6-mm long, whose walls were lined with a 10 MBq  $^{63}\text{Ni}$  radioactive foil, emitting low energy beta particles. As the drift gas flowed through the chamber, both positive and negative reactant ions were formed. These reactant ions then interacted with neutral sample vapors to produce compound specific product ions.

The electric field in the detector's ionization chamber was normally zero, but at 20 ms intervals, short potential pulses were applied across the chamber. A "kick-out" pulse of 0.2 ms created an electric field that forced the ions through an open grid electrode "E1" and into the ion drift region, where the ions were propelled towards the collector electrode by a constant and continuous electric field. The square-wave kick-out pulse had an amplitude of 1600 V. The ions then traveled to the collector electrode through the drift region where their arrival times were recorded.

The IMS drift tube had a length of 3.9 cm, a voltage of 980 V, and a temperature of  $205 \pm 5^{\circ}\text{C}$ . The electric field established across the drift tube was  $251 \text{ V cm}^{-1}$  and the drift gas flow rate into the IMS was  $900 \text{ mL min}^{-1}$ . Pressure in the drift tube during mobility measurements varied from 698 to 703 Torr. Table 2 summarizes the operating conditions and drift gases used in these studies.

All mobility data were collected by the Itemiser's software. Under normal operating procedures an average of four scans was taken for each spectrum. Each spectrum (a combination of four scans) was displayed in near real time. The spectrum view mode was used to collect all data in this study and the software displayed 70 IMS spectrum (each a combination of four scans) on the screen over 2 s. Each IMS spectrum selected within the 70 sets can be considered to occur at a specific time within a 2 s integration/analysis time interval.

## 2.2. Materials and reagents

Explosive compounds studied were 2,4,6-trinitrotoluene, 2,4,6-TNT; cyclotrimethylenetrinitramine, RDX; pentaerythritol tetranitrate, PETN; 1,3,5-trinitrobenzene, 1,3,5-TNB; 1,3-dinitrobenzene, 1,3-DNB; 2,3-dinitrotoluene, 2,3-DNT;

Table 2  
TD-IMS operating conditions summary

Drift tube length	3.9 cm
Reaction region length	6 mm
Drift tube voltage	980 V
Kick-out pulse	0.2 ms every 20 ms interval
Electric field	$251 \text{ V cm}^{-1}$
Drift tube temperature	$205 \pm 5^{\circ}\text{C}$
Drift tube pressure	698–703 Torr
Desorption unit temperature	220 $^{\circ}\text{C}$
Sample ionization	$^{63}\text{Ni}$ foil
Sample acquisition	Surface filters or air collection
Drift gas flow	$0.9 \text{ L min}^{-1}$
Sampling time	5 s
Analysis time	2 s
Data processing	Microsoft Excel 2003
Detection mode	Positive ion mode ( $\text{NH}_3$ dopant) negative ion mode ( $\text{CH}_2\text{Cl}_2$ dopant)
Drift gases	Helium; air; nitrogen; carbon dioxide; nitrous oxide; argon; neon; sulfur hexafluoride

2,4-dinitrotoluene, 2,4-DNT and 2,6-dinitrotoluene, 2,4-DNT. Drug compounds studied were cocaine; amphetamine, AMP; methamphetamine, METHAM; heroin; morphine, MORPH; tetrahydrocannabinol, THC; methylenedioxyamphetamine (MDMA) and 2,4-lutidine. Chemicals chosen for these studies were obtained from Sigma Aldrich Chemical Company (St. Louis, MO). Sample solutions were prepared by dilution with methanol (HPLC grade, J.T. Baker, Phillipsburgh, NJ).

## 2.3. Experiments

Liquid samples of drugs and explosives were prepared at  $50 \mu\text{g mL}^{-1}$  and 2,4-lutidine prepared at  $93 \mu\text{g mL}^{-1}$ . One microliters sample volume corresponding to 50 ng of drug or explosive and 93 ng of 2,4-lutidine was deposited onto a clean sampling filter. All injections on filters were allowed to dry before being introduced to the instrument. The methanol solvent evaporated rapidly at room temperature leaving the analyte of interest on the surface of the filters. The filters were then placed in the detection slot of the vapor desorption unit for a sampling time of 5 s. The sampling time was the time allowed to heat the filters before desorption. Filters were cleaned by desorption in the instrument before their first use. Measurements were taken in triplicates with blank measurements taken between runs. Experiments were conducted to determine ion mobilities and evaluate mobility ratios in different drift gases for identification of explosives and drugs.

## 2.4. Calculations

All reduced mobility constants ( $K_0$ ) were calculated from experimentally determined drift times ( $t_d$ ). The reduced mobility constants were calculated with reference to TNT ion for the negative ion mode and 2,4-lutidine for the positive ion mode using Eq. (1) to correct for variations in temperature, pressure

and drift field.

$$K_{0(\text{unknown})} = \frac{\text{drift time}_{\text{std}}}{\text{drift time}_{\text{unknown}}} \times K_{0(\text{std})} (\text{cm}^2 \text{V}^{-1} \text{s}^{-1}) \quad (1)$$

where  $1.54 \pm 0.02 \text{ cm}^2 \text{V}^{-1} \text{s}^{-1}$  was the  $K_0$  value used for the standard TNT and  $1.95 \pm 0.01 \text{ cm}^2 \text{V}^{-1} \text{s}^{-1}$  was the  $K_0$  value used for the standard 2,4-lutidine in air, respectively [37].

### 3. Results and discussion

#### 3.1. Drift gases

Eight drift gases (helium, air, nitrogen, neon, argon, carbon dioxide, nitrous oxide and sulfur hexafluoride) were initially chosen for study with the IMS instrument in the positive and negative ion modes. However, instrumental limitations related to the hardware and software design were observed with helium, argon, neon and SF<sub>6</sub>.

With argon and neon, a high current was observed for the background. Fig. 2 is an example response from background spectra with argon as drift gas. The high current background that occurred when using argon or neon was contributed by “penning ionization” [38]. Upon collisions with beta particles, argon and neon form neutral metastables which can be carried through the ion gates and into the drift region of the spectrometer with the carrier gas flow. Ionization in the drift region can occur through the “penning ionization” process as shown below.



Because the drift gas flow of the Itemiser is concurrent with ion flow, the metastable gas was swept into the drift region of the Itemiser and ions formed in the drift region through the penning ionization process created high background current and noise which interfered with the spectrum.

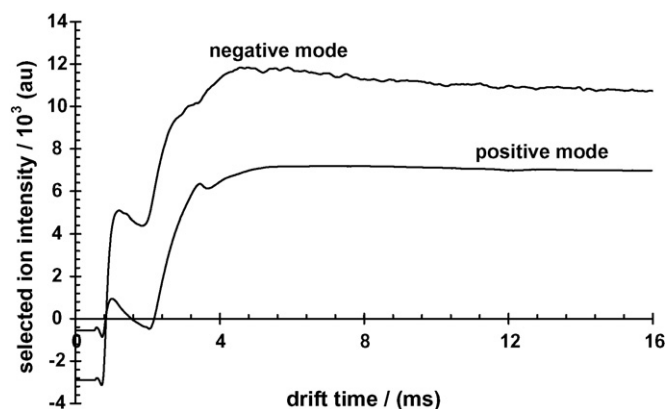


Fig. 2. Ion mobility spectra illustrating the limitations of the instrumentation design when using argon as drift gas.

With helium drift gas, ions drifted too fast to be recognized by the system’s computer. Thus, helium was eliminated from the studies. The problem associated with SF<sub>6</sub> was that the software could not display spectra beyond 16.5 ms. Because, SF<sub>6</sub> had the highest polarizability of the drift gases investigated, ion drifts were too slow to be recorded by the instrument’s software. Although the reactant ion peak (RIP) was measurable in SF<sub>6</sub>, product ion peaks occurred after the instrument’s drift time cut off. These limitations in instrument and software design reduced the drift gases available for this investigation to air, nitrogen, carbon dioxide and nitrous oxide.

#### 3.2. Reduced mobilities in alternate drift gases

##### 3.2.1. Reactant ions

Due to the high proton affinity of ammonia and the high electron affinity of methylene chloride, which were used as dopants in this study, background spectra of ammonium ion (NH<sub>4</sub><sup>+</sup>) for the positive ion mode and chloride ion (Cl<sup>-</sup>) in the negative ion

Table 3

Database of reduced mobility values for drugs and explosives in different drift gases obtained from IMS

Compound	MWt/g mol <sup>-1</sup>	$K_0$ (Air) <sup>a</sup> [lit $K_0$ ]	$K_0$ (N <sub>2</sub> ) <sup>a</sup> [lit $K_0$ ]	$K_0$ (CO <sub>2</sub> ) <sup>a</sup>	$K_0$ (N <sub>2</sub> O) <sup>a</sup>
Cl <sup>-</sup>	35.5	3.05 [3.06]	3.02 [3.01]	1.34	1.37
1,3-DNB	168	1.71	1.71	0.98	1.02
2,3-DNT	182	1.66	1.63	0.97	1.00
2,4-DNT	182	1.68 [1.67]	1.67 [1.61]	1.00	1.02
2,6-DNT	182	1.67 [1.65]	1.66 [1.61]	1.00	1.02
1,3,5-TNB	213	1.69	1.70	1.01	1.03
RDX	222	1.47 [1.44]	1.47 [1.49]	0.94	0.95
TNT	227	1.54 [1.53]	1.54	0.96	0.96
PETN	316	2.53 [2.51]	2.53 [2.51]	1.33	1.33
NH <sub>4</sub> <sup>+</sup>	18	2.98	2.96	1.46	1.44
AMP	135	1.66 [1.68]	1.67 [1.67]	1.02	1.00
METHAM	149	1.63 [1.63]	1.64 [1.64]	1.03	1.00
MDMA	193	1.47 [1.47]	1.47	0.94	0.92
Morphine	285	1.23 [1.19]	1.23 [1.21]	0.85	0.83
Cocaine	303	1.17 [1.17]	1.18 [1.16]	0.80	0.78
THC	314	1.06 [1.06]	1.06 [1.04]	0.75	0.74
Heroin	369	1.06 [1.04]	1.06 [1.09]	0.79	0.77
2,4-Lutidine	107	1.95 [1.95]	1.95 [1.95]	1.20	1.18

<sup>a</sup>  $K_0$  values are in  $\text{cm}^2 \text{V}^{-1} \text{s}^{-1}$ .

mode were observed. The product ions reported in this study resulted from the ion-molecular gas phase reaction of these reactant ions with the neutral vapors of the drugs and explosives introduced into the IMS. Table 3 lists molecular weights of the drugs and explosives investigated along with the  $K_0$  values of their product ions. For many of these drugs and explosives, reduced mobilities in these alternate drift gases have not been previously reported.

### 3.2.2. Product ions from drugs

2,4-Lutidine with a known reduced mobility of  $1.95 \pm 0.01 \text{ cm}^2 \text{ V}^{-1} \text{ s}^{-1}$  in air was used as the daily standard to insure that the IMS unit was responding properly. Despite numerous IMS investigations with 2,4-lutidine, its  $K_0$  values in carbon dioxide and nitrous oxide had not been reported previously. They were determined to be  $1.20 \pm 0.02$  and  $1.18 \pm 0.01 \text{ cm}^2 \text{ V}^{-1} \text{ s}^{-1}$ , respectively.

The differences in  $K_0$  values for a specific drug in different drift gases can be attributed to the difference in polarizability of the drift gases and thus the differences in interactions between the analytes and the drift gasses. As expected, mobility decreased as drift gas polarizability and mass of the ion increased. Increase in drift gas polarizability has the effect of greater interaction between the drift gas and the established electric field across the drift tube. This effect will result in ions drifting slowly in the IMS drift tube, accounting for a decreased reduced mobility value. On the other hand, as the size of the ion increases, the collision cross-section and thus the ionic radii of the ions increases, resulting in a decreased reduced mobility value.

Fig. 3 shows positive mode IMS spectra of amphetamine (AMP) and methamphetamine (METHAM) in the four drift gases studied. The ammonium reactant ion peak migrated in air and nitrogen with a time of  $3.09 \pm 0.01$  and  $3.12 \pm 0.01$  ms, respectively. In carbon dioxide and nitrous oxide the RIP had much longer migration times of  $6.32 \pm 0.02$  and  $6.41 \pm 0.03$  ms, respectively. Similarly, the response ions of both AMP and METHAM migrated with much longer times in the more

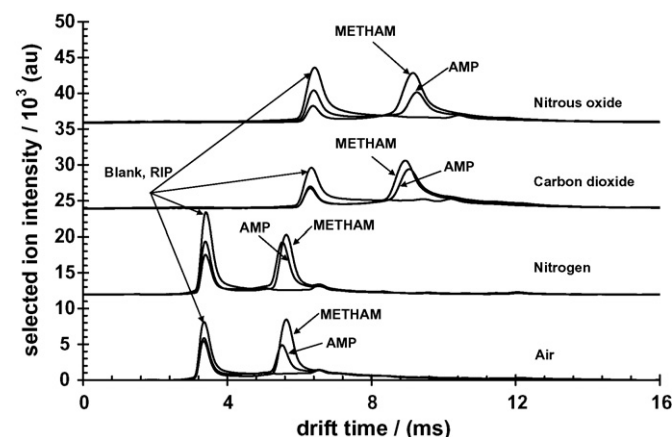


Fig. 3. Ion mobility spectra for AMP and METHAM in different drift gases: air, nitrogen, carbon dioxide and nitrous oxide. The spectra demonstrated that as the polarizability of the drift gas increases, mobility decreases. Furthermore the arrival times of the pair of compounds were inverted as drift gas changes from low to high polarizability.

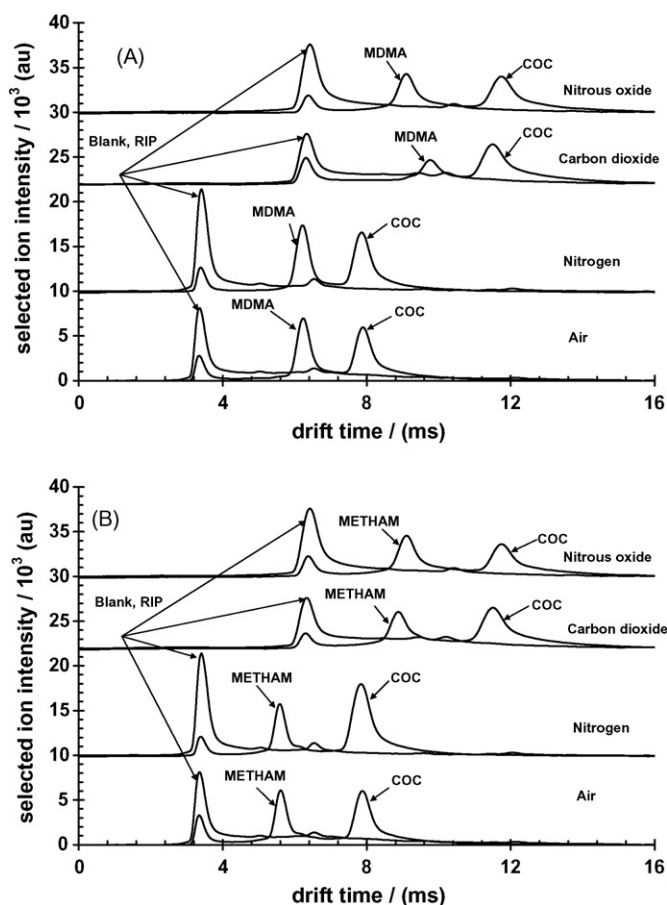


Fig. 4. Ion mobility spectra of (A) MDMA and cocaine mixtures and (B) METHAM and cocaine mixtures. The results demonstrated the pattern of responses obtained for drug mixtures in different drift gases: air, nitrogen, carbon dioxide and nitrous oxide.

polarizable drift gases. The product ion for AMP migrated at  $5.55 \pm 0.01$ ,  $5.53 \pm 0.01$ ,  $9.08 \pm 0.01$  and  $9.27 \pm 0.01$  ms in air, nitrogen, carbon dioxide and nitrous oxide, respectively. On the other hand, the product ion of METHAM migrated at  $5.66 \pm 0.01$ ,  $5.63 \pm 0.01$ ,  $8.97 \pm 0.01$  and  $9.19 \pm 0.01$  ms in air, nitrogen, carbon dioxide and nitrous oxide, respectively. Note that in air AMP had a faster drift time than METHAM while in carbon dioxide it had a slower drift time, demonstrating that these two drugs exhibited different interactions with low and high polarizable drift gases.

Fig. 4(a and b) provides other example spectra of drug mixtures using MDMA:Cocaine and METHAM:Cocaine. As with the AMP and METHAM examples above an increase in drift gas polarizability increased migration times. Reduced mobilities for these drugs in the different gases are given in Table 3. As shown previously, the mobilities of each of these drugs changed as a function of drift gas polarizability.

### 3.2.3. Product ions from explosives

In the negative mode with  $\text{CH}_2\text{Cl}_2$  as the dopant gas, TNT was used as the mobility standard and its  $K_0$  values in both carbon dioxide and nitrous oxide were reported for the first time as  $0.96 \pm 0.01$  and  $0.96 \pm 0.01 \text{ cm}^2 \text{ V}^{-1} \text{ s}^{-1}$ , respectively.

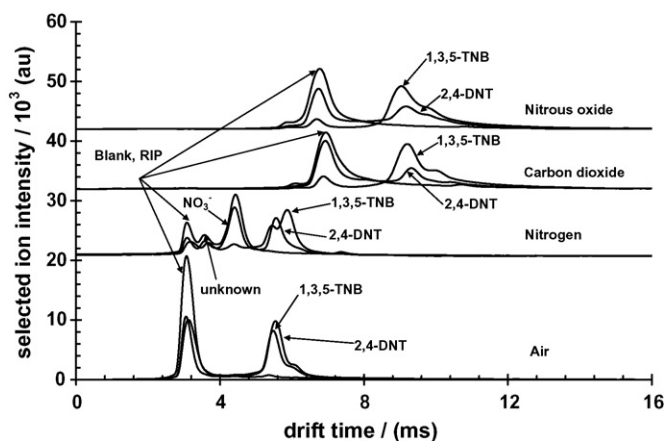


Fig. 5. Ion mobility spectra for 1,3,5-trinitro benzene (1,3,5-TNB) and 2,4-dinitro toluene (2,4-DNT) in different drift gases: air, nitrogen, carbon dioxide and nitrous oxide. The spectra demonstrated that as the polarizability of the drift gas increases, mobility decreases. Furthermore the arrival times of the pair of compounds switches as drift gas changes from low to high polarizability.

Fig. 5 shows examples of negative ion mobility spectral overlays of a background, 1,3,5-trinitro benzene (1,3,5-TNB) and 2,4-dinitro toluene in the different drift gases. When operating in the negative mode, the reactant ion peak is the  $\text{Cl}^-$  ion. Drift times for the reactant ion peak were  $3.05 \pm 0.02$ ,  $3.08 \pm 0.01$ ,  $6.92 \pm 0.01$  and  $6.77 \pm 0.03$  ms in air, nitrogen, carbon dioxide and nitrous oxide, respectively. These drift times produced the following respective reduced mobility values:  $3.05 \pm 0.03$ ,  $3.01 \pm 0.02$ ,  $1.34 \pm 0.01$  and  $1.37 \pm 0.01$   $\text{cm}^2 \text{V}^{-1} \text{s}^{-1}$ . These values compared well with those reduced mobility values reported previously in the literature for chloride ion in air and nitrogen of  $3.06 \pm 0.02$  and  $3.01 \pm 0.01$   $\text{cm}^2 \text{V}^{-1} \text{s}^{-1}$ , respectively [37]. The mobilities of  $\text{Cl}^-$  ion in drift gases of carbon dioxide and nitrous oxide have not previously been reported in the literature. In these studies they were measured to be  $1.34 \pm 0.02$   $\text{cm}^2 \text{V}^{-1} \text{s}^{-1}$  in carbon dioxide and  $1.37 \pm 0.01$   $\text{cm}^2 \text{V}^{-1} \text{s}^{-1}$  for nitrous oxide, respectively. Similar to  $\text{Cl}^-$  ion, the response ions of both 1,3,5-TNB and 2,4-DNT migrated with much longer times in the more polarizable drift gases. The product ion for 1,3-TNB migrated at  $5.49 \pm 0.02$ ,  $5.45 \pm 0.02$ ,  $9.22 \pm 0.02$  and  $9.03 \pm 0.02$  ms in air, nitrogen, carbon dioxide and nitrous oxide, respectively. On the other hand, the product ion of 2,4-DNT migrated at  $5.54 \pm 0.01$ ,  $5.56 \pm 0.01$ ,  $9.32 \pm 0.01$  and  $9.11 \pm 0.01$  ms in air, nitrogen, carbon dioxide and nitrous oxide, respectively. As with the case of the drugs AMP and METHAM, 1,3,5-DNB had a faster drift time than 2,4-DNT in air while in carbon dioxide 1,3,5-DNB had a slower drift time than 2,4-DNT.

Similarly to the positive mode data, the mobility of product ions decreased as the polarizability of the drift gases increased. With the negative ion studies, however, some deviations were observed with respect to the mass of an explosive ion and the expected  $K_0$  value. For example the highest mass of explosives studied was that for PETN with molecular weight of  $316 \text{ g mol}^{-1}$ . PETN however showed the highest  $K_0$  value for all explosives studied. The response ion for PETN was identified by drift time to be that of  $\text{NO}_2^-$  ion. In this investigation,

the thermal desorber was operated at  $220^\circ\text{C}$  using the drugs mode desorber rather than at  $180^\circ\text{C}$  normally used for explosive detection. Thus, the  $\text{NO}_2^-$  ion may have resulted from thermal decomposition of PETN.

The chloride ion, as well as the product ions of 1,3-DNB, 2,3-DNT, 2,4-DNT, 2,6-DNT, 1,3,5-TNB and RDX were all found to drift slower in carbon dioxide than in nitrous oxide while the product ions of 2,4,6-TNT and PETN produced similar drift times in carbon dioxide to those in nitrous oxide (see Table 3).

### 3.3. Relative mobilities of ions in different drift gases

While it is clear from the previous discussion that ion mobility values of a given analyte ion will decrease with increasing mass and polarizability of the drift gas, it also appears that these increases may not be proportional for all ions. If they were proportional, as determined by Russell and co-workers [36] and Karpas and Berant [35] for ions of similar structure, then alternate drift gases would be of little use for effecting novel separations or for use as a confirmatory test in the field. One easy way to determine the proportionality of mobilities in various drift gases is to plot mobility with respect to drift gas polarizability. Plots of reduced mobility versus drift gas polarizability were linear with correlation coefficients  $\geq 0.99$ . The linear regression data summarized from these plots are shown in Table 4. The slopes of these plots provide information on proportionality. If the slopes are the same, then the mobilities are proportional with polarizability and no separation or identification advantages exists with changes in drift gases. As can be clearly seen from the table, the slopes for some compounds vary significantly while others are similar.

The smaller, more compact ions such as  $\text{Cl}^-$ ,  $\text{NH}_4^+$  and  $\text{NO}_2^-$  (the product ion from PETN) where the charge density is

Table 4

Linear regression data for plots of reduced mobility vs. polarizability of four drift gases (air, nitrogen, carbon dioxide & nitrous oxide) obtained from explosive and drug ions

Compound	MWt/g mol <sup>-1</sup>	Reduced mobility		
		(-) Slope	Intercept	R <sup>2</sup>
$\text{Cl}^-$	35.5	$1.36 \pm 0.03$	$5.33 \pm 0.40$	0.99
1,3-DNB	168	$0.57 \pm 0.02$	$2.68 \pm 0.30$	0.99
2,3-DNT	182	$0.53 \pm 0.01$	$2.55 \pm 0.21$	0.99
2,4-DNT	182	$0.53 \pm 0.01$	$2.59 \pm 0.22$	0.99
2,6-DNT	182	$0.53 \pm 0.01$	$2.58 \pm 0.24$	0.99
1,3,5-TNB	213	$0.54 \pm 0.03$	$2.63 \pm 0.41$	0.99
RDX	222	$0.42 \pm 0.01$	$2.19 \pm 0.21$	0.99
TNT	227	$0.46 \pm 0.01$	$2.31 \pm 0.32$	1.00
PETN	316	$0.96 \pm 0.02$	$4.18 \pm 0.41$	0.99
$\text{NH}_4^+$	18	$1.22 \pm 0.02$	$5.07 \pm 0.13$	1.00
AMP	135	$0.53 \pm 0.01$	$2.58 \pm 0.21$	1.00
METHAM	149	$0.49 \pm 0.02$	$2.49 \pm 0.10$	1.00
MDMA	193	$0.44 \pm 0.02$	$2.23 \pm 0.10$	1.00
Morphine	285	$0.31 \pm 0.03$	$1.77 \pm 0.20$	1.00
Cocaine	303	$0.31 \pm 0.01$	$1.70 \pm 0.10$	1.00
THC	314	$0.25 \pm 0.01$	$1.50 \pm 0.20$	1.00
Heroin	369	$0.22 \pm 0.02$	$1.44 \pm 0.10$	1.00
2,4-Lutidine	107	$0.61 \pm 0.01$	$2.99 \pm 0.10$	1.00

Table 5  
Relative mobility ratios for drugs

Compound	$K_0$ (Air)/ $K_0$ (Air)	$K_0$ (N <sub>2</sub> )/ $K_0$ (Air)	$K_0$ (CO <sub>2</sub> )/ $K_0$ (Air)	$K_0$ (N <sub>2</sub> O)/ $K_0$ (Air)
NH <sub>4</sub> <sup>+</sup>	1.00 ± 0.01	0.99 ± 0.01	0.49 ± 0.01	0.48 ± 0.01
2,4-Lutidine	1.00 ± 0.01	1.00 ± 0.01	0.62 ± 0.01	0.61 ± 0.01
AMP	1.00 ± 0.01	1.01 ± 0.01	0.61 ± 0.01	0.60 ± 0.01
METHAMP	1.00 ± 0.01	1.01 ± 0.01	0.63 ± 0.01	0.61 ± 0.01
MDMA	1.00 ± 0.01	1.00 ± 0.01	0.64 ± 0.01	0.63 ± 0.01
Morphine	1.00 ± 0.01	1.00 ± 0.01	0.69 ± 0.01	0.67 ± 0.01
Cocaine	1.00 ± 0.01	1.01 ± 0.01	0.68 ± 0.01	0.67 ± 0.01
THC	1.00 ± 0.01	1.00 ± 0.01	0.71 ± 0.01	0.70 ± 0.01
Heroin	1.00 ± 0.01	1.00 ± 0.01	0.75 ± 0.01	0.73 ± 0.01

high, produced the larger slopes of 1.36, 1.22 and 0.96, respectively. Larger product ions, where the charge density is relatively low, produced the smaller slopes (0.22 for heroin) and were less affected by the polarizability of the drift gas. Thus, it would seem that ions with high charge density are capable of more efficiently polarizing gases with high polarizability than are ions with a lower charge density.

Table 4 provides a wealth of information with respect to the separation and identification of ions by the use of alternate drift gases. In summary, there are three conditions of interest:

- (1) When both the slope and intercept of reduced mobility versus polarizability plots are the same, no separation or qualitative information is possible by varying the drift gas. Compounds which fall into this category include the dinitrotoluenes. They all have slopes of 0.53 and intercepts of 2.55–2.59.
- (2) When the slope is the same but the intercepts are different, ions can be separated by IMS in all gases but no qualitative information is obtained by varying the drift gas. An example of this class would be morphine and cocaine. Both have slopes of 0.31 but they have intercepts of 1.77 and 1.70, respectively. These drugs can be separated in all drift gases but varying the drift gas does not provide additional information on their identity.
- (3) The third case is where ions have a different slope. In this case, ions can potentially be separated in one gas but not in another and changes in drift gas provide additional qualitative information. Compounds which fall into this classification include heroin and cocaine where the slopes are 0.22 and 0.31, respectively. Other examples of this class

of compounds include DNT and RDX with slopes of 0.53 and 0.42; DNT and TNT with slopes of 0.53 and 0.46 and TNT and PETN with slopes of 0.46 and 0.96.

Changes in relative mobilities of ions in one drift gas relative to another allow the use of alternate drift gases for compound confirmation. Tables 5 and 6 provide mobility ratios relative to air for the drugs and explosives tested in this study. For example, the ratio of the reduced mobilities of the product ion for cocaine in carbon dioxide to that in air was determined to be  $0.68 \pm 0.01$  and that for amphetamine was found to be  $0.61 \pm 0.01$ . Thus, by comparing the two drugs in the two different gases, additional qualitative information can be obtained. If an ion mobility peak has the same mobility as amphetamine in air and the same relative mobility as amphetamine in carbon dioxide then the probability that the ion producing this peak was the product ion for the drug amphetamine is higher than if only the mobility peak in air is used as the qualifying data.

Even when relative mobilities are similar such as the case with amphetamine and methamphetamine clear distinctions can be made in the spectrum. For example, the carbon dioxide/air relative mobilities of amphetamine and methamphetamine were found to be  $0.61 \pm 0.01$  and  $0.63 \pm 0.01$ , from the spectra shown in Fig. 3. It was clear that the compounds reversed elution patterns from gases of high to low polarizability. In air the amphetamine eluted before the methamphetamine while in carbon dioxide it eluted after the methamphetamine.

While the example of amphetamine and methamphetamine is one in which the relative mobilities are similar, the example of THC and Heroin provide a clear example of the effect of alternate drift gas on relative mobilities. The carbon dioxide/air

Table 6  
Relative mobility ratios for explosives

Compound	$K_0$ (Air)/ $K_0$ (Air)	$K_0$ (N <sub>2</sub> )/ $K_0$ (Air)	$K_0$ (CO <sub>2</sub> )/ $K_0$ (Air)	$K_0$ (N <sub>2</sub> O)/ $K_0$ (Air)
Cl <sup>-</sup>	1.00 ± 0.01	0.99 ± 0.01	0.44 ± 0.01	0.45 ± 0.01
1,3-DNB	1.00 ± 0.02	1.00 ± 0.02	0.57 ± 0.02	0.60 ± 0.02
2,3-DNT	1.00 ± 0.02	0.98 ± 0.02	0.58 ± 0.02	0.60 ± 0.02
2,4-DNT	1.00 ± 0.01	0.99 ± 0.01	0.60 ± 0.01	0.61 ± 0.01
2,6-DNT	1.00 ± 0.01	0.99 ± 0.01	0.60 ± 0.01	0.61 ± 0.01
1,3,5-TNB	1.00 ± 0.02	1.01 ± 0.02	0.60 ± 0.02	0.61 ± 0.02
RDX	1.00 ± 0.01	1.00 ± 0.01	0.64 ± 0.01	0.65 ± 0.01
TNT	1.00 ± 0.01	1.02 ± 0.01	0.64 ± 0.01	0.64 ± 0.01
PETN	1.00 ± 0.02	1.00 ± 0.02	0.53 ± 0.02	0.53 ± 0.02

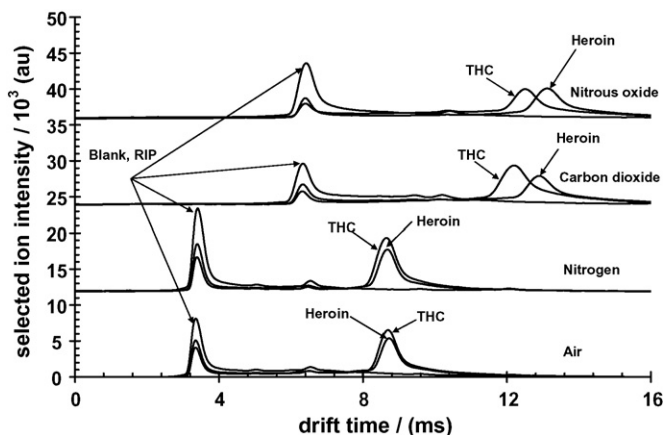


Fig. 6. Ion mobility spectra of heroin and tetrahydrocannabinol (THC) in different drift gases: air, nitrogen, carbon dioxide and nitrous oxide. The spectra illustrates the two compounds can be resolved with high-polarizability drift gases carbon dioxide and nitrous oxide.

relative mobility of THC was measured to be  $0.71 \pm 0.01$  and the relative mobility of heroin was  $0.75 \pm 0.01$ . As shown in Fig. 6, THC and heroin could not be separated in air but were well separated in carbon dioxide and nitrous oxide.

#### 4. Conclusion

Reduced mobility values for drugs and explosives measured in various drift gases indicate that relative mobilities of some drugs and explosives vary significantly and reproducibly. This variance in relative mobility among drift gases demonstrated that confirmatory tests for explosive or drug detection may be performed rapidly in the field by simply changing drift gas composition. For example, a small carbon dioxide cylinder could be attached to the back of a commercial IMS unit and used to switch between air and carbon dioxide drift gases to confirm results for drugs and explosives and reduce the incidence of false positive responses. In addition, the choice of drift gas can have a modest effect on separation selectivity (similar to GC stationary phases), in some cases enabling the resolution of hard-to-resolve compounds by the prudent choice of the IMS drift gas.

The use of secondary drift gases for confirmation is somewhat limited in IMS instruments with low resolving powers such as those currently used in the field. Instruments with higher resolving powers, however, would reduce the number of false positive responses to drugs and explosives due to better ion mobility discrimination between the target compound and interfering ions as well as the potential of using secondary gases for added identity confirmation.

#### Acknowledgements

The authors acknowledge GE Security for partial support of this project. We particularly thank Dr. Paul H. Haigh, Dr. Ching Wu and Mr. Robert Baker for their support in this investigation. We also thank Dr. Maggie Tam for discussions and her input into this manuscript.

#### References

- [1] M.J. Cohen, F.W. Karasek, *J. Chromatogr. Sci.* 8 (1970) 330–337.
- [2] A.B. Kanu, H.H. Hill, *Lab Plus Int.* 18 (April/May (2)) (2004) 20–26.
- [3] G. Gillen, C. Mahoney, S. Wight, R. Lareau, *Rapid Commun. Mass Spectrom.* 20 (12) (2006) 1949–1953.
- [4] J. Luong, R. Gras, R. Van Meulebroeck, *J. Chromatogr. Sci.* 44 (5) (2006) 276–282.
- [5] J.I. Baumbach, *Anal. Bioanal. Chem.* 384 (5) (2006) 1059–1070.
- [6] I.A. Buryakov, *Tech. Phys. Lett.* 32 (1) (2006) 67–69.
- [7] I.A. Buryakov, NATO Science Series, II: Mathematics, Physics and Chemistry (Vapor and Trace Detection of Explosives for Anti-Terrorism Purposes) 167 (2004) 113–121.
- [8] V.M. Gruznov, M.N. Baldin, V.G. Filonenko, NATO Science Series, II: Math., Phys. Chem. (Vapor and Trace Detection of Explosives for Anti-Terrorism Purposes) 167 (2004) 87–99.
- [9] J.K. Likhnauth, N.H. Snow, *J. Chromatogr. A* 1105 (1–2) (2006) 33–38.
- [10] V.S. Pershenkov, A.D. Tremasov, V.V. Belyakov, A.U. Razvalyayev, V.S. Mochkin, *Microelectron. Reliab.* 46 (2–4) (2006) 641–644.
- [11] K.B. Pfeifer, S.B. Rohde, K.A. Peterson, A.N. Rumpf, *IJIMS* 7 (2) (2004) 52–58.
- [12] A.J. Marr, D.M. Groves, *IJIMS* 6 (2) (2003) 59–62.
- [13] J.L. Neves, P.E. Haigh, C. Wu, W.J. McGann, *IJIMS* 6 (2) (2003) 1–3.
- [14] J.M. Perr, K.G. Furton, J.R. Almirall, *J. Sep. Sci.* 28 (2) (2005) 177–183.
- [15] H. Koyuncu, E. Seven, A. Calimli, *Turk. J. Chem.* 29 (3) (2005) 255–264.
- [16] R. Lareau, NATO Science Series, II: Math., Phys. Chem. (Electronic Noses & Sensors for the Detection of Explosives) 159 (2004) 289–299.
- [17] K.L. Linker, C.A. Brusseau, M.-A. Mitchell, D.R. Adkins, K.B. Pfeifer, A.N. Rumpf, S.B. Rohde, Annual Meeting Proceedings of the Institute of Nuclear Materials Management 44th, 2003, pp. 38–42.
- [18] G.A. Eiceman, J.A. Stone, *Anal. Chem.* 76 (21) (2004) 390A–397A.
- [19] J.K. Likhnauth, N.H. Snow, *J. Sep. Sci.* 28 (7) (2005) 612–618.
- [20] A. Miki, M. Tatsuno, M. Katagi, M. Nishikawa, H. Tsuchihashi, *Jpn. J. Forensic Toxicol.* 15 (2) (1997) 142–143.
- [21] J.J. Carroll, T. Le, R. DeBono, *Am. Lab.* 36 (4) (2004) 32–34.
- [22] R. Debono, S. Stefanou, M. Davis, G. Walia, *Pharm. Technol. North Am.* 26 (4) (2002), 72,74,76,78.
- [23] A.H. Lawrence, *Anal. Chem.* 61 (4) (1989) 343–349.
- [24] T. Keller, A. Keller, E. Tutsch-Bauer, F. Monticelli, *Forensic Sci. Int.* 161 (2–3) (2006) 130–140.
- [25] A.B. Kanu, P.E. Haigh, H.H. Hill Jr., *Anal. Chim. Acta* 553 (1–2) (2005) 148–159.
- [26] E.E. Tarver, *Sensors* 4 (1–3) (2004) 1–13.
- [27] G.A. Eiceman, Z. Karpas, *Ion Mobility Spectrometry*, second ed., CRC Press, Taylor & Francis, Boca Raton, FL, 2005.
- [28] S. Rokushika, H. Hatano, H.H. Hill, *Anal. Chem.* 58 (2) (1986) 361–365.
- [29] H.W. Ellis, R.Y. Pai, I.R. Gatland, E.W. McDaniel, R. Wernlund, M.J. Cohen, *Anal. Chem.* 64 (1976) 3935–3941.
- [30] G.R. Asbury, H.H. Hill, *Anal. Chem.* 72 (3) (2000) 580–584.
- [31] L.M. Matz, H.H. Hill, I.W. Beegle, I. Kanik, *J. Am. Soc. Mass Spectrom.* 13 (2002) 300–307.
- [32] M.F. Mesleh, J.F. Hunter, A.A. Shvartsburg, G.C. Schatz, M.F. Jarrold, *J. Phys. Chem.* 100 (1996) 16082–16086.
- [33] A.A. Shvartsburg, M.F. Jarrold, *Chem. Phys. Lett.* 261 (1996) 86–91.
- [34] A.A. Shvartsburg, S.V. Mashkevich, K.W.M. Siu, *J. Phys. Chem. A* 104 (2000) 9448–9453.
- [35] Z. Karpas, Z. Berant, *J. Phys. Chem.* 93 (1989) 3021–3025.
- [36] B.T. Ruotolo, J.A. McLean, K.J. Gillig, D.H. Russell, *J. Mass Spectrom.* 39 (2004) 361–367.
- [37] C. Shumate, R.H. St Louis, H.H. Hill Jr., *J. Chromatogr.* 373 (1986) 141–173.
- [38] B. Lescop, M.B. Arfa, Coz G. Le, M. Cherid, G. Sinon, G. Fanjoux, A. Le Nadan, F. Tuffin, *J. Phys. II France* 7 (1997) 1543–1554.



## Monitoring of environmental phenolic endocrine disrupting compounds in treatment effluents and river waters, Korea

Eun-Joung Ko<sup>a</sup>, Kyoung-Woong Kim<sup>b,\*</sup>, Seo-Young Kang<sup>b</sup>, Sang-Don Kim<sup>b</sup>,  
Sun-Baek Bang<sup>b</sup>, Se-Yeong Hamm<sup>a</sup>, Dong-Wook Kim<sup>c</sup>

<sup>a</sup> Division of Earth Environmental System, Pusan National University, Jangjun-dong, Geumjeong Gu, Busan, Republic of Korea

<sup>b</sup> International Environmental Research Center, Gwangju Institute of Science and Technology, 1 Oryong-dong Buk-gu, Gwangju, Republic of Korea

<sup>c</sup> Department of Environmental Engineering, Kongju National University, 275, Bundae-dong, Cheonan, Republic of Korea

Received 25 January 2007; received in revised form 19 April 2007; accepted 19 April 2007

Available online 27 April 2007

### Abstract

The last two decades have witnessed growing scientific and public concerns over endocrine disrupting compounds (EDCs) that have the potential to alter the normal structure or functions of the endocrine system in wildlife and humans. In this study, the phenolic EDCs such as alkylphenol, chlorinated phenol and bisphenol A were considered. They are commonly found in wastewater discharges and in sewage treatment plant. In order to monitor the levels and seasonal variations of phenolic EDCs in various aquatic environments, a total of 15 water samples from the discharged effluent from sewage and wastewater treatment plants and river water were collected for 3 years. Ten environmental phenolic EDCs were determined by GC–MS and laser-induced fluorescence (LIF). GC–MS analysis revealed that most abundant phenolic EDCs were 4-*n*-heptylphenol, followed by nonlyphenol and bisphenol A during 2002–2003, while 4-*t*-butylphenol and 4-*t*-octylphenol were newly detected in aquatic environments in 2004.

The category of phenolic EDCs showed similar fluorescence spectra and nearly equal fluorescence decay time. This makes it hard to distinguish each phenolic EDC from the EDCs mixture by LIF. Therefore, the results obtained from LIF analysis were expressed in terms of the fluorescence intensity of the total phenolic EDCs rather than that of the individual EDC. However, LIF monitoring and GC–MS analysis showed consistent result in that the river water samples had lower phenolic EDCs concentration compared to the effluent sample. This revealed a lower fluorescence intensity and the phenolic EDCs concentration in summer was lower than that in winter. For the validation of LIF monitoring for the phenolic EDCs, the correlation between EDCs concentration acquired from GC–MS and fluorescence intensity from LIF was obtained ( $R=0.7379$ ). This study supports the feasibility of the application of LIF into EDCs monitoring in aquatic systems.

© 2007 Elsevier B.V. All rights reserved.

**Keywords:** Endocrine disrupting compounds (EDCs); Effluent and river water samples; GC–MS; Laser-induced fluorescence (LIF); Seasonal variation

### 1. Introduction

For the past several decades, human activities have increased the production of many xenobiotics, indicating unknown fates in the natural water system. The compelling evidence has been accumulated showing that some of these natural and synthetic chemical compounds can mimic or antagonize the normal functioning of endocrine systems and can cause reproductive and immune system problems in wildlife [1–4]. These chemicals

are generally considered to be endocrine disrupting chemicals (EDCs). Regarding various EDCs, phenolic compounds known as xenoestrogens, such as alkylphenols and bisphenol A, are not produced naturally. It means that their presence in the environment is solely a consequence of anthropogenic activity. Alkylphenols (APs) in environments are mainly originated from the degradation of alkylphenol polyethoxylates (APEs), which have been used as nonionic surfactants or detergents in industries and households [1,5–6]. Bisphenol A is released through its use in polycarbonate plastics, epoxy resins and phenoxy resins, which are utilized in food storage containers and in dental sealants [7]. These phenolic EDCs have been introduced into the aquatic system and organisms not only through the

\* Corresponding author. Tel.: +82 62 970 2442; fax: +82 62 970 2434.  
E-mail address: [kwkim@gist.ac.kr](mailto:kwkim@gist.ac.kr) (K.-W. Kim).

discharge from industrial and municipal wastewater treatment plant effluents, but also due to direct discharge such as through pesticides [8–10]. Also, several studies have examined the occurrence and distribution of PCBs, PAHs and APs in sediment and water samples from Lake Shihwa, Masan Bay, Heyongsan River and Ulsan Bay in Korea [11–14]

This globally increased concern toward EDCs induced a necessity to develop highly sensitive and specific analytical tools for their determination in environmental samples. The analytical determination of EDCs has been dominated by chromatographic methods (GC and LC) coupled to sensitive and specific detection systems, such as MS. It has also been preceded by complicated, time- and labor-consuming sample preparation [15–17].

Fluorescence spectroscopy using laser as light sources has been recognized as a promising analytical tool for *in situ* environmental analysis to overcome the limitation of the traditional monitoring techniques using GC and LC. Even though these excellent laboratory techniques can be developed for the selective analysis of EDCs, environmental monitoring still requires fast, selective and sensitive *in situ* pollutant detection [18,19].

Most aromatic hydrocarbons are excited in the ultraviolet and visible spectral range, and the high intensity of their fluorescence signals can be used for the detection of these contaminants. Especially polycyclic aromatic hydrocarbons (PAHs) was successfully detected in water samples such as river near former gaswork location [20–24] and soil samples [25] at a high level of sensitivity by using the laser-induced fluorescence (LIF) technique in combination with fiber optic guidance of the exciting laser beam and of the induced fluorescence light. The LIF monitoring techniques provide significant advantages, such as

reduced time and cost of the analysis, and bypass the complicated experimental procedures, such as sampling, clean up and extraction. As a portable, and power independent system, it can also be easily used for continuous *in situ* monitoring [19,21–24]. However, it is rare that the application of LIF into phenolic compounds monitoring except for laboratory experiments of single phenol molecule detection limits [19]. Therefore, in this study, a LIF method as powerful tools for monitoring phenolic compounds was examined.

The class of target phenolic EDCs, which was used in this study, is chlorophenols, bisphenol A and alkylphenol. The objectives of this study were to monitor the level of environmental phenolic EDCs in various aquatic samples and to investigate the feasibility of the LIF application into *in situ* monitoring of phenolic EDCs in the water system. For the validation of the LIF application to EDC monitoring, the relationship between analytical results of total phenolic EDCs concentrations by GC–MS and LIF intensity was also compared for the 15 water samples from sewage and wastewater treatment plants and river system.

## 2. Experimental

### 2.1. Chemicals and reagents

All reagents were of analytical reagent grade. The phenolic EDCs studied were: 2,4-dichlorophenol, 4-*tert*-butylphenol, 4-*n*-butylphenol, 4-*n*-hexylphenol, 4-*n*-heptylphenol, nonylphenol, 4-*n*-octylphenol, pentachlorophenol, and bisphenol A. All of the phenols were purchased from the Aldrich Chemical Co.

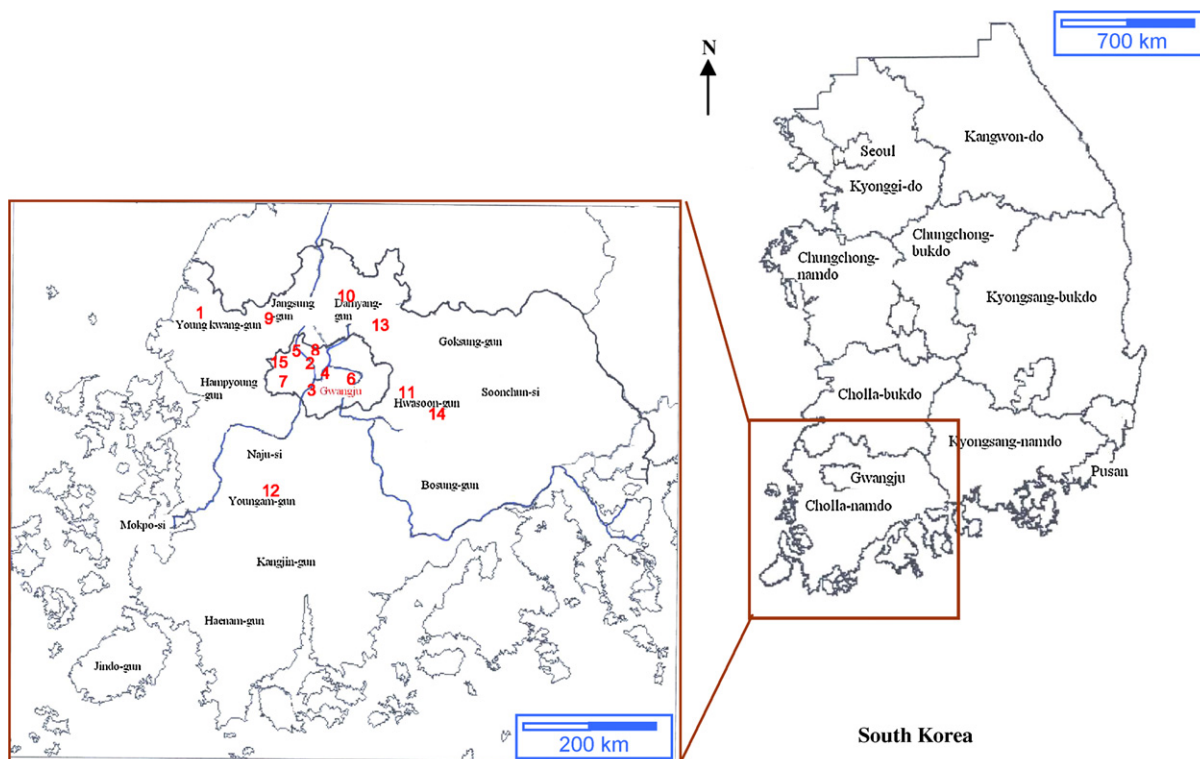


Fig. 1. The location of 15 sampling sites.

Table 1  
List of the 15 water samples used for phenolic EDC monitoring

Sample no.	Sampling sites	Remark <sup>a</sup>	Sampling time				
			2002	2003	2004		
			September	October	February	May	August
1	Yeonwoo Bridge, Watan-chun, Youngkwang	R	✓	✓	✓	✓	✓
2	Songjung Bridge, Hwangryoung River	R	✓	✓	✓	✓	✓
3	Hanam (II) Bridge, Geugrak River	R	✓	✓	✓	✓	✓
4	Sandong Bridge, Youngsan River	R	✓	✓	✓	✓	✓
5	Sochon Bridge, Hwangryoung River	R	–	–	✓	✓	✓
6	Chipyung-dong, Gwangju	S	✓	✓	✓	✓	✓
7	Songdae, Gwangju	S	–	–	✓	✓	✓
8	GIST, Gwangju	S	✓	✓	✓	✓	✓
9	Jangsung, Chonnam	S	✓	✓	✓	✓	✓
10	Damyang, Chonnam	S	✓	✓	✓	✓	–
11	Hwasoon, Chonnam	S	✓	✓	✓	✓	✓
12	Youngam, Chonnam	W	–	–	✓	✓	✓
13	Gumsung, Damyang, Chonnam	W	–	–	✓	✓	✓
14	Dongmeon, Hwasoon, Chonnam	W	–	–	✓	✓	✓
15	Sochon, Gwangju	W	–	–	✓	–	✓

<sup>a</sup> R: sample from river; S: effluent sample from sewage treatment plant; W: effluent sample from wastewater treatment plant.

Stock standard solutions were prepared by dissolving 10 µg of each target compound into 10 ml of dichloromethane (DCM) and stored in an amber glass vial at –20 °C. The working standard solutions were further diluted from the stock solution with dichloromethane (DCM) and placed in a dark glass bottle and stored at 4 °C.

## 2.2. Sample preparation

Aquatic samples were collected from fifteen sites. Five water samples were collected from local rivers (Youngsan, Geugrak, Hwangryoung River and Watan-chun). Six samples were collected from local sewage treatment plants (Gwangju, GIST (Gwangju Institute of Science and Technology), Songdae, Jangsung, Damyang and Hwasoon), and four samples were also collected from local wastewater treatment plants (Youngam, Gumsung, Dongmeon and Sochon) (Fig. 1). Details about sampling site and times were described in Table 1. Fig. 2 shows a flow chart detailing pretreatment prior to the use of GC–MS in EDC monitoring. Each sample was prepared and extracted in duplicate to be used for GCMS analysis and for the LIF analysis.

## 2.3. GC–MS analysis

Aqueous samples were analyzed for the phenolic EDCs using an HP 5890 capillary GC instrument equipped with a Shimadzu QP5000 mass selective detector (MS) in the selective ion monitoring (SIM) mode. System control and data acquisition were performed with the HP MSD Chemstation containing the Wiley Library. The selected ion groups and the retention time of each target compound are listed in Table 2. One microliter of samples was injected through an autosampler AOC-17 (Shimadzu) into the HP-5MS capillary column coated with 5% diphenyl and 95% dimethylpolysiloxane (30 m × 0.25 mm × 0.25 m film thickness). Helium gas was used as a carrier gas at a flow rate of

Table 2  
Selected ion groups for the monitoring of phenolic EDCs

Analyte	Retention time (min)	Quantification ion	Confirmation ion
2,4-Dichlorophenol	10.15	162	63/98/126
4- <i>tert</i> -Butylphenol	11.51	135	107/150/41
4- <i>n</i> -Butylphenol	12.65	107	150/77/121
4- <i>n</i> -Hexylphenol	14.49	107	178/77/39
4- <i>tert</i> -Octylphenol	15.56	135	107/41/119
4- <i>n</i> -Heptylphenol	16.48	107	192/77/41
Nonylphenol	16.79	135	107/149/121
Pentachlorophenol	17.37	266	165/95/202
4- <i>n</i> -Octylphenol	17.41	107	206/96/77
Bisphenol A	21.66	213	228/119/91

1 ml/min. The temperature of the injection port and detector was 280 and 290 °C, respectively. The oven temperature was held at 60 °C for 4 min and increased at a rate of 10 °C/min from 60 to 280 °C, and finally held at 280 °C for 5 min.

Surrogate standards were added to each sample before extraction to confirm the extraction procedure. Procedural blanks, solvent blanks and control samples were included in each batch of analyses. A calibration standard solution of 1 µg/ml was injected in duplicate to monitor the instrumental sensitivity and reproducibility every time before sample analysis.

## 2.4. LIF analysis

The compact LIF system is comprised of four parts: a pulsed UV laser, a fiber-optic probe, a detection unit for time resolved detection and spectrally resolved detection of the fluorescence light, and the control and data acquisition unit (Fig. 3). A diode laser pumped neodymium-doped yttrium aluminium garnet (Nd:YAG) laser deliver 7 ns pulses at 266 nm with energies of 40 µJ at a 100 Hz repetition rate. The detection unit is an optical multi-channel analyzer with a time resolution of 5 ns, which

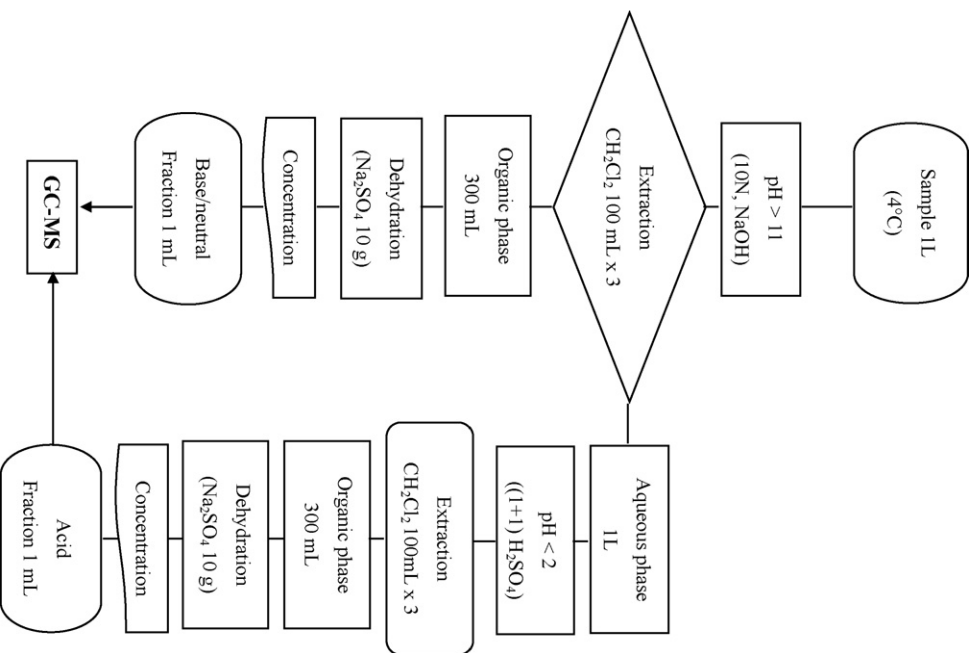


Fig. 2. Analytical protocol used for the pretreatment in the monitoring of EDCs.

consists of a spectrograph, a gateable image intensifier and a charge-coupled device (CCD) camera. Time resolved spectra are recorded by shifting the gate relative to the laser pulse. The spectral resolution is determined over a spectral range from 270 to 600 nm. The fiber was designed with four 400  $\mu\text{m}$  detection fibers around one 600  $\mu\text{m}$  excitation fiber [19,20].

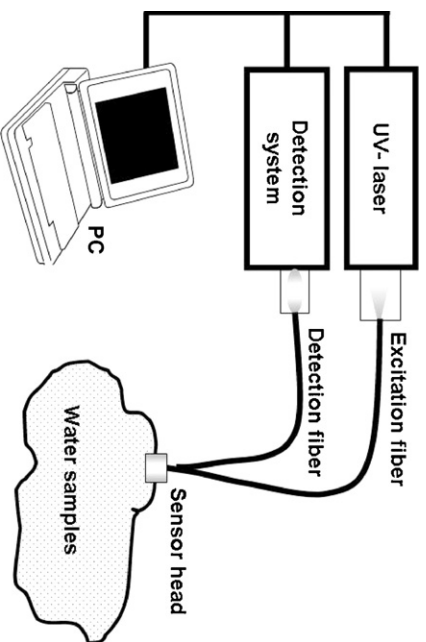


Fig. 3. Schematic diagram of LIF system.

Table 3  
Concentration of detected target phenolic EDCs in water samples during 2002–2003

Sampling time	Concentration of target EDCs ( $\mu\text{g/l}$ )																			
	2,4-Dichlorophenol		4- <i>n</i> -Butylphenol		4- <i>n</i> -Hexylphenol		4- <i>n</i> -Heptylphenol		4- <i>n</i> -Octylphenol		4- <i>t</i> -Butylphenol		4- <i>t</i> -Octylphenol		Nonylphenol		Bisphenol A		Penta-chlorophenol	
	2002	2003	2002	2003	2002	2003	2002	2003	2002	2003	2002	2003	2002	2003	2002	2003	2002	2003	2002	2003
Yeonwoo B (R) <sup>a</sup>	-	-	-	-	-	-	362.7	159.2	-	-	-	-	-	-	135.7	65.9	38.7	36.8	-	-
Songjung B (R)	-	-	-	-	-	-	361.1	166.4	20.9	-	-	-	-	-	244.8	62.8	29	39.4	-	-
Hanam B (R)	-	-	-	-	-	-	399	163.5	-	-	-	-	-	-	-	44.2	24.6	-	-	-
Sandong B (R)	-	-	-	-	-	-	377.3	133.8	-	-	-	-	-	-	182.8	74.4	29.3	20.2	-	-
Sochon B (R)	-	-	-	-	-	-	-	-	-	-	-	-	-	-	-	-	-	-	-	-
Gwangju-CP (S)	-	-	-	-	-	-	345.5	106.5	-	-	29.3	-	-	-	93.8	122.7	43.2	36.6	-	-
Songdea (S) <sup>b</sup>	-	-	-	-	-	-	-	-	-	-	-	-	-	-	-	-	-	-	-	-
GIST (S)	213.4	-	-	-	101.6	-	-	180.6	-	-	218.2	-	185.9	-	299.2	143.8	213.6	34.2	-	-
Jangjung (S)	19.1	-	-	-	-	-	376.4	137.4	-	-	25.7	-	-	-	327.3	110.7	39.3	24.8	54.2	-
Damyang (S)	-	-	-	-	-	-	384.1	162.1	21	-	-	-	-	-	57.4	92.1	39.6	43.5	-	-
Hwasoon (S)	17.4	-	-	-	-	-	333	79.5	-	-	-	-	-	-	186.6	86.4	35.9	46.1	-	-

‘-’: not detected.

<sup>a</sup> R: river.

<sup>b</sup> S: sewage treatment plant.

The EDCs were determined using a LIF system equipped with a fiber optic sensor. The results of the measurement are expressed in a 3D matrix, comprised of the fluorescence intensity ( $I_F$ ) against time and emission wavelength. In order to acquire the characteristic decay time and wavelength coverage of each EDC, the spectra of each EDC sample with 5 mg/l were recorded with the LIF system. For calibration of the LIF system, measurements were conducted using a single phenolic EDC solution and mixtures solution with 0, 10, 50, 100, 200, and 500  $\mu\text{g/l}$ . The detection limits of each EDC and total EDCs were calculated from this linear regression. The detection limits were calculated as the sum of the triple standard deviation of the blank ( $n=8$ ) and the intercept of the calibration plot. Five measurements per each sample from 15 sites were recorded and averaged to get total fluorescence intensity.

### 3. Results and discussion

#### 3.1. GC–MS analysis of phenolic EDCs in aquatic samples

The river, sewage and wastewater treatment plant water samples collected in Chunnam Province, Korea, were analyzed to identify the existence of phenolic EDCs using GC–MS. These monitoring activities regarding phenolic EDCs contamination in the environment were carried out from September 2002 to August 2004. The concentration of 10 phenolic EDCs from 15 sites during 2002–2003 are shown in Table 3.

Below, the discussion is divided two groups. The first group includes the concentration of phenolic EDCs during 2002–2003. The second group includes measurement data set for 2004 to observe seasonal variations. The standard deviation for the duplicate samples was lower than 8%. The recovery of the surrogates

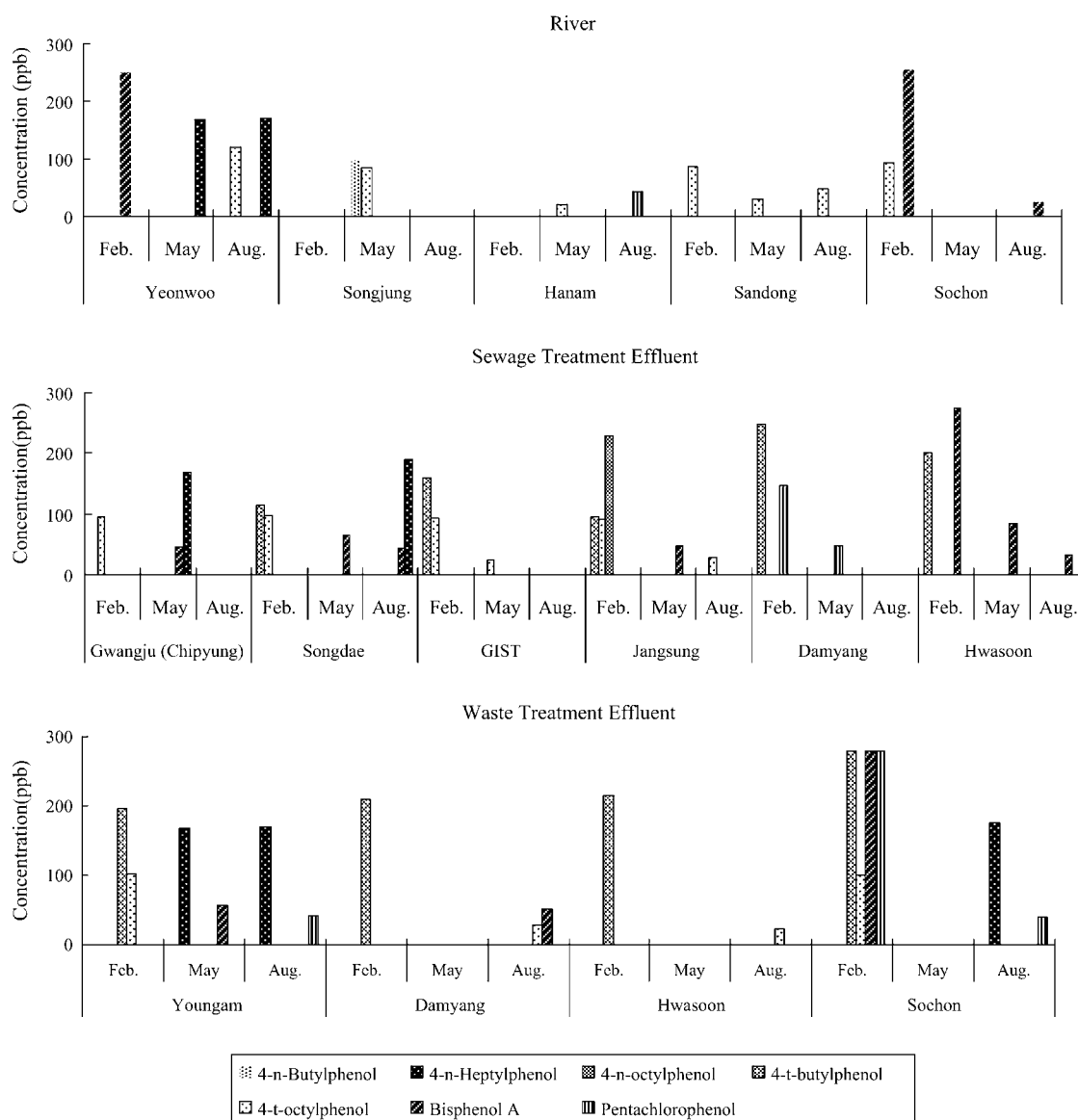


Fig. 4. Seasonal variation of detected target phenolic EDCs during sampling duration 2004.

was also within the range of 75–115%. The detection limit was 10  $\mu\text{g/l}$  for all target phenolic EDCs.

Among the 10 phenolic EDCs studied here, the most abundant compound during the period 2002–2003 was 4-*n*-heptylphenol, with 60% of the samples, followed by nonylphenol and bisphenol A, which were mostly detected in river and sewage treatment effluent samples with 53.3% of the sample size, respectively. Nonylphenol, octylphenol as well as bisphenol A were the mostly detected phenolic compounds in aquatic environment [11–14], and this corresponds with the occurrence of phenolic compounds for Chennai province in this study. It is also interesting that the most abundant compound is 4-*n*-heptylphenol rather than nonylphenol considering that degradation of linear chain isomer is faster than branched. However, the degradation rate is determined by several factors such as the chemical structures of the alkylphenol isomers, activity of amount of microorganisms and surrounding environment [27]. 4-*n*-Heptylphenol was found at the highest concentration in the water samples, except for wastewater treatment water samples, which ranged from 333 to 399  $\mu\text{g/l}$  and from 79.5 to 180.6  $\mu\text{g/l}$  in 2002 and 2003, respectively. Nonylphenol concentration was between 57.4 and 327.3  $\mu\text{g/l}$  and between 44.2 and 143.8  $\mu\text{g/l}$  in 2002 and 2003, respectively. For bisphenol A, the average concentration showed no significant differences in 2002 and 2003, with value of 34.95  $\mu\text{g/l}$  ( $\pm 6.52$ ) and 35.2  $\mu\text{g/l}$  ( $\pm 8.81$ ), respectively except for GIST sewage treatment effluent samples. The concentration of nonylphenol is three times higher than those for Lake shihwa [11]. There is no significant change in water sample from river and sewage treatment plant effluent. This can be explained by the unsuccessful operation of sewage treatment facilities and unpermitted discharges. Also, these water samples were collected from river and sewage treatment plant, indicating that these compounds not originated from industrial application. For other phenolic EDCs, trace levels in the range of non-detectable to 29.3  $\mu\text{g/l}$  were detected in river water as well as in sewage treatment effluent samples, except for 4-*n*-butylphenol. Also, detected compounds were lower than 20% of the sample size. An overall assessment of the results reveals that in 2002 the effluent sample from GIST was the most contaminated sample by target EDCs in this study, with six of the ten target compounds being detected. Furthermore, the concentration of target compounds was significantly higher in the samples from GIST in 2002–2003, in comparison to concentrations measured in other samples. This means that the treatment process was not successful as a means to control the phenolic compounds level. The sewage treatment effluent from Jangsung also had the highest concentration for 4-*n*-heptylphenol as well as nonylphenol, with six of the ten target compounds being detected.

On the other hand, water samples from 15 sites were collected three times (February, May and August) in 2004 to determine the seasonal variation in phenolic EDCs. These results indicated that nonylphenol, one of the most abundant phenolic EDCs during 2002–2003, as well as 2,4-dichlorophenol and 4-*n*-hexylphenol, were not detected in most samples during 2004. Contrarily, 4-*tert*-butylphenol and 4-*tert*-octylphenol newly appeared in 2004, and were not detected in any sample collected during 2003.

The seasonal variation of target compounds from river and effluent samples showed the concentration of EDCs in summer is lower than that in winter in most samples (Fig. 4). The most abundant compound was 4-*tert*-butylphenol, followed by 4-*tert*-octylphenol. 4-*tert*-butylphenol was present in more than 60% of the samples with concentrations ranging from 95 to 280  $\mu\text{g/l}$ . This concentration in river water during the rainy season (May and August), were mostly below their detection limit. The concentration of 4-*tert*-butylphenol was found to be in a range from less than LOD (limit of detection) to 100  $\mu\text{g/l}$  in more than 53% of samples in the dry season (February). Also, it was observed that the frequency and concentration of the phenolic EDCs being detected decreased in the rainy season. It can be explained in part that the degradation rate of alkylphenol is faster in summer than winter [28]. 4-*n*-butylphenol, 4-*n*-octylphenol and pentachlorophenol detected in water samples were mostly less than LOD and few measurable quantities of these compounds were found in less than 11.1% of all water samples with concentrations ranging from 40 to 280  $\mu\text{g/l}$ . Nonylphenol and bisphenol A were continually detected during the period 2004. The high level of bisphenol A was also detected in the dry season and the detectable concentration is almost similar in less than

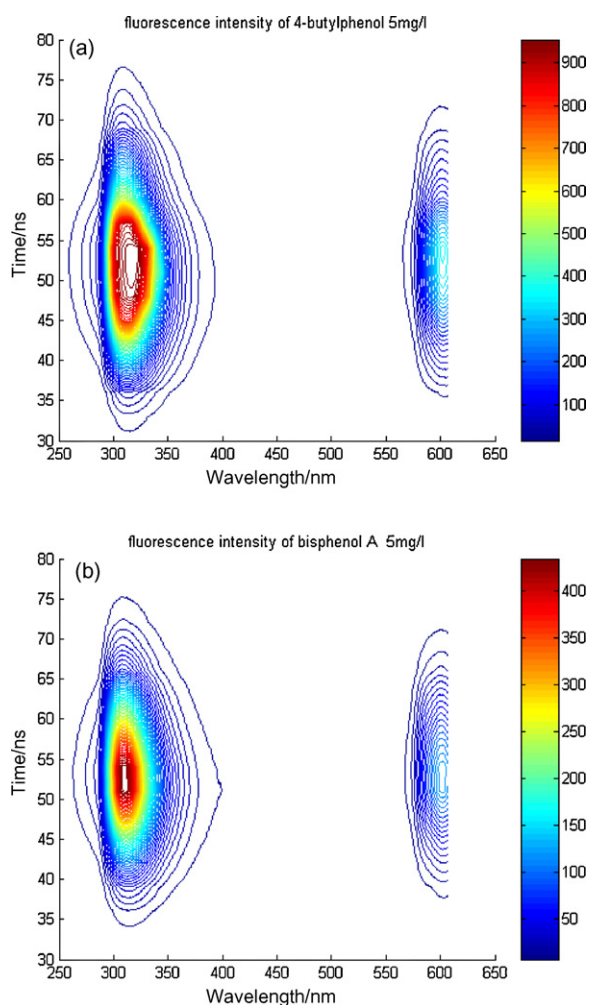


Fig. 5. Fluorescence spectra of (a) 4-butylphenol 5 mg/l and (b) bisphenol A 5 mg/l.

31% of all water samples. However, 4-*n*-heptylphenol showed no significant differences in concentration over the monitoring period of 2003 and 2004.

As a result, the concentrations of target compounds in samples obtained during 2002 were higher than those of 2003–2004, and the levels of target compounds in effluent samples were higher than those of river samples.

### 3.2. LIF spectroscopy monitoring of phenolic EDCs in aquatic samples

The level of each phenolic EDC from standard solution and total phenolic EDCs from the water sample collected from 15 sites were measured with a LIF sensor. It was observed that there are many difficulties when differentiating each phenolic EDC from fluorescent compounds present in the aquatic system. The first reason is that the wavelength coverage of each phenolic EDC is very similar, revealing a characteristic spectra range from 285 to 355 nm with a peak wavelength of 308 nm [30]. Generally, it could be used that the difference in fluorescence decay times in order to distinguish spectrally similar PAHs [24,31]; however, only minor differences are observed in the fluorescence decay times (2.0–2.5 ns) as well as in the emission spectra for phenolic EDCs. Therefore, we consider total phe-

nolic EDCs fluorescence intensity which could be expressed as the concentration of total phenolic EDCs. Furthermore, for dischargeable water quality as well as river water quality, there is no individual standard for the various phenolic EDCs in Korea. Instead, there is a water quality criterion for a class of phenol as a concept of total phenolic compounds for dischargeable water as follows: less than 1 mg/l for clean region and less than 3 mg/l for the other regions. Here, the other fluorescent compounds such as EPA 16 PAH, which could interfere the classification of phenolic compounds from water samples, could be excluded due to their relatively long fluorescence decay time of more than 8ns. For anthracene, with its similar decay time, its characteristic spectra wavelength ranged from 375 to 455 nm, resulting in excluding it from fluorescence spectra of the phenolic EDCs. In addition, chemometric method using time resolved data from LIF analysis was successfully applied for qualification of PAHs in environmental samples [26,31].

The other difficulty is the detection of chlorophenols, including the PCPs (pentachlorophenol) and 2-4-dichlorophenol of interest in this study. Their fluorescence was negligible compared to the other classes of phenolic EDCs due to the existence of chlorine on the aromatic benzene ring hindering the fluorescence [29]. Therefore, the total ten phenolic EDCs fluorescence intensity was not taken into account. Given this, only the

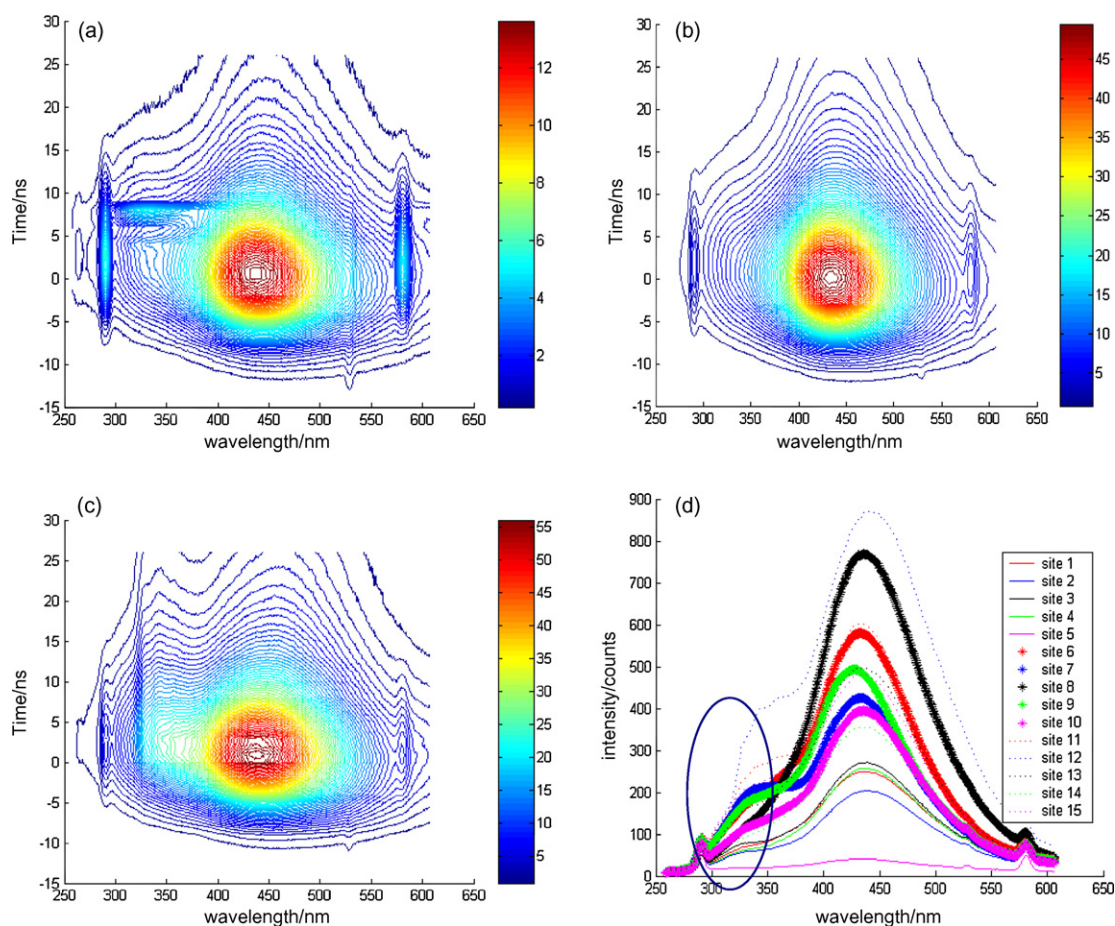


Fig. 6. Fluorescence spectra of EDCs from (a) sample from river, (b) effluent sample from sewage treatment plant, and (c) effluent sample from wastewater treatment plant and (d) fluorescence intensity ( $I_{F, 285-355}$ ) according to 15 field sites (2004. 2).

fluorescence intensity of phenolic EDCs, including bisphenol A and seven alkylphenols, was considered in this LIF monitoring.

Fig. 5 shows the fluorescence spectra of phenolic EDCs (4-butylphenol and bisphenol A) after 266 nm excitation via optical fiber. This fluorescence spectrum was scanned from 250 to 650 nm, with the total wavelength range provided from LIF. According to the type of alkylphenol, the quantum yield is definitely different. As alkyl substitution on the aromatic ring induced the change in the extinction coefficient and decay time, it was observed that the phenolic EDCs with smaller molecular weight produce a higher quantum yield [29].

For the calibration curve and spectra recognition of total phenolic EDCs, the wavelength coverage ranging from 285 to 355 nm was considered and the fluorescence intensity was integrated over this wavelength range. For each single phenolic EDC solution and total mixture solution including eight alkylphenol of interest in this study, the linear regression for the fluorescence intensity and the concentration of alkylphenol were satisfactory for the observed range from 0 to 500  $\mu\text{g/l}$  ( $R \geq 0.99$ ). Five times measurements for 100  $\mu\text{g/l}$  of each single phenolic EDC solution was recorded and the reproducibility of LIF analysis was obtained from the standard deviation (2.7–9.1%). For the phenolic EDCs mixture solution, the minimum distinguishable analytical signal (fluorescence threshold)  $S_m$  and the limit of detection were 2495.04 counts (a.u.) and 31.02  $\mu\text{g/l}$ , respectively. This detection limits were calculated as the sum of the triple standard deviation of the blank ( $n=8$ ) and the intercept of the calibration curve. Signals exceeding the fluorescence threshold were taken into account [19].

The fluorescence spectra of water samples from river, sewage treatment plants and wastewater treatment plants are shown in Fig. 6. Fig. 6(a) and (c) revealed a short fluorescence from 285 to 355 nm together with rather unstructured fluorescence from 355 to 550 nm. This was high background fluorescence resulted from humic substances that are also excited by the UV laser light [32]. There are also peaks at 290 and 580 nm, as well as 532 nm, which correspond to the Raman-scattered laser light in water and the elastic Rayleigh scattering [29].

The fluorescence intensity of the total phenolic EDCs according to the site categories and seasonal variation are given in Fig. 7. The y-axis fluorescence intensity was calculated by subtracting the spectral area (355–550 nm) induced by humic substances from the integrated total intensity (area) over wavelength coverage (285–355 nm) of total phenolic EDCs to consider possible overlapped fluorescence spectra near 355 nm. We assumed the raw fluorescence spectra obtained from LIF measurement comprised of the multi peaks and each one has a Gaussian shape. A multi-peak fit was performed for 2D spectra of each sample and the broad spectra area due to humic substance was successively removed. As with similar procedures, Raman-scattered laser lights were also removed from fluorescence spectra of target phenolic EDCs [32].

The water samples collected in February and August 2004 were examined using the LIF system. The seasonal variation of EDCs by LIF monitoring demonstrated that the concentra-

tion of EDCs in summer (rainy season) was lower than that in winter (dry season). The effluent sample also had higher fluorescence intensity, implying the existence of high phenolic EDC concentration compared to the river sample.

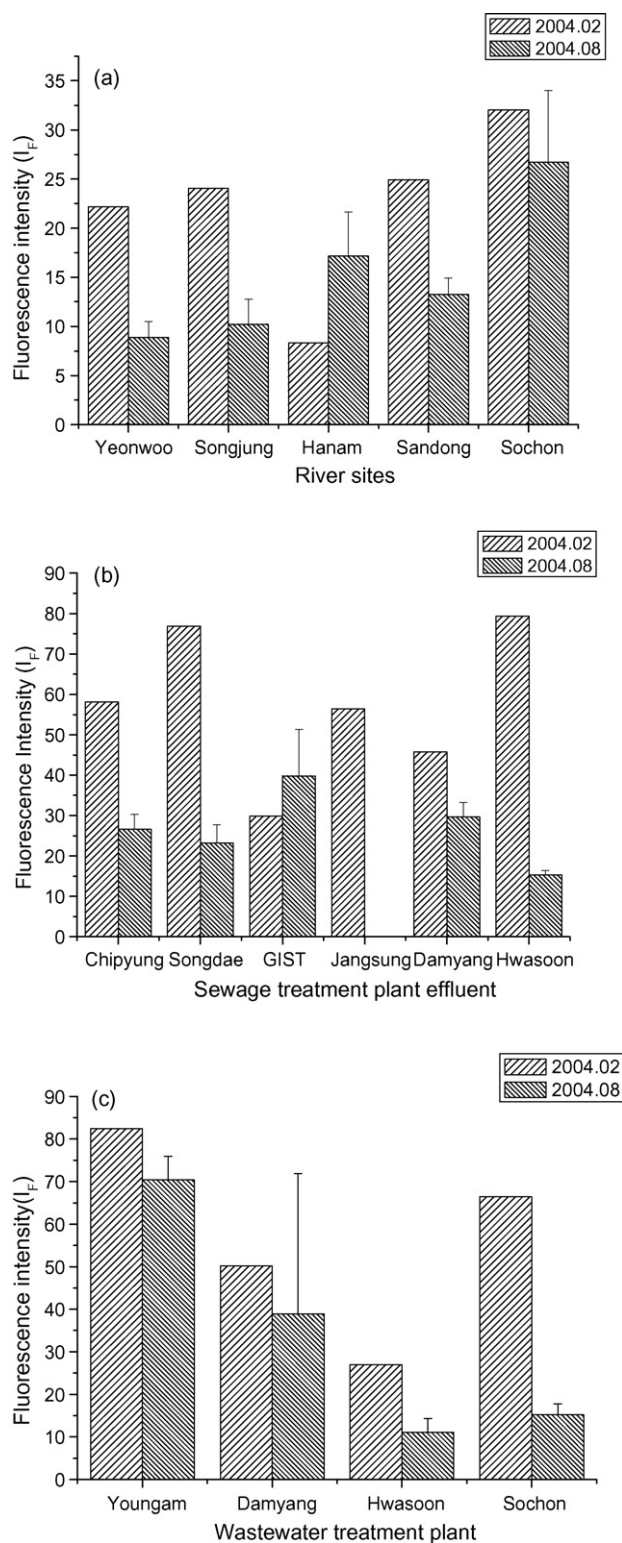


Fig. 7. Seasonal LIF intensity variation of EDCs from 15 sampling sites in 2004: (a) sample from river, (b) effluent sample from sewage treatment plant and (c) effluent sample from wastewater treatment plant.



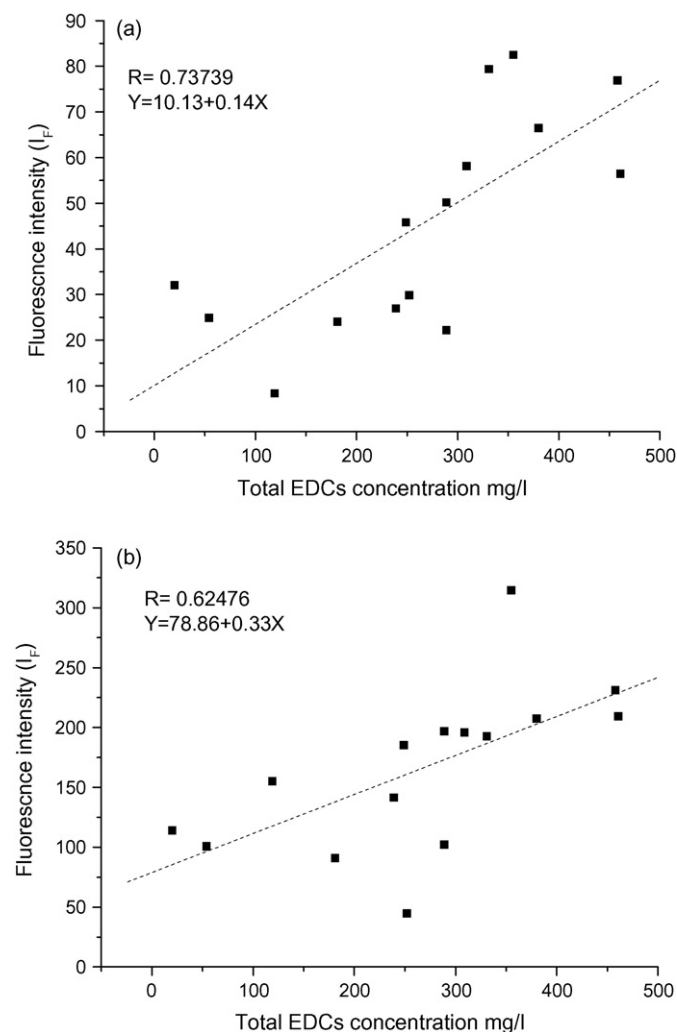


Fig. 8. The correlation between total fluorescence intensity from LIF analysis results and total concentration of EDCs from GC–MS analysis: (a) spectra area subtracting humic substance effect; (b) total integrated spectra area (20004.02).

All data were compared with results of the GC–MS analysis of the same samples. However, it should be taken into account that the relative quantum yield of each EDC is different. This makes it difficult to correlate the total phenolic EDCs concentration and total fluorescence intensity. In the case of chlorophenols, fluorescence was almost not detected. However, 4-*n*-butylphenol, 4-*tert*-butylphenol and bisphenol A showed 2–3 times higher fluorescence intensity compared to the other alkylphenols. It could be explained as an alkyl substitution on the aromatic ring [29]. For samples obtained during January 2004, the relationship between the eight phenolic EDCs concentration and total fluorescence intensity was plotted. In the rainy season, more phenolic EDCs were detected in relatively high levels by GC–MS. 4-*t*-Butylphenol, 4-*t*-octylphenol and bisphenol A were mainly considered in this regression and relatively high quantum yields were also observed except for 4-*t*-octylphenol. The linear regression result showed relatively moderate *R* value ( $=0.73739$ ) (Fig. 8). At low concentration of EDCs, the linear regression between the concentration and intensity of pheno-

lic EDCs was not successfully fitted. This observation can be explained by the relatively high detection limit of phenolic EDCs solution. In cases where the humic substance effect is excluded, the enhanced regression result was shown.

For LIF application into the detection/monitoring of phenolic EDCs in aquatic environment, there is some problem such as selectivity. However, time resolved analysis can be a solution to distinguish the PAH and humic acid, which can fluoresce, from the phenolic EDCs of interest. Considering the most abundant phenolic EDCs such as nonylphenol, bisphenol A, the comparison of fluorescence intensity of nonylphenol and that of total phenolic EDCs can be also indicator for the presence of phenolic EDCs in aquatic environment. In a future study, semi-quantification with weighting factor for specific phenolic EDCs such as nonylphenol and bisphenol A will be evaluated.

#### 4. Conclusions

The extraction and analysis of phenolic EDCs using GC–MS was carried out and the target compounds were also determined by laser-induced fluorescence (LIF) spectroscopy. The monitoring of alkylphenols, chlorophenols and bisphenol A was conducted with water samples collected from rivers as well as sewage and wastewater treatment plants. GC–MS analysis revealed that the concentrations of targeted phenolic EDCs in samples obtained during 2002 were higher than those obtained during 2003 and 2004, and the levels of targeted compounds in most effluent samples were relatively higher than those of river samples. During 2002–2003, bisphenol A, 4-*n*-heptylphenol, and nonylphenol were the most abundant compounds founded in high levels, while 4-*tert*-butylphenol and 4-*tert*-octylphenol were newly observed with bisphenol A and 4-*n*-heptylphenol within the samples. The other phenolic compounds were detected in less than 20% of the sample size and mostly below the detection limit. The seasonal variation of target compounds from river and effluent samples showed lower levels of EDCs in the rainy season than those in the dry season in 2004.

Mixtures of phenolic EDCs showing similar fluorescence spectra and nearly equal decay times are difficult to be discriminated into the single EDCs components. However, the results of LIF are comparable to the results of GC–MS, showing a consistent trend in terms of seasonal variation and site categories. Furthermore, LIF system is powerful tool for on-line/*in situ* contaminant detection and monitoring of phenolic compounds in aquatic environment, providing significant advantages, such as reduced time and cost of the analysis, and bypass the complicate experimental procedures, including sampling, clean up and extraction [21–24].

Therefore, the development of the representative indicators revealing the existence of EDCs or the consideration of weighting factors for the semi-quantification analysis can be helpful to assess the phenolic EDCs in the water system. The LIF can be used for the potential real-time *in situ* monitoring technique of phenolic EDCs in the aquatic system.

## Acknowledgements

This research was financially supported by International Environmental Research Center (UNU and GIST Joint Programme) through the Ministry of Science and Technology, Korea, and Brain Korea 21 program (Coastal Environmental System School, Pusan National University).

## References

- [1] A.C. Nimrod, W.H. Benson, *Crit. Rev. Toxicol.* 26 (1996) 335–364.
- [2] J.W. Birkett, J.N. Lester, *Endocrine Disruptors in Wastewater and Sludge Treatment Processes*, Lewis Publishers, Boca Raton, 2003.
- [3] C.G. Naylor, J.P. Mieux, W.J. Adams, J.A. Weeks, F.J. Castaldi, R.R. Romano, *J. Am. Oil Chem. Soc.* 69 (1992) 695–703.
- [4] C.R. Tyler, S. Jobling, J.P. Sumpter, *Crit. Rev. Toxicol.* 28 (1998) 319–361.
- [5] D.Y. Shang, R.W. Macdonald, M.G. Ikonou, *Environ. Sci. Technol.* 33 (1999) 1366–1372.
- [6] R. White, S. Jobling, S.A. Hoare, J.P. Sumpter, M.G. Parker, *Endocrinology* 135 (1994) 175–182.
- [7] S.C. Nagel, F.S. Saal, K.A. Thayer, M.G. Dhar, M. Boechler, W.V. Welshons, *Environ. Health Perspect.* 105 (1997) 70–76.
- [8] M. Ahel, W. Giger, *Chemosphere* 26 (1993) 1471–1478.
- [9] S.A. Snyder, T.L. Keith, E.M. Snyder, T.S. Gross, K. Kannan, J.P. Giesy, *Environ. Sci. Technol.* 33 (1999) 2814–2820.
- [10] T. Suzuki, T. Nakagawa, I. Takano, *Environ. Sci. Technol.* 38 (2004) 2389–2396.
- [11] D.H. Li, M.S. Kim, J.-R. Oh, J.N. Park, *Chemosphere* 56 (2004) 783–790.
- [12] J.S. Khim, K. Kannan, D.L. Villeneuve, C.H. Koh, J.P. Giesy, *Environ. Sci. Technol.* 33 (1999) 4199–4205.
- [13] C.-H. Koh, J.S. Khim, K. Kannan, D.L. Villeneuve, K. Senthilkumar, J.P. Giesy, *Environ. Pollut.* 132 (2004) 489–501.
- [14] J.S. Khim, K.T. Lee, K. Kannan, D.L. Villeneuve, J.P. Giesy, C.-H. Koh, *Arch. Environ. Contamin. Toxicol.* 40 (2001) 141–150.
- [15] B.L.L. Tan, M.A. Mohd, *Talanta* 61 (2003) 385–391.
- [16] H.-B. Lee, T.E. Peart, M.L. Svoboda, *J. Chromatogr. A* 1094 (2005) 122–129.
- [17] M.I.H. Helaleh, Y. Takabayashi, S. Fujii, T. Korenaga, *Anal. Chim. Acta* 428 (2001) 227–234.
- [18] R. Kotzick, R. Niessner, Fresenius, *J. Anal. Chem.* 354 (1996) 72–76.
- [19] P. Karlitschek, F. Lewitzka, U. Buenting, M. Niederkrueger, G. Marowsky, *Appl. Phys. B* 67 (1998) 497–504.
- [20] G. Hillrichs, P. Karlitschek, W. Neu, *SPIE* 2293 (1994) 178–184.
- [21] J.L. Whitcomb, A.J. Bystol, A.D. Campiglia, *Anal. Chim. Acta* 464 (2002) 261–272.
- [22] M.U. Kumke, H.-G. Loehmannsroeben, Th. Roch, *J. Fluoresc.* 5 (1995) 139–153.
- [23] T. Baumann, S. Haaszio, R. Niessner, *Water Res.* 34 (2000) 1318–1326.
- [24] W. Schade, J. Bublitz, *Environ. Sci. Technol.* 30 (1996) 1451–1458.
- [25] H.-G. Loehmannsroeben, T. Roch, R.G. Schaefer, R.H. Schultz, H. Vereecken, *SPIE* 3107 (1997) 3107–3127.
- [26] F. Lewitzka, U. Buenting, P. Karlitschek, M. Niederkrueger, G. Marowsky, *SPIE* 3821 (1999) 331–338.
- [27] M. Hawrelak, E. Bennett, C. Metcalfe, *Chemosphere* 39 (1999) 745–752.
- [28] M.A. Manzano, J.A. Perales, D. Sales, J.M. Quiroga, *Water Res.* 33 (1999) 2593–2600.
- [29] I.B. Berlman, *Handbook of Fluorescence Spectra of Aromatic Molecules*, Academic Press, New York, 1971.
- [30] N.J. Turro, *Modern Molecular Photochemistry*, University Science Book, 1991.
- [31] R. Niessner, U. Panne, H. Schroeder, *Anal. Chim. Acta* 255 (1991) 231–243.
- [32] J. Bublitz, M. Dickenhausen, M. Gretz, S. Todt, W. Schade, *Appl. Optic.* 34 (1995) 3223–3233.

## Transfer assessment of fipronil residues from feed to cow milk

J. Le Faouder<sup>a</sup>, E. Bichon<sup>a</sup>, P. Brunschwig<sup>b,1</sup>, R. Landelle<sup>c,2</sup>, F. Andre<sup>a</sup>, B. Le Bizec<sup>a,\*</sup>

<sup>a</sup> LABERCA, Ecole Nationale Vétérinaire de Nantes, Route de Gachet, Atlanpôle La Chantrerie, BP 50707, 44087 Nantes Cedex 03, France

<sup>b</sup> Institut de l'Élevage, 9 rue André Brouard, 49100 Angers, France

<sup>c</sup> Chambre d'Agriculture du Maine et Loire, Ferme Expérimentale des Trinottières, 49140 Montreuil-sur-Loire, France

Received 24 November 2006; received in revised form 17 April 2007; accepted 30 April 2007

Available online 22 May 2007

### Abstract

Fipronil, a phenylpyrazole insecticide introduced for pest control on a broad range of crops, can also affect non-target insects such as honeybees. More widely, non-target environment such as milk produced by dairy cows fed with maize silage from treated seeds (=silage T) can be affected. To assess the potential transfer of fipronil residues (sulfone, sulfide, fipronil, desulfinyl and amide), a methodology including gas chromatography coupled with tandem mass spectrometry (GC–MS/MS) analysis was developed and validated according to the 2002/657/EC decision, in order to reach a level of quantification below  $0.1 \mu\text{g L}^{-1}$  in milk and  $0.1 \mu\text{g kg}^{-1}$  in plants. Twelve dairy cows were fed with silage T during 4 months. Concentration of fipronil in treated seeds was estimated at  $1 \text{ g kg}^{-1}$ , whereas silage from these seeds contained  $0.30 \pm 0.05 \mu\text{g kg}^{-1}$  of dry material of fipronil,  $0.13 \pm 0.03 \mu\text{g kg}^{-1}$  of dry material of sulfone. Sulfide residues were below the limit of quantification. Silage from untreated seeds (=silage U) presented traces of fipronil and sulfone, respectively at  $0.04 \pm 0.06$  and  $0.02 \pm 0.03 \mu\text{g kg}^{-1}$  of dry material. Contribution of fipronil residues from supplies was insignificant. During administration of silage T, only sulfone residues were quantified in milk. The average concentration was  $0.14 \pm 0.05 \mu\text{g L}^{-1}$ . Before and after administration, sulfone residues were detected but not quantifiable ( $<0.025 \mu\text{g L}^{-1}$ ). Our results suggest a transfer of fipronil from feed to milk under its sulfone form. Moreover, traces of fipronil residues in maize U, soya, wheat and straw show a diffuse contamination of this pesticide in the environment.

© 2007 Elsevier B.V. All rights reserved.

**Keywords:** GC–MS/MS; Transfer; Fipronil; Cow milk

### 1. Introduction

Fipronil, ( $\pm$ )-5-amino-1-(2,6-dichloro- $\alpha,\alpha,\alpha$ -trifluoro-*p*-tolyl)-4-trifluorométhylsulfanyl – pyrazole-3-carbonitrile, a phenylpyrazol insecticide (Rhône-Poulenc Agro) is used for the control of many soil and foliar insects on a variety of crops [1] and can also be formulated as flea and tick sprays for pets. However, fipronil is highly toxic to non-target environment and a lot of questions remain unanswered, particularly the one linked to the behavior of honeybees exposed to sublethal doses of fipronil [2–4].

In this survey, we focused on the study of milk, which can be considered as a non-target compartment when dairy cows

are fed with maize silage from treated seeds (silage T). Data on fipronil excretion in milk are not available, but the metabolic pathway of fipronil in rats (urine and faeces), and data pertaining to the degradation of fipronil in soil are presented [5–6]. This information enabled us to select the fipronil metabolites and degradation products which were the most relevant to our study (Fig. 1).

Considering the low systemic property of fipronil ( $K_{ow} = 3.5$ ) [7], very low levels of fipronil residues were expected in plants and milk (below  $0.1 \mu\text{g kg}^{-1}$ ). Few analytical methods for the determination of this compound and its residues have been reported. Morzycka [8] proposed a matrix solid-phase dispersion (MSPD) and gas chromatography nitrogen phosphorous detector (GC–NPD) method for the determination of fipronil residues in honeybees. For animal tissues, methods with gas chromatography coupled to mass spectrometry (GC–MS) and electron capture detector (GC–ECD) [9] are proposed. The detection in soils can be conducted using solid-phase microextraction (SPME) GC–MS [10], GC–MS [11] and GC–ECD [11–13]. In plants, methods by GC–MS [9,11] and GC–ECD [11,13]

\* Corresponding author. Tel.: +33 2 40 68 78 80; fax: +33 2 40 68 78 78.

E-mail addresses: [philippe.brunschwig@inst-elevage.asso.fr](mailto:philippe.brunschwig@inst-elevage.asso.fr) (P. Brunschwig), [richard.landelle@maine-et-loire.chambagri.fr](mailto:richard.landelle@maine-et-loire.chambagri.fr) (R. Landelle), [laberca@vet-nantes.fr](mailto:laberca@vet-nantes.fr) (B. Le Bizec).

<sup>1</sup> Tel.: +33 2 41 18 61 76; fax: +33 2 41 18 61 61.

<sup>2</sup> Tel.: +33 2 41 76 60 22; fax: +33 2 41 76 22 12.

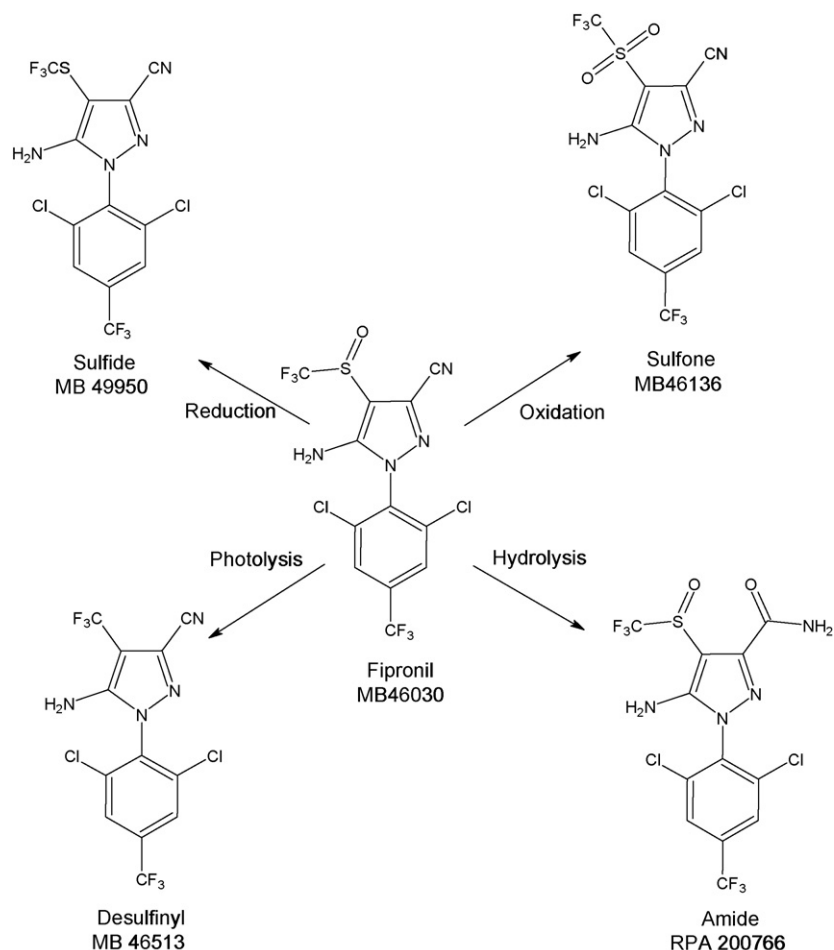


Fig. 1. Relevant metabolites or degradation products of fipronil.

have also been reported. In order to quantify fipronil residues in the various matrices selected for this survey (plants, milk, water), we first had to develop efficient methods of extraction and purification. Then, we decided to base the measurement of fipronil residues on to gas chromatography coupled to mass spectrometry (triple quadrupole device). Methods were validated according to the 2002/657/EC decision [14]. Animal experiment was conducted in an experimental farm according to French rules, and all the parameters were recorded.

## 2. Experimental

### 2.1. Experimental farm

#### 2.1.1. Animals

Twelve pregnant dairy cows were selected in an experimental farm of the Maine et Loire Chamber of Agriculture for their calving between 25 August and 24 September 2004. These cows were therefore at their early stages of lactation, which meant that they could be monitored over 6 months.

#### 2.1.2. Feeds

Maize silage constituted the main part of the dairy cows intake (80% of the total dry material (DM)). A little straw (2%) was

also given to ensure proper rumination. Soya cakes constituted 12–15% of the diet DM according to the protein level needed to obtain the yearly dairy reference delivery of milk. Wheat (3%) could also be given when the feeding value of the silage was changed. Mineral feeds (calcium carbonate and 7P/23Ca/5Mg) and urea represented approximately 2.5% of the intake. The quantity of drink water was evaluated from the DM quantity daily ingested by cows. A “food period” is the unit of time during which the composition of the total intake of the dairy cows remains unchanged. The main periods of the experimentation were characterized by the following elements (Fig. 2). From 14 September 2004 to 30 September 2004 silage U was given. After a transition period of 2 weeks with an increased quantity of silage T in the diet, only silage T was given from 14 October 2004 to 05 January 2005. The period from 06 January 2005 to 20 January 2005 was a transition between silage T and silage U. At last a return to silage U was made from 21 January 05 to 21 March 2005. The other food periods consisted in minor changes in the nature or proportion of the food extracts used to complete the intake.

#### 2.1.3. Milk production

The daily quantity of milk was controlled during the whole experiment for each cow. The content of milk in fat and protein was weekly analysed for each cow.

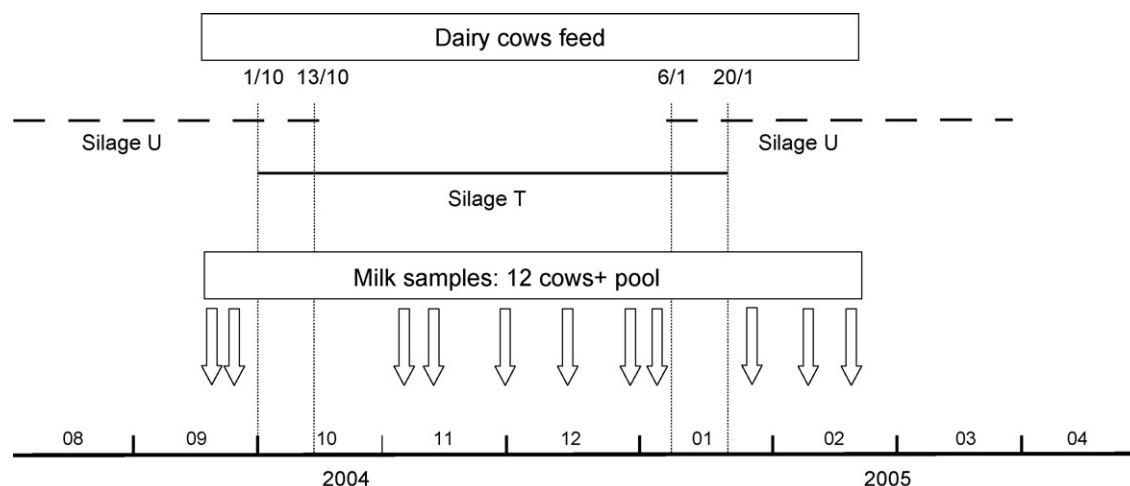


Fig. 2. Scheme of the experimentation (silage U = silage from untreated seeds; silage T = silage from treated seeds).

## 2.2. Chemicals

Fipronil and its metabolites (desulfinyl, sulfone and sulfide) were purchased from Accustandard (New Market, USA). Amide and 4,4'-DDE-d<sub>8</sub> were acquired from CIL (Sainte Foy la Grande, France) and Tebufenpyrad from Riedel de Haën (Hanover, Germany). The solvents used were of pestipur<sup>®</sup>-grade quality and purchased from SDS (Peypin, France) for methanol, ethylacetate, acetonitrile and isooctane. Ammonium hydroxide and sodium sulfate were of analytical-grade quality and purchased from Merck (VWR, Nogent sur Marne, France). Ultrapure water (>14 MΩ) was used. The solvents for gas chromatography (ethylacetate, toluene and tetrahydrofuran) were from Fluka (St. Quentin Fallavier, France). The solid-phase extraction (SPE) columns (Atoll XC: 500 mg/6 mL, Florisil: 1000 mg/6 mL) were from Interchim (Montluçon, France).

## 2.3. Instrumentation

For GC–MS/MS analysis, a gas chromatograph (Agilent, 6890 Series) with split/splitless injector and a programmable oven was coupled to a Quattro-micro triple quadrupole analyzer (Waters, Micromass) operating in electron ionisation mode. Gas chromatography was performed on a non-polar column OV1 (30 m × 0.25 mm × 0.25 μm) purchased from Interchim (Montluçon, France). The injector temperature was kept at 250 °C and used in the splitless mode (1 min) and the transfer

line temperature was set at 320 °C. For the chromatographic separation of fipronil residues, the oven temperature was increased from 70 °C (3 min) to 210 °C (0 min) at 20 °C/min, then to 225 °C (0 min) at 5 °C/min and finally to 320 °C (7 min) at 20 °C/min. Mass spectra were recorded in the multiple reaction monitoring (MRM) mode (Table 1).

## 2.4. Methodology

Methods are described in Fig. 3.

### 2.4.1. Sample preparation

**2.4.1.1. Plants.** Internal standard (tebufenpyrad) was added to 4 g of dried and ground plant (maize, soya, wheat, straw, etc.). Seed, plant and maize silage were dried for 2 days in an oven at 80 °C before grinding. Supplies like wheat and soya cakes did not follow this process because unnecessary.

**2.4.1.2. Milk.** pH of 10 mL milk sample was adjusted at 10 (±0.3) with ammonia 32%. Internal standard was added.

**2.4.1.3. Mineral feeds.** The sample was prepared from 4 g of mineral feeds to which internal standard was added.

**2.4.1.4. Water.** Internal standard was added to 40 mL of Water. Purification of water was carried out on an Atoll XC SPE.

Table 1  
Diagnostic transitions for fipronil, metabolites and degradation products

Analyte	Transition 1	Collision energy (eV)	Transition 2	Collision energy (eV)	RT (min ± 0.2)	Dwell time (ms)	Acquisition window
Desulfinyl	388 > 333	15	333 > 231	20	12.9	150	1
Sulfide	351 > 255	15	420 > 351	10	14.1	100	2
Fipronil	367 > 213	20	367 > 255	15	14.3	100	2
DDE-d8 (ES)	326 > 254	20			15.1	80	3
Sulfone	383 > 255	15	452 > 383	5	15.5	110	3
Amide	385 > 368	10	368 > 213	20	16.5	100	4
Tebufenpyrad (IS)	333 > 171	15			17.0	150	5

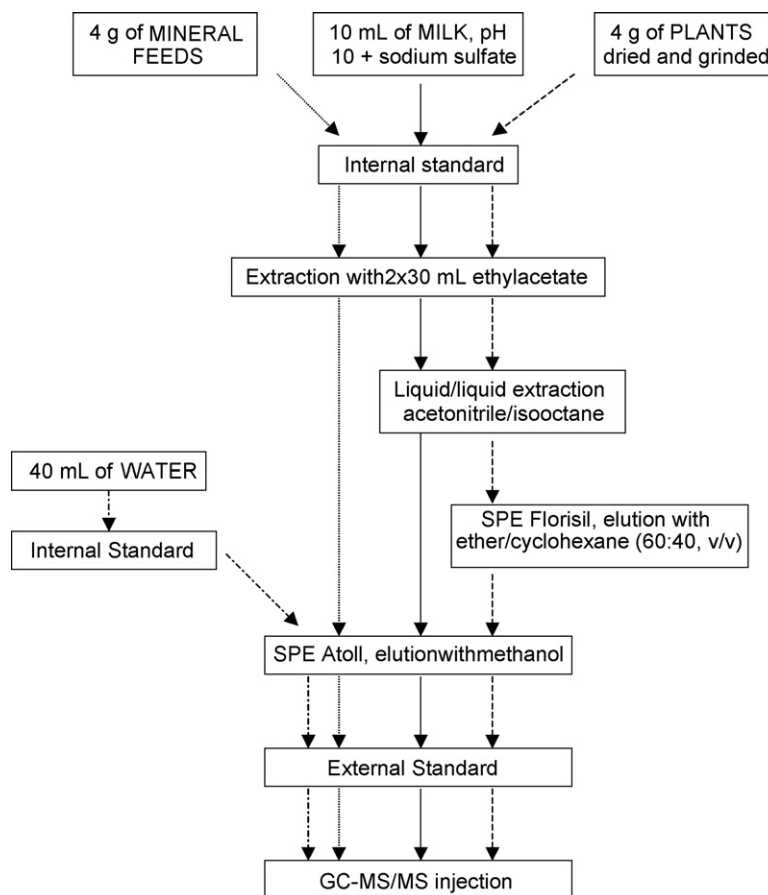


Fig. 3. Procedure for analysis of fipronil residues in milk, water, plant and mineral feed samples.

#### 2.4.2. Extraction

The sample was extracted twice with 30 mL of ethylacetate. The extract was dried under a gentle nitrogen stream until fat residue for milk and to dryness for the other matrices.

#### 2.4.3. Fat removal

Six milliliters of isooctane and 1 mL (for milk) or 2 mL (for plant) of acetonitrile were added. After blending and centrifugation, the acetonitrile phase was retrieved and isooctane phase was re-extracted with 1 mL of acetonitrile. Both polar phases were combined and washed with 1 mL of isooctane. Isooctane was discarded and polar solvent was evaporated to dryness under a gentle nitrogen stream.

#### 2.4.4. Solid-phase extraction

**2.4.4.1. Florisil (for plant).** Florisil phase was conditioned with 12 mL of cyclohexane. The dry extract was restored in 500  $\mu$ L of cyclohexane, deposited on to the column and directly collected in an identified tube. The tube was washed with 500  $\mu$ L of cyclohexane which were laid down on the column. Analytes were eluted with 6 mL of an ether/cyclohexane mixture (60:40, v/v). Solvent was evaporated under a gentle nitrogen stream.

**2.4.4.2. Atoll XC (for all samples).** The column was conditioned with 6 mL of methanol and 6 mL of water. For water, the 40 mL sample was applied. For the other matrices, the dry extract

was restored in 5 mL of a methanol/water mixture (0.5:10; v/v) and applied. The column was then washed with 6 mL of a methanol/water mixture (70:30; v/v). Analytes were eluted with 10 mL of methanol. The external standard (DDE- $d_8$ ) was added. The extract was evaporated to dryness under a gentle nitrogen stream, restored in 80  $\mu$ L of ethyl acetate and transferred in a GC-vial.

#### 2.5. Validation of the method

Validation was carried out in accordance with the 2002/657/EC decision in order to evaluate the performances of the method. Various criteria were monitored:

- **Linearity:** From the calibration curves obtained for each analyte, regression parameters (determination coefficient  $R^2$ , slope ( $a$ ) and intercept ( $b$ )) were determined. These curves were obtained based on seven samples from a pool spiked at different concentrations.
- **Identification criteria:** Repeatability of retention time and signals (standard deviation of retention times, absolute amplitudes of signals and relative intensities in-between two relevant transitions) was assessed for each analyte. These values were calculated from 20 spiked samples.
- **Performance limits:** Values of trueness, decision limit ( $CC\alpha$ ) and detection capability ( $CC\beta$ ) were calculated for each ana-

lyte from 20 blank samples and 20 spiked samples. Trueness is the difference between the added concentration and the calculated concentration. Decision limit ( $CC\alpha$ ) means the limit at and above which it can be concluded with an error probability of  $\alpha$  that a sample is non-compliant. Detection capability ( $CC\beta$ ) means the smallest content of the substance that may be detected, identified and/or quantified in a sample with an error probability of  $\beta$ . This means that the detection capability is the concentration at which the method is able to detect permitted limit concentrations with a statistical certainty of  $1 - \beta$ .

- **Recovery yield:** Six blank samples were extracted and purified according to the protocol. Analytes were added before injection. The signals of each analyte were compared with those from the same samples spiked at the beginning of the processing.

### 3. Results and discussion

#### 3.1. Validation results

For the validation step, blank samples were needed but a “fipronil residues noise” appeared in the majority of the samples. In order to avoid other sources of contamination, a complete cleaning of the work station (work tables, pipettes, dryers, vacuum system, etc.) was carried out and new standard solutions were prepared. A blank sample of water was added in each series to check any contamination occurring in the purification process. No critical step was identified excepting possible minor contamination during extraction process. The contamination of the Quattro-Micro instrument was also considered, but

injections of ethyl acetate between every injection of standard solution or spiked sample permitted to check contamination. Finally, the difficulty was to find blank material because of the widespread fipronil contamination at concentrations below  $10 \text{ ng kg}^{-1}$  in milk and plants. To avoid the “fipronil residue noise”, the sensitivity of the method was decreased, in order to observe only concentrations higher than  $10 \text{ ng kg}^{-1}$ . After several tests on samples, the solution selected consisted in diluting the final extract in  $80 \mu\text{L}$  (instead of  $15 \mu\text{L}$ ) and injecting  $1 \mu\text{L}$  (instead of  $3 \mu\text{L}$ ). 1/80th of the extract was injected in the final method used (method 2) instead of 1/5th in the first method used (method 1). The  $CC\alpha$  and  $CC\beta$  values were determined for method 1 (Table 2). For milk, the  $CC\alpha$  values obtained were lower than  $10 \text{ ng L}^{-1}$ , corresponding to the value expected for a relevant method and the  $CC\beta$  values obtained were lower than  $50 \text{ ng L}^{-1}$ . For plants,  $CC\alpha$  values obtained were lower than  $10 \text{ ng kg}^{-1}$ , and  $CC\beta$  values lower than  $60 \text{ ng kg}^{-1}$  excepted for amide compound.

For method 2, limit of detection (LOD) and limit of quantification (LOQ) were determined for a signal to noise ratio of 3 for respectively the most intense transition and the less intense transition. In this way, LOD in milk for fipronil, sulfone, sulfide and desulfinyl was  $0.01 \mu\text{g L}^{-1}$  and LOQ was  $0.025 \mu\text{g L}^{-1}$ . In plants, LOD for fipronil, sulfone, sulfide and desulfinyl was  $10 \text{ ng kg}^{-1}$  and LOQ was  $50 \text{ ng kg}^{-1}$ . All these values were four times higher for the amide metabolite. The method 2 was evaluated with an extraction of 12 milk samples and 16 plant samples considered as blank and spiked at  $\text{LOQ} \times 2$  for milk and  $\text{LOQ} \times 2.5$  for plants. Repeatability and trueness were assessed at these concentrations (Table 3). For repeatability, some standard deviation values were found above 20% for milk and above

Table 2  
 $CC\alpha$  and  $CC\beta$  values determined during the validation process (method 1)

Analyte	Signal 1 (detection, screening)		Signal 2 (identification, confirmation)	
	$CC\alpha$ ( $\text{ng L}^{-1}$ )	$CC\beta$ ( $\text{ng L}^{-1}$ )	$CC\alpha$ ( $\text{ng L}^{-1}$ )	$CC\beta$ ( $\text{ng L}^{-1}$ )
<b>Milk</b>				
Desulfinyl	0.4	1.0	0.8	2.1
Sulfide	0.4	1.1	0.5	1.3
Fipronil	1.4	9.5	7.4	43.9
Sulfone	1.1	4.7	1.7	7.5
Amide	1.3	7.5	5.8	27.2
Minimum	0.4	1.0	0.5	1.3
Maximum	1.4	9.5	7.4	43.9
Analyte	Signal 1 (detection, screening)		Signal 2 (identification, confirmation)	
	$CC\alpha$ ( $\text{ng kg}^{-1}$ )	$CC\beta$ ( $\text{ng kg}^{-1}$ )	$CC\alpha$ ( $\text{ng kg}^{-1}$ )	$CC\beta$ ( $\text{ng kg}^{-1}$ )
<b>Plants</b>				
Desulfinyl	1.09	2.00	3.66	7.26
Sulfide	1.04	2.27	1.06	2.19
Fipronil	5.63	9.42	29.4	58.7
Sulfone	1.71	3.63	4.20	7.99
Amide	11.8	22.5	71.6	332
Minimum	1.04	2.00	1.06	2.19
Maximum	11.8	22.5	71.6	332

Table 3  
Validation parameters for milk and plants (Method 2)

Analyte	Validation criteria				
	$R^2$	$a$	$b$	Repeatability (%)	Trueness (%)
<b>Milk</b>					
Desulfinyl	0.97	0.007	0.035	16.8	-11.6
Sulfide	0.991	0.011	0.029	14.8	-7.4
Fipronil	0.993	0.005	0.010	15.2	-3.2
Sulfone	1.000	0.007	0.066	22.6	18.3
Amide	0.982	0.014	-0.024	12.3	117.7
Minimum	0.982	0.005	-0.024	12.3	-11.6
Maximum	1.000	0.014	0.066	22.6	117.7
<b>Plants</b>					
Desulfinyl	0.992	0.004	0.018	33.8	-15.2
Sulfide	0.990	0.010	0.008	15.0	12.7
Fipronil	0.969	0.003	0.035	47.1	23.3
Sulfone	0.960	0.008	-0.150	15.8	25.9
Amide	0.893	0.001	0.030	46.0	23.6
Minimum	0.893	0.001	-0.150	15.0	-15.2
Maximum	0.992	0.010	0.035	47.1	25.9

40% for plants, but at concentrations below  $1 \mu\text{g kg}^{-1}$ , non-target values are given in the 2002/657/EC decision. Therefore, trueness values were found between -50 and +20% according to the guideline, excepted for the amide. This could be a prob-

lem for a precise quantification of this compound. Moreover, a range of six samples spiked from 0 to  $150 \text{ ng L}^{-1}$  in milk and 0 to  $375 \text{ ng kg}^{-1}$  in plants for all residues and from 0 to  $600 \text{ ng L}^{-1}$  in milk and 0 to  $1500 \text{ ng kg}^{-1}$  in plants for amide residue was extracted to check the linearity of the method. For all analytes, determination coefficients as well as slopes and intercepts were determined (Table 3). The abundance of each molecule was reported to the internal standard. The linearity of the method was good because  $R^2$  values were generally above 0.98. The amide metabolite was still the critical compound of the method.

### 3.2. Analytical results

#### 3.2.1. Results on maize

Samples of untreated and treated maize have been taken twice in full field at flowering time and before harvest. The other samples have been achieved in silos. For each sampling date, six replicates were sampled separately in order to ensure the heterogeneity of the matrix. Mean and standard deviations calculated are presented on graphs. In the untreated maize (Fig. 4), traces of fipronil and sulfone were identified in some samples. The respective average concentrations were  $0.09 (\pm 0.10) \mu\text{g kg}^{-1}$  and  $0.11 (\pm 0.02) \mu\text{g kg}^{-1}$  of DM at flowering time,  $0.07 (\pm 0.07) \mu\text{g kg}^{-1}$  and  $0.09 (\pm 0.03) \mu\text{g kg}^{-1}$  of DM before harvest and  $0.04 (\pm 0.06) \mu\text{g kg}^{-1}$  and  $0.02 (\pm 0.03) \mu\text{g kg}^{-1}$  of DM in silage (last

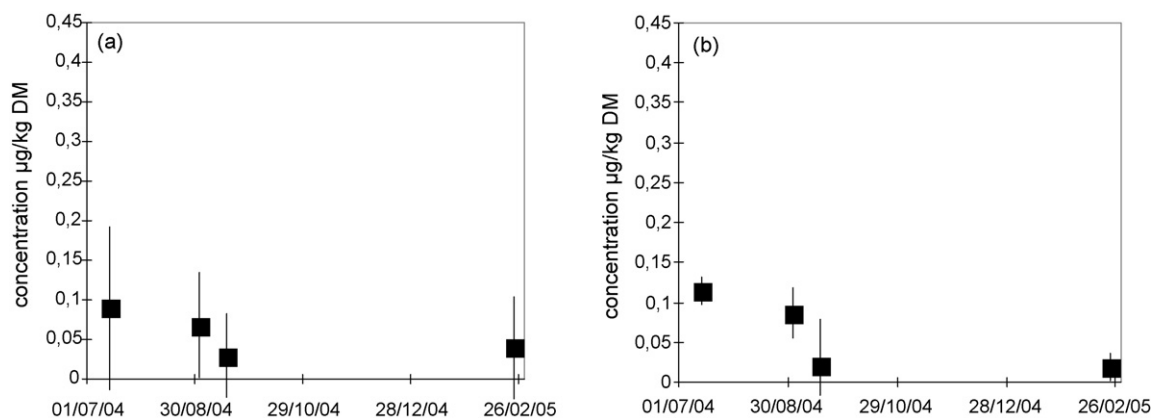


Fig. 4. Fipronil (a) and sulfone (b) concentrations in maize U samples; standard deviation is indicated for each series of measurement.

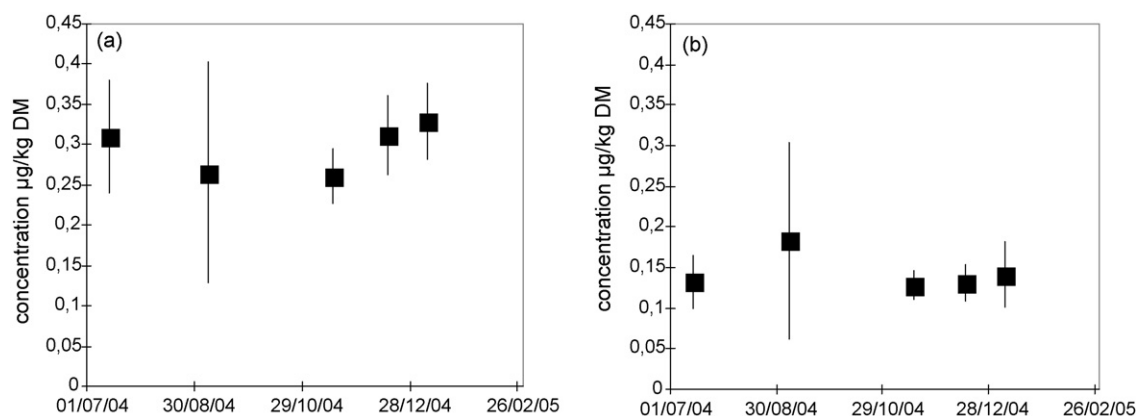


Fig. 5. Fipronil (a) and sulfone (b) concentrations in maize T samples; standard deviation is indicated for each series of measurement.



two samples). The standard deviation values were relatively high because no residues were found in some samples.

Concentration of fipronil in treated seeds was evaluated at  $1 \text{ g kg}^{-1}$ . In maize from these seeds (Fig. 5), traces of fipronil and sulfone were identified in all samples at respective average concentrations of  $0.31 (\pm 0.07)$  and  $0.13 (\pm 0.03) \mu\text{g kg}^{-1}$  of DM at flowering time,  $0.26 (\pm 0.14)$  and  $0.18 (\pm 0.12) \mu\text{g kg}^{-1}$  of DM before harvest and  $0.30 (\pm 0.05)$  and  $0.13 (\pm 0.03) \mu\text{g kg}^{-1}$  of DM in silage (last three samples). Non-quantifiable traces of the sulfide residue were detected.

The total concentration in fipronil residues (fipronil + sulfone) was found seven times higher in silage T than in silage U. And it was found two times higher in the maize T than in the maize U at flowering time and before harvest.

### 3.2.2. Results on other supplies

Even if maize silage was the main component of the dairy cow diet, other supplies such as water, straw, mineral or corrective feeds were characterized in term of fipronil metabolites. LOD and LOQ for supplies were comparable to those observed for plants. Fipronil, sulfone and desulfinyl were sometimes detected and quantified. 3/5 straw samples presented fipronil residues (between LOD and  $0.18 \mu\text{g kg}^{-1}$ ). Concerning corrective feeds, samples contained traces of fipronil residues were: 2/5 brown soya cakes (between LOD and LOQ), 2/5 soya cakes (between LOD and  $0.66 \mu\text{g kg}^{-1}$ ), 1/2 wheat (between LOD and LOQ). For mineral feeds, fipronil residues were not found in the 7P/23Ca/5Mg mixture. Residues were not detected in water samples. Magnesia, salt and urea, which account for a very small part of the intake, have not been analysed. 8/31 samples of supplies analysed presented traces of fipronil residues. Concentrations were generally not quantifiable: concentrations were above LOQ in three samples (two straw samples and one soya cakes sample).

### 3.2.3. Results on milk

Only the sulfone residue was quantified in milk (Fig. 6). Before consumption of silage T, milk did not present quantifiable traces of sulfone (concentration  $< 0.025 \mu\text{g L}^{-1}$ ). During the 3 months of silage T diet, the average concentration of sulfone in milk was  $0.14 \pm 0.05 \mu\text{g L}^{-1}$  and the maximal concentra-

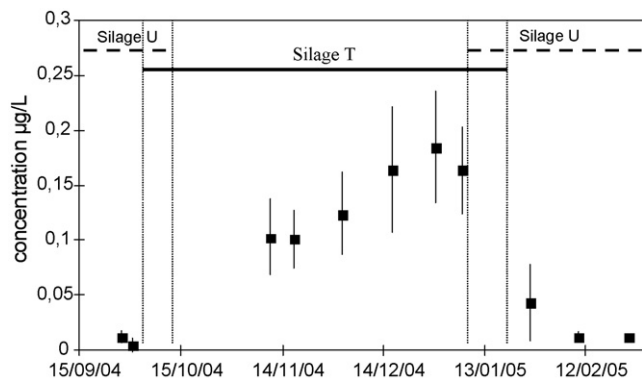


Fig. 6. Sulfone concentration in milk samples (silage U = silage from untreated seeds; silage T = silage from treated seeds).

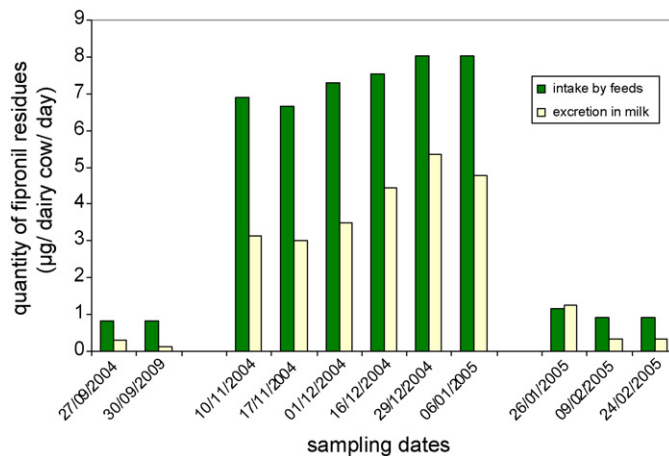


Fig. 7. Fipronil residues—intake by feeds and excretion in milk.

tion measured was found up to  $0.28 \mu\text{g L}^{-1}$ . Sulfide and amide metabolites were sometimes detected, but the results were not quantifiable. After a return to silage U feeding, a fast decrease (over 1 month) in sulfone concentrations was observed. The last samples presented non-quantifiable doses of this compound. Fipronil and desulfinyl forms have never been detected in milk.

### 3.2.4. Balance between food contribution and excretion in milk (Fig. 7)

Food consumption and milk production have been registered for the cattle. During the survey, milk production was found constant; quantitatively speaking, feed consumption was found maximal in October to November ( $\pm 21 \text{ kg}$  of DM/dairy cow per day, half of the cows being in their early stage of lactation). For the purpose of this study, it was decided that, when a sample presented a lower concentration than the LOQ, value for concentration was assigned to  $\text{LOQ}/2$ . Concentration in fipronil residues was higher in maize T than in maize U. Concentration of fipronil residues in supplies was generally not quantifiable. Supplies constituted only 20% of the total intake. So their contribution in term of fipronil residues in dairy cows diet was non-significant. Excretion of these residues in milk increased in the same proportions, but always remained lower than the quantity of residues ingested by cows during the same period. One month after returning to silage U feeding, excretion of residues in milk went back to the initial values.

## 3.3. Discussion

First of all, transfer from seeds to plants has been demonstrated. The concentration of fipronil residues remained higher in the treated samples than in the untreated ones at every steps (flowering time, before harvest, silage). The transfer of fipronil by xylem was also demonstrated in sunflower by Aajoud et al. [15]. Concentration of fipronil in treated seeds was evaluated at  $1 \text{ g kg}^{-1}$ . This semi-quantitative value was found very close to the French homologation value of  $2.5 \text{ g kg}^{-1}$  of seeds.

Secondly, the transfer of fipronil residues from silage T to milk via dairy cows feed has been demonstrated. The concen-

tration of sulfone in milk increased significantly when cows were fed with silage T. All of the ingested fipronil residues were not totally excreted in milk. The remainder could be excreted by other routes (urine, faeces), or bio-accumulated by the dairy cows especially in the adipose tissue. Fipronil was excreted in milk as sulfone form, the main metabolite of fipronil, which presents the same activity than the parent compound. Sulfone toxicity has been found higher for fresh-water invertebrates, fishes and avian species [6] than fipronil. Fipronil has never been detected in milk, which demonstrated the relevance to monitor metabolites as well for a complete risk assessment of the substance.

Another question raised by our study is the diffuse contamination of the environment by fipronil residues. During validation steps (cf. Section 3.1), several commercially branded milk and silages of various origins contained ultra-traces of fipronil residues. During the experimentation, fipronil was found in maize T. Normally fipronil is supposed to be weakly systemic, so its presence in plant was not expected. More surprisingly, it was present in some samples of maize U. This presence could be explained by the relative proximity of the two fields of the experimentation (500 m). The contamination could not come from a presence of fipronil residues in the experimental field because previous crops had never been treated with fipronil. Few samples of supplies like straw, soya cakes and wheat presented also traces of fipronil residues. In milk, the sulfone metabolite was quantified when cows were fed with silage T and sulfone traces were also detected when feed consisted in silage U. Feeds contamination was wider than expected.

In France, fipronil has been temporarily authorized for use since 1996. In February 2004, the Ministry of Agriculture decided to suspend this authorisation, still allowing farmers to use the treated seeds available. Analyses were carried out between November 2004 and May 2005, fipronil was thus possibly used in the vicinity of the experimental fields. Moreover, some gardening products and pet treatments contain fipronil. So there are several potential ways of contamination of the environment by fipronil. Indeed, the “fipronil noise” observed is very low (around  $10 \text{ ng kg}^{-1}$ ).

#### 4. Conclusions

Specific and sensitive methods have been developed and validated according to the 2002/657/EC directive. LOQ was

$0.025 \mu\text{g L}^{-1}$  in milk and  $0.05 \mu\text{g kg}^{-1}$  in plants for all compounds except for the amide residue which values were found four times higher. At these concentrations we were able to detect ultra traces of fipronil residues in several incurred biological matrices. Thus transfer of fipronil residues from seeds to plants until milk via dairy cows feed based on silage T was demonstrated. When cows were fed with silage U, sulfone concentration in milk was lower than LOQ. When feed consisted in silage T, average concentration in milk was  $0.14 \pm 0.05 \mu\text{g L}^{-1}$ . After a return to silage U feeding, a decrease (over 1 month) of sulfone concentrations was observed.

#### Acknowledgement

We would like to thank the “Région Pays de la Loire” for supporting the financial aspects of this project.

#### References

- [1] C. Tomlin, *The Pesticide Manual: A World Compendium*, 11th ed., British Crop Protection Council, 1997.
- [2] A.K. El Hassani, M. Dacher, M. Gauthier, C. Armengaud, *Pharmacol. Biochem. Behav.* 82 (2005) 30.
- [3] M.E. Colin, J.M. Bonmatin, I. Moineau, C. Gaimon, S. Brun, J.P. Vermandere, *Arch. Environ. Contam. Toxicol.* 47 (2004) 387.
- [4] A. Decourtye, J. Devilliers, E. Genecque, K. Le Menach, H. Budzinski, S. Cluzeau, M.H. Pham-Delègue, *Arch. Environ. Contam. Toxicol.* 48 (2005) 242.
- [5] Advisory Committee on Pesticides, *Evaluation on fipronil use as a public hygiene insecticide*, 187 (1999).
- [6] C.C.D. Tingle, J.A. Rother, C.F. Dewhurst, S. Lauer, W.J. King, *Rev. Environ. Contam. Toxicol.* 176 (2003) 1.
- [7] R.H. Bromilow, K. Chamberlain, A.A. Evans, *Weed Sci.* 38 (1990) 305.
- [8] B. Morzycka, *J. Chromatogr. A* 982 (2002) 267.
- [9] D. Hainzl, J.E. Casida, *Proc. Natl. Acad. Sci. U.S.A.* 93 (1996) 12764.
- [10] J.L. Vilchez, A. Prieto, L. Araujo, A. Navalon, *J. Chromatogr. A* 919 (2001) 215.
- [11] H. Fenet, E. Beltran, B. Gadji, J.F. Cooper, C.M. Coste, *J. Agric. Food Chem.* 49 (2001) 1293.
- [12] G.G. Ying, R. Kookana, *Aust. J. Soil Res.* 40 (2002) 1095.
- [13] Z. Pei, L. Yitong, L. Baofeng, J. Gan, *Chemosphere* 57 (2004) 1691.
- [14] 2002/657/EC Commission Decision implementing Council Directive 96/23/EC concerning the performance of analytical method and the interpretation of results. *Official Journal of the European Communities*, 17.08.2002, L221/8.
- [15] A. Aajoud, M. Raveton, H. Aouadi, M. Tissut, P. Ravanel, *J. Agric. Food Chem.* 54 (14) (2006) 5055.

# Precise and accurate determination of lead isotope ratios in mining wastes by ICP-QMS as a tool to identify their source

E. Marguí<sup>a</sup>, M. Iglesias<sup>a</sup>, I. Queralt<sup>b</sup>, M. Hidalgo<sup>a,\*</sup>

<sup>a</sup> Department of Chemistry, University of Girona, Campus Montilivi, 17071 Girona, Spain

<sup>b</sup> Institute of Earth Sciences “Jaume Almera”, CSIC, Solé Sabarís s/n, 08028 Barcelona, Spain

Received 19 July 2006; received in revised form 26 April 2007; accepted 30 April 2007

Available online 10 May 2007

## Abstract

A methodology for a precise and accurate determination of lead isotope ratios in mining wastes by inductively coupled plasma quadrupole-based mass spectrometry (ICP-QMS) has been developed. The study of instrumental bias factors led to the conclusion that internal correction to compensate mass discrimination is required as well as an interference equation correction when Hg is present. The proposed method has been applied to determine lead isotope ratios in several mining wastes, soils and sediments collected at three mining areas in Spain (Aran Valley, Cartagena and Osor).

Statistical analysis highlights that  $^{206}\text{Pb}/^{207}\text{Pb}$  and  $^{208}\text{Pb}/^{207}\text{Pb}$  lead isotope ratios can be used as a fingerprint of mining waste origin which is related to the geological age of the lead ore.

On the other hand, no statistically significant isotopic differences between original ore samples (galena) and processing wastes within a mining district were found, corroborating a unique lead source. Moreover, the lead isotopic composition of soil and sediment samples collected at the studied mining areas is close to that determined in the mining tailings from the same areas, suggesting that the unusual high content of lead in these samples is derived from mining activities rather than from other lead sources.

© 2007 Elsevier B.V. All rights reserved.

**Keywords:** Lead isotope ratios; Mining wastes; ICP-MS

## 1. Introduction

The element lead is naturally occurring with four isotopes:  $^{204}\text{Pb}$  (1.4%),  $^{206}\text{Pb}$  (24.1%),  $^{207}\text{Pb}$  (22.1%) and  $^{208}\text{Pb}$  (52.4%). The ratio between Pb isotopes varies in different geological environments as  $^{206}\text{Pb}$  and  $^{207}\text{Pb}$  are formed by the decay of  $^{238}\text{U}$  and  $^{235}\text{U}$  while  $^{208}\text{Pb}$  is a product of the radioactive decay of  $^{232}\text{Th}$ .  $^{204}\text{Pb}$  is the only lead isotope that is not originated by decay [1].

In this sense, the relative abundance of lead isotopes is dependent on factors such as the relative concentration of Pb, Th and U present in the initial mixture, the half lives of the decay processes and the period of time over which the decay proceeds [2]. Lead isotopic composition is therefore representative of their origin and has been used in different studies mainly to identify sources of lead contamination in different matrices including sediments

[3], soils [2], river water [4], peat bogs [5,6], tree rings [7,8], mussels [9] and tap water [10].

Precise and accurate isotope ratio measurements have traditionally been carried out by thermal ionisation mass spectrometry (TIMS). Recently, inductively coupled plasma source mass spectrometry (ICP-MS) have increasingly been used in isotope ratio measurement. Although ICP-MS cannot achieve the precision and accuracy in isotope ratio measurement attainable in TIMS, the technique can still play an important role due to its fast sample throughput, low sample analysis cost, instrument robustness and simplified sample preparation. The lower precision obtained by ICP-MS compared to TIMS can be explained considering that the isotopes are usually measured sequentially.

Improved precision can be afforded by Multi-Collector ICP-MS instrumentation which combines ICP-source advantages with simultaneous detection [11]. However, these systems are more expensive than quadrupole-based ICP-MS instruments and they are not widely available. For this reason, some works have been focused on the use of quadrupole mass analysers. These instruments were specifically designed for the scanning

\* Corresponding author. Tel.: +34 972418190; fax: +34 972418150.

E-mail address: [manuela.hidalgo@udg.es](mailto:manuela.hidalgo@udg.es) (M. Hidalgo).

of relatively large mass ranges, therefore, they are inherently less stable than magnetic sector mass analysers and less well suited to highly precise and accurate isotope ratio measurements [12]. However, the precision attained with this instrumentation (R.S.D.  $\sim$  0.1–0.5%) is normally sufficient for isotope ratio measurements for many of environmental surveys [3,13]. Some recent studies have been conducted in order to improve ICP-QMS performance when measuring isotope ratios [14–16].

In this work, a methodology for a precise and accurate determination of lead isotope ratios by inductively coupled plasma quadrupole-based mass spectrometry (ICP-QMS) has been developed in order to study the isotopic composition differences between similar mining wastes collected at three abandoned Pb–Zn mining areas in Spain (Aran Valley, Cartagena and Osor). For this purpose, lead isotope ratios of original Pb ore samples and mining processing wastes collected from each of these areas were measured. The determined isotopic composition was also compared to that determined in several soil and sediment samples from the same areas in order to assess the more probable source of the unusual high lead content in these samples.

## 2. Experimental

### 2.1. Instrumentation

A quadrupole-based ICP-MS system (Agilent 7500c, Agilent Technologies, Tokyo, Japan) equipped with an octapole collision reaction cell was used for the isotope ratio measurements. In this work, the collision/reaction cell acts only as an ion focussing lens since it was not filled with any pressurised gas.

In the configuration used, a quartz concentric nebuliser, a scott type double path spray chamber, a shielded torch system and an electron multiplier detector were employed. Typical operating parameters were selected based on the manufacturer's recommended procedures (Table 1). Scan conditions were adjusted in order to obtain optimum precision and accuracy, as discussed later.

A sequential inductively coupled plasma atomic emission spectrometer (ICP-OES, Liberty LR, Varian) with a V-groove nebuliser was used for the analysis of lead concentrations in sample digests.

An ETHOS PLUS Millestone microwave with HPR-1000/10S high pressure rotor (Soriso, Bergamo, Italy) was employed for acid digestion of samples.

### 2.2. Chemicals and reagents

In all analytical work, Suprapur nitric acid (Merck, Darmstadt, Germany), hydrochloric acid (Trace Select, Fluka, Dorset, UK) and ultrapure water obtained from a Milli-Q purifier system (Millipore Corp., Bedford, MA) were used.

The certified reference material NIST SRM 981 ("Common Lead Isotopic Standard", National Institute of Standards and Technology, Gaithersburg, MD, USA) was employed to test the mass bias correction and the whole isotopic measurement procedure developed.

Table 1  
Operating parameters settings for the Agilent 7500c ICP-MS

RF power	1500 W
Gas flow rates	
Plasma	15 l min <sup>-1</sup>
Makeup	0.1 l min <sup>-1</sup>
Nebulizer	1.17 l min <sup>-1</sup>
Sampling cone	Ni, 1 mm aperture diameter
Skimmer cone	Ni, 0.4 mm aperture diameter
Ion lenses	
Extract lens	3.2 V
Einzel lens (1, 2 and 3)	–80 V, 10 V, –80 V
Octapole parameters	
OctP RF	190 V
OctP bias	–7.8 V
Quadrupole parameters	
AMU gain	127 V
AMU offset	124 V
QP bias	–5 V
Detector parameters	
Discriminator	8 mV
Analog HV	1670 V
Pluse HV	1060 V

Tl isotopes were used as internal standard. All working solutions were prepared from a Tl stock solution of  $1000 \pm 0.5 \mu\text{g ml}^{-1}$  (Spectroscan, Technolab AS, Norway). On the other hand, an Hg stock solution of  $1000 \pm 0.5 \mu\text{g mL}^{-1}$  (Spectroscan, Technolab AS, Norway) was employed to study the isobaric interference from <sup>204</sup>Hg on <sup>204</sup>Pb measurements.

Lead content in sample digests were determined using a Pb stock solution of  $1000 \pm 0.5 \mu\text{g mL}^{-1}$  (Pure Chemistry, ROMIL, UKAS calibration).

### 2.3. Sample collection and treatment

The study was involved in three abandoned mining areas in Spain located in the Aran Valley (north Pyrenean Range), in Cartagena (Murcia province) and in Osor (Girona province) (Fig. 1). In all of these areas, Galena (PbS) and Sphalerite (ZnS) were the principal minerals extracted to recover lead and zinc as valuable products. During the period of mining activity the mineral from Val d'Aran and Osor was extracted from the mines underground and was concentrated using flotation techniques [17], whereas Cartagena mining area was one of the most representative open cast mining areas in the country. Since the mining districts closure (at the end of the 20th century) the mines and the areas affected by the mining operations (including the mineral treatment factories) have not been reclaimed and, at present, the areas surrounding the factories are still covered by the remains of ore concentrates and wastes, which have become an important source of lead contamination [18,19]. Even now, when torrential rains occur, the remaining tailings from the Cartagena mining district continue to enter the Mar Menor lagoon through the called "wadis" leading to a continuous sediment pollution [20].

In the present work, different kind of samples were collected in the mining areas of study including mining wastes of different

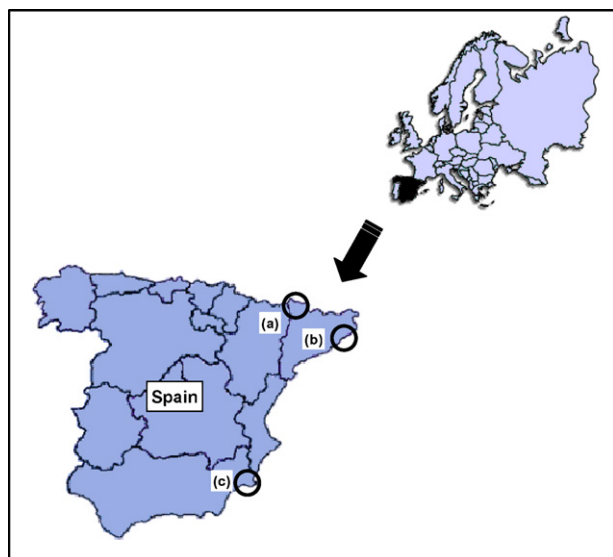


Fig. 1. Location of the studied mining districts: Val d'Aran (a), Osor (b), Cartagena (c).

characteristics, original Pb ore samples and soils and sediments “likely” contaminated by mining activities.

Specifically, sampling of the mining wastes was performed at three sites in the Val d'Aran, two in Cartagena and four in Osor. From the first mining district eleven samples were collected including two samples of the ore vein (galena), eight samples of wastes from an old landfill where the remains of the Pb–Zn concentrates were disposed of, and one mining tailing from a mining dump. In the Cartagena area, a total of eleven samples were collected, nine tailings from several ponds (fine wastes accumulations) and two marine sediment samples likely

contaminated by mining activities. Finally, from the Osor area seven samples were collected including two wastes from a mining dump, two wastes from a landfill with the remains of the Pb–Zn concentrates, one sample of the ore vein (galena) and two soils likely contaminated by mining activities. Therefore, a total of 29 samples were collected for the later lead isotopic analysis. A summary of the location and main characteristics of the collected samples is displayed in Table 2.

All samples were collected using a polypropylene shovel, and subsequently transferred to clean polypropylene bags. In the laboratory, the wastes were oven-dried (50 °C), sieved (<500 μm) and stored in polypropylene containers until analysis.

About 500 mg of sample was weighted and placed in a PTFE reactor and 4 ml HNO<sub>3</sub> (65%) and 12 ml HCl (37%) were added. Then the reactor was sealed and heated following a two stage digestion microwave program which consists of a first step of 5 min to reach 180 °C and a second step of 10 min at 180 °C. After cooling, sample digests were filtered through a whatman 42 filter, transferred into a 25 ml flask and brought to volume with MilliQ water. Then, lead content of the digest was determined by ICP-OES. The experimental procedure was evaluated by using the sediment material BCR-701 from the Community Bureau of Reference (BCR, now the Standards, Measurements and Testing Programme).

The isotopic reference material NIST SRM 981, available in the form of wire, was also treated using the above described digestion method followed by appropriate dilution with Milli-Q water.

Blank digestions were carried out for each set of analysis and the resulting solutions were used throughout all experiments for blank corrections.

Table 2  
Location and main characteristics of the analysed samples

Sample location	Type	Number of samples	<sup>a</sup> [Pb] mg kg <sup>-1</sup>
Val d'Aran mining district	Ore vein (galena)	2	Min. 86000 ± 4000 Max. 87000 ± 4000 Mean 86500
	Pb–Zn concentrate remains	8	Min. 8300 ± 200 Max. 130000 ± 4000 Mean 50600
	Mining dump	1	20000 ± 1000
Cartagena mining district	Fine waste accumulations (ponds)	9	Min. 2700 ± 100 Max. 21000 ± 500 Mean 8800
	Marine sediments	2	Min. 2000 ± 20 Max. 5000 ± 40 Mean 3500
Osor mining district	Ore vein (galena)	1	330000 ± 3000
	Pb–Zn concentrate remains	2	Min. 28000 ± 600 Max. 38970 ± 20 Mean 33500
	Mining dump	2	Min. 320 ± 10 Max. 2050 ± 40 Mean 1180
	Soils	2	Min. 770 ± 10 Max. 1200 ± 100 Mean 990

<sup>a</sup> Results are expressed as mean of two replicates with the corresponding standard deviation.

#### 2.4. Statistical analysis

The statistical analysis of the obtained results was performed using the program SPSS 12.0 for Windows®. Data interpretation was carried out by using discriminating and cluster analysis [21].

In the discriminating analysis performed a set of functions based on linear combinations of the predictor variables (lead isotope ratios) was generated to provide the best discrimination between groups (lead sources). On the other hand, cluster analysis was employed as statistical procedure to form groups of similar objects (samples) according to their isotopic composition.

### 3. Results and discussion

The operating conditions for ICP-MS measurements were optimised daily by using a solution containing  $10 \mu\text{g L}^{-1}$  of Li, Tl, Y, Ce and Co and monitoring the intensities of the isotopes  $^{205}\text{Tl}$ ,  $\text{Y}^{89}$ ,  $\text{Li}^7$ , and the intensities at mass 156 (corresponding to  $^{140}\text{Ce } ^{16}\text{O}^+$ ) and mass 70 (corresponding to  $^{140}\text{Ce}^{2+}$ ) so as to monitor percentage of doubly charged ions and of oxide ions, respectively.

In addition, every working day, a  $30 \mu\text{g L}^{-1}$  lead solution (NIST SRM 981) was analysed in order to check the sensitivity and the resolution of lead isotope peaks to address peak tailing effects coming from adjacent peaks.

The potential of the different lenses in the ion optics play an important role in isotope ratio measurements as it has been quoted in previous works [12,22]. In Fig. 2 the measured  $^{206}\text{Pb}/^{208}\text{Pb}$  isotope ratio is plotted versus the potential of the Einzel 2 lens in the Agilent 7500c quadrupole ICP-MS. As it is shown, by only increasing the Einzel 2 lens potential from +5 to +16 V the measured  $^{206}\text{Pb}/^{208}\text{Pb}$  ratio decreases by about 2%. The ion lenses settings, selected to obtain maximum analyte signal intensity, are collected in Table 1.

Quality assurance of the isotope ratios measurements involved the evaluation of the main parameters affecting accuracy and precision of analytical data, including scan conditions (Precision) and dead time, mass bias and interference effects (Accuracy).

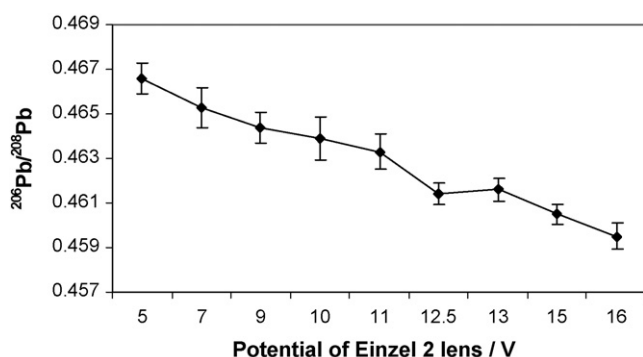


Fig. 2. Dependence of the measured  $^{206}\text{Pb}/^{208}\text{Pb}$  ratio ( $30 \mu\text{g L}^{-1}$  NIST SRM 981) on the potential of the Einzel 2 lens of the Agilent 7500c quadrupole ICP-MS (potential of other lenses: Extract: 3.2 V, Einzel 1:  $-80$  V, Einzel 3:  $-80$  V). Error bars represent the standard deviation between five replicates.

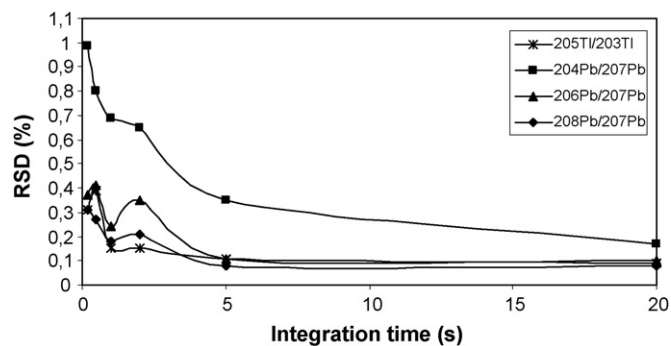


Fig. 3. Integration time vs. relative standard deviation (R.S.D.) using a NIST SRM 981 solution (lead concentration of  $20 \mu\text{g L}^{-1}$ ) spiked with  $20 \mu\text{g L}^{-1}$  of Tl (internal standard).

#### 3.1. Precision

The precision of isotope ratio measurements is influenced by noise and instability originated in both the ICP and the quadrupole mass filter [23].

It should be noted that in the present study, a concentric nebuliser in the self-aspiration mode was used for sample introduction, so discrete noise components caused by rotation of the peristaltic pump rollers were effectively eliminated. Radiofrequency power and gas nebuliser flow rates were also selected so as to minimise relative standard deviation (R.S.D.), see Table 1.

Moreover, integration time for each isotope ratio was optimised in respect to the lowest R.S.D. obtainable as detailed in Fig. 3. All measurements were done using three points per peak and five replicates of each sample. As expected, the higher the integration time the lower the standard deviation until a constant value was reached; from these results, an integration time of five seconds was fixed for all the isotopes except for  $^{204}\text{Pb}$  which requires a longer time to get a similar precision. Ten seconds were finally chosen as a compromise between precision and analysis time.

As a result, a total time of 9 min was needed for each sample analysis obtaining R.S.D. values which are in agreement with those reported in the literature using other quadrupole based instruments (R.S.D.  $\approx 0.1\%$  except in the case of isotope ratios involving  $^{204}\text{Pb}$ , R.S.D.  $\approx 0.2\text{--}0.3\%$ ) [22,24].

#### 3.2. Accuracy

To achieve good accuracy of isotope ratio measurements by ICP-MS three important instrumental bias factors have been studied and properly corrected, including dead time of the detection system, the mass discrimination mainly due to the space charge effects as well as spectral interferences.

##### 3.2.1. Mass discrimination

Mass discrimination is an instrumental bias as a result of a different transmission of ions according to their masses from the point at which they enter the sampling device until they are finally detected by the electron multiplier [23]. Several different processes contribute to this deviation including mass fractionation in the sampling processes or space charge effects in the

Table 3  
Comparison of relative errors  $(R_{\text{corrected}} - R_{\text{certified}})/R_{\text{certified}}$  (%) in estimation of mass bias corrections (lineal, potential and exponential algorithms) using the NIST-981 ( $30 \mu\text{g L}^{-1}$  Pb) and Tl ( $20 \mu\text{g L}^{-1}$ ) as internal standard ( $^{203}\text{Tl}/^{205}\text{Tl}$ )

	Lineal	Potential	Exponential
Bias factor ( $K$ )	$K = \frac{R_{\text{exp}} - R_{\text{theo}}}{R_{\text{theo}} \Delta M}$	$K = \left( \frac{R_{\text{exp}}}{R_{\text{theo}}} \right)^{\frac{1}{\Delta M}} - 1$	$K = \frac{-1}{\Delta M} \ln \left( \frac{R_{\text{exp}}}{R_{\text{theo}}} \right)$
Corrected isotope ratio	$R_c = \frac{R_{\text{exp}}}{1 + K(\Delta M)}$	$R_c = \frac{R_{\text{exp}}}{(1 + K)^{\Delta M}}$	$R_c = \frac{R_{\text{exp}}}{e^{K \Delta M}}$
$K$	-0.0043	-0.0043	-0.0043
$^{204}\text{Pb}/^{207}\text{Pb}$	-0.062	-0.077	-0.077
$^{206}\text{Pb}/^{207}\text{Pb}$	0.18	0.18	0.18
$^{208}\text{Pb}/^{207}\text{Pb}$	-0.0088	-0.0088	-0.0097

$R_{\text{exp}}$  (experimental isotope ratio),  $R_{\text{theo}}$  (theoretical isotope ratio),  $R_c$  (corrected isotope ratio),  $\Delta M$  (mass difference between the isotopes involved in the ratio),  $K$  (mass bias factor).

region of the skimmer cone (due to the preferential transport of heavier isotopes) [25].

Instrumental mass bias may be corrected by using a certified isotopic standard (external correction) or by the measurement of an isotope ratio of an element with known isotopic composition in the same mass range, as an internal standard. The bias is then applied as a part of a mathematical model (linear, power or exponential algorithm) to correct the analyte ratio [11].

In the present work, mass bias correction has been carried out by internal correction using Tl as internal standard ( $^{203}\text{Tl}/^{205}\text{Tl}$ ). It has to be kept in mind that using internal correction inaccuracies may be introduced as the isotopes used to calculate the bias have masses, ionisation characteristics and isotopic abundances that are different to the analyte isotopes [26].

It is known that the use of an inappropriate mathematical model in estimation of mass bias may lead to a certain degree of inaccuracy. Consequently, the different correction algorithms (lineal, power or exponential) were tested, so as to study its suitability in our particular case, by using thallium for the correction of lead isotope ratios measured for NIST SRM 981. Results obtained in the comparison study are summarised in Table 3. As it is shown, the relative errors after correction are very similar using the three fitting functions leading to the conclusion that any of the three algorithms are valid for correction of mass bias. Finally, the power law function was selected for measurements since it is one of the most commonly used according to the literature [20].

In Fig. 4 measured, corrected and certified values for each isotope ratio studied are displayed. As it is shown, measured value deviations from the certified values, which result from mass bias drift, range from 0.4 to 2%, whereas after correction, the errors are reduced to 0.01–0.1%. Thus, the internal correction used in this study efficiently eliminates the mass bias drift effect.

In order to compute the propagated uncertainty on the lead isotope ratios corrected for mass bias, the uncertainty on the mass discriminating factor ( $K$ ) has to be taken into account. According to the expressions used in the potential correction (see Table 3), the propagated uncertainty results in:

$$S(R_{\text{Pb}(c)}) = R_{\text{Pb}(c)} \sqrt{\left( \frac{S(R_{\text{Pb}(\text{exp})})}{R_{\text{Pb}(\text{exp})}} \right)^2 + \left( \frac{S(R_{\text{Tl}(\text{exp})})}{R_{\text{Tl}(\text{theo})} e^{\Delta M_{\text{Pb}}/\Delta M_{\text{Tl}} (\ln R_{\text{Tl}(\text{exp})}/R_{\text{Tl}(\text{theo})})} \right)^2} \quad (1)$$

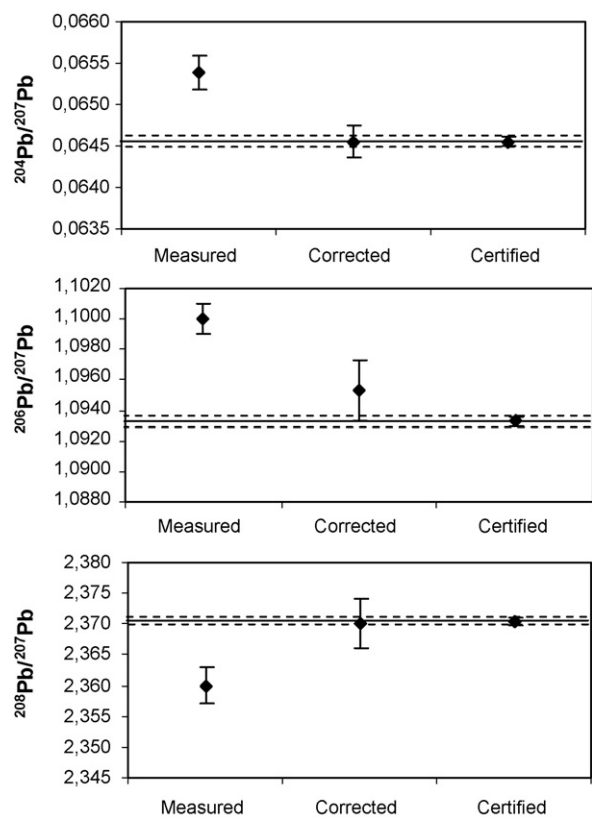


Fig. 4. Comparison of measured, corrected (Thallium internal correction) and certified lead isotope ratios using a  $30 \mu\text{g L}^{-1}$  NIST SRM 981 solution spiked with  $20 \mu\text{g L}^{-1}$  of thallium ( $n=5$ , straight lines represent the certified isotopic values obtained by TIMS and broken lines display the respective 95% confidence ranges).

where  $S$ : standard deviation,  $R_{\text{Pb}(c)}$ : corrected lead isotope ratio for mass bias,  $R_{\text{Pb}(\text{exp})}$ : measured lead isotope ratio,  $R_{\text{Tl}(\text{exp})}$ : measured Tl isotope ratio ( $^{203}\text{Tl}/^{205}\text{Tl}$ ),  $R_{\text{Tl}(\text{theo})}$ : theoretical Tl isotope ratio ( $^{203}\text{Tl}/^{205}\text{Tl}$ ),  $\Delta M$ : mass difference between the isotopes involved in the ratio.

Therefore, despite that the internal correction increased the accuracy of the isotope ratio values, the precision decreased due

to the additional deviations of thallium isotope measurements. In the present study, the overall precision of bias corrected Pb isotope ratios (expression 1) ranges from 0.15–0.18%, except for the ratios involving  $^{204}\text{Pb}$  that present higher values ( $\approx 0.3\%$ ) due to the lower abundance of this isotope. Analogous R.S.D. values have been reported by other authors using similar instrumentation [4].

### 3.2.2. Dead time

The electron multiplier detector employed in this study could use an analog mode (high concentrations) or a pulse counting mode (low concentrations) for ion signal measurement. For our purposes, the detection was made in all cases using the pulse mode so as to work under more sensitive conditions.

Firstly, it was necessary to study which was the maximum lead concentration that can be measured before the instrument automatically switches to the analog mode. For this purpose, solutions containing increasing concentrations of common lead (NIST SRM 981) spiked with  $20\ \mu\text{g L}^{-1}$  of Tl were measured and the “corrected” isotope ratios were plotted with the corresponding confidence range ( $n=5$ , 95% confidence level), see Fig. 5.

The results obtained showed that concentrations lower than  $50\ \mu\text{g L}^{-1}$  should be used since at higher levels the more abundant lead isotope ( $^{208}\text{Pb}$ ) is already measured in the analog mode. On the other hand, at  $10\ \mu\text{g L}^{-1}$  the measured uncertainty is noticeable, particularly for the less abundant isotope ( $^{204}\text{Pb}$ ). Consequently, a working range from 20 to  $50\ \mu\text{g L}^{-1}$  was used throughout this work (Fig. 5).

It is important to note that at high count rates different effects can cause pulse counting systems to register fewer events than actually occur [25]. As a consequence, signal responses become non-linear above certain concentration level (dead time of the detector). As it can be seen in Fig. 5, from 20 to  $50\ \mu\text{g L}^{-1}$ , the dependence of isotope ratios upon analyte concentration is non-existent, suggesting that at this lead levels dead time correction of the detector was not necessary.

### 3.2.3. Interferences

The measurement of  $^{204}\text{Pb}$  by mass spectrometry is subject to an isobaric interference from  $^{204}\text{Hg}$  [27]. Owing to the possible presence of this metal in the mining waste samples studied, the measured  $^{204}\text{Pb}$  ion beam was corrected for the Hg contribution.

Two expressions were evaluated to correct the measured intensity at mass 204 by measuring the ion beam of  $^{202}\text{Hg}$ :

$$^{204}\text{Pb} = I(204) - \frac{\text{Abundance}(^{204}\text{Hg})}{\text{Abundance}(^{202}\text{Hg})} \times I(^{202}\text{Hg}) \quad (2)$$

$$^{204}\text{Pb} = I(204) - \left( \frac{\text{Abundance}(^{204}\text{Hg})/\text{Abundance}(^{202}\text{Hg})}{1 + K\Delta M} \right) \times I(^{202}\text{Hg}) \quad (3)$$

where  $\text{Abundance}(^{204}\text{Hg})/\text{Abundance}(^{202}\text{Hg}) = 0.23$ .

The mass discrimination factor between 202 and 204 masses (expression 3) was neglected since a preliminary study indicated

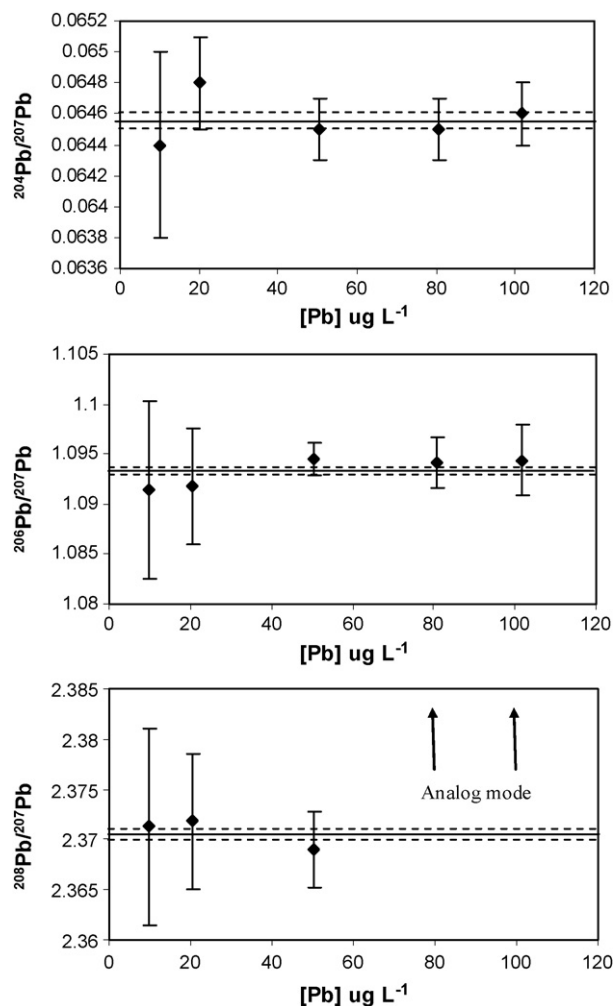


Fig. 5. Lead isotope ratios dependence on analyte concentration. Straight lines represent the certified isotopic values (NIST SRM 981) and broken lines display the respective 95% confidence range.

that isotope lead ratios obtained with and without mass bias correction were found not to be significantly different at 95% confidence level. According to that, it was considered appropriate to use the expression 2 for  $^{204}\text{Pb}$  ion beam correction, due to its higher simplicity.

Table 4 collects the isotope ratio values attained with a  $20\ \mu\text{g L}^{-1}$  lead solution spiked up to  $20\ \mu\text{g L}^{-1}$  using an Hg solution of  $10\ \text{mg L}^{-1}$ , after and before mercury correction. Results clearly demonstrate the necessity of  $^{204}\text{Pb}$  ion beam correction for the Hg contribution. Besides, the isotope ratio values obtained after Hg correction are in agreement to those measured for a solution without Hg, leading to the conclusion of the effectiveness of the equation used for  $^{204}\text{Hg}$  correction.

On the other hand, it is necessary to assess whether matrix interferences make a significant contribution to the offset of the mass discrimination corrected isotope ratio from its true value. This may be done by scanning the mass region of interest for a procedural blank. In this study, no correction for matrix interferences was considered necessary as lead concentration in procedural blank solutions represents  $<0.2\%$  of the Pb content in samples. Besides, Tl content measured in a procedural blank



Table 4

Effect of 204 ion beam correction for  $^{204}\text{Hg}$  contribution using a NIST SRM 981 solution of  $20\ \mu\text{g L}^{-1}$  ( $n = 5$ , 95% confidence level)

	$^{204}\text{Pb}/^{207}\text{Pb}$	$^{204}\text{Pb}/^{206}\text{Pb}$	$^{204}\text{Pb}/^{208}\text{Pb}$
With Hg before correction <sup>a</sup>	$0.1574 \pm 0.0004$	$0.1203 \pm 0.0003$	$0.0628 \pm 0.0002$
With Hg after correction <sup>a</sup>	$0.0630 \pm 0.0002$	$0.0482 \pm 0.0001$	$0.0252 \pm 0.0001$
Without Hg before correction	$0.0633 \pm 0.0003$	$0.0483 \pm 0.0003$	$0.0253 \pm 0.0002$
Without Hg after correction	$0.0632 \pm 0.0003$	$0.0483 \pm 0.0003$	$0.0252 \pm 0.0001$

<sup>a</sup> NIST SRM 981 solution was spiked to  $20\ \mu\text{g L}^{-1}$  with a high purity Hg solution.

( $[\text{Tl}] < 0.07\ \mu\text{g L}^{-1}$ ) indicated that its contribution to the isotopic measurement was also negligible.

### 3.3. Reproducibility

As mentioned previously, the whole procedure developed was evaluated using the isotopic standard NIST SRM 981, and all the lead isotope ratios of this standard were determined every working day. The results of the determinations during a four month period ( $n = 10$ ) are presented in Fig. 6 with the corresponding confidence range ( $n = 5$ , 95% confidence level).

The standard deviation for long-term measurements was slightly lower than that obtained for short-term (a single working day) measurements, with a R.S.D. values ranging from 0.11 to 0.14%, except for the ratios involving  $^{204}\text{Pb}$  which presents a R.S.D. values from 0.21 to 0.27%.

A similar study was performed measuring the lead isotope ratios of a mining waste sample on three different days over a period of three month (see Table 5). As it is shown, results obtained for measurements ( $n = 5$ ) on three different days agree well and no statistically significant differences at the 95% confidence level were found.

### 3.4. Application of lead isotope ratios to real samples

A characteristic feature of all the samples collected in the three mining districts studied is the large amount of lead, ranging from 0.03 up to 13 wt.%. Therefore, after measurement of the Pb concentration in sample digests, the solutions were adjusted to have a lead concentration of about  $30\ \mu\text{g L}^{-1}$ , according to the suitable working range (from  $20\ \mu\text{g L}^{-1}$  to  $50\ \mu\text{g L}^{-1}$ ) established previously.

Once dilutions were performed, they were spiked with a high purity Tl solution to  $20\ \mu\text{g L}^{-1}$  so as to correct for mass bias drift. It is relevant to note that diluted digests spiking was carried out just before the analysis to avoid possible redox reactions under

Table 5

Variation of lead isotope ratios of a mining waste sample observed over a period of three months

	$^{204}\text{Pb}/^{207}\text{Pb}$	$^{206}\text{Pb}/^{207}\text{Pb}$	$^{208}\text{Pb}/^{207}\text{Pb}$
Initial	$0.0640 \pm 0.0005$	$1.155 \pm 0.004$	$2.439 \pm 0.007$
1 month	$0.0640 \pm 0.0006$	$1.155 \pm 0.007$	$2.439 \pm 0.012$
3 month	$0.0643 \pm 0.0008$	$1.147 \pm 0.013$	$2.431 \pm 0.016$

Data are expressed as the mean value of five replicates with the respective 95% confidence range.

laboratory conditions that can greatly affect the precision and accuracy of Pb and Tl isotope ratio values [27].

For each sample, two independent replicates were pre-treated and analysed five times separately. The mean value and respective confidence level (95% confidence level) were then calculated. To avoid sample-to-sample memory effects a rinse step of 20 s using Milli-Q water was performed.

Quality assurance (precision and accuracy) of the measuring procedure was addressed by analysing a  $30\ \mu\text{g L}^{-1}$  NIST SRM

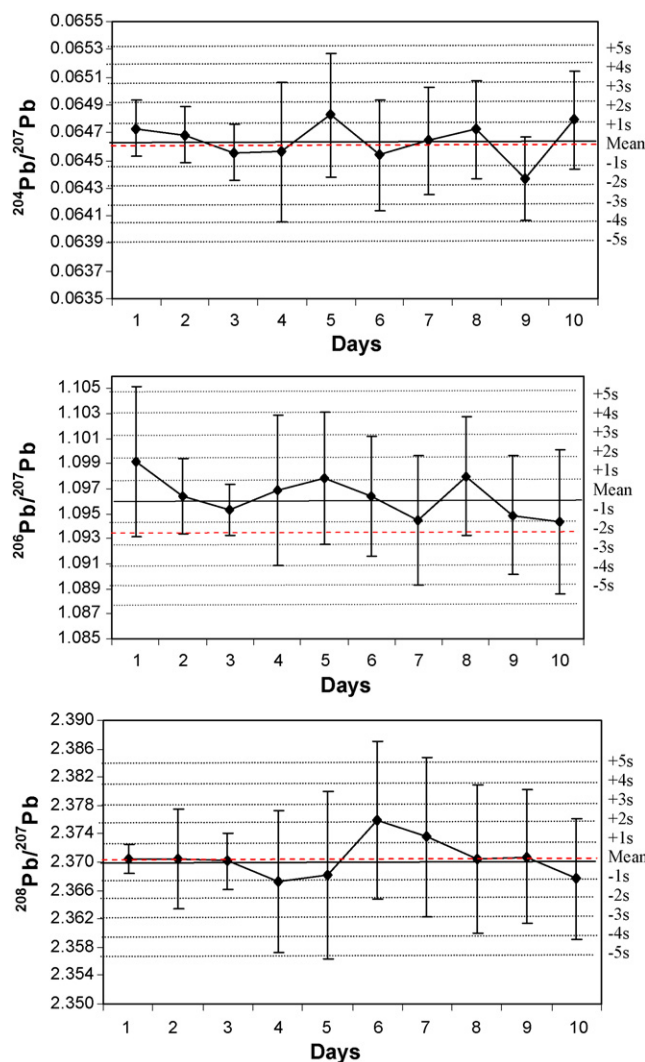


Fig. 6. Variation of the lead isotope ratios ( $30\ \mu\text{g L}^{-1}$  NIST SRM 981 solution) observed over a period of four months ( $s$  = standard deviation of the mean, discontinuous line represent certified values).

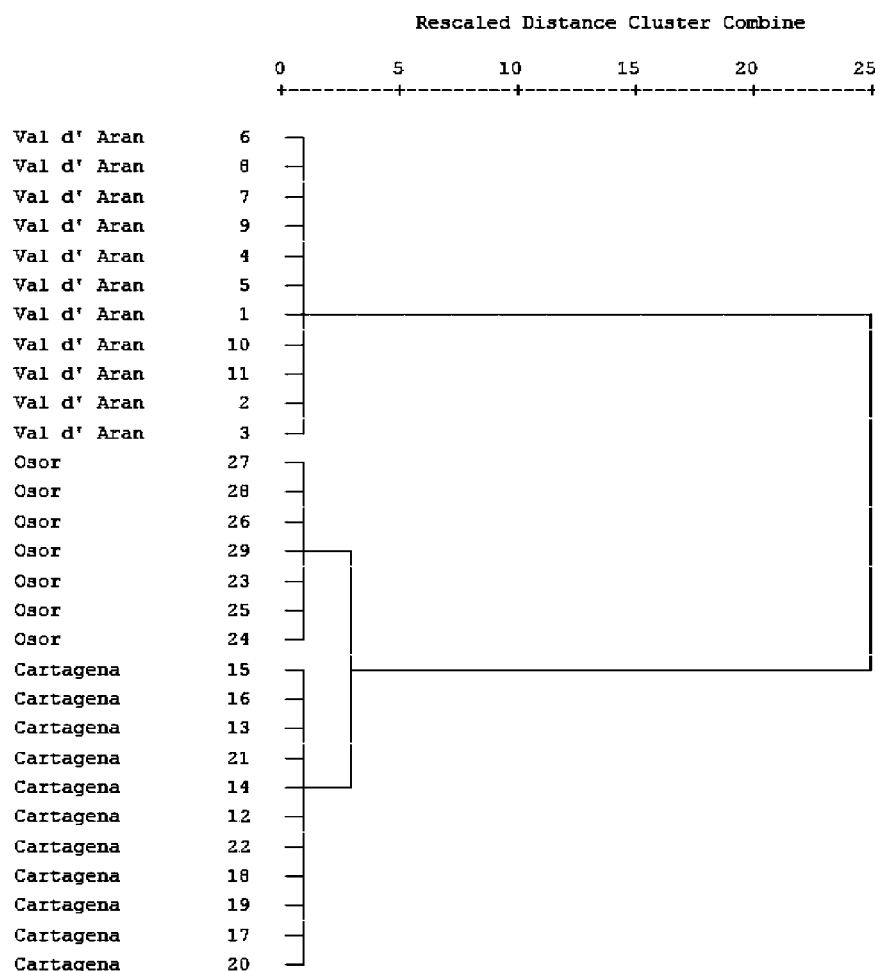


Fig. 7. Dendrogram (Ward's method of agglomeration and square Euclidean distances) showing clustering of mining districts ( $n = 29$ ).

981 solution at the beginning and at the end of the analysis of each batch of samples.

Study of the possible differentiation of the different mining wastes from the areas studied was performed on the basis of the results of all the possible lead isotope ratios measured in the collected samples by using cluster analysis. Square Euclidean distances were used as a similarity measurement and the Ward's method as agglomeration rule. Results obtained are displayed as a dendrogram in Fig. 7. At a cursory glance, three clearly distinct groups can be observed corresponding to the different mining districts where samples were collected. Besides, it would appear that mining waste samples from Val d'Aran are substantially different to those collected at the other two locations.

In order to establish the minimum lead isotope ratios that could also allow distinguishing between mining districts, a discrimination analysis using Wilk's lambda method was performed. Two functions based on linear combinations of the  $^{206}\text{Pb}/^{207}\text{Pb}$  and  $^{208}\text{Pb}/^{207}\text{Pb}$  variables were generated (Table 6) indicating that  $^{206}\text{Pb}/^{207}\text{Pb}$  and  $^{208}\text{Pb}/^{207}\text{Pb}$  are highly indicative of mining waste samples origin and using only this two isotope ratios is possible to discriminate properly between the mining areas (Fig. 8). This point is the main interest for isotopic analysis by techniques less sensitive and precise than thermal ionisation mass spectrometry as ICP-MS, since 206, 207 and 208 isotopes

are easier determined than  $^{204}\text{Pb}$  due to the lower abundance of this isotope.

If the plot  $^{206}\text{Pb}/^{207}\text{Pb}$  versus  $^{208}\text{Pb}/^{207}\text{Pb}$  is performed, the points which represent samples from the three mining areas studied really fall into three separated groups (Fig. 9). All the tailings from Val d'Aran can be assembled in a single group with ranges in Pb ratios from  $1.153 \pm 0.004$  to  $1.159 \pm 0.006$  ( $^{206}\text{Pb}/^{207}\text{Pb}$ ) and from  $2.436 \pm 0.009$  to  $2.441 \pm 0.009$  ( $^{208}\text{Pb}/^{207}\text{Pb}$ ). In a similar way, the samples collected at Osor join together with values ranging from  $1.182 \pm 0.009$  to  $1.186 \pm 0.008$  ( $^{206}\text{Pb}/^{207}\text{Pb}$ ) and from  $2.47 \pm 0.01$  to  $2.48 \pm 0.02$  ( $^{208}\text{Pb}/^{207}\text{Pb}$ ). Finally, samples from Cartagena are located at the upper part of the graph with typical

Table 6  
Standardised coefficients and explained variance from the functions obtained with the discriminating analysis

	Function	
	1	2
Variance (%)	98.2	1.8
$^{206}\text{Pb}/^{207}\text{Pb}$	-0.421	1.005
$^{208}\text{Pb}/^{207}\text{Pb}$	0.755	0.785

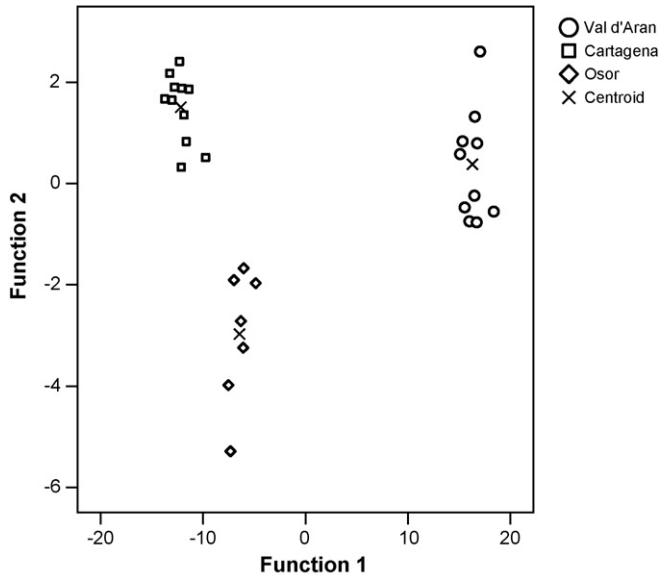


Fig. 8. Discriminating analysis (Wilks' Lambda method) of lead isotope ratios in mining waste samples ( $n=29$ ).

values from  $1.193 \pm 0.004$  to  $1.200 \pm 0.003$  ( $^{206}\text{Pb}/^{207}\text{Pb}$ ) and from  $2.48 \pm 0.01$  to  $2.490 \pm 0.007$  ( $^{208}\text{Pb}/^{207}\text{Pb}$ ).

From Fig. 9 it could be seen a linear tendency ( $R^2=0.9821$ ) between  $^{206}\text{Pb}/^{207}\text{Pb}$  and  $^{208}\text{Pb}/^{207}\text{Pb}$  ratios. This fact could be explained taking into account the possible variations of the relative abundance of lead isotopes over the time, as commented in the introduction section. Old lead ores were formed at an early stage in the earth's evolution so the decay of Th and U contribute little to the lead before these elements become isolate from the lead ore. Thus, as a general rule, old lead ores are generally characterised by low  $^{206}\text{Pb}/^{207}\text{Pb}$  ratios, whereas more radiogenic samples of lead, those that have been mixed with thorium and uranium for a long period of time, have ratios of 1.18 and above [28]. According to that, it could be deduced that galena (lead ore) from Val d'Aran is more ancient than those from Cartagena and Osor, which present higher radio-

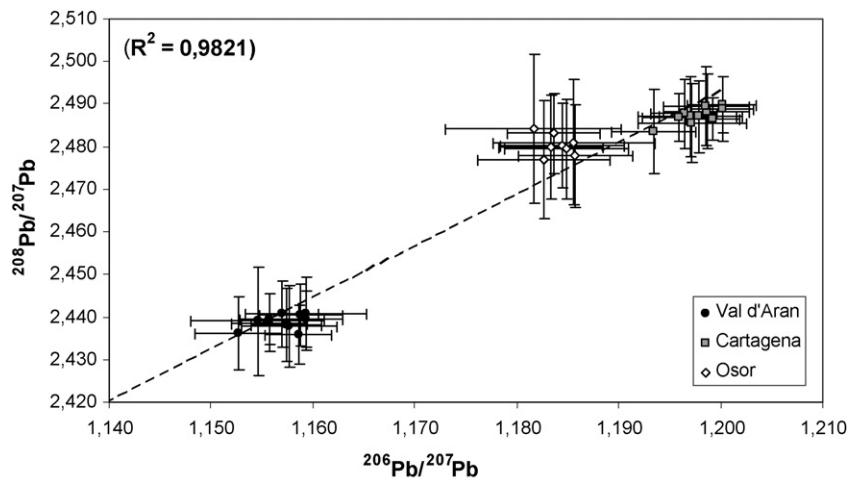


Fig. 9. Plot of  $^{206}\text{Pb}/^{207}\text{Pb}$  vs.  $^{208}\text{Pb}/^{207}\text{Pb}$  for mining waste samples studied ( $n=29$ ). Error bars (95% confidence range) are based on results from two independent replicates of each sample analysed five times separately.

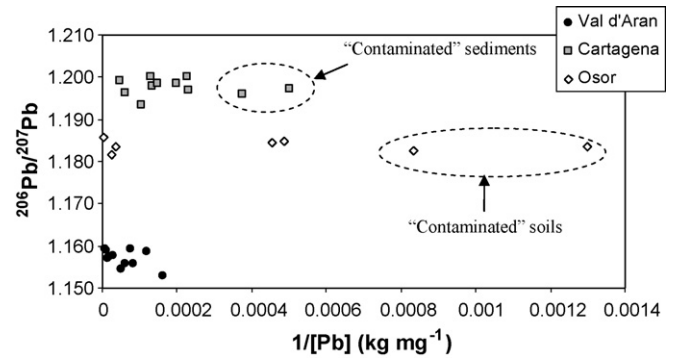


Fig. 10. Relationship between  $^{206}\text{Pb}/^{207}\text{Pb}$  ratio and the Pb content ( $\text{mg kg}^{-1}$ ) for analysed samples.

genic isotope ratios. Moreover, it would seem that geological age of lead ores from Cartagena and Osor are similar because of the similarity between the respective isotope ratios. These statements are consistent with the geological data for the age of the ore deposits in the Eastern part of Spain. Whilst Val d'Aran deposits were formed during Cambro-Ordovician time (about 450–550 Ma old) [18], the mineral deposits of Osor and Cartagena were generated during the Tertiary and the calculated ages are quite younger than for Val'Aran deposits (approximately 45–50 Ma for Osor [19] and 7–11 Ma for the Cartagena ores [29]).

It is interesting to note that despite we can differentiate clearly between the mining wastes from the studied mining areas (which is related to the geological age of lead ores), the Pb isotopic composition of the different kind of samples within a mining district (galena ore, processing wastes, "contaminated mining samples") is indistinguishable leading to the conclusion that lead in the samples is derived from the same source of lead. The dependence of isotope ratios upon analyte concentration (Fig. 10) is non-existent suggesting that different sort of samples within the same area could be identified taking into account their lead content. In this case, "likely" contaminated soil and sediment samples from Cartagena and Osor present similar  $^{206}\text{Pb}/^{207}\text{Pb}$

ratios to the mining wastes but their lower lead content allow distinguishing them from the mining waste samples. On the other hand, resemblance between isotopic composition of soils and sediments and that from mining tailings pointed out the contamination of these samples by mining activities. However, it has to be kept in mind that other source of lead pollution such as the past leaded-petrol emissions could not be excluded. According to that a leaded-petrol sample was analysed and the obtained results were of a low lead ratios ( $^{206}\text{Pb}/^{207}\text{Pb} = 1.080 \pm 0.004$ ,  $^{208}\text{Pb}/^{207}\text{Pb} = 2.374 \pm 0.008$ ), as reported in other works [8,30]. Taking into account that the ratios determined in soil and sediment samples are substantially higher than that determined in the petrol sample, we can suggest that the unusual high content of Pb in these samples are derived from mining activities rather than from other lead sources.

#### 4. Conclusions

The results of this investigation highlight that ICP-MS technique provides sufficient precision and accuracy to satisfactorily determinate lead isotope ratios in mining wastes as a tool to identify their source, provided that instrument bias factors are properly studied and corrected.

By only monitoring  $^{206}\text{Pb}/^{207}\text{Pb}$  and  $^{208}\text{Pb}/^{207}\text{Pb}$  ratios in mining waste samples it was feasible to identify properly mining lead origin which is related to the geological age of lead ore. The data showed that the Pb isotopic composition of the different kind of samples within a mining district (galena ore and processing wastes) is indistinguishable and close to that determined from soils and sediments from the same areas, suggesting that the high lead content in these samples is derived from the mining operations.

#### Acknowledgements

The authors express their sincere gratitude to Giovanni Pardini belonging to the Soil Science Unit (University of Girona) for his help during the sampling campaign in the Osor mining district.

This study was financed by the Spanish National Research Programme (CGL2004-05963-C04-03/HDI). E. Marguí gratefully acknowledges a grant from The Autonomous Government of Catalonia (Ref. 2002FI 00577).

#### References

- [1] I.T. Platzner, *Modern Isotope Ratio Mass Spectrometry*, John Wiley & Sons, Wiley, England, 1997.
- [2] J.R. Bacon, N.S. Dinev, *Environ. Pollut.* 134 (2005) 247.
- [3] P. Négrel, W. Kloppmann, M. Garcin, D. Giot, *Appl. Geochem.* 19 (2004) 957.
- [4] R. Kurkjian, C. Dunlap, A.R. Flegal, *Appl. Geochem.* 19 (2004) 1567.
- [5] A. Martínez Cortizas, E. García-Rodeja, X. Pontevedra Pombal, J.C. Nóvoa Muñoz, D. Weiss, A. Cheburkin, *Sci. Total Environ.* 292 (2002) 33.
- [6] B.P. Jackson, P.V. Winger, P.J. Lasier, *Environ. Pollut.* 130 (2004) 445.
- [7] R. Bindler, I. Renberg, J. Klaminder, O. Emteryd, *Sci. Total Environ.* 319 (2004) 173.
- [8] D.J. Bellis, K. Satake, C.W. McLeod, *Sci. Total Environ.* 321 (2004) 105.
- [9] M. Labonne, D.B. Othman, Jean-Marc Luck, *Chem. Geol.* 181 (2001) 181.
- [10] Z. Cheng, K.A. Foland, *Appl. Geochem.* 20 (2005) 353.
- [11] C.P. Ingle, B.L. Sharp, M.S.A. Horstwood, R.R. Parrish, D. John Lewis, *J. Anal. At. Spectrom.* 18 (2003) 219.
- [12] L.A. Allen, J.J. Leach, R.S. Houk, *Anal. Chem.* 69 (1997) 2384.
- [13] A.A. Meharg, D.J. Pain, R.M. Ellam, R. Baos, V. Olive, A. Joynson, N. Powell, A.J. Green, F. Hiraldo, *Sci. Total Environ.* 300 (2002) 81.
- [14] A.S. Al-Ammar, R.M. Barnes, *J. Anal. At. Spectrom.* 16 (2001) 327.
- [15] Q. Xie, R. Kerrich, *J. Anal. At. Spectrom.* 17 (2002) 69.
- [16] C.M. Almeida, M.T.S.D. Vasconcelos, *J. Anal. At. Spectrom.* 16 (2001) 607.
- [17] A.F. Marques, I. Queralt, M.L. Carvalho, M. Bordalo, *Spectrochim. Acta Part-B* 58 (2003) 2191.
- [18] I. Pujals, *Las mineralizaciones de sulfuros en el Cambro-Ordovícico de la Val d'Aran (Pirineo Central, Lérida)*, Doctoral Thesis, Faculty of Sciences, Autonomous University of Barcelona, Spain, 1992.
- [19] J.M. Mata-Perelló, *Els minerals de Catalunya*, Doctoral Thesis, Faculty of Geology, University of Barcelona, Spain, 1981.
- [20] L. Marín Guirao, A. Marín Atucha, J. Lloret Barba, E. Martínez López, A.J. García Fernández, *Mar. Environ. Res.* 60 (2005) 317.
- [21] M.J. Norusis, *SPSS® for Windows™, Professional Statistics™, Release 6.0*, SPSS Inc., 1993.
- [22] K.G. Heumann, S.M. Gallus, G. Rädlinger, J. Vogl, *J. Anal. At. Spectrom.* 13 (1998) 1001.
- [23] I.S. Begley, B.L. Sharp, *J. Anal. At. Spectrom.* 12 (1997) 395.
- [24] I. Feldmann, N. Jakubowski, C. Thomas, D. Stuewer, Fresenius, *J. Anal. Chem.* 365 (1999) 422.
- [25] C. Latkoczy, T. Prohaska, G. Stingeder, M. Teschler-Nicola, *J. Anal. At. Spectrom.* 13 (1998) 561.
- [26] M.F. Thirlwall, *Chem. Geol.* 184 (2002) 255.
- [27] G.D. Kamenov, P.A. Mueller, M.R. Perfit, *J. Anal. At. Spectrom.* 19 (2004) 1262.
- [28] J.R. Bacon, *J. Environ. Monit.* 4 (2002) 291.
- [29] I.S. Oen, J.C. Windt, T.G.M. Winnubst, P. Kagern, *Epigenetic lead-zinc mineralization in Miocene pebbly mudstones, Sierra de Cartagena, Spain*, *Mineralium Deposita* 10 (1975) 362.
- [30] G. Charalampides, O. Manoliadis, *Environ. Int.* 28 (2002) 147.

# Complete quality analysis of commercial surface-active products by Fourier-transform near infrared spectroscopy

Juan Fco. Martínez-Aguilar<sup>a,\*</sup>, Emma L. Ibarra-Montaña<sup>b</sup>

<sup>a</sup> *Facultad de Estudios Superiores Cuautitlán, Universidad Nacional Autónoma de México, Av. Primero de Mayo s/n, Cuautitlán Izcalli, Estado de México, Mexico*

<sup>b</sup> *Departamento de Química Analítica, Cognis Mexicana, Calzada de la viga s/n, Ecatepec, Estado de México, Mexico*

Received 29 January 2007; received in revised form 1 May 2007; accepted 2 May 2007

Available online 10 May 2007

## Abstract

Using proper calibration data Fourier-transform near infrared spectroscopy is used for developing multivariate calibrations for different analytical determinations routinely used in the surfactants industry. Four products were studied: oleyl-cetyl alcohol polyethoxylated, cocamidopropyl betaine (CAPB), sodium lauryl sulfate (SLS) and nonylphenol polyethoxylated (NPEO). Calibrations for major as well as very low concentrated compounds were achieved and every model was validated through linearity, bias, accuracy and precision tests, showing good results and the viability of NIR spectroscopy as a full quality control method for this products. Duplicate and complete analysis on a single sample takes at most 3 min, requiring neither sample preparation nor the use of reagents. The analytical reference procedures involved in this work represent the typical ones used in the industry and the NIR method shows good results in the analysis of components with weight concentrations less than 1%.

© 2007 Elsevier B.V. All rights reserved.

**Keywords:** NIR spectroscopy; Surfactants industry; Multivariate calibration; NIR validation

## 1. Introduction

Surfactants are used in different areas. Although more known for their cleaning capacity, they can also act as emulsifying, foaming, wetting or even bactericide agents, depending on their composition. In order to carry out those functions, surfactants must fulfil some quality requirements, which in the industry are evaluated with standardized analytical methods [1–3]. Among them are liquid extraction, volumetric and gravimetric analyses, chromatography and even MIR spectroscopy; yet those methods can be very time-consuming and need reagents and solvents that increase costs besides probably being environmentally harmful.

In the past years near infrared spectroscopy along with chemometrics have proved to solve that kind of problems and constitute together a faster, less costly and not polluting analytical method in many areas of chemistry. However, its application for quality control of surfactants has only dealt with the determination of major components [1,4]. In the real world, commercial samples require determinations that have to do with concentra-

tions and analytes that are considered too low or not suitable for a technique like NIR. In this work, we show that NIR spectroscopy can provide good results in the analysis of these materials, studying some of the most important and representative products of the industry and exploring its applicability for determining even very low concentration constituents, provided that they have a relationship with the active, main compounds of the surfactants, making possible a complete quality analysis.

### 1.1. Theory

In the near infrared zone, analytical signals (absorbance measures) arise as a result of overtones and combination bands of C–H, O–H, N–H and S–H bonds. The spectral range goes from 14300 to 4000  $\text{cm}^{-1}$ . With the aid of chemometric tools like partial least squares regression (PLSR) it is possible to build calibration models using most of the information contained in the absorption spectra for getting a relationship between the analytical responses and the analyte concentration, obtained with a reference method. In order to select the appropriate dimension of the calibration models, we have used the Haaland and Thomas criterion via a leave-one-out cross validation [5]. The

\* Corresponding author. Tel.: +52 55 56223794; fax: +52 55 56223723.  
E-mail address: [elcuaderno@yahoo.com.mx](mailto:elcuaderno@yahoo.com.mx) (J.Fco. Martínez-Aguilar).

Table 1  
Analytical determinations and reference procedures performed on the studied products

Product	Determination	Analytical method
OC-AEO	Hydroxyl number	Esterification with phthalic anhydride in pyridine and titration with NaOH
CAPB solution	CAPB content	Titration with HClO <sub>4</sub> of the basic solution in CHCl <sub>3</sub> -ethylene glycol monomethyl ether
	Solids	Karl-Fischer titration with CH <sub>3</sub> OH as solvent
	Glycerol	Oxidation with periodate and titration with NaOH
	NaCl	Mohr titration
SLS solution	SLS content	Epton titration with benzalkonium chloride
	Lauryl alcohol	HPLC quantification
	NaCl	Mohr titration
	Sulfates	Precipitation titration with Pb <sup>2+</sup>
NPEO solution	Solids	Weighting of the residue after a 30 min heating period at 125 °C

prediction error sum of squares (PRESS) gives a measure of the difference between the predicted and the actual concentrations and it can be used to determine the number of components that better model the data. However, looking just for the number of factors that gives the minimum PRESS can lead to overfitting. A better choice is to calculate the quotient of the PRESS values obtained with fewer factors and the minimum PRESS. From these values an *F* ratio probability is calculated and, to select the more parsimonious model, the model with the smallest PRESS not significantly greater than the global PRESS minimum is adopted. The *F*-test is carried out with *m* and *m* degrees of freedom (*m* is the number of calibration samples) and  $\alpha = 0.25$  as it has been suggested and used elsewhere. It is important to mention that in order to prepare suitable training sets the collection of analysed samples was accomplished during a 1-year period. It ensures not just taking into account more differences within the production processes than the different batches alone but also expands the calibration ranges and allows building more robust models. The availability of the samples was nevertheless limited and the obtained test sets did not cover all the range of concentrations. Having these facts it was decided to use a full cross validation, which uses every sample to build the calibration models at the same time that test them. As they originate from different batches and the method leaves one sample out a time the possibility of introducing bias is minimized. The equation that regression gives for predicting concentration of unknowns is  $\hat{y} = b_0 + \mathbf{x}^T \mathbf{b}$ , where  $\mathbf{x}^T$  indicates the transpose of the  $\mathbf{x}$  vector representing the spectrum of a sample,  $\hat{y}$  indicates the estimated concentration,  $b_0$  is a constant and  $\mathbf{b}$  represents the predictor function [6,7].

## 2. Experimental

### 2.1. Instrumentation and software

The absorbance spectra were collected with an FT-NIR model MPA spectrometer from Bruker Optiks, equipped with a thermoelectrically cooled InGaAs detector. Each spectrum was the average of 32 scans measured over the spectral range from 12800 to 4000  $\text{cm}^{-1}$ , having a resolution of 4  $\text{cm}^{-1}$ . The measurements were performed in a temperature-controlled cell holder with a pathlength of 6 mm.

### 2.2. Samples and evaluated parameters

Four products, provided by industry, were studied: oleyl-cetyl alcohol polyethoxylated (OC-AEO, polyethoxylated mixture of both alcohols), cocamidopropyl betaine (CAPB), sodium lauryl sulfate (SLS) and nonylphenol polyethoxylated (NPEO). OC-AEO is a white solid, CAPB and SLS are manufactured as aqueous solutions while NPEO has a water content less than 30%. Table 1 summarizes the parameters habitually tested for each product as well as a brief description of the analysis method currently used. For each product, 30 samples were used as calibration set, every sample corresponding to a different production batch of the respective product, guaranteeing in this way the modelling of variations within samples due to the raw material and the process itself.

## 3. Results and discussion

### 3.1. Calibration for oleyl-cetyl alcohol polyethoxylated

Fig. 1 shows the average spectrum of OC-AEO. The feature around 8227  $\text{cm}^{-1}$  can be assigned to the CH symmetric stretching second overtone of CH<sub>2</sub>. The broad feature from 7400 to 6200  $\text{cm}^{-1}$  is due to the overlapping of the OH stretching first overtone, combination bands of CH vibrations of the CH<sub>2</sub> group and the first overtone of OH stretching modes of hydrogen bond. The strong band at 5782  $\text{cm}^{-1}$  is due to the CH antisymmetric stretching first overtone of CH<sub>2</sub>, which overlaps with the symmetric stretching mode. Bands at 5180 and 4880  $\text{cm}^{-1}$  can be assigned to the OH combination bands of water and

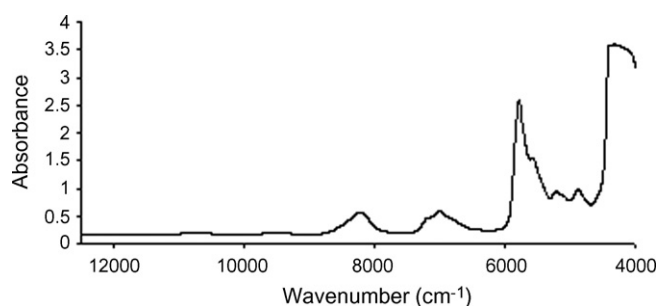


Fig. 1. Average absorbance spectrum of OC-AEO.

Table 2  
OC-AEO, parameters of hydroxyl number calibration

	Hydroxyl number
Spectral range	7500–5450 $\text{cm}^{-1}$
Signal processing	First derivative
Factors	9
RMSECV	$5.7 \times 10^{-3}$ mol/kg
Outliers	2

hydroxyl group, respectively. Finally, the intense feature beyond  $4600 \text{ cm}^{-1}$  is assigned to the overlapping of combination bands of  $\text{H}_2\text{O}$ ,  $\text{CH}_2$  and  $\text{CH}_3$ .

Table 2 shows the optimal parameters encountered for building the calibration model for hydroxyl number. Although near infrared spectroscopy has been studied for its application in this determination [7,8] in order to replace the annoying and time-consuming esterification-titration method, reports present the use of the bands around 7100 or  $4880 \text{ cm}^{-1}$ . In our case the spectral range selected covers the former feature as well as the CH first overtones of  $\text{CH}_2$ , since the hydroxyl number has a high correlation with the degree of ethoxylation and it improves the performance of the model, as Table 4 shows (repeatability CV of 0.88% and intermediate precision CV of 1.56%).

PLSR offers the opportunity to detect outlying calibration samples that can be damaging for the model, either because they are observations apart from the rest (high leverage values) or the instrumental data are poorly predicted (high spectral residuals). Samples with leverage significantly larger than the rest have a marked influence on the model and have to be examined. The practical limit is three times the mean leverage [9]. With respect to the spectral residuals, it is possible to recognize outliers by employing an  $F$ -test comparing the individual squared spectral residual with the mean of all others. An  $F$  ratio probability is calculated with the  $F$  values and 1,  $m-1$  degrees of freedom, having a limit of 0.99. Concentration outliers are detected in a similar manner, calculating the squared differences between the reference and the estimated concentrations. In our models, some of the discarded samples had extreme leverage values that, although being well predicted, are definitely far from the rest of the calibration samples and have been removed in order to have a well-spanned calibration set. Others are concentration outliers whose reference method is thought to be affected by some interferences caused by the storage time, especially the lauryl alcohol values in the CAPB solution. In the case of hydroxyl number there was also a spectral residual.

Reducing too much the size of the calibration set could affect its quality for predicting new concentrations. However, the size of calibration sets with the ranks used according to Tables 2, 5, 7 and 9 are well accepted for exploring the applicability of the developed multivariate calibrations models [6,9]. The factors respond not just to the variations of the measured constituents but also to chemical and physical interferences. In this sense, it is important to remark that the analysed commercial samples have a relatively high viscosity that varies from sample to sample and also causes the formation of tiny bubbles during homogenization and transfer to vials. These factors along

with the small variations in temperature have to be modelled. Moreover, many of the constituents are not the major ones in the samples, and their spectra, being very water-like, reflect just weak features due to the organic main constituents, which in turn are correlated with the minor compounds. In fact, water could be considered as a chemical interference, very strong in these cases. However, we can see that for calibrating solids content in CAPB and NPEO solutions the number of factors is smaller, as the reference method has to do precisely with the determination of water content turning it in some way into the target compound.

Table 3 shows the intercept and slope values of the regression of the results provided by the NIR method versus the results obtained with the reference one. The calibration model covers the hydroxyl number range of 0.6128–0.7059 mol KOH/kg.

In order to evaluate linearity, we have used the Durbin-Watson (DW) test at a significance level  $\alpha$  of 0.025, applied to the residuals from the linear regression between the estimated NIR values and the reference ones [10]. Null hypothesis is that they do not have serial correlation. The value of the DW statistic  $d$  is compared with upper ( $d_U$ ) and lower ( $d_L$ ) bounds and is expected to have the property  $d_L < d < 4 - d_L$  and  $d_U < d < 4 - d_U$  for not rejecting the null hypothesis at level  $2\alpha = 0.05$ . Results are indicated in Table 4.

Once linearity has been examined, bias is then tested via the elliptical joint confidence region (EJCR) for the true intercept ( $b_0$ ) and slope ( $b_1$ ) of the linear regression. In an ideal situation the intercept ( $b_0$ ) of the regression line should be 0 and the slope ( $b_1$ ) should be 1. The null hypothesis that  $b_0 = 0$  and  $b_1 = 1$  is tested by an  $F$ -test. If the  $F$  calculated has an associated significance level  $\alpha$  superior to 5% it can be concluded that the point (0,1) is inside the EJCR and that there is no evidence for constant and proportional systematic errors [11].

Accuracy is one of the most important parameters of a calibration model. One of the used criterion for evaluate this aspect is the RMSECV value, and we have added in the tables the relative error of prediction REP (%). Another method for testing accuracy has been the paired  $t$ -test between NIR and reference results of nine determinations of samples from different production batches. In the full cross validation each sample is treated as

Table 3  
Slope and intercept of the regression of NIR vs. reference values for the performed analyses

Product	Determination	NIR vs. reference values regression	
		$b_1$ (intercept)	$b_0$ (slope)
OC-AEO	Hydroxyl number	0.1451	0.9961
	CAPB content	0.2470	0.9921
CAPB solution	Solids	0.1935	0.9949
	Glycerol	0.0527	0.9805
	NaCl	0.0265	0.9948
SLS solution	SLS content	0.2970	0.9900
	Lauryl alcohol	0.0031	0.9931
	NaCl	0.0005	0.9976
	Sulfates	0.0050	0.9912
NPEO solution	Solids	0.3577	0.9950

Table 4  
OC-AEO, validation results

	Hydroxyl number
Linearity (DW test)	$d = 2.44$ $d_U = 1.37, d_L = 1.22$ $d_L < d < 4 - d_L, d_U < d < 4 - d_U$
Test of bias	94.3%
Accuracy	$\bar{d} = -0.172$ S.D. = 0.812 tcalc = 0.635 tcrit = 2.306
REP	0.89%
Repeatability	Mean: 36.75 S.D. = 0.323 CV = 0.88%
Intermediate precision	Mean: 37.1 S.D. = 0.578 CV = 1.56%

independent one time and allows to explore the performance of the model without wasting data for testing only. In our case every sample originates from different batches and were collected over a 1-year period so that the model is tested over the whole concentrations range and considers the possible variations within the production processes over time. Linearity is then evaluated between the predicted and actual concentrations, although it will be a good practice to examine the results over new samples as its availability is reached whereupon also another measure of accuracy (predicted *versus* actual values) would be possible.

Repeatability has been assessed analysing a single sample six times on the same day. Intermediate precision was evaluated by two different analysts measuring the hydroxyl number on 3 consecutive days. Samples are new, independent from the calibration set and from the one used for testing accuracy. Results of standard deviation (S.D.) and percent coefficient of variation (CV) for these analyses are listed in Table 4.

### 3.2. Calibration for cocamidopropyl betaine solution

This product has a typical composition of 40% of solids and 60% of water. Having the latter one of the most intense bands in the near infrared zone, the average spectrum showed in Fig. 2 becomes very water-like. Signal at  $10280 \text{ cm}^{-1}$  and the broad feature from  $9000$  to  $7800 \text{ cm}^{-1}$  are assigned to the OH second overtone and combination bands of water, respectively. The latter is here heavily overlapped with the CH stretching sec-

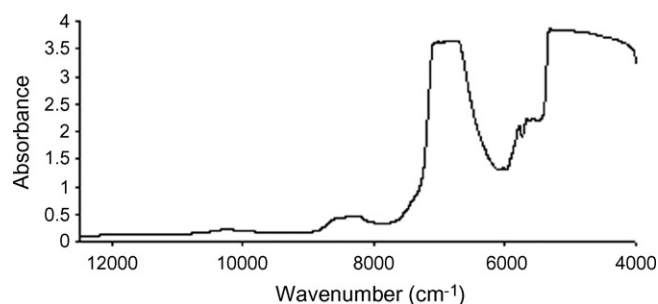


Fig. 2. Average absorbance spectrum of CAPB solution.

ond overtones of  $\text{CH}_2$  and  $\text{CH}_3$  groups. Water gives rise to two very strong signals at  $6897$  and  $5154 \text{ cm}^{-1}$ , due to the OH stretching first overtone and the OH stretching + OH bending mode, respectively. Nevertheless, the very broad features in the range of  $7800$ – $6100 \text{ cm}^{-1}$  and  $5400$ – $4000 \text{ cm}^{-1}$  are known to be caused by multiple overlapping bands of various modes of water (in this case another groups like  $\text{CH}_2$  and  $\text{CH}_3$  also take part), rather than the single ones mentioned. The weak shoulder around  $7430 \text{ cm}^{-1}$  is ascribed to the OH symmetric stretching + OH bending + rotational mode [7].

In the spectral range of  $6100$ – $5400 \text{ cm}^{-1}$  arise four weak signals. Features at  $5784$  and  $5673 \text{ cm}^{-1}$  are due to the  $\text{CH}_2$  group (CH antisym. stretching and CH symmetric stretching first overtone, respectively). Water gives rise to another feature at  $5564 \text{ cm}^{-1}$ , a combination band. Finally, the very weak feature at  $6019 \text{ cm}^{-1}$  is assigned to the betaine group.

### 3.3. CAPB content

Table 5 shows the parameters used for building the calibration models for each determination that CAPB solution requires. CAPB content is estimated using most of the variables present in the spectrum but the most intense water bands have been discarded for they present too high absorbance values, which are noisier and less reproducible. First derivative was performed along with vector normalization, which corrects multiplicative effects (probably small different sample thickness) just like other data pretreatment like minimum–maximum normalization or even multiplicative signal correction, MSC [6,7]. Model built with only first derivative gives an RMSECV slightly higher ( $8.47 \times 10^{-3} \text{ mol/kg}$ ).

Table 3 lists the correlation results between the NIR and reference values for the CAPB content as well as the other worked determinations. The calibration model covers a concentration

Table 5  
CAPB solution, parameters of the respective calibrations

	CAPB content	Solids	Glycerol	NaCl
Spectral range	$9626$ – $7498 \text{ cm}^{-1}$ , $6102$ – $5774 \text{ cm}^{-1}$	$11300$ – $7498 \text{ cm}^{-1}$	$11300$ – $7498 \text{ cm}^{-1}$	$11300$ – $7498 \text{ cm}^{-1}$
Signal processing	First derivative + VN	First derivative + MSC	Minimum–maximum normalization	Minimum–maximum normalization
Factors	9	6	9	9
RMSECV	$7.9 \times 10^{-3} \text{ mol/kg}$	0.327%	$7.2 \times 10^{-3} \text{ mol/kg}$	$8.7 \times 10^{-3} \text{ mol/kg}$
Outliers	2	2	2	0

VN, vector normalization; MSC, multiplicative signal correction.



Table 6  
CAPB solution, validation results

	CAPB content	Solids	Glycerol	NaCl
Linearity (DW test)				
$d$	1.68	1.70	2.22	1.74
$d_U$	1.37	1.37	1.37	1.38
$d_L$	1.22	1.22	1.22	1.25
	$d_L < d < 4 - d_L$		$d_U < d < 4 - d_U$	
Test of bias	90.8%	93.8%	75.4%	92.7%
Accuracy				
$\bar{d}$	0.270	-0.138	-0.040	0.002
S.D.	0.476	0.197	0.057	0.036
tcalc	1.702	2.101	2.105	0.185
tcrit	2.306	2.306	2.306	2.306
REP	0.92%	0.81%	2.28%	0.95%
Repeatability				
Mean	28.53	37.05	2.75	4.88
S.D.	0.118	0.059	0.025	0.010
CV	0.4%	0.16%	0.9%	0.2%
Intermediate precision				
Mean	28.21	36.85	2.91	5.16
S.D.	0.221	0.089	0.044	0.019
CV	0.78%	0.24%	1.5%	0.37%

range of 0.7927–0.9892 mol/kg (28.5–35.6%), and the validation results for this and the rest of NIR determinations for CAPB solution are listed in Table 6.

### 3.4. Solids

Results of water content determined by Karl–Fischer titration were subtracted from the unitary value to obtain the solids content values. In this case, the model has a better RMSECV using the OH second overtone of water and, compared with the CAPB content determination, discarding some features due to CH<sub>2</sub>, the weak ones between the two very broad signals due to water. The concentration range goes from 35.92 to 44.06%. It is necessary to mention that even though this and the two next determinations do not use the weak signals in the range of 6100–5400 cm<sup>-1</sup>, the CAPB content is primarily predicted by using those variables, as the predictor function in Fig. 3 shows. Therefore, a compromise between the signal intensities must be fulfilled: increasing the

pathlength increases the intensity of the feature due to the OH second overtone of water, which is used for predicting solids, glycerol and NaCl, but instead of improving the weak signals in the spectral range mentioned above, used for CAPB content prediction, a distortion due to water absorption occurs. Using a shorter pathlength vanishes those features as well as the signal of the water second overtone. The pathlength used allows a complete quality evaluation of the product in a single exposure, without affecting the method performance (see Table 6).

### 3.5. Glycerol and NaCl

Although glycerol is a compound whose NIR spectra could be readily correlated with concentration, its weight content in the CAPB solution is low (2–4%). For NaCl there are not even absorbance features that could be ascribed to it. However, these two compounds are known to have a stoichiometric-type relationship with the betaine, derived from the production process,

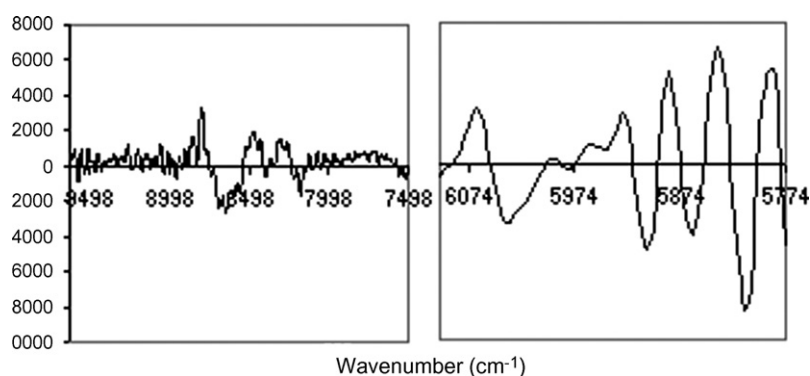


Fig. 3. Predictor function for CAPB content determination.

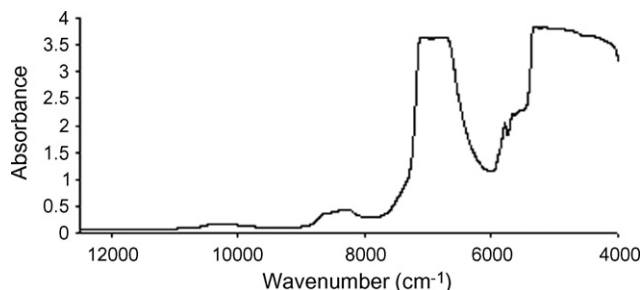


Fig. 4. Average absorbance spectrum of SLS solution.

which allows us to build their respective calibration model. Both determinations are better performed choosing a spectral range similar to that of solids content. The concentration range is 0.2696–0.3576 mol/kg for glycerol and 0.8085–1.0325 mol/kg for NaCl. Table 6 shows that the proposed method completely accomplishes the common confidence standards in precision tests (repeatability CV of 0.2% and intermediate precision CV of 0.37% for NaCl, for example) for these minor components. The relations of content between the main and low concentrated components vary between ranges that have been contemplated in the training set. Although the controlled production processes are not expected to provide abnormal samples that differ greatly from the ones in the calibration group, these could be easily identified by means of the chemometric tools like leverage and spectral residuals.

### 3.6. Calibration for sodium lauryl sulfate solution

As Fig. 4 illustrates, the spectrum of this product is also very water-like, although in comparison with the CAPB solution the betaine feature around 6019  $\text{cm}^{-1}$  does not appear.

### 3.7. SLS content

The parameters used in the calibration for SLS content as well as those for lauryl alcohol and NaCl are summarized in Table 7. The content of SLS is modelled using a combination of  $\text{CH}_2$  and water absorptions. Correlation results between NIR and reference analyses are shown in Table 3. SLS content ranges from 0.9212 to 1.1215 mol/kg (26.5–32.3%); validation results are listed in Table 8.

### 3.8. Lauryl alcohol, NaCl and sulfates content

These three components have typical weight concentrations less than 1% in the SLS solution. As we can see in Table 7 their content are predicted using most of the variables in the spectrum including the four weak ones between 6100 and 5400  $\text{cm}^{-1}$ . Establishing a proper calibration for them implies a necessary relationship of content with the major constituents of the product, otherwise a reliable calibration model would be very improbable. Validation results in Table 8 confirm that the model is not supported by a chance correlation but by a true causal connection between absorbance and concentration values, obtaining what could be named SLS-dependent mod-

Table 7  
SLS solution, parameters of the respective calibrations

	SLS content	Lauryl alcohol	NaCl	Sulfates
Spectral range	9414.6–7498 $\text{cm}^{-1}$ , 5778–5500 $\text{cm}^{-1}$	11200–7498 $\text{cm}^{-1}$ , 6102–5500 $\text{cm}^{-1}$	9400–7498 $\text{cm}^{-1}$ , 6102–5446 $\text{cm}^{-1}$	11200–7498 $\text{cm}^{-1}$ , 6102–5446 $\text{cm}^{-1}$
Signal processing	First derivative	Minimum–maximum normalization	MSC	First derivative
Factors	5	9	9	9
RMSECV	$5.7 \times 10^{-3}$ mol/kg	$3.8 \times 10^{-4}$ mol/kg	$3.6 \times 10^{-4}$ mol/kg	$6.1 \times 10^{-4}$ mol/kg
Outliers	1	3	2	2

Table 8  
SLS solution, validation results

	SLS content	Lauryl alcohol	NaCl	Sulfates
Linearity (DW test)				
$d$	2.18	1.82	1.93	1.93
$d_U$	1.38	1.36	1.37	1.37
$d_L$	1.24	1.21	1.22	1.22
	$d_L < d < 4 - d_L$		$d_U < d < 4 - d_U$	
Test of bias	85.3%	91.8%	97.3%	93.4%
Accuracy				
$\bar{d}$	0.310	0.012	0.001	0.004
S.D.	0.507	0.101	0.012	0.022
tcalc	1.834	0.356	0.272	0.549
tcrit	2.306	2.306	2.306	2.306
REP	0.54%	1.48%	0.97%	1.95%
Repeatability				
Mean	30.13	0.65	0.19	0.37
S.D.	0.038	0.0045	0.0016	0.0035
CV	0.12%	0.69%	0.84%	0.92%
Intermediate precision				
Mean	30.2	0.53	0.21	0.42
S.D.	0.069	0.006	0.003	0.006
CV	0.24%	1.15%	1.40%	1.52%

els. Concentration range is 0.0119–0.0395 mol/kg for the lauryl alcohol calibration model, 0.0263–0.0480 mol/kg for NaCl and 0.0220–0.0518 mol/kg for sulfates. These very low concentration components are primarily predicted using the weak CH<sub>2</sub> stretching overtones that appear in the spectrum, similarly to the case of CAPB content (Fig. 3). Then, a proper pathlength is again needed to get good signal intensities in all of the spectral ranges used for the four determinations. In order to save time and money it is important that the method is able to give the values of all the required parameters of a product without the necessity to change vials. The 6 mm pathlength was found suitable for this purpose. Again, accuracy and precision requirements are totally fulfilled (Table 8).

### 3.9. Calibration for nonylphenol polyethoxylated solution

Fig. 5 shows the average absorbance spectrum of the NPEO solution. The water content is lower than in the two previous cases but the strong signal between 5400 and 4700 cm<sup>-1</sup> and the feature around 6900 cm<sup>-1</sup> still appear. In addition to the features

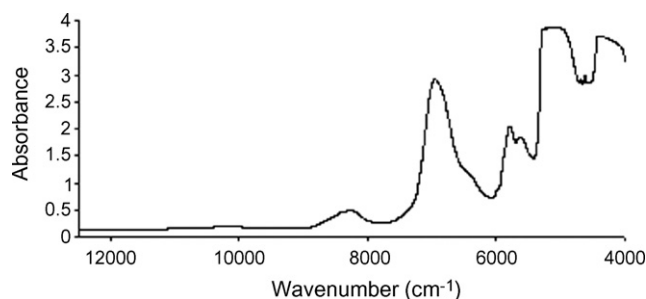


Fig. 5. Average absorbance spectrum of NPEO solution.

caused by overtones and combination bands of CH vibrations of CH<sub>3</sub> and CH<sub>2</sub> groups, the spectrum shows other weak features at 5990 and 4620 cm<sup>-1</sup>, that can be ascribed to aromatic CH bonds.

### 3.10. Solids content

Table 9 lists the parameters used in the calibration for solids content. Most of the variables are taking into account, except those with absorbance values greater than 3. The correlation results between NIR and reference method is shown in Table 3, and the validation results are listed in Table 10. Solids content ranges from 69.35 to 72.82%. We have endeavoured to have suitable concentration ranges by collecting appropriate samples in the stated period of time. The range of solids content as well as of the other determinations is subjected to be expanded as the production process makes the samples available, allowing in this way to get more robust models.

Obtained results express the feasibility of NIR spectroscopy for carrying out a total quality profile determination of the commercial surface-active products. It saves large amounts of time in the analysis of the studied surfactants. Running all the analytical procedures pointed in Table 1, for example, takes up to 3 h

Table 9  
NPEO solution, parameters of solids content calibration

	Solids content
Spectral range	11000–7498 cm <sup>-1</sup> , 6102–5450 cm <sup>-1</sup>
Signal processing	First derivative + normalization
Factors	6
RMSECV	0.094%
Outliers	1

Table 10  
NPEO solution, validation results

	Solids content
Linearity (DW test)	$d = 1.55$ $d_U = 1.38, d_L = 1.24$ $d_L < d < 4 - d_L, d_U < d < 4 - d_U$
Test of bias	95.1% $\bar{d} = 0.152$
Accuracy	S.D. = 0.199 $t_{calc} = 2.283$ $t_{crit} = 2.306$
REP	0.13%
Repeatability	Mean: 71.68 S.D. = 0.048 CV = 0.07%
Intermediate precision	Mean: 71.72 S.D. = 0.085 CV = 0.12%

for single determinations. This time is reduced to just 12 min, making duplicated analyses on the four samples. The analysis is non-destructive and does not require any complicated sample treatment.

#### 4. Conclusions

Multivariate calibration models developed with the use of Fourier-transform near infrared spectroscopy have shown good results in all of the determinations needed for the studied commercial surface-active products, which are some of the most important in the industry and whose quality control system needs to deal with very low concentration constituents. Obtaining a full quality profile for those materials of high water content in just

a single exposure is made possible with the use of a 6 mm path-length. Calibrations for minor components take advantage of the relationship of content between the constituents.

The calibration models fulfill the linearity requirement and no evidence for systematic errors was found. Moreover, results from the developed models are not significantly different from those provided by the reference methods and show good repeatability and intermediate precision. The former has a coefficient of variation less than 1% in all cases while the latter does not double repeatability. After further tests and the expansion of the calibration sets the NIR method could replace the reference ones and be used as a quality control tool that is much faster, does not require sample preparation and avoids the need for solvents and reagents.

#### References

- [1] T. Schmitt, *Analysis of Surfactants*, second ed., Marcel Dekker, New York, 2001, pp. 1–128, 293–335, 490–514.
- [2] AOCS, *Official Methods and Recommended Practices of the AOCS*, fifth ed., American Oil Chemists' Society, Champaign, Illinois, 1998.
- [3] D.O. Hummel, *Handbook of Surfactant Analysis*, second ed., Wiley, New York, 2000, pp. 171–237.
- [4] P.L. Walling, J.M. Dabney, *J. Soc. Cosmet. Chem.* 37 (1986) 445.
- [5] D.M. Haaland, E. Thomas, *Anal. Chem.* 60 (1988) 1193.
- [6] H. Martens, T. Næs, *Multivariate Calibration*, Wiley, New York, 1989, pp. 116–125, 254–296.
- [7] H.W. Siesler, Y. Ozaki, S. Kawata, H.M. Heise, *Near-Infrared Spectroscopy*, Wiley-VCH, Weinheim, 2002, pp. 179–182, 216–222.
- [8] C.L. Hilton, *Anal. Chem.* 31 (1959) 1610.
- [9] K.R. Beebe, R.J. Pell, M.B. Seasholtz, *Chemometrics: A Practical Guide*, Wiley, New York, 1998, pp. 278–337.
- [10] N. Draper, H. Smith, *Applied Regression Analysis*, third ed., Wiley, New York, 1998, pp. 179–193.
- [11] D.L. Massart, B.G.M. Vandeginste, L.M.C. Buydens, S. de Jong, P.J. Lewi, J. Smeyers-Verbeke, *Handbook of Chemometrics and Qualimetrics (part A)*, Elsevier, Amsterdam, 1997, pp. 189–194.

# Study of the phenolic composition of spanish and italian monocultivar extra virgin olive oils: Distribution of lignans, secoiridoidic, simple phenols and flavonoids

Maria Jesus Oliveras-López<sup>a</sup>, Marzia Innocenti<sup>b</sup>, Catia Giaccherini<sup>b</sup>,  
Francesca Ieri<sup>b</sup>, Annalisa Romani<sup>b</sup>, Nadia Mulinacci<sup>b,\*</sup>

<sup>a</sup> Department of Nutrition and Food Science, University of Granada, Campus Universitario de Cartuja – 18071 Granada, Spain

<sup>b</sup> Department of Pharmaceutical Science, University of Florence, Via Ugo Schiff 6, 50019, Sesto F. no (Firenze), Italy

Received 20 December 2006; received in revised form 11 April 2007; accepted 30 April 2007

Available online 10 May 2007

## Abstract

The aim of the present study was to compare the phenolic content in selected monocultivar extra virgin olive oils. Analyses were carried out by HPLC/DAD/MS on Picual, Picuda, Arbequina and Hojiblanca oils from Spain and Seggianese and Taggiasca oils from Italy. Oils from cultivar Picual showed similar characteristics to those of Seggianese oils, with total amounts of secoiridoids of 498.7 and 619.2 mg/L, respectively. The phenolic composition of Arbequina oils is close to that of the Taggiasca variety with lignans among the main compounds. The determination of free and linked OH–Tyr, by way of an acid hydrolysis, represents a rapid and suitable method, especially when standards are not available, to determine antioxidant potentialities in terms of MPC, particularly for fresh extra virgin olive oils rich in secoiridoidic derivatives.

© 2007 Elsevier B.V. All rights reserved.

**Keywords:** Extra virgin olive oil; Secoiridoids; Minor polar compounds; Picual; Taggiasca; HPLC/DAD/ESI/MS

## 1. Introduction

Extra virgin olive oil is becoming increasingly more relevant in the diet of several countries due to its beneficial effects on human health. Some of these effects are associated with extra virgin olive oil's content of phenolic compounds and a high amount of oleic acid and tocopherols [1–5]. The amount and composition of phenolic compounds in virgin olive oil depends on several factors such as olive cultivar [6], degree of maturation and agronomic and technological aspects of production [6–8]. Phenolic compound content is an important parameter for the evaluation of virgin olive oil quality as phenols largely contribute to oil flavour and taste [9] as long as it is protected from auto-oxidation [8,10–13]. Virgin olive oil contains a large number of phenolic compounds including phenyl alcohols, such as tyrosol

(Tyr) and hydroxytyrosol (OH–Tyr), phenolic acids, flavonoids, like luteolin and apigenin [6,14,15], as well as other more complex secoiridoid derivatives from oleuropein and ligstroside [10,16]. Since 2000, the presence of lignans in the phenolic fraction, with (+)-pinoselinol and (+)-1-acetoxypinoselinol as major components, has been described in some olive oils [17–19].

The application of techniques such as HPLC–DAD and HPLC–MS has made it possible to recognize novel bioactive molecules from extra virgin olive oil and to better compare the phenolic profiles in order to explain biological activities of olive oil. Among phenols from olive fruit and virgin olive oil a special significance has been revealed for those with the *o*-diphenolic group, mainly OH–Tyr and oleuropein derivatives, which have shown antiatherogenic effects [4,20] and an antioxidant capacity higher than that of other known antioxidants such as Vitamins E and C [21–23].

In the present work, the phenolic fraction of eleven Spanish and Italian monocultivar extra virgin olive oils has been characterized, with the qualitative and quantitative contents of minor polar compounds (MPC) evaluated and compared.

*Abbreviations:* MPC, minor polar compounds; EVOOS, extra virgin olive oils; OH-tyrhydroxytyrosol; Tyr; tyrosol; 3,4 DHPE-EDA, deacetoxyoleuropein aglycone; 3,4 DHPE-EA, oleuropein aglycone; EA, elenolic acid

\* Corresponding author.

E-mail address: [nadia.mulinacci@unifi.it](mailto:nadia.mulinacci@unifi.it) (N. Mulinacci).

The total amounts of OH-Tyr and Tyr, including their bound forms, were evaluated after a quantitative chemical hydrolysis.

Although the antioxidant content of virgin olive oil is actually widely researched, it is necessary to compare in detail the phenolic profile of diverse monocultivar oils to better correlate their differences among in vitro and in vivo effects.

## 2. Experimental

### 2.1. Olive oil samples

Samples deriving from several cultivars and obtained by traditional and an innovative milling dual-phase system were analyzed.

#### 2.1.1. Picual

Samples of oils from the Andalucía region (Spain) were classified as Pa, Pb, Pc, Pd, Pa-04 (Table 1). Four of these olive oils were harvested in November 2003 (Pa, Pb, Pc, Pd), whereas one of them was a fresh oil (Pa-04); all the Picual oils were from the north of Granada. Samples Pc and Pd came from the same farm and Pa and Pb were purchased from the market. Pd was obtained from an experimental mill characterised by the use of roller blades, a system (Lacerator) which does not involve the complete crushing of olive stones.

#### 2.1.2. Other Spanish cultivars

Pda, Hj, Ab were commercial extra virgin olive oils from Picuda, Hojiblanca and Arbequina varieties respectively obtained from fruits harvested in November 2003. The Hojiblanca and Arbequina oils were from the area near Malaga, the Picuda oil was from the north of Granada, all these products were obtained by dual system milling processes.

#### 2.1.3. Italian olive oils

Two Taggiasca olive oil samples were from Liguria: the fruits were harvested in december 2003 (Tg) and december 2004 (Tg-04). The Seggianese oil (Sg-04) was obtained from fruits harvested in Tuscany near Grosseto, and milled in the first two weeks of November 2004.

## 2.2. Sample preparation

### 2.2.1. Liquid-liquid extraction

A volume of 20 mL of each oil sample was extracted with 60 mL of EtOH/H<sub>2</sub>O 70:30 v/v; the water was acidified by formic acid (pH=2.5). Defatting with *n*-hexane (20 mL × 3) was performed to completely remove the lipid fraction. The raw alcoholic extract of each sample was dried under vacuum (28 °C) and redissolved in 2 mL of the extraction mixture (MPC extract) and then analysed by HPLC/DAD and HPLC/MS.

### 2.2.2. Acid hydrolysis

This type of hydrolysis was carried out according to a previous paper [24]. Samples of 200 µL were drawn from the MPC

Table 1  
Picual olive oil samples analyzed in our study and milling processes applied

	Samples			
	Pa	Pb	Pc	Pd
Origin area	D.O. Sierra de Segura Orcera (Jaén)	D.O. Montes de Granada Iznalloz (Granada)	D.O. Montes de Granada Iznalloz (Granada)	D.O. Montes de Granada Iznalloz (Granada)
Milling date	1–15 November 2003	15–30 November 2003	15–30 November 2003	15–30 November 2003
Type of mill	Alfa-Laval 750,000 kg/h Continuous dual-phase system	Pieralisi 700,000 kg/h Continuous dual-phase system	Pieralisi 700,000 kg/h Continuous dual-phase system	Lacerator 700,000 kg/h Experimental model based on rollers
Milling temperature	18–22 °C	<28 °C	<28 °C	<28 °C
Type of conservation	Bottled under N <sub>2</sub> atmosphere Stored at 4 °C in darkness	Stored at 4 °C in darkness	Stored at 4 °C in darkness	Stored at 4 °C in darkness
Water addition	0–10% volume (depends on olive paste humidity)	0–10% volume (depends on olive paste humidity)	0–10% volume (depends on olive paste humidity)	No
Filter	3 days of decanting and filtered after	Filter	Decanting. Filter no.	Decanting; filter no.
Olive quantity	2000 kg/h	3000 kg/h	3000 kg/h	3000 kg/h
				Pa-04
				D.O. Sierra de Segura Orcera (Jaén)
				1–15 November 2004
				Alfa-Laval 750,000 kg/h
				Continuous dual-phase system
				18–22 °C
				Bottled under N <sub>2</sub> atmosphere
				Stored at 4 °C in darkness
				0–10% volume (depends on olive paste humidity)
				3 days of decanting and filtered after
				2000 kg/h

extract and added with 200  $\mu\text{L}$  of  $\text{H}_2\text{SO}_4$  2 N. The samples were maintained in an oven for 2 h at 80  $^\circ\text{C}$ , then diluted with 200  $\mu\text{L}$  of ethanol to clarify the sample. The final solution (600  $\mu\text{L}$ ) was filtered by a syringe on a 0.45  $\mu\text{m}$  regenerated cellulose filter before the HPLC/DAD/MS analysis.

### 2.2.3. Basic hydrolysis

Samples of 300  $\mu\text{L}$  were drawn from the MPC extract and added to 300  $\mu\text{L}$  of KOH 5.0 N in MeOH. The samples remained at 37  $^\circ\text{C}$  for 3 h and then were acidified with 140  $\mu\text{L}$  of HCl

10 N and added with 160  $\mu\text{L}$  of ethanol to obtain a solution to be directly analyzed by HPLC/DAD/MS [16].

### 2.3. HPLC/DAD/MS analysis

All reagents used were of analytical grade. Phenolic compounds were identified by comparison with pure standards, UV spectra, relative  $t_R$  and mass spectra in API/ES.

Analysis of the MPC extract was performed on an Agilent 1100 liquid chromatograph equipped with a 1100 autosampler,

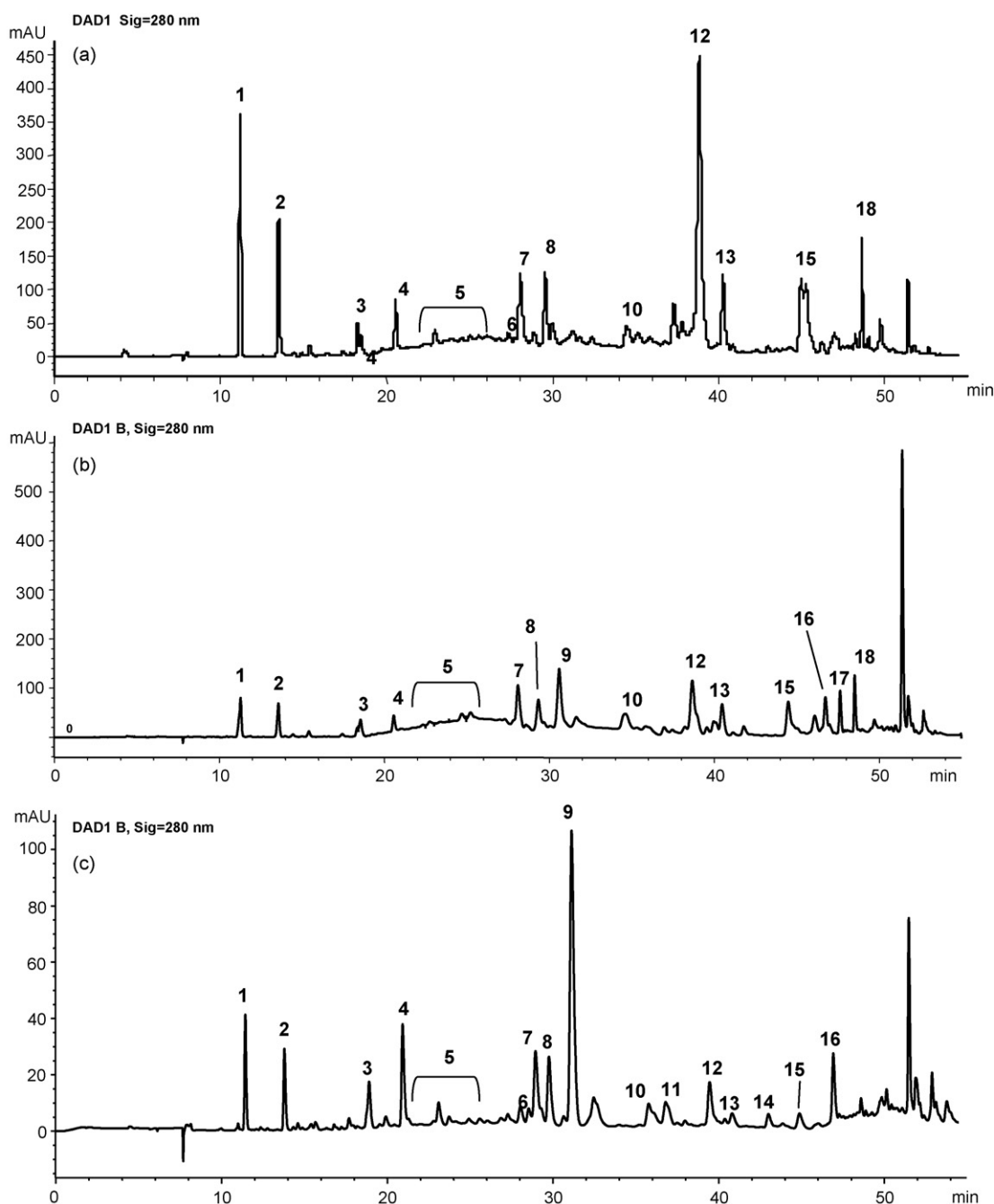


Fig. 1. HPLC–DAD profiles at 280 nm, obtained from Pa (a), Sg (b) and Ab (c) extra virgin olive oil extracts. Compounds: 1, OH–Tyr; 2, Tyr; 3, Tyr derivatives; 4, 5, 7, 11, 13–18, secoiridoidic derivatives; 6, luteolin; 8, pinoresinol; 9, acetoxypinoresinol; 10, impure apigenin; 12, 3,4-DHPE-EA.

column heater module, binary pump and DAD; the MS detector was a HP 1100 MSD API-electrospray, all from Agilent Tech. (Palo Alto, AC, USA). The Luna RP18 (Phenomenex-Torrance CA) column, 250 mm × 4.6 mm (5 μm), was used to quantify all the phenolics, with the exception of deacetoxyoleuropein aglycon (3,4 DHPE-EDA) and elenolic acid (EA). These latter compounds were quantified by the use of a LiChrosorb RP18 (Merk Hibar) column, 250 mm × 4.6 mm (5 μm), according to Mulinacci et al. [16]. For both the columns the eluents were H<sub>2</sub>O at pH 3.2 by formic acid (A) and acetonitrile (B). The analyses carried out on the Luna column were executed applying a multistep linear solvent gradient as follow: from A 100% to A 85% in 5 min; 10 min to A 70% then a plateau of 5 min to A 65% in 5 min and a plateau of the same time; 7 min to A 55% and a plateau for 5 min to B 100% within 5 min, and a final plateau of 3 min. Total time of analysis 50 min, equilibration time 20 min, oven temperature 26 °C; flow rate 0.8 mL min<sup>-1</sup>.

The operative conditions of the MS detector were capillary voltage from 3000 to 3500 V, working in negative and positive ionization, with a variable fragmentor (80–200 V).

#### 2.4. Quantitative evaluation

The quantitative evaluation of individual phenols was performed using four-point regression curves ( $r^2 = 0.999$ ) through the use of authentic standards. Oleuropein was purchased from Extrasynthese (Geney, France), Tyr was from Sigma-Aldrich (St. Louis, MO, USA) and OH-Tyr was purchased from Cayman Chemical (SPI-BIO, Europe). The Tyr and OH-Tyr amounts were calculated at 280 nm using Tyr as reference. The aldehydic form of elenolic acid (EA) linked to OH-Tyr (3,4-DHPE-EDA) and the other secoiridoids were calculated at 280 nm, using oleuropein as standard. The EA was evaluated at 240 nm, using oleuropein as standard. For 3,4-DHPEA-EDA and EA the following correction factors of the molecular weight (MW) were applied respectively: 320/540 and 242/540 (540 = MW of oleuropein). Luteolin and apigenin, usually present in the extra-virgin olive oil in a very low amount (less than 2–3% of the total MPC [16]), were evaluated measuring their absorbance at 350 nm. The total flavonoidic content was determined by the sum

of apigenin and luteolin calculated using luteolin as external standard at the same wavelength, without applying correction factors of the molecular weight.

### 3. Results and discussion

The main findings from this research evidenced interesting differences with regard to the MPC content among these eleven monocultivar extra virgin olive oils. Fig. 1 shows some representative HPLC/DAD profiles at 280 nm, obtained for the MPC extracts from Pa (a), Sg (b) and Ab (c) EVOOs. The HPLC profiles of the MPC fractions were similar and sometimes overlapped for the Pc and Pd samples and for Hj and Ab, while the quantitative amounts presented notable variations. Table 2 reports the content of phenolic compounds present in the MPC fraction of the analyzed Spanish and Italian monocultivar virgin oils. The data are expressed in mg/L of oil and represent mean ± S.D. of three different extracts.

For the Picual cultivar, the studied oils have specific profiles and a total of 45 compounds were detected and quantified; most of them were recognized as secoiridoidic derivatives, others as lignans, flavonoids and simple phenols. The differences among the selected Picual oils can be mainly related to the production area ripening degree and the milling process according to previous data relating to other cultivars [7,25,26]. According to previous results [27], the oleuropein aglycone (3,4-DHPEA-EA) (Rt 38.8 min) was the main secoiridoidic compound found in all the analyzed Picual oils. The UV spectrum was similar to that of oleuropein, with  $\lambda_{\text{max}}$  at 235 and 280 nm and its MS spectrum in negative ionization mode (Fig. 2), according to previous data [28], exhibited the presence of OH-Tyr group. This compound was detected in all the analysed oils, although in Ab in a very low amount.

The secoiridoidic derivatives of oleuropein and ligstroside are often the main phenolic compounds in fresh olive oils [6,15–17]. As expected, the fresh oils Sg-04 and Pa-04 showed the highest values of secoiridoids, up to 85 and 92% of total MPC, respectively (Fig. 3). Moreover, it is known that olive oils with a high content of secoiridoid derivatives with phenolic group show a higher stability [16,17]. In this way, Sg-04 and Pb oils presented

Table 2  
Phenolic compounds concentrations (mg/L) in different Spanish and Italian monocultivar extra virgin olive oil<sup>a</sup>

	OH-Tyr	Tyr	Total secoir <sup>b</sup>	EA	Flavonoidic compounds	Pinoresinol	Acetoxypinoresinol
Pa	17 ± 2	10 ± 1	357 ± 44	67 ± 14	2.4 ± 0.3	23.2 ± 1.2	n.d. <sup>c</sup>
Pb	23 ± 8	11 ± 3	401 ± 31	113 ± 24	0.76 ± 0.1	10.9 ± 0.2	n.d.
Pc	3.8 ± 0.4	22 ± 1	123 ± 15	25 ± 2	1.6 ± 0.6	n.d.	n.d.
Pd	22 ± 2	55 ± 4	133 ± 2	115 ± 23	1.26 ± 0.03	n.d.	n.d.
Pda	2.9 ± 0.1	2.8 ± 0.1	79 ± 1	17.4 ± 0.1	1.54 ± 0.03	5.3 ± 0.3	11 ± 0
Hj	4.6 ± 0.2	2.9 ± 0.0	133 ± 4	41 ± 1	1.43 ± 0.01	12 ± 0	26 ± 0
Ab	2.3 ± 0.3	1.8 ± 0.2	61 ± 9	11 ± 2	1.1 ± 0.1	12 ± 1	77 ± 5
Tg	8.1 ± 0.7	14 ± 1	119 ± 5	22 ± 8	2.3 ± 0.2	7.5 ± 0.3	48 ± 0
Pa-04	1.7 ± 0.1	3.3 ± 0.1	499 ± 4	18 ± 1	2.4 ± 0.1	14 ± 2	8.4 ± 0.6
Tg-04	0.6 ± 0.1	1.9 ± 0.2	171 ± 3.3	47 ± 2.9	1.5 ± 0.1	8.2 ± 0.2	160 ± 3
Sg-04	5.5 ± 0.1	4.6 ± 0.1	619 ± 128	37 ± 25	2.4 ± 0.3	30 ± 1	40 ± 1

<sup>a</sup> Means ± S.D. of three determinations.

<sup>b</sup> With phenolic group (calculated at 280 nm).

<sup>c</sup> n.d. = not detected.



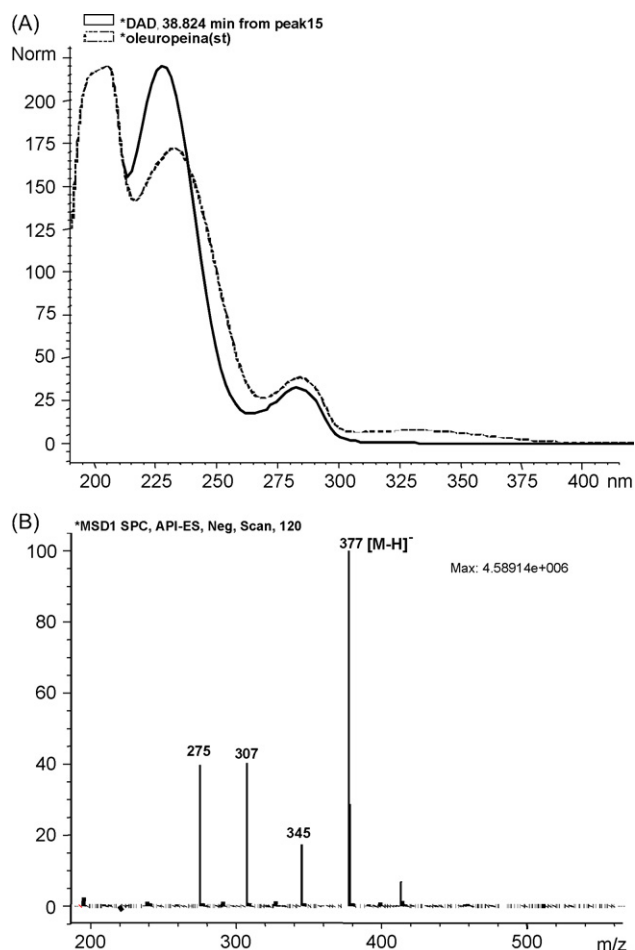


Fig. 2. UV-vis (A) and MS (B) spectra of the oleuropein aglycone with  $t_r$  38.8 min (compound 12).

the highest percentage of 3,4-DHPE-EDA, respect to total secoiridoids, instead, it was not present in Pc, Pd, Pda samples (Fig. 4).

The other major phenols identified in these extra virgin olive oils were lignans, compounds highlighted for the first time in EVOOs in 2000 [17,18]. Their UV-vis spectra are very similar to those of the secoiridoidic compounds, making therefore very difficult their discrimination. Consequently, a quantitative basic hydrolysis, according to a previous proposed method [24],

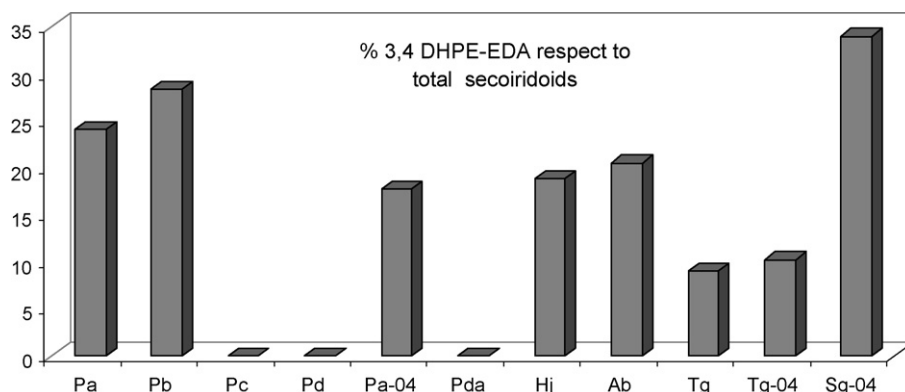


Fig. 4. Percentage of 3,4-DHPE-EDA respect to total secoiridoids in all the studied oils. The results are an average of three different determination.

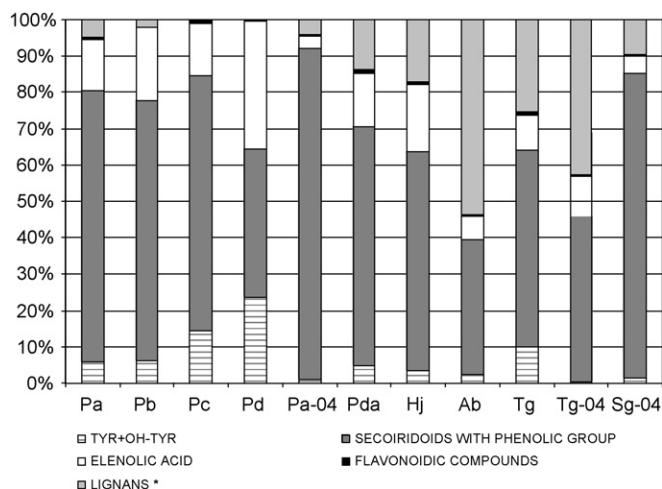


Fig. 3. MPC content expressed as percentage  $\Sigma$  of five different chemical classes: Tyr+OH-Tyr (dark-grey); flavonoidic compounds (black); EA (white); secoiridoidic molecules (hatching); \*pinosresinol and acetoxypinosresinol (grey).

was also applied to better estimate the lignan content in the analysed oils. The pinosresinol was found at low concentrations with respect to the total phenols (2–5%) and was not detected in two of the tested Picual oils (Pc and Pd) together with the acetoxypinosresinol. From our data all the “non Picual” oils analyzed contained lignans, which were found in considerable quantities in Ab, Tg-04 and Tg. Acetoxypinosresinol was the main compound in Taggiasca and Arbequina varieties, in contrast with the Picual cultivar. Our results (Fig. 3 and Table 2) clearly illustrate that oils containing higher amounts of lignans, generally, show lower levels of secoiridoids, especially of oleuropein aglycone. The main simple phenols found in Picual monocultivar virgin olive oil are Tyr and OH-Tyr, ranging between 5 and 23% and with regard to the flavonoidic compounds the quantity of luteolin was always higher than apigenin, found in traces. The total amounts in Picual oils range between 2.4 and 0.76 mg/L, and reach 2.4 mg/L for Sg-04. These results confirm this chemical class as a minor constituent of the MPC fraction, as previously described for other extra virgin olive oils [6,16,27].

As reported in Fig. 5, the total content of MPC from the 2004 crop season EVOOs showed the highest levels, as they were

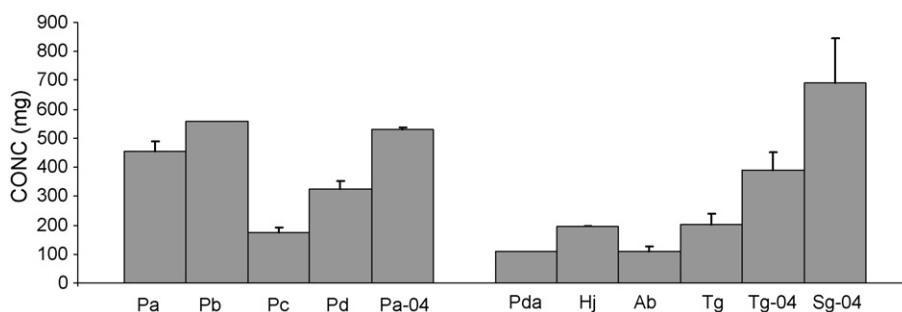


Fig. 5. A comparison of the total MPC content (mg/L) determined for all the analysed oils. The data are an average of three different determination.

Table 3

Quantitative data expressed in mg/L of OH-Tyr and Tyr after acid hydrolysis in all the considered oils

	mg/L <sup>a</sup> ± S.D.										
	Pa	Pb	Pc	Pd	Pda	Hj	Ab	Tg	Pa-04	Tg-04	Sg-04
OH-Tyr after A.H.	226 ± 17	289 ± 67	54 ± 10	64 ± 18	47 ± 0	77 ± 5	42 ± 1	46 ± 10	139 ± 11	11 ± 1	161 ± 4
Tyr after A.H.	109 ± 10	149 ± 18	78 ± 20	100 ± 28	48 ± 0	46 ± 2	24 ± 0	85 ± 20	82 ± 7	34 ± 1	97 ± 3
OH-Tyr/Tyr	2.1	1.9	0.7	0.6	1.0	1.7	1.7	0.6	1.7	0.3	1.7

<sup>a</sup> Data are means ± S.D. of three determinations.

fresh oils rather than one-year-old olive oils. Among these the highest contents were related to Pb, Pa-04 and Sg-04.

It has been suggested that the phenolic profile could be used to classify virgin olive oils according to their fruit variety. The feasibility of cultivar classification from the HPLC phenolic compound profile, in particular for Arbequina, Hojiblanca and Picual varieties, is clear for some authors [25,27,29]. In fact, according to these authors, the phenolic profile of Picual virgin olive oils is midway between those of Cornicabra and Hojiblanca (similar to Arbequina); Picual and Cornicabra are the two Spanish varieties richest in phenolic compounds. Relating to the Tuscany cultivar it can be said that the Sg-04 fresh oil presented the highest level of total MPC among all the considered varieties (Table 2 and Fig. 5) in agreement with our recently published results related to EVOOs obtained from the same cv [30].

### 3.1. Total content of OH-Tyr

The acidic hydrolysis treatment has been proposed as a quantitative method for the identification of the real OH-Tyr/Tyr ratio [24], including both the free forms and those linked to the secoiridoidic nucleus. In fact, spiking tests previously carried out adding oleuropein to MPC fractions of commercial oils, showed % recoveries of OH-Tyr from 97 to 103% [24]. This hydrolysis can also be applied to evaluate the antioxidant capacity in terms of *ortho*-diphenols and to collect useful information to forecast an oil's resistance to ageing. The wide number of secoiridoidic derivatives present in highly variable concentrations in the MPC fraction makes it difficult to identify and to select all the structures with a catecolic nucleus. Moreover, the determination of the secoiridoidic molecules in the MPC extracts can be complicated by the fact that these compounds are not

commercially available as pure standards. The only exception being oleuropein, the bitter glycoside of the fruit, which is almost completely transformed during milling processes and therefore present only in trace amounts in extra virgin olive oil [25]. It is important to discriminate between molecules having the Tyr and those with the OH-Tyr group, as free OH-Tyr is biologically more interesting mainly for its antioxidant capacity, as widely reported [1,2,4].

The data from the complete quantitative hydrolysis of secoiridoid derivatives are reported in Table 3. The highest concentrations of OH-Tyr were found in Picual oils, Pa and Pb and the considerable prevalence of OH-Tyr compared to Tyr should be pointed out. The ripening degree and the applied technology (Table 1) not only influenced the total amount of phenols in the oils, as previously reported [26], but it also modified the relative concentration of the different secoiridoids.

## 4. Conclusions

An in-depth quali-quantitative study of the phenolic compounds can be employed, together with other parameters, to classify Spanish and Italian oils in accordance with their cultivar and milling processes. Oils from cultivar Picual showed similar characteristics to those of Seggianese oils, while the phenolic composition of Arbequina oils is close to that of the Taggiasca variety. The results obtained from this study highlight that Picual and Seggianese EVOOs show higher amounts of total OH-Tyr than Arbequina, Picuda, and Taggiasca cultivars.

The determination of free and linked OH-Tyr, through the use of an acid hydrolysis, represents a rapid and suitable method to determine antioxidant potentialities in terms of MPC, particularly for fresh extra virgin olive oils rich in secoiridoidic derivatives.

## Acknowledgements

This work was partially supported by the Italian M.I.U.R. (Ministero Istruzione Università e Ricerca). We are also grateful to Ente Cassa di Risparmio di Firenze for supplying a part of the instrumentation used for this research.

## References

- [1] R.W. Owen, A. Giacosa, W.E. Hull, B. Haubner, B. Spiegelhalder, H. Bartsch, *Eur. J. Cancer* 36 (2000) 1235.
- [2] R.W. Owen, W. Mier, A. Giacosa, W.E. Hull, B. Spiegelhalder, H. Bartsch, *Food Chem. Toxicol.* 38 (2000) 647.
- [3] F. Visioli, C. Galli, F. Bornet, A. Mattei, R. Patelli, G. Galli, D. Caruso, *FEBS* 468 (2000) 159.
- [4] F. Visioli, C. Galli, *Crit. Rev. Food Sci. Nutr.* 42 (2002) 209.
- [5] E. Miró-Casas, M.I. Covas Planells, M. Fitó Colomer, M. Farré-Albadalejo, J. Marrugat, M.C. De la Torre, *Eur. J. Clin. Nutr.* 57 (2003) 186.
- [6] P. Pinelli, C. Galardi, N. Mulinacci, F.F. Vincieri, A. Cimato, A. Romani, *Food Chem.* 80 (2003) 331.
- [7] E. Gimeno, M.E. Fitó, R.M. Lamuela-Raventós, A.I. Castellote, M. Covas, M. Farre, M.C. De la Torre Boronat, M.C. López-Sabater, *Eur. J. Clin. Nutr.* 56 (2002) 114.
- [8] A. Van der Sluis, M. Dekker, N. Van Boekel, *J. Agric. Food Chem.* 53 (2005) 1073.
- [9] F. Gutiérrez-Rosales, J.J. Ríos, L. Gómez-Rey, *J. Agric. Food Chem.* 51 (2003) 6021.
- [10] M. Servili, G.F. Montedoro, *Eur. J. Lipid Sci. Technol.* 104 (2002) 602.
- [11] J. Velasco, C. Dobarganes, *Eur. J. Lipid Sci. Technol.* 104 (2002) 661.
- [12] J.R. Morelló, S. Vuorela, M.P. Romero, M.J. Motilva, M. Heinonen, *J. Agric. Food Chem.* 53 (2005) 2002.
- [13] R. Mateos, M. Trujillo, C. Pérez-Camino, W. Moreda, A. Cert, *J. Agric. Food Chem.* 53 (2005) 5766.
- [14] F. Pirisi, F.P. Cabras, C. Falqui, M. Migliorini, M. Muggelli, *J. Agric. Food Chem.* 48 (2000) 1191.
- [15] A. Romani, P. Pinelli, N. Mulinacci, C. Galardi, F.F. Vincieri, L. Liberatore, A. Cichelli, *Chromatographia* 53 (2001) 279.
- [16] N. Mulinacci, C. Giaccherini, M. Innocenti, A. Romani, F.F. Vincieri, F. Marotta, A. Mattei, *J. Sci. Food Agric.* 85 (2005) 662.
- [17] M. Brenes, F.J. Hidalgo, A. García, J.J. Ríos, P. García, R. Zamora, A. Garrido, *J. Am. Oil Chem. Soc.* 77 (2000) 715.
- [18] R.W. Owen, W. Mier, A. Giacosa, W.E. Hull, B. Spiegelhalder, H. Bartsch, *Clin. Chem.* 46 (2000) 976.
- [19] R. Mateos, J.L. Espartero, M. Trujillo, J.J. Ríos, M. León-Camacho, F. Alcudia, *A. Cert, J. Agric. Food Chem.* 49 (2001) 2185.
- [20] E.A. Miles, P. Zoubouli, P.C. Calder, D. Phil, *Nutrition* 21 (2005) 389.
- [21] R. Mateos, M.M. Domínguez, J.L. Espartero, A. Cert, *J. Agric. Food Chem.* 51 (2003) 7170.
- [22] M. Bouaziz, R.J. Grayer, M. Simmonds, M. Damak, S. Sayadi, *J. Agric. Food Chem.* 53 (2005) 236.
- [23] F. Paiva-Martins, M.H. Gordon, *J. Agric. Food Chem.* 53 (2005) 2704.
- [24] N. Mulinacci, C. Giaccherini, F. Ieri, A. Romani, F.F. Vincieri, *J. Sci. Food Agric.* 86 (2006) 757.
- [25] M.D. Salvador, F. Aranda, S. Gómez-Alonso, G. Fregapane, *Food Chem.* 80 (2003) 359.
- [26] M. Servili, R. Selvaggini, S. Esposito, A. Taticchi, G.F. Montedoro, G. Morozzi, *J. Chromatogr. A* 1054 (2004) 113.
- [27] A. García, M. Brenes, C. Romero, P. García, A. Garrido, *Eur. Food Res. Technol.* 215 (2002) 407.
- [28] D. Caruso, R. Colombo, R. Patelli, F. Giavarini, G. Galli, *J. Agric. Food Chem.* 48 (2000) 1182.
- [29] S. Gómez-Alonso, M.D. Salvador, G. Fregapane, *J. Agric. Food Chem.* 50 (2002) 6812.
- [30] F. Franconi, R. Coinu, S. Carta, P. Urgeghei, F. Ieri, N. Mulinacci, A.L. Romani, *J. Agric. Food Chem.* 54 (2006) 3121.

# A novel amperometric sensor for the detection of difenidol hydrochloride based on the modification of $\text{Ru}(\text{bpy})_3^{2+}$ on a glassy carbon electrode

Wen Pan, Xiaoli Chen, Manli Guo, Yan Huang, Shouzhuo Yao\*

*College of Chemistry & Chemical Engineering, Hunan University, Changsha, China*

Received 14 November 2006; received in revised form 13 April 2007; accepted 18 April 2007

Available online 27 April 2007

## Abstract

An amperometric sensor for the detection of difenidol, a tertiary amine-containing analyte, was proposed. Ruthenium(II) tris(bipyridine)/multi-walled carbon nanotubes/Nafion composite film was suggested to modify the glassy carbon electrode. The modified electrode was shown to be an excellent amperometric sensor for the detection of difenidol hydrochloride. The linear range is from  $1.0 \times 10^{-6}$  to  $3.3 \times 10^{-5}$  M with a correlation coefficient of 0.998. The limit of detection was  $5 \times 10^{-7}$  M, which was obtained through experimental determination based on a signal-to-noise ratio of three. The sensor was employed to the determination of the active ingredients in the tablets containing difenidol hydrochloride.

© 2007 Published by Elsevier B.V.

*Keywords:* Amperometric detection; Carbon nanotube;  $\text{Ru}(\text{bpy})_3^{2+}$ ; Difenidol hydrochloride

## 1. Introduction

In recent years, many approaches [1–8] have been presented to immobilize  $\text{Ru}(\text{bpy})_3^{2+}$  and its derivatives on various electrode surfaces as a way to develop cost-effective, regenerable chemical and biosensors. Electrogenerated chemiluminescence (ECL) from  $\text{Ru}(\text{bpy})_3^{2+}$  ion-exchanged in carbon nanotube (CNT)/perfluorosulfonated ionomer composite films was also reported [8]. Nafion is an effective ion exchanger for  $\text{Ru}(\text{bpy})_3^{2+}$ , and so  $\text{Ru}(\text{bpy})_3^{2+}$  could be strongly incorporated into the Nafion film. But the rate of charge transfer was relatively slow in pure Nafion film, so CNT was adopted to interfuse in the Nafion to quicken the transfer of charge.

There are also many reports on the detection of tertiary amine-containing analytes based on the ECL produced by their interaction with  $\text{Ru}(\text{bpy})_3^{2+}$  at an electrode surface. Complex apparatus is required to combine the end-column  $\text{Ru}(\text{bpy})_3^{2+}$  ECL detector with flowing system, e.g. high-performance liquid chromatograph [9–11], flow injection [12–14] or capillary electrophoresis device [15–19]. These methods were proved to have high resolving power and require small sample volume, but

they also have some marked disadvantages, such as vast waste of costly reagent  $\text{Ru}(\text{bpy})_3^{2+}$ , costliness of the employed apparatus and the fussy manipulation.

In this paper, a simple and sensitive method was put forward to overcome these disadvantages with the modification of  $\text{Ru}(\text{bpy})_3^{2+}$  on a glassy carbon electrode. Only a simple electrochemical apparatus is required for the detection of tertiary amine-containing analytes. The new method can be used to replace the ECL method, which does not fit due to the low ECL efficiency of these analytes. To the best of our knowledge, there is no report in the literature on the amperometric detection of tertiary amine-containing analytes only with the  $\text{Ru}(\text{bpy})_3^{2+}$ -modified electrode. There is a paper [20] referring to the electrical current intensity produced by the interaction of tertiary amine-containing analytes with  $\text{Ru}(\text{bpy})_3^{2+}$  in the ECL detector coupled with capillary electrophoresis, but no detailed relation between electrical current intensity and the concentration of analytes was investigated.

Difenidol hydrochloride is used to relieve or prevent nausea, vomiting and dizziness caused by certain medical problems. As far as we know, there is scarcely a report on its determination with a sensitive analytical method except for our previous work [21], which must waste vast valuable ECL reagent  $\text{Ru}(\text{bpy})_3^{2+}$  for its determination employing the end-column  $\text{Ru}(\text{bpy})_3^{2+}$  ECL detector combined with the capillary electrophoresis sys-

\* Corresponding author. Fax: +86 731 8821848.  
E-mail address: [szyao@hnu.cn](mailto:szyao@hnu.cn) (S. Yao).

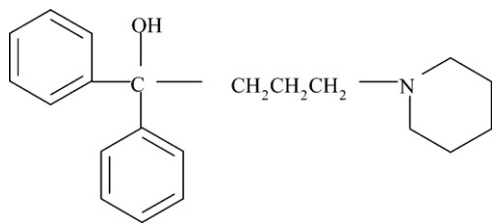


Fig. 1. Molecular structure of difenidol.

tem. Since difenidol contains a tertiary amine group in its molecular structure (Fig. 1), it was selected as a representative to study the amperometric detection of tertiary amine-containing analytes. Dealing with the amperometric detection of difenidol hydrochloride, a detailed study on the optimization of the critical parameters was conducted. This method was successfully applied to the determination of the active ingredients in the commercial ‘difenidol hydrochloride’ tablets.

## 2. Experimental

### 2.1. Reagents

Difenidol hydrochloride was extracted from ‘difenidol hydrochloride 25 mg’ Tablets with an average tablet weight of 0.13 g purchased from Hunan Qianjin Pharmaceutical Co. Ltd. (Hunan, China). The tablets were ground to fine powder in a mortar and extracted successively with ethanol and water, respectively, with each extraction step followed by filtering and rotary evaporation. The resulting powder was recrystallized twice from water and dried under vacuum. Nafion (perfluorinated ionexchange powder, 5 wt% solution in a mixture of lower aliphatic alcohols and water) was obtained from Aldrich. Multi-walled carbon nanotubes (MWNTs, 10–20 nm in diameter) purchased from Shenzhen Nanotech Port Co., Ltd. (Shenzhen, China) were purified and treated to take negative charge as reported previously [22]. Tris(2,2'-bipyridyl)ruthenium(II) chloride hexahydrate was from J & K Chemical Company. All chemicals used were of analytical grade. Double-distilled water was used to prepare solutions in this work. The buffer solutions with a series of pH values were prepared from  $\text{Na}_2\text{HPO}_4$  and  $\text{KH}_2\text{PO}_4$ . The stock solution of 0.01 M difenidol hydrochloride was prepared, stored at 4 °C in a refrigerator, and diluted to prepare standard solutions with a series of concentrations before use.

### 2.2. Apparatus

Cyclic voltammetric and amperometric experiments were carried out on CHI 660B electrochemical analyzer. A three-electrode system was used with the modified glassy carbon electrode as the working electrode, a Ag/AgCl reference electrode (KCl saturated) and a platinum counter electrode.

### 2.3. Preparation of the amperometric sensor

MWNTs suspension (0.5 mg/mL) in double-distilled water was ultrasonically mixed with 5 wt% Nafion solution in the pro-

portion of nine to one by volume for about 30 min to form a homogeneous, well-distributed solution of the MWNTs/Nafion complex. Before modification, the glassy carbon (GC) electrode (3 mm in diameter) was polished with 1.0 and 0.3  $\mu\text{m}$  aluminum slurry, respectively, cleaned under sonication in water for 10 min, and then activated by cyclic voltammetry. The  $\text{Ru}(\text{bpy})_3^{2+}$ -modified electrode was fabricated by dropping 5  $\mu\text{L}$  of the MWNTs/Nafion complex on the pretreated GC electrode and then dipping the electrode into 1 mM  $\text{Ru}(\text{bpy})_3^{2+}$  solution for 30 min after evaporation of the solvents on the electrode. For comparison, 5  $\mu\text{L}$  of 0.5 wt% pure Nafion solution was employed to fabricate  $\text{Ru}(\text{bpy})_3^{2+}$ -modified electrode without MWNTs using the above-mentioned method.

## 3. Results and discussion

### 3.1. Comparison of electrochemical behaviors of modified electrodes

Different kinds of modified electrodes were investigated and their electrochemical responses were studied and compared.

#### 3.1.1. Cyclic voltammograms of $\text{Ru}(\text{bpy})_3^{2+}$ immobilized on the GC electrode

Cyclic voltammograms in 67 mM phosphate buffer solution (pH 7.4) at the bare GC electrode, MWNTs/Nafion composite film-modified electrode before and after immersing in  $\text{Ru}(\text{bpy})_3^{2+}$  solution are shown in Fig. 2. There is a pair of large redox peaks related to  $\text{Ru}(\text{bpy})_3^{2+}/\text{Ru}(\text{bpy})_3^{3+}$  redox transition in the cyclic voltammogram of the MWNTs/Nafion composite film-modified electrode after immersing in  $\text{Ru}(\text{bpy})_3^{2+}$  solution (curve d), while no peak is found on the bare GC and MWNTs/Nafion modified electrodes (curves a and b, respec-

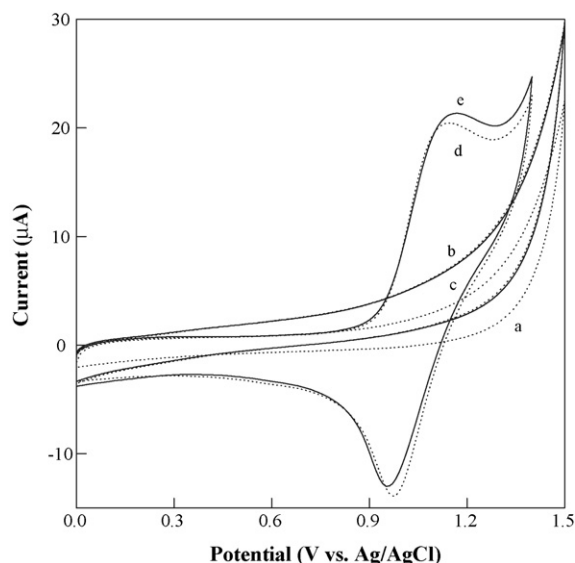


Fig. 2. Cyclic voltammograms in 67 mM phosphate buffer solution (pH 7.4) at a scan rate of 50 mV/s in the presence of 0 mM (a, b, d) and 1.0 mM (c, e) difenidol hydrochloride at the bare GC electrode (a), MWNTs/Nafion composite film-modified electrode before (b, c) and after (d, e) immersing in  $\text{Ru}(\text{bpy})_3^{2+}$  solution.

tively). It can be concluded that  $\text{Ru}(\text{bpy})_3^{2+}$  can easily move into the MWNTs/Nafion composite film on the GC electrode while immersing the electrode into  $\text{Ru}(\text{bpy})_3^{2+}$  solution. A pair of redox peaks can also be observed at the  $\text{Ru}(\text{bpy})_3^{2+}$ /Nafion electrode, but the peak currents are relatively smaller. The MWNTs in the composite film can quicken the electron transfer of  $\text{Ru}(\text{bpy})_3^{2+}$ , and, thus, result in the larger redox current of  $\text{Ru}(\text{bpy})_3^{2+}$  than that of the electrode only modified by  $\text{Ru}(\text{bpy})_3^{2+}$ /Nafion film. When the modified electrodes were repeatedly cycled in the potential range from 0.0 to 1.5 V at a scan rate of 50 mV/s for 50 cycles, the anodic peak currents decreased by 16 and 57% at the  $\text{Ru}(\text{bpy})_3^{2+}$ /MWNTs/Nafion and  $\text{Ru}(\text{bpy})_3^{2+}$ /Nafion electrodes, respectively, which indicates that the  $\text{Ru}(\text{bpy})_3^{2+}$ /MWNTs/Nafion electrode has a better stability.

The voltammetric behavior of  $\text{Ru}(\text{bpy})_3^{2+}$ /MWNTs/Nafion composite film-modified electrode in phosphate buffer solution (pH 7.4) at different scan rates were investigated. It was found that the peak current increased directly with the potential scan rate. Within the tested range from 50 to 250 mV/s, the peak current is in direct proportionality with the potential scan rate. A linear relationship between the anodic peak current and potential scan rate was deduced:

$$I_{\text{pa}} = 18.13 + 0.11v \quad (r = 0.9883) \quad (1)$$

where  $I_{\text{pa}}$  is the anodic peak current ( $\mu\text{A}$ ) and  $v$  is the potential scan rate (mV/s). Therefore, the electron transfer process of  $\text{Ru}(\text{bpy})_3^{2+}$  immobilized on the modified electrode can be considered as a surface eT process.

### 3.1.2. Electrocatalytic oxidation of difenidol at $\text{Ru}(\text{bpy})_3^{2+}$ -modified electrode

To investigate the response of the modified electrode to the addition of difenidol hydrochloride, cyclic voltammetric measurements were carried out in phosphate buffer solution (pH 7.4) at the  $\text{Ru}(\text{bpy})_3^{2+}$ /MWNTs/Nafion composite film-modified electrode in the presence of 1 mM difenidol hydrochloride. For comparison, the cyclic voltammetry of the MWNTs/Nafion modified electrode in the presence of 1 mM difenidol hydrochloride was also performed, and the corresponding results are also shown in Fig. 2. No obvious change in the cyclic voltammogram can be observed at the MWNTs/Nafion modified electrode upon the addition of 1 mM difenidol hydrochloride (curve c). While at the  $\text{Ru}(\text{bpy})_3^{2+}$ /MWNTs/Nafion composite film-modified electrode, the addition of difenidol hydrochloride into the phosphate buffer solution induced the increase of the anodic peak current and the simultaneous decrease of cathodic peak current (curve e). This phenomenon is in accordance with an electrocatalytic reaction mechanism which is expressed in Fig. 3. The immobilized  $\text{Ru}(\text{bpy})_3^{2+}$  was firstly oxidized to  $\text{Ru}(\text{bpy})_3^{3+}$ , which reacted subsequently with difenidol and reversed to the reductive state. Hence, the amount of  $\text{Ru}(\text{bpy})_3^{2+}$  on the electrode increased, resulting in the increase in the oxidation current and the decrease in the reduction current. As a result, the modified electrode can be used as an amperometric sensor for the determination of difenidol.

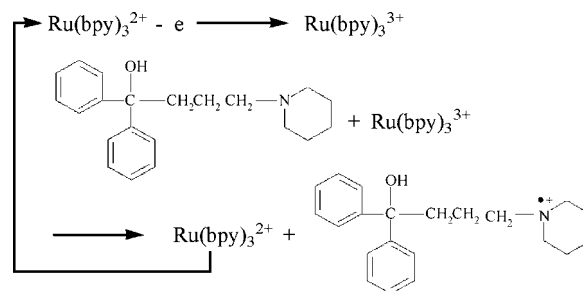


Fig. 3. Electrocatalytic mechanism of  $\text{Ru}(\text{bpy})_3^{2+}$  to the oxidation of difenidol.

## 3.2. Optimization of experimental conditions

To obtain a better result in the detection of difenidol hydrochloride by the above-mentioned amperometric sensor, some parameters were investigated in details, including the applied potential at the working electrode and the pH value of the supporting electrolyte.

### 3.2.1. Effect of the applied potential

The effect of the applied potential on the amperometric response of the composite film modified electrode to difenidol hydrochloride was investigated. It was found that with the increase of the applied potential from 0.90 to 1.20 V, the current intensity increased and reached a maximum value at 1.12 V, which is close to the potential of the oxidation peak of  $\text{Ru}(\text{bpy})_3^{2+}$  immobilized in the MWNTs/Nafion film in the cyclic voltammogram, then decreased rapidly. So, 1.12 V was selected as the optimized potential in the following experiments.

### 3.2.2. Effect of the solution pH value

The current responses for difenidol hydrochloride with the pH change of the phosphate buffer solution used in the amperometric detection were investigated. It was found that the current response increased with the pH value from 6.0 to 7.4, and then decreased markedly. Hence, pH 7.4 was selected as the optimal pH value of phosphate buffer solution for the detection of difenidol with the  $\text{Ru}(\text{bpy})_3^{2+}$ /MWNTs/Nafion film modified electrode.

## 3.3. Standard concentration curves of difenidol hydrochloride

The amperometric method employed for the detection of difenidol hydrochloride is based on the electrocatalytic property of the immobilized  $\text{Ru}(\text{bpy})_3^{2+}$  to the oxidation of difenidol. Under the optimized experimental conditions (pH 7.4, applied potential 1.12 V), amperometric responses of the MWNTs/Nafion,  $\text{Ru}(\text{bpy})_3^{2+}$ /Nafion, and  $\text{Ru}(\text{bpy})_3^{2+}$ /MWNTs/Nafion-modified electrodes to the successive additions of difenidol hydrochloride into 4 mL buffer solution were measured and the corresponding results are presented in Fig. 4. As shown in Fig. 4, neglectable current response can be observed at the MWNTs/Nafion film modified electrode upon the addition of difenidol hydrochloride (curve a). The current responses obtained at the  $\text{Ru}(\text{bpy})_3^{2+}$ /Nafion elec-

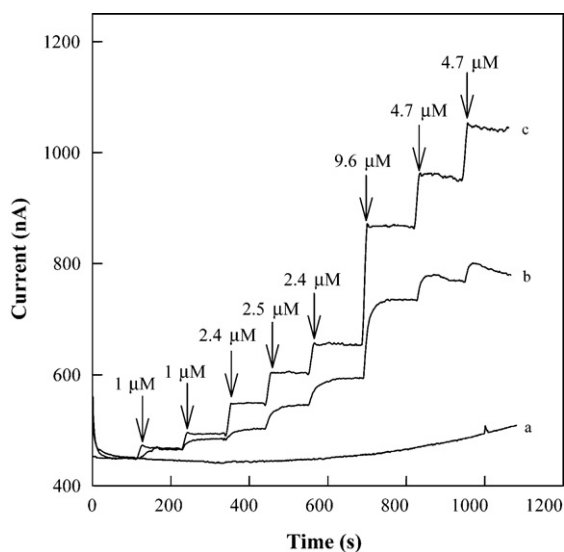


Fig. 4. Amperometric response of (a) MWNTs/Nafion, (b)  $\text{Ru}(\text{bpy})_3^{2+}/\text{Nafion}$  and (c)  $\text{Ru}(\text{bpy})_3^{2+}/\text{MWNTs}/\text{Nafion}$  modified electrodes to the successive additions of difenidol hydrochloride in phosphate buffer solution (pH 7.4) at an applied potential of 1.12 V.

trode are satisfactorily high (curve b). These results indicate that the immobilized  $\text{Ru}(\text{bpy})_3^{2+}$  plays a dominant role in the amperometric response, and the response current due to the direct oxidation of difenidol at the modified electrode was neglectable. The existence of MWNTs in the composite film facilitates the electron transfer between  $\text{Ru}(\text{bpy})_3^{2+}$  and the surface of GC electrode, thus, a largest current response was observed at the  $\text{Ru}(\text{bpy})_3^{2+}/\text{MWNTs}/\text{Nafion}$ -modified electrode (curve c). The relationship between the response current at the  $\text{Ru}(\text{bpy})_3^{2+}/\text{MWNTs}/\text{Nafion}$  film modified electrode and the concentration of difenidol is plotted in Fig. 5. It can be seen that the current response increases linearly with the concentration in the range from  $1.0 \times 10^{-6}$  to  $3.3 \times 10^{-5}$  M. The linear

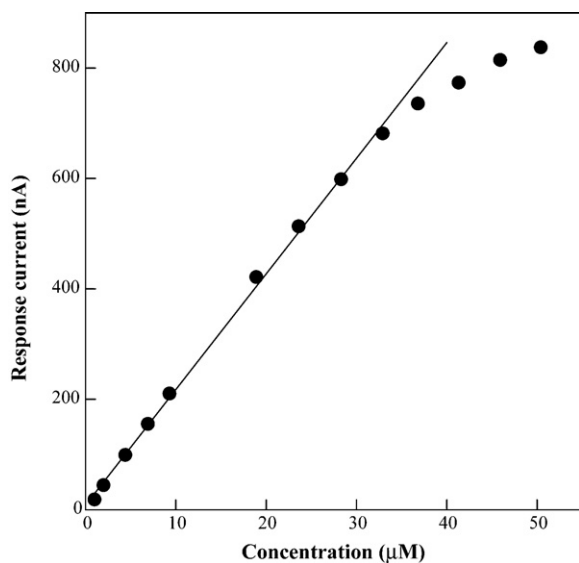


Fig. 5. The relationship between response current and difenidol hydrochloride concentration. pH value of the phosphate buffer solution: 7.4; applied potential: 1.12 V.

Table 1  
Determination of difenidol hydrochloride in tablets

No	Content labeled (mg/tablet)	Content found (mg/tablet) <sup>a</sup>	R.S.D. (%)
050502	25	25.71	3.3
050317	25	24.25	3.6
050107	25	24.90	3.2

<sup>a</sup> Average value of five measurements.

regression equation is presented as follows:

$$\Delta I = 8.14 + 20.97C \quad (r = 0.9983) \quad (2)$$

where  $\Delta I$  is the current response (nA) and  $C$  is the concentration of difenidol hydrochloride ( $\mu\text{M}$ ). The limit of detection (LOD) is  $0.5 \mu\text{M}$  based on the signal-to-noise ratio of 3. The relative standard deviation (R.S.D.) of the current response for  $2.5 \times 10^{-5}$  M difenidol hydrochloride is 6%, while the recovery of difenidol hydrochloride at  $2.5 \times 10^{-6}$ ,  $7.5 \times 10^{-6}$ ,  $1.25 \times 10^{-5}$ ,  $1.75 \times 10^{-5}$ ,  $2.5 \times 10^{-5}$  and  $2.75 \times 10^{-5}$  M were 93, 106, 98, 103, 95 and 106%, respectively. Hence, this method is considered as a sensitive and reliable analytical approach for the determination of difenidol hydrochloride.

#### 3.4. The analysis of drug tablets

Three batches of drug tablets of “difenidol hydrochloride 25 mg” were purchased and were analyzed by the above-mentioned method. Five pieces of tablets were selected at random from every batch and then were ground to powder in a mortar. A part of the obtained powder was weighed, treated with water under sonication for 10 min, and then filtered through a  $0.22 \mu\text{m}$  membrane. The filtrate was analyzed using the  $\text{Ru}(\text{bpy})_3^{2+}/\text{MWNTs}/\text{Nafion}$ -modified electrode. The content of difenidol hydrochloride was determined using the standard calibration curve. The result is presented in Table 1. It can be seen that the contents obtained by the proposed method are close to the labeled value.

## 4. Conclusion

The proposed amperometric method for the detection of difenidol hydrochloride is simple, reproducible and sensitive. Parameters influencing the amperometric response of the  $\text{Ru}(\text{bpy})_3^{2+}/\text{MWNTs}/\text{Nafion}$ -modified electrode were optimized. The calibration curve over the range from  $1.0 \times 10^{-6}$  to  $3.3 \times 10^{-5}$  M was linear with a correlation coefficient of 0.998 and a detection limit of  $5 \times 10^{-7}$  M ( $S/N=3$ ). The sensor was employed to the determination of the active ingredients in the tablets containing difenidol hydrochloride. It is suggested that such kind of sensor can also be used for the detection of other tertiary amine-containing analytes.

## Acknowledgements

This work was supported by the Research Fund for the Doctoral Program of Higher Education (no. 20030523017) and the

National Natural Science Foundation of China (no. 20335020 and 20575019).

## References

- [1] H.N. Choi, S.H. Cho, W.Y. Lee, *Anal. Chem.* 75 (2003) 4250.
- [2] X. Sun, Y. Du, S.J. Dong, E.K. Wang, *Anal. Chem.* 77 (2005) 8166.
- [3] J. Premkumar, S.B. Khoo, *Electrochem. Commun.* 6 (2004) 984.
- [4] S.N. Ding, J.J. Xu, H.Y. Chen, *Electrophoresis* 26 (2005) 1737.
- [5] Z.H. Guo, Y. Shen, M.K. Wang, F. Zhao, S.J. Dong, *Anal. Chem.* 76 (2004) 184.
- [6] A. Mugweru, J.F. Rusling, *Anal. Chem.* 74 (2002) 4044.
- [7] H.Y. Wang, G.B. Xu, S.J. Dong, *Electroanalysis* 14 (2002) 853.
- [8] Z.H. Guo, S.J. Dong, *Anal. Chem.* 76 (2004) 2683.
- [9] J.B. Noffsinger, N.D. Danielson, *J. Chromatogr. A* 387 (1987) 520.
- [10] W.Y. Lee, T.A. Nieman, *J. Chromatogr. A* 659 (1994) 111.
- [11] K. Uchikura, M. Kirisawa, A. Sugii, *Anal. Sci.* 9 (1993) 121.
- [12] J.B. Noffsinger, N.D. Danielson, *Anal. Chem.* 59 (1987) 865.
- [13] L. He, K.A. Cox, N.D. Danielson, *Anal. Lett.* 23 (1990) 195.
- [14] A.W. Knight, G.M. Greenway, *Analyst* 120 (1995) 2543.
- [15] X.H. Sun, J.F. Liu, W.D. Cao, X.R. Yang, E.K. Wang, Y.S. Fung, *Anal. Chim. Acta* 470 (2002) 137.
- [16] J.L. Yan, J.F. Liu, W.D. Cao, X.H. Sun, X.R. Yang, E.K. Wang, *Microchem. J.* 76 (2004) 11.
- [17] J.F. Liu, W.D. Cao, X.R. Yang, E.K. Wang, *Talanta* 59 (2003) 453.
- [18] W.D. Cao, X.R. Yang, E.K. Wang, *Electroanalysis* 16 (2004) 169.
- [19] J.F. Liu, W.D. Cao, H.B. Qiu, X.H. Sun, X.R. Yang, E.K. Wang, *Clin. Chem.* 48 (2002) 1049.
- [20] H.B. Qiu, X.B. Yin, J.L. Yan, X.C. Zhao, X.R. Yang, E.K. Wang, *Electrophoresis* 26 (2005) 687.
- [21] W. Pan, Y.G. Liu, Y. Huang, S.Z. Yao, *J. Chromatogr. B* 831 (2006) 17.
- [22] M. Guo, J. Chen, J. Li, L. Nie, S. Yao, *Electroanalysis* 16 (2004) 1992.



Short communications

# Instrumental neutron activation analysis of mass fractions of toxic metals in plastic

Kwangwon Park, Namgoo Kang\*

*Division of Metrology for Quality Life, Korea Research Institute of Standards and Science, 1 Doryong-Dong, Yuseong-Gu, Daejeon 305-340, South Korea*

Received 23 March 2007; received in revised form 20 April 2007; accepted 21 April 2007  
Available online 5 May 2007

## Abstract

It is very challenging to decompose a plastic product for the purpose of analysis of hazardous elements contained. To circumvent such technical problem, it is imperative that an analyst employ a nondestructive analytical method free of any pretreatments. The analytical results of the concentrations of toxic metals such as Cd and Cr in polypropylene for seven samples at two different levels were obtained using the instrumental neutron activation analysis. This work was intended ultimately to establish certified reference materials (CRMs) of these metals in the polypropylene, traceable to the SI. The uncertainties associated with the analytical procedures were estimated in accordance with the ISO guideline. The results were subsequently validated by a comparison with those for CRM-680 and –681 of the Bureau Communautaire de Reference (BCR), which demonstrated acceptable agreement within their uncertainty ranges.

© 2007 Elsevier B.V. All rights reserved.

*Keywords:* Neutron activation analysis; Hazardous element; Certified reference material; Polypropylene; Uncertainty

## 1. Introduction

Strict environmental regulations have placed technical barriers on the international trade of many industrial products. Such regulations include the programs of the European Union (EU) for Restriction of Hazardous Substances in electrical and electronic products (RoHS) [1], a directive on Waste from Electric and Electronic Equipment (WEEE) [2], and Registration, Evaluation, and Authorization of Chemicals (REACH) [3]. Electrical and electronic products containing above the allowable levels of Cd, Cr(VI), Pb, Hg, polybrominated biphenyl (PBB), and polybrominated biphenyl ether (PBBE) began being banned from the EU starting from July 2006. The regulation limits of hazardous metals specify 100 mg/kg for Cd and 1000 mg/kg for Cr(VI), Hg, and Pb. A number of products are being affected, ranging from computers and telecommunications equipment to domestic appliances, electronic tools, toys, and automatic dispensers. The primary constituents of electric and electronic goods are plastic polymers and metals. Chemical analyses

of the polymers have been conducted extensively by manufacturing companies, industrial laboratories, and regulatory sectors.

However, there are no internationally approved analytical methods to determine hazardous metals in polymers. In order to certify polypropylene (PP) reference materials, the materials are usually pretreated using a microwave-assisted acid digestion method and then are analyzed by isotope dilution mass spectrometry (IDMS) [4] and inductively coupled plasma/optical emission spectrometry (ICP/OES). It is thus imperative that prior to analysis, such analytical approach require chemical dissolution of solid samples, which step is very tedious and time-consuming. Unlike other analytical methods, the instrumental neutron activation analysis (INAA) [5] has an advantage of a nondestructive characteristic, which enable an analyst to measure the elements of interest in a polymer without pretreatments, which may break the chain of traceability and cause additional sources of uncertainties. Although INAA as a primary method render an analyst to conduct rapid, reliable, accurate, and sensitive determinations of many elements in complex matrices including various polymers and resins, this method has also some shortcomings. Pb cannot be determined by INAA because no suitable nuclides exist for this element. In addition, Hg deter-

\* Corresponding author. Tel.: +82 42 868 5221; fax: +82 42 868 5042.  
E-mail address: [nkang@kriss.re.kr](mailto:nkang@kriss.re.kr) (N. Kang).

mination is inaccurate because of potential volatilization in the course of sample irradiation.

An alternative approach to fortifying reliability of analytical results is to employ certified reference materials (CRMs). To date, very little is known about the availability of CRMs for the analysis of toxic metals in polymers. Rare examples of these are PP CRMs of pellet type provided by the Bureau Communautaire de Reference (BCR) and acrylonitrile–butadiene–styrene CRMs of pellet and disc types prepared by National Metrology Institute of Japan (NMIJ).

In order to imminently cope with such technical barriers in international trade, Korea Research Institute of Standards and Sciences (KRISS) started to develop plastic CRMs containing low and high levels of hazardous substances. As a preliminary application of the INAA to the determination of hazardous materials in a polymer, the present communication is intended to report the analytical results of Cd and Cr in PP. Additionally, the measurement uncertainties related to each analytical step were estimated following International Organization of Standards (ISO) Guide [6].

## 2. Theoretical background

The INAA depends on the irradiation of a stable nuclide  ${}^A Z$  with neutrons using the  ${}^A Z(n, \gamma) {}^{A+1} Z$  nuclear reaction. Once the production  ${}^{A+1} Z$  is  $\gamma$ -ray emitter, a  $\gamma$ -ray detection system can be employed to measure both intensity and energy of the  $\gamma$ -rays used to indicate the target nuclide  ${}^A Z$ , and to determine the concentration of the element in the sample. The analytical sensitivity is based primarily upon the abundance of the isotope  ${}^A Z$ , the neutron capture cross section of  ${}^A Z$ , the  $\gamma$ -ray emission branching ratio of  ${}^{A+1} Z$ , and the interferences from other  $\gamma$ -rays in the sample. The INAA as an absolute method can be employed without standard materials. If associated uncertainty parameters to obtain accurate analytical results are largely unknown, any absolute method could produce appreciable levels of uncertainties. High-accuracy INAA thus almost always uses a ratio method (a comparator technique) by which the sample is compared with a standard of the quantity to be measured.

By means of  $\gamma$ -rays spectrometry, the INAA procedure compares the neutron-induced activities in an unknown sample with those induced in a standard with known composition. The widely known equation of a comparator technique is [7]:

$$C_x = C_c \frac{m_c}{m_x} \frac{A_{0,x}}{A_{0,c}} R_\theta R_\phi R_\sigma R_\varepsilon \quad (1)$$

where  $C_x$  is the mass fraction of sample in  $\mu\text{g/g}$ ,  $C_c$  is the mass fraction of standard in  $\mu\text{g/g}$ ,  $m_x$  and  $m_c$  are the masses of sample and standard used in g,  $R_\theta$  is the ratio of isotopic abundances for sample and standard,  $R_\phi$  is the ratio of neutron fluences (including neutron self shielding),  $R_\sigma$  is the ratio of effective cross sections,  $R_\varepsilon$  is the ratio of counting efficiencies (differences due to geometry and  $\gamma$ -ray self shielding). The decay corrected counting rates for the indicator  $\gamma$ -ray of sample  $A_{0,x}$  and of standard  $A_{0,c}$  are derived from the measurement. Hence, the decay-corrected  $\gamma$ -ray counting rate ( $A_0$ ) for a measured

nuclide is estimated by the following equation:

$$A_0 = \frac{N_c \lambda e^{\lambda t_D}}{(1 - e^{-\lambda t_C})} \quad (2)$$

where  $N_c$  is the number of counts in indicator  $\gamma$ -ray peak,  $\lambda$  is the decay constant for indicator nuclide is  $\ln 2/t_{1/2}$ ,  $t_D$  is the time elapsed between the end of activation and the start of counting, and  $t_C$  is the time of counting.

## 3. Experimental

### 3.1. Preparation of samples

National Research Center for CRMs (NRCCRM) provided fourteen samples in two different types of PP (seven samples for each category) for the purpose of an international comparison of standard materials between China, Korea, and Japan. These materials are of pellet type in which the concentrations of Cd and Cr were 1000 mg/kg for Cr, Hg, Pb and 100 mg/kg Cd (high levels), and 100 mg/kg for Cr, Hg, Pb, and 10 mg/kg Cd (low levels). The homogeneity tests of the materials were performed by NRCCRM with inductively coupled plasma–atomic emission spectrometry (ICP/AES) The results showed about 2–3% of relative standard deviation (R.S.D.) with 0.2 g of a sample.

### 3.2. INAA procedure

The comparator INAA method was applied to the analysis of Cr and Cd in the solid PP samples. Seven test portions of about 30 mg were taken from high-level samples while approximately 60 mg were taken from low-level ones. The test portions were embedded into about 300 mg cellulose filter aid ashless powder (Whatman catalog # 1700025) and pressed into pellets of 13 mm diameter and 1.5 mm thickness under 2 metric tons of pressure. The test samples were sealed in an envelope made of 6  $\mu\text{m}$  PP film. These sealed samples were packaged with linear polyethylene (LPE) film.

A portion of aliquots of the comparator as an assay standard was taken from the KRISS primary reference solution and subsequently were dropped onto 55 mm diameter filter papers (Whatman # 41). After air-drying and palletizing, the standards were prepared in the same manner to the samples. The size of pellets was 13 mm diameter by 1.5 mm thickness.

The irradiation time was 4 h in the IP-hole #4 of the KAERI research reactor, HANARO, at a neutron fluence rate of  $1.30 \times 10^{14} \text{ n cm}^{-2} \text{ s}^{-1}$ . The samples, standards and blanks were stacked in the center of the irradiation container (rabbit). After irradiation, the outer PP film was removed and the samples, standards and blanks were counted using a HPGe detector (GEM 30, EG&G Ortec, Oak Ridge, TN, 1.85 keV resolution at 1332.5 keV and 30% relative efficiency, 60 peak-to-compton ratio) with a 16K channel analyzer. After cooling for 4 d, counting time was 80,000 s. All counts were carried out at 10 cm distance from the detector to reduce uncertainties due to differences in counting geometry. The  $\gamma$ -ray energy used for the determinations 320.1 and 336.3 keV for  ${}^{51}\text{Cr}$  ( $t_{1/2} = 27.7 \text{ d}$ ) and  ${}^{115}\text{Cd}$  ( $t_{1/2} = 53.47 \text{ h}$ ). The  $\gamma$ -ray spectra of the irradiated samples

Table 1  
Standard uncertainty budget for low-level Cr determination in polypropylene CRM candidates by INAA

Parameter	Symbol	Unit	Description	Value	Standard uncertainty	Relative standard uncertainty (%)
<b>Mass</b>						
	$C_c$	mg/kg	Comparator mass fraction	115.4	0.152	0.132
	$m_x$	mg	Sample mass*	50.94	0.006	0.012
	$m_c$	mg	Comparator mass*	51.6	0.044	0.085
<b><math>A_0</math> parameter</b>						
	$N_x$		Sample counts*	475863	904	0.19
	$N_c$		Comparator counts*	151043	634	0.42
	$\lambda$	d <sup>-1</sup>	Decay constant	0.025	0.000072	0.289
	$t_{D,x}$	d	Decay time of sample	4.21	2.3E-05	0.0005
	$t_{D,c}$	d	Decay time of comparator	19.29	2.3E-05	0.0001
	$t_{C,x}$	d	Elapsed time of sample	0.579	2.3E-05	0.0039
	$t_{C,c}$	d	Elapsed time of comparator	0.231	2.3E-05	0.0099
<b>Ratio uncertainty</b>						
	$R_\theta$		Ratio of isotope abundance	1	0	0
	$R_\phi$		Ratio of neutron flux	1.002	0.003	0.3
	$R_\sigma$		Ratio of cross section	1	0	0
	$R_e$		Ratio of efficiency	0.9978	0.0001	0.012
<b>Results</b>						
	$C_x$ (mg/kg)		Sample mass fraction		101.24	
	$u$ (rel.), %		Relative standard uncertainty		0.42	
	$u_c$ (mg/kg)		Measurement standard uncertainty		0.43	

Asterisks indicate Type A uncertainties while the other uncertainties belong to Type B.

were counted at a high counting rate in the  $\gamma$ -ray spectrometer. Since a counting loss frequently occurs because of a pulse pile-up from the high counting rate, a loss-free counting system was installed in the  $\gamma$ -ray spectrometer in order to correct this counting loss. The DSPEC system (DSPEC-PRO Trade Mark, EG&G Ortec) was run with a Gaussian amplifier at 12- $\mu$ s shaping time.

#### 4. Results and discussion

The analytical results and associated uncertainty components as to high-level Cd in PP is presented in Table 1. The comparator INAA has the sources of measurement uncertainties from each step in the procedures which were categorized into sample preparation, irradiation, and  $\gamma$ -ray spectrometry [8]. Virtually all

recognizable effects on the final results were taken into account to obtain the overall uncertainty. As the mathematical relationships described in (1) and (2) contain the terms of multiplication and division of quantities, the measurement standard uncertainty can be expressed as the square root of the sum of the squares of each relative standard uncertainty.

The overall results with regard to high-level Cd in PP for seven samples are displayed in Table 2. In addition, the measurement standard uncertainties were estimated for the samples of low-level Cd, low-level Cr, and high-level Cr. Consequently, the final combined standard uncertainty ( $u_c$ ) of high-level Cd in PP was obtained by combining the pooled measurement standard uncertainty and the standard deviation of mass fractions of seven high-level Cd samples. The pooled measurement uncertainty due to systematic effects was calculated by averaging the

Table 2  
Determination of low-level Cr in polypropylene CRM candidates by INAA

Sample ID	Mass fraction (mg/kg)	Measurement standard uncertainty (mg/kg)
171	101.24	0.43
421	97.86	0.42
713	99.51	0.42
844	96.17	0.41
901	100.67	0.43
1193	95.91	0.41
1212	97.45	0.41
Pooled measurement standard deviation		0.42
Mean of mass fractions ( $C_x$ ), mg/kg		98.40
Standard deviation of mass fractions ( $u_R$ ), mg/kg		2.12
Combined uncertainty ( $u_C$ ), mg/kg		2.16
Coverage factor, $k$		2
Expanded uncertainty ( $U$ ), mg/kg (at 95% level of confidence)		4.31 (4.38 %, relative)

Table 3  
Analytical results of Cd and Cr in polypropylene CRM candidates by INAA

Sample	Element	Mass fraction, (mg kg <sup>-1</sup> )	Expanded uncertainty at 95% level of confidence (mg kg <sup>-1</sup> )
High-level sample	Cd	88.3	5.0
	Cr	974.7	51.8
Low-level sample	Cd	9.0	0.5
	Cr	98.4	4.3

measurement standard uncertainties of the seven samples. The standard deviation (2.12 mg/kg) of mass fractions of the seven samples (Table 2) was regarded as the uncertainty associated with homogeneity between the samples used, which is called between-bottle uncertainty [5]. Our analytical results show the relative standard deviation of 2.2%, which was located within the reported range of about 2–3% by NRCCRM. The between-bottle uncertainty was the major contributor to the final combined standard uncertainty. Finally, the expanded uncertainty was estimated by multiplying the combined uncertainty with a coverage factor (*k*) of 2 at 95% confidence level. The overall results and uncertainties for Cd and Cr at low and high levels are summarized in Table 3.

Since there is no PP CRMs available, our obtained analytical results were validated by the standard reference materials made of polyethylene (BCR 680 at high level and BCR 681 at low level) provided by the Bureau Communautaire de Reference (BCR) [9] were analyzed in the same manner. The reference values using BCR materials showed the following results of mass fractions:  $140.8 \pm 2.5$  mg/kg for Cd and  $114.6 \pm 2.6$  mg/kg for Cr at the high level;  $21.7 \pm 0.71$  mg/kg for Cd and  $17.7 \pm 0.6$  mg/kg for Cr at the low level. Our measured results obtained were  $138.4 \pm 1.95$  mg/kg for Cd and  $113.6 \pm 1.5$  mg/kg for Cr at the high level while  $20.5 \pm 0.5$  mg/kg for Cd and  $19.1 \pm 0.4$  mg/kg for Cr at the low level. The comparison shows acceptable agreement within given uncertainties between our samples and BCR materials.

## 5. Conclusions

The overall results demonstrate that the comparator INAA procedures employed in this initial study may be a viable alternative to the conventional analytical approaches for the measurements of toxic substances in plastics. Our future study will focus on searching for a method to be capable of measuring Hg in plastic materials.

## References

- [1] Official Journal of the European Union, L37/19, Directive 2002/95/EC of the European Parliament and of the Council on the Restriction of the Use of Hazardous Substances in Electrical and Electronic Equipment, 2001.
- [2] European Commission Environment Directorate-General XI, Proposal for a Directive on Waste from Electrical and Electronic Equipment (WEEE), third Draft Version, 1998.
- [3] P. Short, Europe Readies Chemical Rules, Chemical Engineering and News, December 11, 2006 (<http://www.cen-online.org/>).
- [4] C.J. Park, S.A. Yim, J. Anal. Atom. Spectrom. 14 (1999) 1061.
- [5] M.D. Glascock, H. Neff, Meas. Sci. Technol. 13 (2003) 1516.
- [6] ISO/IEC Guide 34, Quality System Guidelines for the Production of Reference Materials, ISO, Geneva, 1996.
- [7] R. Zeisler, N. Vajda, G. Lamaze, G.L. Molnar, Handbook of Nuclear Chemistry, vol. 3, Kluwer Academic Publishers, 2003, p. 303.
- [8] A. Lamberty, W. Van Borm, Ph. Quevauviller, The certification of mass fraction of As, Br, Cd, Cl, Cr, Hg, Pb and S in two polyethylene CRMs: BCR-680 and BCR-681, bcr information reference materials, European Commission, 2001.
- [9] M. Balla, Zs. Molnár, Á. Kőrös, J. Radioanal. Nucl. Chem. 259 (2004) 395.

# Liquid-phase microextraction and GC for the determination of primary, secondary and tertiary aromatic amines as their iodo-derivatives

Kishan Reddy-Noone, Archana Jain, Krishna K. Verma\*

*Department of Chemistry, Rani Durgavati University, Jabalpur 482001, Madhya Pradesh, India*

Received 3 February 2007; received in revised form 24 April 2007; accepted 24 April 2007

Available online 6 May 2007

## Abstract

Presence of iodine in aromatic amines, introduced by their reaction with iodine, and other electron withdrawing substituents such as chlorine and nitro, has been found to afford excellent liquid-phase microextraction (LPME) in toluene and separation by gas chromatography in the determination of primary, secondary and tertiary aromatic amines. The effect is due to decreased basic nature of amines when electronegative substituents are present. Single drop microextraction (SDME) of the amines in 2  $\mu\text{l}$  of toluene and injection of the whole extract into GC, or LPME into 50  $\mu\text{l}$  of toluene and injection of 2  $\mu\text{l}$  of extract, were used. LPME has been found more robust and to give better extraction in shorter period than SDME. In SDME–GC–FID, the average correlation coefficient was 0.9939 and average limit of detection 25  $\mu\text{g l}^{-1}$  (range 12–61  $\mu\text{g l}^{-1}$ ) whereas the corresponding values in LPME–GC–MS were, respectively, 0.9953 and 33  $\text{ng l}^{-1}$  (range 18–60  $\text{ng l}^{-1}$ ). The method has been applied to determine aromatic amines in river water, dye factory effluents and food dye stuffs. The LPME was found as robust, rugged and simple extraction method. © 2007 Elsevier B.V. All rights reserved.

**Keywords:** Iodination; Primary, secondary and tertiary aromatic amines; Liquid-phase microextraction; Gas chromatography–flame ionization or mass spectrometric detection

## 1. Introduction

Aromatic amines widely occur in nature and are substances of concern due to their toxicity and persistence in the environment. Aromatic amines are useful industrial chemicals, which can be transformed into a multitude of products such as pesticides, pharmaceuticals, explosives, rubber, epoxy polymers, azo dyes and aromatic polyurethanes [1]. Aromatic amines are highly toxic to human beings and some of these compounds have been classified as carcinogens [2,3]. Owing to their high solubility in water, amines can easily permeate through soil and contaminate groundwater. Amines have been detected in rivers Rhine and Elbe between 1 and 30  $\mu\text{g l}^{-1}$  level [4]. These compounds can contribute significantly to the taste and odour of water even at their trace level [5,6]. A number of aromatic amines have been detected in the particulate phase of cigarette smoke [7,8], and in indoor and outdoor air [9]. Amines and/or their metabolites have been found in the urine or blood of persons without known

exposure and in human milk [10]. The EU [11,12] has included many anilines in the list of priority pollutants which should be monitored in environmental waters.

Chromatographic separation and quantification of aromatic amines is hampered by their polarity, which can cause tailing and irreversible adsorption. The mass spectra of amines are often not ideal for their characterization, especially if these compounds are present in low concentration [13]. Derivatization is therefore recommended to enhance extraction efficiency and improve chromatographic performance [13,14]. Perfluoroacylation is most often used [15,16], but there are reported derivatization to Schiff bases with pentafluorobenzaldehyde [17], *N*-benzamides with benzoyl chloride [18], and isobutyloxycarbonyl compounds with isobutyl chloroformate [19,20]. *N*-Allyl-*N'*-arythiureas, formed by the reaction of aromatic amines with allyl isothiocyanate, were subjected to pyrolysis and determined as aryl isothiocyanates [21]. Halogenation of aromatic amines enabled the use of electron capture detection. This, nuclear bromination worked well with many amines [22–24], however, problems are inevitable due to side-chain bromination of alkyl anilines, and bromination at ortho and para carboxyl or sulfonic groups, which are knocked off, giving the same product

\* Corresponding author.

E-mail address: [arichna@sancharnet.in](mailto:arichna@sancharnet.in) (K.K. Verma).

from more than one compound [25]. Thus, reaction with bromine of aniline, sulfanilic acid, anthranilic acid, 4-aminobenzoic acid give the same product, viz., 2,4,6-tribromoaniline. Replacement of amino group by iodine through diazotization and substitution of diazo group by reaction with iodide at elevated temperature results in much greater electron affinity, at least by a factor of 150 [26,27]. However, under these conditions, diazo group can also be replaced by hydroxyl group giving phenols, and in real environmental samples, that also contain chloride and bromide, other halo-compounds are side-products [28]. Excepting bromination, none of these methods is applicable to secondary and tertiary aromatic amines, and in our experience nuclear bromination has uncertain stoichiometry [29,30] that complicates chromatography.

Halogenation decreases basic properties of aromatic amines and this has two-fold advantage of increased recovery during sample preparation and improved chromatography. Difficulty is encountered with underivatized aniline and alkyl anilines which are more basic. Nuclear iodination has been examined in this work as an alternative derivatization reaction. Iodination is a relatively moderate process, albeit, it is not subjected to side-reactions. Iodoanilines are not naturally encountered in real environmental samples. Liquid-phase microextraction of the derivatives and analysis by GC–MS resulted in recovery of analytes, their peak shapes and chromatographic separation that were better than obtained with underivatized amines; GC–FID could also be used but the sensitivity is lower. The method has been found to be applicable to primary, secondary and tertiary aromatic amines.

## 2. Experimental

### 2.1. Standards and solvents

Analytical grade standards of the aromatic amines used in this work were obtained from BDH, Dorset, UK. Standard solution ( $1000 \text{ mg l}^{-1}$ ) of each aromatic amine was prepared in acetonitrile and stored in a refrigerator when not in use. Working solutions were prepared by sequentially diluting the stock solutions. The reagent solution was prepared by grinding together 0.320 g of iodine and 0.5 g of potassium iodide (Merck, Mumbai, India), and dissolving the mass in 100 ml of deionized water. Phosphate buffer contained 4 g each of  $\text{KH}_2\text{PO}_4$  and  $\text{K}_2\text{HPO}_4$  (Qualigens, Mumbai, India) in 100 ml water and was adjusted between pH 6 and 7. 2,4,6-Tribromoaniline (Aldrich, Milwaukee, WI, USA), 100 mg in 100 ml of acetonitrile, was used as an internal standard. All solvents used for extraction were obtained from Merck, Mumbai, India.

### 2.2. Instrumentation

The GC–FID analysis was performed using Hewlett Packard 5890 series II gas chromatograph (Agilent Technologies Inc., Palo Alto, CA). The separation of iodo-phenols was performed on a HP-5 (5% phenyl substituted methylpolysiloxane),  $30 \text{ m} \times 0.32 \text{ mm}$ ;  $0.25 \text{ } \mu\text{m}$  film thickness, capillary column. Nitrogen (99.999%) was used as carrier gas at a flow rate of

$3 \text{ ml min}^{-1}$ . The GC–MS instrumentation consisted of Hewlett Packard G1800B GCD system (HP 5890 series II with a quadrupole mass detector). HP-5,  $30 \text{ m} \times 0.25 \text{ mm}$ ;  $0.25 \text{ } \mu\text{m}$  film thickness, capillary column and helium (99.999%) carrier gas at a flow rate of  $1 \text{ ml min}^{-1}$  were used. The GC–MS transfer line was maintained at  $300 \text{ }^\circ\text{C}$ , electron ionization at  $70 \text{ eV}$  and the mass spectrum scanned from  $m/z$  45–450. Chromatographic data were acquired using HP ChemStation software G1074B version A.01.00. The injector temperature was maintained at  $250 \text{ }^\circ\text{C}$  and all injections were made in splitless mode. Extraction vials, 4 ml, with PTFE silicon septum and screw cap with a hole (Supelco),  $8 \text{ mm} \times 1.5 \text{ mm}$ , magnetic stir bars coated with PTFE, magnetic stirrer and in-house made syringe stand were used. Diffuse Reflectance, model DRS-8000, and FTIR spectrometer, model 8400S Shimadzu Corporation Analytical and Measuring Instruments Division, Kyoto, Japan, was used.

### 2.3. Procedure

#### 2.3.1. Method involving SDME

A  $0.5\text{--}2 \text{ ml}$  aliquot of sample solution containing  $0.03\text{--}10 \text{ mg l}^{-1}$  of aromatic amine was mixed with  $800 \text{ } \mu\text{l}$  of phosphate buffer,  $200 \text{ } \mu\text{l}$  of iodine and  $2 \text{ } \mu\text{l}$  of the internal standard, and diluted to  $3.5 \text{ ml}$  with de-ionized water in the extraction vial. The solution was mixed well and kept for 5 min at the ambient temperature ( $26 \text{ }^\circ\text{C}$ ). A portion of  $250 \text{ } \mu\text{l}$  of 0.5% ascorbic acid was added to reduce the surplus iodine from reaction, and the solution made alkaline by addition of  $250 \text{ } \mu\text{l}$  of 5 M sodium hydroxide. For SDME, the needle of a  $10 \text{ } \mu\text{l}$  Hamilton syringe containing  $2 \text{ } \mu\text{l}$  of toluene was penetrated through the septum of the vial until the tip protruded 1 cm below the meniscus of solution. The plunger was suspended to form a drop hanging at the tip of needle. After 15 min of equilibration (stir rate 300 rpm), the drop was retracted back into the syringe and immediately transferred to the injection port of GC for analysis.

#### 2.3.2. Method involving LPME

A  $0.5\text{--}2 \text{ ml}$  aliquot of the combined standard solution containing  $0.1 \text{ } \mu\text{g}\text{--}10 \text{ mg l}^{-1}$  of aromatic amine was mixed in a 5 ml standard flask having a ground glass stopper with  $800 \text{ } \mu\text{l}$  of phosphate buffer,  $200 \text{ } \mu\text{l}$  of iodine and  $2 \text{ } \mu\text{l}$  of the internal standard, and diluted to  $3.5 \text{ ml}$  with deionized water. The solution was mixed well and kept for 5 min at the ambient temperature ( $26 \text{ }^\circ\text{C}$ ). Thereafter, the reaction solution was mixed with  $250 \text{ } \mu\text{l}$  of ascorbic acid and  $250 \text{ } \mu\text{l}$  of 5 M sodium hydroxide, and diluted to  $5 \text{ ml}$  with deionized water. A  $50\text{-}\mu\text{l}$  portion of toluene was added to the flask and shaken vigorously for about 1 min. The flask was kept undisturbed for the toluene droplets to coalesce and settle as a separate layer on the top of the aqueous phase. A  $2 \text{ } \mu\text{l}$  portion of organic phase was carefully withdrawn by a  $5 \text{ } \mu\text{l}$  Hamilton syringe and injected into the GC.

## 3. Results and discussion

Chromatogram obtained after iodination of a range of anilines and their SDME is shown in Fig. 1, and compared with

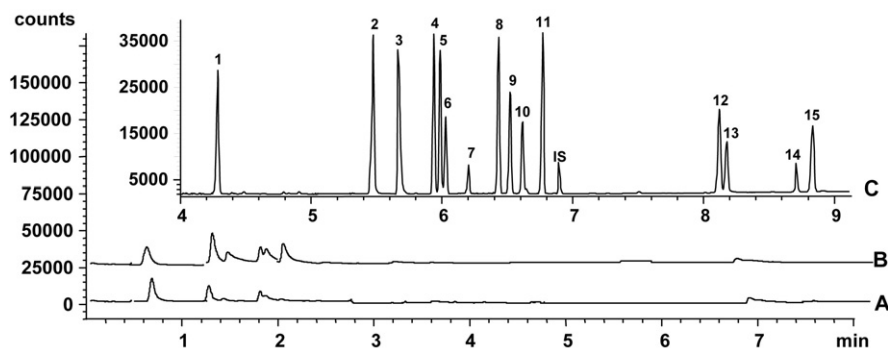


Fig. 1. GC–FID for anilines. (A) Chromatogram of the anilines,  $5 \text{ mg l}^{-1}$  each, spiked in deionised water and extracted with  $2 \mu\text{l}$  of toluene without derivatization; (B) chromatogram of anilines without derivatization and direct injection of standard into GC; and (C) chromatogram of a mixture of anilines,  $1 \text{ mg l}^{-1}$  each, after their derivatization and extraction with  $2 \mu\text{l}$  of toluene. Peaks identification (as their iodo-derivatives; underivatized mentioned in parentheses), 1 = 4-chloroaniline (uniodinated); 2 = aniline; 3 = 3-nitroaniline (uniodinated); 4 = *N*-methylaniline; 5 = 2-toluidine; 6 = *N,N*-dimethylaniline; 7 = 2-chloroaniline; 8 = 2,6-dimethylaniline; 9 = *N,N*-diethylaniline; 10 = 3-chloroaniline; 11 = 4-aminobiphenyl; 12 = 3,5-dinitroaniline (uniodinated); 13 = 2,4-dinitroaniline (uniodinated); 14 = 3,5-dimethylaniline; 15 = 3-anisidine; and IS (internal standard) = 2,4,6-tribromoaniline. GC oven temperature,  $100^\circ\text{C}$  for 3 min, increased to  $210^\circ\text{C}$  at  $70^\circ\text{C min}^{-1}$ , held for 0.5 min, ramped to  $260^\circ\text{C}$  at  $10^\circ\text{C min}^{-1}$ .

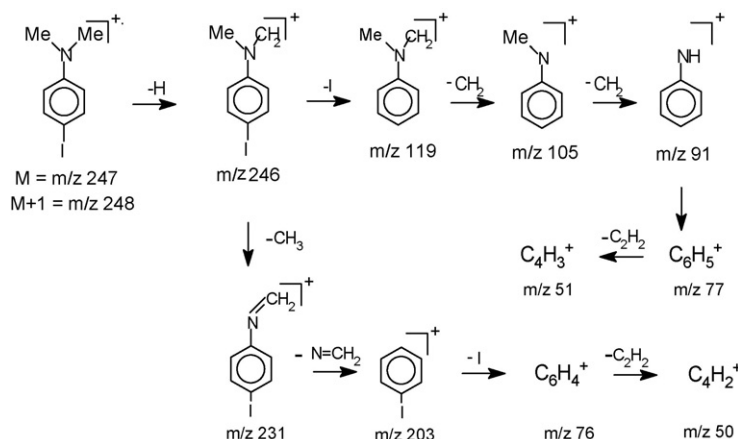
those obtained when a standard solution was directly injected into the GC (to reveal the chromatographic behaviour of anilines) or was spiked to water, subjected to SDME in toluene and the extract chromatographed (to establish extraction recovery). Indeed, derivatization to iodo-derivatives has clear advantage of superior extraction efficiency and better chromatographic performance for aniline or alkyanilines. Owing to the presence of electron withdrawing substituents, such as nitro and chlorine (in para position), in the nucleus (which reduce basic character), many anilines have inherent capability of showing both above advantages and their incapability to undergo iodination is not a shortcoming. From an analytical point of view, it is a methodology of interest that allows the determination, in the same chromatogram, of mixtures of aromatic amines with substituents of different nature.

### 3.1. Reaction condition

Preliminary experiments were performed in order to study the influence of diverse parameters on the derivatization process. Three parameters, iodine volume, reaction solution pH

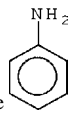
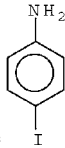
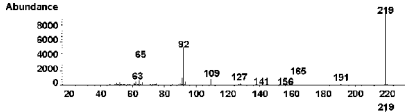
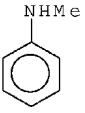
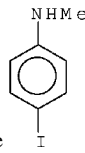
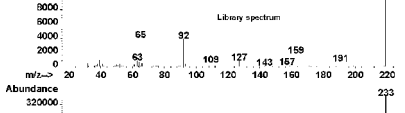
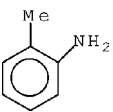
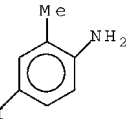
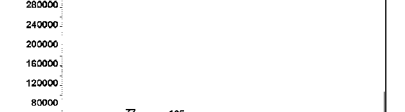
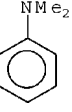
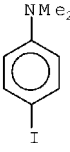
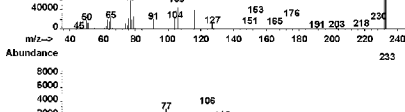
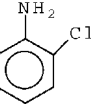
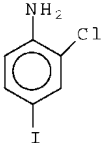
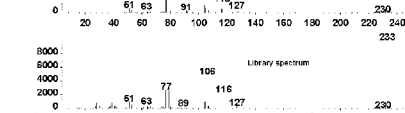
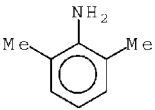
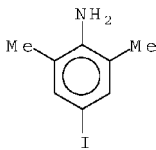
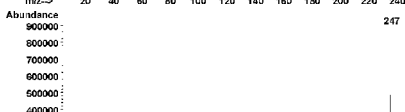
and time were investigated to achieve the highest derivatization yield. Optimum derivatization yield was found in pH range 6–7.5; phosphate buffer of pH 6–7 was used in subsequent experiments. One of the important factors affecting the yields of iodo-derivative is the amount of iodine used. The derivatization yield was observed to constantly increase with iodine in range 0.2–0.4 ml. Volumes higher than this produced precipitation, ostensibly, due to formation of charge-transfer complex between substituted aniline and iodine. Therefore, 0.4 ml of iodine was used for iodination, and the excess of iodine from reaction was reduced by addition of ascorbic acid. During the study of the effect of time on iodination, the reaction was found to be complete within 5 min and there was no further increase in peak area ratios after 5 min. A reaction time of 5 min was optimum. The iodo derivatives formed by aromatic amines and their mass spectra obtained by GC–MS are given in Table 1. A probable fragmentation pattern for 4-iodo-*N,N*-dimethylaniline is shown in Scheme 1.

The reaction chemistry was validated by synthesis of 4-iodoaniline under the recommended condition of derivatization. Into a 250 ml beaker, were placed 7 g of freshly distilled aniline,



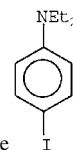
Scheme 1. A probable fragmentation pattern for 4-iodo-*N,N*-dimethylaniline.

Table 1  
Iodo derivatives of aromatic amines and their mass spectra

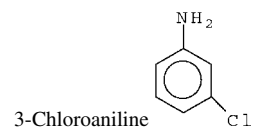
Compd. no.	Amines	Iodo-product	Electron ionization mass spectra of iodo derivative
2	Aniline 	4-Iodoaniline 	
4	<i>N</i> -Methylaniline 	4-Iodo- <i>N</i> -methylaniline 	
5	2-Toluidine 	4-Iodo-2-toluidine 	
6	<i>N,N</i> -Dimethylaniline 	4-Iodo- <i>N,N</i> -dimethylaniline 	
7	2-Chloroaniline 	2-Chloro-4-iodoaniline 	
8	2,6-Dimethylaniline 	4-Iodo-2,6-dimethylaniline 	



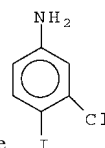
9

4-Iodo-*N,N*-diethylaniline

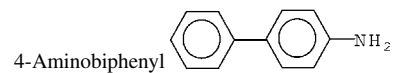
10



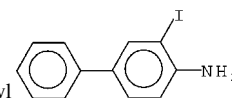
3-Chloro-4-iodoaniline



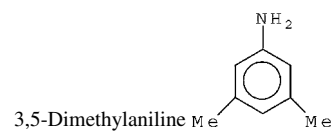
11



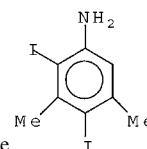
3-Iodo-4-aminobiphenyl



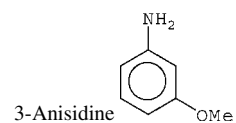
14



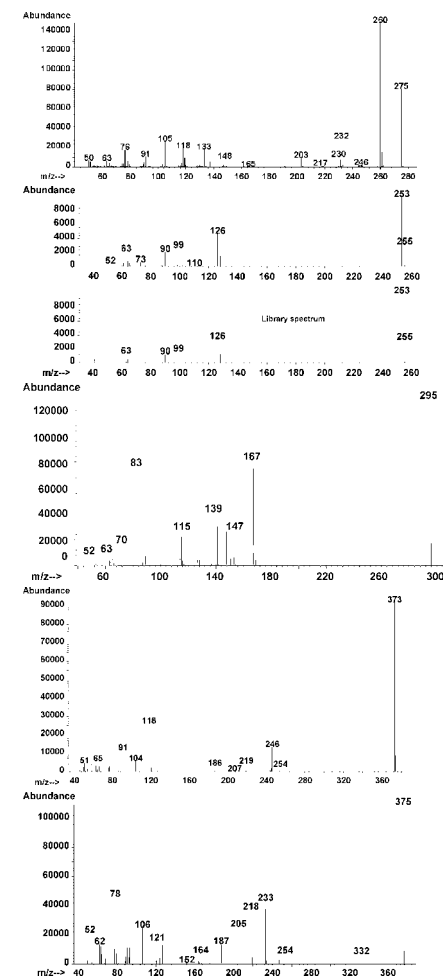
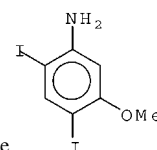
3,5-Dimethyl-4,6-diiodoaniline



15



4,6-Diiodo-3-methoxyaniline



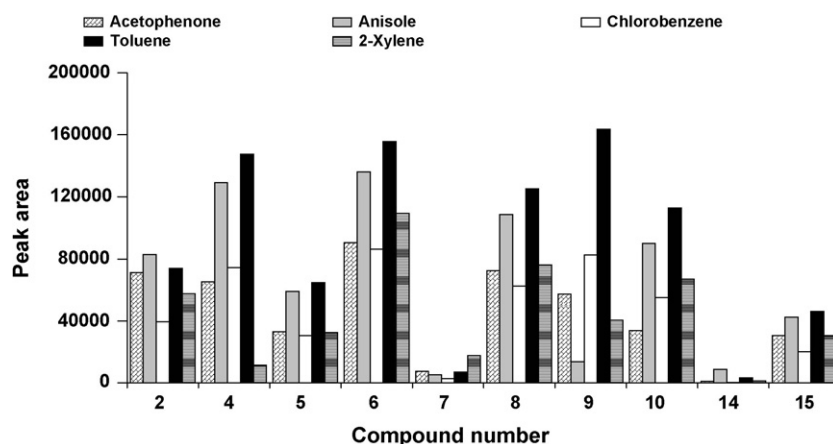


Fig. 2. Effect of different organic solvents on the SDME efficiency. Concentration of analytes:  $100 \mu\text{g l}^{-1}$ ; solvent volume:  $2 \mu\text{l}$ ; solution temperature:  $30^\circ\text{C}$ ; extraction time: 15 min. Compound number as in Fig. 1.

6 g each of potassium dihydrogenphosphate and dipotassium hydrogenphosphate, and 150 ml of deionized water. The mixture was cooled to about  $15^\circ\text{C}$  in ice-bath and stirred well to dissolve the solid and disperse aniline into fine droplets. To the stirred mixture was added 18 g of powdered resublimed iodine in small portions of 2–3 g during a period of 20 min. The stirring was continued for further 15 min by which time the colour of free iodine practically disappeared. The crude 4-iodoaniline was filtered under vacuum, drained and dried in the air. The crude product was mixed with 75 ml of light petroleum, b.p.  $60\text{--}80^\circ\text{C}$ , in a 250 ml round bottomed flask fitted with a water condenser and refluxed for about 15 min. The clear hot solution was decanted into a beaker, placed in a freezing mixture and stirred. The 4-iodoaniline crystallized out almost immediately as colourless needles. The product was filtered, washed with two 5 ml portions of chilled light petroleum and dried in shade. The yield of 4-iodoaniline, m.p.  $63^\circ\text{C}$ , was 12 g (80%). FT-IR,  $3400, 3306 \text{ cm}^{-1}$ , N–H asymmetric and symmetric stretch;  $3198 \text{ cm}^{-1}$ , Fermi resonance band with overtone of  $1620 \text{ cm}^{-1}$ ;  $1620 \text{ cm}^{-1}$ , N–H bending;  $1500 \text{ cm}^{-1}$ , aromatic ring C=C stretch;  $1283 \text{ cm}^{-1}$ , C–N stretch,  $1100 \text{ cm}^{-1}$ , para substituted iodobenzene.

The synthesis yield validated the formation of predicted iodoaniline at higher concentration level. Formation of mono- or poly-iodoanilines was confirmed by the full scanned range of mass spectra of each derivative. Di-iododerivative was found to be formed by 3,5-dimethylaniline and 3-anisidine owing to the ring activation for electrophilic iodination by their substituents, and to the availability of ortho and para positions to these group for iodination reaction. The yields of derivatization reaction for the compounds of interest at investigated concentrations, similar to those found in environmental samples, was determined by comparison of the peak area ratios of the given anilines (after derivatization) to that of the internal standard with those found by using equal molar concentrations of the authentic iodo-anilines. The agreement was in the range 98.2–101.4%, which served to indicate the quantitative nature of the derivatization.

### 3.2. Optimization of extraction

Several parameters which control SDME such as nature of extracting solvent, time, stirring and ionic strength of solution, etc. have been separately evaluated to optimize the extraction condition. Five water immiscible solvents (Fig. 2) were chosen to select the best one for extraction. The data indicated the best extraction recovery obtained for most of the compounds by using toluene. Separate extractions were carried out for duration of 2–20 min; the extraction profiles showed that optimum was attained in 15 min for all amines (Fig. 3). Stability of drop in SDME is important when solution are stirred; in the present work stirring at 300 rpm allowed optimum preconcentration and drop stability. Addition of salt (sodium chloride) has been used in classical solvent extraction to facilitate mass transfer of analyte into the organic solvent. However, in SDME, the relative peak areas of analytes decreased with increase in salt concentration. Similar observations have earlier been reported [31–34] and a plausible explanation given [35].

LPME with organic solvent in the standard flask and withdrawal of microliter portion of extract settled in the flask above the meniscus mark for analysis by GC has previously been used by us as a convenient method of sample preparation [36,37].

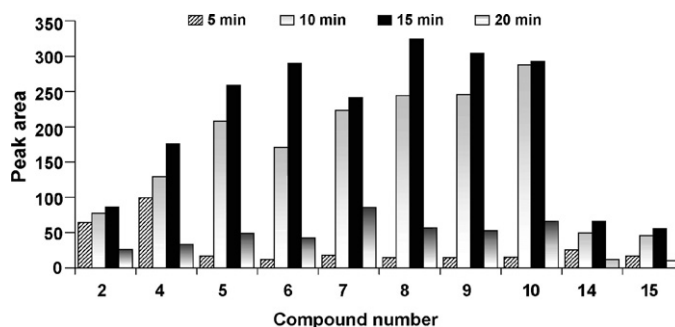


Fig. 3. Effect of extraction time on the SDME efficiency. Concentration of analytes:  $100 \mu\text{g l}^{-1}$ ; solvent volume:  $2 \mu\text{l}$ ; solution temperature:  $30^\circ\text{C}$ . Compound number as in Fig. 1.

Toluene gave optimum extraction in comparison to other solvents as were used in SDME. With conventional 5 ml standard flask, down to 50  $\mu\text{l}$  of solvent could be used conveniently. The peak areas were found to decrease with larger volume of organic solvent. Shaking for 1 min was optimum for complete extraction. Contrary to the SDME, and similar to classical solvent extraction, analyte mass transfer to organic phase is favoured by high salt concentration in this method of LPME. Thus, LPME was robust, rugged and simple extraction method.

### 3.3. Calibration graph and detection limits

The analytical performance of the present method was validated for its linearity, precision and limit of detection. The calibration data and detection limits of aromatic amines in the SDME/GC–FID and LPME/GC–MS, and selected ions used for mass detection and quantification are given in Table 2. Each point of the calibration graph corresponded to the mean value obtained from three independent area measurements, and each calibration graph was constructed with eight concentration levels. The limit of detection ( $S/N=3$ ) was estimated as three times the standard deviation obtained in eight replicate analyses of lowest concentration level in the rectilinear calibration graph. In SDME–GC–FID, the average correlation coefficient was 0.9939 (range 0.9907–0.9990) and average limit of detection  $25 \mu\text{g l}^{-1}$  (range 12–61  $\mu\text{g l}^{-1}$ ), whereas the corresponding values in LPME–GC–MS were, respectively, 0.9953 (range 0.9928–0.9992) and  $33 \text{ ng l}^{-1}$  (range 18–60  $\text{ng l}^{-1}$ ). The higher sensitivity in GC–MS is due to efficiency of both LPME and MS detection.

Stability of solutions is often regarded as part of measure of ruggedness of the method. Standards of amines were analyzed over a period of 3 months, the solutions being stored in freezer when not in use. The peak area ratios were within  $\pm 4\%$  between freshly prepared stock solutions and the aged ones stored at least up to 2 months. Up to 10% changes that were made deliberately on experimental parameters such as iodine concentration, reaction and extraction time, and GC mobile phase flow rate did

not affect the results by more than  $\pm 5\%$ , and this supported the robustness of the method.

### 3.4. Real sample analysis

In order to investigate the applicability of the present SDME method in real sample analysis, determination of amines in sea water, Ganga and Narmada River waters, Jabalpur city tap water and a dye factory effluent samples was performed by standard addition technique. The analytes were added to real water samples at concentration level of  $0.1 \text{ mg l}^{-1}$  and analyzed by GC–FID after derivatization. The recovery results take into account the amounts of amines that were originally present in the sample. The method gave overall recovery of 97% (range 92–104%;  $n=6$ ). The average R.S.D. was found to be 8.1% (range 3.5–14.5%).

Two synthetic food dye stuffs, tartrazine and sunset yellow FCF, were obtained from the local market and the proposed method was applied to determine the presence of free aromatic amines in them. A known quantity of dye stuff, 10 mg, was dissolve in 50 ml of deionized water (acidified with 1 ml of 0.1 M sulfuric acid) and a 5 ml portion of this solution was loaded on a  $\text{C}_{18}$  cartridge (500 mg, Alltech, Deerfield, IL) that was previously activated by passing 5 ml each of methanol and deionized water, and allowed to flow under a mild positive pressure. Thereafter, the sorbent was washed with 1 ml of 0.1 M sulfuric acid; the eluate and washing were combined together and subjected to derivatization and analysis by LPME–GC–MS. The dye stuffs were found to retain strongly on  $\text{C}_{18}$  sorbent whereas aromatic amines could be easily eluted. The free amines (as iodo-derivatives) were identified by their full scan mass spectra. 2-Toluidine ( $5.72 \mu\text{g g}^{-1}$ ; R.S.D., 8.4%) and *N,N*-diethylaniline ( $8.35 \mu\text{g g}^{-1}$ ; R.S.D., 7.5%) were detected in sunset yellow FCF, and 2-toluidine ( $9.84 \mu\text{g g}^{-1}$ ; R.S.D., 7.8%) in tartrazine. Standard addition of detected amine at  $50 \mu\text{g g}^{-1}$  each to the dye stuff produced average recovery of 94.2% (range 89.5–115.8%) with R.S.D. of 8.6% (range 5.5–9.7%).

Table 2  
Calibration data and detection limits in the determination of aromatic amines

	Aromatic amine	SDME–GC–FID			LPME–GC–MS			
		Range ( $\text{mg l}^{-1}$ )	$R^2$	LoD ( $\mu\text{g l}^{-1}$ )	Range ( $\mu\text{g–mg l}^{-1}$ )	$R^2$	LoD ( $\text{ng l}^{-1}$ )	Ions quantitated ( <i>m/z</i> )
1.	4-Chloroaniline	0.05–7	0.9967	28	0.1–8	0.9946	30	92.127
2.	Aniline	0.04–8	0.9948	21	0.1–10	0.9990	25	92.219
3.	3-Nitroaniline	0.05–8	0.9975	25	0.1–8	0.9992	60	92.138
4.	<i>N</i> -Methylaniline	0.05–10	0.9976	61	0.1–10	0.9959	18	106.233
5.	2-Toluidine	0.09–10	0.9929	12	0.1–10	0.9898	19	106.233
6.	<i>N,N</i> -Dimethylaniline	0.09–10	0.9962	21	0.1–10	0.9936	25	119.247
7.	2-Chloroaniline	0.05–9	0.9908	19	0.1–8	0.9968	27	90.253
8.	2,6-Dimethylaniline	0.05–10	0.9990	17	0.1–8	0.9959	28	120.247
9.	<i>N,N</i> -Diethylaniline	0.03–10	0.9907	12	0.1–8	0.9929	25	260.275
10.	3-Chloroaniline	0.05–7	0.9828	50	0.1–7	0.9928	30	126.253
11.	4-Aminobiphenyl	0.09–10	0.9978	25	0.2–9	0.9984	52	167.295
12.	3,5-Dinitroaniline	0.05–10	0.9876	25	0.2–8	0.9956	50	153.183
13.	2,4-Dinitroaniline	0.05–10	0.9985	25	0.2–8	0.9895	55	153.183
14.	3,5-Dimethylaniline	0.09–10	0.9888	32	0.1–10	0.9979	32	118.373
15.	3-Anisidine	0.09–8	0.9969	12	0.1–8	0.9974	30	233.375

#### 4. Conclusions

Broad and tailing peaks, and poor resolution obtained in the GC of aromatic amines have been avoided by nuclear iodination of primary, secondary and tertiary aromatic amines. The iodinated amines, and those which are already having electron withdrawing substituents such as nitro group and chlorine show excellent preconcentration by LPME in toluene. The method is applicable to polluted waters and food dye stuffs. Simplicity of operation, short analysis time and low consumption of solvent are the main advantages of the present technique.

#### Acknowledgement

A.J. thanks the Department of Science & Technology, New Delhi, for the award of a research grant under Women Scientist Scheme (SR/WOS-A/CS-02/2004).

#### References

- [1] P.F. Vogt, J.J. Gerialis, Ullman's Encyclopedia of Industrial Chemistry, Vol. A2, fifth ed., VCH, Weinheim, 1985, p. 37.
- [2] T.S. Scott, Carcinogenic and Chronic Toxic Hazards of Aromatic Amines, Elsevier, Amsterdam, 1962.
- [3] L. Fishbein, Toxicol. Environ. Chem. Rev. 3 (1980) 145.
- [4] F. Sacher, S. Lenz, H.-J. Brauch, J. Chromatogr. A 764 (1997) 85.
- [5] R.M. Riggin, C.C. Howard, Anal. Chem. 51 (1979) 210.
- [6] A. Asthana, D. Bose, A. Durgbanshi, S.K. Sanghi, W.Th. Kok, J. Chromatogr. A 895 (2000) 197.
- [7] C. Patrianakos, D. Hoffmann, J. Anal. Toxicol. 3 (1979) 150.
- [8] C.J. Smith, G.L. Dooly, S.C. Moldoveanu, J. Chromatogr. A 991 (2003) 99.
- [9] G. Palmiotto, G. Pieraccini, G. Moneti, P. Dolora, Chemosphere 43 (2001) 355.
- [10] L.S. DeBruin, J.B. Pawliszyn, P.D. Josephy, Chem. Res. Toxicol. 12 (1999) 78.
- [11] Directive 2002/72/EC of 6 August 2002 relating to plastic materials and articles intended to come into contact with foodstuffs, Official J. Eur. Communities, L 220, 2002, p. 18.
- [12] Directive 2002/61/EC of 19 July 2002 amending for the nineteenth time Council Directive 76/76/EEC relating to restrictions on the marketing and use of certain dangerous substances and preparations (azo colourants), Official J. Eur. Communities, L 243, 2002, p. 15.
- [13] K. Blau, J. Halket (Eds.), Handbook of Derivatives for Chromatography, second ed., Wiley, Chichester, 1993, pp. 31, 131, 157.
- [14] H. Kataoka, J. Chromatogr. A 733 (1996) 19.
- [15] H.-B. Lee, J. Chromatogr. A 457 (1983) 267.
- [16] M. Longo, A. Cavallaro, J. Chromatogr. A 753 (1996) 91.
- [17] K.-J. Chia, S.-D. Huang, J. Chromatogr. A 1103 (2006) 158.
- [18] S. Mishra, V. Singh, A. Jain, K.K. Verma, Analyst 126 (2001) 1663.
- [19] M. Akyuz, S. Ata, J. Chromatogr. A 1129 (2006) 88.
- [20] M. Akyuz, Talanta 71 (2007) 486.
- [21] V. Singh, M. Gupta, A. Jain, K.K. Verma, J. Chromatogr. A 1010 (2003) 243.
- [22] T.C. Schmidt, R. Hass, E. von Low, K. Steinbach, Chromatographia 48 (1998) 436.
- [23] T.C. Schmidt, R. Hass, K. Steinbach, E. von Low, Fresenius J. Anal. Chem. 357 (1997) 909.
- [24] R. Hass, T.C. Schmidt, K. Steinbach, E. von Low, Fresenius J. Anal. Chem. 359 (1997) 497.
- [25] S. Siggia, J.G. Hanna, Quantitative Organic Analysis via Functional Groups, fourth ed., John Wiley, New York, 1979, pp. 57–62, 532, 565–566.
- [26] T.C. Schmidt, M. Less, R. Hass, E. von Low, K. Steinbach, G. Stork, J. Chromatogr. A 810 (1998) 161.
- [27] M. Less, T.C. Schmidt, E. von Low, G. Stork, J. Chromatogr. A 810 (1998) 173.
- [28] J. March, Advanced Organic Chemistry, Reactions, Mechanisms and Structure, fourth ed., John Wiley, New York, 2001, pp. 669, 670.
- [29] K.K. Verma, A.K. Gupta, Anal. Chem. 54 (1982) 249.
- [30] K.K. Verma, A. Jain, S.K. Sanghi, Analyst 112 (1987) 1051.
- [31] K.D. Buchholz, J. Pawliszyn, Anal. Chem. 66 (1994) 160.
- [32] E. Psillakis, N. Kalogerakis, J. Chromatogr. A 907 (2001) 211.
- [33] D.A. Lambropoulou, T.A. Albanis, J. Chromatogr. A 1049 (2004) 17.
- [34] M.C. Lopez-Bianco, S. Blanco-Cid, B. Cancho-Grande, J. Simal-Gandara, J. Chromatogr. A 984 (2003) 245.
- [35] M. Gupta, A. Jain, K.K. Verma, Talanta 71 (2007) 1039.
- [36] A. Jain, R.M. Smith, K.K. Verma, J. Chromatogr. A 760 (1997) 319.
- [37] S. Mishra, V. Singh, A. Jain, K.K. Verma, Analyst 125 (2000) 459.

## Micropumping multicommutation turbidimetric analysis of waters

Eva Ródenas-Torralla<sup>a</sup>, Ángel Morales-Rubio<sup>a,\*</sup>, André F. Lavorante<sup>a,1</sup>,  
Boaventura Freire dos Reis<sup>b</sup>, Miguel de la Guardia<sup>a</sup>

<sup>a</sup> *Departamento de Química Analítica, Universitat de València, 50 Dr. Moliner St., 46100 Burjassot, Valencia, Spain*

<sup>b</sup> *Department of Analytical Chemistry, Centre for Energy Nuclear in Agriculture,  
University of Sao Paulo, P.O. Box 96, 13400-970 Piracicaba, Brazil*

Received 2 February 2007; received in revised form 27 April 2007; accepted 30 April 2007

Available online 22 May 2007

### Abstract

A micropumping multicommutation manifold to perform turbidity determinations in waters is described. The procedure is based on the use of a combination of hydrazine sulfate and hexamethylenetetramine, to obtain an external standard of nephelometric turbidity units (NTU), which could compare the absorbance measurements at high wavelengths for samples with a calibration line obtained from a concentrated formazine standard diluted on-line. To minimize sample and reagent consumption and waste generation, the flow system was designed with two solenoid micro-pumps, one of them for the alternative introduction of the formazine standard and samples and the other one for the water carrier. The multicommutation approach makes possible the on-line dilution of a single standard to obtain the external calibration. The linear response was ranged up to 160 NTU. The coefficient of variation was estimated as 1.6 and 3.2% for 10 and 100 mm flow cell, respectively, for solutions containing 40 NTU ( $n = 10$ ). Approximately, 60 determinations can be carried out per hour with limit of detection values of 1 and 0.1 NTU, consuming only 160 or 240  $\mu\text{L}$  formazine solution and generating 1.8 or 2.0 mL waste per determination, using measurement cells of 10 and 100 mm optical pathlength, respectively. The procedure was successfully applied to 11 different water samples. Recovery studies were carried out and results obtained were between  $97.5 \pm 0.2$  and  $100 \pm 1\%$ . The development of a homebuilt light emitting diode (LED)-based portable flow analysis instrument was checked for in situ turbidimetric measurements, providing this equipment a LOD value of 0.09 NTU working with a blue LED at 464 nm and a LOD value of 0.1 NTU working with an IR LED.

© 2007 Elsevier B.V. All rights reserved.

**Keywords:** Multicommutation; Solenoid micro-pump; Turbidimetry; Long optical pathway; Light emitting diode-based photometer

### 1. Introduction

Turbidity analysis is an optical measurement of scattered light. When light is passed through a water sample, particles in the light path change the direction of the light, scattering it and decreasing the incident radiation to the detector. If the turbidity is low, most of the light will continue in the original direction. Light scattered by particles allows the particles to be detected in water, just as sunlight can illuminate dust particles in the air.

In 2002, the EPA published the LT1ESWTR (Long Term 1 Enhanced Surface Water Treatment Rule) mandating that turbidities in combined filtered effluents must read at or below 0.3

nephelometric turbidity units (NTU) [1–3]. To achieve the EPA's goal, constant turbidity monitoring of filtered water is critical. This monitoring is often accomplished with the use of on-line turbidity meters at water treatment plants and with specially designed portable instruments in the field [4].

Turbidimetric methods are widely used in water analysis and for the control of treatment processes. Moreover, the concentration of a variety of ions can be determined using suitable precipitation reagents to form suspensions [5]. Sulfate determination through turbidity measurements has been made in waters, wines and plant digests, by using flow injection analysis (FIA) [6,7], sequential injection analysis (SIA) [8–10], multicommutated flow injection analysis (MCFIA) [11] and monosegmented flow (MSFA) [12].

On the other hand, turbidimetric measurements have been used to locate potential precipitants in soft drinks and alcoholic beverages [13,14], in waters [9,15] and as an environmental analytical tool to measure suspended solids in waters [16,17].

\* Corresponding author. Tel.: +34 96354399734; fax: +34 963544838.

E-mail address: [angel.morales@uv.es](mailto:angel.morales@uv.es) (Á. Morales-Rubio).

<sup>1</sup> Present address: Departamento de Química Fundamental, Universidade Federal de Pernambuco, Rua Luiz Freire, s/n, CEP 50740-550, Recife-PE, Brazil.

They have been also used to measure suspended particles in gases, like smog and fog [18]. Even turbidity analysis is becoming the method of choice for biomass determination in order to alert against emerging pathogens such as *Cryptosporidium* and *Giardia* [19].

Turbidimetry has been widely used as detection method in flow analysis. Although FIA is the most widely used technique, there are three papers in the literature which use multicommution to implement methods for determining the turbidity of solutions [11,12,16]. However, two of these papers made a turbidimetric determination of sulfate [11,12] and the other one used a dye solution, prepared by dissolving bromocresol green in disodium tetraborate solution [16]. Nevertheless, in our best knowledge, there is a lack of compact low-cost systems which could be used for fully mechanized control of water turbidity, and in fact not any paper of multicommution which uses formazine solution to make turbidimetric analyses was found.

In the present paper, it has been developed a micropumping multicommuted strategy to made turbidity measurements using two different cells of 10 and 100 mm optical pathway length. Solenoid micro-pumps were employed to minimize reagent consumption and waste generation. Turbidity was determined at 464 nm and data for samples were calibrated based on the absorbance of a concentrated formazine standard solution diluted on-line. Finally, the portable flow analysis light emitting diode (LED)-detector described in earlier studies for in situ spectrophotometric measurements [20] was adapted to do the turbidimetric measurements.

## 2. Experimental

### 2.1. Apparatus

The flow system comprised two solenoid micro-pumps Biochem 090SP with a nominal volume of 8  $\mu\text{L}$  per pulse (Boonton, NJ, USA), flow lines of 0.8 mm i.d. PTFE tubing and a Y-confluence connector made on acrylic. A Pentium 133 MHz microcomputer was employed for system controlling by a parallel interface through a software written in Quick Basic. A lab-made electronic interface, analogous to that previously described [21,22], was used to generate the electric potential and current required to switch the solenoid micro-pumps (12 V, *ca.* 100 mA). Measurements were made with a Hewlett-Packard Model 8452A diode array spectrophotometer equipped with a 10 mm optical path and 50  $\mu\text{L}$  inner volume flow cell (Waldbronn, Germany) and a homemade 100 mm long path and 315  $\mu\text{L}$  inner volume flow cell.

The compact homemade LED photometer employed was described in detail by Ródenas-Torralba et al. [20], being used as light source an infrared LED (>800 nm) and alternately four visible LEDs of blue ( $\lambda = 464$  nm), yellow ( $\lambda = 512$  nm), green ( $\lambda = 562$  nm) and red ( $\lambda = 650$  nm) color.

### 2.2. Reagents and solutions

All solutions were prepared with deionized water (18.2 M $\Omega$  cm) and analytical grade chemicals. A 4000 NTU formazine

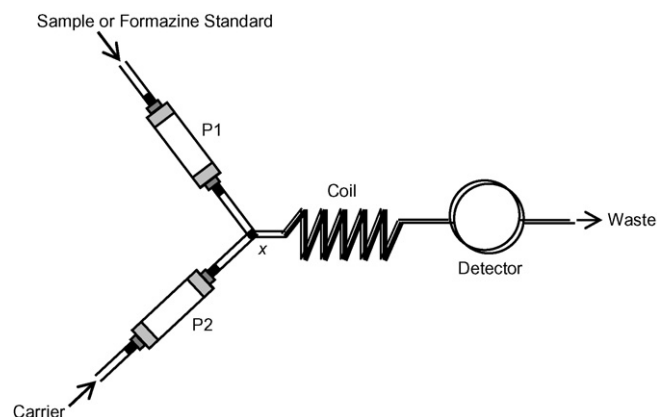


Fig. 1. Multicommuted flow system employed for the turbidimetric measurements. P1 and P2—solenoid micro-pumps; LED detector; x—confluence point.

stock suspension was prepared by mixing equal volumes of 10,000  $\mu\text{g mL}^{-1}$  hydrazine sulfate solution,  $\text{N}_2\text{H}_4\text{H}_2\text{SO}_4$ , and 100,000  $\mu\text{g mL}^{-1}$  hexamethylenetetramine,  $(\text{CH}_2)_6\text{N}_4$ , both from Aldrich (Steinheim, Germany). After that, the mixture was let to stand for 48 h at 24–26  $^\circ\text{C}$  in a topaz bottle before the measurements at 710 nm. Deionized water was used as a carrier.

Eleven water samples from different origin like puddle, tap, heating bath, radiator and waste were analyzed. Tap water samples were obtained from Burjassot and Valencia cities, in Spain.

### 2.3. Flow procedure

The flow system manifold was designed employing two solenoid micro-pumps, which were assembled to allow the handling of two solutions: P1 for formazine stock standard or sample solutions and P2 to introduce a carrier deionized water flow.

When the solenoid of a micro-pump was energized (ON) a sucking action was carried out, thus permitting the solution insertion into the micro-pump chamber through the input channel. When the applied voltage was turned OFF, the inner diaphragm go back to rest position and the fluid was dispensed through the output channel.

The solenoid micro-pumps were arranged as shown in Fig. 1, employing one device for each solution handled, during 0.1 s ON and 0.1 s OFF. This 0.1 s/0.1 s (ON/OFF) sequence means that the 8  $\mu\text{L}$  internal volume of the micropumps was filled in 0.1 s (ON) and emptied in 0.1 s (OFF). The devices were operated at 5 Hz.

The multicommuted system was operated as described in Table 1. Samples were introduced into the manifold through micropump P1 and diluted 1:1 with deionized water using micropump P2 till to obtain an enough volume to fill the measurement cell. After that, micropump was energized alone to transport the sample plugs to the detector and to wash the measurement cell. Each step was repeated until to complete the number of pulses.

Forty and sixty total pulses of sample plus deionized water (step 1) were enough to obtain stable measurements of 1:1 dispersed samples using the 10 and 100 mm length cell, respectively. Sample zone was transported by 200 or 250 pulses of

Table 1  
Solenoid micro-pumps switching course for turbidimetric measurements<sup>a</sup>

Step	Description	P1	P2	Total pulses
1	Sample or formazine standard introduction Deionized water introduction	ON/OFF OFF	OFF ON/OFF	40/60 <sup>b</sup>
2	Transport to the detection cell and system washing	OFF	ON/OFF	200/250 <sup>c</sup>
3	Cleaning	ON/OFF	OFF	Variable <sup>d</sup>
4 <sup>e</sup>	Standardization using stock formazine solution	ON/OFF OFF	OFF ON/OFF	40/60 <sup>b</sup>

<sup>a</sup> ON/OFF indicate a 0.1 s/0.1 s pulse of the solenoid micro-pump.

<sup>b</sup> 40 or 60 pulses depending on the cell employed, 10 or 100 mm, respectively.

<sup>c</sup> 200 or 250 pulses depending on the 10 or 100 mm optical pathway cell, respectively.

<sup>d</sup> The number of pulses for cleaning the tube of sample or standard in each case is variable and is made after three replicate measurements of the same solution.

<sup>e</sup> For standardization two alternative strategies could be followed: (i) the insertion of 40/60 pulses of standards of different concentration of formazine and water in a 1 pulse P1 + 1 pulse P2 sequence or (ii) the on-line dilution of a 200 NTU formazine standard using 1:1, 1:2, 1:3, 1:4, 1:5, 2:3 dilution through the use of 1 pulse P1 + 1 pulse P2, 1 pulse P1 + 2 pulse P2, 1 pulse P1 + 3 pulse P2, 1 pulse P1 + 4 pulse P2, 1 pulse P1 + 5 pulse P2, 2 pulse P1 + 3 pulse P2, till to reach a total number of 40/60 pulses.

carrier water towards the detector where transient signal measurements were made (step 2). After obtaining three replicates of each sample it was introduced a cleaning step (step 3) throughout the activation of micro-pump P1. With the new sample or the standard, the cleaning step was made after every three measurements of the same solution in order to avoid cross contamination between samples and to avoid memory effects. Turbidity measurements were established at 464 nm wavelength and no correction of the baseline was necessary.

For calibration, it can be made alternatively two strategies: (i) the introduction of 40/60 total pulses of formazine standards of different concentration following the same sequence described for samples introduction or (ii) the on-line dilution of a 200 NTU stock standard formazine solution.

In the second case, a 4th step different pulses of P1 and P2 in 1:1, 1:2, 1:3, 1:4, 1:5 and 2:3 relationship allowed the dispersion through the coil of the stock standard in order to obtain the appropriate calibration line. In fact, 1 pulse P1 + 1 pulse P2, 1 pulse P1 + 2 pulse P2, 1 pulse P1 + 3 pulse P2, 1 pulse P1 + 4 pulse P2, 1 pulse P1 + 5 pulse P2, 2 pulse P1 + 3 pulse P2, were repeated as new sequences to reach the different NTU levels.

#### 2.4. Batch reference procedure

Independent solutions of different formazine standard concentration (up to 1000 NTU) were directly introduced into the 10 mm spectrophotometric cell and absorbance measurements were made at 710 nm by using the diode array spectrophotometer. Samples were measured in the same way as standards and data interpolated in the external calibration line.

### 3. Results and discussion

#### 3.1. Stability of formazine standards

Fig. 2 shows the intervals of time in which the different concentrations of formazine solutions could be employed for turbidimetric measurements. As can be seen, formazine solutions from 0.1 to 4 NTU were only stable for 1 day, from 6 to

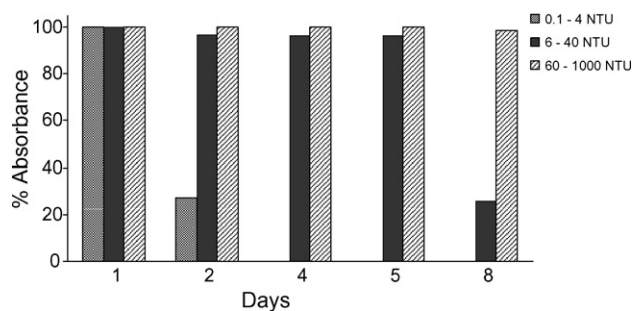


Fig. 2. Study of the stability of different formazine standard solutions.

40 NTU were stable for 5 days and from 60 to 1000 NTU were stable at least for a week. So, it can be concluded that the use of a single concentrate, and high stable, formazine standard solution could be the best strategy to establish the appropriate calibration line by on-line dilution, confirming the potentiality of the multicommutation systems for in-line standards preparation [23].

#### 3.2. Effect of sampling cycles

Fig. 3 shows the effect of the number of sample pulses on the signal response. As can be seen, after a linear response till

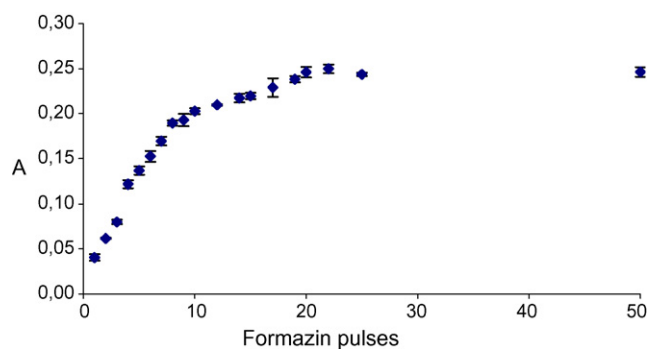


Fig. 3. Effect of pulses on absorbance signal. Experimental conditions using a 10 mm optical path flow cell, 150 cm coil length, 0.1 s/0.1 s (ON/OFF), 1:1 relation between formazine:H<sub>2</sub>O and 200 NTU formazine concentration. Each pulse corresponds to 8  $\mu$ L volume.

10 formazine pulses it happens a lost of linear response with the increasing of number of pulses, as reported before in several studies [24,25]. Twenty pulses were selected as the most suitable volume to achieve the maximum sensitivity in a shorter as possible period of time and using the measurement cell of 10 mm optical path length, thus involving a total of 40 alternative pulses of P1 and P2.

### 3.3. Analytical features

Table 2 shows the analytical features of the different procedures assayed. Multicommutation procedure using a 10 mm flow injection cell provides calibration equations of the same order than the batch mode. Nevertheless, multicommutation using a 100 mm cell increases the sensitivity 4.4 times. The best alternative was the on-line standard dilution, reducing the linear range up to 160 NTU. For the external calibration by on-line dilution, a formazine standard of 200 NTU was introduced by using the 1:1, 1:2, 1:3, 1:4, 1:5 and 2:3, dilutions between standard and water throughout alternating the sequence of different number of pulses though P1 and P2 micro-pumps to build the whole calibration line. Moreover, this proposed method reduces the formazine consumption and the waste volume to 1.8 mL, maintaining other analytical features like limit of detection LOD, repeatability established for the relative standard deviation R.S.D. and sampling throughput. Therefore, it can be concluded that multicommutation approach using an on-line standard dilution offers a sustainable alternative to the batch method in terms of reagents consume and solutions handling by the operator. Nevertheless, multicommutation with a 100 mm cell provides a LOD of *ca.* 0.1 NTU, 10 times better than the batch one using 10 mm cell, and a R.S.D. of 3.2%.

### 3.4. Analysis of samples

The proposed procedure was applied to the turbidity analysis of 11 water samples and results are shown in Table 3. The correlation between data obtained by multicommutation (10 mm cell) procedure ( $y$ ) and batch measurements ( $x$ ) provided an equation  $y = (1.00 \pm 0.01)x + (0.04 \pm 0.05)$ , with a correlation coefficient of 0.9991. The correlation between multicommutation (100 mm cell) ( $z$ ) and batch procedure ( $x$ ) provided an equation  $z = (1.00 \pm 0.01)x + (0.05 \pm 0.05)$ , with a correlation coefficient of 0.9991, and the correlation between multicommutation using on-line standard dilution (10 mm cell) ( $w$ ) and batch procedure ( $x$ ) provided an equation  $w = (1.00 \pm 0.01)x + (-0.01 \pm 0.04)$ , with a correlation coefficient of 0.9998, thus evidencing the good comparability of all approaches and confirming the validity of the multicommutation procedure in front of the in batch measurements. Student's  $t$  calculated values for the slopes (0.0, 0.0 and 0.0) and for the intercepts (0.8, 1.0 and 0.25) was in all cases lower than the theoretical  $t$  value (1.734) for a 95% probability level and 18 degree freedom. It can be concluded that the accuracy of the developed procedure is comparable to that found in-batch on using the same reaction and in multicommutation flow analysis.

Table 2  
Comparison of the analytical features achieved by the proposed method (10 and 100 mm flow cell) and batch procedure for turbidimetric measurements in water samples

	Batch mode 10 mm cell		Multicommutation 10 mm flow cell		Multicommutation 100 mm flow cell	
	Direct analysis		Direct analysis		Direct analysis	
	Linear range (NTU)	Calibration equation	Linear range (NTU)	Calibration equation	Linear range (NTU)	Calibration equation
	0–1000	$y = (0.00158 \pm 0.00001)x + (0.001 \pm 0.003)$	0–1000	$y = (0.001685 \pm 0.000008)x + (0.0017 \pm 0.0005)$	0–1000	$y = (0.0074 \pm 0.00003)x + (0.002 \pm 0.001)$
$R$	0.9996		0.99995		0.997	
LOD (NTU)	1.0		1.0		0.1	
R.S.D. (%) <sup>a</sup>	1.6		1.6		3.2	
Working range (NTU)	0–8		0–8		0–8	
Calibration equation	$y = (0.0019 \pm 0.00002)x + (0.001 \pm 0.002)$		$y = (0.00157 \pm 0.000008)x + (0.002 \pm 0.003)$		$y = (0.008 \pm 0.001)x + (0.001 \pm 0.001)$	
$R$	0.9994		0.9998		0.9994	
LOD (NTU)	1.1		1.0		0.15	
R.S.D. (%) <sup>b</sup>	1.8		1.6		2.9	
Injection frequency (h <sup>-1</sup> )	60		60		60	
Sample rate (h <sup>-1</sup> )	18		18		18	
Waste volume (mL) <sup>c</sup>	4		1.8		2.0	
Hydrazine sulfate (mg) <sup>d</sup>	16.61		0.66		0.997	
Hexamethylenetetramine (mg) <sup>d</sup>	166.10		6.64		9.966	

<sup>a</sup> Data obtained for a standard of 40 NTU ( $n = 10$ ).

<sup>b</sup> Data obtained for a standard of 5 NTU ( $n = 10$ ).

<sup>c</sup> Per determination.

<sup>d</sup> Per calibrate prepared: sum of the amount of each standard, including replicates, employed.

<sup>e</sup> It was employed a standard of 200 NTU.



Table 3  
Determination of turbidity in water samples

	Batch (NTU)	Multicommutation (NTU)	
		10 mm cell	100 mm cell
Tap water Burjassot	<LOD	<LOD	0.20 ± 0.08
Tap water Valencia	<LOD	<LOD	0.10 ± 0.05
Puddle water	1.0 ± 0.1	1.1 ± 0.1	1.1 ± 0.1
Heating bath water	4.9 ± 0.1	5.11 ± 0.09	5.1 ± 0.2
Radiator water 1	4.31 ± 0.09	4.2 ± 0.1	4.2 ± 0.2
Radiator water 2	4.72 ± 0.08	4.6 ± 0.1	4.8 ± 0.1
Radiator water 3	3.1 ± 0.1	3.1 ± 0.1	3.1 ± 0.1
Waste water 1	5.55 ± 0.05	5.6 ± 0.1	5.5 ± 0.2
Waste water 2	<LOD	<LOD	<LOD
Waste water 3	3.0 ± 0.1	3.0 ± 0.2	3.2 ± 0.1
Waste water 4	3.9 ± 0.1	3.9 ± 0.2	3.9 ± 0.1

Mean values and standard deviation of  $n = 3$  independent analysis.

On the other hand, Table 4 shows the recovery studies made on the Burjassot tap water samples spiked with known amounts of formazine solution corresponding to 10–150 NTU. It can be observed that recovery values between 96.8 and 101% were found for all the different approaches tested.

### 3.5. Development of a low-cost LED-based turbidimeter

Based on our previous experience on developing a low-cost LED-based spectrophotometer [20] and incorporating to the aforementioned equipment the multicommutation set-up described before and the long path length cell, it has been evaluated the use of different color LEDs and IR LED for turbidity measurements.

As it can be seen in Table 5, similar figures of merit than those obtained with a spectrophotometer were obtained using a LED photometer.

On comparing the analytical features obtained as a function of the LED wavelength it can be concluded that the best sensitivity was obtained on using the blue LED. However, LOD and R.S.D. values found were of the same order for all the LEDs assayed. So, and in order to avoid interferences for the water color, the use of high wavelength LEDs and specially that of IR emitting light can be recommended.

## 4. Conclusions

Multicommutation offers a sustainable and environmentally friendly alternative to the previously proposed methods for

Table 4  
Recovery values ( $n = 3$ ) for turbidimetric measurements in Burjassot tap water using both, the batch and the multicommutation methods

Spiked level (NTU)	Recovery %		
	Batch	Multicommutation	
		10 mm cell	100 mm cell
10	101 ± 1	100 ± 1	99.1 ± 1
50	97.5 ± 1.0	97.5 ± 0.2	96.8 ± 0.9
100	99.6 ± 0.4	98.8 ± 0.1	99.5 ± 0.9
150	99.0 ± 0.8	99.2 ± 0.1	98.5 ± 0.9

Table 5  
Analytical features of the LED-based turbidimeter as a function of the specific light source employed

	Light source			
	Blue LED 464 nm	Yellow LED 512 nm	Green LED 562 nm	Red LED 650 nm
Linear range (NTU)	0–25	0–25	0–25	0–25
Calibration equation	$y = (0.0090 \pm 0.0001)x + (0.002 \pm 0.002)$	$y = (0.0040 \pm 0.0001)x + (0.0019 \pm 0.0007)$	$y = (0.0069 \pm 0.0001)x + (0.0023 \pm 0.0004)$	$y = (0.0042 \pm 0.0001)x + (0.0049 \pm 0.0008)$
R	0.9995	0.9994	0.9998	0.9997
LOD (NTU)	0.09	0.13	0.11	0.11
R.S.D. (%) <sup>a</sup>	1.0	1.5	2.0	2.0

Experiment conditions: a 100 mm length cell and the multicommutation conditions included in the text for spectrophotometric measurements.

<sup>a</sup> Data obtained for a standard of 5 NTU ( $n = 10$ ).

turbidity measurements in waters, reducing the reagent consumption and waste generation.

Moreover, multicommutation permitted us to do the on-line dilution from one formazine standard, avoiding the manipulation of solutions and their contact with the operator and providing sustainable environmental results.

Additionally, multicommutation using a 100 mm optical pathway cell can allow reducing the limit of detection and to increase the sensitivity.

The incorporation of a LED-based photometer as detector provides low cost and portable equipment with a total weight circa 3 kg and which can be fed by 12 V batteries thus offering a cheap and sustainable alternative to instruments and methods availables.

### Acknowledgements

Authors acknowledge the financial support from The Ministerio de Educación, Cultura y Deporte ref. PHB2002-0054-PC, from CAPES/MECD (Brazil) process number 042/03 and CAPES/MECD (proc. BEX 0211/06-0) for grant to André F. Lavorante.

### References

- [1] U.S. EPA, Long Term 1 Enhanced Surface Water Treatment Rule, Final Rule, 40 CFR Part 9, 141 and 142, Vol. 67, No. 9, EPA 815-z-02-001, January 14, 2002, p 1814.
- [2] U.S. EPA, Methods for Chemical Analysis of Water and Wastes, Method 180.1, Determination of Turbidity by Nephelometry, Rev 2, Cincinnati, OH, August 1993.
- [3] International Standards Organization, Water Quality–Determination of Turbidity, ISO 7027, Geneva, Switzerland, 1999.
- [4] [http://www.process-controls.com/Metex/HF\\_Scientific/micro\\_200\\_industrial\\_turbidimeter.htm](http://www.process-controls.com/Metex/HF_Scientific/micro_200_industrial_turbidimeter.htm).
- [5] I.P.A. Morais, I.V. Tóth, A.O.S.S. Rangel, Spectrosc. Lett. 39 (2006) 547.
- [6] J.F. Van Staden, Fresenius J. Anal. Chem. 310 (1982) 239.
- [7] F.J. Krug, E.A.G. Zagatto, B.F. Reis, O. Bahia, A.O. Jacintho, S.S. Jorgensen, Anal. Chim. Acta 145 (1983) 179.
- [8] J.F. Van Staden, R.E. Taljaard, Anal. Chim. Acta 331 (1996) 271.
- [9] I.P.A. Morais, M.R.S. Souto, T.I.M.S. Lopes, A.O.S.S. Rangel, Water Res. 37 (2003) 4243.
- [10] H.R. Silva, M.A. Segundo, A.O.S.S. Rangel, J. Braz. Chem. Soc. 14 (2003) 59.
- [11] J.A. Vieira, B.F. Reis, E.A.M. Kronka, A.P.S. Paim, M.F. Giné, Anal. Chim. Acta 366 (1998) 251.
- [12] J.A. Vieira, I.M. Raimundo, B.F. Reis, Anal. Chim. Acta 438 (2001) 75.
- [13] N.E. Llamas, M.S. Di Nezio, M.E. Palomeque, B.S.F. Band, Anal. Chim. Acta 539 (2005) 301.
- [14] T. Zhao, J.Y. Zhang, X.G. Cheng, X.G. Chen, Z.D. Hu, J. Agric. Food Chem. 52 (2004) 3688.
- [15] P.J. Barter, T. Deas, New Zealand J. Mar. Freshwater Res. 37 (2003) 485.
- [16] M. Hulsmann, M. Bos, W.E. Van der Linden, Anal. Chim. Acta 324 (1996) 13.
- [17] J. Hodge, B. Longstaff, A. Steven, P. Thornton, P. Ellis, I. McKelvie, Mar. Pollut. Bull. 51 (2005) 113.
- [18] J.N.G. Paniz, E.M.M. Flores, V.L. Dressler, A.F. Martins, Anal. Chim. Acta 445 (2001) 139.
- [19] [http://www.warws.com/Downloads/Turbidiy.article.REV\\_10.pdf](http://www.warws.com/Downloads/Turbidiy.article.REV_10.pdf). Consulted September 2006.
- [20] E. Ródenas-Torralba, F.R.P. Rocha, B.F. Reis, A. Morales-Rubio, M. de la Guardia, J. Autom. Meth. Manage. Chem. 2006 (2006) 1.
- [21] F.R.P. Rocha, E. Ródenas-Torralba, A. Morales-Rubio, M. de la Guardia, Anal. Chim. Acta 547 (2005) 204.
- [22] B.F. Reis, M.F. Giné, E.A.G. Zagatto, J.L.F.C. Lima, R.A.S. Lapa, Anal. Chim. Acta 293 (1994) 129.
- [23] F.R.P. Rocha, C.M.C. Infante, W.R. Melchert, Spectrosc. Lett. 39 (2006) 651.
- [24] E. Ródenas-Torralba, A. Peláez-Hernández, C. Morales-Rubio, A. Morales-Rubio, M. de la Guardia, Spectrosc. Lett. 39 (2006) 683.
- [25] E. Ródenas-Torralba, B.F. Reis, A. Morales-Rubio, M. de la Guardia, Talanta 66 (2005) 591.

# Laser induced-thermal lens spectrometry after cloud point extraction for the determination of trace amounts of rhodium

N. Shokoufi, F. Shemirani\*

*Department of Analytical Chemistry, Faculty of Chemistry, University College of Science,  
The University of Tehran, P.O. Box 14155-6455, Tehran, Iran*

Received 1 January 2007; received in revised form 18 April 2007; accepted 19 April 2007  
Available online 27 April 2007

## Abstract

A new combination method, employing thermal lens spectrometry (TLS) after cloud point extraction (CPE), has been developed for the preconcentration and determination of rhodium. TLS and CPE methods have good matching conditions for the combination because TLS is a suitable method for the analysis of low volume samples obtained after CPE.

Rhodium was complexed with 1-(2-pyridylazo)-2-naphthol (PAN) as a complexing agent in an aqueous medium and concentrated by octylphenoxypolyethoxyethanol (Triton X-114) as a surfactant. After the phase separation at 50 °C based on the cloud point extraction of the mixture, the surfactant-rich phase was dried and the remaining phase was dissolved using 20  $\mu\text{L}$  of carbon tetrachloride. The obtained solution was introduced into a quartz micro cell and the analyte was determined by laser induced-thermal lens spectrometry (LI-TLS). The single laser TLS was used as a sensitive method for the determination of Rhodium-PAN complex in 20  $\mu\text{L}$  of the sample. Under optimum conditions, the analytical curve was linear for the concentration range of 0.5–50  $\text{ng mL}^{-1}$  and the detection limit was 0.06  $\text{ng mL}^{-1}$ . The enhancement factor of 450 was achieved for 10 mL samples containing the analyte and relative standard deviations were lower than 5%. The developed method was successfully applied to the extraction and determination of rhodium in water samples.

© 2007 Elsevier B.V. All rights reserved.

**Keywords:** Thermal lens spectrometry; Cloud point extraction; Rhodium; Laser

## 1. Introduction

The use of surfactants in analytical chemistry provides a lot of possibilities [1,2]. Separation and preconcentration based on the cloud point extraction emerges as an important practical technique. Aqueous solutions of most non-ionic surfactants possess the ability to decrease their solubility rapidly and become turbid when they are heated above a temperature called the cloud point temperature ( $t_c$ ) [3,4]. For higher temperatures (above  $t_c$ ) two distinct phases are formed; one consisting of almost the entire surfactant and the other containing a small portion equal to the critical micellar concentration (cmc) [5,6]. The mechanism of this separation is attributed to the rapid increase in the aggregation number of the surfactant's micelles due to an increase in the temperature [7,8]. During their formation, the surfactant micelles have proved to entrap several hydrophobic

substances, isolating them from the bulk aqueous solution [5,9]. The centrifugation and decantation of the aqueous phase can easily separate the two phases. The species that can interact with micellar systems either directly or after being derivatized, become concentrated in a small volume of the surfactant-rich phase which can subsequently be analyzed using analytical systems such as AAS, ETAAS, ICP, GC, HPLC, CE and spectrophotometry [10–16].

Spectrophotometric methods are the most commonly used techniques and continue to enjoy wide popularity. The common availability of the instrumentation, the simplicity of the procedures, speed, precision and accuracy of the technique still make spectrophotometric methods attractive. The spectrophotometric analysis has been used for cloud point extraction of trace metal ions such as Zn, Cd, Cu, Ni [17,18], U [19,20], Er [21], Gd [22], Al [23] and Co [24].

Thermal lens spectrometry as an indirect spectrophotometry has many advantages over direct spectrophotometry such as high sensitivity, low volume analysis and organic solvent enhancement effect. The thermal lens effect has been success-

\* Corresponding author.

E-mail address: [shemiran@khayam.ut.ac.ir](mailto:shemiran@khayam.ut.ac.ir) (F. Shemirani).

fully applied to the spectrometric measurement of trace amounts of analytes [25–28]. The absorption of the laser beam with Gaussian profile by the analyte produces temperature gradient in sample. This temperature gradient leads to the refractive index gradient that corresponds to the formation of thermal lens in solution. The strength of the lens is determined by its effect on the divergence of the same laser beam [26] or on the divergence of a second laser beam [28]. A steady-state condition is obtained when the rate of laser heating equals the rate of heat loss due to the thermal conductivity of the solvent and the finite temperature rise. The build-up of the lens can take place on time scales from tens of microseconds to hundreds of milliseconds, depending on the thermo-optical properties of the solvent and the radius of the laser beam through the sample [25,29]. Thermal lens takes time to develop into its full strength of thermal effect in solution (steady-state) [30], afterwards the thermal lens effect needs some time to relax in the solution [31]. The maximum signal is obtained when the steady-state condition is applied.

The lack of tunability of the laser source precludes the measurement of spectra, therefore the selectivity of a method must be provided by chemical means, e.g., chromogenic reaction or separation technique, while the thermal lens apparatus acts as a sensitive, quantitative system.

The aim of this research is to combine thermal lens spectrometry, as a high sensitive method, with cloud point extraction for determination of rhodium. This combination is favorable because TLS is a suitable determination method for low volume of the remained phase obtained after CPE and for organic solvents used to dissolve the remaining analyte phase. Furthermore, we would like to use low power laser, discrete wavelength and continuous-wave lasers because lasers of this type are inexpensive and accessible. In this work, we used thermal lens spectrometry after cloud point extraction in order to determine rhodium for the first time.

Rhodium is present at about  $0.001 \mu\text{g mL}^{-1}$  in the crust of the earth. Rhodium metal is known for its stability in corrosive environments, physical beauty and unique physical and chemical properties. Recent interest in the medical and industrial significance of rhodium has been accompanied by an increasing interest in determination at low levels. The determination of rhodium has been studied in different techniques and samples [32,33]. Spectrophotometric determination of rhodium with PAN in organic solvent was previously reported [34]. Rhodium(III) reacts with PAN as a  $\text{ML}_2$  water-insoluble complex.

In the present work, we report on the results obtained for the preconcentration and determination of rhodium by CPE/LI-TLS. The proposed method was applied to the determination of rhodium in water samples.

## 2. Experimental

### 2.1. Thermal lens spectrometer setup

A single laser thermal lens spectrometer was designed and developed in our laboratory (Fig. 1). The He–Ne laser (632.8 nm, 5 mW,  $\text{TEM}_{00}$ ) was used as pump/probe source. The laser beam

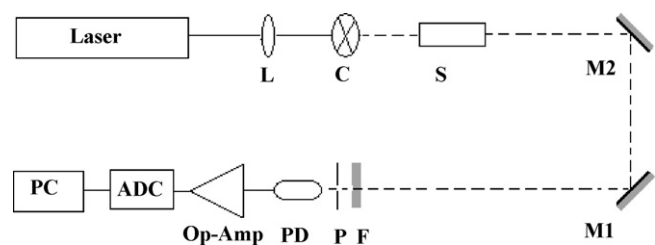


Fig. 1. Schematic diagram of single-laser thermal lens spectrometer: L, lens; C, chopper; S, sample microcell; M1 and M2, mirror; F, filter; P, pinhole; PD, photodetector; Op-Amp, operational amplifier; ADC, analog digital converter; PC, personal computer.

was focused by an 18 cm focal length lens and passed through the cylindrical microcell located at the confocal distance. The laser beam was allowed to irradiate the sample and blocked using a chopper with an electronic controller. After filtration, the beam intensity change was measured through 1 mm pinhole with a photo-detector that was located at a 2 m distance from the sample cell. The output signal from the photo-detector was amplified by an operation amplifier and it was digitized by the analog to digital converter (ADC). The digital signals were processed in personal computer by laboratory developed software in the Delphi 7 program environment.

### 2.2. Thermal lens signal calculation

Under CW-laser excitation, the intensity measured at the beam center,  $I(t)$ , will initially ( $t=0$ ) reflect only the Beer's law response of the sample. After sufficient time, when a steady state temperature difference is reached, the intensity at the detector,  $I(\infty)$ , will depend on the optical arrangement of the system. An optimum configuration which minimizes  $I(\infty)$  is obtained when the sample is placed one confocal length beyond the beam waist formed by a long focal length lens. In this configuration, using a  $\text{TEM}_{00}$  laser beam to probe a sample whose length,  $L$ , is sufficiently small ( $L \ll 2\pi w_0^2 n/\lambda$ , where  $w_0$  is the beam waist,  $n$  the refractive index, and  $\lambda$  is the laser wavelength), the following expression governs the initial and final intensities.

$$\text{TL}_{\text{signal}} = \frac{I(0) - I(\infty)}{I(\infty)} = -\frac{2.303(\text{dn}/\text{dT})PA}{\lambda k} \quad (1)$$

$$E = -\frac{\text{dn}/\text{dT}}{\lambda k} P \quad (2)$$

where  $P$  is the power of laser,  $\text{dn}/\text{dT}$  the change in solvent refractive index with temperature,  $\lambda$  the laser wavelength,  $k$  the thermal conductivity,  $E$  the enhancement of this effect relative to Beer's law behavior and  $A$  is the absorbance of the sample. This expression assumes that all of the absorbed light is converted into heat [24].

The intensity of laser beam passing through the microcell was measured during the thermal lens effect at initial time ( $I(0)$ ), and steady state time ( $I(\infty)$ ). Then thermal lens signal ( $\text{TL}_{\text{signal}}$ ) was calculated by Eq. (1). For each sample, the signal was derived from the average of three recordings of the thermal lens signals.

### 2.3. Reagents and solutions

All chemicals used were of analytical reagent grade. The non-ionic surfactant TritonX-114 was obtained from Sigma (NJ, USA). Stock standard solution of rhodium at a concentration of  $1000 \mu\text{g mL}^{-1}$  was prepared from  $\text{RhCl}_3 \cdot 4\text{H}_2\text{O}$  (PROLABO, Paris, France). Working standard solutions were obtained by appropriate dilution of the stock standard solution. A solution of  $5.0 \times 10^{-4} \text{ mol L}^{-1}$  PAN was prepared in pure ethanol (Merck, Darmstadt, Germany). The materials and vessels used for the trace analysis were kept in 10% nitric acid for at least 24 h and subsequently washed four times with doubly distilled water.

### 2.4. Apparatus

Thermostatic bath (Fision-Germany, model HAKKE-N3) maintained at the desired temperature was used for cloud point extraction experiments, and phase separation was performed using a centrifuge (DAMON/IEC division, USA). Atomic absorption spectrometer (Perkin-Elmer, model 1100B) equipped with the electro thermal system was used for the determination of rhodium. A  $20 \mu\text{L}$  quartz Suprasil cylindrical microcell with 10 mm light path was used as a determination cell (Hellma, GmbH).

### 2.5. Procedures

For the rhodium–PAN complex formation, an aliquot of 10 mL solution containing rhodium and  $7.5 \times 10^{-6} \text{ mol L}^{-1}$  PAN was adjusted to pH 4.0 and was kept for 30 min in the boiling water bath. Afterward for cloud point extraction, 0.7 mL Triton X-114 (1.0%, w/v) was added to the solution and it was kept for 10 min in the thermostatic bath at  $50^\circ\text{C}$ . Since the surfactant density is higher than water, the surfactant-rich phase typically settles through the aqueous phase. The separation of the phase was accelerated by centrifuging at 2500 rpm for 10 min. On the cooling stage in an ice-bath, the surfactant-rich phase became viscous. Then, the aqueous phase was separated by simple decantation. Later, surfactant rich phase was heated in oven at  $100^\circ\text{C}$  to remove the remaining water. Twenty microliters of carbon tetrachloride were added to the remaining phase and then the sample was introduced into the  $20 \mu\text{L}$  micro cell located at the thermal lens spectrometer. Thermal lens spectrometer was set at wavelength of 632.8 nm and chopper frequency of 0.5 Hz. The intensity of the detector over time was obtained during thermal lens effect for each sample and then the thermal lens signal was calculated by Eq. (1).

## 3. Results and discussion

### 3.1. Selection of wavelength

The absorption spectrum of rhodium–PAN complex was studied in the remaining phase after dissolving with carbon tetrachloride. This complex exhibits absorption in the wavelength range of 600–660 nm in the surfactant rich phase while Triton X-114 and PAN do not have any absorption at this range. This

is a well-matched range to the wavelength of the He–Ne laser at 632.8 nm.

### 3.2. Time of steady-state thermal lens

The steady-state thermal lens effect is due to the formation of the temperature dependent refractive index gradient. In order to optimize the required time for the steady-state thermal lens effect the laser beam path to the sample was continuously blocked and opened by a chopper at different frequencies. The intensity of detector output over time was evaluated for  $10 \text{ ng mL}^{-1}$  of rhodium–PAN complex after CPE at 632.8 nm laser wavelength. It was found that the frequency of 0.5 Hz (time of 2 s) is suitable for the steady-state condition which is favorable to build up and decay the thermal lens effect.

### 3.3. Time of heating and its effect on complex formation

The formation of rhodium–PAN complex is very slow at the room temperature, so the color formation is very slow. The color begins to form about 2 min after the solution is heated in a boiling water bath. To determine the optimum time of the color formation, samples containing  $30 \text{ ng mL}^{-1}$  rhodium and  $7.5 \times 10^{-6} \text{ mol L}^{-1}$  PAN were prepared and placed in a boiling water bath for varying lengths of time. Then the samples were cooled in tap water and cloud point extraction procedure was carried out by addition of 0.7 mL of Triton X-114 1% (w/v) to each sample. The surfactant rich phase was separated after CPE and dissolved in carbon tetrachloride, and then its thermal lens signal was measured afterwards. The negligible increase in  $\text{TL}_{\text{signal}}$  on the heating of samples longer than 30 min does not merit the increased time for analysis, thus a heating time of 30 min is recommended.

### 3.4. Effect of pH

The thermal lens signal of rhodium after CPE as a function of the pH was performed using hydrochloric acid and potassium hydroxide at the pH range of 1–7. Separation of metal ions by the cloud point method involves prior formation of a complex with sufficient hydrophobicity to be extracted into the small volume of surfactant-rich phase. Extraction yield depends on the pH at which complex formation is carried out. The Effect of pH on the thermal lens signal of rhodium–PAN complex was evaluated for 10 mL of  $10 \text{ ng mL}^{-1}$  rhodium at 0.07% (w/v) Triton X-114 and  $7.5 \times 10^{-6} \text{ mol L}^{-1}$  PAN conditions. The results showed that the signal increases with the increase of pH up to 3; thereafter, the signal is almost constant up to pH 5. Hence pH 4 was chosen.

### 3.5. Effect of PAN concentration

The thermal lens signal of rhodium as a function of the complexing agent concentration was evaluated. The variation of the thermal lens signal over the PAN concentration was evaluated in the range of  $1 \times 10^{-6}$  to  $25 \times 10^{-6} \text{ mol L}^{-1}$  for 10 mL aliquots of solutions containing  $30 \text{ ng mL}^{-1}$  rhodium and 0.07% (w/v) Triton-X114 at pH of 4. The  $\text{TL}_{\text{signal}}$

increased as the concentration of PAN increased from  $1 \times 10^{-6}$  to  $5 \times 10^{-6}$  mol L<sup>-1</sup> and reached the highest in the range of  $5 \times 10^{-6}$  to  $10 \times 10^{-6}$  mol L<sup>-1</sup>, then decreased after  $10 \times 10^{-6}$  mol L<sup>-1</sup> of the PAN concentration. Therefore, a PAN concentration of  $7.5 \times 10^{-6}$  mol L<sup>-1</sup> was employed for the other experiments.

### 3.6. Effect of Triton X-114 concentration

A successful cloud point extraction would be that which maximizes the extraction recovery through minimizing the phase volume ratio. We evaluated the effect of the surfactant concentration in the range of 0.01–0.2% (w/v) Triton X-114 on the thermal lens signal for 10 mL of 30 ng mL<sup>-1</sup> rhodium at  $7.5 \times 10^{-6}$  mol L<sup>-1</sup> PAN and pH 4.0 conditions. It is found that the thermal lens signal is approximately constant and high in the range of 0.04–0.10% (w/v), so an amount of 0.07% (w/v) Triton X-114 was chosen for subsequent experiments. The signal decreases with the increase of the Triton X-114 concentration (over 0.1% (w/v)) due to an increase in the volume and the viscosity of the remaining phase.

### 3.7. Effect of equilibration temperature and time

It is suitable to choose the shortest equilibration time and the lowest possible equilibration temperature which ensures completion of phase separation in the cloud point extraction. An excellent thermal lens signal was obtained for the equilibration temperature from 40 to 80 °C. Therefore, temperature of 60 °C was used in subsequent experiments. The dependence of thermal lens signal upon incubation time was studied in the range of 5–15 min and the optimum time of 10 min was chosen as a suitable time.

### 3.8. Effect of organic solvent

A general trend in Eq. (1) shows the enhancement of thermal lens signal is obtained for the smaller thermal conductivity ( $k$ ) and the larger absolute amount of temperature dependent refractive index ( $dn/dT$ ). The order of magnitude of  $E$  predicts that the organic solvent will produce enhancement for TLS relative to Beer's law. As it is shown in Table 1, organic solvents have better thermo-optical properties than the water medium at thermal lens spectrometry [26,35–37]. We have calculated  $E$  parameter for organic solvents and water at 632.8 nm and 5 mW (Table 1). The results show that the  $E$  parameter for non-polar organic solvent

is higher than those of polar organic solvents and water. Therefore, it may be advantageous to use organic solvents to improve the sensitivity of TLS method after CPE. For this reason, the remaining phase after cloud point extraction was dissolved in 20  $\mu$ L of organic solvent. Suitable solvents must dissolve complex or complexes, excess of ligand, surfactant and also they should have good thermo-optical properties.

The effect of organic solvents such as carbon tetrachloride, chloroform, THF, cyclohexane and DMSO were investigated on the thermal lens signal after cloud point extraction for 10 mL of 30 ng mL<sup>-1</sup> rhodium at  $7.5 \times 10^{-6}$  mol L<sup>-1</sup> PAN, 0.07% (w/v) Triton X-114 and pH 4.0 condition. The results show that a good correlation exists between the thermal lens signal obtained for rhodium in various solvents and the calculated  $E$  parameter. Since the thermal lens signal is the highest in the carbon tetrachloride media, it was chosen as a suitable solvent.

### 3.9. Figure of merits

Calibration graph was obtained by preconcentrating 10 mL of samples in the presence of  $7.5 \times 10^{-6}$  mol L<sup>-1</sup> PAN and 0.07% (w/v) Triton X-114 at the pH of 4.0. The remained phases of the samples after CPE were analyzed by the thermal lens spectrometer after dissolving with carbon tetrachloride. Under optimum conditions, the calibration curve was linear from 0.5 to 50 ng mL<sup>-1</sup> with a correlation coefficient of 0.9968 ( $R^2$ ). The linear calibration curve was obtained with an intercept and slope of 0.036 and 0.232, respectively. The limit of detection (LOD) was calculated as the ratio of three times of the blank standard deviation over the slope of the calibration curve. The value of 0.06 ng mL<sup>-1</sup> was obtained for LOD. The relative standard deviations were lower than 5% for five samples subjected to the complete procedure. The enhancement factor, as the ratio of slope of preconcentrated samples to that obtained without preconcentration, was 450.

Table 2 compares the proposed method with those was reported previously for the determination of rhodium after preconcentration procedure. It shows that the proposed method has a low detection limit compared with previous studies and it allows the determination of ng mL<sup>-1</sup> levels of rhodium. Also, TLS requires low volume of the remained phase after CPE (20  $\mu$ L) for determination of analyte in comparison with the other similar determination methods such as FAAS, Spectrophotometry or ICP-AES that they require about 500–5000  $\mu$ L of the remained phase after preconcentration methods, So the remained

Table 1  
Thermo-optical properties and amounts of enhancement parameter for several solvents

Solvent	$dn/dT$ (K <sup>-1</sup> )	$k$ (Wm <sup>-1</sup> K <sup>-1</sup> )	$E^a$
Carbon tetrachloride	$-6.12 \times 10^{-4}$	0.103	46.948
Chloroform	$-6.03 \times 10^{-4}$	0.117	40.722
THF	–	0.126	–
Cyclohexane	$-5.56 \times 10^{-4}$	0.123	35.716
DMSO	–	0.199	–
Water	$-0.91 \times 10^{-4}$	0.598	1.202

<sup>a</sup> Calculated at 632.8 nm and 5 mW of laser.

Table 2  
Comparison of preconcentration-determination methods for rhodium reported in the literature with the proposed method

Determination technique	Preconcentration method	Sample volume (mL)	Solvent volume ( $\mu\text{L}$ )	Enhancement factor	LDR <sup>a</sup> (ng mL <sup>-1</sup> )	LOD <sup>b</sup> (ng mL <sup>-1</sup> )	Reference
FIA-FAAS	SPE	50	–	–	–	8	[38]
ETAAS	IEM <sup>c</sup>	2.4	40	20	0.9–50	0.3	[39]
FAAS	CPE	100	300	50	0.16–1.5	0.052	[40]
Spectrophotometry	SLS <sup>d</sup>	250	5000	40	30–2500	14.4	[41]
Spectrophotometry	LLE	–	–	–	440–4400	–	[42]
LI-TLS	CPE	10	20	450	0.5–50	0.06	Present work

<sup>a</sup> Linear dynamic range.

<sup>b</sup> Limit of detection.

<sup>c</sup> Ion exchange microcolumn.

<sup>d</sup> Solid liquid separation.

phase was dissolved by low volume of solvent in the proposed method.

The proposed method has a high enhancement factor in compare to the other similar methods because of high volume ratio (sample volume to the remained phase volume after CPE).

### 3.10. Interferences

Considering the selectivity provided by the cloud point extraction and thermal lens spectrometry, many anions and cations were evaluated. An ion was considered to interfere when its presence produced a variation of 5% in thermal lens signal of sample. The effect of foreign ions on the preconcentration and determination of rhodium was investigated. Among the tested ions; Sb<sup>5+</sup>, Sb<sup>3+</sup>, Pb<sup>2+</sup>, Mn<sup>2+</sup>, Ca<sup>2+</sup>, Mg<sup>2+</sup>, Na<sup>+</sup>, K<sup>+</sup>, F<sup>-</sup>, Cl<sup>-</sup>, Br<sup>-</sup>, NO<sub>3</sub><sup>-</sup>, SO<sub>4</sub><sup>2-</sup> did not show any interference at a concentration of 500 times higher than rhodium concentration, however Fe<sup>3+</sup>, Cu<sup>2+</sup> and Ni<sup>2+</sup> showed interferences at a concentration of 20 times higher than rhodium concentration and Co<sup>2+</sup>, Pd<sup>2+</sup> showed interference at the same concentration of rhodium.

### 3.11. Analysis of water samples

In order to test the applicability and reliability of the proposed method, tap water, drinking water, dispenser water and seawater samples were analyzed. For this purpose, 10 mL of each sample was preconcentrated with  $7.5 \times 10^{-6}$  mol L<sup>-1</sup> PAN and 0.07% (w/v) Triton X-114 in accordance to the proposed method. For the calibration, the working standard solutions (0.5–50 ng mL<sup>-1</sup>) were subjected to the same preconcentration procedure as used for the sample solutions. The results are shown in Table 3. In all cases the spike recoveries confirmed the reliability of the proposed method. Also, we applied standard addition method for the determination of rhodium in 20 ng mL<sup>-1</sup> spiked real samples mentioned in Table 3. The results showed that the obtained concentrations were in the range of 19.4–20.5 ng mL<sup>-1</sup> that good recoveries (97–102.5%) were achieved for analyzed samples.

We carried out determination of rhodium by ETAAS after CPE for samples detailed in Table 3. The results confirm the accuracy of CPE/TLS method for rhodium preconcentration and

Table 3  
Determination of rhodium in the real and spiked samples after CPE

Sample	Spiked (ng mL <sup>-1</sup> )	TLS		ETAAS	
		Found (ng mL <sup>-1</sup> ) <sup>a</sup>	Recovery (%)	Found (ng mL <sup>-1</sup> ) <sup>a</sup>	Recovery (%)
Tap water <sup>b</sup>	–	N.D	–	N.D	–
	15.0	15.3 ± 0.31	102.0	14.9 ± 0.25	99.3
	30.0	30.9 ± 0.40	103.0	30.4 ± 0.25	101.3
Drinking water <sup>b</sup>	–	N.D	–	N.D	–
	20.0	19.8 ± 0.43	99.0	20.4 ± 0.25	102.0
	40.0	40.1 ± 0.39	100.2	40.2 ± 0.25	100.5
Dispenser water <sup>b</sup>	–	N.D	–	N.D	–
	20.0	19.9 ± 0.39	99.5	20.6 ± 0.25	103.0
	40.0	39.9 ± 0.44	99.7	39.3 ± 0.25	98.2
Sea water <sup>b</sup>	–	N.D	–	N.D	–
	15.0	15.2 ± 0.25	101.3	14.6 ± 0.25	97.3
	30.0	30.1 ± 0.30	100.3	30.3 ± 0.25	101.0
Synthetic sample <sup>c</sup>	20.0	19.9 ± 0.30	99.5	20.5 ± 0.25	102.5
	40.0	39.7 ± 0.23	99.2	39.3 ± 0.25	98.2

<sup>a</sup> Mean ± S.D. (n = 3).

<sup>b</sup> The concentration of Cu<sup>2+</sup>, Fe<sup>3+</sup>, Ni<sup>2+</sup> were lower than 100 ng mL<sup>-1</sup> and Co<sup>2+</sup>, Pd<sup>2+</sup> were not detected.

<sup>c</sup> Sb<sup>3+</sup>, Pb<sup>2+</sup>, Mn<sup>2+</sup>, Ca<sup>2+</sup> and Mg<sup>2+</sup> 2000 ng mL<sup>-1</sup> of each cation; Na<sup>+</sup> and K<sup>+</sup> 10,000 ng mL<sup>-1</sup> of each.

determination. Since no real samples were available for testing the validity of the proposed method, we analyzed rhodium in synthetic samples.

#### 4. Conclusions

The use of laser induced-thermal lens spectrometry as an alternative determination method after the cloud point extraction for the trace determination of rhodium was proposed. The laser induced-thermal lens spectrometry as a sensitive spectrometry method is suitable for analysis of low volume of the remained phase after the cloud point extraction. The use of organic solvent after CPE is not only suitable for dissolving the remained phase (metal complex and surfactant) but also enhance the thermal lens signal. The cloud point extraction is an easy, safe, rapid and inexpensive method for the preconcentration and separation of trace metals from aqueous solutions to low volume organic phase.

This combination method exhibits high enhancement factor (450) as a result of the preconcentration enhancement factor in CPE and the enhancement factor of organic solvent effects in TLS.

The proposed combination method for rhodium offers a good sensitivity, because LI-TLS is suitable for the determination of analyte after CPE in comparison to the other detection systems such as FAAS, ICP/OES and UV/vis spectrophotometer.

On the other hand, in addition to simplicity and low cost, this method is comparable with the other sensitive methods such as ETAAS and ICP-MS for rhodium determination.

The proposed method was applied for the determination of trace amounts of rhodium in spiked water samples.

#### Acknowledgement

Support of this investigation by the Research Council of The University of Tehran through Grant is gratefully acknowledged.

#### References

- [1] Q. Fang, M. Du, C.W. Huie, *Anal. Chem.* 73 (2001) 3502.
- [2] J.L. Manzoori, A. Bavili-Tabrizi, *Microchem. J.* 72 (2002) 1.
- [3] B.M. Cordero, J.L.P. Pavon, C.G. Pinto, E.F. Laespada, *Talanta* 40 (1993) 1703.
- [4] H. Watanabe, H. Tanaka, *Talanta* 25 (1978) 585.
- [5] M.J. Schick (Ed.), *Non-ionic Surfactants*, Marcel Dekker, New York, 1987.
- [6] K.L. Mittal (Ed.), *Solution Chemistry of Surfactants*, Plenum, New York, 1979.
- [7] M.J. Rosen, *Surfactants and Interfacial Phenomena*, Wiley, New York, 1987.
- [8] V. De Giorgio, *Physics of Amphiphiles: Micelles, Vesicles and Microemulsions*, North Holland, Amsterdam, 1985, p. 303.
- [9] F. Xia, R.M. Cassidy, *Anal. Chem.* 63 (1991) 2883.
- [10] C.D. Stalikas, *Trends Anal. Chem.* 21 (2002) 343.
- [11] R.C. Martínez, E.R. Gonzalo, B.M. Cordero, J.L.P. Pavon, C.G. Pinto, E.F. Laespada, *J. Chromatogr. A* 902 (2000) 251.
- [12] C.G. Pinto, J.L.P. Pavon, B.M. Cordero, E.R. Beato, S.S. Sanchez, *J. Anal. At. Spectrom.* 11 (1996) 37.
- [13] M.C.C. Oliveros, O.J. de Blas, J.L.P. Pavon, B.M. Cordero, *J. Anal. At. Spectrom.* 13 (1998) 547.
- [14] E.K. Paleologos, C.D. Stalikas, S.M. Tzouwara-Karayanni, G.A. Pilidis, M.I. Karayannis, *J. Anal. At. Spectrom.* 15 (2000) 287.
- [15] E.K. Paleologos, C.D. Stalikas, M.I. Karayannis, *Analyst* 126 (2001) 389.
- [16] D.L. Giokas, E.K. Paleologos, S.M. Tzouwara-Karayanni, M.I. Karayannis, *J. Anal. At. Spectrom.* 16 (2001) 521.
- [17] J. Miura, H. Ishii, H. Watanabe, *Bunseki Kagaku* 25 (1976) 808.
- [18] H. Watanabe, T. Saitoh, T. Kamidate, K. Haraguchi, *Mikrochim. Acta* 106 (1992) 83.
- [19] M.E.F. Laespada, J.L.P. Pavon, B.M. Cordero, *Analyst* 118 (1993) 209.
- [20] F. Shemirani, R. Rahnama Kozani, M.R. Jamali, Y. Asadi, M.R. Milani, *Sep. Sci. Technol.* 40 (2005) 2527.
- [21] M.F. Silva, L.P. Fernandez, R.A. Olsina, D. Stacchiola, *Anal. Chim. Acta* 342 (1997) 229.
- [22] M.F. Silva, L.P. Fernandez, R.A. Olsina, *Analyst* 123 (1998) 1803.
- [23] L. Sombra, M. Luconi, M.F. Silva, R.A. Olsina, L.P. Fernandez, *Analyst* 126 (2001) 1172.
- [24] A. Safavi, H. Abdollahi, M.R. Hormozi Nezhad, R. Kamali, *Spectrochim. Acta A* 60 (2004) 2897.
- [25] J.P. Gordon, R.C.C. Leite, R.S. Moore, S.P.S. Porto, J.R.J. Whinnery, *Appl. Phys.* 36 (1965) 3.
- [26] N.J. Dovichi, J.M. Harris, *Anal. Chem.* 51 (1979) 728.
- [27] T. Imasaka, K. Miyaishi, N. Ishibashi, *Anal. Chim. Acta* 115 (1980) 407.
- [28] J.P. Haushalter, M.D. Morris, *Appl. Spectrosc.* 34 (1980) 445.
- [29] N.J. Dovichi, J.M. Harris, *Anal. Chem.* 53 (1981) 106.
- [30] R.O. Carman, P.L. Kelley, *Appl. Phys. Lett.* 12 (1968) 241.
- [31] J.M. Harris, N.J. Dovichi, *Anal. Chem.* 52 (1980) 695A.
- [32] C. Bosch Ojeda, F. Sanchez Rojas, *Talanta* 67 (2005) 1.
- [33] C. Bosch Ojeda, F. Sanchez Rojas, *Talanta* 68 (2006) 1407.
- [34] J.R. Stokely, W.D. Jacobs, *Anal. Chem.* 35 (1963) 149.
- [35] C.D. Tran, *Anal. Chem.* 60 (1988) 182.
- [36] H. Zhang, G. Zhao, H. Ye, X. Ge, S. Cheng, *Meas. Sci. Technol.* 16 (2005) 1430.
- [37] S.E. Bialkowski, *Chemical Analysis*, vol. 134, Wiley, New York, 1996, p. 426.
- [38] I.A. Kovalev, L.V. Bogacheva, G.I. Tsylin, A.A. Formanovsky, Y.A. Zolotov, *Talanta* 52 (2000) 39.
- [39] F.S. Rojas, C.B. Ojeda, J.C. Pavon, *Anal. Lett.* 37 (2004) 2685.
- [40] K. Suvardhan, K.S. Kumar, D. Rekha, P. Subrahmanyam, K. Kiran, B. Jayaraj, S. Ramanaiah, K. Janardhanam, P. Chiranjeevi, *Microchim. Acta*, 2006 (online).
- [41] J.P. Pancras, B.K. Puri, *Anal. Sci.* 15 (1999) 575.
- [42] D.K. Das, *Z. Fresenius, Anal. Chem.* 318 (1984) 612.



# Determination of lithium in pharmaceutical formulations used in the treatment of bipolar disorder by flow injection analysis with spectrophotometric detection

Cássia Maria L. da Silva, Vanessa G.K. Almeida, Ricardo J. Cassella\*

*Departamento de Química Analítica, Universidade Federal Fluminense, Outeiro de São João Batista s/n, Centro, Niterói/RJ, 24020-150, Brazil*

Received 23 January 2007; received in revised form 30 March 2007; accepted 7 April 2007

Available online 24 April 2007

## Abstract

In this work, a flow injection system with spectrophotometric detection was developed for the determination of lithium in pharmaceutical formulations used in the treatment of bipolar disorder. Reaction between Quinizarine (1,4-dihydroxyanthraquinone) and Li(I) ion in alkaline medium containing dimethylsulfoxide (DMSO) was explored for this purpose. The flow system was optimized regarding to its chemical (DMSO, Quinizarine and NaOH concentrations and sample pH) and physical parameters (sample loop volume, carrier flow rate and reactor length) in order to establish better conditions in terms of sensitivity and sampling frequency. The results obtained showed that the concentration of DMSO in the reagent solution presents remarkable influence on the magnitude of analytical signal. Chemical species that could be found in the formulations such as Na(I), K(I), Mg(II), Ca(II), Ti(IV), Cl<sup>-</sup>, CO<sub>3</sub><sup>2-</sup> e sodium dodecylsulfate were tested as possible interfering ions. Among them, only non-monovalent cations presented noticeable interference on lithium signal. However, they were not found in concentrations high enough to cause interference in the determination of lithium in the samples. Sample preparation was performed by sonicating a slurry prepared by dispersing 100 mg of powdered sample in 15 mL of 0.10 mol L<sup>-1</sup> HCl solution. Results obtained by developed methodology were not statistically different from those obtained by flame emission spectrometry. In the optimized conditions the method presented a linear range of 5–40 mg L<sup>-1</sup> and a relative standard deviation of 3.6% at 5 mg L<sup>-1</sup> Li concentration. Detection and quantification limits were 0.54 and 1.8 mg L<sup>-1</sup>, respectively. Sampling frequency, calculated as the time interval passed between two consecutive injections, was 60 samples per hour. The methodology was successfully applied in the determination of lithium in three commercial samples.

© 2007 Elsevier B.V. All rights reserved.

**Keywords:** Lithium; Flow injection analysis; Spectrophotometry; Quinizarine

## 1. Introduction

Bipolar disorder, also known as manic-depressive illness, is a brain disorder that causes unusual shifts in a person mood, energy, and ability to function. It can result in damaged relationships, poor job or school performance, and even suicide [1]. Lithium salts have widely been employed in the control of the symptoms of bipolar disorder [2–5]. However, some cases of death and severe intoxication derived from the bad use of lithium salts are related in the literature [6].

In the organism, lithium produces, partially, the effects of sodium, magnesium and calcium cations in celular processes [7],

being efficient in the control of bipolar disorder symptoms when found at plasmatic concentrations higher than 0.50 mmol L<sup>-1</sup>. However, when found at concentrations above 1.5 mmol L<sup>-1</sup> lithium yields several toxic effects, which denotes a strait therapeutic window [8]. Lithium does not produce remarkable psychotropic effects in healthy people when found at plasmatic concentrations around 1 mmol L<sup>-1</sup>, but in this situation some biochemical alterations can be detected. When supplied at toxic levels, Li can cause several neurological effects, varying from confusion to convulsion and even death, when plasmatic concentrations achieve 2–2.5 mmol L<sup>-1</sup> [9]. In front of this scenario, there is a growing interest to determine Li concentration in biological fluids and drugs used for bipolar disorder control, mainly because of the already mentioned strait therapeutic window.

Various analytical techniques such as flame photometry [10–13], FAAS [14,15], ETAAS [16–19], ICP OES [20,21],

\* Corresponding author.

E-mail address: [cassella@vm.uff.br](mailto:cassella@vm.uff.br) (R.J. Cassella).

ICP-MS [22], fluorimetry [23,24], and potentiometry with ion selective electrodes [25–27] have been used for Li monitoring in different kinds of samples. Some few spectrophotometric methods are found in the current literature [28–33], but only one regarding to on-line determination of lithium [34]. Even so, this work reports the measurement of Li after a liquid–liquid extraction employing a reagent synthesized in the own laboratory.

Some of the fluorimetric and spectrophotometric methods utilized Quinizarine (1,4-dihydroxyanthraquinone) as reagent. Román-Ceba et al. [23] used Quinizarine as reagent for Li determination in acetone/water medium by fluorimetry. They observed various interference problems and recommended previous separation of Li from matrix before instrumental measurement. In order to avoid such interferences, Cuadros-Rodríguez et al. [24] followed this recommendation and performed a fluorimetric determination of Li carrying out the extraction of Li-Quinizarine complex with TBP. Samples of mineral water, pharmaceutical formulations and biological materials were analyzed in this work.

Spectrophotometric determination of lithium with Quinizarine reagent was performed by Gámiz-Gracia et al. [33] in a batch mode. They optimized experimental conditions employing a three variable Doehlert design and the method was applied for lithium determination in pharmaceutical formulations and blood serum. Several solvent mixtures were tested and DMSO/H<sub>2</sub>O 90:10% (v/v) was chosen as the best condition for the methodology. However, the whole analytical methodology was extremely slow and required intense manipulation of samples and reagents, since the general procedure recommends the manual mixing of several solutions and the preparation of samples by digestion of tablets (in the case of pharmaceutical formulations) with 1 mol L<sup>-1</sup> HCl solution.

The goal of this work was to develop and optimize a flow injection system for rapid and reliable determination of Li in pharmaceutical formulations by spectrophotometry with Quinizarine. Several parameters that could affect the performance of the FIA system were evaluated as well as the effect of possible interfering species and the sample preparation approach.

## 2. Experimental

### 2.1. Apparatus

Absorbance spectra were recorded in a Femto 800 XI (São Paulo, Brazil) spectrophotometer with a resolution of 1 nm and a standard glass cuvette of 10-mm optical path. This equipment was coupled to a PC for data acquisition and treatment.

The set-up consisted of a Femto 700 Plus (São Paulo, Brazil) UV–vis spectrophotometer equipped with a Hellma (Jamaica, NY, USA) standard glass flow cell of 80- $\mu$ L internal volume and 10-mm optical path. The instrument was set at 590 nm for all absorbance measurements and the peaks were recorded by coupling the spectrophotometer to a PC equipped with a FIA peak acquisition software provided by own Femto. A Milan BP-206 (Curitiba, Brazil) peristaltic pump, equipped with flexible Tygon<sup>®</sup> tubes, was used to propel all solutions and a Rheodyne

5041 (Cotati, CA, USA) six-port valve was employed to inject samples and standard solutions into the system. The manifold was built up with PTFE tubes with 0.8 mm bore and with a laboratory-made polypropylene connection (inverted Y shape).

Flame atomic emission measurements were carried out with a Perkin-Elmer (Norwalk, CT, USA) Analyst 100 spectrometer operating at emission mode. The instrument was operated at conditions suggested by the manufacturer (670.8 nm; air-acetylene flame and slit width of 0.7 nm).

Adjustments and measurements of pH were carried out with an Analyser 300 (São Paulo, Brazil) potentiometer equipped with a combined glass electrode (Ag/AgCl as reference). A Fanem Excelsa II centrifuge (São Paulo, Brazil) and an ultrasonic cleaner bath Unique USC 1400 (São Paulo, Brazil) were employed for sample preparation.

### 2.2. Reagents and solutions

Purified water obtained in a Simplicity Milli-Q Water System (Saint Quentin, Yvelines, France) was used to prepare all solutions. All reagents were of analytical grade unless otherwise mentioned.

Lithium standard stock solution of 1000 mg L<sup>-1</sup> concentration was prepared by dissolving 3.103 g of LiCl (Vetec, Rio de Janeiro, Brazil) in exactly 500 mL of pure water. Standard Li(I) solutions employed every day were prepared by adequate dilution of the stock standard solution.

Reagent solution was prepared by dissolving 12.5 mg of Quinizarine (1,4-dihydroxyanthraquinone, Acros, St. Louis, USA) in a mixture of 125 mL of dimethylsulfoxide (DMSO) and 5 mL of a 1 mol L<sup>-1</sup> NaOH solution. After total solubilization of Quinizarine, the solution obtained was transferred to a 250-mL volumetric flask and the volume was completed up to the mark with water. The stability of this solution was not longer than 24 h. This way, the reagent solution was prepared daily just before use.

Solvents acetone and DMSO used were of pesticide grade and supplied by Vetec (Rio de Janeiro, Brazil).

### 2.3. Flow system operation

In the developed flow system, depicted in Fig. 1b, the loop (215  $\mu$ L) was filled with sample (or standard solutions) while the water carrier stream (C, 1.50 mL min<sup>-1</sup>) was mixed with the reagent solution (R<sub>1</sub>, 2.0 mL min<sup>-1</sup>), yielding a final stream that allowed the establishment of the baseline. By valve switching, the sample was injected into the carrier stream, and the formed sample zone flowed to the confluence point *x* (inverted Y) where it was mixed with the reagent stream. The final stream then flowed to the stitched reactor (40 cm, which corresponds to 200  $\mu$ L) where the reaction between Quinizarine and Li(I) ions took place. After color development, the dispersed sample zone reached the measuring cell positioned in the optical path of the spectrophotometer (D) and the absorbance was continuously monitored at 590 nm, yielding a transient signal. The peak height was employed as quantitative variable.

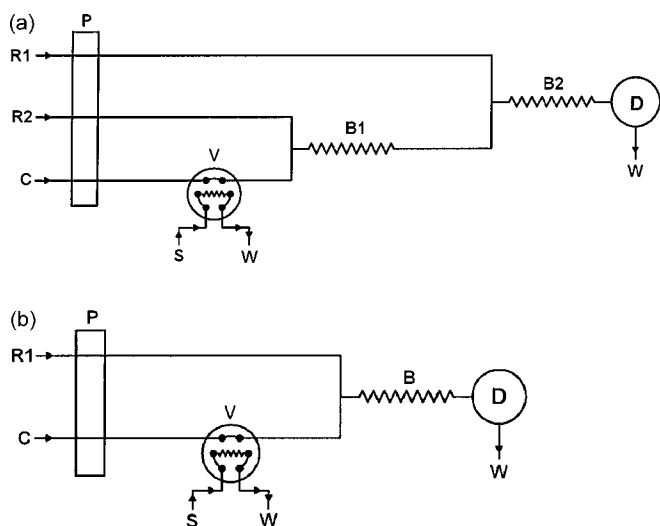


Fig. 1. (a) Initial FIA system mounted for the spectrophotometric determination of Li in pharmaceutical formulations. R<sub>1</sub> = reagent solution (1.5 mL min<sup>-1</sup>, 15% (v/v) acetone + 1.0 × 10<sup>-4</sup> mol L<sup>-1</sup> Quinizarine + 1% (w/v) Triton X-100), R<sub>2</sub> = NaOH solution (0.5 mL min<sup>-1</sup>, 0.010 mol L<sup>-1</sup>), C = carrier solution (2.0 mL min<sup>-1</sup>, water), B<sub>1</sub> = coil reactor (50 cm), B<sub>2</sub> = coil reactor (50 cm), S = sample (175 μL), P = peristaltic pump, V = six-port injection valve, D = detector (spectrophotometer at 590 nm), W = waste. (b) Configuration of the final FIA system obtained after optimization process. R<sub>1</sub> = reagent solution (2.0 mL min<sup>-1</sup>, 50% (v/v) DMSO + 2.0 × 10<sup>-4</sup> mol L<sup>-1</sup> Quinizarine + 2.0 × 10<sup>-2</sup> mol L<sup>-1</sup> NaOH), C = carrier solution (water, 1.5 mL min<sup>-1</sup>), B = stitched reactor (40 cm), S = sample (215 μL), P = peristaltic pump, V = six-port injection valve, D = detector (spectrophotometer at 590 nm), W = waste.

#### 2.4. Sample preparation

Three commercial samples of pharmaceutical formulations purchased in the local market were analyzed in this work. Lithium (found as Li<sub>2</sub>CO<sub>3</sub>) was extracted from samples by simple leaching with HCl solution. For this task, around 100 mg of powdered sample were accurately weighed in 25 mL glass flasks and then 15 mL of 0.10 mol L<sup>-1</sup> HCl solution were added. The slurry obtained was sonicated for 10 min in the center of an ultrasonic bath and, after elapsed this time, it was centrifuged for 20 min at 3500 rpm. Lithium was determined in the solution after suitable dilution with pure water employing the developed FIA system and flame emission spectrometry. The determination of lithium in the samples followed two strategies: (i) evaluation of each individual tablet (three tablets of each sample) and (ii) evaluation of a set of 10 tablets of each sample (four aliquots per set). In both cases, the same procedure described above was employed.

### 3. Results and discussion

This study was performed taking into consideration four steps: (i) mounting and testing initial configuration of the flow system; (ii) optimization of the chemical and flow variables of the FIA system; (iii) evaluation of possible interferences and; (iv) evaluation of sample preparation before analysis and validation.

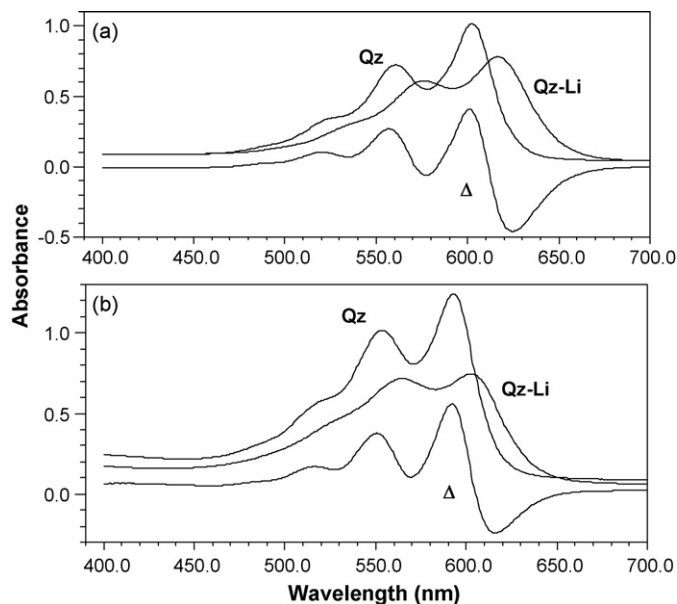


Fig. 2. Evaluation of the influence of the nature of the solvent on the spectroscopic behavior of Quinizarine and Quinizarine–Li complex. (a) DMSO and (b) acetone. Experimental conditions: 5.0 × 10<sup>-4</sup> mol L<sup>-1</sup> Quinizarine (in Qz and Qz–Li), 5.0 × 10<sup>-3</sup> mol L<sup>-1</sup> NaOH (in Qz and Qz–Li) and 10 mg L<sup>-1</sup> Li (in Qz–Li).

#### 3.1. Tests for the establishment of the initial configuration of the FIA system

Before designing and mounting the flow system to be employed for Li(I) determination, a detailed study about the solvent system suitable to carry out Li(I) Quinizarine reaction was performed. For this purpose, the effect of nature (acetone or DMSO) and concentration of the solvent were evaluated in static (off-line) mode. The results obtained in this experiment are shown in Figs. 2 and 3. As can be seen in Fig. 2, in a medium containing 90% (v/v) concentration of solvent, similar sensitivity can be attained by the use of acetone or DMSO. It was also verified that greater separation of the absorption spectrum of the complex (Qz–Li) in relation to reagent alone (Qz) was obtained when DMSO was employed. This could indicate that the use of DMSO is more suitable for spectrophotometric determination of lithium by Quinizarine method due to lower interference of reagent on the optimum wavelength for the measurement of the complex.

In terms of solvent concentration (Fig. 3), highest absorbance values were observed for increasing concentrations of solvent. In this case, acetone showed to be more suitable for analytical purposes since higher absorbance was verified when it was used. This way, the initial manifold of the FIA system was mounted employing acetone as solvent for the reagent solution. Such manifold is shown in Fig. 1a.

Employing acetone as solvent for the reagent solution an intense baseline oscillation was verified for the system, probably due to the formation of small bubbles in the reagent stream. This phenomenon occurred because of volatilization of acetone (boiling point 56.5 °C at 1 atm) by the heat released by friction of Tygon<sup>®</sup> tubes with metallic rollers of the peristaltic pump.

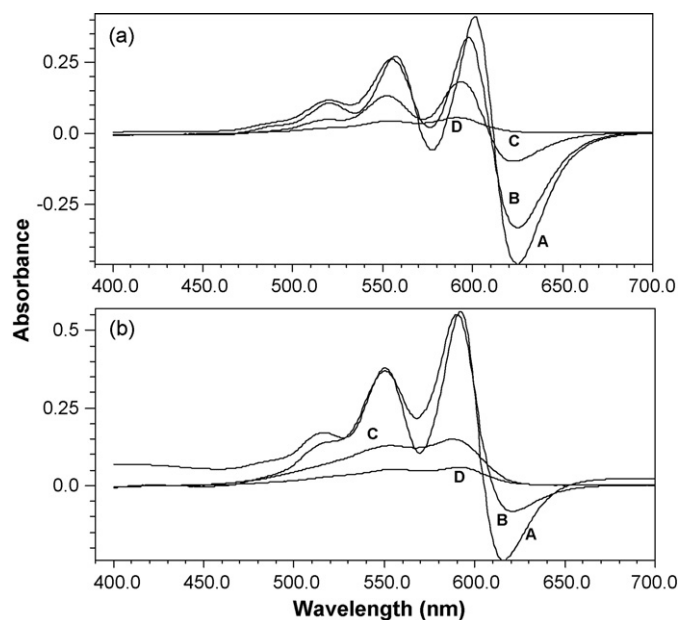


Fig. 3. Evaluation of the influence of the solvent concentration (A=90% (v/v), B=75% (v/v), C=50% (v/v) and D=25% (v/v)) on the difference spectra. (a) DMSO and (b) acetone. Experimental conditions: in all cases,  $5.0 \times 10^{-4} \text{ mol L}^{-1}$  Quinizarine,  $5.0 \times 10^{-3} \text{ mol L}^{-1}$  NaOH and  $10 \text{ mg L}^{-1}$  Li.

Another problem verified in the first manifold (Fig. 1b) was the low solubility of the Quinizarine in the medium containing 15% (v/v) acetone and Triton X-100, added to increase the solubility of Quinizarine in water. This situation could create constraints in the application of the methodology since the amount of Li to be determined could be limited by the low concentration of reagent. So, the project of FIA system was changed, assuming the configuration shown in Fig. 1b. In this new configuration, NaOH was added to the reagent solution and the acetone was replaced by DMSO as solvent due to the lowest volatility of DMSO (boiling point  $189^\circ\text{C}$  at 1 atm). In these conditions, the solubility of Quinizarine in the reagent solution was increased by the presence of NaOH and the problem related to bubbles formation was eliminated by the use of DMSO. Also, in order to promote a more efficient mixture between carrier/sample and reagent streams, the coil reactor was replaced by a stitched one. The final FIA system was then optimized in relation to chemical (DMSO, Quinizarine and NaOH concentrations and sample pH) and flow (sample volume, reactor length and carrier flow rate) variables using the univariate approach.

### 3.2. Optimization of chemical variables

The influence of the DMSO concentration on the absorbance signals produced by the analyte was studied in the range of 5–50% (v/v). As in the initial experiments, the concentration of solvent presented remarkable influence on analytical signals (Fig. 4) obtained with the FIA system. Such signals increased with the increase of DMSO concentration. Concentrations higher than 50% (v/v) were not tested in order to avoid fast damage of Tygon<sup>®</sup> tubes of the peristaltic pump and to avoid excessive increase of the viscosity of the reagent solution,

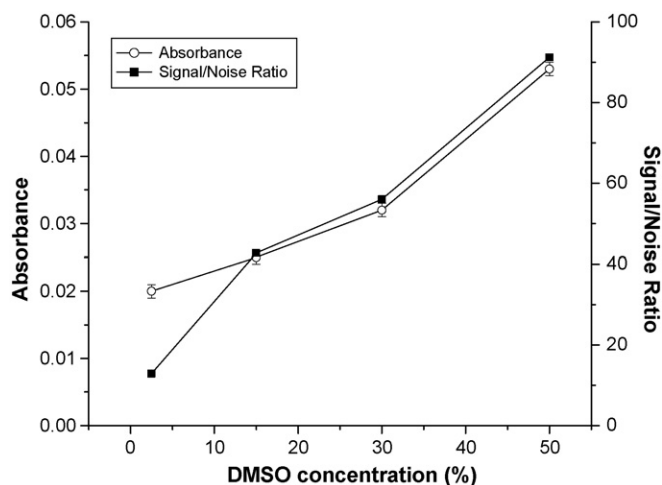


Fig. 4. Influence of DMSO concentration on analytical signal of Li in the flow system.  $R_1$  ( $2.0 \text{ mL min}^{-1}$ ) =  $1.0 \times 10^{-4} \text{ mol L}^{-1}$  Quinizarine +  $0.010 \text{ mol L}^{-1}$  NaOH, C = carrier (water,  $2.1 \text{ mL min}^{-1}$ ), B = 50 cm, S =  $175 \mu\text{L}$  and Li =  $25 \text{ mg L}^{-1}$  (at natural pH).

which could result in a poor mixture of this solution with carrier stream in the confluence point. This way, a DMSO concentration of 50% (v/v) was chosen for the system. It is important to remark that even with this high concentration of DMSO, minimum baseline noise was observed proving that efficient mixture between reagent and carrier streams was attained.

Quinizarine concentration was studied between  $5.0 \times 10^{-5}$  and  $2.5 \times 10^{-4} \text{ mol L}^{-1}$  and highest sensitivity was verified for Quinizarine concentrations equal or higher than  $2.0 \times 10^{-4} \text{ mol L}^{-1}$  (Fig. 5). However, when the FIA system was operated with Quinizarine solutions with concentration higher than this value it produced analytical signals with poor precision probably because of the increase of baseline noise due to low intensity of the radiation that achieves the detector. This way, a Quinizarine concentration of  $2.0 \times 10^{-4} \text{ mol L}^{-1}$  was selected

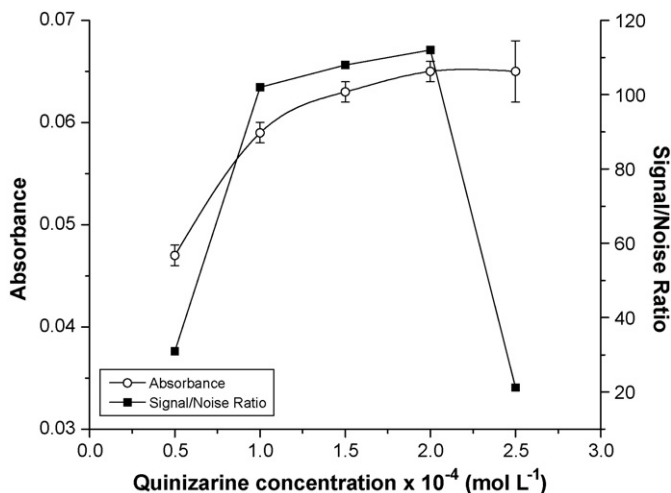


Fig. 5. Influence of Quinizarine concentration on analytical signal of Li in the flow system.  $R_1$  ( $2.0 \text{ mL min}^{-1}$ ) = 50% (v/v) DMSO +  $0.010 \text{ mol L}^{-1}$  NaOH, C = carrier (water,  $2.1 \text{ mL min}^{-1}$ ), B = 50 cm, S =  $175 \mu\text{L}$  and Li =  $25 \text{ mg L}^{-1}$  (at natural pH).

for the method due to the lower ratio signal/noise observed at this concentration.

The function of NaOH in the reagent solution, together with sample pH, was to provide a medium sufficiently alkaline to allow the reaction between Quinizarine and Li(I) ions. This way, its effect on analytical signal was investigated in the range of  $1.0 \times 10^{-2}$  to  $3.0 \times 10^{-2}$  mol L<sup>-1</sup>, always maintaining standard Li solution with this original pH (around 7.0). The magnitude of analytical signal only varied around 4% along the range investigated, evidencing that this parameter has not noticeable influence on method. Then, the NaOH concentration of  $2.0 \times 10^{-2}$  mol L<sup>-1</sup>, located in the middle of the range evaluated, was chosen for all further experiments. In this same sense, the influence of sample pH was evaluated. Lithium standard solutions with pH between 2.0 and 12 (adjusted with NaOH and/or HCl diluted solutions) were injected into the system. Constant signals were observed in the range 4.0–12. However, for sample pH lower than 3.0 an abrupt decrease of the signal was verified, probably due to the decrease of pH of the reaction medium formed from mixture of reagent and carrier/sample streams. In this condition of low sample pH, the consumption of NaOH present in the reagent solution was enhanced, causing a decrease in the final pH of the medium, which was not suitable to promote Quinizarine-Li(I) reaction.

### 3.3. Optimization of flow variables

In flow systems, the sample volume injected controls the amount of analyte inserted for reaction. In a general way, when sample volume is increased the analytical signal is also increased. This behavior occurs up to a limit, that is achieved when the central region of the analytical zone no longer suffer additional dispersion. In the present case, sample loops with volumes varying from 115 to 315  $\mu$ L were tested. The absorbance signal increased up to 215  $\mu$ L and after this value, no remarkable gain in sensitivity was observed. Additionally, for volumes higher than this, the time spent to complete the transient signal was high, which decreased the sampling frequency of the system. This way, a sample volume of 215  $\mu$ L was chosen for the system.

The length of the reactor controls the reaction time between reagent and sample (analyte) inside the FIA system and also the mixture between such streams. For longest reactors, the contact time between Quinizarine and Li(I) ions is enhanced, allowing that reaction could achieve its equilibrium before sample zone passing through flow cell thus providing highest sensitivity for the methodology. Also, in this situation, the mixture of carrier (sample) and reagent streams is improved, which minimizes the baseline noise. On the other hand, excessive increase of this variable can cause decrease of analytical signal due to the increase of sample plug dispersion. In the present case, stitched reactors with lengths ranging from 10 to 70 cm (50–350  $\mu$ L) were evaluated and no noticeable variation in the signal was recorded. This fact proves that reaction between Quinizarine and Li(I) is fast enough to be applied in a flow system. In order to maintain a compromise between higher sampling frequency and better mixture, a stitched reactor with 40 cm was chosen.

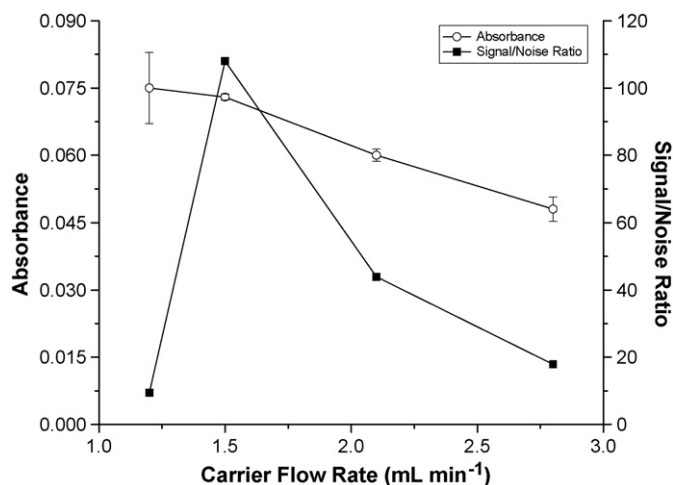


Fig. 6. Influence of sample pH on analytical signal of Li in the flow system.  $R_1$  ( $2.0 \text{ mL min}^{-1}$ ) = 50% (v/v) DMSO +  $2.0 \times 10^{-4}$  mol L<sup>-1</sup> Quinizarine +  $0.020 \text{ mol L}^{-1}$  NaOH, C = carrier (water,  $2.0 \text{ mL min}^{-1}$ ), B = 50 cm, S = 215  $\mu$ L and Li = 25 mg L<sup>-1</sup> (at natural pH).

As the same way of reactor length, the carrier flow rate controls the reaction time. Also, this parameter influences the dilution of sample plug inside the system, affecting the magnitude of analytical signal. In order to evaluate the effect of carrier flow rate on sensitivity, it was tested between 1.2 and  $2.8 \text{ mL min}^{-1}$ . As can be seen in Fig. 6, highest absorbance signals were recorded for lowest carrier flow rates. This behavior can be credited to the lower dilution imposed to sample zone when carrier flow rate decreases. It is also important to remark that for  $1.20 \text{ mL min}^{-1}$  carrier flow rate an intense variation of the baseline was recorded, causing a poor precision for the measurements performed in this condition. This can be attributed to the high absorbance of the baseline due to the high concentration of the Quinizarine in the final stream. In this situation the detector of the spectrophotometer received low intensity radiation, enhancing the electronic noise. Also, a carrier flow rate of  $0.70 \text{ mL min}^{-1}$  was tested but it was not possible to adjust a stable baseline for the system at this condition. In this context, a carrier flow rate of  $1.5 \text{ mL min}^{-1}$  was established for the system due to better signal to noise ratio observed in this condition (Fig. 6).

### 3.4. Interference study

In this study, possible interfering species usually present in pharmaceutical formulations as inert concomitants were tested. Such substances were classified in three groups: (i) cations, (ii) anions and (iii) surfactants. Na(I), K(I), Mg(II), Ca(II) and Ti(IV) were tested in the first group, while carbonate and chloride were evaluated in the second group. Only sodium dodecylsulfate was investigated as surfactant since it was found in all three commercial pharmaceutical formulations under study as wetting agent.

In the group of cations, Na(I) and K(I) were tolerated up to concentrations of 500 and 400 mg L<sup>-1</sup>, respectively, taking as interference a variation of signal higher than 5% in relation to a

signal produced by a standard solution of  $25 \text{ mg L}^{-1}$  Li. These values do not take into account the amount of Na(I) already present in the system due to the NaOH in the reagent solution.

In relation to divalent cations, both Mg(II) and Ca(II) were tolerated up to concentration much lower than Na(I) and K(I). Ca(II) did not cause any interference on  $25 \text{ mg L}^{-1}$  Li when found at  $2.5 \text{ mg L}^{-1}$ . It is important to remark that in all these cases (Na, K and Ca) a negative interference was observed, probably due to the consumption of Quinizarine reagent. The behavior of signal in presence of Mg(II) was totally different. A little increase of the signal was verified with the increase of Mg(II) concentration up to  $1 \text{ mg L}^{-1}$ , probably due to the formation of small amounts of a Quinizarine–Mg complex that absorbs in the wavelength chosen for measurements. However, when the concentration of Mg(II) was increased to levels higher than  $1 \text{ mg L}^{-1}$  there was an abrupt decrease of the absorbance signal down to negative values. This probably occurred due to the formation of great amounts of Quinizarine–Mg complex that presents poor solubility in the reaction medium, which consumed practically all Quinizarine supplied by reagent solution [35]. This hypothesis was confirmed visually since the deep blue Qz–Mg precipitate formed was retained in the stitched reactor. In the case of Ti(IV), employed as  $\text{TiO}_2$  in the formulations, no interference was verified when found in concentrations up to  $1 \text{ mg L}^{-1}$ . For concentrations higher than this value, a soft decrease of signal was observed. None of the cationic species selected as possible interfering specie seems to present any problem for Li determination by the developed procedure, especially because the most important of them (Ca, Mg and Ti) are found as practically insoluble compounds in the formulations (magnesium and calcium estearates, talc and titanium dioxide), being not available in solution after sample treatment.

The evaluation of carbonate interference was tested in the range  $5\text{--}500 \text{ mg L}^{-1}$ . This anion was chosen because Li is found in the formulations as  $\text{Li}_2\text{CO}_3$ . No variation of signal was verified for carbonate concentrations up to  $100 \text{ mg L}^{-1}$ , which are much higher than that found in final solutions resulting from sample treatment. In turn, chloride did not interfere in any of the concentrations tested (up to  $5000 \text{ mg L}^{-1}$ ), turning possible the use of HCl for sample acid treatment before injection into the system. Sodium dodecylsulfate was tolerated in concentrations as high as  $700 \text{ mg L}^{-1}$ , being observed a decrease of Li signal ( $25 \text{ mg L}^{-1}$ ) of 9% for  $800 \text{ mg L}^{-1}$  SDS. How these high concentrations of SDS are not usually found in the commercial formulations, this component was not considered an important interference for the developed method.

### 3.5. Evaluation of sample preparation conditions

Once Li is found in the samples as  $\text{Li}_2\text{CO}_3$ , an acid treatment with HCl solution was selected as alternative for Li leaching from solid matrix by simple dissolution of the respective carbonate. For this purpose, around 100 mg of the three samples were dispersed in 15 mL of HCl solutions with different concentrations and sonicated for 10 min in order to evaluate the

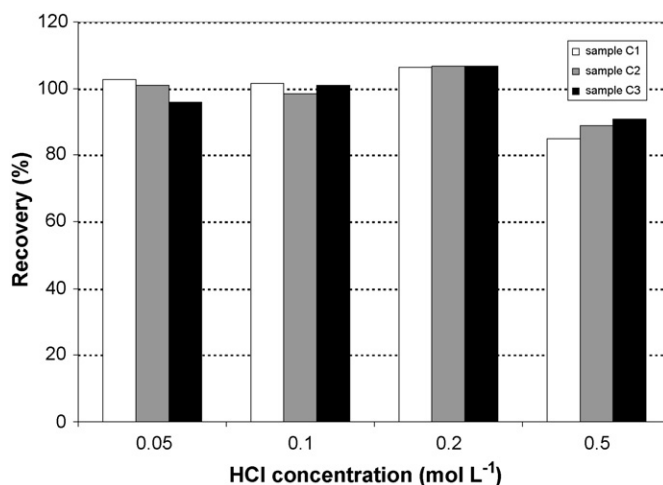


Fig. 7. Effect of HCl concentration used for Li extraction on its determination in the samples. Recovery calculated against data obtained by flame emission spectrometry.

efficiency of such solutions to extract Li from samples and the suitability of the final medium for the spectrophotometric detection of Li using the developed FIA system. The results obtained in this experiment are presented in Fig. 7. As can be seen, quantitative recoveries (in relation to flame emission spectrometry) were obtained when HCl solutions with  $0.05$  and  $0.10 \text{ mol L}^{-1}$  were employed. Higher recoveries (around  $106 \pm 1\%$ ) were verified when a  $0.20 \text{ mol L}^{-1}$  HCl solution was utilized. This result can be related to an excessive leaching of Mg in the conditions of high acidity, since all of three samples had high amounts of magnesium estearate as lubricant. How this interfering specie causes a positive interference on Li signal, this could explain the verification of recoveries higher than 100%. On the other hand, when a  $0.5 \text{ mol L}^{-1}$  HCl solution was used, the recoveries (around  $88.2 \pm 3.1\%$ ) were lower than 100%, denoting that a negative interference occurred. In this case, the unsuitable result can be attributed to the low pH verified in the final solution injected into the system, which was lower than 3.0, a pH range where Li signal decreases.

## 4. Method evaluation

### 4.1. Analytical characteristics

Under optimized conditions, the proposed method was able to produce analytical fits with good linearity in the range  $5\text{--}40 \text{ mg L}^{-1}$  Li with a typical equation  $A = (0.0029 \pm 0.0002) [\text{Li} (\text{mg L}^{-1})] + (0.001 \pm 0.004)$  and a correlation coefficient of 0.9991. Detection limit ( $3\sigma$  criterion) and quantification limit ( $10\sigma$  criterion) derived from 10 measurements of blank solution were  $0.54$  and  $1.8 \text{ mg L}^{-1}$ , respectively. Although these limits can be considered relatively high when compared with those reported in the literature for flame emission spectrometry [12,13], ETAAS [17], ICP OES [20,21], fluorimetry [24] or even potentiometry with ion-selective electrodes [25], all in the  $\mu\text{g L}^{-1}$  range, they were sufficiently low to allow the analy-

Table 1  
Results obtained in the determination of lithium carbonate in individual tablets

Sample	FIA (mg Li <sub>2</sub> CO <sub>3</sub> /pill)	Flame emission (mg Li <sub>2</sub> CO <sub>3</sub> /pill)	Declared values (mg Li <sub>2</sub> CO <sub>3</sub> /pill)
C <sub>1</sub>	308 ± 16 (5.2%)	310 ± 15 (4.8%)	300
C <sub>2</sub>	300 ± 12 (4.0%)	300 ± 11 (3.7%)	300
C <sub>3</sub>	478 ± 14 (2.9%)	479 ± 11 (2.3%)	450

Results are expressed as mean ± standard deviation ( $n = 3$ ). Coefficient of variation is between parentheses.

sis of pharmaceutical formulations containing Li (as Li<sub>2</sub>CO<sub>3</sub>). A RSD of 3.6% at 5 mg L<sup>-1</sup> was also derived from 10 measurements of the solution. A sampling frequency of 60 h<sup>-1</sup> was calculated, taking into consideration a time passed between two consecutive injections.

The amount and nature of the waste generated by FIA system was critically evaluated. In the present case, around 210 mL of effluent were wasted per hour of operation of the system. This effluent contained 60 mL of DMSO, 96 mg of NaOH and 5.8 mg of Quinizarin, and is related to 60 determinations of Li. Taking this same number of determinations into account for the manual procedure reported by Gámiz-Gracia et al. [33] it is possible to calculate that 129 mL of DMSO are wasted as well as 14.4 mg of Quinizarine, 3 mg of NaOH and 15.9 mg of Na<sub>2</sub>CO<sub>3</sub>. As can be noted, the developed flow system results in a less toxic effluent for the same number of determinations, since the amounts of DMSO and Quinizarine are much lower than those observed for the manual procedure.

#### 4.2. Application

Three commercial samples of pharmaceutical formulations containing lithium were analyzed by the developed methodology in order to prove its applicability. Results were compared with those obtained by flame emission spectrometry. Two approaches were utilized in the determination of Li in the samples: (i) analysis of individual tablets and (ii) analysis of a set of 10 tablets. As can be seen in Tables 1 and 2, in both cases, the results obtained by the FIA system agreed statistically with those obtained by flame emission spectrometry when applying a paired *t*-test at 95% confidence level.

In the first case (Table 1), the experimental value of *t* was 1.73 and the critical value of *t* is 4.30. In the second case (Table 2), the experimental value of *t* was 0.87, while the critical value of *t* is 3.18. This way, in both cases the null hypothesis is maintained.

Also, applying a correlation test, the following equations were obtained—for the first case: FIA = (1.0004 ± 0.0099) FES + (0.857 ± 3.689),  $r = 0.9999$  and for the second case:

Table 2  
Results obtained in the determination of lithium carbonate in the set of 10 tablets

Sample	FIA (mg/g Li <sub>2</sub> CO <sub>3</sub> )	Flame emission (mg/g Li <sub>2</sub> CO <sub>3</sub> )	Difference (%)
C <sub>1</sub>	772 ± 39 (5.0%)	771 ± 33 (4.3%)	0.13
C <sub>2</sub>	754 ± 40 (5.3%)	756 ± 42 (5.6%)	-0.23
C <sub>3</sub>	714 ± 19 (2.7%)	715 ± 26 (3.6%)	-0.14

Results are expressed as mean ± standard deviation ( $n = 4$ ). Coefficient of variation is between parentheses.

FIA = (0.975 ± 0.045) FES + (1.90 ± 3.38),  $r = 0.9989$ , where FIA is the result obtained by the developed procedure and FES is the result obtained by standard method of flame emission spectrometry.

The results also show that no significant differences in the contents of Li<sub>2</sub>CO<sub>3</sub> in the different tablets of same samples were observed. This conclusion is supported on the low coefficients of variation (2.3–5.2%) obtained for the content of the active principle in the individual tablets of each sample (Table 1).

The contents of Li<sub>2</sub>CO<sub>3</sub> in the samples C<sub>1</sub> and C<sub>3</sub> were 2.7% and 6.2%, respectively, higher than those declared by the manufacturer. However, such values still are in conformity with Brazilian Pharmacopeia, which recommends that the content of active principle be between 85 and 115% of the declared value [36].

#### 5. Conclusions

The proposed methodology developed here proved to be successful for the determination of Li in pharmaceutical formulations employed in the treatment of bipolar disorder. The system presented adequate sensitivity and selectivity, allowing the determination of Li at levels under those found in the samples. Comparison between the developed FIA system and flame emission spectrometry revealed that the proposed methodology does not provide results statistically different from those obtained by this reference technique.

One of the main advantages of the developed methodology is the minimum sample treatment required (10 min sonication of a slurry containing 100 mg of sample plus 15 mL of 0.1 mol L<sup>-1</sup> HCl solution) before injection into the system, which improves the whole analytical throughput. Besides the high sampling frequency of the FIA system (60 samples h<sup>-1</sup>) makes the procedure very suitable for routine analysis in quality control laboratories.

#### Acknowledgment

The authors would like to thank to CNPq (Conselho Nacional de Desenvolvimento Científico e Tecnológico) for the financial support and for the fellowships.

#### References

- [1] M. Spearing, Bipolar Disorder, Publication no. 02-3679, National Institute of Mental Health (USA), 2002.
- [2] M.E. Thase, G.S. Sachs, Biol. Psychiatry 48 (6) (2000) 558.
- [3] G.S. Sachs, M.E. Thase, Biol. Psychiatry 48 (6) (2000) 573.
- [4] R.F. Prien, J.M. Himmelhoch, D.J. Kupfer, J. Affect. Disord. 15 (1988) 9.

- [5] R.F. Prien, D.J. Kupfer, P.A. Mansky, J.G. Small, V.B. Tuason, C.B. Voss, W.E. Johnson, *Arch. Gen. Psychiatry* 41 (1984) 1096.
- [6] R.J. Baldessarini, in: A.G. Gilman, L.S. Goodman, T.W. Rall, F. Murad (Eds.), *The Pharmacological Basis of Therapeutics*, 7th ed., Macmillan Publishing Company, New York, USA, 1985.
- [7] C.J. Phiel, P.S. Klein, *Ann. Rev. Pharm. Toxicol.* 41 (2001) 789.
- [8] A. Korolkovas, *Dicionário Terapêutico Guanabara*, 1st ed., Guanabara Koogan, 2000.
- [9] M.M. Dale, J.M. Ritter, P. Gardner, H.P. Rang, *Pharmacology*, 4th ed., Churchill Livingstone, UK, 2001.
- [10] P. Popov, V. Otruba, L. Sommer, *Clin. Chim. Acta* 154 (1986) 223.
- [11] M. Sampson, M. Ruddel, R.J. Elin, *Clin. Chem.* 40 (1994) 869.
- [12] H. Matusiewicz, *Anal. Chim. Acta* 136 (1982) 215.
- [13] I. Dol, M. Knochen, E. Vieras, *Analyst* 117 (1992) 1373.
- [14] B.F. Rocks, R.A. Sherwood, C. Riley, *Clin. Chem.* 28 (1982) 440.
- [15] R.A. Sherwood, B.F. Rocks, C. Riley, *Analyst* 110 (1985) 493.
- [16] S. González, M. Navarro, H. López, M.C. López, V. Pérez, *J. Assoc. Off. Anal. Chem. Int.* 83 (2000) 377.
- [17] A.V. Flores, C.A. Pérez, M.A.Z. Arruda, *Talanta* 62 (2004) 619.
- [18] J.L. Magnin, L.A. Decosterd, C. Centeno, M. Burnier, J. Diezi, *J. Biol. Pharm. Acta Helv.* 71 (1996) 237.
- [19] G.A. Trapp, *Anal. Biochem.* 148 (1985) 127.
- [20] C.W. McLeod, P.J. Worsfold, A.G. Cox, *Analyst* 109 (1984) 327.
- [21] P. Leflon, R. Plaquet, F. Rose, G. Herndon, N. Ledeme, *Anal. Chim. Acta* 327 (1996) 301.
- [22] H. Vanhoe, C. Vandecasteele, J. Versieck, R. Dams, *Anal. Chim. Acta* 244 (1991) 259.
- [23] M. Román-Ceba, A. Fernández-Gutiérrez, C. Marín-Sánchez, *Microchem. J.* 32 (1985) 286.
- [24] L. Cuadros-Rodríguez, C. Jiménez-Linares, M. Román-Ceba, *Fresen J. Anal. Chem.* 356 (1996) 320.
- [25] M. Cretin, L. Alern, J. Bartoli, P. Fabry, *Anal. Chim. Acta* 350 (1997) 7.
- [26] A.O. Okorodudu, R.W. Burnett, R.B. McComb, G.N. Bowers Jr., *Clin. Chem.* 36 (1990) 104.
- [27] R.Y. Xie, G.D. Christian, *Anal. Chem.* 58 (1986) 1806.
- [28] J.K. Trautman, V.P.Y. Gadzekpo, G.D. Christian, *Talanta* 30 (1983) 587.
- [29] J.C. Thompson, *Clin. Chim. Acta* 327 (2003) 149.
- [30] R.H. Christenson, J.J. Mandichak, S.H. Duh, J.M. Augustyn, J.C. Thompson, *Clin. Chim. Acta* 327 (2003) 157.
- [31] Y.A. Ibrahim, A.H.M. El-Waby, N. Barsoum, A.A. Abbas, S.K. Kella, *Talanta* 47 (1998) 1199.
- [32] E. Chapoteau, B.P. Czech, W. Zazulak, A. Kumar, *Clin. Chem.* 38 (1992) 1654.
- [33] L. Gámiz-Gracia, L. Cuadros-Rodríguez, M. Román-Ceba, *Talanta* 44 (1997) 75.
- [34] K. Kimura, S. Iketani, H. Sakamoto, T. Shono, *Analyst* 115 (1991) 1251.
- [35] F. Feigl, V. Anger, *Spot Tests in Inorganic Analysis*, 6th ed., Elsevier Publishing Company, Amsterdam, Netherlands, 1972.
- [36] *Farmacopéia Brasileira*, 4th ed., Editora Atheneu, São Paulo, 1988.



# One single LC–MS/MS analysis for both phenolic components and tanshinones in *Radix Salviae Miltiorrhizae* and its medicinal products

Jian-lin Wu<sup>a</sup>, Ling Pui Yee<sup>a</sup>, Zhi-Hong Jiang<sup>b</sup>, Zongwei Cai<sup>a,\*</sup>

<sup>a</sup> Department of Chemistry, Hong Kong Baptist University, Kowloon Tong, Kowloon, Hong Kong, SAR, China

<sup>b</sup> School of Chinese Medicine, Hong Kong Baptist University, Kowloon Tong, Kowloon, Hong Kong, SAR, China

Received 19 December 2006; received in revised form 17 April 2007; accepted 18 April 2007

Available online 1 May 2007

## Abstract

A LC–MS/MS method was developed for the separation and simultaneous determination of phenolic components including danshensu, protocatechuic acid, protocatechuic aldehyde and caffeic acid as well as tanshinones including cryptotanshinone, tanshinone I and tanshinone IIA in samples of *Radix Salviae Miltiorrhizae* and *Salviae Miltiorrhizae* tablet. Triple quadrupole mass spectrometry was optimized in both positive and negative ion multiple reaction monitoring modes for the simultaneous quantitative analysis of the two different types of active components by using a time-segment program. The method gave recoveries of 85.4–106.4% with relative standard deviations of 2.4–8.0% for the spiked herb samples. The limits of detection were 0.30–0.83  $\mu\text{g/g}$  for the analysis of 1.0 g *Radix Salviae Miltiorrhizae* or tablet samples.

© 2007 Elsevier B.V. All rights reserved.

**Keywords:** *Radix Salviae Miltiorrhizae*; Danshen; Phenolic acids; Tanshinones; LC–MS/MS

## 1. Introduction

*Radix Salviae Miltiorrhizae* Bunge (Danshen in Chinese) is one of the most popular herbs used in many traditional Chinese medicines that have been commonly applied for promoting blood circulation to remove blood stasis, relieving vexation, nourishing the blood and cooling the blood to relieve carbuncles [1–4]. Major ingredients of Danshen can be classified into water-soluble components that include danshensu, protocatechuic acid, protocatechuic aldehyde and caffeic acid, as well as lipid-soluble components including cryptotanshinone, tanshinone I and tanshinone IIA (Fig. 1).

Analysis of the active components of Danshen has become more and more important due to its increasing popularity and its intensive applications in medicinal chemistry and the pharmaceutical industry. Several reversed-phase HPLC and TLC methods have been developed for determining some of the active components of Danshen. An isocratic reversed-phase HPLC

method was described to measure lithospermic acid B and rosmarinic acid in the dried tissues of the calluses, regenerated plantlets, or cultivated plants of Danshen Bunge [5]. Gradient reversed-phase HPLC methods have also been used for analyzing lithospermates and rosmarinates in an aqueous extract of *Cordia spinescens* [6] and rosmarinic acid, lithospermic acid and lithospermic acid B in root hair cultures of *Ocimum basilicum* [7]. A TLC-based method was reported for the determination of rosmarinic acid and caffeic acid in five *Salvia* species [8]. A method combining TLC and FAB-MS techniques was applied for identifying lithospermic acid B in the aqueous extract of Danshen Bunge [9] as well as rosmarinic acid and caffeic acid in *Sanicula europaea* L. [10]. Isocratic reversed-phase HPLC methods were also reported for the determination of cryptotanshinone, tanshinone I and tanshinone IIA in Danshen Bunge [11,12]. Recently, several studies focusing on the simultaneous determination of cryptotanshinone, tanshinone I and tanshinone IIA, as well as the water-soluble components, by using HPLC–UV and HPLC–MS were reported [13,14]. However, the methods either lacked specificity or had unbalanced sensitivity for the targeted components because the water-soluble and lipid-soluble components are significantly chemically dif-

\* Corresponding author. Tel.: +852 34117070; fax: +852 34117348.

E-mail address: [zwcai@hkbu.edu.hk](mailto:zwcai@hkbu.edu.hk) (Z. Cai).

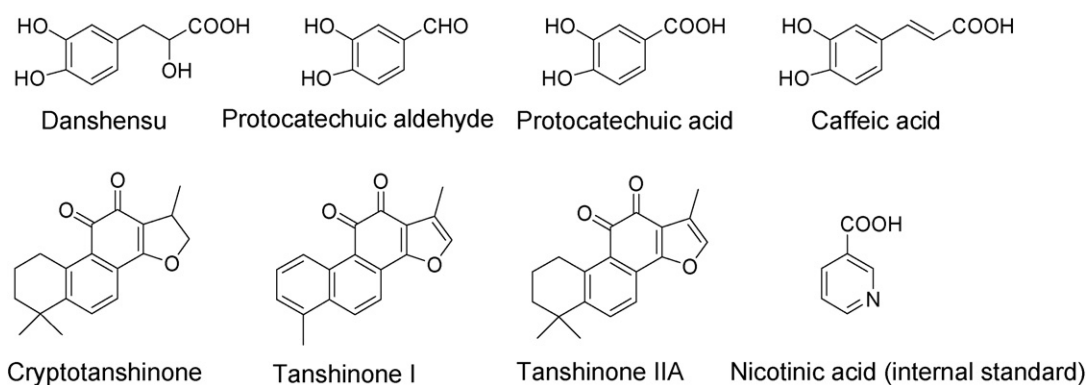


Fig. 1. Chemical structures of danshensu, protocatechuic acid, protocatechuic aldehyde, caffeic acid, cryptotanshinone, tanshinone I, tanshinone IIA and internal standard nicotinic acid.

ferent. Furthermore, most of reported methods had too high detection limits for phenolic compounds that exist in Danshen at much lower levels compared to other water-soluble acids. When electrospray LC–MS was used, positive ion mode provided good sensitivity for the tanshinones while negative ion mode suited better for the phenolic components. In this study, a time-segment program in multiple-reaction-monitoring mode was developed for the simultaneous LC–MS/MS analysis of Danshen and medicinal products. MS parameters under the positive and negative electrospray ionization conditions were optimized for achieving good sensitivity for both phenolic compounds and tanshinones in one single analytical run.

## 2. Experimental

### 2.1. Chemicals and materials

All chemicals used were of analytical grade unless specified. Formic acid, ammonium formate, HPLC-grade acetonitrile and methanol were purchased from BDH Laboratory Supplies (Poole, England). Deionized water was cleaned with a Milli-Q water purification system (Millipore, France) prior to the use as HPLC mobile phase. Nicotinic acid was purchased from Sigma (USA) and used as the internal standard. Danshensu (3-(3,4-dihydroxyphenyl) lactic acid), protocatechuic acid, protocatechuic aldehyde, caffeic acid, cryptotanshinone, tanshinone I and tanshinone IIA were purchased from the National Institute for the Control of Pharmaceutical and Biological Products (Beijing, China). All of the Danshen standards were stored in the dark. Danshen originated from Sichuan, China was obtained from the Chinese Medicine Clinics, School of Chinese Medicine, Hong Kong Baptist University. The Danshen tablet was purchased from a local Chinese herb store.

### 2.2. Sample preparation

Individual stock standard solutions were prepared by dissolving each standard of the Danshen components in 10 ml of methanol at a concentration of 1.00 mg/ml for nicotinic acid (internal standard); 0.60 mg/ml for danshensu; 2.35 mg/ml for protocatechuic acid; 1.11 mg/ml for protocatechuic aldehyde;

1.08 mg/ml for caffeic acid; 1.00 mg/ml for cryptotanshinone; 0.19 mg/ml for tanshinone I; and 0.25 mg/ml for tanshinone IIA. A standard mixture was prepared by diluting the individual stock standard solutions in 50% ACN and 50% 10 mM ammonium formate with 0.5% formic acid to give the concentrations of the phenolic components at 100 ng/ $\mu$ l and the tanshinones at 50 ng/ $\mu$ l. Seven calibration standard mixtures were prepared by diluting 25  $\mu$ l, 50  $\mu$ l, 250  $\mu$ l, 500  $\mu$ l, 1000  $\mu$ l, 2000  $\mu$ l and 5000  $\mu$ l of the standard mixture in 5 ml of the ammonium buffer solution.

Twenty Danshen tablets were powdered and homogenized. Six powdered tablet samples (1.0 g each) were accurately weighed. The sample was extracted with 50 ml of methanol by using an ultrasonic bath for 1 h after the internal standard addition. The extract was centrifuged at 10,000 rpm for 15 min. The supernatant was evaporated and dried by nitrogen blow-down. The dried residue was dissolved in 1 ml of the formate buffer. Finally, the extract was filtered with a 0.45- $\mu$ m filter and 10  $\mu$ l was analyzed by using LC–MS/MS for the Danshen components.

Three Danshen samples were pounded and homogenized by using a cyclone mill fitted with 0.45-mm seize screen (Waring Commercial, USA). The powdered samples were freeze-dried in a freeze-dryer (Heto-holten, Denmark). Three portions (1.0 g each) of the homogenized herb powder were accurately weighted. After the internal standard addition, the sample was prepared with the method described for the Danshen tablets and then analyzed by LC–MS/MS for the Danshen components.

## 3. Validation study

The linear dynamic range, limit of detection (LOD), recovery and precision were evaluated for the method developed. Due to lack of blank matrix, the linearity of calibration curve was tested with standard analysis. However, spiked matrix samples were analyzed for investigating the matrix suppression during the LC–MS/MS analysis. LOD for each analyte were measured at the signal-to-noise ration of 3:1. Recovery and precision were examined by using the spiked samples with the tablet and herb matrix. The Danshen tablet and herb samples were added with

the known amounts of nicotinic acid, danshensu, protocatechuic acid, protocatechuic aldehyde, caffeic acid, cryptotanshinone, tanshinone I and tanshinone IIA (standard addition analysis) and reanalyzed. The percentage recovery and precision of the samples were calculated.

A portion of 1.0 g of the Danshen tablet and herb matrix was each spiked with 100.0  $\mu\text{g/g}$  nicotinic acid, 100.0  $\mu\text{g/g}$  danshensu, 750.0  $\mu\text{g/g}$  protocatechuic acid, 330.0  $\mu\text{g/g}$  protocatechuic aldehyde, 970.0  $\mu\text{g/g}$  caffeic acid, 630.0  $\mu\text{g/g}$  cryptotanshinone, 320.0  $\mu\text{g/g}$  tanshinone I and 880.0  $\mu\text{g/g}$  tanshinone IIA. Six replicated samples were extracted and analyzed with the same procedures for obtaining recovery and precision data. Because the matrices contained the targeted analytes, the recovery was therefore calculated upon the subtraction of the averaged levels of each analyte. The spiked samples were also evaluated for intra- and inter-day stability. After the initial analysis, the sample extracts were kept in the HPLC autosampler for 24 h and. Reinjection was then performed for the LC–MS/MS quantitative analysis.

### 3.1. LC–MS/MS analysis

A Hewlett-Packard 1050 HPLC was used for the HPLC analysis. An Alltima C18 column (250 mm  $\times$  2.1 mm i.d., 5  $\mu\text{m}$ ) with a guard column of the same packing material was used for the separation. Gradient elution of A (10 mM ammonium formate and 0.5% formic acid) and B (acetonitrile) started with 10% B for 20 min, increased to 70% within 1 min and then hold for 34 min. The flow rate was 0.2 ml/min. The sample injection amount was 10  $\mu\text{l}$ . Under the HPLC conditions, the phenolic compounds and the tanshinones were well separated into two groups.

The MS experiments were conducted on a Perkin-Elmer PE-Sciex API 365 triple quadrupole mass spectrometer equipped with a Turbo-ion spray interface. The MS and MS/MS parameters were optimized with representative reference compounds by direct infusion. Negative ion mode was used to monitor phenolic compounds for the first 25 min. Positive ion mode was used for analyzing tanshinones from 25 min to 55 min. During the LC–MS/MS analysis, a time-segment program was developed to switch the ionization mode from negative to positive at the retention time of 25 min. Both positive and negative ion modes were performed with multiple-reaction-monitoring (MRM) for the quantitative analysis. The MS and MS/MS spectra of the internal standard and the seven Danshen components were acquired

by direct infusion of each standard in methanol with the concentration of 5  $\mu\text{g/ml}$  at the flow rate of 5  $\mu\text{l/min}$ . The MRM quantitative ions were then selected from the MS/MS results.

Nicotinic acid (MW = 123), danshensu (MW = 198), protocatechuic acid (MW = 154), protocatechuic aldehyde (MW = 138) and caffeic acid (MW = 180) were detected in the negative. Cryptotanshinone (MW = 296), tanshinone I (MW = 276), tanshinone IIA (MW = 294) were detected in the positive. Typical MS conditions of each component in Danshen and the internal standard were showed in Table 1.

## 4. Results and discussion

### 4.1. LC–MS/MS with time-segment program

Negative electrospray ionization (ESI) was found to provide better sensitivity for the phenolic components of Danshen than the positive ion mode. On the other hand, positive ESI provided better sensitivity for the tanshinones. Thus, conventional LC–MS method using one ionization mode may not provide unique good sensitivity for both of the water-soluble and lipid-soluble components. In order to achieve low detection limits required for supporting pharmaceutical studies of Danshen and its related medicines, double injection was previously needed for the LC–MS analysis with respective positive and negation ionization mode. This analytical procedure with two injections was time- and resource consuming. Thus, we have investigated the feasibility of developing a time-segment program applying the different ionization mode of ESI in one single LC–MS run [15,16].

HPLC conditions were optimized in order to separate the two groups of compounds. Under the current HPLC conditions, retention times of the targeted Danshen components were obtained from multiple injections of inter- and intra-day during the entire method development and sample analysis time period. Danshensu, protocatechuic acid, protocatechuic aldehyde and caffeic acid, cryptotanshinone, tanshinone I and tanshinone IIA had retention time at 5.1 min, 8.8 min, 13.2 min, 17.6 min, 36.3 min, 38.8 min and 45.5 min, respectively. The data indicated that the phenolic acids and tanshinone components from Danshen were well separated, allowing the application of the time-segment program for the simultaneous analysis. Because the phenolic compounds were eluted first, negative ion mode was applied for the 1st time-segment running to the chromatographic retention time at 25 min. The ionization mode was then

Table 1  
Typical MS/MS conditions of the Danshen components and the internal standard

Component	Ionspray voltage (V)	Orifice voltage (V)	Collision voltage (eV)	MS/MS transition
Danshensu	–4200	–26	–13	197 > 179
Protocatechuic acid	–4200	–21	–17	153 > 109
Protocatechuic aldehyde	–4200	–31	–25	137 > 108
Caffeic acid	–4200	–16	–19	179 > 135
Nicotinic acid	–4200	–21	–15	122 > 78
Cryptotanshinone	4800	56	29	297 > 251
Tanshinone I	4800	56	25	277 > 249
Tanshinone IIA	4800	51	25	295 > 277

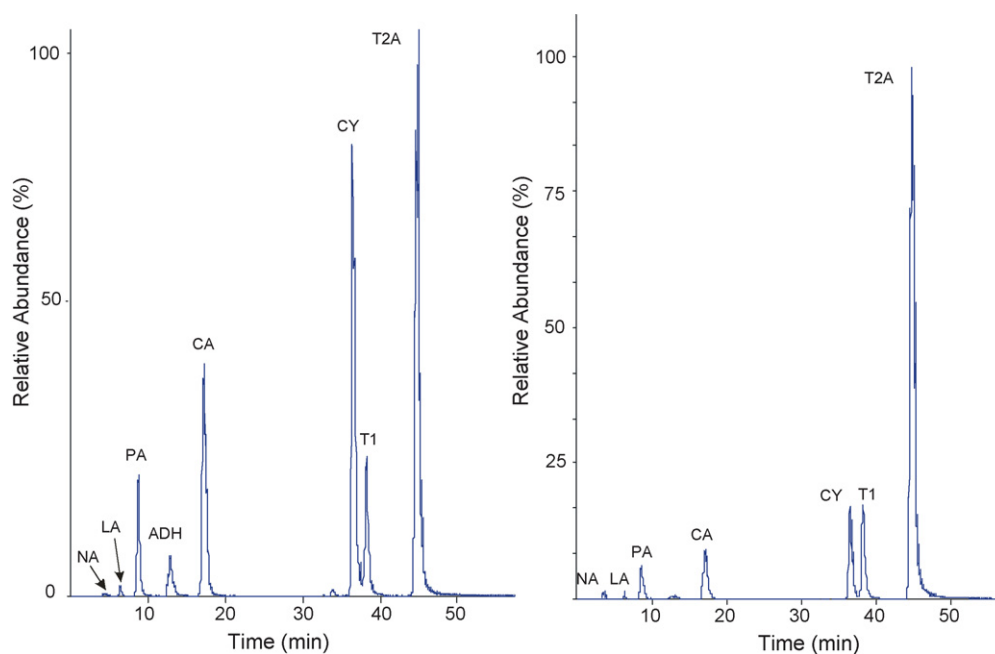


Fig. 2. TIC chromatograms obtained from the MRM analysis of the spiked matrix sample of Danshen herb (left) and the Danshen tablet sample (right). The spiked levels of the components were described in Section 2. Nicotine acid (NA, the internal standard), danshensu (LA), protocatechuic acid (PA), protocatechuic aldehyde (ADH), caffeic acid (CA) were analyzed with negative electrospray ionization, while cryptotanshinone (CY), tanshinone I (T1) and tanshinone IIA (T2A) were determined with positive ionization mode.

switched to positive ionization mode for the analysis of tanshinones. MRM quantitative ions were selected for each of the time segments. The selection of the quantitative ions was based on the criteria of the highest peak intensity and lowest cross-talk or interference.

#### 4.2. Identification of the Danshen components in Danshen herbs and tablet

The applicability of the developed LC–MS/MS method with time-segment program was examined with the analysis of the *Salviae miltorrhiza* herb and tablet samples. By using the HPLC conditions developed in the reversed-phase LC–MS/MS method, both the phenolic compounds and the tanshinones were successfully separated and identified simultaneously (Fig. 2). The retention times of the Danshen components are listed in Table 2. The Danshen components in the herb and tablet samples were identified by matching their retention times and confirmed

by interpreting and comparing the MS/MS spectra with those of the corresponding standards. Fig. 3 shows the MS/MS spectra of caffeic acid and cryptotanshinone obtained from the analysis of the tablet sample. The LC–MS analysis of caffeic acid (MW = 180.2) produced a negative ion of  $m/z$  179.1, corresponding to the  $[M - H]^-$  precursor ion. Subsequent product ion scan of this precursor ion produced a fragmentation pattern dominated by an ion at  $m/z$  135.0. The identification of caffeic acid in the tablet sample was done with the detection of the MS/MS ion at the retention time at 17.6 min (Table 2). Similarly, cryptotanshinone (MW = 296.4) was identified in the tablet sample at 36.3 min. However, a positive ion of  $m/z$  297.3 corresponding to the  $[M + H]^+$  precursor ion was detected in the LC–MS analysis because positive ion mode was applied (Fig. 3). The MS/MS analysis of cryptotanshinone produced dominate fragment ions at  $m/z$  279.0 and  $m/z$  251.0. Other components in the Danshen herb and tablet samples were identified in a similar way.

Table 2  
Method validation data of the Danshen active components from the analysis of matrix spiked samples

Component	Retention time (min)	LOD ( $\mu\text{g/g}$ )	Herb		Tablet	
			Recovery (%)	R.S.D. <sup>a</sup> (%)	Recovery (%)	R.S.D. <sup>a</sup> (%)
Danshensu	5.1	0.30	106.4	5.2	94.2	4.7
Protocatechuic acid	8.8	0.56	101.4	2.4	98.1	3.0
Protocatechuic aldehyde	13.2	0.68	97.2	7.7	90.1	5.8
Caffeic acid	17.6	0.44	103.2	8.0	101.6	6.5
Cryptotanshinone	36.6	0.61	85.4	3.4	89.2	4.8
Tanshinone I	38.8	0.52	104.9	3.2	92.6	3.0
Tanshinone IIA	45.5	0.83	91.1	2.4	94.1	2.1

<sup>a</sup>  $n = 6$ .

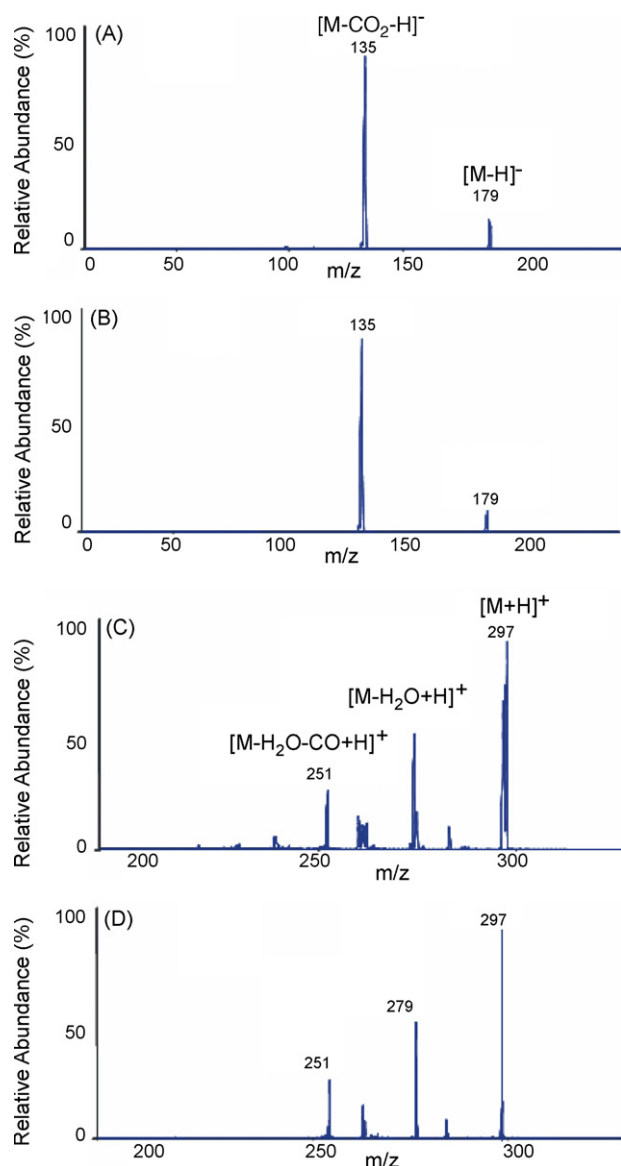


Fig. 3. MS/MS spectra obtained from the analysis Danshen tablet sample for caffeic acid (A) and cryptotanshinone (C), compared with the standard spectra of caffeic acid (B) and cryptotanshinone (D).

#### 4.3. Quantitative analysis of the Danshen components in Danshen herbs and tablet

Internal standard method was used for the sample analysis. Calibration curves of the seven Danshen standards were constructed using the raw data from the LC–MS/MS experiments. Linear calibration curves with the correlation coefficients ranging from 0.9960 to 0.9992 were obtained from 0.5 ng/ $\mu$ l to 100 ng/ $\mu$ l and from 0.25 ng/ $\mu$ l to 50 ng/ $\mu$ l for phenolic components and tanshinones, respectively. Although the calibration curves were obtained with the standard analysis due to the lack of matrix blank, the potential signal suppression was tested with the analysis of matrix spiked samples. The obtained results indicated matrix interference was minimal due the application of MS/MS modes with high specificity. In particular, no detectable cross-interference was found around the retention time of each

Table 3

Results of the simultaneous determination of the Danshen active components in Danshen herb and tablet samples

Component	$C_{\text{Herb}}$ (mg/g <sup>a</sup> )	$C_{\text{Tablet}}$ (mg/g) <sup>a</sup>
Danshensu	0.10	0.089
Protocatechuic acid	0.020	0.008
Protocatechuic aldehyde	0.014	ND <sup>b</sup>
Caffeic acid	0.080	0.036
Cryptotanshinone	0.37	0.11
Tanshinone I	0.081	0.060
Tanshinone IIA	1.20	1.02

<sup>a</sup> Data were averaged from the analyses of three homogenized samples.

<sup>b</sup> ND: not detected.

Danshen component. The calibration standards were repeatedly analyzed during the entire 8-month study period for testing the stability of the Danshen components and the reproducibility of the LC–MS/MS analysis. Variation of less than 5% in relative standard deviation was obtained, indicating the good stability of Danshen components under the conditions for standard solutions as well as the excellent analytical reproducibility.

The detection limits defined as signal-to-noise ratio of 3 ranged from 0.03 ng/ $\mu$ l to 0.12 ng/ $\mu$ l when the injection volume of standard solutions was 10  $\mu$ l, which corresponded to the method detection limits 0.30  $\mu$ g/g to 0.83  $\mu$ g/g when 1.0 g of the Danshen herb or tablet sample was analyzed. The recoveries of the seven Danshen compounds were determined from the analysis of the spiked samples. Table 2 listed the recovery data that ranged between 85.4% and 106.4% and the relative standard deviations of 2.4% and 8.0% ( $n=6$ ) for the Danshen herb matrix. Better recovery and precision data were received for the spiked Danshen tablet samples. The inter-day stability test conducted by re-injecting the extracts of the spiked samples next day showed no notable variations (less than 2%) for both recovery and precisions data.

The applicability of the developed method was further evaluated through the analysis of real Danshen samples, although only selected and limited Danshen herbs and tablet samples were analyzed. The internal calibration curves were applied for the determination of the targeted components. While this study mainly focuses on the LC–MS/MS method development for the simultaneous determination of the two different types of Danshen components by using a time-segment program for switching ESI polarity, levels of the seven Danshen components were measured at sub- to low mg/g. The obtained data indicated that the level profiles of the herb and tablet were significantly different (Table 3). Considering the statement claimed by the manufacturer that the tablet was made of Danshen herb, the different component profiles might be attributed from the possible degradation of some active components during the medicinal manufacturing treatment. Various sources of Danshen products may also give different levels of active components.

## 5. Conclusion

The developed method with a time-segment enabled the application of positive and negative ESI-MS for the analysis of

phenolic acids and tanshinone components in one single HPLC run. The method gave good recovery and precision, and was successfully applied for the simultaneous determination of the two different types of components in Danshen herb and tablet samples. The developed technique provides rapid and sensitive analysis of Danshen and its related medicinal products for quality control and authentication.

### Acknowledgement

The authors would like to acknowledge the financial supports for this study from the Research Grant Council, University Grants Committee of Hong Kong (HKBU2014/05M).

### References

- [1] H.B. Li, F. Chan, *J. Chromatogr. A* 925 (2001) 109–114.
- [2] X. Pan, G. Niu, H. Liu, *J. Chromatogr. A* 922 (2001) 371–375.
- [3] Pharmacopoeia Committee of the Health Ministry of the People's Republic of China (Ed.), *Pharmacopoeia of People's Republic of China*, vol. 1, Guangdong Scientific Technologic Publisher, Guangdong, 2000.
- [4] R. Kasimu, K. Tanaka, Y. Tezuka, Z.N. Gong, J.X. Li, P. Basnet, T. Namba, S. Kadota, *Chem. Pharm. Bull.* 46 (1998) 500–504.
- [5] M. Satoshi, G. Yuri, S. Yukihiro, *J. Nat. Products* 57 (6) (1994) 817–823.
- [6] N. Nakamura, S. Kojima, Y.A. Lim, M.R. Meselhy, M. Hattori, M.P. Gupta, M. Correa, *Phytochemistry* 46 (1997) 1139–1141.
- [7] H. Tada, Y. Murakami, T. Omoto, K. Shimomura, K. Ishimaru, *Phytochemistry* 42 (1996) 431–434.
- [8] G. Janicsak, I. Mathe, *Chromatographia* 46 (5/6) (1997) 322–324.
- [9] K. Kamata, T. Iizuka, M. Nagai, Y. Kasuya, *G. Pharma.: Vascular Syst.* 24 (1993) 977–981.
- [10] A. Nazly, G. Nezhun, K. Avni, P. Thitima, P. John, S. Qiu, C. Geoffrey A, *J. Nat. Products* 60 (11) (1997) 1170–1173.
- [11] W.M.A. Niessen, *Liquid Chromatography—Mass Spectrometry*, in: *Chromatogr. Sci. Series*, vol. 79, second ed., Marcel Dekker Inc., New York, NY, 1999.
- [12] H.T. Liu, K.T. Wang, H.Y. Zhang, X.G. Chen, Z.D. Hu, *Analyst* 125 (2000) 1083–1086.
- [13] Z. Shi, J. He, T. Yao, W. Chang, M. Zhao, *J. Pharm. Biomed. Anal.* 37 (2005) 481.
- [14] J.L. Zhang, M. Cui, Y. He, H.L. Yu, D.A. Guo, *J. Pharm. Biomed. Anal.* 36 (2005) 1029–1035.
- [15] E. Fung, Z. Cai, A. Sinhababu, *J. Chromatogr. B* 754 (2001) 285–293.
- [16] K.C. Lee, J.L. Wu, Z. Cai, *J. Chromatogr. B* 843 (2006) 247–251.

# Study of the interactions of berberine and daunorubicin with DNA using alternating penalty trilinear decomposition algorithm combined with excitation–emission matrix fluorescence data

A-Lin Xia, Hai-Long Wu\*, Shu-Fang Li, Shao-Hua Zhu,  
Yan Zhang, Qing-Juan Han, Ru-Qin Yu

*State Key Laboratory of Chemo/Biosensing and Chemometrics, College of Chemistry and Chemical Engineering,  
Hunan University, Changsha 410082, China*

Received 27 January 2007; received in revised form 6 April 2007; accepted 6 April 2007  
Available online 24 April 2007

## Abstract

Studies of interactions between drugs and DNA are very interesting and significant not only in understanding the mechanism of interaction, but also for guiding the design of new drugs. However, until recently, mechanisms of interactions between drug molecules and DNA were still relatively little known. It is necessary to introduce more simple methods to investigate the mechanism of interaction. In this study, the interactions of daunorubicin (DNR) or berberine (BER) with DNA and the competitive interactions of DNR and BER with DNA have been studied by alternating penalty trilinear decomposition algorithm (APTLD) combined with excitation–emission matrix fluorescence data. The excitation and emission spectra as well as the relative concentrations of co-existing species in different reaction and equilibrium mixtures can be directly and conveniently obtained by the APTLD treatment. The results obtained are valuable for providing a deeper insight into the interaction mechanism of DNR and BER with DNA. It is proved that the fluorescence spectrum of complex DNR–DNA is different from that of DNR. Furthermore, the present method provides a new way to search for a new non-toxic, highly efficient fluorescent probe. For controversial interaction mechanism of the drugs and DNA, it can provide a helpful verification.

© 2007 Published by Elsevier B.V.

**Keywords:** Drug; DNA; Interaction; APTLD; Daunorubicin; Berberine

## 1. Introduction

Chemotherapy is an important part of the program for cancer treatment. A lot of compounds have been developed as potential candidates for anticancer drugs, but only a handful of them have become effective clinical drugs [1,2]. The development of new drugs requires that the underlying mechanism of the drug action at the cellular and molecular levels be better understood. The study on the interaction of small molecules with DNA is of great importance in many areas [1–11]. Many anticancer drugs are known to interact with deoxyribonucleic acid (DNA) to exert their biological activities. Generally, DNA-acting anticancer drugs can be classified into three categories. Drugs of the first category form covalent linkages with DNA. Drugs of

the second category form noncovalent complexes with DNA by either intercalation or groove-binding. Drugs of the final category cause DNA backbone cleavages [2].

Daunorubicin (DNR) is an anthracycline antibiotic with antiproliferative and anticancer activity, which is linked by the formation of intercalative complexes with DNA and the inhibition of both DNA and RNA synthesis [9–11]. Berberine, an alkaloid, is the active component of *Coptis chinensis*, which is a traditional Chinese medicine. It is initially used as an antibiotic and has a wide range of pharmacological activities, including antisecretory, anti-inflammatory, antimicrobial, antimalarial as well as anticancer properties and cardiovascular actions [12–18]. Despite its slightly buckled structure due to the partial saturation of the central ring, berberine has been previously characterized as a DNA intercalating agent and as a cationic ligand, electrostatic forces play an important role in its interaction with DNA [19–25]. However, the intercalation mechanism initially proposed [26] contradicted a minor groove orientation

\* Corresponding author. Fax: +86 731 8821818.  
E-mail address: [hlwu@hnu.cn](mailto:hlwu@hnu.cn) (H.-L. Wu).

mechanism recently proposed on the basis of NMR analyses [27].

It is very interesting and significant that interactions between drugs and DNA are studied for understanding the mechanism of interaction and guiding the design of new drugs. The interactions between drugs and DNA have been studied with structural tools, including high resolution X-ray diffraction and NMR spectroscopy [28] and utilizing Scatchard plot [29]. However, until recently, relatively little was known as far as the detailed interactions between DNA (including some unusual structures) and drug molecules. It is necessary to introduce more simple methods to investigate the mechanism of interaction.

With the development of modern high-order analytical instruments and data collection techniques, in particular the application of chemometrics methods dealing with three-way data set [30–40], it becomes possible to study the interactions between drugs and DNA, and one can conveniently predict the interaction model of the drug of interest with DNA even when there exists a complicated chemical equilibrium in the mixtures. The attractive predominance lies in the fact that the decomposition of a three-way data array is often unique, allowing relative concentrations and profiles (in the spectral, time, pH or other domains) of individual components in a complex system to be extracted directly. The type of studies is especially valuable for guiding the use of clinical drugs and the design of new drugs.

The interactions of DNR and berberine (BER) with DNA have been studied in the present paper. Chemical structures of DNR and BER are characterized in Fig. 1. A series of three-way data arrays has been obtained by excitation–emission fluorescence spectroscopy and resolved by the APTLD algorithm [30]. The results revealed that relative concentrations, excitation and emission spectra profiles of individual components in interaction systems can be conveniently achieved and provide valuable information for a deeper insight into the interaction mechanisms of DNR and BER with DNA.

## 2. Theory

The  $K$  size of matrices  $I \times J$  of the excitation–emission fluorescence spectra are obtained by measuring  $K$  equilibrium mixtures containing  $N$  fluorescing components at  $I$  excitation

and  $J$  emission wavelengths. A three-way data array  $\underline{\mathbf{X}}$  is obtained with dimensions  $I \times J \times K$ . According to the trilinear model, i.e. PARAFAC model [41], each element  $x_{ijk}$  of the data array  $\underline{\mathbf{X}}$  has the form:

$$x_{ijk} = \sum_{n=1}^N a_{in} b_{jn} c_{kn} + e_{ijk},$$

$$(i = 1, 2, \dots, I; \quad j = 1, 2, \dots, J; \quad k = 1, 2, \dots, K) \quad (1)$$

where  $x_{ijk}$  is the element  $(i, j, k)$  of  $\underline{\mathbf{X}}$ ,  $N$  denotes the number of factors, which should correspond to the total number of detectable species, including component(s) of interest and background as well as unknown interferences;  $e_{ijk}$  the element of an  $I \times J \times K$  three-way residual array  $\underline{\mathbf{E}}$ ;  $a_{in}$  the element  $(i, n)$  of an  $I \times N$  matrix  $\mathbf{A}$  corresponding to excitation spectra profiles of  $N$  species;  $b_{jn}$  the element  $(j, n)$  of a  $J \times N$  matrix  $\mathbf{B}$  corresponding to emission spectra profiles of  $N$  species;  $c_{kn}$  the element  $(k, n)$  of a  $K \times N$  matrix  $\mathbf{C}$  corresponding to relative concentrations of  $N$  species.

Regardless of scaling and permutation, the decomposition of the trilinear model proposed above will be unique and no free rotations provided that  $k_1 + k_2 + k_3 \geq 2N + 2$  [41–43], where  $k_1$ ,  $k_2$  and  $k_3$  are  $k$ -ranks of  $\mathbf{A}$ ,  $\mathbf{B}$  and  $\mathbf{C}$ , respectively. In other words, the profile matrices  $\mathbf{A}$ ,  $\mathbf{B}$  and  $\mathbf{C}$  will be resolved in a unique way.

The APTLD algorithm [30] is an alternative one and used to solve the PARAFAC model by utilizing alternating least-squares principle and the alternating penalty constraints to minimize three different alternating penalty (AP) errors simultaneously. It assumes the loadings in two modes and then estimates the unknown set of parameters of the last mode until optimizing the residuals of the model. For detail information of the APTLD algorithm, one could refer to the literature [30]. The number of responsive factors ( $N$ ) can be estimated by several methods. In this study, core consistency diagnostic (CORCONDIA) [44], which compares the results from the core matrix of the Tucker3 and PARAFAC models with different factors attempted, and ADD-ONE-UP [45], which unfolds the three-way data along with the two orders into two cube matrices and then runs PARAFAC algorithm twice to compare the residuals of different factors, were used to estimate the chemical rank of three-way data arrays.

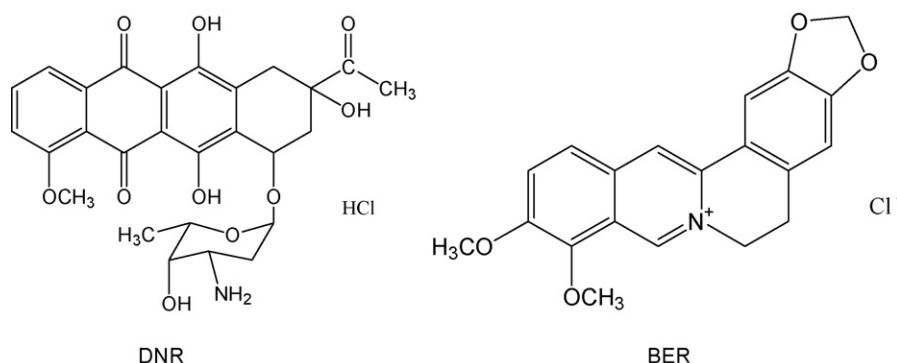


Fig. 1. Chemical structures of DNR and BER.





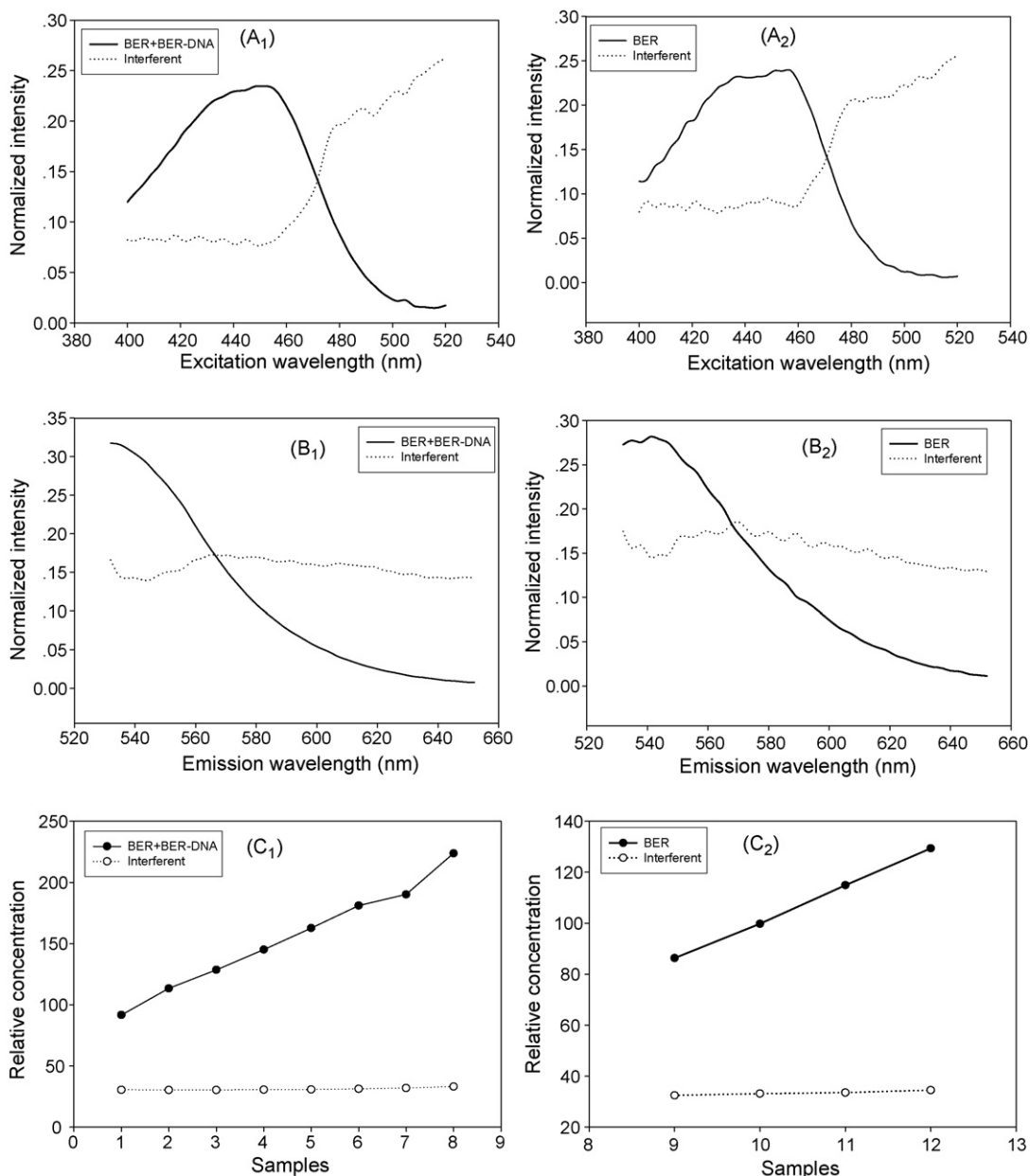


Fig. 2. Resolved excitation–emission spectral and relative concentration profiles of each component using APTLD when the chosen factor number was two.

ment is possibly contributed to the model for interferent. In order to confirm it, a data array produced by the samples of Nos. 9–12 was analyzed using APTLD. The profiles resolved by APTLD are shown in Fig. 2. One observes that the excitation and emission spectra of BER and BER–DNA are almost the same and the interferent is assuredly present in chemical BER purchased, but its fluorescence is very weak. Furthermore, it is seen from Fig. 2(C<sub>1</sub>) and (C<sub>2</sub>) combined with Table 1 that the fluorescence is largely enhanced when BER binds to DNA and the fluorescence yield of BER in the absence of DNA is poor.

#### 4.2. Interaction of DNR and DNA

Nos. 13–24 samples were measured and a three-way data array was produced. Two components are obtained for the model

using CORCONDIA and ADD-ONE-UP. A component is contributed to the model for DNR. A possible component is complex DNR–DNA. When APTLD algorithm runs with two components for the three-way data array measured, the resolved profiles are shown in Fig. 3(A<sub>1</sub>)–(C<sub>1</sub>). The results revealed that the resolved DNR spectral profiles are nearly the same as actual ones.

To distinguish whether another component is complex DNR–DNA, not the impurity from chemical DNR, a data array produced by the samples of Nos. 25–28 only containing DNR was analyzed using APTLD. One factor is obtained for the model using CORCONDIA and ADD-ONE-UP. It has been proved that when the component number estimated for a complex system is more than or equal to the real one, the APTLD algorithm is a robust method. Therefore, in order to fully illuminate that

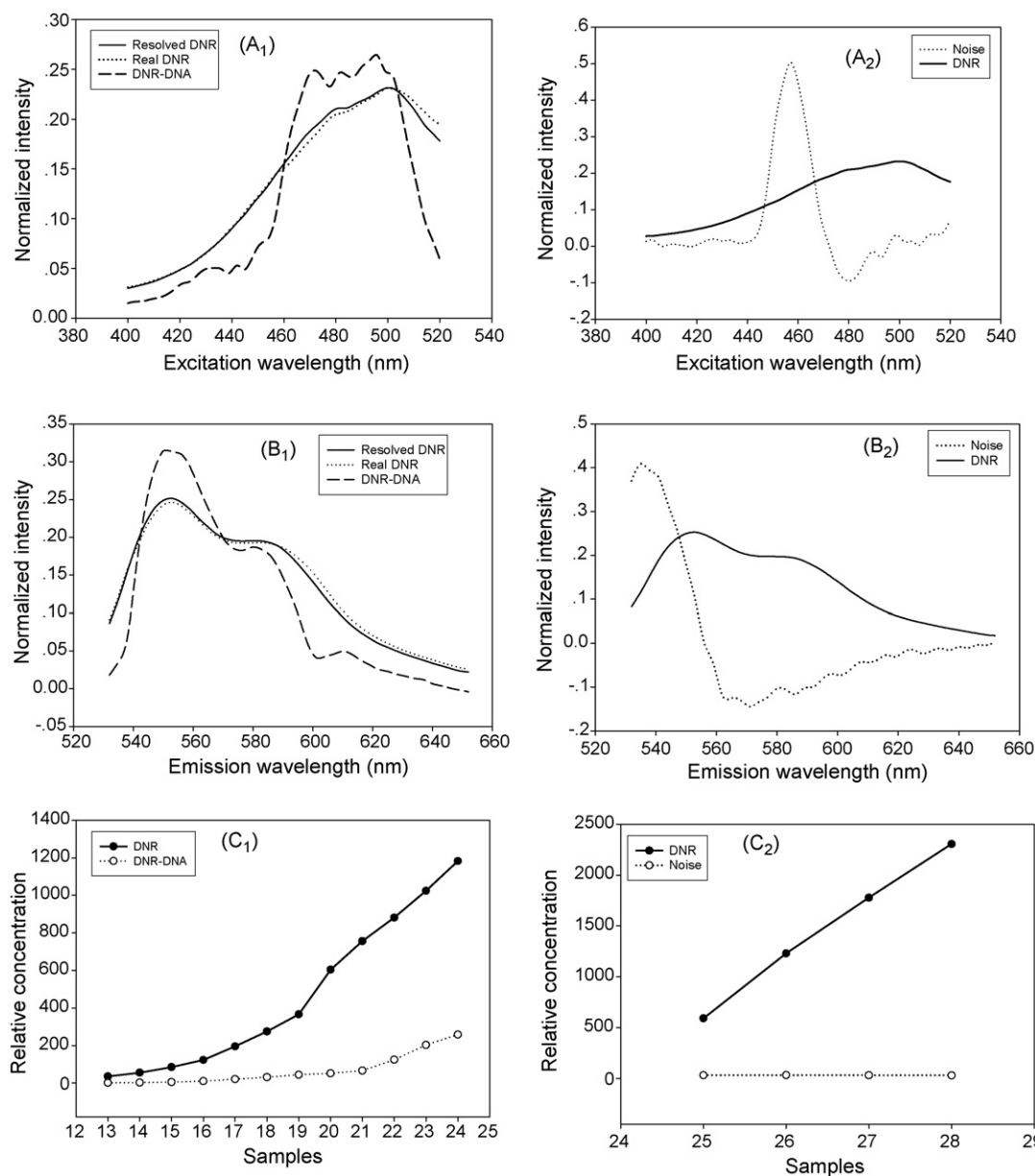


Fig. 3. Actual spectral profiles of DNR and resolved excitation–emission spectral and relative concentration profiles of each component using APTLD when the chosen factor number was two ( $N=2$ ).

another component is not the impurity from chemical DNR, two factors are still chosen. It is seen from Fig. 3(A<sub>2</sub>)–(C<sub>2</sub>) that relative concentrations of another component are nearly equal to zero and it is fitting pseudo component. Fig. 3 combined with Table 1 shows that the fluorescence spectrum of complex DNR–DNA is similar to and different from that of DNR. Furthermore, its fluorescence is far weaker than that of DNR, which is also consistent with the conclusion that the interaction of DNR with DNA is a complex reaction with quenching of the fluorescence [46].

Interestingly, Angeloni et al. [47] studied the interaction between adriamycin and DNA and reported that the fluorescence spectrum of complex adriamycin–DNA is different from that of adriamycin. However, for DNR, similar conclusion can be simply obtained by three-way analysis.

#### 4.3. Competitive interaction of DNR and BER with DNA

Aiming to study competitive interaction of DNR and BER with DNA, Nos. 29–39 samples contain the same initial amount of DNA and BER, and only the initial concentration of DNR varied and increased gradually (see Table 3). The samples were measured on fluorescence spectrophotometer and produced a three-way data array. After CORCONDIA and ADD-ONE-UP were used to estimate the chemical rank, two components were acquired. However, from Fig. 4, it is obviously seen that there are three components in the system. It is possibly owed to the fact that the two methods estimating the chemical rank are required to run PARAFAC which bears two-factor degeneracy [48,49] and is not satisfactory in dealing with high multicollinearity. It can be the optimum number of components for PARAFAC. Interest-

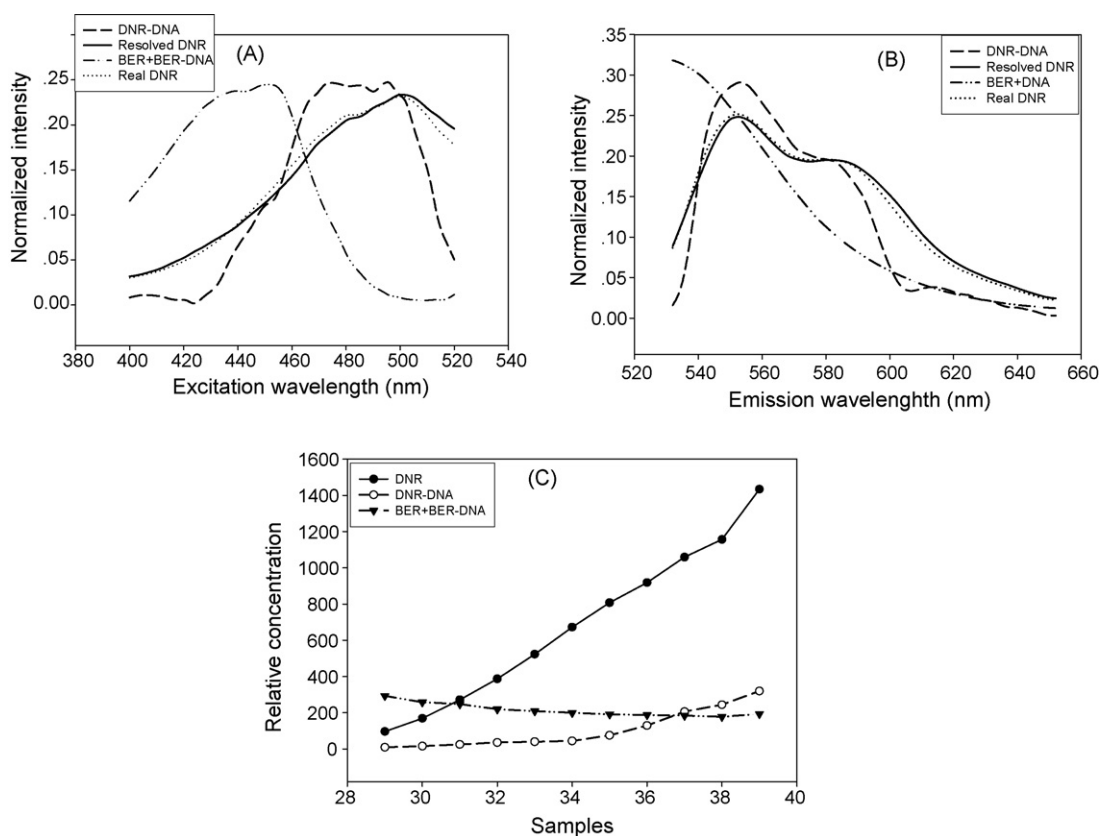


Fig. 4. Actual spectral profiles of DNR and resolved excitation–emission spectral and relative concentration profiles of each component using APTLD when the chosen factor number was three ( $N=3$ ).

ingly, when APTLD replaces PARAFAC in the two methods, the estimated number of components was three. The result reveals APTLD can overcome high multicollinearity to some extent. Therefore, it is reasonable that the number of components was chosen as three for APTLD, i.e. DNR, DNR–DNA and BER–DNA. As for the impurity from chemical BER, the poor fluorescence results in its burial in strong fluorescence environment.

Fig. 4 shows resolved profiles of each component using APTLD and actual excitation and emission spectra profiles of DNR. Fig. 1 demonstrates that a possible interaction between DNR and BER can be ruled out. Combined with above results, one can confirm that the resolved spectral and concentration profiles correspond to that of DNR, DNR–DNA and BER–DNA (Fig. 4). It can be seen from Fig. 4(C), the relative concentration of DNR and DNR–DNA increased gradually and the relative concentration of BER–DNA decreased gradually when the initial concentration of DNR increased gradually. The phenomena illuminated that the equilibrium concentration of complex DNR–DNA and free BER increased gradually with the increase of initial concentration of DNR. One can assume that the interaction of DNR and BER with DNA possesses a competitive mechanism, that is, the interactions are a pair of the parallel competitive reactions. It is well known that the interaction of DNR with DNA follows the intercalation model and then that DNR is an intercalator [9,10]. Consequently, one can think that DNR intercalates into the same base sites of DNA as the bound

BER and the interaction mechanism of BER and DNA is the same interaction model of DNR and DNA, that is, BER being an intercalator and intercalating between the base pairs of doublestranded DNA, which is also consistent with the conclusions from the literatures [19–25].

Interestingly, Krey et al. [26] studied the interaction between BER and DNA and reported that the interaction mechanism belonged to the intercalation mechanism. However, it contradicted a minor groove orientation mechanism recently proposed on the basis of NMR analyses [27]. In present study, the results demonstrate that the interaction mechanism of BER and DNA is the intercalation model. In addition, all results display that the analysis of three-way data array can provide more direct visualization of the equilibrium state of the system studied, as compared with the traditional method using Scatchard plot [29] or others. It is significant to apply clinical drugs and design new drugs.

## 5. Conclusions

Several data arrays have been analyzed by APTLD combined with excitation–emission matrix fluorescence. The results presented demonstrated that the method can conveniently achieved and provide valuable information from complex systems. Accordingly, the strategy of using this chemometric tool can redound to study of the interaction mechanisms between drugs and DNA. It can be proved that the fluorescence spectrum

of complex DNR–DNA is different from that of DNR. Moreover, for controversial interaction mechanism of BER and DNA, the method can provide a helpful proof that BER is an intercalator. Consequently, BER can be widely applied as a non-toxic fluorescent probe to replace highly toxic fluorescent probe, such as ethidium bromide. To search for a new non-toxic, highly efficient fluorescent probe, the present method can provide a new way.

### Acknowledgements

The authors would like to thank the National Nature Science Foundation of China (Grant Nos. 20475014 and 20435010) and the Nature Science Foundation of Hunan Province for financial support.

### References

- [1] J.W. Lown (Ed.), *Anthracycline and Anthracenedione-Based Anticancer Agents*, Elsevier, Amsterdam, 1988.
- [2] W. Priebe (Ed.), *Anthracyclines Antibiotics. New Analogs, Methods of Delivery, and Mechanisms of Action*, American Chemical Society, Washington, DC, 1995.
- [3] X.X. Dai, Y.F. Li, W. He, Y.F. Long, C.Z. Huang, *Talanta* 70 (2006) 578.
- [4] Y.Q. Li, Y.J. Guo, X.F. Li, J.H. Pan, *Talanta* 71 (2007) 123.
- [5] C.L. Tong, Z. Hu, W.P. Liu, *Talanta* 71 (2007) 816.
- [6] P. Palaska, E. Aritzoglou, S. Girousi, *Talanta* 72 (2007) 1199.
- [7] T.A. Ivandini, K. Honda, T.N. Rao, A. Fujishima, Y. Einaga, *Talanta* 71 (2007) 648.
- [8] L. Guo, W.J. Dong, X.F. Tong, C. Dong, S.M. Shuang, *Talanta* 70 (2006) 630.
- [9] F. Zunino, A. Di Marco, A. Zaccara, R.A. Gambetta, *Biochim. Biophys. Acta* 607 (1980) 206.
- [10] D.C. Ward, E. Reich, I.H. Goldberg, *Science* 149 (1965) 1259.
- [11] N.S. Mizuno, B. Zakis, R.W. Decker, *Cancer Res.* 35 (1975) 1542.
- [12] E.K. Marinova, D.B. Nekoosa, D.N. Popover, G.B. Gallagher, N.D. Ivanovska, *Immunopharmacology* 48 (2000) 9.
- [13] H. Zhou, S. Mineshita, *J. Pharmacol. Exp. Ther.* 294 (2000) 822.
- [14] W.H. Ko, X.Q. Yao, C.W. Lau, W.I. Law, Z.Y. Chen, W. Kwok, K. Ho, Y. Huang, *Eur. J. Pharmacol.* 399 (2000) 187.
- [15] N. Mitani, K. Murakami, T. Yamaura, T. Ikeda, I. Saiki, *Cancer Lett.* 35 (2001) 165.
- [16] W.A. Creasey, *Biochem. Pharmacol.* 28 (1979) 1081.
- [17] T.C. Birdsall, G.S. Kelly, *Alt. Med. Rev.* 2 (1997) 94.
- [18] C.W. Lau, X.Q. Yao, Z.Y. Chen, W.H. Ko, Y. Huang, *Cardiovasc. Drug Rev.* 19 (2001) 234.
- [19] M.W. Davidson, I. Lopp, S. Alexander, W.D. Wilson, *Nucl. Acids Res.* 4 (1977) 2697.
- [20] M. Cushman, F.W. Dekow, L.B. Jacobsen, *J. Med. Chem.* 22 (1979) 331.
- [21] M. Maiti, K. Chaudhuri, *Indian J. Biochem. Biophys.* 18 (1981) 245.
- [22] D. Debnath, G.S. Kumar, R. Nandi, M. Maiti, *Indian J. Biochem. Biophys.* 26 (1989) 201.
- [23] G.S. Kumar, D. Debnath, M. Maiti, *Anticancer Drug Des.* 7 (1992) 305.
- [24] G.S. Kumar, D. Debnath, A. Sen, M. Maiti, *Biochem. Pharmacol.* 46 (1993) 1665.
- [25] Y. Qin, J.Y. Pang, W.H. Chen, Z.W. Cai, Z.H. Jiang, *Bioorg. Med. Chem.* 14 (2006) 25.
- [26] A.K. Krey, F.E. Hahn, *Science* 166 (1969) 755.
- [27] S. Mazzini, M.C. Belluci, R. Mondelli, *Bioorg. Med. Chem. Lett.* 11 (2003) 505.
- [28] X.L. Yang, A.H.-J. Wang, *Pharmacol. Ther.* 83 (1999) 181.
- [29] J.B. Lepecq, C. Paoletti, *J. Mol. Biol.* 27 (1967) 87.
- [30] A.L. Xia, H.L. Wu, D.M. Fang, Y.J. Ding, L.Q. Hu, R.Q. Yu, *J. Chemom.* 19 (2005) 65.
- [31] H.L. Wu, M. Shibukawa, K. Oguma, *J. Chemom.* 12 (1998) 1.
- [32] K.S. Booksh, Z. Lin, Z. Wang, B.R. Kowalski, *Anal. Chem.* 66 (1994) 2561.
- [33] Z.P. Chen, H.L. Wu, R.Q. Yu, *J. Chemom.* 15 (2001) 439.
- [34] H.P. Xie, X. Chu, J.H. Jiang, H. Cui, G.L. Shen, R.Q. Yu, *Spectrochim. Acta Part A* 59 (2003) 743.
- [35] Y.X. Tan, J.H. Jiang, H.L. Wu, H. Cui, R.Q. Yu, *Anal. Chim. Acta* 412 (2000) 195.
- [36] A.L. Xia, H.L. Wu, D.M. Fang, Y.J. Ding, L.Q. Hu, R.Q. Yu, *Anal. Sci.* 22 (2006) 1189.
- [37] J.H. Jiang, H.L. Wu, Z.P. Chen, R.Q. Yu, *Anal. Chem.* 71 (1999) 4254.
- [38] L.Q. Hu, H.L. Wu, J.H. Jiang, Y.J. Ding, A.L. Xia, R.Q. Yu, *Anal. Bioanal. Chem.* 384 (2006) 1493.
- [39] Y. Zhang, H.L. Wu, A.L. Xia, S.H. Zhu, Q.J. Han, R.Q. Yu, *Anal. Bioanal. Chem.* 386 (2006) 1741.
- [40] Y. Zhang, H.L. Wu, A.L. Xia, Q.J. Han, H. Cui, R.Q. Yu, *Talanta* 72 (2007) 926.
- [41] R.A. Harshman, *UCLA Working Papers in Phonetics*, 16(1970) 1.
- [42] P. Geladi, *Chemom. Intell. Lab. Syst.* 7 (1989) 11.
- [43] C.J. Appellof, E.R. Davidson, *Anal. Chem.* 53 (1981) 2053.
- [44] R. Bro, H.A.L. Kiers, *J. Chemom.* 17 (2003) 274.
- [45] Z.P. Chen, Z. Liu, Y.Z. Cao, R.Q. Yu, *Anal. Chim. Acta* 444 (2001) 295.
- [46] D. Vedaldi, F. Dallacqua, S. Caffieri, G. Rodighiero, *Farmaco. Ed. Sci* 37 (1982) 571.
- [47] L. Angeloni, G. Smulevich, M.P. Marzocchi, *Spectrochim. Acta* 38A (1982) 213.
- [48] B.C. Mitchell, D.S. Burdick, *Chemom. Intell. Lab. Syst.* 20 (1993) 149.
- [49] W.S. Rayens, B.C. Mitchell, *Chemom. Intell. Lab. Syst.* 38 (1997) 173.

# Simultaneous determination of nine aristolochic acid analogues in medicinal plants and preparations by high-performance liquid chromatography

Jinbin Yuan<sup>a,b</sup>, Lihua Nie<sup>a</sup>, Deyu Zeng<sup>c</sup>, Xubiao Luo<sup>d</sup>, Fei Tang<sup>a</sup>, Li Ding<sup>a</sup>,  
Qian Liu<sup>a</sup>, Manli Guo<sup>a</sup>, Shouzhuo Yao<sup>a,\*</sup>

<sup>a</sup> State Key Laboratory of Chemo/Biosensing & Chemometrics, Chemistry & Chemical Engineering College, Hunan University, Changsha 410082, PR China

<sup>b</sup> Key Laboratory of Modern Preparation of TCM, Ministry of Education, Jiangxi University of Traditional Chinese Medicine, Nanchang 330004, PR China

<sup>c</sup> Cancer Hospital of Hunan Province, Changsha, 410006, PR China

<sup>d</sup> Environmental & Chemical Engineering College, Nanchang Institute of Aeronautical Technology, Nanchang 330063, PR China

Received 5 March 2007; received in revised form 13 April 2007; accepted 18 April 2007

Available online 5 May 2007

## Abstract

By optimizing the extraction, separation and analytical conditions, a simple, reliable and effective high-performance liquid chromatography method coupled with photodiode array detector (HPLC–DAD) is presented for simultaneous determination of nine aristolochic acid (AA) analogues, i.e., AA I, AA II, AA C, AA D, 7-OH AA I, aristolic acid, AL II, AL III and AL IV, in twelve medicinal herbs and two preparations. The separation was completed on a C18 column with aqueous methanol containing 0.2% (V/V) acetic acid as mobile phase. Linearities of around two orders of magnitude were obtained with correlation coefficients exceeding 0.9950. Satisfactory intra-day and inter-day precisions were achieved with R.S.D.s less than 4.35%, and the average recovery factors obtained were in the range of 88.4–98.8%. The proposed method appears to be suitable for use as a tool for safety assurance and quality control for commercially available suspect samples containing aristolochic acid analogues.

© 2007 Published by Elsevier B.V.

**Keywords:** Aristolochic acid analogues; HPLC; *Aristolochiaceae*; Traditional chinese medicine; Herbal preparation

## 1. Introduction

Aristolochic acid (AA) analogues are known to be present in *Aristolochiaceae* plants including *Aristolochia* and *Asarum* genera [1,2]. A number of *Aristolochiaceae* plants and their preparations have been used in traditional and folk medicines in many countries as anti-inflammatory agents for arthritis, gout, rheumatism and diuresis [2–5]. Some North American species have been used for the treatment of snakebites. About 29 aristolochic acids (AAs) and 23 aristololactams (ALs) had been found in *Aristolochiaceae* plants until 2000 [2]. Among them, six AAs, namely AA I, II, C, D, 7-OH AA I and aristolic acid, and four ALs, namely, AL I, II, III and IV, are the main active constituents (Fig. 1).

The anti-inflammatory properties of AA had encouraged its use in various drug formulations in Germany [6] until it was iden-

tified as a potential carcinogen in rodents by Mengs [7–9]. In 1993, cases of rapidly progressive renal fibrosis found in young Belgian women were reported to be associated with aristolochic acids [10]. Since then, the so-called “Chinese herbs nephropathy” (CHN) was used all around the world. The term “CHN” is very prejudicial and has finally been corrected as “AAN” (aristolochic acid nephropathy). During the following years, the analogues were found to be nephrotoxic [10–14], carcinogenic [13–16] and mutagenic [17,18]. Balachandran et al. indicated that the analogues have more or less cytotoxic effect [19]. Therefore, the use of *Aristolochia* genera in herbal medicines is no longer permitted in many countries due to the toxicity of the aristolochic acid constituents. In TCM, *Aristolochia* species are also considered to be interchangeable with other commonly used herbal ingredients and substitution of one plant species for another is an established practice. Herbal ingredients are traded using their common Chinese Pinyin name and this may lead to confusion. Therefore, it is necessary to develop an analytical method which can be used to confirm the absence or presence of aristolochic acid analogues in any drug products.

\* Corresponding author. Tel.: +86 731 8821968; fax: +86 731 8821848.  
E-mail addresses: [kings008@gmail.com](mailto:kings008@gmail.com) (J. Yuan), [szyao@hnu.cn](mailto:szyao@hnu.cn) (S. Yao).

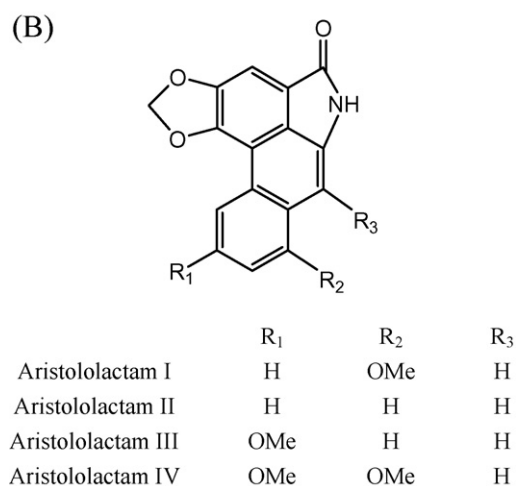
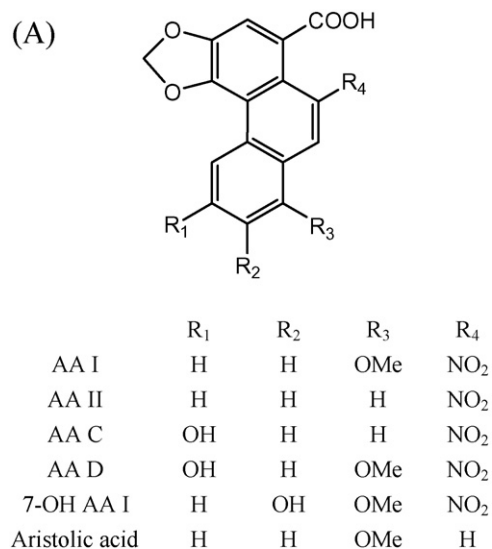


Fig. 1. Structures of aristolochic acids (A) and aristololactams (B).

In the past years, many attempts have been made to assay the active component in *Aristolochiaceae* by various methods including thin layer chromatography (TLC) [20–22], ultraviolet spectrophotometry (UV) [23], high-performance liquid chromatography coupled to a UV detector (HPLC–UV) [22,24–28] or to a mass spectrometer (HPLC–MS) [25,29–32], and capillary electrophoresis (CE) [33–35]. However, most of these methods focus on the analyses of AA I and/or AA II in samples, and various HPLC–MS [22,29–31] or HPLC–MS/MS [30–32] methods aim to obtain lower detection limit or elucidate the structures of AAs. As mentioned above, all AA analogues are more or less cytotoxic [19] and coexist in various *Aristolochiaceae* plants [1,2]. So it is more interesting to separate and analyze AA analogues as many as possible.

Very recently, several reports have been published on analysis of more than three compounds [26,31,36]. Detection of aristolochic acid I, tetrandrine and fangchinoline in medicinal plants by HPLC was reported by Koh et al. [36]. Simultaneous determination of five aristolochic acids and two aristolo-

lactams in *Aristolochia* plants were investigated by HPLC method with acetonitrile–phosphoric acid buffer as the eluent [26]. Wei et al. [29] detected the six main aristolochic acids by HPLC–DAD–ESI/MS with a relatively long analysis time.

This work focuses on developing a simple, effective and reliable method to screen AA analogues in various herbal plants and their preparations. Influencing factors such as the extraction methods, column temperature, mobile phase and gradient elution program were investigated carefully regarding to the complexity of various samples. The optimum separation was obtained with gradient methanol–water (both contain 0.2% acetic acid) system. The developed method was successfully applied to the simultaneous quantitative determination of the nine aristolochic acid analogues in nine *Aristolochiaceae* plants, three substituents and two herbal preparations.

## 2. Experimental

### 2.1. Instrumentation

A Waters (Waters Corp., Milford, MA, USA) 600 liquid chromatographic system interfaced to a 2996 photodiode array detector (DAD) was controlled by a Masslynx V4.0 workstation (Micromass UK Ltd., Manchester, UK). An Agilent (Agilent Corp., Wilmington, Delaware) XDB-C18 analytical column (150 mm × 4.6 mm, 4 μm particle size) was used.

### 2.2. Chemicals and reagents

The reference standards (Fig. 1) of AA I, AA II, AA C, AA D, 7-OH AA I, aristolochic acid, AL II, AL III and AL IV were purchased from Herbwild Scientific & Technical Development Center (Beijing, China). The purities of all the standards were not less than 98%. HPLC-grade acetonitrile and methanol were from Tedia Company, Inc. (Fairfield, OH, USA). Ultrapure water was prepared using an Aike purification system (Chengdu, China). Other reagents were of analytical grade, including methanol and acetic acid.

### 2.3. Materials

Herbs such as Guanmutong (the stems of *Aristolochia manshuriensis* Kom.), Madouling (the fruits of *Aristolochia contorta* Bunge), Guangfangji (the roots of *Aristolochia fangchi*), Qingmuxiang (the roots of *Aristolochia debilis*), Tianxianteng (the herbs of *Aristolochia debilis*), Fangji (the roots of *Stephania tetrandra* S. Moore), Chuanmutong (the stems of *Clematis armandii* Franch), Yunmuxiang (the roots of *Saussurea lappa* C.B. Clarke), Xungufeng (the herbs of *Aristolochia mollissima* Hance) and Xixin (the herbs of *Asarum heterotropoides* Fr. Schmidt var. *mandshuricum* (Maxim.) Kitag.), and two herbal preparations, namely Guanxin Suhe Wan and Qinglin Keli were purchased from drug stores all around China. Among them, Fangji, Chuanmutong and Yunmuxiang are used sometimes as the substituents of Guangfangji, Guanmutong and Qingmuxiang, respectively.

## 2.4. Standard solutions and calibration curves

Each standard (5 mg) was placed in a 5-mL volumetric flask with 4 mL of methanol. After the solids had been dissolved under sonication, the solution was diluted to volume with methanol to give the stock solution.

The mixed standard stock solution was prepared by accurately adding appropriate volume of each standard stock solution into a 10-mL volumetric flask. The concentration ( $\mu\text{g mL}^{-1}$ ) of each compound was: AL III (69.0), AA C (125), AL IV (92.5), 7-OH AA I (83.0), AA D (86.0), AL II (96.1), AA II (210), AA I (172) and aristolochic acid (120). A series of working standard solutions with gradient concentration was obtained by diluting the mixed standard stock solution. All the solutions were stored in a refrigerator at 4 °C and brought to room temperature before use.

Calibration curves ( $y = ax + b$ ) were constructed by plotting the peak areas ( $y$ ) versus the concentrations ( $x$ ) of the calibration standards.

## 2.5. Preparation of sample solutions

### 2.5.1. Guanmutong, guangfangji, qingmuxiang, fangji and chuanmutong

In a 10-mL polypropylene centrifuge tube, 0.3 g of powdered herbal sample was weighed, 6 mL methanol was added and sonicated for 15 min before centrifugation at  $3100 \times g$  for 10 min. Methanol extraction was repeated three times. The extracts were combined and concentrated in a rotary evaporator. Methanol was used to dilute the concentrated solution under sonication, and the volume was made up to exactly 10 mL (5 mL for Xixin and Xungufeng).

### 2.5.2. Madouling, tianxianteng, xungufeng, xixin and yunmuxiang

Madouling (0.3 g), Tianxianteng (0.5 g), Xungufeng (0.8 g), Xixin (0.8 g) and Yunmuxiang (0.3 g) were placed in centrifuge tubes, respectively, and 8 mL of *n*-hexane was added to remove the grease. The solution was sonicated for 15 min at room temperature and then centrifuged at  $3100 \times g$  for 10 min. After removal of the supernatant with a pipette, the residue was placed in the vacuum dryer to let the solvent evaporate. The following procedures were similar to the Section 2.5.1.

### 2.5.3. Guanxin suhe wan and qinglin keli

Five pills of Guanxin Suhe Wan were weighed out and ground in mortar, then 1 g was weighed out accurately and placed in a centrifuge tube. The sampling weight of Qinlin Keli was also 1 g. The following procedures were the same as the Section 2.5.2.

## 2.6. HPLC–DAD analysis

Methanol (B) and aqueous solution (A) (both contain 0.2% acetic acid) were used as mobile phase. The gradient elution was programmed as follows: 0–20 min, 30–45% B; 20–35 min, 45–50% B; 35–50 min, 50–80% B; 50–55 min, 80–100% B.

The other analysis conditions were as follows: column temperature, 30 °C; flow rate,  $1.0 \text{ mL min}^{-1}$ ; injection volume, 20  $\mu\text{L}$ ; UV scan, 210–400 nm; detection wavelength, 254 nm. Samples were filtered through 0.45  $\mu\text{m}$  membrane prior to analysis. Some solutions (Madouling, Guanmutong, Guangfangji and Qingmuxiang) were diluted with methanol in order to obtain concentrations within the range of the calibration curve.

## 3. Results and discussion

### 3.1. Optimum separation conditions

In general, AA analogues are difficult to be separated due to their extremely similar structures (Fig. 1). This may be one of the reasons why many reports [23–25,28,30–35] focused on the analysis of AA I, and/or AA II. In most cases, a mixture of acetonitrile and water was utilized as the mobile phase with some special modifiers, such as phosphoric acid [26], trifluoroacetic acid (TFA) [31], formic acid and acetic acid to control pH.

In this work, various conventional mobile phases were tested and optimized across-the-board to obtain the optimum conditions. The chromatographic behaviours were investigated with the following mobile phases: (a) acetonitrile–3.7 mM phosphoric acid buffer [26], (b) 0.1% acetic acid and 0.1% tetrahydrofuran (THF) in water (solvent A)–0.1% acetic acid and 0.1% THF in acetonitrile (solvent B) [29], (c) aqueous acetonitrile containing 0.1% TFA, (d) aqueous methanol containing 0.1% TFA and (e) methanol–water (both contain 0.2% acetic acid), were investigated, respectively. Some peaks of the analytes were overlapped with mobile phases (a), (b), (c) and (d) under various gradient conditions. However, excellent separation for all of compounds explored were achieved with the optimized mobile phase (e). For an analyte-pair difficult to separate, a solvent with relatively weak elution strength may be more appropriate. Moreover, mobile phase (e) is more cheap and friendly to environment. Therefore, mobile phase (e) was adopted in subsequent studies.

In analytical liquid chromatography gradient elution is widely applied to improve the separation of mixtures by varying the solvent strength during the elution process. In the present work the optimum gradient was picked out through a large number of empirical attempts. As can be seen from Fig. 2, nine AA analogues were separated properly with symmetrical peak shapes and adequate resolution with the optimum gradient program described in Section 2.6.

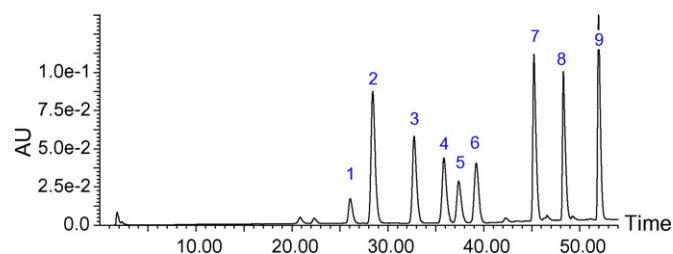


Fig. 2. Chromatograms of mixture standards. (1) AL III; (2) AA C; (3) AL IV; (4) 7-OH AA I; (5) AA D; (6) AL II; (7) AA II; (8) AA I; (9) aristolochic acid.



### 3.2. Extraction conditions

Considering the complexity of samples, various extraction solvents and extraction methods were investigated in detail. It was found that reflux method provided similar extraction efficiency as sonication under this experimental conditions, but was more tedious and time-consuming. So ultrasonication was used in subsequent experiments.

Geoffrey et al. [32] investigated various solvents including water, 0.2 M acetic acid, 0.2 M ammonia, aqueous methanol of different concentration, ethanol and acetone, and picked out 70% methanol as solvent which is similar with the FDA's advice [37]. In our experiments, the above-mentioned solvents and ethyl acetate were investigated, and similar results were obtained. But no significant difference in extraction efficiency was found between methanol and 70% methanol. Moreover, 70% methanol induced more polar impurities which may affect the separation. Thus methanol was used as extraction solvent in our experiments.

Madouling, Tianxianteng, Xungufeng, Xixin, Guanxin Suhe Wan and Qingli Keli contain non-polar compounds such as chlorophyll, terpenes and volatile oils, which should be removed before analysis because they have strong retention on the stationary phase and affect the later separation even the column life. So an additional procedure to degrease was adopted with *n*-hexane. Furthermore, low level AA analogues were found in Xixin and Xungufeng, so more raw samples were required and preconcentration was necessary.

### 3.3. Validation of HPLC assay

#### 3.3.1. Linearity, limit of detection and limit of quantification

The standard curves were calculated via least-square regression with six concentration levels and three injections were examined at each level. Good linear relationships were gained, and the correlation coefficients of all the calibration curves were found to be higher than 0.9950. Detection limits and quantification limits of the investigated compounds were estimated as the minimum concentration giving a signal-to-noise

Table 1

Linear ranges, correlation coefficients, quantification and detection limits for the analogues studied

Compound	Linear range ( $\mu\text{g mL}^{-1}$ )	$r^2$	LOQ (ng/mL)	LOD (ng/mL)
AL III	0.690–69.0	0.9972	65.0	23.6
AA C	0.249–24.9	0.9994	58.2	24.0
AL IV	0.231–23.1	0.9988	35.5	10.6
7-OH AA I	0.166–16.6	0.9950	86.4	31.7
AA D	0.860–86.0	0.9964	72.8	14.7
AL II	0.960–96.0	0.9978	95.5	20.6
AA II	0.420–42.0	0.9950	104	14.6
AA I	0.324–32.4	0.9994	69.5	15.2
Aristolic acid	0.240–24.0	0.9984	84.6	15.0

ratio (S/N) of 3 and 10, respectively. The data are listed in Table 1.

#### 3.3.2. Precision and accuracy

Precision was evaluated with a standard mixture solution of the analogues under the optimal conditions six times in one day for intra-day variation and twice a day on three consecutive days for inter-day variation, expressed as relative standard deviation (R.S.D.). The results are shown in Table 2.

The recovery tests were studied by spiking the known content of the analogues into the real samples. The analogues were added at three concentration levels (approximately equivalent to 0.8, 1.0 and 1.2 times of the concentration of the matrix) with two parallels at each level. The solutions were prepared and quantified in accordance with the Sections 2.5.1 and 2.6, respectively. The recoveries of AA I, AL II, AL III, AL IV and aristolic acid were tested with Tianxianteng as the matrix, and those of AA II, AA C, 7-OH AA I and AA D were done in Madouling. The data are listed in Table 2.

#### 3.3.3. Robustness of column

Three kinds of C18 columns were tested for validation of the robustness including Agilent XDB-C18, Waters Xterra Ms C18 (5  $\mu\text{m}$ , 150 mm  $\times$  3.9 mm) and waters Symmetry C18 (5  $\mu\text{m}$ ,

Table 2

Precision of the intra-day and inter-day measurements and recoveries of the analytical method for AA analogues

Compound <sup>a</sup>	Intra-day <sup>b</sup> (peak areas)		Inter-day <sup>c</sup> (peak areas)		Recovery (%) (mean, $n=6$ )
	$\bar{X} \pm \text{S.D.}$	R.S.D. (%)	$\bar{X} \pm \text{S.D.}$	R.S.D. (%)	
AL III	7562 $\pm$ 128	1.69	7385 $\pm$ 316	4.28	92.4
AA C	51017 $\pm$ 1485	2.91	50873 $\pm$ 2053	4.03	94.8
AL IV	28148 $\pm$ 804	2.86	28950 $\pm$ 924	3.19	89.0
7-OH AA I	25935 $\pm$ 712	2.75	25479 $\pm$ 1104	4.33	94.5
AA D	16146 $\pm$ 396	2.45	16361 $\pm$ 712	4.35	94.6
AL II	23914 $\pm$ 269	1.12	23750 $\pm$ 590	2.48	88.4
AA II	48190 $\pm$ 761	1.58	48460 $\pm$ 1607	3.32	97.7
AA I	38960 $\pm$ 503	1.29	38748 $\pm$ 1437	3.71	98.8
Aristolic acid	52157 $\pm$ 671	1.29	51965 $\pm$ 2005	3.86	98.2

<sup>a</sup> The concentration ( $\mu\text{g mL}^{-1}$ ) of each compound was: AL III (6.90), AA C (12.5), AL IV (9.25), 7-OH AA I (8.30), AA D (8.60), AL II (9.61), AA II (21.0), AA I (17.2) and aristolochic acid (12.0).

<sup>b</sup> The sample was analyzed six times during one day.

<sup>c</sup> The sample was analyzed over three consecutive days.

Table 3

Contents of the nine AA analogues in nine *Aristolochiaceae* plants, three substituents and two preparations, mg g<sup>-1</sup> (crude drug) (n = 3)

No.	Sample	AL III	AA C	AL IV	7-OH AA I	AA D	AL II	AA II	AA I	Aristololic acid	Sum
1	Madouling	Trace	1.33	Trace	0.825	1.37	0.0465	0.325	1.76	0.0624	5.72
2	Guanmutong	–	0.521	–	–	0.472	–	0.958	3.82	–	5.77
3	Guanmutong	–	0.652	–	–	0.497	–	1.30	3.57	–	6.02
4	Guangfangji	–	0.372	–	–	1.25	–	0.986	4.76	–	7.37
5	Qingmuxiang	–	0.854	0.0955	0.615	0.284	0.271	0.875	2.61	–	4.72
6	Tianxianteng	0.0152	0.481	Trace	1.29	0.245	Trace	0.0385	0.175	0.0682	2.24
7	Xungufeng	–	0.147	–	0.0988	0.0438	–	0.0255	0.162	–	0.375
8	Xixin*	–	56.2	–	Trace	46.8	Trace	25.1	69.5	–	198
9	Xixin*	–	43.5	–	28.7	73.5	Trace	17.8	125	–	289
10	Fangji	–	–	–	–	–	–	–	–	–	–
11	Chuanmutong	–	–	–	–	–	–	–	–	–	–
12	Yunmuxiang	–	–	–	–	–	–	–	–	–	–
13	Guanxin Suhe Wan	–	–	–	–	–	–	0.0647	0.0525	3.75	3.87
14	Qinglin Keli	–	–	0.0525	–	0.0582	–	0.0593	0.184	–	0.354

Trace: under quantification limit. –: under detection limit. Xixin\*: μg g<sup>-1</sup> (crude drug).

150 mm × 3.9 mm), and no significant difference was found between them.

### 3.4. Sample analysis

The contents of nine AA analogues in nine *Aristolochiaceae* plants, three substitutes and two herbal preparations were determined with the HPLC method developed as described above. The representative HPLC chromatograms of the nine samples are shown in Fig. 3, respectively. The contents were calculated with external standard method, and the mean values from three parallel determinations are shown in Table 3. It can be seen from Table 3 that the contents of such analogues vary obviously in different plants. Negative results were observed for AA analogues in three substitutes, namely Fangji, Chuanmutong and Yunmuxiang. AA I, AA II, AA C, and AA D were found in the nine *Aristolochiaceae* plants studied, and were the main active compounds. In addition, 7-OH AA I was also the main active constituent of Madouling, Qingmuxiang and Tianxianteng. The other analogues exist in various plants at low levels. In view of variety, Madouling, Tianxianteng and Qingmuxiang contain more components than Guangfangji and Guanmutong

do. Although Xungufeng and Xixin also contain relatively more ingredients than Guanmutong and Guangfangji, where only low contents were found. The total contents of analogues in the seven *Aristolochiaceae* plants decrease in the following order: Guangfangji, Guanmutong, Madouling, Qingmuxiang, Tianxianteng, Xungufeng and Xixin. Complex chromatogram of Xixin was found (Fig. 3(G)). To obtain complete baseline resolution for Xixin, gradient program from 45 to 55 min (refer to Section 2.6) was rectified by lowering the percentage of methanol and lengthening the gradient. The content of Xixin in Table 3 was obtained with the modified gradient condition.

It should be emphasized that the multicomponent analysis is much more important and effective than the detection of AA I and/or AA II alone in the suspected products. As showed in Table 3, the content of AA I and AA II (0.214 mg g<sup>-1</sup> crude drug) is much lower than that of AA C, 7-OH AA I and AA D (2.02 mg g<sup>-1</sup>) in Tianxianteng. The total of AAC, 7-OH AA I and AA D exceeds that of AA I and AA II in Madouling. Even in Guangfangji, Guanmutong and Qingmuxiang, the other compounds could not be neglected. Due to the diversity of species and habitats, the results may be much more complex. There-

Table 4

Comparison between the present method and the previous HPLC methods

Reference	Detection	Mobile phase	Analytes	Matrices	LOD
This work	DAD	Methanol and water (both containing 0.2% HAc)	AA I, AA II, AA C, AA D, 7-OH AA I, Aristolic acid, AL II, AL III and AL IV	12 medicinal plants and 2 preparations	≥ 10.6 ng mL <sup>-1</sup>
[26]	DAD	3.7 mM phosphoric buffer and acetonitrile	AA I, AA II, 9-OH AA I, AA D, AA Va, AL I, and AL II	5 kinds of <i>Aristolochia</i> species	≥ 10.0 ng mL <sup>-1</sup>
[28]	MS	20 mM NH <sub>4</sub> Ac and acetonitrile	AA I and AA II	5 herbal materials and 18 herbal formulations	Not reported
[29]	ESI/MS	Acetonitrile and water (both containing 0.1% HAc and 0.1% tetrahydrofuran)	AA I, AA II, AA C, AA D, 7-OH AA C, aristolic acid,	10 medicinal plants and 6 herbal formulations	Not reported
[30]	ES-ITMS	Methanol and water (containing 1.0 mM NH <sub>4</sub> Ac and 0.2% HAc)	AA I and AA II	Several Chinese herbal remedies	12 ng mL <sup>-1</sup>
[32]	MS/MS	Methanol and 0.1% NH <sub>4</sub> Ac	AA I and AA II	Herbal remedies	10 ng on column

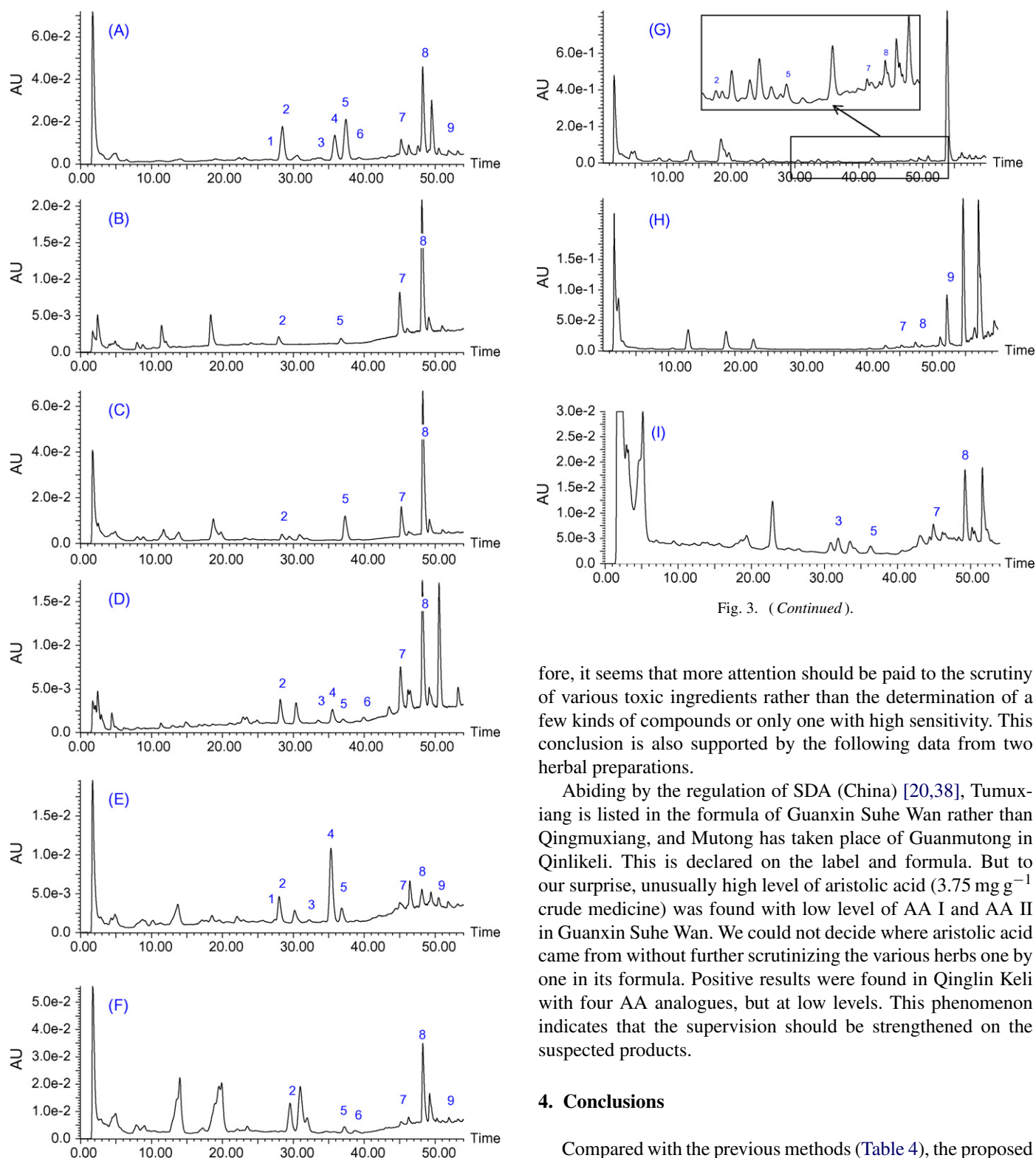


Fig. 3. (Continued).

Fig. 3. Typical chromatograms of samples. (A) Madouling; (B) Guanmutong; (C) Guangfangji; (D) Qingmuxiang; (E) Tianxianteng; (F) Xungufeng; (G) Xixin; (H) Guanxin Suhe Wa; and (I) Qinglin Keli. Peak numbering is the same as in Fig. 2.

fore, it seems that more attention should be paid to the scrutiny of various toxic ingredients rather than the determination of a few kinds of compounds or only one with high sensitivity. This conclusion is also supported by the following data from two herbal preparations.

Abiding by the regulation of SDA (China) [20,38], Tumuxiang is listed in the formula of Guanxin Suhe Wan rather than Qingmuxiang, and Mutong has taken place of Guanmutong in Qinlikeli. This is declared on the label and formula. But to our surprise, unusually high level of aristolic acid ( $3.75 \text{ mg g}^{-1}$  crude medicine) was found with low level of AA I and AA II in Guanxin Suhe Wan. We could not decide where aristolic acid came from without further scrutinizing the various herbs one by one in its formula. Positive results were found in Qinglin Keli with four AA analogues, but at low levels. This phenomenon indicates that the supervision should be strengthened on the suspected products.

#### 4. Conclusions

Compared with the previous methods (Table 4), the proposed HPLC–DAD method was more simple, reliable and effective. The method has been used successfully to the simultaneous determination of six aristolochic acids and three aristolactams in nine *Aristolochiaceae* plants, three substituents and two herbal preparations for the first time. The proposed method appears to be suitable for use as a tool for safety assurance and quality control for commercially available samples.

## Acknowledgements

Some herbal medicines were provided by Institute of Chinese Material Medica, China Academy of Traditional Chinese Medicine and Jiangxi Herbfine Scientific & Technical Co. Ltd. This work was financially supported by the National Basic Research Program (also called 973 Program) (No. 2006CB504701) and the National Natural Science Foundation of China (No. 20575019 and 20335020).

## References

- [1] D.B. Mix, H. Guinaudeau, M. Sharmma, *J. Nat. Prod.* 45 (1982) 657.
- [2] Y. Wang, J.X. Pan, Z.J. Jia, *Nat. Prod. Res. Dev.* 12 (2000) 84.
- [3] Zhonghua Bencao Committee of State Traditional Chinese Medicine Administration, *Zhonghua Bencao*, vol. 3, Shanghai Sci. & Tech. Press, Shanghai, 1999, pp. 463–471 and 477.
- [4] T.S. Wu, Y.Y. Chan, Y.L. Leu, *J. Nat. Prod.* 64 (2001) 71.
- [5] P.M. Shafi, M.K. Rosamma, K. Jamil, P.S. Reddy, *Fitoterapia* 73 (2002) 439.
- [6] R. Kluthe, A. Vogt, S. Batsford, *Drug Res.* 32 (1982) 443.
- [7] U. Mengs, *Arch. Toxicol.* 52 (1983) 209.
- [8] U. Mengs, *Arch. Toxicol.* 59 (1987) 328.
- [9] U. Mengs, *Arch. Toxicol.* 61 (1988) 504.
- [10] J.L. Vanherweghem, M. Depierreux, C. Tielemans, D. Abramowicz, M. Dratwa, M. Jadoul, C. Richard, D. Vandervelde, D. Verbeelen, R. Vanhaelen-Fastre, M. Vanhaelen, *Lancet* 341 (1993) 387.
- [11] C.S. Yang, C.H. Lin, S.H. Chang, H.C. Hsu, *Am. J. Kidney Dis.* 35 (2000) 313.
- [12] B. Li, X.M. Li, C.Y. Zhang, X. Wang, S.Q. Cai, *China J. Chin. Mater Medica* 29 (2004) 78.
- [13] J.L. Nortier, J.L. Vanherweghem, *Toxicology* 181–182 (2002) 577.
- [14] C.L. Cheng, K.J. Chen, P.H. Shih, L.Y. Lu, C.F. Hung, W.C. Lin, J.Y. Gu, *Cancer Lett.* 232 (2006) 236.
- [15] J.L. Nortier, M.C. Munz Martinez, H.H. Schmeiser, V.M. Arlt, C.A. Bieler, M. Petein, M.F. Depierreux, L. De Pauw, D. Abramowitz, P. Vereerstraeten, J.L. Vanherweghem, *New Eng. J. Med.* 342 (2000) 1686.
- [16] M. Stiborova, E. Frei, A. Breuer, C.A. Bieler, H.H. Schmeiser, *Exp. Toxicol. Pathol.* 51 (1999) 421.
- [17] H.H. Schmeiser, B.L. Pool, M. Wiessler, *Carcinogenesis* 7 (1986) 59.
- [18] A. Kohara, T. Suzuki, M. Honma, T. Ohwada, M. Hayashi, *Mutat. Res.* 515 (2002) 63.
- [19] P. Balachandran, F. Wei, R.C. Lin, I. Khan, D.S. Pasco, *Kidney Int.* 67 (2005) 1797.
- [20] Chinese Pharmacopoeia Committee, *The Chinese Pharmacopoeia*, 2000 ed., Chemical Industry Press, Beijing, 2000, p. 31, 39, 41, 114 and 154.
- [21] Chinese Pharmacopoeia Committee, *The Chinese Pharmacopoeia*, 2005 ed., Chemical Industry Press, Beijing, 2005, p. 25, 35, 37 and 101.
- [22] J.R. Ioset, G.E. Raelison, K. Hostettmann, *Food Chem. Toxicol.* 41 (2003) 29.
- [23] M.Y. Shang, J. Li, B. Hu, S. Yang, C.L. Li, J.H. Zheng, *Chin. Tradit. Herb. Drugs* 31 (2000) 899.
- [24] B.T. Schanegerg, I.A. Khan, *J. Ethnopharmacol.* 94 (2004) 245.
- [25] K. Hashimoto, M. Higuchi, B. Makino, I. Sakakibara, M. Kubo, Y. Komatsu, M. Maruno, M. Okada, *J. Ethnopharmacol.* 64 (1999) 185.
- [26] C.Y. Zhang, X. Wang, M.Y. Shang, J. Yu, Y.Q. Xu, Z.G. Li, L.C. Lei, X.M. Li, S.Q. Cai, T. Namba, *Biomed. Chromatogr.* 20 (2006) 309.
- [27] W. Chan, K.M. Hui, W.T. Poon, K.C. Lee, Z.W. Cai, *Anal. Chim. Acta* 576 (2006) 112.
- [28] M.C. Lee, C.H. Tsao, S.C. Lou, W.C. Chuang, S.J. Sheu, *J. Sep. Sci.* 26 (2003) 818.
- [29] F. Wei, X.L. Cheng, L.Y. Ma, W.T. Jin, B.T. Schaneberg, *Phytochem. Anal.* 16 (2005) 222.
- [30] S.A. Chan, M.J. Chen, T.Y. Liu, M.R. Fuh, J.F. Deng, M.L. Wu, S.J. Hsieh, *Talanta* 60 (2003) 679.
- [31] T.T. Jong, M.R. Lee, S.S. Hsiao, J.L. Hsai, T.S. Wu, S.T. Chiang, S.Q. Cai, *J. Pharm. Biomed. Anal.* 33 (2003) 831.
- [32] G.C. Kite, M.A. Yule, C. Leon, M.S.J. Simmonds, *Rapid Commun. Mass Spectrom.* 16 (2002) 585.
- [33] E.S. Ong, S.O. Woo, *Electrophoresis* 22 (2001) 2236.
- [34] W. Li, S.X. Gong, D.W. Wen, B.Q. Che, Y.P. Liao, H.W. Liu, X.F. Feng, S.L. Hu, *J. Chromatogr. A* 1049 (2004) 211.
- [35] S.C. Hsieh, M.F. Huang, B.S. Lin, H.T. Chang, *J. Chromatogr. A* 1105 (2006) 127.
- [36] H.L. Koh, H. Wang, S. Zhou, E. Chan, S.O. Woo, *J. Pharm. Biomed. Anal.* 40 (2006) 653.
- [37] R.A. Flurer, M.B. Jones, N. Vela, L.A. Ciolino, K.A. Wolnik, *The FDA Lab. Inform. Bull.*, 2004, No. 4212, <http://www.cfsan.fda.gov/acrobat/lib4212.pdf>.
- [38] Chinese Pharmacopoeia Committee, *The Chinese Pharmacopoeia*, 2000 ed., 2002 Suppl., Chemical Industry Press, Beijing, 2002, p. 3.

## Determination of afloqualone in human plasma using liquid chromatography/tandem mass spectrometry: Application to pharmacokinetic studies in humans

Hwi-yeol Yun<sup>a</sup>, Seo-pan Lee<sup>a</sup>, Hae Hum Jeong<sup>b</sup>, Young-ran Yoon<sup>c</sup>,  
Soo Jung Sohn<sup>d</sup>, Sang Kyum Kim<sup>a</sup>, Wonku Kang<sup>b</sup>, Kwang-il Kwon<sup>a,\*</sup>

<sup>a</sup> College of Pharmacy, Chungnam National University, Daejeon, Korea

<sup>b</sup> College of Pharmacy, Catholic University of Daegu, Kyungbuk, Korea

<sup>c</sup> Clinical Trial Center, Kyungpook National University Hospital, Daegu, Korea

<sup>d</sup> Division of Bioequivalence, Korea Food and Drug Administration, Seoul, Korea

Received 27 February 2007; received in revised form 18 April 2007; accepted 18 April 2007

Available online 1 May 2007

### Abstract

Two methods for determining the central-acting muscle relaxant afloqualone in human plasma were developed and compared using API2000 and API4000 liquid chromatography tandem mass spectrometry (LC/MS/MS) systems. In the API2000 LC/MS/MS system, afloqualone and the internal standard methaqualone were extracted from plasma using a methyl-tertiary ether. After drying the organic layer, the residue was reconstituted in a mobile phase (0.1% formic acid–acetonitrile:0.1% formic acid buffer, 80:20 v/v) and injected onto a reversed-phase C<sub>18</sub> column. The isocratic mobile phase was eluted at 0.2 ml/min. The ion transitions monitored in multiple reaction-monitoring mode were  $m/z$  284 → 146 and 251 → 117 for afloqualone and methaqualone, respectively.

Sample preparation for the API4000 LC/MS/MS system involved simple protein precipitation with an organic mixture (methanol:10% ZnSO<sub>4</sub> = 8:2). The ion transitions monitored in multiple reaction-monitoring mode were  $m/z$  284 → 146 and 251 → 131 for afloqualone and methaqualone, respectively.

In both assays, the coefficient of variation of the precision was less than 11.8%, the accuracy exceeded 91.5%, the limit of quantification was 0.5 ng/ml, and the limit of detection was 0.1 ng/ml for afloqualone. Two methods were used to measure the plasma afloqualone concentration in healthy subjects after a single oral 20-mg dose of afloqualone. During subsequent application of the methods, we observed that high-concentration plasma samples (>7 ng/ml) prepared using the protein precipitation method resulted in about 20% higher afloqualone concentrations than with plasma samples prepared using the liquid–liquid extraction method. We believe that this phenomenon was related to the cleanness of the sample and its chemical nature.

© 2007 Elsevier B.V. All rights reserved.

**Keywords:** Afloqualone; LC/MS/MS; Pharmacokinetic; API2000; API4000; Matrix effect

### 1. Introduction

Afloqualone, 6-amino-2-fluoromethyl-3-(*o*-tolyl)-4-(3*H*)-quinazolinone, is a centrally acting muscle relaxant that inhibits mono- and polysynaptic reflexes (Fig. 1) [1]. After a single oral dose of 20-mg afloqualone, the peak afloqualone concentration in healthy humans is about 18 ng/ml at 2 h, and its plasma terminal half-life is about 7 h [2].

Several methods for determining afloqualone in biological fluids have been published, including thin layer chromatography (TLC) [3] and gas chromatography (GC)/mass detection (MS) [4]. However, the TLC-based methods might not be sufficiently selective and sensitive for routine analysis of the drug in plasma, and the disadvantage of GC/MS methods lies in the elaborate sample preparation required.

High-performance liquid chromatography (HPLC) with tandem mass spectrometry (MS/MS) detection has played a prominent role in analytic studies and has high sensitivity and accuracy. However, no reports have been published on the quantification of afloqualone using LC/MS/MS. Therefore,

\* Corresponding author. Tel.: +82 42 821 5937; fax: +82 42 823 6781.  
E-mail address: [kwon@cnu.ac.kr](mailto:kwon@cnu.ac.kr) (K.-i. Kwon).

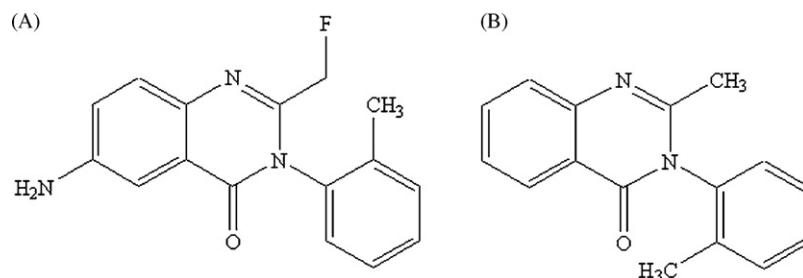


Fig. 1. Molecular structures of afloqualone (A) and the internal standard methaqualone (B).

we developed two new methods for determining afloqualone in human plasma using LC/MS/MS with API2000 and API4000 LC/MS/MS systems.

## 2. Experimental

### 2.1. Reagents and materials

Afloqualone and methaqualone (IS, internal standard) were purchased from Sigma (St. Louis, MO, USA). The HPLC-grade diethylether was obtained from Merck (Darmstadt, Germany). All other chemicals and solvents were of the highest analytical grade available.

### 2.2. Characterization of the product ions using MS/MS

In both the API2000 and API4000 systems, solutions containing 1 µg/ml each of afloqualone and the IS were infused into the mass spectrometer separately at a flow rate of 10 µl/min to characterize the product ions of each compound. The precursor ions,  $[M+H]^+$ , and pattern of fragmentation were monitored using positive ion mode. The major peaks observed in the MS/MS scan were used to quantify afloqualone and the IS [5,6].

### 2.3. Preparation of standards and quality controls

To determine afloqualone using the API2000 and API4000 LC/MS/MS systems, afloqualone and the IS were dissolved in methanol at 1 mg/ml each. The afloqualone standard solution was serially diluted with methanol and added to drug-free plasma to obtain concentrations of 0.5, 0.75, 1, 5, 10, 25, and 50 ng/ml. A calibration graph was derived from the peak area ratios of afloqualone to the IS using a linear regression. All solutions were stored at 4 °C and protected from light.

Quality controls were prepared daily in 450 µl of blank human plasma by adding 50 µl of standard solution. Controls were prepared for low (0.5 ng/ml afloqualone), intermediate (0.75 and 25 ng/ml afloqualone), and high (50 ng/ml afloqualone) concentrations to evaluate the intra- and inter-day precision and accuracy of the assay method. The calibration equation was validated when the relative difference between the theoretical and back-calculated concentrations of each sample of the calibration set did not exceed 20% at the lowest concentration and 15% at the other concentrations.

### 2.4. Analytical system

The plasma afloqualone concentrations were quantified using LC/MS/MS with PE SCIEX API 2000 or API4000 LC/MS/MS systems (Sciex Division of MDS, Toronto, Canada) equipped with an electrospray ionization interface used to generate positive ions  $[M+H]^+$ .

In the API2000 LC/MS/MS system, the compounds were separated on a reversed-phase column (Gemini C<sub>18</sub> 50 × 4.60 mm 5 µm; Phenomenex, Torrance, CA, USA) with an isocratic mobile phase consisting of 0.1% formic acid in acetonitrile and purified water (80:20%, v/v). The mobile phase was eluted at 0.2 ml/min using an Agilent 1100 series pump (Agilent Technologies, Palo Alto, CA, USA). The turbo ion spray interface was operated in positive ion mode at 5500 V and 500 °C. The operating conditions were optimized by flow injection of a mixture of all analytes as follows: nebulizing gas flow, 1.04 L/min; auxiliary gas flow, 4.0 L/min; curtain gas flow, 1.44 L/min; collision gas (nitrogen) pressure,  $5 \times 10^{-5}$  Torr; orifice voltage (declustering potential), 66 V; ring voltage (focusing potential), 370 V; entrance potential, 12 V; collision energy, 41 V; and collision exit potential, 6.0 V.

The afloqualone was quantified using multiple reaction monitoring of the protonated precursor ion and the related product ion using the internal standard method with peak area ratios. The mass transitions used for afloqualone and the internal standard were  $m/z$  284 → 146 and 251 → 117, respectively (dwell time, 150 ms).

In the API4000 LC/MS/MS system, the compounds were separated on a reversed-phase column (Xterra<sup>®</sup> RP C<sub>18</sub> 2.1 × 50 mm 3.5 µm; Waters, Milford, MA, USA) with an isocratic mobile phase consisting of methanol and 0.1% formic acid in purified water (75:25%, v/v). The mobile phase was eluted at 0.3 ml/min using an Agilent 1100 series pump. The turbo ion spray interface was operated in positive ion mode at 5500 V and 450 °C. The operating conditions were optimized by flow injection of a mixture of all of the analytes and were as follows: nebulizing gas flow, 1.04 L/min; auxiliary gas flow, 4.0 L/min; curtain gas flow, 1.44 L/min; collision gas (nitrogen) pressure,  $5 \times 10^{-5}$  Torr; orifice voltage (declustering potential), 816 V; ring voltage (focusing potential), 370 V; entrance potential, 10 V; collision energy, 39 V; and collision exit potential, 10 V. Afloqualone was quantified by multiple reaction monitoring of the protonated precursor ion and the related product ion using the internal standard method with peak area ratios. The

mass transitions used for afloqualone and the internal standard were  $m/z$  284  $\rightarrow$  146 and 251  $\rightarrow$  131, respectively (dwell time, 150 ms).

The resolution conditions for quadrupoles and the software used to analyze the data were the same in both the API2000 and API4000 LC/MS/MS systems. Quadrupoles Q1 and Q3 were set on unit resolution and the analytical data were processed using Analyst software (version 1.4.1; Applied Biosystems, Foster City, CA, USA) in the API2000 and API4000 LC/MS/MS systems.

### 2.5. Sample preparation for the API2000 system

One hundred microliters of internal standard (100 ng/ml) were added to 500  $\mu$ l of plasma, followed by a 10-min liquid–liquid extraction with 5 ml of methyl *tert*-butyl ether. The organic layer was separated and evaporated under a gentle stream of nitrogen at about 40 °C. The residue was reconstituted into 100  $\mu$ l of mobile phase by vortex mixing for 15 s; 10  $\mu$ l of this solution were injected into the column.

### 2.6. Sample preparation for the API4000 system

Sample preparation involved simple protein precipitation with an organic mixture (methanol:10% ZnSO<sub>4</sub> = 8:2). Aliquots (100  $\mu$ l) of human plasma were precipitated by adding 10  $\mu$ l of internal standard working solution (50 ng/ml) and 100  $\mu$ l of organic mixture. The sample was vortexed for 10 s and centrifuged at 1700  $\times$  *g* for 10 min. The upper layer was transferred into injector vials and a 10- $\mu$ l aliquot was injected into the column.

### 2.7. Validation procedure

The validation parameters were selectivity, precision, and accuracy. Ten batches of blank heparinized human plasma were screened to determine the specificity. The extraction recoveries of afloqualone were calculated by comparing the peak area ratio measured for the standard solution considering condensation with that obtained for plasma extracts after the extraction procedure. The precision and accuracy of the intra- and inter-day assay validation were estimated using the inverse prediction of the concentration of the quality controls from the calibration curve [7,8]. Samples for stability test were prepared at two different levels (1 and 10 ng/ml) and kept on the storage conditions in Table 3, respectively. Analysis was done in triplicate at each concentration levels. The stability of short-term, long-term, freeze-thaw and extracted sample were calculated using the ratio of standard samples to processed samples.

### 2.8. Clinical application

Seven healthy subjects who gave written informed consent took part in this study. Health problems, drug or alcohol abuse, and abnormalities in laboratory screening values were exclusion criteria. The study protocol was approved by the Korea Food and Drug Administration (KFDA) and the Ethics Committee of the

Clinical Trial Center at Kyungpook National University Hospital (Daegu, Korea).

After an overnight fast, all the subjects were given a single oral 20-mg dose of afloqualone. Blood samples (6 ml) were taken before and 0.5, 1, 1.5, 2, 3, 4, 6, 8, 10, 12, and 24 h after drug administration. The plasma was separated by centrifugation at 1360  $\times$  *g* for 10 min and stored at –70 °C until analysis.

### 2.9. Pharmacokinetic analysis

The pharmacokinetic analysis was performed using non-compartmental methods. The area under the plasma concentration-versus-time curve (AUC) was calculated using the trapezoidal rule and extrapolated to infinity. The time course of the plasma afloqualone concentration was used to determine the maximum plasma concentration ( $C_{\max}$ ) and the time ( $T_{\max}$ ) to reach  $C_{\max}$ . The elimination rate constant ( $k_{\text{el}}$ ) was obtained by linear regression of the terminal phase, and the calculated elimination half-life ( $t_{1/2}$ ) was  $0.693/k_{\text{el}}$  [9].

## 3. Results and discussion

### 3.1. Mass spectra

In the API2000 LC/MS/MS system, the precursor ions for afloqualone and methaqualone and their corresponding product ions were determined from spectra obtained during the infusion of standard solutions into the mass spectrometer; we used an electrospray ionization source, which operated in positive ionization mode with nitrogen as collision gas Q2 of a MS/MS system. Afloqualone and methaqualone produced mainly protonated molecules at  $m/z$  284 and 251, respectively. Both product ions were scanned in Q3 after collision with nitrogen in Q2 at  $m/z$  146 and 117 for afloqualone and methaqualone, respectively (Fig. 2A).

In the API4000 LC/MS/MS system, afloqualone produced the same protonated molecules and product ions as in the API2000 LC/MS/MS system. Methaqualone also produced the same protonated molecules as in the API2000 LC/MS/MS system, although the product ion was scanned more sensitively at  $m/z$  131 than at  $m/z$  117 in the API2000 LC/MS/MS system (Fig. 2B).

### 3.2. Determination of afloqualone

The retention times of afloqualone and the internal standard (methaqualone) in humans were approximately 3.5 and 4.0 min, respectively, in the API2000 LC/MS/MS system. Fig. 3A and B show typical chromatograms for blank plasma and plasma spiked with 5 ng/ml afloqualone, respectively. The plasma sample from a study participant is shown in Fig. 3C.

In the API4000 system, the retention times of afloqualone and the internal standard (methaqualone) were approximately 0.70 and 0.78 min, respectively. Fig. 4A and B show typical chromatograms for blank plasma and plasma spiked with 5 ng/ml afloqualone, respectively. The plasma sample from a study participant is shown in Fig. 4C.

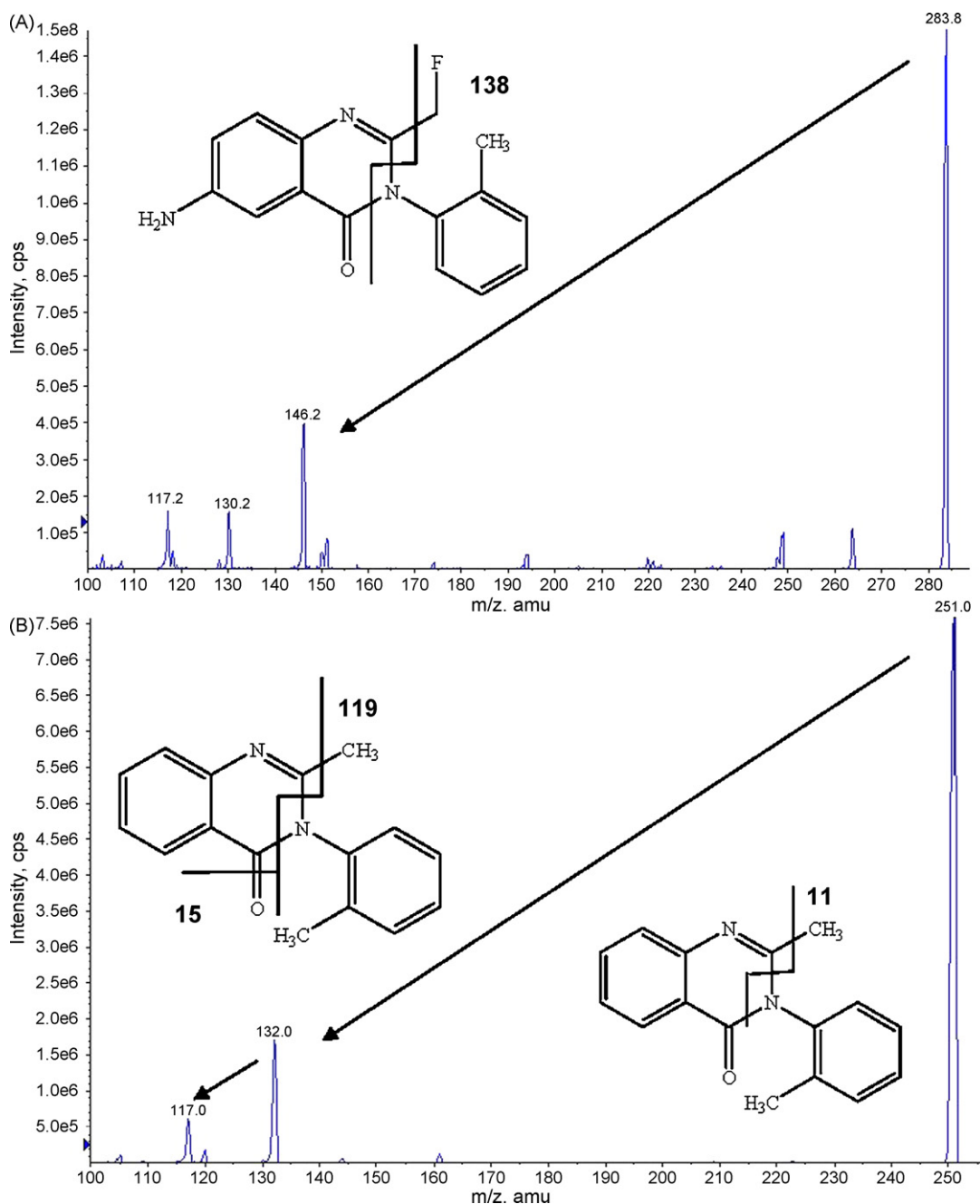


Fig. 2. Mass–mass spectra of afloqualone (A) and methaqualone (B) using electrospray ionization mode.

### 3.3. Linearity and detection limit

The calibration curve of afloqualone gave a reliable response from 0.5 to 50 ng/ml in both systems. The mean equation of the regression line was  $y = 0.0633x + 0.0075$  (slope range, 0.0588–0.0666; intercept range,  $-0.0039$  to  $0.0095$ ;  $r^2 > 0.999$ ) and the limit of detection was 0.1 ng/ml at a signal-to-noise (S/N) ratio of 3 in the API2000 system.

In the API4000 LC/MS/MS system, the mean equation was  $y = 0.0291x + 0.0018$  (slope range, 0.0268–0.0312; intercept range,  $-0.0054$  to  $0.0153$ ;  $r^2 > 0.999$ ) and the limit of detection was 0.1 ng/ml.

### 3.4. Precision and accuracy

The intra- and inter-day precision and accuracy of our two methods for afloqualone are listed in Tables 1 and 2, respectively. The afloqualone coefficients of variation of the precision of the intra- and inter-day validation under the API2000 LC/MS/MS system conditions were less than 7.9 and 11.8%, respectively. The method exceeded 98.5% accuracy for afloqualone.

Under the API4000 system conditions, the afloqualone coefficients of variation for the precision of the intra- and inter-day validation were less than 11.3 and 10.4%,



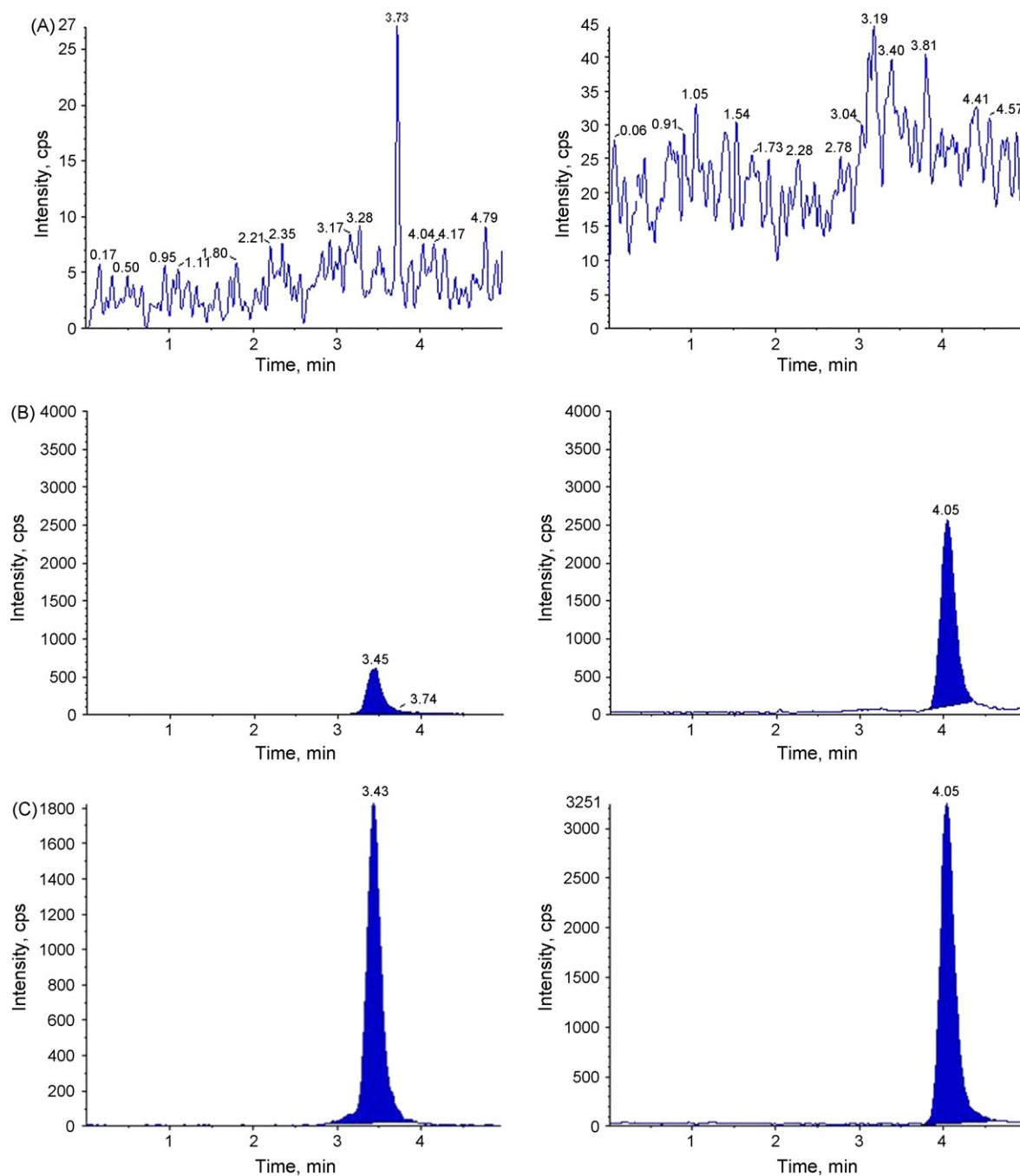


Fig. 3. Chromatograms of afloqualone (left) and the internal standard methaqualone (right) using the API2000 LC/MS/MS system. (A) Blank plasma; (B) plasma spiked with 5 ng/ml afloqualone and 100 ng/ml internal standard; (C) plasma sample of subject #5, 1 h after a single oral 20-mg dose of afloqualone.

respectively. The method exceeded 94.8% accuracy for afloqualone.

### 3.5. Stability

The stability of afloqualone in plasma was investigated using the API2000 LC/MS/MS system. The stability results are summarized in Table 3. The afloqualone in human plasma was stable over the short-term (6 h at room temperature), long-term (30 days at  $-70^{\circ}\text{C}$ ), for three freeze/thaw cycles, and during extraction (48 h at  $4^{\circ}\text{C}$ ).

### 3.6. Pharmacokinetics of afloqualone

All seven enrolled subjects completed the study. The compound was tolerated very well under both the fed and fasting conditions. No subject exhibited any clinically important changes in vital signs or electrocardiogram and blood chemistry parameters during the study.

Fig. 5 shows the time course of the afloqualone plasma concentrations after a single oral 20-mg dose of afloqualone. The pharmacokinetic parameters are listed in Table 4.

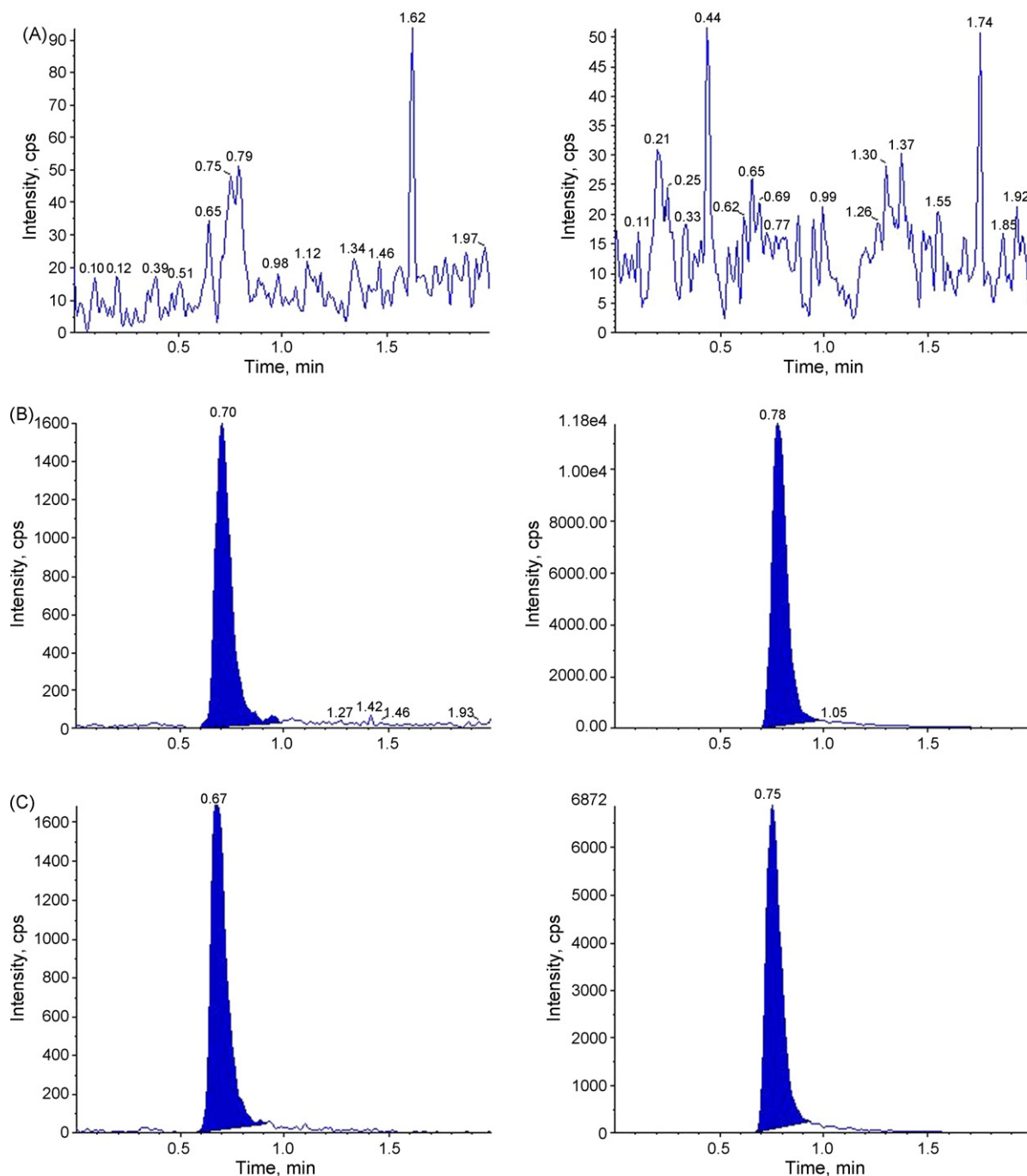


Fig. 4. Chromatograms of afloqualone (left) and the internal standard methaqualone (right) using the API4000 LC/MS/MS system. (A) Blank plasma; (B) plasma spiked with 5 ng/ml afloqualone and 100 ng/ml internal standard; (C) plasma sample of subject #5, 1 h after a single oral 20-mg dose of afloqualone.

### 3.7. Effects of the sample preparation methods

We have already discussed two methods for quantifying afloqualone in human plasma. However, during subsequent application of the methods, we observed that high-concentration plasma samples (>7 ng/ml) prepared with the protein precipitation method resulted in concentrations of afloqualone that were about 20% higher than for plasma samples prepared with the liquid–liquid extraction method (Fig. 5). Instability was eliminated as a cause because our experiments established stability

throughout the study. In addition, the recoveries of afloqualone and methaqualone (IS) were eliminated as a factor because both compounds had similar recoveries. Therefore, we suspected that ion suppression arising from the different methods of sample preparation caused this inaccuracy.

### 3.8. Assessing the matrix effect in a bio-analysis

The matrix effect was checked with five different lots of normal control heparinized plasma using the API2000 LC/MS/MS

Table 1  
The precision and accuracy of the intra-day afloqualone assay using the API2000 and API4000 LC/MS/MS systems ( $n=5$ )

Afloqualone added (ng/ml)	Measured (ng/ml) (mean $\pm$ S.D.)	CV (%)	Accuracy (mean (%) $\pm$ S.D.)
API2000			
0.5	0.5 $\pm$ 0.1	7.2	104.0 $\pm$ 9.1
0.75	0.7 $\pm$ 0.1	7.9	98.5 $\pm$ 9.0
25	24.6 $\pm$ 1.1	4.5	98.5 $\pm$ 4.5
50	50.2 $\pm$ 2.3	4.6	100.5 $\pm$ 4.7
API4000			
0.5	0.5 $\pm$ 0.1	8.4	94.8 $\pm$ 7.9
1	1.0 $\pm$ 0.1	5.9	103.4 $\pm$ 6.1
25	25.0 $\pm$ 2.0	7.8	100.1 $\pm$ 7.8
50	48.9 $\pm$ 3.0	6.1	97.9 $\pm$ 5.9

Table 2  
The precision and accuracy of the inter-day afloqualone using the API2000 and API4000 LC/MS/MS systems ( $n=5$ )

Afloqualone added (ng/ml)	Measured (ng/ml) (mean $\pm$ S.D.)	CV (%)	Accuracy (mean (%) $\pm$ S.D.)
API2000			
0.5	0.5 $\pm$ 0.1	1.3	97.9 $\pm$ 7.6
0.75	0.7 $\pm$ 0.1	5.4	91.9 $\pm$ 5.8
25	22.9 $\pm$ 2.7	11.8	91.5 $\pm$ 10.9
50	48.0 $\pm$ 4.5	9.3	95.9 $\pm$ 8.9
API4000			
0.5	0.5 $\pm$ 0.1	6.8	102.2 $\pm$ 7.9
1	1.0 $\pm$ 0.1	7.4	96.3 $\pm$ 7.6
25	25.0 $\pm$ 2.6	10.4	100.0 $\pm$ 10.4
50	51.9 $\pm$ 5.0	9.7	102.0 $\pm$ 9.9

system. Both low-quality controls (LQCs) and high-quality controls (HQCs) were prepared from different lots of plasma and checked for inaccuracy in all of the quality control (QC) samples. In the QC samples, a matrix effect or interference from endogenous compounds was detected from two different LQCs and four different HQCs (Table 5).

The plasma concentrations were found to be 4.0% higher than 0.5 ng/ml in the LQC samples. Conversely, we observed that the plasma concentrations were 4.1% lower than the expected plasma concentration (50 ng/ml) in the HQC samples.

### 3.9. Testing the effects of the sample preparation method in the API4000 system

The following experiments were performed to test the effect of the different sample preparation methods on the electrospray

Table 3  
Stability of afloqualone

Stability experiments (afloqualone)	Storage conditions	Stability (%) $\pm$ S.D. (1 ng)	Stability (%) $\pm$ S.D. (10 ng)
Benchmark	Room temperature (6 h)	96.1 $\pm$ 2.5	104.6 $\pm$ 8.8
Process (extracted sample)	4 °C, for 48 h	106.8 $\pm$ 8.3	103.5 $\pm$ 7.6
Freeze/thaw stability in plasma	After the third FT cycle at $-70$ °C	98.0 $\pm$ 3.9	106.0 $\pm$ 7.9
Long-term stability in human plasma	For 30 days at $-70$ °C	101.1 $\pm$ 6.8	99.8 $\pm$ 6.5

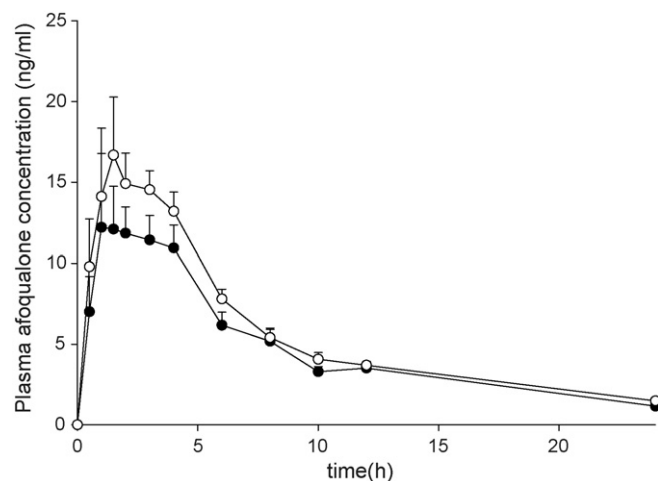


Fig. 5. Time course of the plasma concentration in healthy subjects after a single oral 20-mg dose of afloqualone. Each point represents the mean  $\pm$  S.E. ( $n=7$ ). (●) Observed plasma afloqualone concentration using the API2000 LC/MS/MS system; (○) observed plasma afloqualone concentration using the API4000 LC/MS/MS system.

Table 4  
Pharmacokinetics of afloqualone after a single 20-mg dose ( $n=7$ )

Model independent parameters (mean $\pm$ S.E.)	API2000 LC/MS/MS system	API4000 LC/MS/MS system
	AUC <sub>24h</sub> (ng h/ml)	109.6 $\pm$ 11.5
AUC <sub>inf</sub> (ng h/ml)	124.2 $\pm$ 11.3	152.8 $\pm$ 12.1
C <sub>max</sub> (ng/ml)	17.2 $\pm$ 3.6	19.7 $\pm$ 3.4
T <sub>max</sub> (h)	1.6 $\pm$ 0.3	2.0 $\pm$ 0.4
t <sub>1/2</sub> (h)	8.6 $\pm$ 0.8	9.7 $\pm$ 0.4

ionization response. We used plasma samples from three healthy subjects prepared using the two methods described above, and the plasma afloqualone concentrations were quantified using the API4000 system. Fig. 6 shows the time course of the afloqualone plasma concentrations using the two sample preparation methods. Scatterplots of the plasma concentration using the simple liquid–liquid extraction method versus the plasma concentration using simple protein precipitation are shown Fig. 7. The pharmacokinetic parameters are listed in Table 6. We observed that the high-concentration plasma samples ( $>7$  ng/ml) prepared using the protein precipitation method resulted in afloqualone concentrations that were about 17% higher than for plasma samples prepared with the liquid–liquid extraction method (Fig. 6).

Table 5  
Matrix effect in five different lots of plasma for afloqualone using the API2000 LC/MS/MS system

	Lot					Mean
	1	2	3	4	5	
Afloqualone (0.5 ng/ml)						
Cal. conc. (ng/ml)	0.5	0.5	0.5	0.6	0.6	0.5
RE (%)	-8.0	-4.0	8.0	10.0	14.0	4.0
Afloqualone (50 ng/ml)						
Cal. conc. (ng/ml)	55.3	47.7	47.8	43.4	45.6	48.0
RE (%)	10.5	-4.7	-4.3	-13.2	-8.7	-4.1

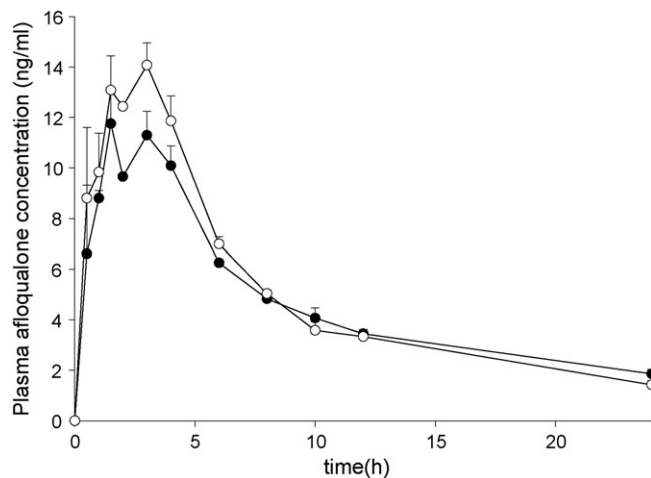


Fig. 6. Time course of the plasma concentration in healthy subjects after a single oral 20-mg dose of afloqualone using the API4000 LC/MS/MS system. Each point represents the mean  $\pm$  S.E. ( $n = 3$ ). (●) Observed plasma afloqualone concentration using the liquid–liquid extraction method; (○) observed plasma afloqualone concentration using protein precipitation.

The results of this study indicate that protein precipitation caused the least initial signal loss in the high-concentration plasma samples ( $>7$  ng/ml). Consequently, a pronounced ion suppression phenomenon was recorded in the liquid–liquid

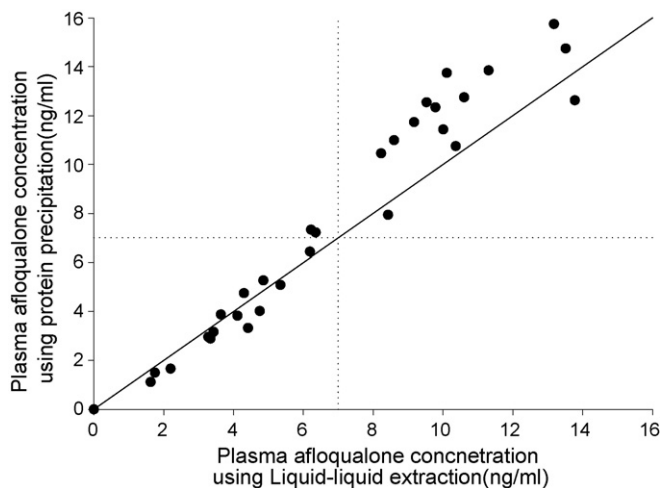


Fig. 7. Scatterplots of the plasma concentration using the simple liquid–liquid extraction method versus plasma concentration using simple protein precipitation (solid line, line of unity; dashed line, 7 ng/ml plasma concentration line).

Table 6  
Pharmacokinetics of afloqualone after a single 20-mg dose using the protein precipitation and liquid–liquid extraction methods ( $n = 3$ )

Model independent parameters (mean $\pm$ S.E.)	Protein precipitation	Liquid–liquid extraction
	$AUC_{24h}$ (ng h/ml)	$89.5 \pm 16.4$
$AUC_{inf}$ (ng h/ml)	$112.8 \pm 15.3$	$121.7 \pm 15.2$
$C_{max}$ (ng/ml)	$14.1 \pm 0.9$	$12.6 \pm 1.1$
$T_{max}$ (h)	$3.0 \pm 0.0$	$2.0 \pm 1.0$
$t_{1/2}$ (h)	$6.3 \pm 1.8$	$8.7 \pm 2.3$

extraction processed samples. A possible explanation for this follows. On visual inspection, the final solution prepared using protein precipitation was clearer than the final solution produced using liquid–liquid extraction. The volume of the plasma samples (500  $\mu$ l) using liquid–liquid extraction was greater than with protein precipitation (100  $\mu$ l). This difference in sample volume affected how clean the plasma samples were. In Bonfiglio et al. [10], one solution for the ion suppression problem was to use cleaner sample preparation methods whenever possible to eliminate some of the interfering plasma components. Although these different sample treatment methods caused differences in response suppression, the results of Bonfiglio et al. suggest that the chemical nature of the compound has more of an effect on the amount of response suppression than the sample preparation method itself [10].

#### 4. Conclusion

In conclusion, the protein precipitation method caused the least response suppression (matrix effect) in the analysis of afloqualone in plasma, while the liquid–liquid extraction samples showed high ion suppression, especially at high afloqualone concentrations. In addition, the protein precipitation sample preparation method is less expensive and faster than the liquid–liquid extraction method. Therefore, we recommend using the protein precipitation method for analyzing afloqualone in human plasma.

#### Acknowledgement

This study was supported by a grant from the Korea Food and Drug Administration (KFDA).

**References**

- [1] H. Kaji, T. Kume, *Drug Metab. Dispos.* 33 (2005) 60–67.
- [2] Arobest<sup>®</sup> Tablet Insert Paper, Hanil Pharm., Suwon, Korea.
- [3] S. Furuuchi, M. Otsuka, Y. Miura, S. Harigaya, *Drug Metab. Dispos.* 11 (4) (1983) 371–376.
- [4] M. Otsuka, S. Furuuchi, S. Usuki, S. Nitta, S. Harigaya, *J. Pharm. Dyn.* 6 (1983) 708–720.
- [5] N.V.S. Ramakrishna, K.N. Vishwottam, M. Koteswara, S. Manoj, M. Santosh, J. Chidambara, B. Sumatha, D.P. Varma, *J. Pharmaceut. Biomed.* 40 (2006) 360–368.
- [6] R.K. Trivedi, R.R. Kallem, R. Mullangi, N.R. Srinivas, *J. Pharmaceut. Biomed.* 39 (2005) 661–669.
- [7] W. Kang, H.Y. Yun, K.H. Liu, K.I. Kwon, J.G. Shin, *J. Chromatogr. B* 805 (2004) 311–314.
- [8] M.H. Yun, K.I. Kwon, *J. Pharmaceut. Biomed.* 40 (2006) 168–172.
- [9] L. Shargel, A. Yu, *Applied Biopharmaceutics and Pharmacokinetics*, fourth ed., Appleton & Lange, Stamford, CT, 1999.
- [10] R. Bonfiglio, R.C. King, T.V. Olah, K. Merkle, *Rapid Commun. Mass Spectrom.* 13 (1999) 1175–1185.